Quorum Sensing as a Potential Biomarker Target to Diagnose *Staphylococcus aureus* Infections

Carla Ferrero Ruedas

UNIVERSITAT DE BARCELONA
FACULTAT DE FARMÀCIA I CIÈNCIES DE L'ALIMENTACIÓ

"Quorum Sensing as a Potential Biomarker Target to Diagnose *Staphylococcus aureus* Infections"

"El Quorum Sensing com a possible biomarcador per al diagnòstic d'infeccions per *Staphylococcus aureus*"

Carla Ferrero Ruedas

2025

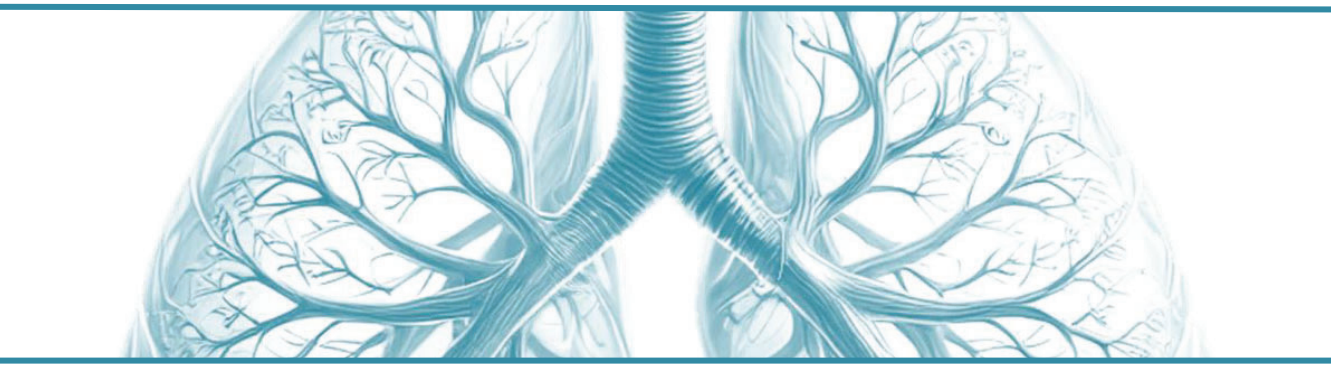



UNIVERSITAT DE BARCELONA

Facultat de Farmàcia
i Ciències de l'Alimentació

Doctoral program in Biotechnology

"Quorum Sensing as a Potential Biomarker Target to Diagnose *Staphylococcus aureus* Infections"

"El Quorum Sensing com a possible biomarcador per al diagnòstic d'infeccions per *Staphylococcus aureus*"

"Dissertation presented by Carla Ferrero in fulfillment of the requirements for the degree of doctor by Universitat de Barcelona"

PhD candidate
Carla Ferrero Ruedas

Supervisors:

Prof. Mª Pilar Marco Colás
Research Professor
Head of Nanotechnology for Diagnostic group,
IQAC-CSIC

Dr. J-Pablo Salvador
Tenured Scientist
Nanotechnology for Diagnostic group
IQAC-CSIC

Tutor:
Prof. Verónica Noé Mata
Department of Biochemistry and Physiology
Faculty of Pharmacy
University of Barcelona

AGRADECIMIENTOS

Han sido años de esfuerzo, superación y crecimiento. A veces el camino fue un paseo, otras una carrera de obstáculos. Hubo días en los que dudé de mí misma, pero siempre tuve en mente una frase: *"Algún día diré: no fue fácil, pero lo logré."* Hoy, al escribir estas líneas, puedo decir con orgullo que ese día ha llegado.

Esta tesis es mucho más que un trabajo académico. Es el reflejo de caídas, aprendizajes, risas, lágrimas y, sobre todo, de todas las personas que han estado ahí, con paciencia y apoyo incondicional.

Pilar, desde el primer día he admirado el alto nivel y la profesionalidad que tanto tú como los integrantes del equipo demuestran cada día. Ha sido una gran oportunidad de aprendizaje y de crecimiento profesional, una experiencia que ha transformado mi manera de enfrentar los retos. Todo esto no habría sido posible sin tu apoyo, tu calidez humana y el trato cercano que me has brindado durante estos años.

Pablo, mi estimado colaborador, muchas gracias por confiar en mí, por dedicarme tu tiempo y por darme la libertad de poder proponer nuevas ideas, que han enriquecido enormemente mi capacidad de razonar y encontrar nuevas soluciones. Has sido para mí un gran mentor y una fuente de inspiración, siempre con cercanía y humor.

Gracias, Nuria, por enseñarme todo sobre cultivo celular y producción de anticuerpos. Aprendí de la mejor. Lluïsa, aunque no trabajamos juntas directamente, siempre estuviste dispuesta a ayudar y a aportar soluciones en cada momento. Gracias por tu enorme implicación. Roger, además de ser un investigador excepcional, aportaste humor en los momentos difíciles. Es una pena que no pudieras acompañarme hasta el final de este recorrido, pero siempre es una alegría verte.

Dicho esto, también quiero agradecer al resto de miembros del Nb4D por su apoyo incondicional. Desde el primer día me han acogido y han conseguido que me sienta como en CASA. Es un grupo increíblemente profesional y multidisciplinar, lleno de conocimientos y grandes científicos, pero, sobre todo, he encontrado en ellos una FAMILIA que me ha arropado y acompañado en cada paso de este camino.

Todos vosotros habéis endulzado esta etapa de mi vida con vuestra calidez y complicidad. No han faltado las horas de "terapia grupal", donde cada uno confesaba tener más "taritas" que el anterior. Juntos hemos compartido momentos de fatiga, risas, confesiones, cotilleos y viajes, construyendo recuerdos inolvidables que siempre llevaré conmigo. Gracias por convertir esta experiencia en algo mucho más grande que una tesis.

Nere, mi niña, mi compañera de fatigas. No se me ocurre mejor persona con quien haber trabajado codo con codo. Has sido un apoyo incondicional y una gran amiga. Hemos compartido momentos increíbles y también difíciles, y eso ha hecho que nuestro vínculo sea aún más fuerte. Siento que me entiendes, que somos un equipo y que siempre puedo contar contigo. Eres luz, desprendes una energía increíble y sé que esta amistad no se perderá con el tiempo. Te quiero mucho, maiti.

Irenita, me cuesta creer cómo alguien puede dejar una huella tan grande en tan poco tiempo. Desde que llegaste, congeniamos como si nos conociéramos de siempre. Tus abrazos, tu humor, tus momentos de telenovela y tu enorme sensibilidad han sido un pilar clave en esta etapa final. Cada día contigo ha tenido un toque especial, y solo puedo agradecerte por estar ahí, por las risas y por recordarme lo bonito que es encontrar personas como tú en el camino.

Juantxi, mi hermanito de tesis. Hemos vivido de todo juntos: una pandemia, clonajes interminables, escapadas, cotilleos diarios y viajes inolvidables. Me alegro de haber compartido estas experiencias contigo, de haber creado recuerdos únicos y, sobre todo, de habernos apoyado en el día a día. Más allá de la ciencia, ha habido risas, desahogos y una complicidad que solo crece con el tiempo. Te tengo mucho cariño, gracias por estar siempre ahí.

Marcus, desde que llegaste al grupo, revolucionaste el Nb4D. Tus preguntas y conversaciones han abierto debates interminables nos han hecho replantearnos demasiadas cosas. Me has ayudado a centrarme, a conocerme mejor y a conoceros aún mejor a todos vosotros. Has sido ese toque de cercanía que rompe barreras, siempre con humor y autenticidad. Me alegro de haber hecho "Historia" juntos y, aunque fuiste el primero en volar, sé con certeza que esto es un hasta siempre.

Deivid, algún día descubriré el secreto de tu eterna juventud y tu energía inagotable. Si algo tengo claro, es que estos años no habrían sido lo mismo sin ti. Cada día a tu lado tiene su toque de humor, desde tus expresiones pegadizas hasta tu incansable búsqueda de "miseria humana". Nos das vida, nos ayudas a quitarle peso a las preocupaciones, nos animas a conocer mundo y nos alegras cada día con tu forma única de ser. Contigo he aprendido, junto con el refranero español completo, que hay que vivir sin miedo y actuar con rapidez porque, al fin y al cabo, *"la vida es esto".* Eres único, no cambies nunca.

Fran, mi project manager de confianza, compañero de piscina, repostero experto y catador de pizzas. En cada vivencia compartida has estado ahí, siempre atento, ofreciendo tu ayuda y pensando en el bien del grupo. Has sido el pegamento que nos ha mantenido unidos, esa pieza clave que hace que todo funcione mejor. Gracias por tu empatía, por esas conversaciones que arreglan el mundo y por hacer de esta etapa algo aún más especial. Me alegro de haber coincidido contigo en este camino.

Monsis, has sido como una madre para mí. Más allá de ser una gran investigadora, eres una persona increíble: fuerte, valiente, empática y siempre con una sonrisa. Gracias por tu apoyo incondicional, por los saludos mañaneros, los abrazos en el pasillo y por preguntarme *"¿qué tal estás?"* con ese cariño genuino que tanto te define. Pequeños gestos que han significado muchísimo y me han hecho sentir arropada.

Mis nenitas, sois fantásticas. Juntas sois imparables, complementándoos a la perfección, pero cada una tiene una esencia única que hace especial al grupo. Ido, me alegro de haber compartido estos años contigo y de haber descubierto aún más la gran persona que eres. Carismática y divertida, pero con esa calma que transmite paz. Andrius, tu cercanía y humor hicieron que conectar contigo fuera fácil desde el primer momento. Lidia, tu energía, tu personalidad arrolladora y tu generosidad hacen que todo el mundo se sienta bien a tu lado. Gracias a las tres por vuestra alegría contagiosa y por hacer de este grupo algo aún más especial.

Juli, con tu acento nos cautivaste y con tu humor nos conquistaste. Gracias por esas charlas interminables, desde cotilleos hasta debates científicos que siempre derivaban en temas inesperados. Contigo nunca faltaron las risas ni la diversión, y cada momento compartido ha sido único. Desde ser tu fan #1 y seguirte hasta

Madrid hasta acabar rodeada de plumas en carnaval, hay recuerdos que siempre quedarán grabados. Me alegro muchísimo de haber compartido esta etapa contigo.

Gemmita, aunque no compartimos tanto tiempo juntas, cada momento contigo estuvo lleno de risas y buen humor. Tu energía, tu sonrisa y tu actitud positiva hicieron que encajaras en el grupo desde el primer día, como si siempre hubieras estado con nosotros. Y aunque el tiempo fue corto, sigues presente en cada anécdota donde tu alegría y stickers para partirse de risa dejaron huella.

Quiero agradecer a todas las personas que han pasado por el Nb4D y con quienes he tenido la suerte de coincidir. Gracias por hacer que cada día de trabajo fuera más especial, por las risas, los momentos compartidos y por estar siempre dispuestos a ayudar. Enrique, Luciano, Joel, Eva, Ástrid, Bárbara, Ana, Melek, Fabiola, Bet, cada uno ha dejado su huella en esta etapa. También a las incorporaciones más recientes. Tamás, Romi, Min y Samuele, gracias por formar parte de esta aventura.

También quiero dar las gracias a Imanol. Aunque ya lo sabes, aunque nos distanciemos, para mí seguirás siendo familia. No has sido solo mi pareja, sino también mi amigo, mi compañero de piso, mi hombro en el que llorar y un apoyo incondicional en los momentos más difíciles. Gracias por haber estado siempre ahí y por creer en mí incluso cuando yo dudaba.

Marc, gracias por aparecer en mi vida. Como siempre decimos, nos hacemos bien el uno al otro, y de alguna forma consigues sacar lo mejor de mí. Contigo todo ha sido más fácil. Me has hecho reír, desconectar, probar deportes y actividades nuevas, e incluso temer por mi vida al sobrepasar badenes o escalar montañas entre desfiladeros. Has sido clave en esta recta final, con tus llamadas interminables y ese toque de humor que tanto me gusta. Gracias por todos los momentos vividos y por lo que aún nos queda por construir juntos.

Chiara, cariño, llegaste a mi vida de forma inesperada, pero qué suerte haberte conocido y haber compartido este tiempo juntas. Más que una compañera de piso, te has convertido en una amiga que hace de nuestra casa un verdadero hogar. Gracias por tu humor, por tu personalidad tan alegre y cercana, por los ratitos compartiendo una copa vino y viendo una peli juntas, por tus consejos y por estar siempre ahí.

Gracias a mis neskas, Meri, Patri, Maider, Yangxi, Joha y Nago. Aunque nos separen más de 600 km, sé que siempre podré contar con vosotras. Esta tesis lleva un pedacito de cada conversación, cada palabra de aliento y cada momento en el que, pese a la distancia, habéis estado cerca.

También gracias a todos esos amigos que, de una forma u otra, han formado parte de este proceso, compartiendo risas, desahogos y compañía, haciendo que este camino fuera mucho más especial.

Por último, gracias a mi familia, la más increíble que podría imaginar. Aita, ama, gracias por dejarme volar y ser mi mayor apoyo, pese a la distancia. Siempre sois mi refugio. Maritxu, mi canija, eres un ejemplo de esfuerzo y alegría, y me recuerdas lo importante que es vivir con ilusión. Gracias también a mi yaya Cloti, que es como una segunda madre; a mi yayo Eliseo, que siempre creyó en mí; y a mis yayos Etel y Toño, por sus llamadas constantes y esos *"te quiero"* que significan tanto. A toda mi familia, gracias por ser ese núcleo donde siempre encuentro cariño y apoyo incondicional.

Todos vosotros habéis sido parte de esta aventura, y solo puedo estar agradecida por la suerte inmensa que tengo de teneros cerca, de sentirme tan querida. No sabéis lo afortunada que me siento. ¡Muchas gracias!

Carla

THESIS ABSTRACT

Staphylococcus aureus is a Gram-positive bacterium capable of causing a wide range of infections, from minor skin conditions to severe diseases like pneumonia and sepsis. Its adaptability, virulence factors, and the emergence of multidrug-resistant strains, such as methicillin-resistant *S. aureus* (MRSA), pose significant global health challenges. Current diagnostic methods, such as culture-based techniques, are time-consuming, delaying treatment and contributing to antimicrobial resistance.

This research focuses on developing immunochemical diagnostic tools to detect *S. aureus* infections rapidly and effectively. The work targets the main quorum sensing (QS) system of this bacterium, known as the accessory gene regulator (*agr*) system, which coordinates the production of virulence factors through autoinducing peptides (AIPs). AIPs are presented as biomarkers for detecting infections, phenotyping strains based on their *agr* group, and guiding therapeutic strategies.

To achieve these goals, monoclonal and polyclonal antibodies against AIPs were developed and implemented in ELISAs. These assays demonstrated exceptional sensitivity, with low IC_{50} values (20.41 nM for AIP1o; 2.70 nM for AIP2o; 6.54 nM for AIP3c; and 2.19 nM for AIP3o), exceeding traditional detection methods like mass spectrometry. Additionally, the ELISAs were successfully adapted for detecting AIPs in bacterial culture media, providing rapid results within 2–3 hours.

The study also addressed the challenges of analyzing AIPs in complex biological samples like bronchial aspirates (BAS). Various sample preparation strategies, including enzymatic treatments and immunoaffinity purification techniques, were evaluated. Immunoaffinity spin columns (ISCs) emerged as a scalable and robust method for AIP purification, enabling accurate detection in clinical respiratory samples.

This work represents a significant advancement in diagnostic technology *for S. aureus*, offering rapid, sensitive, and clinically relevant tools. Further research is needed to validate these methods and expand their application, but they hold

great promise for improving patient outcomes and combating antimicrobial resistance.

Key words: *S. aureus*, Quorum sensing, AIPs, ELISA.

RESUMEN DE LA TESIS

Staphylococcus aureus es una bacteria Gram-positiva capaz de causar un amplio rango de infecciones, desde afecciones cutáneas leves hasta enfermedades graves como neumonía y sepsis. Su adaptabilidad, factores de virulencia y la aparición de cepas multirresistentes, como *S. aureus* resistente a meticilina (MRSA), representan importantes desafíos para la salud global. Los métodos diagnósticos actuales, como las técnicas basadas en cultivos, son laboriosos y consumen tiempo, lo que retrasa el tratamiento y contribuye a la resistencia antimicrobiana.

Esta investigación se centra en desarrollar herramientas de diagnóstico inmunoquímico para detectar infecciones por *S. aureus* de manera rápida y efectiva. El trabajo se enfoca en el principal sistema de quorum sensing (QS) de esta bacteria, conocido como el regulador génico accesorio (*agr* según sus siglas en inglés), que coordina la producción de factores de virulencia a través de los péptidos autoinductores (AIPs). Los AIPs se presentan como biomarcadores para detectar infecciones, fenotipar cepas según su grupo *agr* y guiar estrategias terapéuticas.

Para alcanzar estos objetivos, se desarrollaron anticuerpos monoclonales y policlonales contra los AIPs, que se implementaron en ensayos ELISA. Estos ensayos demostraron una sensibilidad excepcional, con valores de IC_{50} bajos (20,41 nM para AIP1o; 2,70 nM para AIP2o; 6,54 nM para AIP3c; y 2,19 nM para AIP3o), superando métodos de detección tradicionales como la espectrometría de masas. Además, los ELISAs se adaptaron con éxito para detectar AIPs en medios de cultivo bacteriano, proporcionando resultados rápidos en tan solo 2-3 horas.

El estudio también abordó los desafíos de analizar AIPs en muestras biológicas complejas como aspirados bronquiales (ABs). Se evaluaron diversas estrategias de preparación de muestras, incluidos tratamientos enzimáticos y técnicas de purificación por inmunoafinidad. Las columnas de inmunoafinidad por centrifugación (aquí denominadas ISCs) se destacaron como un método escalable y robusto para purificar AIPs, permitiendo una detección precisa en muestras respiratorias clínicas.

Este trabajo representa un avance significativo en las tecnologías de diagnóstico para *S. aureus*, ofreciendo herramientas rápidas, sensibles y clínicamente relevantes. Si bien se requiere más investigación para validar estos métodos y ampliar su aplicación, muestran un gran potencial para mejorar los resultados de los pacientes y combatir la resistencia antimicrobiana.

Palabras clave: *S. aureus*, Quorum sensing, AIPs, ELISA.

RESUM DE LA TESI

Staphylococcus aureus és una bactèria Gram-positiva capaç de causar una àmplia varietat d'infeccions, des d'afectacions cutànies lleus fins a malalties greus com pneumònia i sèpsia. La seva adaptabilitat, els seus factors de virulència i l'aparició de soques multiresistents, com *S. aureus* resistent a la meticilina (MRSA), representen importants reptes per a la salut global. Els mètodes diagnòstics actuals, com les tècniques basades en cultius, són laboriosos i requereixen molt de temps, fet que retarda el tractament i contribueix a la resistència antimicrobiana.

Aquesta investigació se centra en desenvolupar eines de diagnòstic immunoquímic per detectar infeccions per *S. aureus* de manera ràpida i efectiva. El treball es focalitza en el principal sistema de quorum sensing (QS) d'aquesta bactèria, conegut com el regulador genètic accessori (*agr*, per les seves sigles en anglès), que coordina la producció de factors de virulència a través dels pèptids autoinductors (AIPs). Els AIPs es presenten com a biomarcadors per detectar infeccions, fenotipar soques segons el seu grup *agr* i guiar estratègies terapèutiques.

Per assolir aquests objectius, es van desenvolupar anticossos monoclonals i policlonals contra els AIPs, que es van implementar en assajos ELISA. Aquests assajos van demostrar una sensibilitat excepcional, amb valors d'IC_{50} baixos (20,41 nM per a AIP1o; 2,70 nM per a AIP2o; 6,54 nM per aAIP3c; y 2,19 nM per a AIP3o), superant mètodes de detecció tradicionals com l'espectrometria de masses. A més, els ELISAs es van adaptar amb èxit per detectar AIPs en medis de cultiu bacterià, proporcionant resultats ràpids en tan sols 2-3 hores.

L'estudi també va abordar els reptes d'analitzar AIPs en mostres biològiques complexes com aspirats bronquials (ABs). Es van avaluar diverses estratègies de preparació de mostres, inclosos tractaments enzimàtics i tècniques de purificació per immunoafinitat. Les columnes d'immunoafinitat per centrifugació (anomenades ISCs) van destacar com un mètode escalable i robust per purificar AIPs, permetent una detecció precisa en mostres respiratòries clíniques.

Aquest treball representa un avenç significatiu en les tecnologies de diagnòstic per a *S. aureus*, oferint eines ràpides, sensibles i clíniques. Tot i que cal més recerca per validar aquests mètodes i ampliar-ne l'aplicació, mostren un gran

potencial per millorar els resultats dels pacients i combatre la resistència antimicrobiana.

Paraules clau: *S. aureus*, Quorum sensing, AIPs, ELISA.

TABLE OF CONTENTS

1 INTRODUCTION

1.1 INFECTIOUS DISEASES

Infectious diseases are caused by pathogenic microorganisms, including bacteria, viruses, fungi, and parasites. These pathogens invade a host organism, multiply, and disrupt normal physiological functions, leading to various clinical manifestations. Infectious diseases can affect multiple organ systems and result in a wide range of symptoms depending on the pathogen involved, the route of infection, and the host's immune response[1].

1.1.1 INFECTION PATHWAYS AND TRANSMISSION

Pathogens can enter the body through several routes, each associated with different types of infections (see Figure 1.1). One common pathway is the respiratory tract, where pathogens such as the Influenza virus A or *Mycobacterium tuberculosis* are inhaled through **droplets or aerosols**, resulting in respiratory infections[2]. Afterwards, pathogens are disseminated when an infected person coughs, sneezes, or even talks and they can remain in the air for extended periods, increasing the risk of transmission, especially in enclosed spaces[3].

The gastrointestinal tract is another significant location to suffer infections. Pathogens like *Vibrio cholerae* or *Salmonella enterica* enter the body through contaminated **food or water**. Poor sanitation and hygiene practices are key factors that facilitate the transmission of these diseases, particularly in areas with inadequate access to clean water[4].

Skin and mucous membranes also serve as entry points for pathogens. Bacterial infections, such as those caused by Herpes simplex virus (HSV) and *Staphylococcus aureus,* can occur when the skin is broken or wounded, allowing the bacteria to penetrate and infect the underlying tissues[5]. Similarly, sexually transmitted infections such as *Neisseria gonorrhoeae* and *Chlamydia trachomatis* are spread through mucous membranes during contact with infected bodily fluids[5, 6].

Vector-borne pathway involves pathogens being carried from one host to another through vectors like mosquitoes. Diseases such as malaria, zika and

dengue fever are spread by mosquitoes as intermediaries, transmitting thosee pathogen from an infected person or animal to a new host[7].

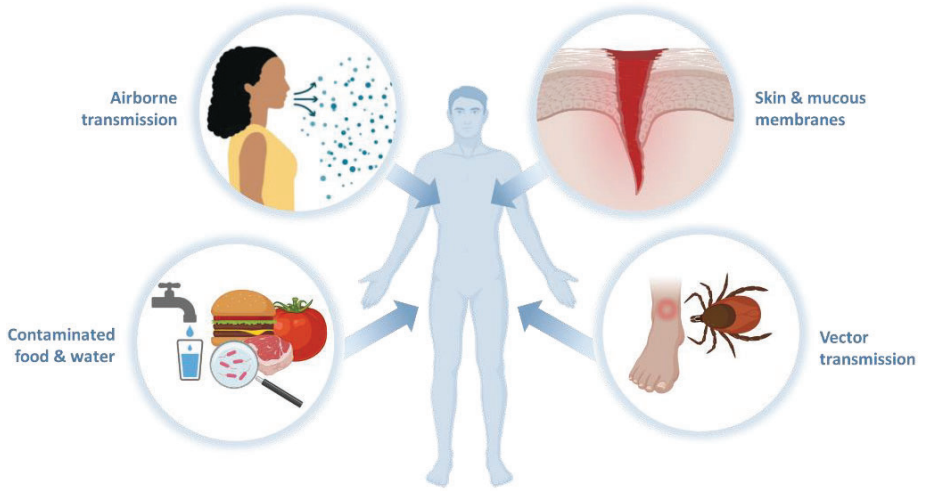

Figure 1.1. *Main transmission routes. The figure illustrates the primary pathways for disease transmission: airborne, contaminated food and water, skin and mucous membranes, and vectors.*

There are various ways in which infectious diseases can spread. On one side, **direct transmission** occurs when pathogens move directly from one individual to another, such as through body fluids like blood, saliva, or mucus. This mode includes person-to-person contact (touching, kissing, or sexual interactions). Diseases like HIV and certain respiratory illnesses like influenza can be transmitted efficiently in this manner due to the easy transfer of viruses present in body fluids during close physical interactions.

On the other side, **indirect transmission** involves pathogens surviving on surfaces or objects (known as fomites) before infecting a new host when they come into contact with these contaminated surfaces. Diseases like norovirus and some forms of influenza can spread this way, especially in crowded or unsanitary environments[8].

Several **factors** influence how efficiently a **pathogen spreads**, which **pathogen characteristics** are fundamental. For instance, the infectious dose is the minimum number of organisms required to cause infection, varies significantly between pathogens. Highly contagious pathogens like measles have a low infectious dose, meaning only a few viral particles are needed to infect a person, allowing rapid spread within susceptible populations[9].

Another important characteristic is the ability of the pathogen to **survive outside the host**, which plays a crucial role in its transmission potential. Pathogens that can remain viable for extended periods on surfaces or in the environment have a higher chance of infecting new hosts, specially in areas with frequent human contact[10]. Some examples of bacteria that can survive for extended periods on inert surfaces, posing a significant challenge particularly in hospital environments, include *S. aureus*, *Pseudomonas aeruginosa*, and *Acinetobacter baumannii*[11]. Additionally, **high mutation rates**, especially in viruses like influenza[12], allow pathogens to adapt quickly to host immune defenses, increasing their transmissibility. Such genetic adaptability is a key factor in the virus's ability to cause recurrent seasonal outbreaks and pandemics. The frequent genetic changes, known as antigenic drift, result in the emergence of new viral variants that evade immunity developed from previous infections or vaccinations, highlighting the importance of continuous monitoring and vaccine updates to control these outbreaks[13].

Virulence factors play a pivotal role in facilitating the initial stages of infection. For instance, adhesins that help pathogens attach to host cells, like pili, fimbriae or proteoglycans, are critical in linking the pathogen to host cell receptors, initiating the infection process[14]. Such mechanisms not only play a crucial role in the pathogen’s ability to evade immune responses and proliferate, but also increase its capacity to spread efficiently within susceptible populations[15].

Host factors significantly impact the transmissibility of infectious diseases. Individuals with weakened immune systems, due to factors like age, malnutrition, or immunocompromising conditions such as HIV, are more vulnerable to infections[16]. These individuals often experience a higher severity of disease and may contribute to increased transmission rates within communities as pathogens can spread more easily in such hosts.

Additionally, high **population density** and close **human contact**, common in urban settings, amplify the spread of infections, particularly those transmitted through respiratory droplets or direct contact. **Travel and commerce** between countries have made the spread of infectious diseases much more complex, speeding up the propagation of infections across frontiers. This was demonstrated by the rapid global spread of COVID-19, as the SARS-CoV-2 managed to spread from China to all around the world within 3 to 4 months[17].

These activities create opportunities for rapid transmission of respiratory diseases and other infections that spread through close human interaction[18].

Finally, **environmental factors** such as sanitation, hygiene practices, and access to clean water critically determine how infectious diseases spread. In regions with poor sanitation, waterborne diseases like cholera become prevalent as pathogens easily contaminate water supplies. Seasonal variations, temperature, and humidity also affect vector populations and the stability of airborne particles, influencing the spread of infections like malaria and influenza[19].

1.1.2 INVASION MECHANISMS AND IMMUNE RESPONSE

At the cellular and molecular levels, pathogens employ a variety of mechanisms to colonize and invade host tissues. **Bacteria**, for example, produce **virulence factors** such as toxins, adhesins, and enzymes that facilitate attachment to host cells and evasion of the immune system[20]. These virulence factors enable bacteria to break down host barriers, such as epithelial layers and extracellular matrix components, and manipulate host signalling pathways to promote their survival and replication[21]. In the case of **viruses**, the infection often begins with the **attachment to specific receptors** on the host cell surface, followed by entry, replication, and subsequent release of new viral particles that propagate the infection[22].

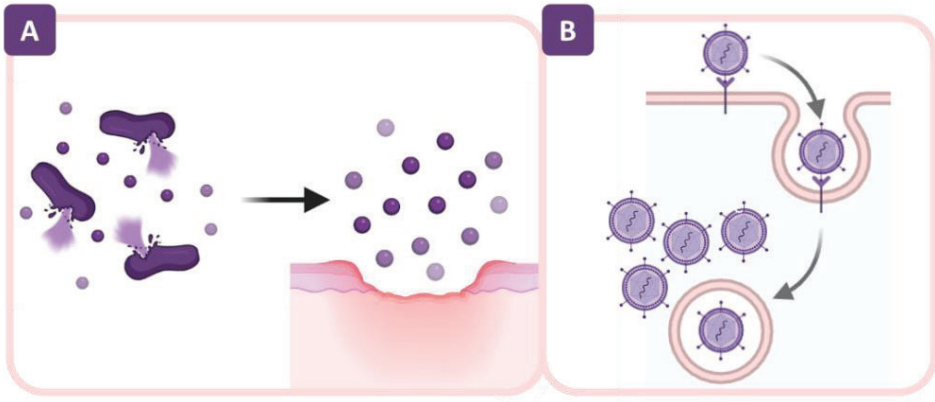

Figure 1.2. *Invasion mechanisms of bacteria vs. viruses. A) Bacteria use virulence factors like toxins, adhesins, and enzymes to attach to host cells, evade the immune system, and break down barriers, promoting survival and replication. B) Viruses infect host cells by binding to specific receptors, entering the cell, replicating, and releasing new viral particles to spread the infection.*

The immune system plays a crucial role in the **host's defence** against infectious agents. The first line of defense is provided by **innate immunity**, which includes soluble components like complement proteins and cytokines, cellular reactions like neutrophils and macrophages, and physical barriers like skin and mucous membranes[23]. **Adaptive immunity**, involving T and B lymphocytes, is more specific and develops a memory response that enhances protection upon re-exposure to the same pathogen[24]. An illustration comparing the main components of the immune system is shown in Figure 1.3. Despite these defences, pathogens have evolved strategies to evade immune detection and neutralization. For instance, some bacteria can form biofilms, complex communities encased in a protective matrix, which can resist antimicrobial treatment and immune clearance. Viruses may alter their surface proteins through antigenic variation, complicating recognition by the immune system.

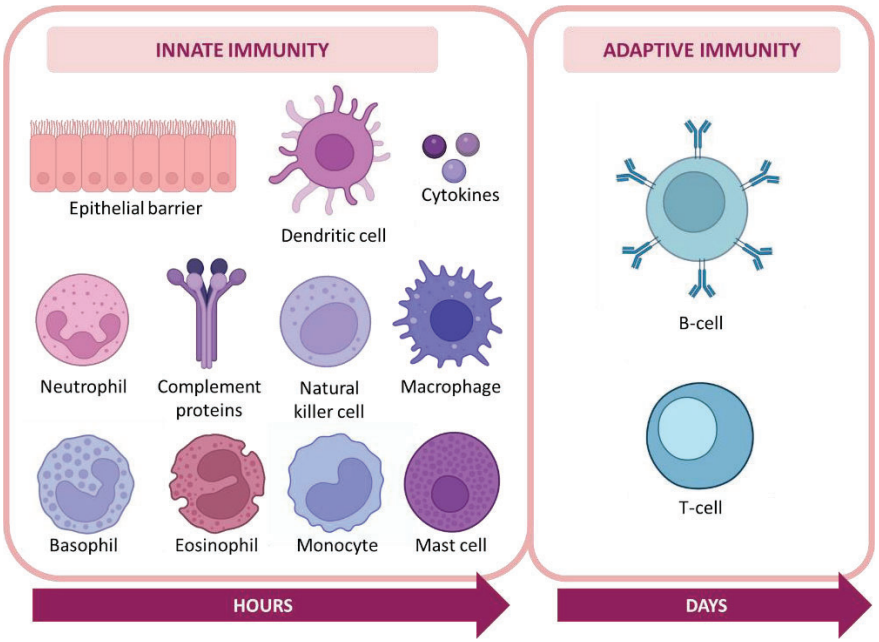

Figure 1.3. *Immune system overview. The figure highlights the two main components of the immune system: innate immunity and adaptive immunity. Innate immunity acts within the first hours of exposure and includes physical barriers (skin and mucous membranes), soluble components (complement proteins and cytokines), and various immune cells such as neutrophils, basophils, eosinophils, macrophages, dendritic cells, mast cells, monocytes, and natural killer cells. Adaptive immunity, which develops over days, is mediated by B and T lymphocytes. Adapted from Ernst, L. M., et al.[25].*

1.1.3 CLINICAL MANIFESTATIONS

Infectious diseases can present a wide range of clinical manifestations, which vary based on the pathogen and the affected organ systems. **Localized symptoms** often occur when infections are confined to a specific area, such as the skin or respiratory tract. Skin infections may cause redness, swelling, and pus formation[5], while respiratory infections typically present with symptoms like coughing, difficulty breathing, and chest pain[26].

In contrast, some infectious diseases lead to **systemic symptoms**, affecting the entire body. These symptoms include fever, fatigue, and muscle aches, indicating the body's immune response to the infection. In severe cases, when pathogens spread throughout the body, they can cause organ failure or septic shock, which is life-threatening[27].

Certain pathogens can establish **chronic or latent infections**, where they persist within the host for extended periods. For example, *M. tuberculosis* and HSV can remain dormant for years. While these infections may be asymptomatic initially, they can reactivate later, leading to chronic health issues such as tuberculosis or recurrent herpes outbreaks[28].

1.1.4 INCIDENCE

Infectious diseases have been one of the **main causes of morbidity and mortality** throughout human history and their incidence is determined by a number of factors, such as **microbial evolution**, **environmental changes**, and **human behaviour.** Although public health and medicine have made great progress, infectious diseases remain a major global health concern, accounting for millions of cases and deaths annually. As, reported by The World Health Organization (WHO), communicable diseases such as tuberculosis, HIV/AIDS, malaria, and respiratory infections continue to cause significant mortality (see Figure 1.4).

The global burden of infectious diseases varies significantly by region. In **lower-income countries**, particularly in sub-Saharan Africa and parts of Asia, infectious diseases spread easily due to poor sanitation, restricted access to treatment and malnutrition, worsening health and further limiting health and economic

resources[29, 30]. For instance, **respiratory infections** such as pneumonia and influenza are major contributors, causing an estimated **2.5 million deaths annually**, particularly in children under five and elderly populations in low-income regions[31]. In 2021, **tuberculosis** remained a leading respiratory infection, responsible for **1.4 million deaths**, predominantly in sub-Saharan Africa and Southeast Asia[32].

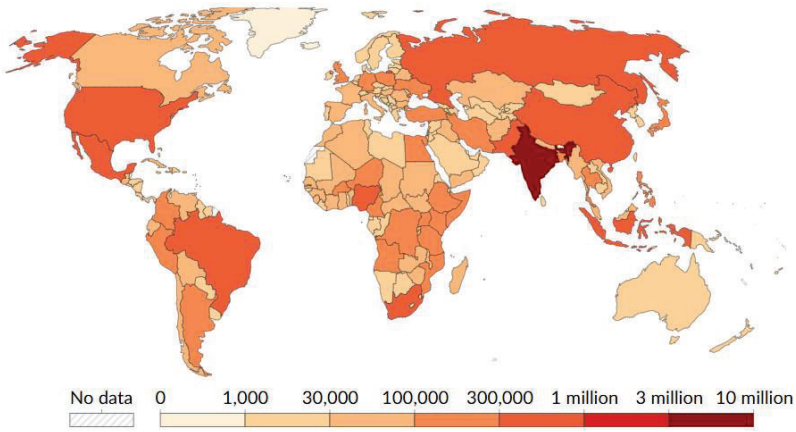

Figure 1.4. *Deaths caused by infectious diseases in 2021. The figure illustrates the global impact of infectious diseases. Although the burden varies across regions, it remains a significant concern worldwide. Retrieved from IHME, Global Burden of Disease[33].*

Specifically, lower respiratory tract infections (**LRTIs**), often exacerbated by poor air quality and limited access to healthcare, have significantly impacted vulnerable populations. According to the WHO, household air pollution, mainly from cooking with solid fuels like biomass and coal, is a major contributor to these infections. In 2020, household **air pollution** caused approximately 3.2 million deaths globally, with 21 % of these attributed to **LRTIs**[34]. This includes 44 % of pneumonia deaths in children under five, highlighting a critical health risk for young children in low-resource environments where clean cooking technologies are limited[35].

Moreover, **malaria** caused around 619,000 deaths globally in 2021, with over 95 % of cases occurring in African countries[36]. **Diarrheal diseases**, closely linked to poor sanitation and unsafe drinking water, accounted for over 1.5 million deaths, mostly among children under five in low-resource settings. These examples reflect the close relationship between socioeconomic factors and infectious

diseases, highlighting the urgent need for targeted interventions and resources to combat the burden of infectious diseases in vulnerable populations.

1.1.5 IMPACT

The impact of infectious diseases can be manifested at many different levels, affecting public healthcare systems, social institutions, economy and individual health. The incidence of communicable diseases has a huge impact on **public healthcare systems**, leading to various significant effects. Pandemics and epidemics impose pressure on healthcare systems by overcrowding clinics and hospitals, running out of medical supplies, and wearing out medical personnel. For example, the COVID-19 pandemic revealed vulnerabilities in even the most sophisticated healthcare systems, causing significant disruptions to standard medical services[30].

The effects of infectious diseases are broad and varied in terms of the **economy**. Through a number of different processes, outbreaks can result in large economic losses. For instance, the COVID-19 pandemic's estimated trillion-dollar global economic impact accounts for healthcare costs as well as the massive company closures and interruptions to commerce and travel[37, 38].

Additionally, infectious diseases have a significant **social impact**. In order to restrict the spread of diseases, public health responses can adopt measures like social distancing and quarantine, which may have an impact on **day-to-day activities** and **social life**. In addition, some diseases can lead to behavioral changes and increased public awareness, which promotes a culture of preventive care and health consciousness. For example, the widespread mask use and more concious and frequent hand-cleaning COVID-19 pandemic's have had a favourable long-term impact on public health practices. Additionaly, access to healthcare can be more difficult for vulnerable populations such as the elderly people and those with limited economic resources. This emphasizes the need for customized assistance and interventions to guarantee equal access to everyone[39, 40].

1.1.6 TREATMENT AND CONTROL

The treatment, prevention, and control of infectious diseases require a comprehensive approach that combines **medical interventions**, **public health strategies**, and **behavioral modifications** (see Figure 1.5). Effective management not only involves addressing existing infections but also preventing their spread and minimizing the risk of outbreaks.

Treatment strategies vary depending on the pathogen type (bacteria, viruses, fungi, or parasites) and the severity of the disease. **Antibiotics** are fundamental for bacterial infections, targeting specific bacterial functions like cell wall synthesis or protein production. However, the rise of antibiotic resistance due to misuse and overuse has become a significant global health issue, making the development of new drugs and alternative therapies essential[41, 42].

Antiviral medications, on the other hand, are crucial for managing viral infections like HIV, influenza, and hepatitis, targeting various stages of the viral life cycle to inhibit replication and reduce disease severity. For example, antiretroviral therapy has significantly improved HIV management by lowering viral loads and preventing progression[43]. Additionally, **antifungal** and **antiparasitic** treatments are used for infections like candidiasis and malaria, demonstrating the need for diverse therapeutic tools to combat different pathogens.

Prevention is equally important in managing infectious diseases. In order to lessen the effects of the risks of infectious diseases and to **protect global health**, persistent efforts and international cooperation are essential. A variety of strategies must be used to mitigate the effects of infectious diseases, such as reinforcing public health infrastructure, advancing surveillance, and improving healthcare systems[44]. Furthermore, decreasing the prevalence and consequences of infectious diseases in groups that are already vulnerable requires addressing **socioeconomic factors** of health[45].

Vaccination remains one of the most effective measures, as it boosts immunity and reduces disease incidence. Global **vaccination** efforts have drastically reduced the prevalence of diseases such as measles, influenza, and COVID-19, demonstrating their critical role in preventing outbreaks and maintaining public health. For example, routine immunization programs have led to a significant decline in the incidence of measles and other vaccine-preventable diseases,

preventing millions of cases annually[46]. Similarly, the COVID-19 vaccination campaigns have been instrumental in reducing the spread, hospitalizations, and deaths associated with the virus, highlighting the importance of widespread vaccination in controlling pandemics[47].

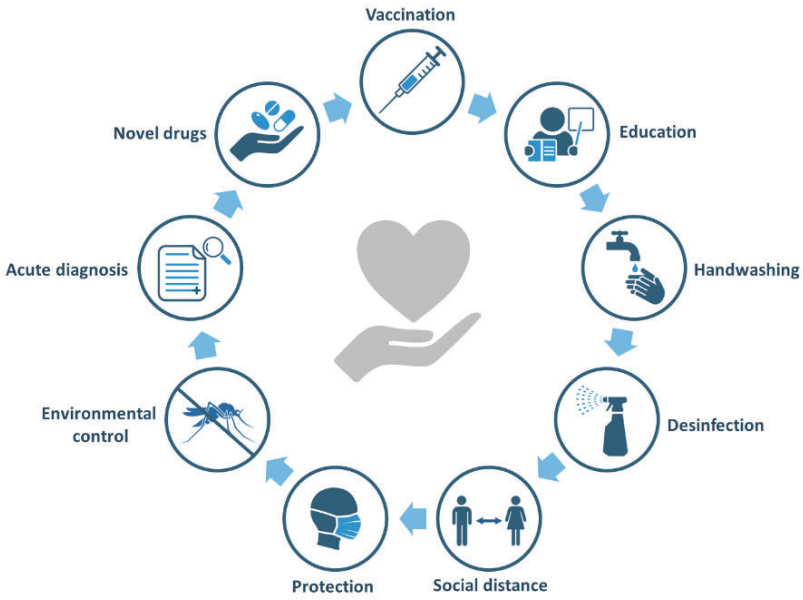

Figure 1.5. *Key measures to control infectious diseases*.

Alongside vaccination, **hygiene and sanitation** are essential, especially in regions with inadequate infrastructure. Implementing basic hygiene practices like handwashing and improving sanitation facilities can significantly reduce the spread of waterborne diseases like cholera, which are prevalent in areas lacking clean water access[48].

Environmental control measures, such as vector control, are also vital in preventing diseases transmitted by insects, like malaria and dengue. Utilizing insecticide-treated bed nets, habitat control, and spraying insecticides effectively reduce mosquito populations, limiting transmission opportunities[36]. These preventive efforts highlight the importance of targeted interventions that address the specific transmission dynamics of different pathogens.

In terms of disease control, **surveillance and monitoring** are fundamental for early detection and outbreak management. Public health authorities rely on laboratory diagnostics and data monitoring to quickly respond to emerging

threats, preventing widespread transmission[49]. **Quarantine and isolation** are also critical strategies, particularly during outbreaks of highly contagious diseases like COVID-19. These measures, when implemented effectively, can significantly reduce the spread of infections by separating infected individuals from the general population[50].

Moreover, **antimicrobial stewardship** programs are essential in combating the rise of antibiotic resistance. These programs focus on optimizing antibiotic use and monitoring resistance patterns, ensuring the long-term effectiveness of current treatments while promoting the development of new antimicrobials[51]. This integrated approach, which combines monitoring, targeted treatment, and preventive strategies, is crucial for the exhaustive management of infectious diseases.

The discovery and development of **novel drugs and therapeutic strategies** is also ongoing. Latest research focuses on antiviral and monoclonal antibody therapies, as well as on developing novel antimicrobials to combat resistant bacteria. Strategies under study to improve the treatment of infections include **reformulating** current drugs and creating **novel antimicrobial agents**[52].

Additionally, **improving diagnostic procedures** is a crucial element for controlling infectious diseases. Quick and precise diagnosis allows for early identification and treatment, **reducing** the **severity and spread** of infections. Studies have shown that the implementation of rapid diagnostic techniques in healthcare settings significantly enhances patient outcomes by enabling quicker, more precise identification of pathogens and appropriate treatment adjustments. For example, incorporating rapid diagnostic tools in ICUs has been linked to shorter hospital stays and reduced healthcare costs, highlighting their importance in controlling infectious diseases efficiently[53].

1.2 BACTERIAL INFECTIONS

Bacterial infections occur when pathogenic bacteria invade and multiply within a host, disrupting normal physiological functions. Bacteria are **unicellular microorganisms**, and while many are part of the normal flora, pathogenic bacteria can lead to disease. Factors such as the pathogen's virulence

mechanisms, the host's immune status, and the genetic variations in both host and pathogen play crucial roles in determining infection outcomes[54]. Different bacterial strains can exhibit diverse virulence factors, influencing the severity and progression of infections depending on the host's immune system's ability to respond effectively. For instance, host factors like chronic diseases or immunocompromised conditions, like diabetes or HIV, significantly increase susceptibility to severe bacterial infections and impact the host's immune response capabilities[15].

Bacteria are classified into **two major groups** based on the composition of their cell walls: Gram-positive and Gram-negative bacteria. This distinction originates from the Gram staining technique, a method developed by Hans Christian Gram in 1884, which differentiates bacteria by the characteristics of their cell wall[55].

Gram-positive bacteria have a thick layer of peptidoglycan, which retains the crystal violet stain used in the Gram staining process, causing these bacteria to appear purple under a microscope. This thick peptidoglycan layer provides structural strength but also makes Gram-positive bacteria more susceptible to certain antibiotics, like penicillin, that target cell wall synthesis[56]. Some common Gram-positive bacteria include *Staphylococcus aureus*, *Streptococcus pneumoniae*, and *Clostridium difficile*. These bacteria are often responsible for infections such as pneumonia, skin infections, and foodborne illnesses[57].

In contrast, **Gram-negative** bacteria have a thinner peptidoglycan layer but possess an outer membrane that contains lipopolysaccharides (LPS). This outer membrane not only acts as an additional barrier but also contributes to the bacteria's resistance to antibiotics and immune evasion. Gram-negative bacteria do not retain the crystal violet stain and instead appear pink or red after the staining process. Common Gram-negative pathogens include *Escherichia coli*, *P. aeruginosa*, and *Neisseria gonorrhoeae*, which are often implicated in urinary tract infections, hospital-acquired infections, and sexually transmitted diseases[58].

Thanks to developments in medical research, especially the development of antibiotics, bacterial infections can be controlled and treated. Misuse of antibiotics, however, can lead to **antimicrobial resistance (AMR)**, complicating the treatment of infections such as MRSA. AMR is the process by which bacteria develop resistance mechanisms to drugs that in previous times were capable of

killing them or limiting their growth[59]. This makes routine treatments ineffective and increases the risk of recurrent infections and transmission. As a consequence, AMR has become a major public health concern, necessitating the development of new antimicrobial strategies.

In recent decades, it is becoming more difficult to treat many bacterial infections due to the significant rise in AMR. The emergence of antibiotic-resistant bacteria is particularly notable in hospital settings, since the regular use of antibiotics favours the formation and spread of resistant strains[60]. AMR is **one of the top ten global public health challenges** that humanity is now facing, according to the World Health Organization[61]. This issue is particularly concerning in the case of some pathogens that cause a large percentage of hospital-acquired infections and can easily evade the effects of antibiotics[62]. These pathogens are grouped by the name of **ESKAPE**, including *Enterococcus faecium*, *S. aureus*, *Klebsiella pneumoniae*, *Acinetobacter baumannii*, *P. aeruginosa*, and *Enterobacter* species (see Figure 1.6).

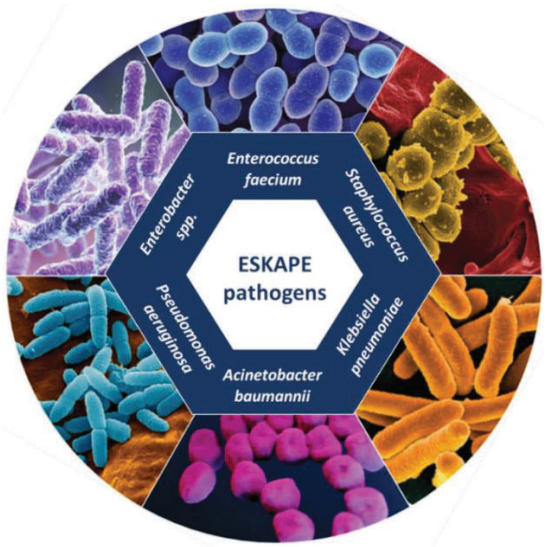

Figure 1.6. *ESKAPE pathogens. Antibiotic-resistant priority bacteria that pose the greatest threat to human health, known as ESKAPE pathogens (E. faecium, S. aureus, K. pneumoniae, A. baumannii, P. aeruginosa, and Enterobacter species) are presented.*

AMR has been recognized by the World Health Organization (WHO) as one of the top ten worldwide public health risks. According to research from the European Centre for Disease Prevention and Control (ECDC) in the European Union (EU)

around **670,000 illnesses annually** are due to antibiotic-resistant bacteria, leading to approximately **33,000 deaths**[63] and healthcare costs over **€1.5 billion**[64]. If adequate measures are not applied, the global economic cost of antibiotic resistance is expected to exceed **$100 trillion by 2050**[65].

The situation in Spain is similar to the overall European background. **Spain** has one of the highest rates of antibiotic resistance in Europe, according to ECDC data. For instance, resistance carbapenems, one of the antibiotics used as a last resort, is especially problematic in *A. baumannii* and *K. pneumoniae*. According to the Ministry of Health in Spain, there were over **4,000 cases** of infections in 2019 that were caused by carbapenem-resistant *Enterobacteriaceae*, most of them linked to *K. pneumoniae*[66].

Globally, the **incidence** of ESKAPE pathogens is **still rising**, with notable geographical differences. According to Suetens et al. (2018), the rate of multidrug-resistant *K. pneumoniae* infections in Europe is reported to be 5.4 per 100,000 population annually, with other countries seeing significantly higher rates[67]. Likewise, MRSA is still one of the main pathogens causing infections linked to healthcare settings[64].

Bacterial infections can affect various parts of the body and are categorized based on the affected organ systems (refer to Figure 1.7). **Urinary tract infections (UTIs)** are among the most common, typically caused by *E. coli*, which enters the urinary tract through the urethra. These infections lead to symptoms such as frequent urination, burning sensation, and in severe cases, kidney infections (pyelonephritis) with symptoms like fever and back pain. Women are more susceptible to UTIs, although men and children can also develop them[68].

Bacterial **infections of the gastrointestinal system** are frequently caused by pathogens like *Salmonella*, *Shigella*, *Campylobacter*, and certain strains of *E. coli*. These bacteria are commonly transmitted through contaminated food or water and can result in symptoms such as diarrhea, vomiting, abdominal cramping, and fever. Severe dehydration is a risk, especially in children, the elderly, or immunocompromised individuals[69]. Another significant gastrointestinal infection is caused by *Helicobacter pylori*, which is linked to chronic gastritis, peptic ulcers, and even gastric cancer[70].

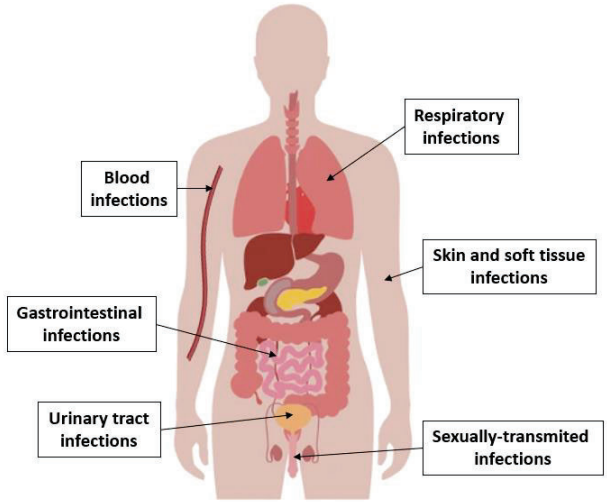

Figure 1.7. *Bacterial infection types according to the anatomical location of the infected site.*

Blood infections, or sepsis, occur when bacteria enter the bloodstream, leading to a systemic inflammatory response. The bacteria most commonly associated with sepsis include both Gram-positive and Gram-negative pathogens. Among Gram-positive bacteria, *S. aureus* and *S. pneumoniae* are frequently implicated. For Gram-negative bacteria, *E. coli* is the most common, followed by *K. pneumoniae* and *P. aeruginosa*. These pathogens are often linked to infections in the lungs, urinary tract, and abdominal regions, which can lead to bloodstream infections and sepsis[71]. This condition presents with fever, confusion, rapid heart rate, and low blood pressure. It is a medical emergency that can result in multi-organ failure if not promptly treated with antibiotics and supportive care.

Sexually transmitted infections are also caused by bacteria and include conditions such as chlamydia, gonorrhea, and syphilis. *Chlamydia trachomatis* and *Neisseria gonorrhoeae* are responsible for chlamydia and gonorrhea, both of which can cause pelvic pain, discharge, and long-term reproductive issues if untreated. Syphilis, caused by *Treponema pallidum*, can progress through various stages, initially presenting with sores and, if left untreated, leading to serious systemic effects such as neurological and cardiovascular damage[72].

Respiratory infections can affect both the upper and lower airways. Upper respiratory infections such as bacterial sinusitis and pharyngitis are primarily caused by *Streptococcus pyogenes*[73]. In contrast, lower respiratory infections,

including pneumonia, are frequently due to *S. pneumoniae* and *Haemophilus influenzae*, which are well-known pathogens involved in community-acquired infections[74]. These bacteria can present with symptoms such as coughing, fever, chest pain, and breathing difficulties. In individuals with chronic respiratory conditions, such as chronic obstructive pulmonary disease (COPD) or cystic fibrosis (CF), or those with weakened immune systems, *S. aureus* and *P. aeruginosa* become significant pathogens[75]. These bacteria often lead to severe and complicated infections, including hospital-acquired pneumonia, due to their ability to resist multiple antibiotics and adapt to host defense

1.3 RESPIRATOTY INFECTIONS

Respiratory infections constitute one of the most serious health threats globally, affecting millions of individuals every year. Both the upper and lower respiratory tracts are susceptible to these infections, causing a wide range of clinical symptoms, from minor illnesses to serious, life-threatening disorders. To effectively prevent and treat them, it is fundamental to understand their epidemiology, impact and effects.

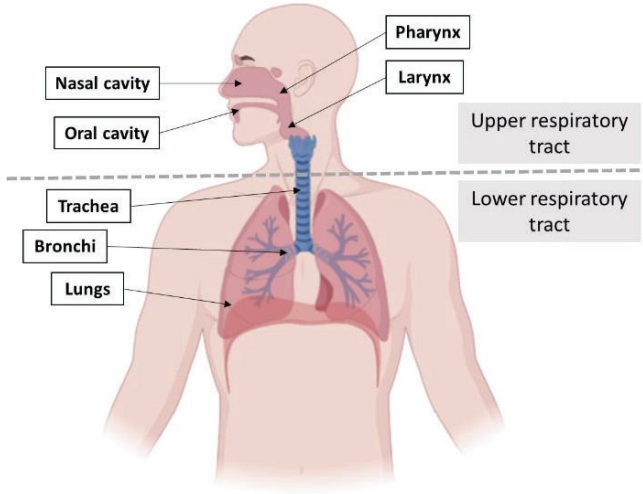

Figure 1.8. *Anatomical Overview of the Respiratory Tract. The respiratory system is divided into the upper and lower respiratory tracts. The upper respiratory tract includes the nasal cavity, oral cavity, pharynx, and larynx. The lower respiratory tract comprises the trachea, bronchi, and lungs.*

Upper respiratory tract infections (URTIs) mostly affect the nose, sinuses, pharynx, and larynx (Figure 1.8). They include the common cold, sinusitis, pharyngitis, and laryngitis. Many URTIs are viral, mostly caused by adenoviruses, coronaviruses, and rhinoviruses. Even though they are usually mild, URTIs can cause severe discomfort, absences from work, and medical visits. Additionally, they exacerbate the clinical scenario or patients suffering other disorders by making them more susceptible to subsequent bacterial infections[76].

Infections of the lower respiratory tract (LRTIs) affect the lungs, trachea, bronchi, and bronchioles (Figure 1.8) and are more severe. Pneumonia, bronchiolitis, and bronchitis are the most common LRTIs. Because of its high rates of morbidity and death, pneumonia is especially alarming when it comes to vulnerable populations, including children, the elderly, and people with underlying affections. Pneumonia continues to be the most common cause of mortality for children under five, causing more than 740,000 deaths per year according to the WHO[77]. LRTIs are a major cause of hospitalization and mortality in adults, especially in the elderly people and immunocompromised patients.

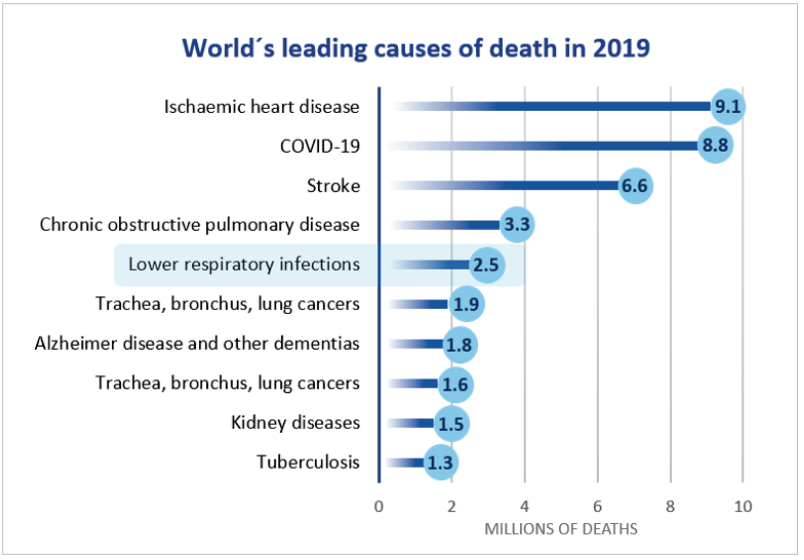

Figure 1.9. *Ranking on the world´s leading causes of death in 2021, with each bar representing the number of deaths in millions. The relevance of lower respiratory tract infections (LTRIs) is evidenced since they are the fifth cause of highest mortality rate globally, excluding COVID-19. Data retrieved from World Health Organization (WHO) (2024)[78].*

Respiratory infections are largely responsible for a great deal of infectious diseases worldwide. Particularly, **LRTIs** remain the deadliest, apart from COVID-19, which caused around 8.8 million deaths in 2021. According to WHO's Global Health Estimates, these infections consistently rank as the **fifth top cause of death globally**, resulting in almost **2.5 million deaths** according to the Global Burden of Disease Study in 2021[78] (see Figure 1.9). In **Europe,** they are a significant public health concern, with LRTIs causing high hospitalizations and mortality rates. In the EU, pneumonia leads to 230,000 hospitalizations annually[79]. In **Spain**, respiratory infections rank among the top causes of death, with pneumonia causing 8.7 thousand deaths in 2022. Recent data show increasing mortality from chronic respiratory disorders (14.8 %) and pneumonia (36.5 %) in early 2023, highlighting their severe impact on healthcare systems[80].

Bacterial respiratory infections, especially those affecting the lower respiratory tract, pose a serious challenge due to their potential complications and the increasing prevalence of AMR. **AMR** is nowadays one of the biggest dangers to global development and public health and it significantly complicates the management of bacterial respiratory infections, reducing the effectiveness of current therapies and raising the possibility of serious consequences. According to estimates, bacterial AMR **contributed** to **4.95 million deaths** worldwide in 2019 and was directly **responsible** for **1.27 million deaths** worldwide[81].

Respiratory infections driven by bacteria resistant to antibiotics are a major concern in Spain, as there are continuously adapting to new antimicrobial drugs. This complicates treatment and promotes the use of more costly, broad-spectrum antibiotics[82].

Initiatives to mitigate the prevalence of respiratory infections include **immunization campaigns**, public health initiatives encouraging good hygiene, improving diagnostic procedures and the creation of novel drugs and therapeutic approaches. Campaigns for immunization are essential for preventing respiratory diseases. As an example, immunizations against pathogens like the influenza virus, *H. influenzae*, and *S. pneumoniae* have greatly decreased their incidence[83].

Equally important are public health campaigns that promote proper hygiene practices like handwashing. Programs that promote hand cleanliness during

epidemics have been found to dramatically lower the spread of respiratory diseases[84].

1.4 *STAPHYLOCOCCUS AUREUS*

S. aureus is a **Gram-positive** bacterium that is part of the normal flora of human skin and mucous membranes. Despite its role as a **commensal** organism, it can also behave as an **opportunistic pathogen**, causing a wide array of infections ranging from minor skin conditions to life-threatening systemic diseases. Its ability to switch from being harmless to causing disease mostly depends largely on the host's immune status and environmental factors.

Morphologically, *S. aureus* is characterized by spherical cells, known as **cocci**, which typically appear in grape-like clusters (see Figure 1.10). This distinctive arrangement results from its irregular pattern of division in multiple planes. *S. aureus* is **non-motile**, meaning it lacks flagella for movement, and it **does not form spores**, which are dormant, resistant structures some bacteria produce to survive harsh conditions. Despite this, the bacterium thrives in various environments due to its metabolic versatility.

Metabolically, *S. aureus* is classified as **facultatively anaerobic**, meaning it can switch between aerobic respiration and fermentation depending on the availability of oxygen. Under oxygen-rich conditions, it uses aerobic respiration to generate energy. However, when oxygen is scarce, it switches to fermentation, producing lactic acid as a byproduct. This metabolic flexibility allows *S. aureus* to survive and grow in both oxygen-rich and oxygen-poor environments, making it adaptable to various niches in the human body and external environments.

One of its key **enzymatic features** is that it is **catalase-positive**, meaning it produces the enzyme catalase, which breaks down hydrogen peroxide into water and oxygen. This helps the bacterium protect itself from oxidative stress, particularly from reactive oxygen species generated by the host immune response. Additionally, *S. aureus* is **coagulase-positive**, a crucial diagnostic trait that differentiates it from other staphylococci. The coagulase enzyme enables

the bacterium to clot plasma, which can protect it from immune system attacks and enhance its ability to establish infections.

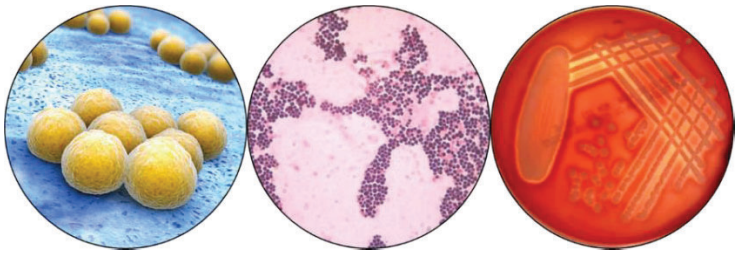

Figure 1.10. *Main phenotypical characteristics of S. aureus. From left to right: 1) Cocci morphology of S. aureus, showing its characteristic grape-like clusters. 2) Gram stain, indicating the bacterium as Gram-positive with a purple dye. 3) S. aureus growth on blood agar, highlighting the presence of hemolysis, evidenced by clear zones around the colonies due to lysis of red blood cells.*

Phenotypically, *S. aureus* forms **golden-yellow colonies** when cultured on nutrient-rich agar, due to the production of carotenoid pigments. These pigments not only give the colonies their characteristic color but also play a role in protecting the bacterium from oxidative damage. On blood agar, it exhibits **beta-hemolysis**, which means it completely lyses red blood cells, creating clear zones around the colonies (see Figure 1.10). This hemolytic activity is another marker of its virulence, as it contributes to tissue destruction and immune evasion. In addition, *S. aureus* ferments mannitol, a sugar alcohol, producing acid as a byproduct. This property is utilized in selective media like Mannitol Salt Agar (MSA) to differentiate it from other bacteria. On MSA, *S. aureus* turns the medium yellow due to the acid produced during **mannitol fermentation**.

The combination of these phenotypic traits, along with its ability to produce a variety of virulence factors and its capacity to form biofilms, make *S. aureus* both a common colonizer of humans and a significant cause of infection in clinical settings.

1.4.1 EPIDEMIOLOGY AND INCIDENCE

S. aureus is a **commensal microorganism** present in **mucous membranes** and **skin** of healthy individuals, but under some circumstances, it can become a strong **opportunistic pathogen** that causes a variety of infections, from minor

skin diseases to potentially fatal systemic infections. **Weak infections**, including folliculitis, impetigo, and abscesses are characterized by provoking localized inflammation. On the other hand, **invasive infections**, such as bacteremia, endocarditis, and pneumonia, can lead to major health risks and need for immediate medical assistance[85]. The epidemiology of *S. aureus* varies significantly based on geography, healthcare settings, and the presence of MRSA strains.

S. aureus is the most prevalent cause of **skin and soft tissue** i**nfections** (SSTIs) globally. It is responsible for a significant number of these infections, with MRSA strains, particularly the USA300 clone, being the dominant cause in community settings[86, 87]. MRSA remains a critical concern due to its resistance to multiple antibiotics, leading to severe and complicated infections. Since the 2000s, the incidence of community-acquired MRSA (CA-MRSA) has increased, contributing to the global burden of *S. aureus* SSTIs[86]. Clinical manifestations range from superficial infections like abscesses and cellulitis to severe cases such as necrotizing fasciitis, which can result in systemic complications and death if not managed promptly.

Notably, *S. aureus* is a major contributor to **nosocomial infections**, particularly in hospital settings[88]. The prevalence of strains with high multidrug-resistant (MDR) profiles associated to hospitals complicates infection control. In addition, significant morbidity, extended hospital admissions, and higher healthcare expenses are associated with *S. aureus* infections in healthcare settings, which carry elevated costs[89].

Globally, *S. aureus* **bloodstream infections**, including bacteremia and endocarditis, represent significant healthcare challenges. The incidence of ***S. aureus* bacteremia** (SAB) is notably high, with estimates around 80 to 190 cases per 100,000 people annually in high-income countries, translating to hundreds of thousands of cases per year. SAB is often associated with substantial morbidity and mortality, particularly in cases leading to deep infections like endocarditis, which occurs in 10-46 % of SAB patients, depending on risk factors such as invasive procedures or underlying heart conditions. SAB has a high fatality rate, with case mortality around 20 % or more in some populations[90].

Infective endocarditis (IE), a severe complication of SAB, has become a leading cause in Western Europe and North America, associated with poor outcomes. IE

is particularly dangerous due to its potential for damaging heart valves and the increased need for extended antibiotic therapy or surgical intervention. These infections place a heavy burden on healthcare systems and emphasize the need for early detection and targeted treatment strategies to reduce morbidity and mortality[90, 91].

S. aureus is also a major cause of **respiratory infections**, particularly in hospital settings. It is frequently associated with hospital-acquired pneumonia (HAP) and ventilator-associated pneumonia (VAP), both of which have high morbidity and mortality rates. In the intensive care unit (ICU), S. aureus can account for up to 20 % of VAP cases. MRSA poses a significant challenge due to its resistance to multiple antibiotics. Community-acquired *S. aureus* infections, while less common, also contribute to pneumonia cases, especially in individuals with underlying health conditions.

1.4.2 PATHOGENESIS

S. aureus often **colonizes the skin and mucous membranes**, where it constitutes part of normal microbiota composition. Its ability to attach to host tissues and evade the reactions of the immune system is crucial to its ability to colonize a host. **Adhesins** are surface proteins that play a crucial role in colonization by facilitating adhesion to host tissues. **Clumping factors** and fibronectin-binding proteins (**FnBPs**) that allow adhesion to extracellular matrix components promote bacterial invasion[92].

S. aureus can produce number of **exotoxins** that greatly contribute to increase its pathogenicity. Superantigens, such as toxic shock syndrome toxin-1 (**TSST-1**), can cause huge T-cell activation and cytokine production, intensifying the inflammatory response and leading to systemic consequences[93]. A common example of a cytotoxin is alpha-hemolysin (**Hla**), which directly attacks host cells and breaks down cell membranes causing tissue damage. **Enterotoxins** are toxins secreted by microorganisms that target the digestive tract. They are often associated with the ingestion of spoiled food or contaminated water, causing intestinal upset[94].

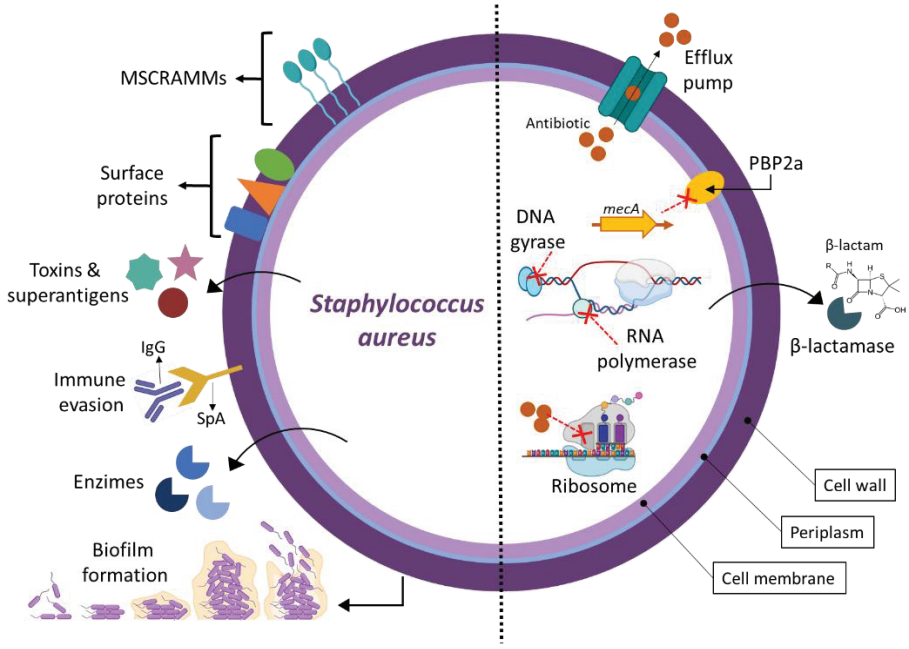

Figure 1.11. *S. aureus virulence factors and antibiotic resistance mechanisms. All virulence factors that contribute to the pathogenicity of this bacterium are shown on the left side, and the mechanisms that confer resistance to antibiotic treatments are shown on the right side. MSCRAMMS: Microbial surface components recognizing adhesive matrix molecules. PBP2a: Penicillin binding protein 2a. Adapted from Wójcik-Bojek, U., et al.[95] and Lade, H. and J.-S. Kim[96].*

The pathogenicity of *S. aureus* is further enhanced by **enzymes**, that help in tissue invasion and immune evasion. **Coagulase** is a crucial enzyme that helps the bacterium evade the immune system forming a fibrin shield around it. According to recent studies, **nucleases, lipases, and proteases** are involved in tissue degradation, nutrient absorption, and immune system regulation in the host[97]. Moreover, **staphylokinase** binds to plasminogen forming active plasmin, a proteolytic enzyme that facilitates bacterial penetration and tissue invassion. Similarly, **hyaluronidase** breaks down hyaluronic acid in connective tissues, facilitating as well bacterial dissemination[98]. *S. aureus* protein A (**SpA**) is a cell-wall-componnet that acts as an important virulence factor. SpA limitis opsonization and phagocytosis by attaching to the Fc region of immunoglobulin G, promoting immune evasion[99].

Another crucial aspect of the pathogenicity of *S. aureus* is its ability to form **biofilms**, complex bacterial colonies embedded in an extracellular matrix

that they produce on their own. The formation of biofilms contributes to the chronicity of infections facilitating bacterial adhesion to surfaces, conferring antibiotic-resistance and protecting bacteria from host immunological responses[100]. All the virulence mechanisms mentioned above are illustrated in Figure 1.11.

1.4.3 MECHANISMS OF ANTIBIOTIC RESISTANCE

Historically, *S. aureus* infections have been successfully treated by a wide range of antibiotics. However, it has shown a remarkable ability to develop resistance to several drugs, making treatment efforts more difficult. The growing incidence of MRSA in healthcare and community environments highlights an urgent necessity to comprehend and address antibiotic resistance in this pathogen.

In order to evade the effects of antibiotics, *S. aureus* has developed a number of defence mechanisms. These processes may be acquired through **horizontal gene transfer** or **mutations**, or they may be **intrinsic**, involving bacterial structural or functional traits that are innate. The process by which resistance develops can include antibiotic **degradation by enzymes**, **modifications to the antibiotic target site**, **alterations in membrane permeability** to avoid the antibiotic from entering and **active efflux** of the antibiotic from the bacterial cell (see Figure 1.11).

The main mechanisms by which *S. aureus* develops and displays resistance to different antibiotic classes are the following:

- **Beta-lactams:** *S. aureus* produces beta-lactamase enzymes as its main defense against antibiotics classified in this group, which include cephalosporins, carbapenems, and penicillins. When the beta-lactam ring is hydrolyzed by these enzymes, the antibiotic loses its effectiveness. The acquisition of the *mecA* gene, which results in a mutated penicillin-binding protein (PBP2a) with a low affinity for beta-lactam antibiotics, provides resistance by enabling cell wall construction to continue even when these antibiotics are present[101].
- **Glycopeptides:** *S. aureus* develops resistance to glycopeptide antibiotics like vancomycin due to modifications in the cell wall structure and

metabolism. VRSA strains result form the acquisiton of *VanA* gene clusters from *Enterococcus* species, leading to the production of peptidoglycan precursors that have a lower affinity for vancomycin[102]. Furthermore, modifications in cell wall production pathways and thicker cell walls are factors that contribute to glycopeptide resistance.

- **Aminoglycosides:** Aminoglycoside resistance in *S. aureus* is primarily mediated by enzymatic modification of antibiotics. The structure of aminoglycosides is altered by enzymes such acetyltransferases, phosphotransferases, and adenylyltransferases, which decreases their affinity for the bacterial ribosome. Additionally, ribosomal protein mutations and efflux pumps have a role in the rise of resistance[103].
- **Macrolides, lincosamides, and streptogramins (MLS):** Methylation of the 23S rRNA target region, mediated by the *erm* genes (erythromycin ribosome methylase), is a common cause of *S. aureus* resistance to MLS antibiotics. because of this alteration, the antibacterial activity is inhibited as they are unable to attach to the ribosome. Antibiotics are actively ejected from the bacterial cell by efflux pumps that are encoded by the *msrA* and *msrB* genes, which also contribute to MLS resistance[104].
- **Quinolones:** Resistance to quinolones, such as ciprofloxacin, relies on mutations in the genes encoding DNA gyrase (*gyrA*) and topoisomerase IV (*grlA* and *grlB*), which are the main targets of these antibiotics. These alterations decrease the binding affinity of quinolones to their respective enzymes, which reduces their inhibitory effect. Resistance can be further increased by plasmid-mediated quinolone resistance genes (*qnr*) and efflux pump overexpression[105].

1.4.4 EVOLUTION AND ADAPTABILITY

S. aureus is an extremely **versatile** bacterium that may cause a wide range of infections, from minor skin infections to serious systemic disorders. Treatment for invasive *S. aureus* infections, including pneumonia, endocarditis, and bacteremia, typically involves the use of **systemic antibiotics**. The main cause of *S. aureus*'s adaptability is its **rapid evolution** and acquisition of genes that confer antibiotic resistance. Broad-spectrum resistance has resulted from this, making management and treatment extremely challenging.

Soon after **penicillin** was initially introduced in the 1940s, treating *S. aureus* infections presented its first significant obstacle. Penicillin was originally quite powerful against *S. aureus*, but as it became widely used, penicillin-resistant forms quickly appeared. More than half of *S. aureus* isolates in hospitals by the late 1940s were resistant to penicillin[106].

Methicillin, a beta-lactam antibiotic resistant to beta-lactamase breakdown, was introduced in 1959 as a response to the widespread beta-lactamase-mediated resistance. MRSA strains were discovered, nevertheless, a few years later. The acquisition of the ***mecA*** gene, which results in the expression of PBP2a protein, provides resistance in these strains[107]. Because of this, methicillin and all other beta-lactam antibiotics became useless against MRSA infections.

When MRSA first appeared, it was found in healthcare environments and resulted in serious nosocomial infections. It was named Healthcare-Acquired MRSA (**HA-MRSA**). As these strains can cause invasive infections and are resistant to various antibiotics, they have been linked to high rates of morbidity and mortality. **CA-MRSA** strains first appeared in the 1990s. These strains caused serious skin and soft tissue infections in healthy people who had not been exposed to healthcare, and they were frequently more virulent than HA-MRSA due to their genetic differences[108].

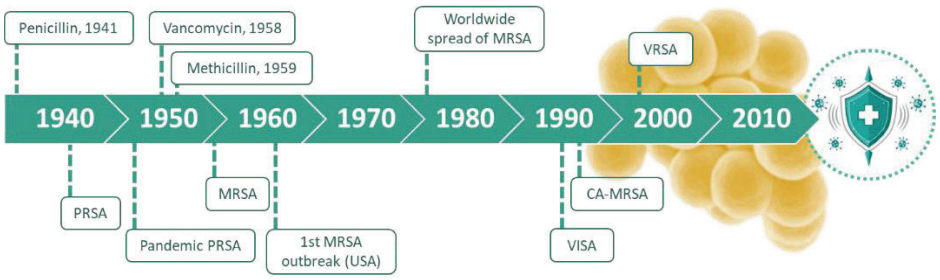

Figure 1.12. *Timeline regarding the rise of new antibiotic therapies and the subsequent emergence of antibiotic-resistant S. aureus. Adapted from McGuinness, W. A., et al.*[102].

An essential antibiotic for the management of MRSA infections is **vancomycin**. However, as a result of *S. aureus* adaptation, vancomycin-intermediate *S. aureus* (**VISA**) and ultimately vancomycin-resistant *S. aureus* (**VRSA**) emerged. The thicker cell walls of VISA strains limit the ability of vancomycin to reach target areas, thus reducing its effectiveness. On the other side, *Enterococcus* species

provided the ***vanA*** gene to VRSA strains, which results in high-level resistance to vancomycin by changing the precursors of the cell wall[109].

In the US, an VRSA infection was documented in 2002 for the firt time. As VRSA has the ability to share resistance genes between distinct bacterial by horizontal gene transfer of, this constituted a serious risk to public health and complicated the treatment options for *S. aureus* infections[110].

More recently, resistance to additional treatments has also been developed by *S. aureus* as a result of antibiotic overuse. Mutations in the 23S rRNA gene have led to the creation of resistant strains of MRSA, which was treated with **linezolid.** Another antibiotic prescribed to treat MRSA, **daptomycin**, has been the target of resistance mechanisms that involve modifications to the charge and fluidity of the cell membrane, which decrease drug binding and, overall, its efficacy[111].

In short, several MDR strains of *S. aureus* have emerged resulting from its rapid evolution and adaptation. It has developed resistance to several antibiotic groups, such as beta-lactams, glycopeptides, tetracyclines, and macrolides, making infection control and treatment more difficult (see Figure 1.12). The constant evolution in response to the emerging antimicrobial drugs from 1940 to the present, highlights how persistent *S. aureus* is in developing resistance mechanisms. To treat the infections driven by this life-threatening pathogen, it is imperative to carry out **continuous surveillance**, study into **novel therapeutic techniques**, provide **early and accurate diagnosis**, and **use existing antibiotics prudently.**

1.5 STATE OF THE ART IN *S. AUREUS* DIAGNOSIS

An **early and precise** diagnosis is essential for providing *S. aureus* with the proper and effective treatment. *S. aureus* infections can spread quickly and even be lethal. Treatment can start as soon possible when a diagnosis is made early and accurately, which may improve patient outcomes. Therefore, in order help in the early detection of *S. aureus* infections, it is imperative to develop diagnostic methods that are more rapid, accurate, and precise[112].

Accurate diagnosis requires a combination of clinical evaluation and laboratory techniques. Because *S. aureus* infections can have a wide range of clinical presentations, an exhaustive diagnostic strategy is required. The conventional diagnostic procedures can involve molecular techniques, immunological assays, metabolic testing, and microbiological cultures, depending on the infection type, its severity and the availability of resources

Improved diagnostic technologies have made it possible to identify and describe *S. aureus* with greater accuracy, which has improved patient outcomes. However, the need for continual **research and innovation** in diagnostic procedures is highlighted by the constant evolution of *S. aureus*, particularly the appearance of novel strains that are both virulent and resistant to treatment. To improve *S. aureu*s infection diagnosis and treatment, new methods and technologies must be integrated into clinical practice.

1.5.1 CURRENT METHODOLOGIES FOR DIAGNOSING *S. AUREUS* INFECTIONS

A combination of microscopy, Gram staining, phenotypic analysis, and culture techniques are used in conventional diagnostic procedures for *S. aureus*. These methods are fundamental to clinical microbiology and are still necessary for accurately diagnosing and identifying *S. aureus* infections. They offer vital information for the detection and treatment of *S. aureus* in clinical settings and are reliable and reasonably priced.

1.5.1.1 Optical Microscopy

When diagnosing bacterial infections in a laboratory setting, microscopy is frequently the **initial step**. To find out if there are any bacteria present, clinical specimens must be directly examined under a microscope. The **morphological** attributes such as the size, shape, and distribution of bacteria reveal quick information about the disease. Typically, *S. aureus* appears as **clusters** of spherical (**cocci**) bacteria that resemble grapes[113].

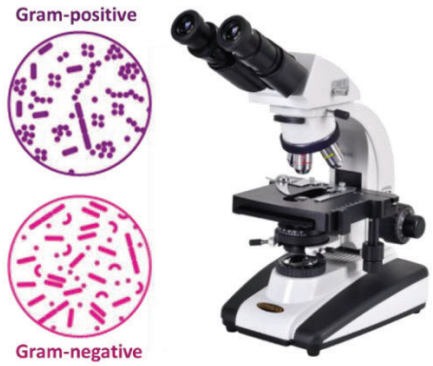

Figure 1.13. *Optical microscopy combined with Gram staining. This diagnostic method reveals bacterial morphology and cell wall characteristics, enabling the differentiation between Gram-positive (purple) and Gram-negative (pink) bacteria.*

Based on the composition of their cell walls, bacteria are categorized using **Gram staining** technique, which usually is the first step in the identification of a bacterial group. The procedure involves staining bacteria with crystal violet dye, then iodine, alcohol decolorization, and safranin counterstaining. As presented in Figure 1.13, under a microscope, *S. aureus* appears as purple, Gram-positive cocci that are grouped together and retain the crystal violet dye[114]. Its unique form helps in distinguishing it from other bacteria.

1.5.1.2 Biochemical Tests

Using **phenotypic** approaches, particular biochemical and physiological features of bacteria are observed. The distinct **metabolic and enzymatic activities** of *S. aureus* can be used to identify it using these techniques.

The **catalase test** (see Figure 1.14) distinguishes between streptococci, which are catalase-negative, and staphylococci, which are catalase-positive. The catalase enzyme breaks down hydrogen peroxide into water and oxygen when it is given to a *S. aureus* culture, which results in fast bubbling[115].

A reliable method for identifying *S. aureus* is the **coagulase test**. Coagulase is an enzyme characteristic which causes clot formation in plasma. There are two different types of coagulase tests: the tube coagulase test, which finds free coagulase, and the slide coagulase test, which finds bound coagulase or clumping

factor. According to Chamberlain *et al.* the presence of *S. aureus* is confirmed by a positive coagulase test[116].

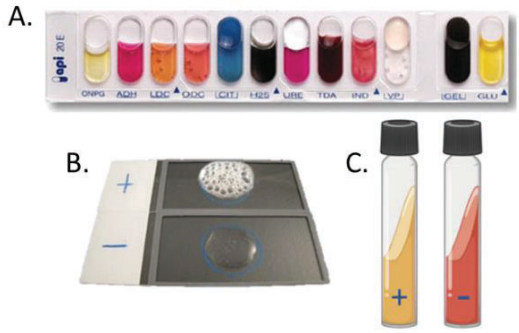

***Figure 1.14**. Biochemical diagnostic tests for bacterial identification. A) API Gallery: a panel of miniaturized biochemical tests to determine metabolic profiles; B) Catalase test: used to identify catalase enzyme activity; C) Mannitol salt agar: a selective and differential medium that indicates mannitol fermentation through a color change.*

Another technique to identify *S. aureus* is using **mannitol salt agar (MSA)** for its growth, as mannitol can be fermented by this bacterium. With the exception of staphylococci, most microorganisms are inhibited by the high salt concentration in MSA. As illustrated in Figure 1.14, when mannitol is fermented by *S. aureus*, acid is produced and the medium turns yellow instead of red[117].

Several FDA-approved **biochemical tests** are commonly used for diagnosing *S. aureus* infections. The API® Staph test strip (bioMérieux) is specifically designed for the identification of *Staphylococcus* species through a series of biochemical reactions (an example from the API gallery can be seen in Figure 1.14. The BBL™ Rabbit Coagulase Plasma (BD) and Remel™ Coagulase Plasma (Thermo Fisher Scientific) tests are used to detect the production of coagulase. Additionally, some reagents such as BD BBL™ Catalase Reagent Droppers (BD) are commercially available to perform catalase tests. Biochemical tests are essential tools in clinical microbiology for the accurate identification and differentiation of *S. aureus*.

1.5.1.3 Microbial Culture: gold standard technique

The benchmark for identifying *S. aureus* infections are culture-based approaches. To **isolate and identify** the pathogen, these procedures involve cultivating the bacteria on certain media. Cultures are normally incubated for 24

to 48 hours at 35 to 37°C. This gives colonies enough time to grow and display distinguishing characteristics.

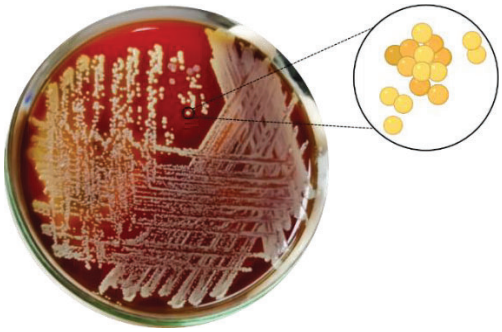

Figure 1.15. *Microbial culture of S. aureus on a blood agar plate, showing its characteristic golden-yellow colonies. A close-up view of one isolated colony highlights the morphology of S. aureus, displaying cocci arranged in clusters.*

As presented in Figure 1.15*, S. aureus* colonies are typically **spherical** and **smooth**. A variety of media, such as blood agar, mannitol salt agar, tryptic soy agar, Baird-Parker agar and chromogenic agar, can be used to cultivate *S. aureus*. **Mannitol salt agar** is selective for staphylococci because to its high salt concentration and differential for *S. aureus* through mannitol fermentation. In contrast, **blood agar** promotes the growth of a broad variety of bacteria and allows the identification of hemolytic activity. Cultured in on blood agar, *S. aureus* forms **golden yellow** color colonies and it usually results in **beta-hemolysis**, showing colorless zone surrounds the bacterial colony due to the total lysis of red blood cells. The hemolytic activity of *S. aureus* is a crucial diagnostic characteristic that helps distinguishing it from other staphylococcal species, many of which display distinct hemolytic patterns.

Due to its high salt concentration and differential for *S. aureus* caused by mannitol fermentation, which causes a change in medium color, **mannitol salt agar** is specific for staphylococci. **Chromogenic agar** creates colonies with distinct colors, making it easier to identify *S. aureus* quickly and precisely. Finally, **Baird-Parker agar** is selective for isolating *S. aureus*, which forms black colonies due to tellurite reduction and clear zones from lecithinase activity.

1.5.1.4 Molecular Diagnostic Techniques

Molecular diagnostic techniques (simpliflied in Figure 1.16) have significantly improved the identification and characterization of *S. aureus*, especially in identifying antibiotic **resistance genes**. These pioneering methodologies, which provide quick and precise results essential for efficient treatment and infection control, include Whole Genome Sequencing (WGS), Real-Time PCR, and Polymerase Chain Reaction (PCR).

Conventional PCR is a technique used to amplify specific DNA sequences to detect genes associated with *S. aureus* and its resistance mechanisms. The identification process typically targets the *nuc* gene, which encodes a thermonuclease unique to this bacterium. Additionally, the *clfA* gene, responsible for clumping factor A, and the *spa* gene, encoding SpA, are often utilized as markers[115].

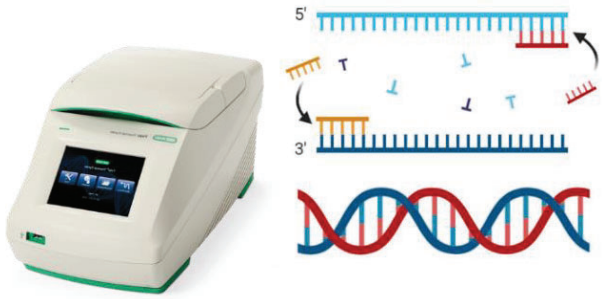

Figure 1.16. *Molecular diagnostic technique using PCR (Polymerase Chain Reaction) for DNA amplification.*

Multiplex PCR, a variation of the conventional method, allows for the simultaneous amplification of multiple targets, facilitating the identification of various virulence factors and resistance genes in a single reaction. This approach is particularly valuable for comprehensive profiling of clinical isolates, as it enables the detection of several genes, including *mecA*, *pvl* (Panton-Valentine leukocidin), and *tsst* (toxic shock syndrome toxin)[118].

Real-time PCR (qPCR), also known as quantitative PCR, is a method that uses fluorescent markers to monitor DNA amplification in real-time. It provides rapid, highly sensitive, and specific results. As in previous techniques, in clinical diagnosis, qPCR assays frecuently target the *nuc* gene, *mecA* gene, and other

resistance determinants, like the *pvl* gene. One key advantage of qPCR is its ability to quantify the bacterial load, which is useful for assessing the severity of an infection and monitoring treatment efficacy[119].

Molecular diagnostic techniques offer great advantages over traditional approaches in several ways. First, they provide data much faster than methods based on culture, which is important for quick clinical decision-making. Because of its extreme **sensitivity** and **specificity**, there is a lower chance of false positives or negatives. The use of these advanced molecular methods in everyday clinical practice improves the ability to diagnose and treat *S. aureus* infections, especially those brought on by **resistant strains**. Further developments in molecular diagnostics could enhance pathogen identification and characterization in terms of precision, speed, and comprehensiveness.

However, molecular diagnostic approaches have drawbacks and limits as well. Certain healthcare facilities might not have access to the **specific equipment** and **trained personnel** needed for these approaches, which can be costly. The sensitivity of molecular approaches can occasionally result in the identification of non-viable bacteria or contaminants, which could lead to false positives. Furthermore, even if these methods enable the quick discovery of resistance genes, there isn't always a correlation between them and phenotypic resistance, which means that the resistance that is really seen in clinical settings could not match the resistance that genetic testing predicts. Because of that, molecular diagnostic techniques must be continuously monitored and correlated with clinical outcomes in order to guarantee their accuracy and reliability.

1.5.1.5 Immunological techniques

Immunological techniques are essential for the rapid and specific diagnosis of *S. aureus* infections. These techniques provide great specificity and sensitivity by precisely using the interaction between antigens and antibodies. Key immunological methods include immunoassays (IFAs), lateral flow assays, western blotting, latex agglutination assays, and the enzyme-linked immunosorbent assays (ELISAs).

1.5.1.5.1 Enzyme-Linked Immunosorbent Assay (ELISA)

ELISA is a widely used versatile laboratory technique used to detect and quantify antigens or antibodies in a sample. In the context of *S. aureus*, ELISA can be employed to identify specific antigens such as SpA, staphylococcal enterotoxins, and clumping factor.

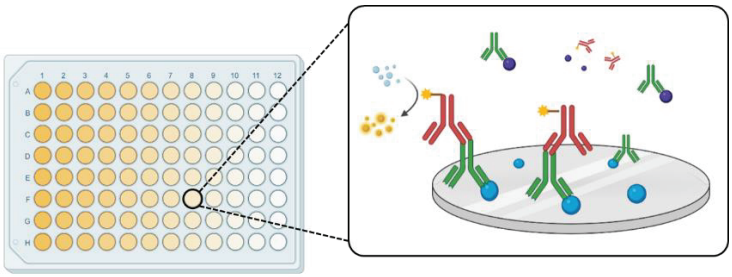

Figure 1.17. *ELISA assay illustrating antigen-antibody interaction. The well displays a colorimetric change triggered by an enzyme, indicating the presence of the target antigen. The intensity of the color correlates with the concentration of the antigen, enabling quantitative measurement.*

As presented in Figure 1.17, the general principle involves binding an antigen or antibody to a solid surface, followed by the addition of a detection antibody linked to an enzyme. The enzyme uses a substrate to catalyze a reaction that results in a quantifiable signal, usually a change in color. Different formats for ELISAs, including as direct, indirect, sandwich, and competitive, can be set up to suit different experimental requirements.

Some examples of FDA-approved ELISA kits for *S. aureus* detection are VIDAS® Staph Enterotoxin II (bioMérieux), RIDASCREEN® SET Total (R-Biopharm), TECRA® Staph Enterotoxin Visual Immunoassay (3M) and Prodesse ProGastro™ SSCS Assay (Hologic). These kits are designed to detect staphylococcal enterotoxins in food samples, helping to identify foodborne pathogens. They are used primarily in food safety testing in order to help avoid foodborne infections and in and clinical diagnostics when a gastrointestinal illness is suspected and *S. aureus* is a potential causative agent.

As displayed above, FDA-approved ELISA kits are mainly focused on enterotoxin detection, which are essential for diagnosing conditions related to food poisoning. However, some kits for diagnosing *S. aureus* infections

targeting detecting SpA, Hla or TSST-1 in clinical samples are now available in the market.

1.5.1.5.2 Latex Agglutination Tests

Using **latex beads coated** with antibodies, latex agglutination tests are fast assays that identify the presence of particular antigens. A visible agglutination that happens when a sample containing *S. aureus* antigens is combined with the latex beads indicates a positive result.

Latex agglutination tests are **rapid** diagnostic methods designed to detect the presence of specific **antigens or antibodies** in a sample. As dis played in Figure 1.18, the test uses latex beads coated with antibodies that match the target molecules. When a sample containing *S. aureus* antigens is mixed with these beads, the interaction between the coated antibodies and the antigens causes the beads to cluster together. This clustering forms a **visible clump**, known as agglutination, indicating a positive result. This reaction occurs quickly, allowing for fast detection, which is particularly useful in clinical and point-of-care settings.

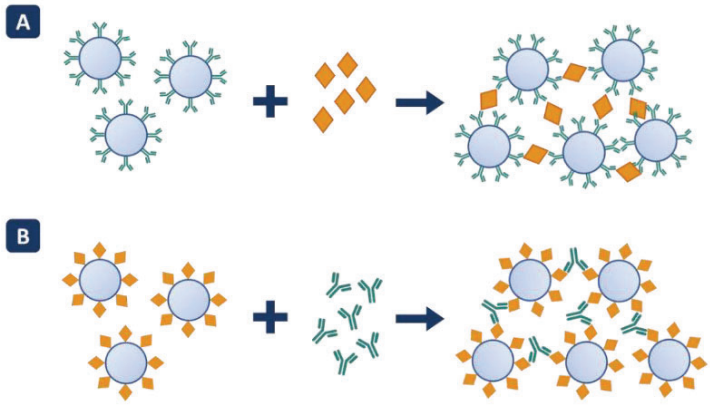

Figure 1.18. *Schematic representation of the latex agglutination test. A) Latex beads coated with specific antibodies bind to target antigens present in the sample. This configuration is commonly used to detect bacterial antigens. B) Latex beads are coated with antigens, allowing for the detection of specific antibodies present in the sample. The antibody-antigen binding results in agglutination, indicating a positive result. Adapted from Alhabbab, R. Y.*[120].

On the other hand, if the goal is to detect antibodies rather than antigens, the beads are coated with the specific antigen instead. If the target antibodies are

present in the sample, they bind to the antigen on the beads, leading to the same agglutination effect. This flexibility makes this technique a versatile and efficient tool for various diagnostic applications (see Figure 1.18).

These assays are frequently used to quickly identify *S. aureus* in clinical samples, such as swabs from wounds, blood, and urine. According to Idelevich et al. (2014), latex agglutination can identify antigens in a matter of minutes, including clumping factor, SpA, and capsular polysaccharides[121]. The FDA has approved the following latex agglutination tests for the quick identification of *S. aureus* in clinical specimens: BD BBL™ Staphyloslide™ Latex Test (BD), Slidex Staph-Kit® (bioMérieux), Staphaurex™ Plus and PASTOREX™ Staph Plus (Bio-Rad) and PathoDX™ Strep Grouping Kit (Remel).

1.5.1.5.3 Immunofluorescence assays (IFA)

Immunofluorescence implies labelling antibodies with **fluorescent dyes** in order to identify certain antigens in a sample. As illustrated in Figure 1.19, **Indirect** immunofluorescence uses a secondary antibody coupled to a fluorophore that binds to the primary antibody, whereas **direct** immunofluorescence uses antibodies directly linked to a fluorophore. Using a fluorescent microscope, it provides spatial information about the **infection site** and *S. aureus* **prevalence** in tissue samples or on glass slides. This method **amplifies the signal**, enhancing the detection sensitivity and visualization of the antigen, detecting even very low antigen concentrations[122].

In clinical diagnostics, IFA specifically targeting *S. aureus* are not as common, with most assays being developed for broader pathogen detection or for use in research rather than routine clinical diagnostics. One example of an Indirect IFA for diagnosing *S. aureus* would be using a specific antibody, such as the BacTrace® Anti-Staphylococcus aureus primary antibody (seracare), and a commercially available fluorescently labeled secondary antibody, like FITC-conjugated anti-goat IgG. The fluorescence indicates the presence of *S. aureus* in the sample under a fluorescence microscope.

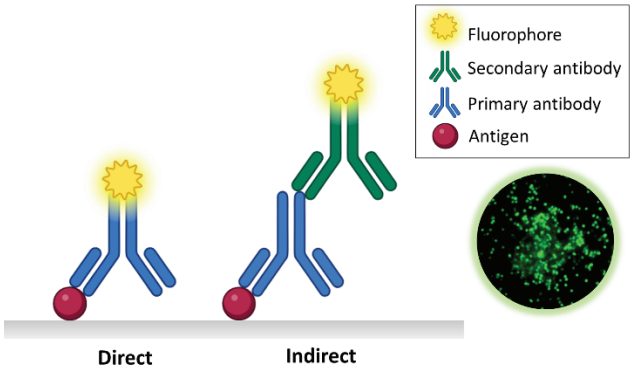

Figure 1.19. *Schematic representation of an Immunofluorescence Assay (IFAs). Direct IFA: fluorescently labeled antibodies specifically bind to target antigens present in the sample. Indirect IFA: Primary antibodies bind to the target antigen, and a secondary antibody, conjugated with a fluorescent dye, recognizes and binds to the primary antibody*.

1.5.1.5.4 Lateral Flow Immunoassay (LFIA)

LFIAs are rapid, portable diagnostic tools widely used for the qualitative or semi-quantitative detection of analytes in complex matrixes. These assays work on the basis of immunochromatography, in which a sample is added to a test strip, and the target analyte binds to specific antibodies or immobilized antigens on the strip. The target and the labeled detection antibodies interact to generate visible lines that indicate the presence or absence of the target when the sample migrates along the strip due to capillary action (see Figure 1.20).

Because of their ease of use, affordability, and their ability to deliver quick results, LFIAs are highly valued in environmental testing, clinical diagnostics, food safety, and at-home health monitoring. Point-of-care testing and screening programs have widely adopted them due to their versatility and ease of use.

An example of an FDA-approved LFIA is BinaxNOW® *S. aureus* Card (Alere), which is a quick diagnostic method for determining this pathogen directly from blood cultures.

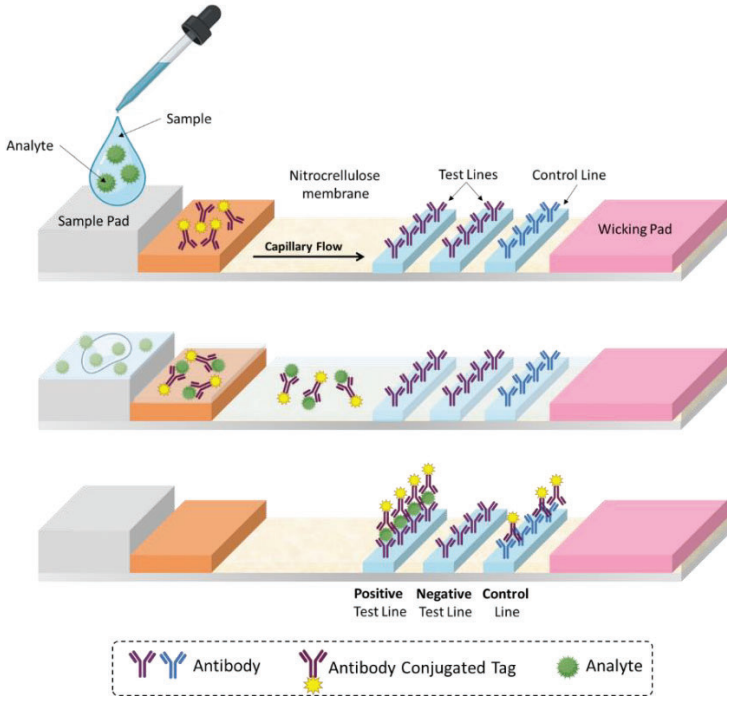

Figure 1.20. *Schematic representation of the Lateral Flow Immunoassay (LFIA) process. 1) The sample containing the analyte flows through the nitrocellulose membrane via capillary action. 2) As it travels, the analyte binds to reporter antibodies (labeled with substances like gold, latex, or fluorophores) and reaches the test line, where specific antibodies capture the analyte, and the control line, containing anti-IgG antibodies that confirm test validity. 3) A visible control line confirms the test functioned correctly. If no line appears at the test site, the result is negative, indicating the analyte is absent. Adapted from Costa, A., et al.*[123].

1.5.1.5.5 Western blotting

Western blotting, also known as immunoblotting, is a widely used analytical technique in molecular biology and biochemistry for detecting specific proteins in a sample. As displayed in Figure 1.21, the process involves separating proteins by gel electrophoresis, typically using SDS-PAGE, based on their molecular weight. The separated proteins are then transferred onto a membrane, usually made of nitrocellulose or polyvinylidene fluoride (PVDF). The membrane is subsequently probed with antibodies specific to the target protein. The presence of the target protein is visualized through a secondary antibody conjugated to an enzyme or fluorescent dye, which produces a detectable signal upon interaction with a substrate.

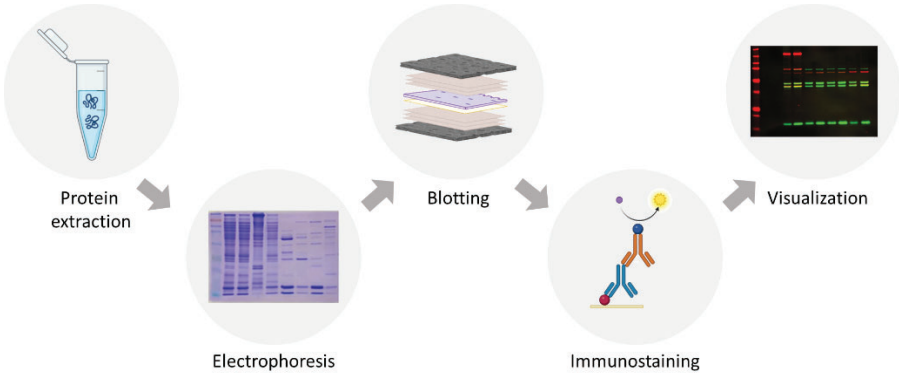

Figure 1.21. *Steps involved in the Western Blot technique. 1) Protein Extraction: Proteins are isolated from the sample. 2) Electrophoresis: Proteins are separated by size on a polyacrylamide gel. 3) Blot Transfer: Separated proteins are transferred onto a membrane, typically PVDF or nitrocellulose. 4) Immunostaining: The membrane is incubated with primary and secondary antibodies to identify target proteins. 5) Visualization: Proteins are detected using chemiluminescence or fluorescence and captured with imaging equipment for analysis.*

This technique is a powerful tool used for confirming the presence of a specific protein, analyzing post-translational modifications, and quantifying protein expression levels in research and diagnostic settings. Its applications span various fields, including immunology, virology, and oncology, where it plays a crucial role in understanding protein function and disease mechanisms. Although there is not any western blotting kit available in the market for the specific identification of *S. aureus*, various reagents and antibodies that can be used to detect certain *S. aureus* proteins via this technique are accessible for furchase.

The use of immunological methods offers multiple benefits. These techniques provide quick results, frequently in a matter of hours, which is essential for prompt clinical decision-making. The sensitivity of immunological assays allows them to detect low quantities of antigens, which makes them appropriate for early diagnosis. The high specificity of antibody-antigen interactions significantly reduces the possibility of false positives. These methods, nevertheless, come with some drawbacks such as their expense due to the need for particular antibodies and to require trained staff. All in all, ongoing developments in immunological assays may improve their precision and consistency, improving the clinical outcomes of patients suffering *S. aureus* infections.

1.5.2 ADVANCES IN DIAGNOSTIC TECHNIQUES

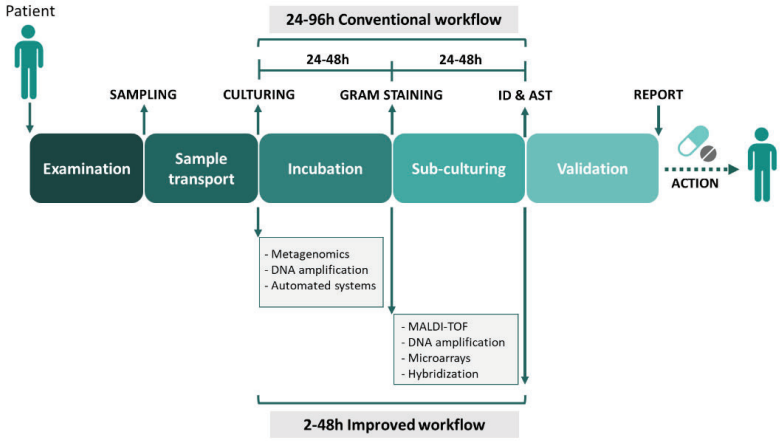

Figure 1.22. *Workflow chart for diagnosing S. aureus infections, comparing conventional and improved workflows. The conventional method, taking 24 to 96 hours, relies on sequential culture steps, isolation, and susceptibility testing. In contrast, the advanced methodology reduces diagnostic time to 2-48 hours by integrating molecular techniques, MALDI-TOF MS for rapid identification, and automated systems that streamline the process.*

Significant progress has been made in the field of infectious disease diagnostic technology. Specifically with regard to *S. aureus*, diagnostic procedures have shown an improvement in accessibility, accuracy, and speed.

Novel sequencing techniques, automated systems, new mass spectrometric approaches and point-of-care (PoC) diagnostics are important areas of innovation. These tools complement traditional techniques, enabling faster and more accurate diagnosis, which are crucial for timely and effective patient management (see Figure 1.22).

1.5.2.1 Mass Spectrometric techniques

Mass spectrometry (MS) determines the mass-to-charge ratio of ions in order to identify and measure compounds. It involves measuring the **mass-to-charge ratios** of charged molecules or fragments of molecules created by ionizing compounds (the underlaying principle is shown in Figure 1.23).

MS is widely used in multiple disciplines. In microbiology, it can be applied or identifying and characterizing microorganisms. Clinical microbiology has seen a rise in the use of **MALDI-TOF MS** (Matrix-Assisted Laser Desorption/Ionization

Time-of-Flight MS) with the goal of accelerating the identification of microorganisms.

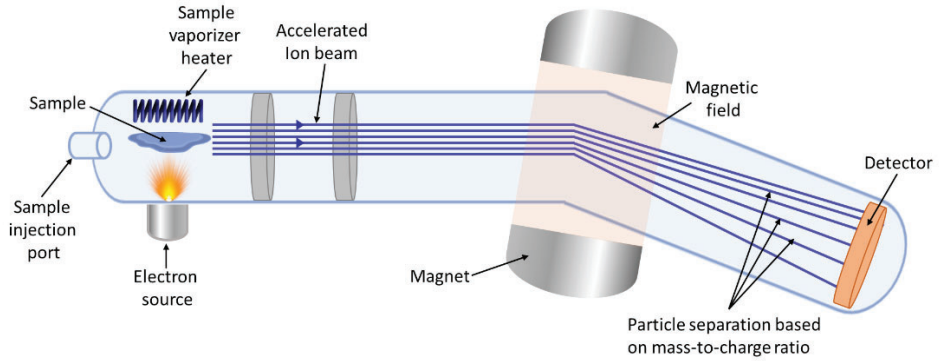

Figure 1.23. *Overview of the principle of mass spectrometry. The process begins with ionization, where sample molecules are charged to form ions. These ions are then accelerated through an electric field and enter the mass analyzer, which separates them based on their mass-to-charge (m/z) ratios. The detector records the ions, creating a spectrum that displays the intensity of each ion signal as a function of the m/z ratio. This allows for precise identification and quantification of molecular components in the sample. Adapted from Vasu, M., et al.*[124].

Briefly, the microbiological sample is first combined with a matrix compound that is capable of absorbing laser light. The sample-matrix mixture is then exposed to a laser shot, which ionizes the microbial proteins in the sample by causing the matrix to absorb energy and transfer it to the sample. After being desorbed from the surface, the ionized molecules go into the gas phase. After that, the ions are forced into a vacuum tube and accelerate in an electric field. Finally, they are measured for their time of flight to a detector, which is a function of their mass-to-charge ratio**.** An illustration presenting the MS principle is shown in Figure 1.23**.**

The **accuracy** and **affordability** of MALDI-TOF MS have improved the identification of *S. aureus* in clinical microbiology. Clinical samples are taken from people who may have an infection with *S. aureus*, such as blood, urine, or wound swabs. However, a significant limitation of these techniques is the requirement to isolate bacterial colonies for identification, meaning that the **samples must first be cultured**, delaying the diagnostic process. Bacterial colonies are then combined with a MALDI matrix. After the mixture is analyzed using MALDI-TOF MS, a mass spectrum representing the distinct protein fingerprint of the bacterial sample is produced. This spectrum is contrasted with spectra of recognized

bacterial species found in a reference database. When the sample spectrum and the database records match, *S. aureus* is identified.

The **Bruker MALDI Biotyper®** and the **bioMérieux VITEK® MS** are two MALDI-TOF MS systems extensively used in clinical laboratories for the identification of *S. aureus* and other pathogens. When compared to conventional approaches, these systems significantly reduce the time necessary for pathogen identification, and they offer considerable advantages by providing results in a matter of minutes. These methods do have several drawbacks, though, in spite of their speed and accuracy. These include the demand for initial sample culturing, the need for specialized equipment and workers with the necessary training, and the high cost of equipment implementation and maintenance.

1.5.2.2 DNA Sequencing

DNA sequencing is a technique used to determine the exact **order of nucleotide bases** (adenine, guanine, cytosine, and thymine) in a DNA molecule (its principles are presented in Figure 1.24).

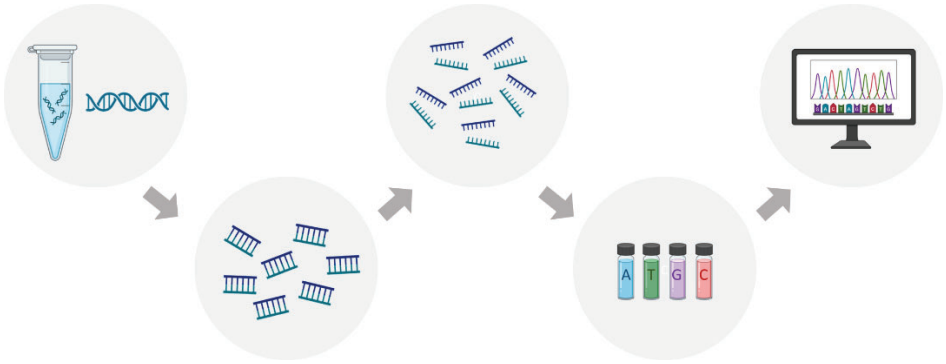

Figure 1.24. *Illustration showing the fundamental principles of DNA sequencing technology. The sequence determination begins with DNA extraction, followed by fragmentation. The DNA fragments are then subjected to sequencing reactions, generating reads that represent the order of nucleotide bases (A, T, C, G). The sequencing data is processed to construct the full DNA sequence, displayed as a chromatogram or readout of nucleotide order. This sequence reveals genetic information, allowing for analysis of genes, mutations, and variations across the DNA sample.*

This process reveals the genetic information encoded within an organism's DNA, allowing for the identification of genes, mutations, and structural variations. It has applications in various fields, including genomics, medical diagnostics,

evolutionary biology, and forensic science. Advances in sequencing technologies have made it faster and more accessible, enabling large-scale genetic studies and personalized medicine approaches.

Treatment strategies and public health initiatives can benefit from the abundance of information that sequencing techniques provide regarding the genetic background of the disease. By WGS, the complete bacterial genome can be analyzed, providing precise information on the genetic composition, resistance mechanisms, and evolutionary relationships. WGS has developed into a vital tool for tracking the transmission of resistance genes, epidemiological studies, and outbreak investigations[125]. The whole genomes of *S. aureus* isolates are sequenced using WGS, which allows it to find all **virulence factors**, **resistance genes**, and possible **routes of transmission**. This high-resolution method is especially helpful in directing focused actions and understanding the **epidemiology** of MRSA and other resistant infections[126].

NGS has enabled extensive investigation of bacterial genomes at high speed and resolution, revolutionizing microbial genomics. With a single experiment, NGS enables the detection of every genomic element linked to virulence factors, antibiotic resistance, and strain typing. This method facilitates epidemiological studies, outbreak investigations, and the development of novel therapeutic options by offering extensive insights into the genetic composition of *S. aureus*[127].

The **Illumina MiSeq™** system is a prime example of the sophisticated NGS capabilities in microbial genome analysis. **Thermo Fisher Scientific Ion Torrent™** Systems, which offer quick and thorough genomic sequencing for a variety of pathogens, including *S. aureus*, and **Oxford Nanopore MinION™**, a portable sequencing device appropriate for field-based genomic analysis, are two additional noteworthy equipments.

1.5.2.3 Automated systems

S. aureus identification in clinical settings is now much more accurate and efficient thanks to automated diagnostic techniques. These systems decrease human error and boost efficiency by combining several diagnostic procedures,

such as sample preparation, amplification, detection, and data analysis, into an effortless workflow.

Because automated diagnostic methods offer **quick**, **precise**, and **high-throughput** solutions, they have revolutionized the diagnosis of *S. aureus*, among other pathogens. These systems, which integrate many diagnostic processes to produce standardized data fast, help with efficient patient care and better clinical outcomes. Some of the most commonly used platforms are shown in Figure 1.25. They do have a few restrictions and drawbacks, though, which need to be taken into account.

Automated diagnostic systems require substantial **financial investment** for purchase, maintenance, and consumables, making them less accessible for smaller or low-resource healthcare facilities. Healthcare staff must undergo significant **training** in order to operate and maintain automated systems, which can be a logistical and economic load. These systems also require **specialized infrastructure**, which may not be available in all healthcare settings. The required facilities may include regulated conditions, continuous electrical supplies, and sufficient space. It can also be necessary to integrate with laboratory information systems.

Figure 1.25. *Overview of automated systems for clinical diagnosis, showing four widely used platforms. On the left, two phenotypic systems are displayed: Vitek® 2 (Cepheid) and Microscan® WalkAway (Beckman Coulter). These systems use panels to identify pathogens and test antimicrobial susceptibility based on the growth of the organisms and their metabolic patterns. On the right, two molecular systems are shown: GeneXpert® and BioFire® FilmArray®, which utilize cartridge-based assays to detect genetic material from pathogens directly. Together, these automated systems exemplify the integration of phenotypic and molecular diagnostics in modern clinical microbiology.*

Despite their high sensitivity, automated systems may not be able to identify low-abundance pathogens or other microorganisms that are not the system's primary target. They are also susceptible to false positives and false negatives, which can result in **missed diagnosis** or unnecessary therapies. Numerous systems are built to identify particular infections or resistance markers, which may require further testing to provide a complete pathogen diagnosis. Moreover, although the analysis time is quite short in many of these systems, an initial **sample culturing** step is still required for most automated methods, which can cause delays in diagnosis and treatment. The time needed for pathogen identification and antibiotic susceptibility testing is increased by the need for culture processes. A summary on the automated systems for detecting *S. aureus* is displayed in Table 1.1.

Ultimately, the use of automated diagnostic systems in healthcare settings has resulted in notable progress in microbial identification and susceptibility testing. However, their processing capacity is limited in some cases and is only valid for some specific sample types, which is a drawback in laboratories with high sample volumes. Likewise, because they are mostly culture-dependent, they do not address the main drawback of conventional approaches, which is the delay in diagnosis. While these automated systems provide valuable and rapid results, it is recommended that the results be interpreted in conjunction with other clinical and laboratory data, and not be used as the unique reference for establishing treatment guidelines. These are, therefore, tools of great clinical value, complementary to conventional diagnostic methods but, up to date, not an alternative to replace them.

Table 1.1. *Comparison of automated systems for S. aureus detection. The name of each product, the manufacturing company, a brief description, type of samples processed, pre-treatment or culturing requirements, assay type, detection and readout principles and assay running time are displayed. N/A: not available.*

Product	Company	Sample	Pre-treatment	Description	Culture	Type/time of culture (h)	Sensitivity	Assay type	Detection principle	Readout principle	Analysis time	Total time
BD Phoenix™ Automated Microbiology System	BD	Blood, urine, wound swabs, respiratory specimens	None	Automates identification and AST of bacteria	Yes	Plates (24-48h)	10^2-10^3 CFU/mL	Phenotypic	Growth-based colorimetric	Automated colorimetric readout	16-24h	40-72h
VITEK® 2 System	bioMérieux	Blood, urine, wound swabs, respiratory specimens	None	Automated platform for microbial ID and AST	Yes	Plates (18-24h)	10^2-10^3 CFU/mL	Phenotypic	Growth-based	Automated	6-18h (2-8 ID; 4-18 AST)	24-42h
MicroScan WalkAway® System	Beckman Coulter	Blood, urine, wound swabs, respiratory specimens	None	Automates bacterial ID and susceptibility testing	Yes	Plates (18-24h)	10^2-10^3 CFU/mL	Phenotypic	Growth-based photometric and fluorometric	Automated photometric and fluorometric	6-18h (2-18 ID; 16-24 AST)	24-42h
BACTEC™ FX Blood Culture System	BD	Blood	None	Detects bacteremia and septicemia	Yes	Hemoculture (24-48h)	1-10 CFU/mL	Phenotypic	Fluorescent sensor	Automated fluorescent readout	12-24h	36-72h
Accelerate Pheno™ System	Accelerate Diagnostics	Blood	None	Rapid ID and AST directly from positive blood cultures	Yes	Blood culture (18-24h)	10^2-10^3 CFU/mL	Phenotypic	Morphokinetic cellular analysis	Automated	1.5h (ID), 5.5h (AST)	20-30h
Cepheid GeneXpert®	Cepheid	Nasal swabs, wound swabs, blood	None	Automated system for rapid detection of MRSA and MSSA	No	N/A	1-10 CFU/mL	Molecular	Real-time PCR	Automated fluorescent readout	60-75 min	1-1.5h
VERIGENE®	Luminex Corporation	Blood, nasal swabs	Minimal (depends on sample)	Molecular diagnostics for pathogen identification and resistance markers.	No	N/A	10^2-10^3 CFU/mL	Molecular	Nucleic acid hybridization and amplification	Automated colorimetric readout	2.5-3 hours	3-4h
cobas® MRSA/SA	Roche Diagnostics	Nasal swabs	None	Automated system for simultaneous detection of MRSA and MSSA.	No	N/A	1-10 CFU/mL	Molecular	Real-time PCR	Automated fluorescent readout	60-90 min	1-2h
BIOFIRE® FILMARRAY®	bioMérieux	Blood, respiratory swabs, wound swabs	Minimal (depends on sample)	Multiplex PCR system for rapid pathogen and resistance gene detection.	No	N/A	1-10 CFU/mL	Molecular	Multiplex PCR	Automated colorimetric and fluorescent readout	1 hour	1-1.5h
BD Max StaphSR assay	BD	Nasal swabs, wound swabs	None	Automated molecular assay for detecting MRSA and MSSA directly from clinical samples.	No	N/A	10^2-10^3 CFU/mL	Molecular	Real-time PCR	Automated fluorescent readout	2 hours	2-3h
QuickFISH Rapid Molecular Pathogen ID System	OpGen	Positive blood cultures	Minimal (sample preparation)	Fluorescent in situ hybridization (FISH) for rapid identification of *S. aureus* directly from positive blood cultures.	Yes	Blood culture (18-24h)	10^2-10^3 CFU/mL	Molecular	Fluorescent in situ hybridization (FISH)	Automated fluorescent readout	20 minutes	18-24h (including culture)
LightCycler® PRO System	Roche Diagnostics	Blood, respiratory swabs, wound swabs	Minimal (sample preparation)	Real-time PCR system for rapid detection and quantification of nucleic acids, including MRSA and MSSA.	No	N/A	1-10 CFU/mL	Molecular	Real-time PCR	Automated fluorescent readout	1-2 hours	1-2h
Staph ID/R Blood Culture Panel	AdvanDx	Positive blood cultures	Minimal (sample preparation)	Multiplex PCR panel for rapid identification of Staphylococci and resistance markers from positive blood cultures.	Yes	Blood culture (18-24h)	10^2-10^3 CFU/mL	Molecular	Multiplex PCR	Automated PCR readout	1 hour	18-24h (including culture)
iCubate iC-GPC Assay™	iCubate	Blood cultures	Minimal (sample preparation)	Multiplex PCR assay for identification of gram-positive cocci, directly from blood cultures.	Yes	Blood culture (18-24h)	10^2-10^3 CFU/mL	Molecular	Multiplex PCR	Automated PCR readout	2-3 hours	20-27h (including culture)
CLART® SeptiBac	Genomica	Blood cultures	Minimal (sample preparation)	Multiplex PCR-based assay for detection of bloodstream infections and resistance markers.	Yes	Blood culture (18-24h)	10^2-10^3 CFU/mL	Molecular	Multiplex PCR	Automated PCR readout	3-4 hours	21-28h (including culture)

1.5.2.4 Point-of-Care testing

Point-of-care (PoC) devices are diagnostic tools designed for use directly at the **site of patient care**, enabling rapid testing and **immediate results** without the need for centralized laboratories. These devices are essential in settings where quick decision-making is crucial, such as in emergency rooms, clinics, or remote areas with limited laboratory access. PoC technology encompasses a wide range of devices, from simple lateral flow assays, like pregnancy tests, to more sophisticated tools like glucometers for blood glucose monitoring, coagulometers for clotting time, pulse oximeters for oxygen saturation, and pulsometers for heart rate tracking (some examples are displayed in Figure 1.26). Their **portability**, **ease of use**, and ability to deliver **accurate**, **real-time data** facilitate faster diagnosis, immediate treatment initiation, and improved patient outcomes.

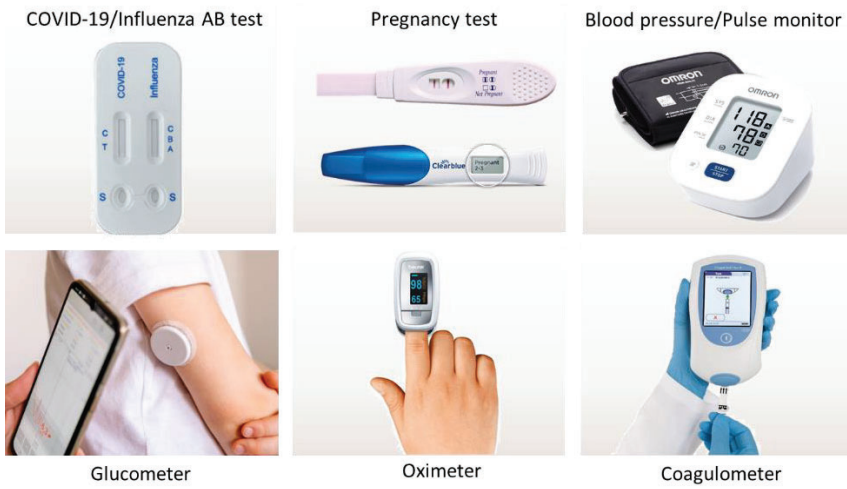

Figure 1.26. *Commonly used point-of-care (PoC) diagnostic technologies. The figure shows a range of PoC devices that facilitate rapid diagnostics at the patient site. Examples include pregnancy and respiratory infection tests (lateral flow assays), glucometers for blood glucose monitoring, coagulometers for assessing blood clotting time, pulse oximeters for measuring oxygen saturation, and pulsometers for heart rate tracking.*

In recent years, PoC devices have also expanded into fields like infectious disease detection, chronic disease management, and genetic testing, driven by advancements in microfluidics, biosensors, and smartphone integration. This

evolution underscores their growing **impact on healthcare** in both high-resource and low-resource settings, making healthcare more accessible and responsive to patient needs.

PoC testing represents a significant advancement in the timely **diagnosis of infectious diseases**, including *S. aureus*, due to its ability to carry out diagnostic tests at or near the site of patient care. This technology is especially useful in situations where laboratory infrastructure is limited, during emergencies, or in remote locations.

For instance, the **Aksense blood-based PoC biosensor** uses electrochemical technology to identify the presence of specific biomarkers or pathogens directly from a blood sample, allowing for quick and accurate diagnosis at the healthcare settings. The system is intended to be portable and easy to use, providing results within minutes, which is crucial for timely decision-making in critical care situations[128]. It has successfully completed clinical validation studies and is now positioned as a market-ready solution for diagnosing bloodstream infections, including those caused by *S. aureus*. This device has been validated through clinical trials involving over 400 patients in intensive care settings, demonstrating high sensitivity and specificity (100 % sensitivity and 91 % specificity) in detecting infections.

The **LabDisk MRSA Detection System** is an additional example. It consists of a microfluidic system for digital single-cell detection that can process nasal swabs directly to identify MRSA. This technology uses recombinase polymerase amplification and fluorescence-based detection to identify MRSA by targeting the *mecA* gene. LabDisk achieves results in under 60 minutes, enhancing the speed of MRSA screening and helping reduce transmission in healthcare settings[129].

A **paper-based** diagnostic devive that uses loop-mediated isothermal amplification (**LAMP**) **for PoC detection of MRSA** in bacterial culture and blood samples in less that 45 minutes has also been recently reported. Designed for PoC settings, it employs a simple color change for visual readout, making it suitable for low-resource environments. The device has been shown to detect the *mecA* gene, specific to MRSA, with 100% specificity and sensitivity compared to qPCR results, being a promising tool for rapid on-site diagnostics of bloodstream MRSA infections[130].

The main benefit of PoC testing is how quickly results are obtained, many times in a matter of minutes. This quick response is essential for **limiting the spread** of infection, **enhancing patient outcomes**, and starting the **right antimicrobial medication**. Furthermore, PoC testing equipment is typically made to be simple to operate, needing little training for medical staff. Their mobility makes it possible to use them in a variety of places, such as field locations, hospitals, and clinics. Moreover, PoC testing **minimizes** delays and possible **sample degradation** by eliminating the need to transport samples to centralized laboratories. This is especially helpful in places with low resources, such rural areas, where access to lab facilities may be restricted.

Despite their advantages, PoC devices face some limitations. The possibility of **reduced sensitivity and specificity** in comparison to centralized laboratory testing is a significant drawback. False positives and false negatives can happen, resulting in treatment choices that are not appropriate. In addition, some other factors, including operator skill and sample quality, might impact the accuracy of PoC testing results.

As a whole, PoC testing for *S. aureus* and other pathogens has a promising future thanks to continuous advances that aim to increase its affordability, accuracy, and simplicity of use. It is anticipated that advancements in lab-on-a-chip and microfluidics technology could improve the capabilities of PoC devices, permitting more comprehensive testing and multiplexing. These innovations enable a wider range of diagnostic capabilities by combining several tests into a single device.

The sensitivity and specificity of PoC devices could improve with further advancements in biosensors and nanotechnology, lowering the possibility of false positives. Furthermore, real-time diagnostic information sharing with electronic health records will become possible by advances in connectivity and data integration, improving patient care and epidemiological tracking.

1.5.3 BIOMARKERS IN *S. AUREUS* DIAGNOSIS

The need for quicker, more precise, and targeted diagnosis of *S. aureus* infections is driving ongoing research into new biomarkers and diagnostic methods, particularly in light of antibiotic-resistant forms. Since biomarkers are

biological molecules indicative of a disease, they are being extensively explored due to their potential utility in the **detection** or **monitoring** of *S. aureus* infections. Biomarkers play, thus, an essential function in the rapid and accurate diagnosis of *S. aureus*. The potential to greatly enhance patient outcomes and diagnostic accuracy for *S. aureus* lies in the development and validation specific biomarkers.

To diagnose infections driven by *S. aureus*, a wide range of biomarker types, including those connected to immunity, molecular biology, and metabolism, have been investigated. Prominent candidates include proteins specific to this bacterium, such as SpA, Clumping factor, Enterotoxins, Exfoliatin, and PVL, as well as other prevalent compounds like hemolysins[131]. As an example, some strains of *S. aureus* produce **PVL**, which is a toxin linked to serious infections of the skin and soft tissues. PCR assays can identify the presence of PVL genes (lukS-PV and lukF-PV), which predicts a higher virulence of the infecting strain[132].

Specific DNA sequences, like the ***mecA*** gene that confers methicillin resistance, the ***blaZ*** gene that confers vancomycin resistance, and the staphylococcal cassette chromosome *mec* (**SCC*mec***) that carries the *mecA* gene, are being studied further[115, 133]. Procalcitonin (**PCT**), interleukin-6 (**IL-6**), and C-reactive protein (**CRP**) are among the host responses that are actively being studied as potential indicators of inflammatory reactions triggered by *S. aureus*[134].

Often used as biomarkers for *S. aureus*, staphylococcal **enterotoxins** are linked to toxic shock syndrome and food poisoning. According to Argudín et al., the presence of *S. aureus* in clinical and dietary samples can be verified using immunoassays that detect enterotoxins A, B, C, D, and E[135]. Another important biomarker that interferes with the immune response is **SpA**, which is frequently found in diagnostic assays. SpA isa surface protein of *S. aureus that* binds to the Fc region of immunoglobulins. During an infection, this protein is actively displayed on the bacterial surface and can be released from the bacterial envelope[136, 137]. As a result, the presence of an active *S. aureus* infection is strongly suggested by its detection.

Teichoic acids, which are found in the cell walls of Gram-positive bacteria such as *S. aureus*, can be identified using a variety of biochemical tests and function as biomarkers for the bacterial presence[138]. PCR can be used to identify the *nuc* gene, which is unique to *S. aureus* and encodes a thermostable nuclease.

According to Becker et al. (2014), this gene is a reliable genetic marker for determining whether *S. aureus* is present in clinical samples[115].

As a biomarker for bloodstream infections carried on by *S. aureus*, lipoteichoic acid (**LTA**), a component of the cell wall, can be found in blood samples[139]. Fibrinogen-binding proteins (**FnBPs**) are also important indicators because they help *S. aureus* adhere to host tissues. Their identification can help with the diagnosis of invasive *S. aureus* infections, such as endocarditis and osteomyelitis[140].

The main benefit of biomarker-based diagnostics over conventional culture methods is their speed at producing data. Because of its extreme sensitivity and specificity, there are fewer false positives and negatives. They can also be employed in a variety of approaches, such as point-of-care testing, which makes them useful instruments for clinical diagnostics. Biomarker-based diagnostics provide benefits, but they can have drawbacks. The variation in biomarker expression between *S. aureus* strains is one of the primary problems, as it can affect the sensitivity and specificity of the assays. Clinical trials and in-depth investigation are further necessary for the creation and validation of novel biomarkers.

Research remains ongoing to meet the urgent need for biomarkers that are **unique to *S. aureus*** and **sensitive in early infections**. Up to now, the studies suggest biomarkers that show promise. Further study is required, nevertheless, in order to evaluate and incorporate these indicators into routine clinical practice and potentially improve patient outcomes.

The goals of future research are to improve current assays and identify new biomarkers. It is thought that developments in proteomics and genomics may yield new biomarkers that will improve the precision of *S. aureus* diagnosis. Moreover, building quick, high-throughput diagnostic platforms might be possible by combining biomarker detection with cutting-edge technologies like **microfluidics** and **lab-on-a-chip** devices.

As an alternative, **Quorum Sensing molecules** (QSms) present a promising potential as diagnostic biomarkers. The advantage of using QSms as biomarkers lies in their ability to reflect bacterial activity and virulence at an early stage, potentially enabling earlier detection of infections before clinical symptoms fully develop. Unlike traditional diagnostic methods that require bacterial culture and

identification, detecting QSMs could offer a more rapid and direct way to identify *S. aureus*. Moreover, since QSMs are involved in regulating critical pathogenic behaviors, their detection might also provide insights into the infection's progression and severity. This makes QSMs valuable not only for rapid diagnosis but also for real-time monitoring of *S. aureus* infections.

1.6 QUORUM SENSING (QS)

QS is a sophisticated **cell-to-cell communication** mechanism used by bacteria to coordinate their collective activities based on **population density.** This procedure comprises the synthesis, release, identification, and reaction to autoinducers, which are small signaling molecules. QS allows bacterial populations to **coordinate processes** including biofilm formation, virulence factor production, bioluminescence, and extracellular enzyme release that are advantageous when carried out collectively[141].

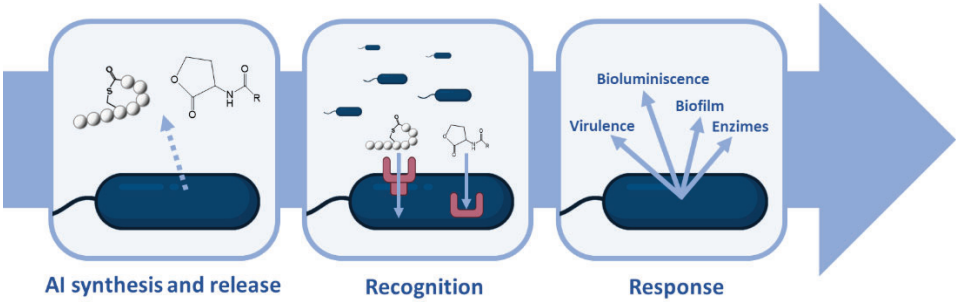

***Figure 1.27**. Summary of the three mains stages of quorum sensing (QS) mechanisms: biosynthesis and extracellular release of autoinducers (AIs), recognition by the surrounding bacteria and response upon reaching a threshold limit. Multiple coordinated actions such as enzyme synthesis and secretion, biofilm formation, bioluminescence and the expression of virulence factors are triggered by QS systems.*

Three essential elements are usually involved in bacterial QS: **autoinducers** (AIs), **receptors**, and **regulatory pathways** (see Figure 1.27). Bacteria produce small signalling molecules, known as AIs, which are released into the environment. The concentration of AIs increases as the bacterial population grows. When they reach a certain threshold, these molecules attach to particular receptor proteins on the bacterial cell surface or inside the cell. The bacterial population can

respond collectively as a result of this binding event, triggering a signal transduction cascade that modifies gene expression[142].

QS was first discovered in the context of **bioluminescence** in marine bacteria, specifically *Vibrio fischeri* and *Vibrio harveyi*[143]. Bioluminescence is the biochemical emission of light by live organisms, primarily observed in marine species like bacteria, dinoflagellates, and some fish, as well as terrestrial organisms such as fireflies. This process results from a chemical reaction involving a substrate called luciferin and an enzyme known as luciferase. In the presence of oxygen, luciferin is oxidized by luciferase, releasing energy in the form of visible light. The function of bioluminescence varies, serving roles in defense, communication, mating, and symbiotic relationships, such as the mutualism seen between *V. fischeri* and marine hosts[144].

The discovery of QS began with the observation that Vibrio species only produced light when they reached a certain population density. This density-dependent behavior suggested that bacterial cells could **communicate to coordinate** their activity. The light production, or bioluminescence, is an energy-intensive process, so the bacteria use QS to ensure that they only activate the genes responsible for light emission when the population is sufficiently large, making the energy expenditure worthy[145].

This discovery not only elucidated the mechanism behind bioluminescence but also laid the foundation for understanding QS as a broader regulatory system. Beyond controlling light production, QS plays a key role in regulating various bacterial processes such as virulence factor expression, motility, and horizontal gene transfer[146].

One of its primary roles is controlling the creation of **virulence factors**, such as the expression of toxins, enzymes, and other chemicals that allow bacteria to invade and damage host tissues effectivelt [147]. By coordinating the production of these components, bacteria can attack the host more efficiently, improving their chances of survival and growth. By synchronizing the release of these components when the bacterial population reaches a critical threshold, QS maximizes the impact of the infection while minimizing the likelihood of early detection by the host immune system, enhancing bacterial survival and growth. For example, *Vibrio cholerae* uses QS to regulate the secretion of cholera toxin, a crucial virulence factor that disrupts intestinal cells, leading to severe diarrhea

and dehydration[148]. Similarly, *S. aureus* utilizes QS to control the production of alpha-hemolysin (hla), which lyses host cells and assists in immune evasion[149].

Enzymes also play a significant role in pathogenicity, and their production is regulated by QS. *P. aeruginosa*, for instance, controls the synthesis of elastase and alkaline protease by its QS mechanisms[150]. Elastase degrades structural proteins such as collagen and elastin, weakening tissues and promoting bacterial penetration, while alkaline protease targets immune components, further enhancing bacterial survival.

Additionally, QS influences the expression of **surface molecules** such as adhesins and invasins, which are vital for bacterial attachment and penetration into host tissues. For instance, in *P. aeruginosa*, QS controls the production of **lectins** (LecA and LecB) and Type IV **pili**, which are vital for adhesion and biofilm formation, enhancing the bacteria's ability to colonize host surfaces effectively[151].

In *E. coli*, particularly uropathogenic strains, QS influences the expression of type 1 and P pili, which facilitate colonization in the urinary tract by adhering to specific receptors in the bladder and kidney[152]. Similarly, in *S. aureus*, the QS modulates the expression of surface adhesins such as Clumping Factor B (**ClfB**) and **FnBPs**. These molecules enable the bacteria to adhere to host tissues and invade, crucially supporting its pathogenicity[149]. Listeria monocytogenes uses QS to regulate invasins like **Internalin A** and **B**, which interact with host cell receptors (such as E-cadherin) to penetrate intestinal epithelial cells, a key step in systemic infection[153].

Iron acquisition, another critical survival strategy, is as well modulated by QS. Bacteria like *P. aeruginosa* uses QS to regulate siderophore production, such as **pyoverdine**, optimizing iron uptake in iron-limited environments like the host body[154].

The formation of **biofilms** and their management and preservation are also controlled by QS mechanisms. A biofilm is a structured community of bacteria attached to a surface and embedded in a self-produced extracellular matrix composed of polysaccharides, proteins, nucleic acids, and lipids [155]. They can be formed on a variety of surfaces, including those found in natural environments like riverbeds and ocean bottoms, as well as on living tissues, medical devices, and industrial equipment[156].

The first step for the creation of a biofilm is the **initial adhesion** of free-floating (planktonic) microbial cells to a surface. This initial attarchment is driven by the synthesis of **adhesins**, which are surface proteins or polysaccharides that help in cell adhesion to the surface. Once bound to a surface, the extracellular matrix is produced, which surrounds the cells and provides structural stability to the biofilm[157]. Subsequently, the biofilm can disperse planktonic cells, leading to propagation and colonization of other tissues or surfaces, further spreading the infection. The main stages of the biofilm life cycle are presented in Figure 1.28.

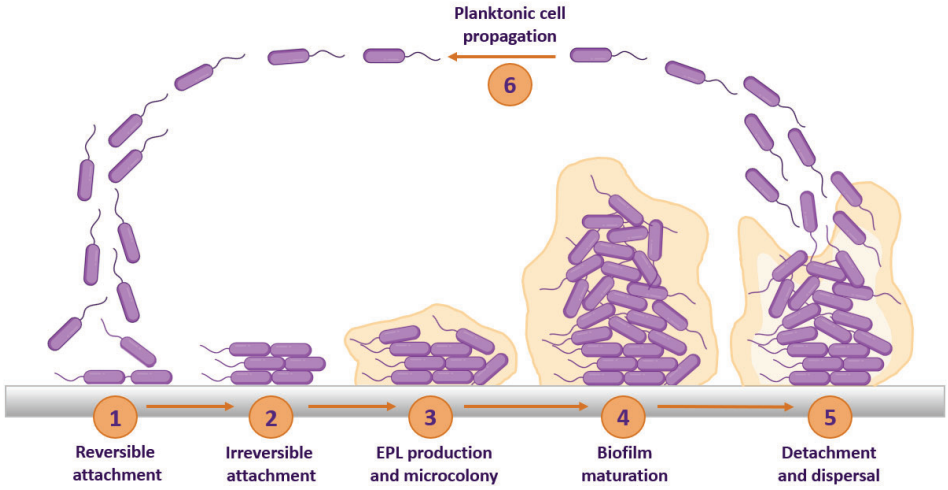

Figure 1.28. *The biofilm life cycle. The biofilm infection life cycle generally follows the steps of attachment (interaction between bacteria and the surface), accumulation (interactions between bacterial cells, forming microcolonies embedded by the extracellular polysaccharide (EPL) they produce and secrete), maturation (formation of a viable 3D structure) and detachment (release from the biofilm) followed by dispersion to surrounding areas.*

As the biofilm develops, the bacteria living inside it experience significant **physiological changes**. These modifications include changes in metabolic activity, gene expression and AMR. Thanks to the biofilm structure, microenvironments with gradients of nutrients, oxygen, and waste products are created. The spacial heterogenicity increases the overall resilence of the biofilm community as it allows different microbial species to live together[158].

The microorganisms living in biofilms benefit from multiple advantages:

- **Protection from environmental stresses:** During an infection, the extracellular matrix serves as a physical barrier that protects the microbial cells from UV radiation, desiccation, and the host immune system.
- **Greater resilience to antimicrobial drugs:** When compared to planktonic cells, biofilms show a significantly higher resilience to antibiotics and disinfectants. The limited ability of antimicrobial agents to diffuse through the matrix, the existence of persistent cells with lower metabolic activity, and the expression of certain resistance genes are the main causes of this increased resistance.
- **Improved nutrient acquisition:** Biofims provide to mirobial cells inside them a continious supply of food resources, as they capture and concentrate nutrients from the surrounding environment.
- **Facilitated genetic exchange:** Within a biofilm, cells are placed very close to each other, facilitating horizontal gene transfer of benecicial features like antibiotic resistance.

QS plays a key role in the coordination of biofilm development, by controlling the synthesis of extracellular polymers and other elements required for maintaining their integrity[159]. It also regulates the acquisition and incorporation of extracellular DNA from the surrounding environment, increasing genetic diversity. This mechanism is reffered as **bacterial competence**[160]. Additionally, **swarming** motility, a collective movement of bacterial cells across surfaces that promotes colonization and infection spread, is regulated by QS[161].

Understanding the production, structure, and behavior of biofilms is essential to prevent and regulate biofilm-related issues. In **industry**, biofilms can cause **biofouling** in pipelines and equipment, leading to blockages, reduced efficiency, and increased maintenance costs, as well as **biocorrosion** that degrades materials and incurs financial burdens[162]. In **healthcare**, biofilms are linked to chronic infections on **medical devices** like catheters and implants, protecting pathogens from antibiotics and immune responses, making them hard to treat[163].

In **environmental settings**, biofilms are crucial for **bioremediation**, enhancing the breakdown of pollutants and toxins in wastewater treatment by providing a stable environment for microorganisms[164]. However, they also present risks when they form in drinking water systems, where they can harbor and protect

harmful pathogens such as *Legionella* and *Pseudomonas* from disinfectants, potentially leading to **waterborne disease** outbreaks[165].

QS also plays a crucial role in **interspecies communication**. In complex habitats like the human gut, soil, and marine ecosystems, different bacterial species can coordinate their activities and coexist in response of the production and detection of different AIs. The dynamics, stability, and general function of microbial communities can be impacted by this interspecies communication[142].

1.6.1 QS IN GRAM-NEGATIVE BACTERIA

The QS system of Gram-negative bacteria includes the synthesis, release, detection, and reaction to AIs, mainly **N-acyl homoserine lactones** (AHLs). These compounds, produced by LuxI-like enzymes, **easily diffuse** bacterial cell membranes. AHLs accumulate in the environment as bacterial populations increase, and once they reach a sufficient concentration, they enter bacterial cells where they bind to **LuxR-type receptor** proteins. As a result of this interaction, the receptors undergo conformational changes that help them interacting with DNA to modify gene expression (see Figure 1.29 A). This coordinated reaction controls the synthesis of virulence factors, the creation of biofilms, and the resistance to antibiotics, among other physiological processes.

The QS systems of some Gram-negative bacteria may have higher complexity. *P. aeruginosa*, for example, employs several interrelated systems, such as LasI/LasR, RhlI/RhlR, and the PQS (*Pseudomonas* Quinolone Signal) system[166]. Similar to this, *Vibrio harveyi* regulates gene expression by combining signals from 3 different AIs to coordinate various physiological mechamisms such as bioluminescence[167].

1.6.2 QS IN GRAM-POSITIVE BACTERIA

Gram-positive bacteria often use **oligopeptide** AIs, which are recognized by a membrane-bound **histidine kinase receptor**. Subsequently, a response regulator that controls gene expression is phosphorylated by the activated receptor. AIs in Gram-positive bacteria require certain **transport mechanisms**

for secretion and detection, being unable to passively diffuse through the thick peptidoglycan barrier (refer to Figure 1.29 B).

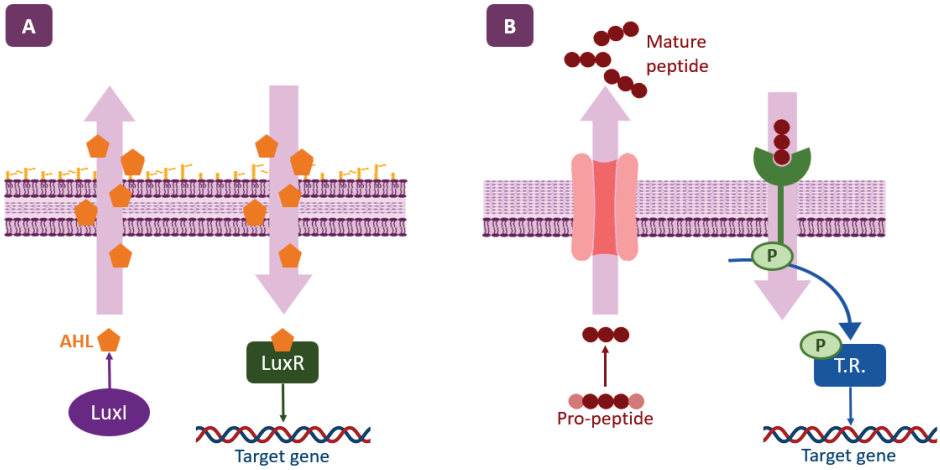

Figure 1.29. *Schematic illustration of quorum sensing (QS) systems in bacteria. A) Gram-negative bacteria: The AI synthase (LuxI) participates in the synthesis of acyl homoserine lactones (AHL). The AHL receptor (LuxR) senses the signaling molecules and interacts with them, contribiuting to the regulation of the target gene. B) Gram-positive barceria: Pro-peptides are synthesized inside the cell and secreted outside in their mature form. Upon reached a thresgold, they interact with a transmembrane histidine kinase receptor activating the target gene expression via autophosphorylation of the trascriptional regulator (T.R.). Adapted from Verbeke, F., et al.*[168].

1.6.3 QS AS A CLINICAL TARGET

From a clinical perspective, QS is of great therapeutic importance as it directly regulates the pathogenesis of many bacterial diseases. One approach that appears to be promising for the development of new antimicrobial medicines is to target QS pathways. It is feasible to reduce bacterial pathogenicity and biofilm formation without completely eliminating the bacteria by **interfering with QS** mechanisms. This reduces the selection pressure for the emergence of antibiotic resistance in bacteria. The main therapeutic approaches targeting QS are illustrated in Figure 1.30, involving the use of compounds that **prevent AI synthesis**, **destroy AIs**, **or prevent receptor binding,** what is known as **Quorum Quenching** (QQ)[169].

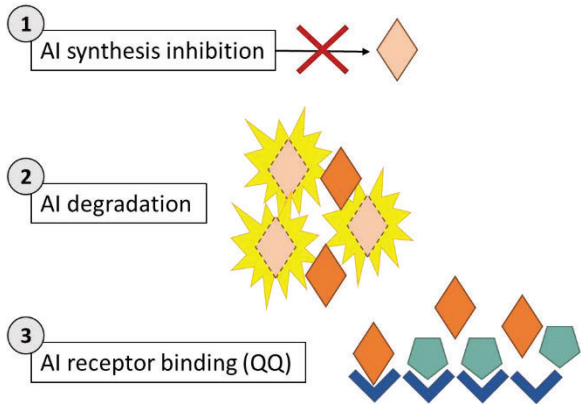

Figure 1.30. *Key therapeutic strategies targeting QS pathways to control bacterial virulence. 1) Inhibition of AI synthesis: prevents the production of QS signaling molecules, blocking communication between bacterial cells and reducing virulence. 2) Degradation of AIs: Enzymes or molecules degrade AIs in the extracellular environment, disrupting bacterial signaling and diminishing coordinated virulence responses. 3) Blocking AI Receptors: Quorum quenching (QQ) agents bind to QS receptors on bacteria, blocking AIs from activating gene expression linked to virulence.*

QS also shows great potential for **diagnostic applications**, especially in detecting bacterial infections early by monitoring QS signaling molecules, such as AIs. These molecules, which bacteria release to coordinate population behaviors like biofilm formation and virulence, can serve as biomarkers for the **presence** and **density** of pathogenic bacteria in clinical samples.

By identifying specific QS signals associated with particular pathogens, diagnostic tools can potentially detect infections **before they reach critical levels**. This may result in the creation of diagnostic instruments that quickly recognize infections and evaluate their seriousness by measuring the concentrations of particular QSMs[170]. Furthermore, QS-based diagnostics could help differentiate between **colonization** and **active infection**, allowing for more targeted treatment approaches and reducing unnecessary antibiotic use (see Figure 1.31). The sensitivity and specificity of QS molecule detection also make it a promising approach for PoC diagnostics, where rapid, accurate bacterial identification is essential.

Comprehending QS is crucial for creating novel treatment approaches to fight bacterial infections and control microbial communities in diverse settings. Likewise, the potential of this communication system for diagnostic applications emphasizes its significance in both clinical and scientific settings.

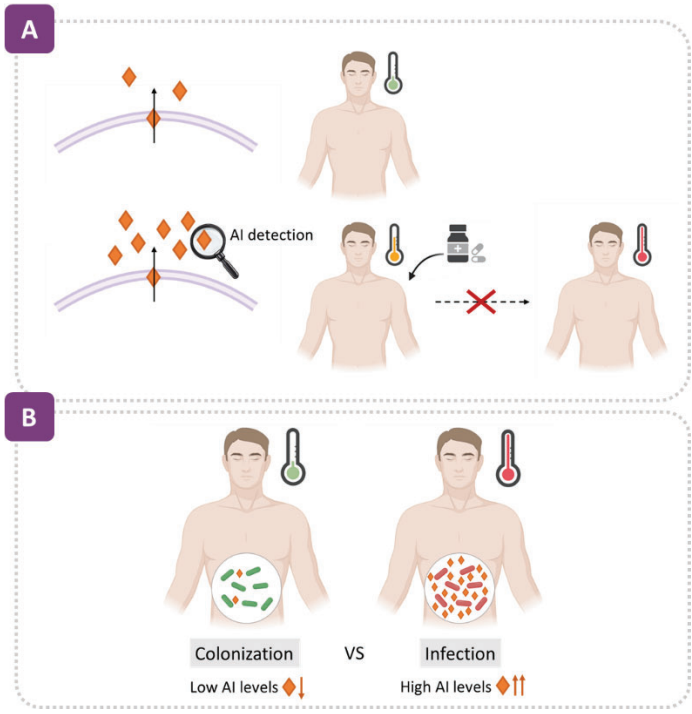

Figure 1.31. *Potential of QS as a diagnostic tool for bacterial infections. A) Early Detection: monitoring QS signaling molecules allows for early diagnosis, identifying infections before symptoms worsen, enabling timely treatment, and improving patient outcomes. B) Differentiation between Colonization and Infection: by detecting specific QS molecules, diagnostics can distinguish between bacterial colonization and active infection, reducing unnecessary antibiotic use.*

1.7 *S. AUREUS* ACCESSORY GENE REGULATOR (*AGR*) QS SYSTEM

In *S. aureus*, QS signals are mainly regulated by the *agr* QS system, a sophisticated macchinery that synchronizes the expression of virulence factors and other behaviours in response to variations in cell density. The system is constituted by genes encoding **downstream effectors**, **signaling molecules**, and **regulatory proteins**[171].

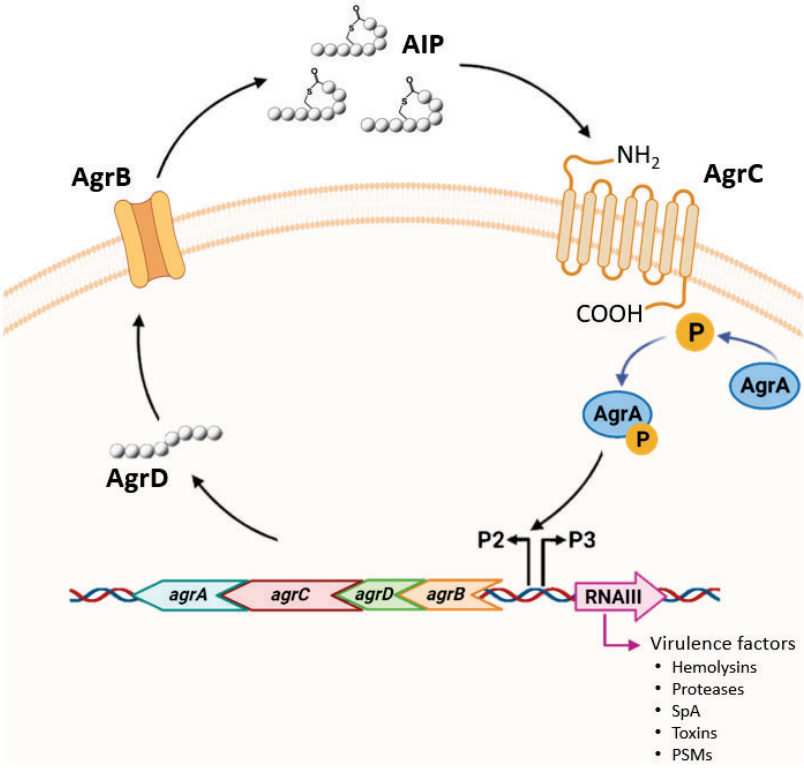

Figure 1.32. *Schematic representation of the S. aureus accessory gene regulatory (agr) QS system. The agr locus contains two distinct transcripts known as RNAII and RNAIII. The RNAII transcript, or operon agrBDCA, encodes the necessary components for AIP synthesis and the activation of the regulatory cascade. AgrD is the precursor peptide of AIP, AgrB is a membrane protease that helps produce AIP, AgrC is a histidine kinase that binds to AIP to activate it, and AgrA is a response regulator that uses the P2 and P3 promoters to drive transcription of RNAII and RNAIII. The main effector of the agr system is a regulatory RNA molecule that is produced by the RNAIII transcript. It works by down-regulating cell surface proteins and up-regulating extracellular virulence factors. Adapted from Novick, R. P. and E. Geisinger*[171].

The *agr* system (illustrated in Figure 1.32) is encoded by ***agr* locus**, which drives to an autoactivation circuit expressed from two divergently transcribed promoters, **P2** and **P3**. The P2 promoter produces the RNAII transcript, which is an operon of four genes (***agrBDCA***), and encodes for the majority of components that are required for *agr* functionality[172].

Briefly explained, **AgrD** is the precursor peptide that is post-translationally modified into an extracellular signal molecule known as autoinducing peptide (**AIP**). AIPs are processed and secreted into the extracellular media by the transmembrane endopeptidase AgrB, which also forms the thiolactone that is

characteristic of AIPs[173]. *S. aureus* has **four** known agr **allelic variants**, each of which results in unique AIP type (1 to 4) with slight variations in amino acid composition (Figure 1.33).

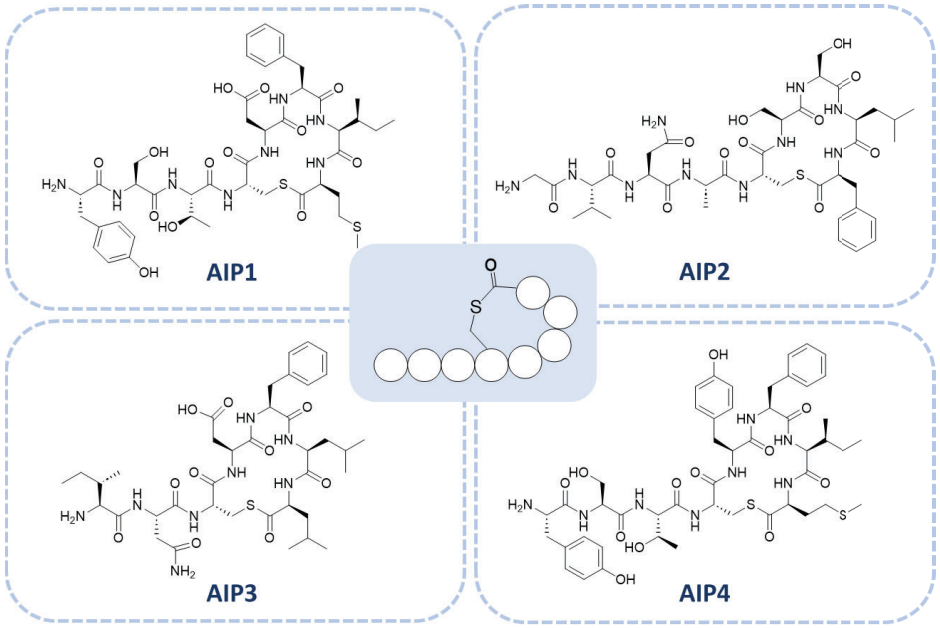

Figure 1.33. *Chemical structures of the four autoinducing peptides (AIPs 1-4) produced by S. aureus. A simplified representation of the overall structure of the AIPs, which consists of seven to nine amino acid residues and their distinctive thiolactone ring, is displayed in the center.*

AIPs are secreted into the **extracellular** environment in their mature form and act as signaling molecules. Once they reach a threshold concentration, AIPs attach to the membrane-anchored histidine kinase **AgrC** receptor anchored in the membrane, leading to its autophosphorylation. The *agr* system of each strain of *S. aureus* specifically recognizes each AIP type, being inhibited by other AIPs. The phosphate group is then transferred to **AgrA**, the response regulator, activating it. Finally, activated AgrA binds to promoters P2 and P3, enhancing the trascription of **RNAIII**, the primary regulatory effector of the *agr* system (see Figure 1.32).

RNAIII plays an essential role in modulating bacterial growth as well as virulence and adherence to host tissues[171]. *S. aureus* first expresses adhesins to facilitate colonization at low cell densities. By upregulating the synthesis of exotoxins and other **virulence factors**, the *agr* system modifies the gene expression profile that

promotes tissue invasion and immune evasion as the bacterial population and AIP concentration rise[173]. Hemolysins, proteases, and phenol-soluble modulins (PSM) cosntitute some of the virulence genes that RNAIII regulates.

Since the pathogenicity of *S. aureus* depends on its capacity to modulate virulence factors, the *agr* system is an important target for both therapeutic and diagnostic purposes. By interfering with QS, attacking the agr system can lower virulence and facilitate the identification and management of infections[169].

Targeting the *agr* system **therapeutically** can reduce virulence and disrupt quorum sensing, which are two promising ways to minimize *S. aureus* infections. By preventing bacteria from coordinating harmful actions, QQ can increase the susceptibility of bacteria to immune responses and drugs. This strategy offers an alternative to conventional antibiotics and may be particularly successful against *S. aureus* strains that are resistant to them[169, 174].

From a **diagnostic** perspective, the *agr* system holds significant promise. Different biomarkers, like RNAIII and AIPs, can be used to identify and track *S. aureus* infections. Detecting these molecules in clinical samples can provide rapid and accurate identification of infections, allowing for timely intervention and treatment. This feature is especially helpful in hospital environments, where early *S. aureus* detection can help stop the infection from spreading thus improving patient outcomes[173, 174]. Moreover, the specificity to a certain AIP type of each *S. aureus* strain improves the accuracy of diagnostic testing and makes targeted treatment approaches possible.

All thing considered, the significance of the *agr* system in controlling *S. aureus* infections is highlighted by its complex function in controlling virulence as well as its potential as a therapeutic target and diagnostic marker. Treatment and early diagnosis of diseases linked to *S. aureus* infections could be significantly improved with further study on the *agr* system and its components.

1.8 STATE OF THE ART ON THE DETECTION OF *S. AUREUS* AIPS

Even though AIPs are essential for bacterial communication and pathogenicity, their identification has received very little attention in the literature. Detecting AIPs poses significant **challenges** due to their chemical composition, low molecular weight, small quantities in bacterial isolates and the complicated matrix environments of clinical samples.

Because AIPs are present in biological samples at **low quantities** and the surrounding matrices are complicated, detecting them is a substantial challenge. These tiny signaling molecules are frequently hidden by **chemical noise**, and the procedure is made more difficult by the requirement for precise sample preparation and specific detection techniques. Moreover, their chemical structure, containing a thiolactone ring-containing, might be **labile**, which makes them susceptible to degradation and complicates their identification. The amount of study conducted in this field has been limited by the inherent challenges in measuring and isolating these peptides.

1.8.1 MS-BASED APPROACHES

Detecting AIPs in staphylococci has advanced dramatically, utilizing sophisticated technologies. Owing to its remarkable sensitivity and specificity, MS has emerged as the reference method for AIP detection. It makes accurate identification and quantification of AIPs possible, making it a key tool for research on bacterial communication and quorum sensing.

Originally, AIPs were found using **single-stage MS** methods. Due to signal suppression effects and low concentrations in the samples, these peptides can be hidden in chemical noise, making it challenging to detect them from extremely complex matrices using these techniques. To get around these restrictions, Kalkum et al. (2003) used MALDI-TOF technology to investigate the presence of AIPs from **bacterial culture supernatants**. The distinct subtypes of AIPs may be definitively identified as well as their structural characteristics thanks to this **multistage MS** technique. Yet the results were only qualitative, which led to the creation of new methods for their quantitative investigation[175].

In 2013, Junio and colleagues used ultrahigh-performance liquid chromatography-high resolving power mass spectrometry (**UHPLC-HRMS**) to undertake quantitative analysis of AIP1. This approach involved substantial pre-treatment procedures like filtration and purification, as well as the requirement to culture *S. aureus*. They used a mutant with a mutation in agr (AH2492), which was unable to make AIP1, to confirm the proper identification of the extra peaks at early detection periods with the same nominal mass of **AIP1**. Upon analysis of the mutant strain's spent medium, no peaks indicating the presence of AIP1 were seen, demonstrating that this peptide was correctly identified. According to their study, AIP1 showed a limit of quantification (LOQ) of 2.6 µM and a limit of detection (LOD) of 0.25 µM, demonstrating the technique's high precision and sensitivity for the effective detection of AIP1 from complex culture spent media[176].

Shortly after, in 2014, Roux et al. investigated the combination of nutritional and population density signals in the control of AIPs by examining the CodY-mediated regulation of the *S. aureus agr* system. For that purpose, both reporter and *S. aureus* control strains culturing was required. In their approach, the methodology previously used for the detection of AIP1[176] was modified to facilitate measurements of the accumulation of **AIP3.** The analysis was made in filtered culture fluids using reversed-phase liquid chromatography (LC) in an ultrahigh-performance liquid chromatograph (**UPLC**) **coupled to** an **Orbitrap** mass spectrometer with an electrospray source. Despite focusing on the regulatory mechanisms, this work highlighted how difficult it is to detect AIP in relation to bacterial growth circumstances and population dynamics. While the study did not offer values on AIP concentration, it made a substantial contribution to the better understanding of the environmental parameters influencing AIP synthesis and the detection of AIP3[177].

Todd et al. (2016) measured the inhibition of quorum sensing quantitatively using hybrid **Quadrupole-Orbitrap** MS. *S. aureus* culturing and sample pre-treatment were also necessary for this technique. With a detection and quantification of range of 3.5 nM and 100 nM, the study offered sensitive quantitative data. *S. aureus* AIP1 was successfully identified and quantified using this method[178].

A method for the identification of AIPs by exploiting their thiolactone functionality for chemoselective trapping and enrichment of the compounds

from the bacterial supernatants was also reported. Standard liquid chromatography-mass spectrometry (**LC-MS**) analysis, guided by genome sequencing data, readily provided the AIP identities. By synthesizing peptides in their original environments, this novel approach improved stability and detection precision with LOD values reaching 12.5 nM for some of the peptides, although no sensitivity values were reported for *S. aureus* AIPs. Rather than focusing on quantification, the approach confirmed the identity of the four existing *S. aureus* AIPs, among other AIPs produces by other staphylococcal species, through broad identification[179].

Using cutting-edge MS techniques, Jones et al. (2020) conducted both targeted and untargeted study of secondary metabolites. Once again, this method needed cultivating *S. aureus* and carefully **pre-treating** culture supernatants in order to identify AIP1, the linear range of instrument response using a concentration range of 10^{-4} to 10 µg × mL^{-1} was established[180].

Even though chromatographic techniques for detecting AIPs have advanced, the investigations that have thus far been reported have primarily concentrated on detecting AIP1 and have not been able to detect the other AIP subtypes that are currently accessible. Therefore, from a therapeutic perspective, the approaches mentioned above cannot rule out a potential *S. aureus* infection because different strains of the bacteria do not all produce the same AIP.

Interestingly, a technique for simultaneously **detecting the four AIP** molecules that are now in use has just been patented. In as little as ten minutes, the UHPLC-MS-based approach can identify any kind of *S. aureus* AIP. Depending on the AIP subtype, the LOD can range from 1 to 6 µg x L^{-1}. This method shows great promise because it can accurately and specifically diagnose infections caused by any strain of *S. aureus* [181]. The main obstacle with the diagnostic procedure described is that samples must be **cultured** for 12 hours. Although the culture period is shorter than for other tests, the diagnosis is as well delayed because of culture necessity. Table 1.2 provides a summary of AIP detection using MS approaches.

Though mass spectrometry offers many benefits, there are still certain limitations when it comes to identifying AIPs. Among these are the requirements for **complex machinery** and **specialized knowledge**, both of which can be expensive and aren't always available in clinical or research settings. Furthermore, even though MS methods have a high sensitivity, signal

suppression and **interference** from complex biological matrices can potentially affect them, which could compromise the precision and dependability of the results.

1.8.2 BIOSENSING SYSTEMS

The development PoC systems is now taking place, with the goal of performing an early diagnosis in medical facilities without requiring sample transportation. For that reason, biosensors have become increasingly attractive as diagnostic instruments due to their accessibility, ease of handling, and potential for downsizing to a compact design[182].

These systems show promise as a replacement for traditional clinical procedures because they offer **higher sensitivity** and **faster** reaction times than standard diagnostic approaches[183]. Similarly, their **accessibility** and **affordability** make them a diagnostic instrument for anyone, particularly in developing countries unable to invest in specialized equipment like those needed for MS methods [184]. The creation of novel biosensors that may be utilized in ordinary clinical settings to diagnose infectious diseases has thus become the focus of the efforts of numerous researchers.

Biosensors are analytical tools that convert a biological response into a signal that can be measured by combining a biological component with a physicochemical detector. They typically consist of **three main components**: a bioreceptor, a transducer, and a signal processor. The **bioreceptor**—which can be an enzyme, antibody, nucleic acid, or cell receptor—specifically binds the target analyte. The **transducer** converts this binding event into an electrical or optical signal. Finally, the **signal processor** amplifies and processes the signal for display or further analysis.

Biosensors can be categorized according the biorecognition element used sucha as enzyme, protein-receptor, DNA-biosensors, whole-cell biosensors, and antibodies. In addition, they can be broadly classified according to their mode of signal transduction into three groups: mass-sensitive, thermal optical, and electrochemical sensors [185]. Refer to Figure 1.34 for a more detailed classification of biosensors.

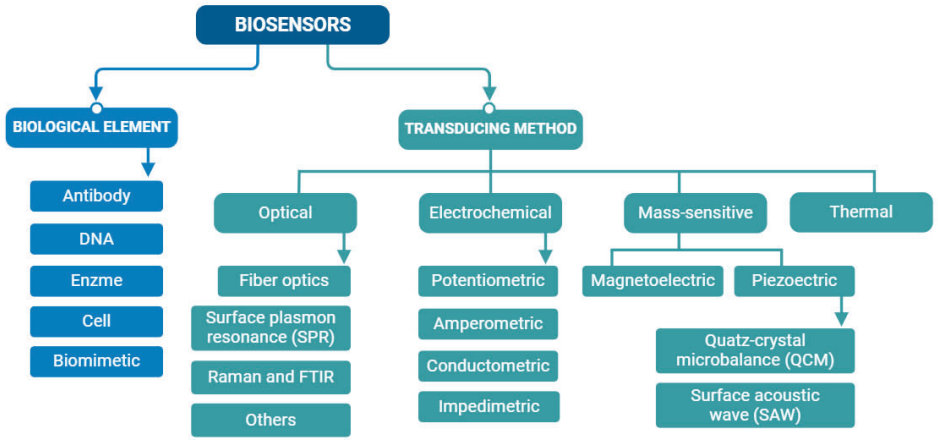

Figure 1.34. *Classification of biosensors based on biological elements and transduction methods. The figure categorizes biosensors according to their biological elements—including enzymes, antibodies, nucleic acids, and cells—which specifically recognize target analytes. It further classifies them by transduction methods: electrochemical, optical and mass-sensitive.*

The most recent developments with regard *to S. aureus* have been concentrated on development of electrochemical and optical biosensors, which have emerged as viable approaches towards its diagnosis. **Electrochemical biosensors** measure changes in electrical properties (like current, voltage, or impedance) upon analyte binding. They are widely used for detecting small molecules and ions due to their high sensitivity, rapid response time, and adaptability to miniaturization. In contrast, **optical biosensors** detect changes in light properties, such as absorbance, fluorescence, or reflectance, upon analyte interaction. They offer high specificity and are often used for detecting biomolecules with fluorescent labels or for real-time monitoring of molecular interactions.

While electrochemical biosensors were the first commercially available sensors and have been the subject of much research for many years, recent trends for detecting AIPs in *S. aureus* have shifted towards the development of optical biosensors. A biorecognition element combined with an optical transducer performs the detection in optical biosensing systems, yielding a quantifiable signal proportional to the amount of analyte detected[186].

Whole cell optical sensors use genetically modified cells that can identify chemicals emitted by pathogens and provide a detectable signal in response. Gram-negative pathogen detection has made considerable use of reporter

bacteria biosensors. Nonetheless, there are yet few applications of these sensing methods for identifying QS compounds from Gram-positive bacteria[168].

Recently, Lubkowicz et al. (2018) developed a novel approach by reprogramming probiotic *Lactobacillus reuteri* as a biosensor for detecting *S. aureus*-derived **AIP1**. This innovative method involved genetic modification of *L. reuteri* to produce a detectable signal in response to AIP-I presence. The technique required culturing both *S. aureus* and the biosensor strain.

For that purpose, the *GusA* gene was placed under the P3 promoter and the regulatory module of the *agr*-I system (*AgrA* and *AgrC*) was introduced under the *L. reuteri* constitutive promoter slp. The GusA gene produces β-glucoronidase, an enzyme that changes 4-nitrophenyl-β-D-glucuronide into the yellow pigment p-nithophenol. Because *L. reuteri* expresses *AgrA* and *AgrC*, it can detect AIP1 and adopts an *agr*-I habit. The production of β-glucoronidase gets impeded when AIP1 is present. As a result, a color change to yellow won't be noticed (see Figure 1.35 for deeper details).

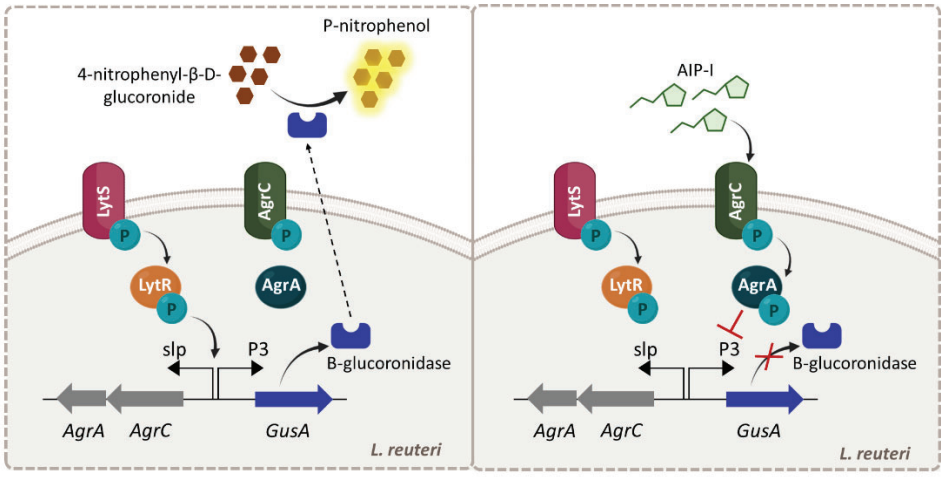

Figure 1.35. *Lactobacillus reuteri reprogrammed as a biosensor for detecting S. aureus AIP1. This biosensor system uses genetically modified L. reuteri to detect AIP1 by inhibiting β-glucuronidase production. In this setup, the GusA gene, which encodes β-glucuronidase, was placed under the P3 promoter, while the agr-I regulatory module (AgrA and AgrC) was introduced under the L. reuteri constitutive promoter slp. In S. aureus, high levels of AIP1 inhibit the P3 promoter; thus, when AIP1 is present, the P3 promoter is repressed, blocking GusA expression and β-glucuronidase production. Without β-glucuronidase, the expected color change to yellow does not occur, signaling S. aureus activity through the absence of color. Adapted from Lubkowicz, D., et al.[187].*

With sensitivity to concentrations as low as 0.5 nM, the technology presented was able to identify AIP1 from bacterial cultures at a nanomolar to micromolar

range. These findings highlight the potential of biosensors for **real-time** AIP **detection** and/or **quantification** in complex samples, enabling the screening of several samples at once[187].

1.8.3 SUMMARY ON AIP DETECTION

The progress made in identifying AIPs in *S. aureus* highlights the necessity of **bacterial culturing**, frequently requiring additional **pre-treatment** procedures to improve detection precision. Even though these methods are quite sensitive and specific, they nonetheless show how difficult it is to find low-abundance peptides in complex biological matrices.

Despite the critical role of AIPs in bacterial communication and virulence, their detection has received relatively little attention in the literature. Because AIPs are present in biological samples at low quantities and the surrounding matrices are complicated, detecting them is a substantial issue. Their detection often requires extensive sample preparation, such as culturing and purification. Moreover, their chemical structure, which may be labile as it contains a thiolactone ring, makes them susceptible to degradation and complicates detection procedures, leading to a delayed diagnosis.

Interestingly, in our group, an immunochemical assay was previously developed to detect AIP4 in culture medium with a limit of detection (LOD) of 0.19 nM[188]. This method is more sensitive than MS-based techniques and biosensors, making it a highly promising approach for AIP detection.

Table 1.2. *Summary of reported S. aureus AIP detection.*

AIP	Detection method	Matrix	LOD (nM)	Author/Year
AIP1, AIP2, AIP3, AIP4	LC-MS/MS	Culture broth	-	Kalkum et al. (2003)[175]
AIP1	LC-MS/MS	Culture broth	250	Junio et al. (2013)[176]
AIP3	LC-MS/MS	Culture broth	-	Roux et al. (2014)[177]
AIP1	LC-MS/MS	Culture broth	3.5	Todd et al. (2016)[178]
AIP1	Colorimetric biosensor	Culture broth	0.5	Lubkowicz et al. (2018)[187]
AIP2	LC-MS/MS	Culture broth	12.5	Gless et al. (2019)[179]
AIP1	LC-MS/MS	Culture broth	-	Jones et al. (2020)[180]
AIP4	Immunochemical	Culture broth	0.19	Montagut et al. (2022)[188]

Detected S. aureus AIP type, detection method used, matrix in which the detection was made, Limit of Detection (LOD) values and the authors and year of publication are shown.

1.9 BIBLIOGRAPHY

1. Iwasaki, A.; Medzhitov, R., Control of adaptive immunity by the innate immune system. *Nat Immunol* **2015,** *16* (4), 343-53.
2. Milton, D. K.; Fabian, M. P.; Cowling, B. J.; Grantham, M. L.; McDevitt, J. J., Influenza virus aerosols in human exhaled breath: particle size, culturability, and effect of surgical masks. *PLoS Pathog* **2013,** *9* (3), e1003205.
3. Gautam, S.; Setu, S.; Khan, M. N. H.; Khan, M. G. Q.; Khan, M. B., Chapter 3 - Microbial aerosols: analytical methods, dispersal mechanisms and health risk assessment. In *Bioaerosols Emission from Anthropogenic Sources*, Singh, N. K.; Sanghvi, G.; Yadav, M., Eds. Woodhead Publishing: 2024; pp 35-62.
4. Lamichhane, B.; Mawad, A. M. M.; Saleh, M.; Kelley, W. G.; Harrington, P. J., 2nd; Lovestad, C. W.; Amezcua, J.; Sarhan, M. M.; El Zowalaty, M. E.; Ramadan, H.; Morgan, M.; Helmy, Y. A., Salmonellosis: An Overview of Epidemiology, Pathogenesis, and Innovative Approaches to Mitigate the Antimicrobial Resistant Infections. *Antibiotics (Basel)* **2024,** *13* (1).
5. Ramsay, I. D.; Török, M. E., Skin and soft tissue infections. *Medicine* **2017,** *45* (11), 699-706.
6. Unemo, M.; Bradshaw, C. S.; Hocking, J. S.; de Vries, H. J. C.; Francis, S. C.; Mabey, D.; Marrazzo, J. M.; Sonder, G. J. B.; Schwebke, J. R.; Hoornenborg, E.; Peeling, R. W.; Philip, S. S.; Low, N.; Fairley, C. K., Sexually transmitted infections: challenges ahead. *The Lancet Infectious Diseases* **2017,** *17* (8), e235-e279.
7. Onen, H.; Luzala, M. M.; Kigozi, S.; Sikumbili, R. M.; Muanga, C. K.; Zola, E. N.; Wendji, S. N.; Buya, A. B.; Balciunaitiene, A.; Viškelis, J.; Kaddumukasa, M. A.; Memvanga, P. B., Mosquito-Borne Diseases and Their Control Strategies: An Overview Focused on Green Synthesized Plant-Based Metallic Nanoparticles. *Insects* **2023,** *14* (3).
8. Kraay, A. N. M.; Hayashi, M. A. L.; Hernandez-Ceron, N.; Spicknall, I. H.; Eisenberg, M. C.; Meza, R.; Eisenberg, J. N. S., Fomite-mediated transmission as a sufficient pathway: a comparative analysis across three viral pathogens. *BMC Infect Dis* **2018,** *18* (1), 540.
9. Anelone, A. J. N.; Clapham, H. E., Measles Infection Dose Responses: Insights from Mathematical Modeling. *Bulletin of Mathematical Biology* **2024,** *86* (7), 85.
10. Wißmann, J. E.; Kirchhoff, L.; Brüggemann, Y.; Todt, D.; Steinmann, J.; Steinmann, E., Persistence of Pathogens on Inanimate Surfaces: A Narrative Review. *Microorganisms* **2021,** *9* (2), 343.
11. Russotto, V.; Cortegiani, A.; Raineri, S. M.; Giarratano, A., Bacterial contamination of inanimate surfaces and equipment in the intensive care unit. *Journal of Intensive Care* **2015,** *3* (1), 54.
12. Yunker, M.; Villafuerte, D. A.; Fall, A.; Norton, J. M.; Abdullah, O.; Rothman, R. E.; Fenstermacher, K. Z. J.; Morris, C. P.; Pekosz, A.; Klein, E.; Mostafa, H. H., Genomic evolution of influenza during the 2023–2024 season, the johns hopkins health system. *Journal of Clinical Virology* **2024,** *174*, 105718.
13. Sanjuán, R.; Domingo-Calap, P., Mechanisms of viral mutation. *Cell Mol Life Sci* **2016,** *73* (23), 4433-4448.
14. Solanki, V.; Tiwari, M.; Tiwari, V., Host-bacteria interaction and adhesin study for development of therapeutics. *International Journal of Biological Macromolecules* **2018,** *112*, 54-64.
15. Soni, J.; Sinha, S.; Pandey, R., Understanding bacterial pathogenicity: a closer look at the journey of harmful microbes. *Front Microbiol* **2024,** *15*, 1370818.
16. Goldstein, I. H.; Bayer, D.; Barilar, I.; Kizito, B.; Matsiri, O.; Modongo, C.; Zetola, N. M.; Niemann, S.; Minin, V. M.; Shin, S. S., Using genetic data to identify transmission risk

factors: Statistical assessment and application to tuberculosis transmission. *PLOS Computational Biology* **2022,** *18* (12), e1010696.
17. Li, R.; Pei, S.; Chen, B.; Song, Y.; Zhang, T.; Yang, W.; Shaman, J., Substantial undocumented infection facilitates the rapid dissemination of novel coronavirus (SARS-CoV-2). *Science* **2020,** *368* (6490), 489-493.
18. Zhang, L.; Han, X.; Wu, J.; Wang, L., Mechanisms influencing the factors of urban built environments and coronavirus disease 2019 at macroscopic and microscopic scales: The role of cities. *Front Public Health* **2023,** *11*, 1137489.
19. Uwishema, O.; Masunga, D. S.; Naisikye, K. M.; Bhanji, F. G.; Rapheal, A. J.; Mbwana, R.; Nazir, A.; Wellington, J., Impacts of environmental and climatic changes on future infectious diseases. *Int J Surg* **2023,** *109* (2), 167-170.
20. Finlay, B. B.; McFadden, G., Anti-immunology: evasion of the host immune system by bacterial and viral pathogens. *Cell* **2006,** *124* (4), 767-82.
21. Reddick, L. E.; Alto, N. M., Bacteria fighting back: how pathogens target and subvert the host innate immune system. *Mol Cell* **2014,** *54* (2), 321-8.
22. Yamauchi, Y.; Helenius, A., Virus entry at a glance. *J Cell Sci* **2013,** *126* (Pt 6), 1289-95.
23. Iwasaki, A.; Medzhitov, R., Regulation of adaptive immunity by the innate immune system. *Science* **2010,** *327* (5963), 291-5.
24. Farber, D. L.; Yudanin, N. A.; Restifo, N. P., Human memory T cells: generation, compartmentalization and homeostasis. *Nat Rev Immunol* **2014,** *14* (1), 24-35.
25. Ernst, L. M.; Casals, E.; Italiani, P.; Boraschi, D.; Puntes, V., The Interactions between Nanoparticles and the Innate Immune System from a Nanotechnologist Perspective. *Nanomaterials* **2021,** *11* (11), 2991.
26. Jiang, M. Y.; Duan, Y. P.; Tong, X. L.; Huang, Q. R.; Jia, M. M.; Yang, W. Z.; Feng, L. Z., Clinical manifestations of respiratory syncytial virus infection and the risk of wheezing and recurrent wheezing illness: a systematic review and meta-analysis. *World J Pediatr* **2023,** *19* (11), 1030-1040.
27. Holub, M.; Pottecher, J.; Herwald, H.; Pasupuleti, M.; Papareddy, P., Editorial: Systemic inflammation in severe infectious diseases. *Front Immunol* **2024,** *15*, 1483682.
28. O'Neill, X.; White, A.; Clancy, D.; Ruiz-Fons, F.; Gortázar, C., The Influence of Latent and Chronic Infection on Pathogen Persistence. *Mathematics* **2021,** *9* (9), 1007.
29. Holmes, K. K.; Bertozzi, S.; Bloom, B. R.; Jha, P.; Gelband, H.; DeMaria, L. M.; Horton, S., Major Infectious Diseases: Key Messages from Disease Control Priorities, Third Edition. In *Major Infectious Diseases*, Holmes, K. K.; Bertozzi, S.; Bloom, B. R.; Jha, P., Eds. The International Bank for Reconstruction and Development / The World Bank© 2017 International Bank for Reconstruction and Development / The World Bank.: Washington (DC), 2017.
30. Global, regional, and national age-sex specific mortality for 264 causes of death, 1980-2016: a systematic analysis for the Global Burden of Disease Study 2016. *Lancet* **2017,** *390* (10100), 1151-1210.
31. World Health Organization (WHO) Pneumonia in children. https://www.who.int/news-room/fact-sheets/detail/pneumonia.
32. World Health Organization (WHO) World health statistics 2024: monitoring health for the SDGs, sustainable development goals. https://www.who.int/publications/i/item/9789240094703.
33. Global Burden of Disease Collaborative Network Global Burden of Disease Study 2021 (GBD 2021). Seattle, United States: Institute for Health Metrics and Evaluation (IHME), 2024. https://vizhub.healthdata.org/gbd-results/.
34. World Health Organization (WHO) Health consequences of air pollution on populations. https://www.who.int/news/item/25-06-2024-what-are-health-consequences-of-air-pollution-on-populations.

35. World Health Organization (WHO) Household air pollution. https://www.who.int/news-room/fact-sheets/detail/household-air-pollution-and-health.
36. World Health Organization (WHO) World malaria report 2022. https://www.who.int/teams/global-malaria-programme/reports/world-malaria-report-2022.
37. Nicola, M.; Alsafi, Z.; Sohrabi, C.; Kerwan, A.; Al-Jabir, A.; Iosifidis, C.; Agha, M.; Agha, R., The socio-economic implications of the coronavirus pandemic (COVID-19): A review. *Int J Surg* **2020,** *78*, 185-193.
38. Cutler, D. M.; Summers, L. H., The COVID-19 Pandemic and the $16 Trillion Virus. *Jama* **2020,** *324* (15), 1495-1496.
39. Hargreaves, J.; Davey, C., Three lessons for the COVID-19 response from pandemic HIV. *Lancet HIV* **2020,** *7* (5), e309-e311.
40. Bavel, J. J. V.; Baicker, K.; Boggio, P. S.; Capraro, V.; Cichocka, A.; Cikara, M.; Crockett, M. J.; Crum, A. J.; Douglas, K. M.; Druckman, J. N.; Drury, J.; Dube, O.; Ellemers, N.; Finkel, E. J.; Fowler, J. H.; Gelfand, M.; Han, S.; Haslam, S. A.; Jetten, J.; Kitayama, S.; Mobbs, D.; Napper, L. E.; Packer, D. J.; Pennycook, G.; Peters, E.; Petty, R. E.; Rand, D. G.; Reicher, S. D.; Schnall, S.; Shariff, A.; Skitka, L. J.; Smith, S. S.; Sunstein, C. R.; Tabri, N.; Tucker, J. A.; Linden, S. v. d.; Lange, P. v.; Weeden, K. A.; Wohl, M. J. A.; Zaki, J.; Zion, S. R.; Willer, R., Using social and behavioural science to support COVID-19 pandemic response. *Nature Human Behaviour* **2020,** *4* (5), 460-471.
41. Ventola, C. L., The antibiotic resistance crisis: part 1: causes and threats. *P t* **2015,** *40* (4), 277-83.
42. Wright, G. D., Something old, something new: revisiting natural products in antibiotic drug discovery. *Can J Microbiol* **2014,** *60* (3), 147-54.
43. De Clercq, E., The design of drugs for HIV and HCV. *Nat Rev Drug Discov* **2007,** *6* (12), 1001-18.
44. Sartelli, M.; Marini, C. P.; McNelis, J.; Coccolini, F.; Rizzo, C.; Labricciosa, F. M.; Petrone, P., Preventing and Controlling Healthcare-Associated Infections: The First Principle of Every Antimicrobial Stewardship Program in Hospital Settings. *Antibiotics (Basel)* **2024,** *13* (9).
45. Ashiru-Oredope, D.; Langford, B. J.; Bonaconsa, C.; Nampoothiri, V.; Charani, E.; Goff, D. A., Global collaborations in antimicrobial stewardship: All hands on deck. *Antimicrob Steward Healthc Epidemiol* **2023,** *3* (1), e66.
46. Talbird, S. E.; Carrico, J.; La, E. M.; Carias, C.; Marshall, G. S.; Roberts, C. S.; Chen, Y. T.; Nyaku, M. K., Impact of Routine Childhood Immunization in Reducing Vaccine-Preventable Diseases in the United States. *Pediatrics* **2022,** *150* (3).
47. Moghadas, S. M.; Vilches, T. N.; Zhang, K.; Wells, C. R.; Shoukat, A.; Singer, B. H.; Meyers, L. A.; Neuzil, K. M.; Langley, J. M.; Fitzpatrick, M. C.; Galvani, A. P., The Impact of Vaccination on Coronavirus Disease 2019 (COVID-19) Outbreaks in the United States. *Clinical Infectious Diseases* **2021,** *73* (12), 2257-2264.
48. Curtis, V.; Cairncross, S., Effect of washing hands with soap on diarrhoea risk in the community: a systematic review. *Lancet Infect Dis* **2003,** *3* (5), 275-81.
49. McGowan, C. R.; Takahashi, E.; Romig, L.; Bertram, K.; Kadir, A.; Cummings, R.; Cardinal, L. J., Community-based surveillance of infectious diseases: a systematic review of drivers of success. *BMJ Glob Health* **2022,** *7* (8).
50. Zhang, R.; Wang, Y.; Lv, Z.; Pei, S., Evaluating the impact of stay-at-home and quarantine measures on COVID-19 spread. *BMC Infect Dis* **2022,** *22* (1), 648.
51. Pallares, C.; Hernández-Gómez, C.; Appel, T. M.; Escandón, K.; Reyes, S.; Salcedo, S.; Matta, L.; Martínez, E.; Cobo, S.; Mora, L.; Marín, A.; Correa, A.; De La Cadena, E.; Rodríguez-Baño, J.; Villegas, M. V., Impact of antimicrobial stewardship programs on antibiotic consumption and antimicrobial resistance in four Colombian healthcare institutions. *BMC Infectious Diseases* **2022,** *22* (1), 420.

52. Majumder, J.; Minko, T., Recent Developments on Therapeutic and Diagnostic Approaches for COVID-19. *Aaps j* **2021,** *23* (1), 14.
53. Messacar, K.; Parker, S. K.; Todd, J. K.; Dominguez, S. R., Implementation of Rapid Molecular Infectious Disease Diagnostics: the Role of Diagnostic and Antimicrobial Stewardship. *J Clin Microbiol* **2017,** *55* (3), 715-723.
54. Ellner, S. P.; Buchon, N.; Dörr, T.; Lazzaro, B. P., Host-pathogen immune feedbacks can explain widely divergent outcomes from similar infections. *Proc Biol Sci* **2021,** *288* (1951), 20210786.
55. Ueber die isolirte Färbung der Schizomyceten in Schnitt- und Trockenpräparaten von Dr. Gram, Kopenhagen. — Fortschritte der Medicin 1884 No. 6. Ref. Dr. Becker. *Deutsche Medizinische Wochenschrift* **1884,** *10*, 234 - 235.
56. Zhydzetski, A.; Głowacka-Grzyb, Z.; Bukowski, M.; Żądło, T.; Bonar, E.; Władyka, B., Agents Targeting the Bacterial Cell Wall as Tools to Combat Gram-Positive Pathogens. *Molecules* **2024,** *29* (17), 4065.
57. Bartlett, J. G., Changing trends in bacterial infections: Staphylococcus aureus, bacterial pneumonia, Clostridium difficile. *Top HIV Med* **2007,** *15* (3), 94-8.
58. Behzadi, P.; Urbán, E.; Matuz, M.; Benkő, R.; Gajdács, M., The Role of Gram-Negative Bacteria in Urinary Tract Infections: Current Concepts and Therapeutic Options. *Adv Exp Med Biol* **2021,** *1323*, 35-69.
59. Holmes, A. H.; Moore, L. S.; Sundsfjord, A.; Steinbakk, M.; Regmi, S.; Karkey, A.; Guerin, P. J.; Piddock, L. J., Understanding the mechanisms and drivers of antimicrobial resistance. *Lancet* **2016,** *387* (10014), 176-87.
60. Laxminarayan, R.; Matsoso, P.; Pant, S.; Brower, C.; Røttingen, J. A.; Klugman, K.; Davies, S., Access to effective antimicrobials: a worldwide challenge. *Lancet* **2016,** *387* (10014), 168-75.
61. WHO publishes list of bacteria for which new antibiotics are urgently needed. . https://www.who.int/news/item/27-02-2017-who-publishes-list-of-bacteria-for-which-new-antibiotics-are-urgently-needed.
62. Santajit, S.; Indrawattana, N., Mechanisms of Antimicrobial Resistance in ESKAPE Pathogens. *Biomed Res Int* **2016,** *2016*, 2475067.
63. Cassini, A.; Högberg, L. D.; Plachouras, D.; Quattrocchi, A.; Hoxha, A.; Simonsen, G. S.; Colomb-Cotinat, M.; Kretzschmar, M. E.; Devleesschauwer, B.; Cecchini, M.; Ouakrim, D. A.; Oliveira, T. C.; Struelens, M. J.; Suetens, C.; Monnet, D. L., Attributable deaths and disability-adjusted life-years caused by infections with antibiotic-resistant bacteria in the EU and the European Economic Area in 2015: a population-level modelling analysis. *Lancet Infect Dis* **2019,** *19* (1), 56-66.
64. European Centre for Disease Prevention and Control (ECDC). Antimicrobial resistance in the EU/EEA (EARS-Net) - Annual Epidemiological Report 2019. . https://www.ecdc.europa.eu/en/publications-data/surveillance-antimicrobial-resistance-europe-2019.
65. World Health Organization (WHO). Antimicrobial resistance. https://www.who.int/news-room/fact-sheets/detail/antimicrobial-resistance#:~:text=In%20addition%20to%20death%20and,year%20by%202030%20(2).
66. Ministerio de Sanidad, Consumo y Bienestar Social (2020). Plan Nacional frente a la Resistencia a los Antibióticos (PRAN) 2019-2021.
67. Suetens, C.; Latour, K.; Kärki, T.; Ricchizzi, E.; Kinross, P.; Moro, M. L.; Jans, B.; Hopkins, S.; Hansen, S.; Lyytikäinen, O.; Reilly, J.; Deptula, A.; Zingg, W.; Plachouras, D.; Monnet, D. L., Prevalence of healthcare-associated infections, estimated incidence and composite antimicrobial resistance index in acute care hospitals and long-term care facilities: results from two European point prevalence surveys, 2016 to 2017. *Euro Surveill* **2018,** *23* (46).

68. Whelan, S.; Lucey, B.; Finn, K., Uropathogenic Escherichia coli (UPEC)-Associated Urinary Tract Infections: The Molecular Basis for Challenges to Effective Treatment. *Microorganisms* **2023,** *11* (9).
69. Bintsis, T., Foodborne pathogens. *AIMS Microbiol* **2017,** *3* (3), 529-563.
70. Reyes, V. E., Helicobacter pylori and Its Role in Gastric Cancer. *Microorganisms* **2023,** *11* (5).
71. Mayr, F. B.; Yende, S.; Angus, D. C., Epidemiology of severe sepsis. *Virulence* **2014,** *5* (1), 4-11.
72. Workowski, K. A.; Bolan, G. A., Sexually transmitted diseases treatment guidelines, 2015. *MMWR Recomm Rep* **2015,** *64* (Rr-03), 1-137.
73. Juhn, Y. J.; Frey, D.; Li, X.; Jacobson, R., Streptococcus pyogenes upper respiratory infection and atopic conditions other than asthma: a retrospective cohort study. *Primary Care Respiratory Journal* **2012,** *21* (2), 153-158.
74. Musher, D. M.; Thorner, A. R., Community-acquired pneumonia. *N Engl J Med* **2014,** *371* (17), 1619-28.
75. Hubert, D.; Réglier-Poupet, H.; Sermet-Gaudelus, I.; Ferroni, A.; Le Bourgeois, M.; Burgel, P.-R.; Serreau, R.; Dusser, D.; Poyart, C.; Coste, J., Association between Staphylococcus aureus alone or combined with Pseudomonas aeruginosa and the clinical condition of patients with cystic fibrosis. *Journal of Cystic Fibrosis* **2013,** *12* (5), 497-503.
76. Eccles, R., Understanding the symptoms of the common cold and influenza. *Lancet Infect Dis* **2005,** *5* (11), 718-25.
77. World Health Organization (2022, November 11). Pneumonia in children. https://www.who.int/news-room/fact-sheets/detail/pneumonia.
78. World Health Organization (WHO), The top 10 causes of death. **2024**.
79. Marshall, D. C.; Goodson, R. J.; Xu, Y.; Komorowski, M.; Shalhoub, J.; Maruthappu, M.; Salciccioli, J. D., Trends in mortality from pneumonia in the Europe union: a temporal analysis of the European detailed mortality database between 2001 and 2014. *Respiratory Research* **2018,** *19* (1), 81.
80. *Instituto Nacional de Estadística. (2023). Defunciones según la causa de muerte. Año 2022 [Press release]*
81. World Health Organization. (November 2023). Antimicrobial Resistance. . https://www.who.int/news-room/fact-sheets/detail/antimicrobial-resistance.
82. Gudiol, C.; Aguilar-Guisado, M.; Azanza, J. R.; Candel, F. J.; Cantón, R.; Carratalà, J.; Garcia-Vidal, C.; Jarque, I.; Lizasoain, M.; Gil-Bermejo, J. M.; Ruiz-Camps, I.; Sánchez-Ortega, I.; Solano, C.; Suárez-Lledó, M.; Vázquez, L.; de la Cámara, R., Executive summary of the consensus document of the Spanish Society of Infectious Diseases and Clinical Microbiology (SEIMC), the Spanish Network for Research in Infectious Diseases (REIPI) and the Spanish Society of Haematology and Haemotherapy (SEHH) on the management of febrile neutropenia in patients with hematological malignancies. *Enfermedades Infecciosas y Microbiología Clínica* **2020,** *38* (4), 174-181.
83. Tripp, R. A.; Stambas, J., Intervention Strategies for Seasonal and Emerging Respiratory Viruses with Drugs and Vaccines Targeting Viral Surface Glycoproteins. *Viruses* **2021,** *13* (4), 625.
84. Veys, K.; Dockx, K.; Van Remoortel, H.; Vandekerckhove, P.; De Buck, E., The effect of hand hygiene promotion programs during epidemics and pandemics of respiratory droplet-transmissible infections on health outcomes: a rapid systematic review. *BMC Public Health* **2021,** *21* (1), 1745.
85. Tong, S. Y.; Davis, J. S.; Eichenberger, E.; Holland, T. L.; Fowler, V. G., Jr., Staphylococcus aureus infections: epidemiology, pathophysiology, clinical manifestations, and management. *Clin Microbiol Rev* **2015,** *28* (3), 603-61.
86. Linz, M. S.; Mattappallil, A.; Finkel, D.; Parker, D., Clinical Impact of Staphylococcus aureus Skin and Soft Tissue Infections. *Antibiotics* **2023,** *12* (3), 557.

87. David, M. Z.; Daum, R. S., Community-associated methicillin-resistant Staphylococcus aureus: epidemiology and clinical consequences of an emerging epidemic. *Clin Microbiol Rev* **2010,** *23* (3), 616-87.
88. Sousa, S. A.; Feliciano, J. R.; Pita, T.; Soeiro, C. F.; Mendes, B. L.; Alves, L. G.; Leitão, J. H., Bacterial Nosocomial Infections: Multidrug Resistance as a Trigger for the Development of Novel Antimicrobials. *Antibiotics* **2021,** *10* (8), 942.
89. Serra-Burriel, M.; Keys, M.; Campillo-Artero, C.; Agodi, A.; Barchitta, M.; Gikas, A.; Palos, C.; López-Casasnovas, G., Impact of multi-drug resistant bacteria on economic and clinical outcomes of healthcare-associated infections in adults: Systematic review and meta-analysis. *PLOS ONE* **2020,** *15* (1), e0227139.
90. Le Moing, V.; Alla, F.; Doco-Lecompte, T.; Delahaye, F.; Piroth, L.; Chirouze, C.; Tattevin, P.; Lavigne, J.-P.; Erpelding, M.-L.; Hoen, B.; Vandenesch, F.; Duval, X.; group, V. s., Staphylococcus aureus Bloodstream Infection and Endocarditis - A Prospective Cohort Study. *PLOS ONE* **2015,** *10* (5), e0127385.
91. Westgeest, A. C.; Buis, D. T. P.; Sigaloff, K. C. E.; Ruffin, F.; Visser, L. G.; Yu, Y.; Schippers, E. F.; Lambregts, M. M. C.; Tong, S. Y. C.; de Boer, M. G. J.; Fowler, V. G., Jr, Global Differences in the Management of Staphylococcus aureus Bacteremia: No International Standard of Care. *Clinical Infectious Diseases* **2023,** *77* (8), 1092-1101.
92. Foster, T. J.; Geoghegan, J. A.; Ganesh, V. K.; Höök, M., Adhesion, invasion and evasion: the many functions of the surface proteins of Staphylococcus aureus. *Nat Rev Microbiol* **2014,** *12* (1), 49-62.
93. Spaulding, A. R.; Salgado-Pabón, W.; Kohler, P. L.; Horswill, A. R.; Leung, D. Y.; Schlievert, P. M., Staphylococcal and streptococcal superantigen exotoxins. *Clin Microbiol Rev* **2013,** *26* (3), 422-47.
94. McGuinness, W. A.; Kobayashi, S. D.; DeLeo, F. R., Evasion of Neutrophil Killing by Staphylococcus aureus. *Pathogens* **2016,** *5* (1).
95. Wójcik-Bojek, U.; Różalska, B.; Sadowska, B., Staphylococcus aureus—A Known Opponent against Host Defense Mechanisms and Vaccine Development—Do We Still Have a Chance to Win? *International Journal of Molecular Sciences* **2022,** *23* (2), 948.
96. Lade, H.; Kim, J.-S., Bacterial Targets of Antibiotics in Methicillin-Resistant Staphylococcus aureus. *Antibiotics* **2021,** *10* (4), 398.
97. Otto, M., Staphylococcal Biofilms. *Microbiology Spectrum* **2018,** *6* (4), 10.1128/microbiolspec.gpp3-0023-2018.
98. Bhattacharya, S.; Ploplis, V. A.; Castellino, F. J., Bacterial plasminogen receptors utilize host plasminogen system for effective invasion and dissemination. *J Biomed Biotechnol* **2012,** *2012*, 482096.
99. Falugi, F.; Kim Hwan, K.; Missiakas Dominique, M.; Schneewind, O., Role of Protein A in the Evasion of Host Adaptive Immune Responses by Staphylococcus aureus. *mBio* **2013,** *4* (5), 10.1128/mbio.00575-13.
100. Schilcher, K.; Horswill, A. R., Staphylococcal Biofilm Development: Structure, Regulation, and Treatment Strategies. *Microbiol Mol Biol Rev* **2020,** *84* (3).
101. Lakhundi, S.; Zhang, K., Methicillin-Resistant Staphylococcus aureus: Molecular Characterization, Evolution, and Epidemiology. *Clin Microbiol Rev* **2018,** *31* (4).
102. McGuinness, W. A.; Malachowa, N.; DeLeo, F. R., Vancomycin Resistance in Staphylococcus aureus. *Yale J Biol Med* **2017,** *90* (2), 269-281.
103. Garneau-Tsodikova, S.; Labby, K. J., Mechanisms of Resistance to Aminoglycoside Antibiotics: Overview and Perspectives. *Medchemcomm* **2016,** *7* (1), 11-27.
104. Miklasińska-Majdanik, M., Mechanisms of Resistance to Macrolide Antibiotics among Staphylococcus aureus. *Antibiotics (Basel)* **2021,** *10* (11).
105. Hooper, D. C.; Jacoby, G. A., Mechanisms of drug resistance: quinolone resistance. *Ann N Y Acad Sci* **2015,** *1354* (1), 12-31.

106. Chambers, H. F., The changing epidemiology of Staphylococcus aureus? *Emerg Infect Dis* **2001,** *7* (2), 178-82.
107. Utsui, Y.; Yokota, T., Role of an altered penicillin-binding protein in methicillin- and cephem-resistant Staphylococcus aureus. *Antimicrob Agents Chemother* **1985,** *28* (3), 397-403.
108. DeLeo, F. R.; Otto, M.; Kreiswirth, B. N.; Chambers, H. F., Community-associated meticillin-resistant Staphylococcus aureus. *Lancet* **2010,** *375* (9725), 1557-68.
109. Howden, B. P.; Davies, J. K.; Johnson, P. D.; Stinear, T. P.; Grayson, M. L., Reduced vancomycin susceptibility in Staphylococcus aureus, including vancomycin-intermediate and heterogeneous vancomycin-intermediate strains: resistance mechanisms, laboratory detection, and clinical implications. *Clin Microbiol Rev* **2010,** *23* (1), 99-139.
110. Dm, S.; Boulton, M.; Stoltman, G.; D, J.; Stobierski, M. G.; W, B.; Hafeez, W.; T, L.; E, F.; R, J.; J, M.; S, C., Staphylococcus aureus Resistant to Vancomycin—United States. *JAMA The Journal of the American Medical Association* **2002,** *288*, 824-825.
111. Fowler, V. G., Jr.; Sakoulas, G.; McIntyre, L. M.; Meka, V. G.; Arbeit, R. D.; Cabell, C. H.; Stryjewski, M. E.; Eliopoulos, G. M.; Reller, L. B.; Corey, G. R.; Jones, T.; Lucindo, N.; Yeaman, M. R.; Bayer, A. S., Persistent bacteremia due to methicillin-resistant Staphylococcus aureus infection is associated with agr dysfunction and low-level in vitro resistance to thrombin-induced platelet microbicidal protein. *J Infect Dis* **2004,** *190* (6), 1140-9.
112. Shanmugakani, R. K.; Srinivasan, B.; Glesby, M. J.; Westblade, L. F.; Cárdenas, W. B.; Raj, T.; Erickson, D.; Mehta, S., Current state of the art in rapid diagnostics for antimicrobial resistance. *Lab Chip* **2020,** *20* (15), 2607-2625.
113. Cheung, G. Y. C.; Bae, J. S.; Otto, M., Pathogenicity and virulence of Staphylococcus aureus. *Virulence* **2021,** *12* (1), 547-569.
114. Chambers, H. F.; DeLeo, F. R., Waves of resistance: Staphylococcus aureus in the antibiotic era. *Nature Reviews Microbiology* **2009,** *7* (9), 629-641.
115. Becker, K.; Heilmann, C.; Peters, G., Coagulase-negative staphylococci. *Clin Microbiol Rev* **2014,** *27* (4), 870-926.
116. El Jakee, J.; Marouf, S.; Ata, N.; Abdel-Rahman, E.; Abd El-Moez, S.; Samy, A.; El-Sayed, W., Rapid Method for Detection of Staphylococcus aureus Enterotoxins in Food. *Global Veterinaria* **2013,** *11*, 335-341.
117. Brown, D. F. J.; Edwards, D. I.; Hawkey, P. M.; Morrison, D.; Ridgway, G. L.; Towner, K. J.; Wren, M. W. D.; on behalf of the Joint Working Party of the British Society for Antimicrobial Chemotherapy, H. I. S.; Association, I. C. N., Guidelines for the laboratory diagnosis and susceptibility testing of methicillin-resistant Staphylococcus aureus (MRSA). *Journal of Antimicrobial Chemotherapy* **2005,** *56* (6), 1000-1018.
118. Dayie, N.; Sekoh, D.; Kotey, F.; Egyir, B.; Tetteh-Quarcoo, P.; Adutwum-Ofosu, K.; Ahenkorah, J.; Osei, M.-M.; Donkor, E., Nasopharyngeal Carriage of Methicillin-Resistant Staphylococcus aureus (MRSA) among Sickle Cell Disease (SCD) Children in the Pneumococcal Conjugate Vaccine Era. *Infectious Disease Reports* **2021,** *13*.
119. Cattoir, V.; Merabet, L.; Djibo, N.; Rioux, C.; Legrand, P.; Girou, E.; Lesprit, P., Clinical impact of a real-time PCR assay for rapid identification of Staphylococcus aureus and determination of methicillin resistance from positive blood cultures. *Clin Microbiol Infect* **2011,** *17* (3), 425-31.
120. Alhabbab, R. Y., Precipitation and Agglutination Reactions. In *Basic Serological Testing*, Alhabbab, R. Y., Ed. Springer International Publishing: Cham, 2018; pp 23-30.
121. Idelevich, E. A.; Walther, T.; Molinaro, S.; Li, X.; Xia, G.; Wieser, A.; Peters, G.; Peschel, A.; Becker, K., Bacteriophage-based latex agglutination test for rapid identification of Staphylococcus aureus. *J Clin Microbiol* **2014,** *52* (9), 3394-8.
122. Im, K.; Mareninov, S.; Diaz, M. F. P.; Yong, W. H., An Introduction to Performing Immunofluorescence Staining. *Methods Mol Biol* **2019,** *1897*, 299-311.

123. Costa, A.; Campos Aguiar, A. C.; Silva, A.; Pereira, D., Point-of-Care Strategies Applied to Malaria Diagnosis. 2021.
124. Vasu, M.; Tara, A.; Chowdary, M., CONVENTIONAL AND LATEST MOLECULAR TECHNIQUES FOR DIAGNOSING LIVESTOCK DISEASES. 2023.
125. Köser, C. U.; Ellington, M. J.; Peacock, S. J., Whole-genome sequencing to control antimicrobial resistance. *Trends Genet* **2014,** *30* (9), 401-7.
126. Turner, N. A.; Sharma-Kuinkel, B. K.; Maskarinec, S. A.; Eichenberger, E. M.; Shah, P. P.; Carugati, M.; Holland, T. L.; Fowler, V. G., Jr., Methicillin-resistant Staphylococcus aureus: an overview of basic and clinical research. *Nat Rev Microbiol* **2019,** *17* (4), 203-218.
127. Dylus, D.; Pillonel, T.; Opota, O.; Wüthrich, D.; Seth-Smith, H. M. B.; Egli, A.; Leo, S.; Lazarevic, V.; Schrenzel, J.; Laurent, S.; Bertelli, C.; Blanc, D. S.; Neuenschwander, S.; Ramette, A.; Falquet, L.; Imkamp, F.; Keller, P. M.; Kahles, A.; Oberhaensli, S.; Barbié, V.; Dessimoz, C.; Greub, G.; Lebrand, A., NGS-Based S. aureus Typing and Outbreak Analysis in Clinical Microbiology Laboratories: Lessons Learned From a Swiss-Wide Proficiency Test. *Front Microbiol* **2020,** *11*, 591093.
128. Aksense Aksense is a blood-based point of care biosensor that saves lives. https://www.aksense.com/what-we-do/.
129. Schulz, M.; Calabrese, S.; Hausladen, F.; Wurm, H.; Drossart, D.; Stock, K.; Sobieraj, A. M.; Eichenseher, F.; Loessner, M. J.; Schmelcher, M.; Gerhardts, A.; Goetz, U.; Handel, M.; Serr, A.; Haecker, G.; Li, J.; Specht, M.; Koch, P.; Meyer, M.; Tepper, P.; Rother, R.; Jehle, M.; Wadle, S.; Zengerle, R.; von Stetten, F.; Paust, N.; Borst, N., Point-of-care testing system for digital single cell detection of MRSA directly from nasal swabs. *Lab Chip* **2020,** *20* (14), 2549-2561.
130. Choopara, I.; Suea-Ngam, A.; Teethaisong, Y.; Howes, P. D.; Schmelcher, M.; Leelahavanichkul, A.; Thunyaharn, S.; Wongsawaeng, D.; deMello, A. J.; Dean, D.; Somboonna, N., Fluorometric Paper-Based, Loop-Mediated Isothermal Amplification Devices for Quantitative Point-of-Care Detection of Methicillin-Resistant Staphylococcus aureus (MRSA). *ACS Sens* **2021,** *6* (3), 742-751.
131. A, G. A.; T, G. V.; Barros-Velázquez, J.; Cañas, B.; Sánchez-Pérez, A.; Calo-Mata, P.; Carrera, M., Staphylococcus aureus Exotoxins and Their Detection in the Dairy Industry and Mastitis. *Toxins (Basel)* **2020,** *12* (9).
132. Shallcross, L. J.; Fragaszy, E.; Johnson, A. M.; Hayward, A. C., The role of the Panton-Valentine leucocidin toxin in staphylococcal disease: a systematic review and meta-analysis. *Lancet Infect Dis* **2013,** *13* (1), 43-54.
133. Andrzejczuk, S.; Cygan, M.; Dłuski, D.; Stępień-Pyśniak, D.; Kosikowska, U., Staphylococcal Resistance Patterns, blaZ and SCCmec Cassette Genes in the Nasopharyngeal Microbiota of Pregnant Women. *Int J Mol Sci* **2023,** *24* (9).
134. Morad, E. A.; Rabie, R. A.; Almalky, M. A.; Gebriel, M. G., Evaluation of Procalcitonin, C-Reactive Protein, and Interleukin-6 as Early Markers for Diagnosis of Neonatal Sepsis. *Int J Microbiol* **2020,** *2020*, 8889086.
135. Argudín, M.; Mendoza, M. C.; Rodicio, M. R., Food poisoning and Staphylococcus aureus enterotoxins. *Toxins (Basel)* **2010,** *2* (7), 1751-73.
136. Schneewind, O.; Missiakas, D. M., Staphylococcal Protein Secretion and Envelope Assembly. *Microbiol Spectr* **2019,** *7* (4).
137. Tam, K.; Torres, V. J., Staphylococcus aureus Secreted Toxins and Extracellular Enzymes. *Microbiol Spectr* **2019,** *7* (2).
138. Di Carluccio, C.; Soriano-Maldonado, P.; Berni, F.; de Haas, C. J. C.; Temming, A. R.; Hendriks, A.; Ali, S.; Molinaro, A.; Silipo, A.; van Sorge, N. M.; van Raaij, M. J.; Codee, J. D. C.; Marchetti, R., Antibody Recognition of Different Staphylococcus aureus Wall Teichoic Acid Glycoforms. *ACS Cent Sci* **2022,** *8* (10), 1383-1392.

139. Algorri, M.; Jorth, P.; Wong-Beringer, A., Variable Release of Lipoteichoic Acid From Staphylococcus aureus Bloodstream Isolates Relates to Distinct Clinical Phenotypes, Strain Background, and Antibiotic Exposure. *Front Microbiol* **2020,** *11*, 609280.
140. Speziale, P.; Pietrocola, G., The Multivalent Role of Fibronectin-Binding Proteins A and B (FnBPA and FnBPB) of Staphylococcus aureus in Host Infections. *Front Microbiol* **2020,** *11*, 2054.
141. Miller, M. B.; Bassler, B. L., Quorum sensing in bacteria. *Annu Rev Microbiol* **2001,** *55*, 165-99.
142. Waters, C. M.; Bassler, B. L., Quorum sensing: cell-to-cell communication in bacteria. *Annu Rev Cell Dev Biol* **2005,** *21*, 319-46.
143. Miyashiro, T.; Ruby, E. G., Shedding light on bioluminescence regulation in Vibrio fischeri. *Mol Microbiol* **2012,** *84* (5), 795-806.
144. Kaskova, Z. M.; Tsarkova, A. S.; Yampolsky, I. V., 1001 lights: luciferins, luciferases, their mechanisms of action and applications in chemical analysis, biology and medicine. *Chem Soc Rev* **2016,** *45* (21), 6048-6077.
145. Ball, A. S.; Chaparian, R. R.; van Kessel, J. C., Quorum Sensing Gene Regulation by LuxR/HapR Master Regulators in Vibrios. *J Bacteriol* **2017,** *199* (19).
146. Frederix, M.; Downie, J. A., Chapter 2 - Quorum Sensing: Regulating the Regulators. In *Advances in Microbial Physiology*, Poole, R. K., Ed. Academic Press: 2011; Vol. 58, pp 23-80.
147. Ng, W. L.; Bassler, B. L., Bacterial quorum-sensing network architectures. *Annu Rev Genet* **2009,** *43*, 197-222.
148. Jung, S. A.; Chapman, C. A.; Ng, W.-L., Quadruple Quorum-Sensing Inputs Control Vibrio cholerae Virulence and Maintain System Robustness. *PLOS Pathogens* **2015,** *11* (4), e1004837.
149. Butrico, C. E.; Cassat, J. E., Quorum Sensing and Toxin Production in Staphylococcus aureus Osteomyelitis: Pathogenesis and Paradox. *Toxins* **2020,** *12* (8), 516.
150. Li, Q.; Mao, S.; Wang, H.; Ye, X., The Molecular Architecture of Pseudomonas aeruginosa Quorum-Sensing Inhibitors. *Marine Drugs* **2022,** *20* (8), 488.
151. Venturi, V., Regulation of quorum sensing in Pseudomonas. *FEMS Microbiology Reviews* **2006,** *30* (2), 274-291.
152. Terlizzi, M. E.; Gribaudo, G.; Maffei, M. E., UroPathogenic Escherichia coli (UPEC) Infections: Virulence Factors, Bladder Responses, Antibiotic, and Non-antibiotic Antimicrobial Strategies. *Front Microbiol* **2017,** *8*, 1566.
153. Riedel, C. U.; Monk, I. R.; Casey, P. G.; Waidmann, M. S.; Gahan, C. G.; Hill, C., AgrD-dependent quorum sensing affects biofilm formation, invasion, virulence and global gene expression profiles in Listeria monocytogenes. *Molecular microbiology* **2009,** *71* (5), 1177-1189.
154. Díaz-Pérez, S. P.; Solis, C. S.; López-Bucio, J. S.; Valdez Alarcón, J. J.; Villegas, J.; Reyes-De la Cruz, H.; Campos-Garcia, J., Pathogenesis in Pseudomonas aeruginosa PAO1 Biofilm-Associated Is Dependent on the Pyoverdine and Pyocyanin Siderophores by Quorum Sensing Modulation. *Microbial Ecology* **2023,** *86* (1), 727-741.
155. Costerton, J. W.; Lewandowski, Z.; Caldwell, D. E.; Korber, D. R.; Lappin-Scott, H. M., Microbial biofilms. *Annu Rev Microbiol* **1995,** *49*, 711-45.
156. Donlan, R. M., Biofilms: microbial life on surfaces. *Emerg Infect Dis* **2002,** *8* (9), 881-90.
157. Stoodley, P.; Sauer, K.; Davies, D. G.; Costerton, J. W., Biofilms as complex differentiated communities. *Annu Rev Microbiol* **2002,** *56*, 187-209.
158. Flemming, H.-C.; Wingender, J., The biofilm matrix. *Nature Reviews Microbiology* **2010,** *8* (9), 623-633.
159. Preda, V. G.; Săndulescu, O., Communication is the key: biofilms, quorum sensing, formation and prevention. *Discoveries (Craiova)* **2019,** *7* (3), e100.

160. Claverys, J. P.; Martin, B.; Håvarstein, L. S., Competence-induced fratricide in streptococci. *Mol Microbiol* **2007,** *64* (6), 1423-33.
161. Daniels, R.; Vanderleyden, J.; Michiels, J., Quorum sensing and swarming migration in bacteria. *FEMS Microbiol Rev* **2004,** *28* (3), 261-89.
162. Huang, S.; Bergonzi, C.; Smith, S.; Hicks, R. E.; Elias, M. H., Field testing of an enzymatic quorum quencher coating additive to reduce biocorrosion of steel. *Microbiol Spectr* **2023,** *11* (5), e0517822.
163. Khatoon, Z.; McTiernan, C. D.; Suuronen, E. J.; Mah, T. F.; Alarcon, E. I., Bacterial biofilm formation on implantable devices and approaches to its treatment and prevention. *Heliyon* **2018,** *4* (12), e01067.
164. Mishra, S.; Huang, Y.; Li, J.; Wu, X.; Zhou, Z.; Lei, Q.; Bhatt, P.; Chen, S., Biofilm-mediated bioremediation is a powerful tool for the removal of environmental pollutants. *Chemosphere* **2022,** *294*, 133609.
165. Erdei-Tombor, P.; Kiskó, G.; Taczman-Brückner, A., Biofilm Formation in Water Distribution Systems. *Processes* **2024,** *12* (2), 280.
166. Kostylev, M.; Kim, D. Y.; Smalley, N. E.; Salukhe, I.; Greenberg, E. P.; Dandekar, A. A., Evolution of the Pseudomonas aeruginosa quorum-sensing hierarchy. *Proceedings of the National Academy of Sciences* **2019,** *116* (14), 7027-7032.
167. Chen, J.; Lu, Y.; Ye, X.; Emam, M.; Zhang, H.; Wang, H., Current advances in Vibrio harveyi quorum sensing as drug discovery targets. *European Journal of Medicinal Chemistry* **2020,** *207*, 112741.
168. Verbeke, F.; De Craemer, S.; Debunne, N.; Janssens, Y.; Wynendaele, E.; Van de Wiele, C.; De Spiegeleer, B., Peptides as Quorum Sensing Molecules: Measurement Techniques and Obtained Levels In vitro and In vivo. *Front Neurosci* **2017,** *11*, 183.
169. Rutherford, S. T.; Bassler, B. L., Bacterial quorum sensing: its role in virulence and possibilities for its control. *Cold Spring Harb Perspect Med* **2012,** *2* (11).
170. Venturi, V., Regulation of quorum sensing in Pseudomonas. *FEMS Microbiol Rev* **2006,** *30* (2), 274-91.
171. Novick, R. P.; Geisinger, E., Quorum sensing in staphylococci. *Annu Rev Genet* **2008,** *42*, 541-64.
172. Novick, R. P., Autoinduction and signal transduction in the regulation of staphylococcal virulence. *Mol Microbiol* **2003,** *48* (6), 1429-49.
173. Thoendel, M.; Kavanaugh, J. S.; Flack, C. E.; Horswill, A. R., Peptide signaling in the staphylococci. *Chem Rev* **2011,** *111* (1), 117-51.
174. Le, K. Y.; Otto, M., Quorum-sensing regulation in staphylococci-an overview. *Front Microbiol* **2015,** *6*, 1174.
175. Kalkum, M.; Lyon, G. J.; Chait, B. T., Detection of secreted peptides by using hypothesis-driven multistage mass spectrometry. *Proc Natl Acad Sci U S A* **2003,** *100* (5), 2795-800.
176. Junio, H. A.; Todd, D. A.; Ettefagh, K. A.; Ehrmann, B. M.; Kavanaugh, J. S.; Horswill, A. R.; Cech, N. B., Quantitative analysis of autoinducing peptide I (AIP-I) from Staphylococcus aureus cultures using ultrahigh performance liquid chromatography-high resolving power mass spectrometry. *J Chromatogr B Analyt Technol Biomed Life Sci* **2013,** *930*, 7-12.
177. Roux, A.; Todd, D. A.; Velazquez, J. V.; Cech, N. B.; Sonenshein, A. L., CodY-mediated regulation of the Staphylococcus aureus Agr system integrates nutritional and population density signals. *J Bacteriol* **2014,** *196* (6), 1184-96.
178. Todd, D. A.; Zich, D. B.; Ettefagh, K. A.; Kavanaugh, J. S.; Horswill, A. R.; Cech, N. B., Hybrid Quadrupole-Orbitrap mass spectrometry for quantitative measurement of quorum sensing inhibition. *J Microbiol Methods* **2016,** *127*, 89-94.
179. Gless, B. H.; Bojer, M. S.; Peng, P.; Baldry, M.; Ingmer, H.; Olsen, C. A., Identification of autoinducing thiodepsipeptides from staphylococci enabled by native chemical ligation. *Nat Chem* **2019,** *11* (5), 463-469.

180. Jones, D. D., Jr.; Caesar, L. K.; Pelzer, C. V.; Crandall, W. J.; Jenul, C.; Todd, D. A.; Horswill, A. R.; Cech, N. B., Targeted and untargeted analysis of secondary metabolites to monitor growth and quorum sensing inhibition for methicillin-resistant Staphylococcus aureus (MRSA). *J Microbiol Methods* **2020,** *176*, 106000.
181. WANG XIN, X. X., WANG YUTANG, ZHANG PENGFEI, GUO CHUNFENG, WU QIAN, ZHANG QIANG Liquid chromatography and mass spectrometry detection method for simultaneously detecting IV AIPs (auto-inducing peptides) signal molecules of staphylococcus aureus. CN106501394, 2018.
182. Yoo, S. M.; Lee, S. Y., Optical Biosensors for the Detection of Pathogenic Microorganisms. *Trends Biotechnol* **2016,** *34* (1), 7-25.
183. Simoska, O.; Stevenson, K. J., Electrochemical sensors for rapid diagnosis of pathogens in real time. *Analyst* **2019,** *144* (22), 6461-6478.
184. Rubab, M.; Shahbaz, H. M.; Olaimat, A. N.; Oh, D. H., Biosensors for rapid and sensitive detection of Staphylococcus aureus in food. *Biosens Bioelectron* **2018,** *105*, 49-57.
185. Alhadrami, H. A., Biosensors: Classifications, medical applications, and future prospective. *Biotechnol Appl Biochem* **2018,** *65* (3), 497-508.
186. Damborský, P.; Švitel, J.; Katrlík, J., Optical biosensors. *Essays Biochem* **2016,** *60* (1), 91-100.
187. Lubkowicz, D.; Ho, C. L.; Hwang, I. Y.; Yew, W. S.; Lee, Y. S.; Chang, M. W., Reprogramming Probiotic Lactobacillus reuteri as a Biosensor for Staphylococcus aureus Derived AIP-I Detection. *ACS Synth Biol* **2018,** *7* (5), 1229-1237.
188. Montagut, E. J.; Acosta, G.; Albericio, F.; Royo, M.; Godoy-Tena, G.; Lacoma, A.; Prat, C.; Salvador, J. P.; Marco, M. P., Direct Quantitative Immunochemical Analysis of Autoinducer Peptide IV for Diagnosing and Stratifying Staphylococcus aureus Infections. *ACS Infect Dis* **2022,** *8* (3), 645-656.

2 CONTEXT SCENARIO, OBJECTIVES AND STRUTURE OF THIS THESIS

2.1 THESIS FRAMEWORK

The present thesis has been developed within the framework of two different research projects:

1. **QS4CF Project. Targeting Quorum Sensing for the Management of Cystic Fibrosis**. (RTI2018-096278-B-C21, MINECO, Dirección General de Investigación Científica y Técnica, Subdirección General de Proyectos de I+D.)

   The **QS4CF** project is a continuation of the precedent **Immuno-QS** project (SAF2015-67476-R), with the same final goal: to advance in the knowledge of the mechanisms involved in the pathogenesis caused by two important microorganisms (*P. aeruginosa* and *S. aureus*) with a clear intention of improving the treatment and the diagnostics of infectious diseases caused by these pathogens, through immunochemical studies of their QS systems as therapeutic and biomarker targets. The project will address three applied objectives: i) generating knowledge on the QS role driving *colonization towards infection* (in collaboration with HGTiP), ii) investigating the potential value of QS molecules as biomarkers of infection in patients suffering respiratory diseases and CF (in collaboration with HGTiP and HUVH) and iii) assessing the potential therapeutic value of the anti-QS antibodies on in *vitro* assays. The selection of the new QS targets was based on the knowledge obtained from the Immuno-QS project, which pointed several relevant targets for *P. aeruginosa* and *S. aureus*. Patients suffering CF were identified as a priority based on the prevalence of infection by these bacteria and the impact in their life expectancy. In this context, PoC devices have been considered in the project as an important need for appropriate CF routine microbiological controls. For this purpose, the project counted with the collaboration of the Bioanalysis and Biosensors group of the University of Alcalá de Henares. Moreover, the above-mentioned clinical groups were also involved.

2. **Targeting-QS. Towards Improved Diagnostic and Therapeutic Strategies for Infectious Diseases Targeting Quorum Sensing.** (PID2021-126357OB-C21, MICIN, Dirección General de Investigación Científica y Técnica, Subdirección General de Proyectos de I+D.)

The **Targeting-QS** project builds on insights from the prior QS4CF initiative, where both participating groups collaborated to advance diagnostic and therapeutic strategies targeting QS molecules in *S. aureus* and other pathogens. This project, led by the Nb4D-CSIC group (Subproject 1) and BBG-UAH (Subproject 2), benefits from the expertise in antibody-based diagnostics and innovative PoC devices of both research groups. The Nb4D-CSIC team focuses on producing immunoreagents against QS molecules, while BBG-UAH specializes in developing PoC devices with optical and electrochemical detection, enabling early, near-patient diagnostics. A key objective of Targeting-QS is to create laboratory-based ELISA and microarray methods alongside PoC arrays for rapid, efficient diagnostics. Collaborations with the Hospital Vall d'Hebron, Hospital Germans Trias i Pujol, and IMIM focus on analyzing QS signatures in respiratory and urinary tract infections to improve diagnostic precision and support antimicrobial resistance tracking. The project also emphasizes social responsibility and innovation by engaging with patient advocacy groups and private sector partners like Werfen and IDNEO, fostering a pathway for clinical translation and social impact. Coordination across teams, stakeholders, and private companies will be maintained through regular meetings, and workshops are planned to disseminate results and explore new scientific and technological applications.

2.2 PRECEDENT WORK IN OUR RESEARCH GROUP

The Nanobiotechnology for Diagnostics (Nb4D) research group has extensive extensive expertise in the rational design and synthesis of haptens, tailored to generate antibodies specifically targeting low-molecular-weight compounds. With a strong focus on immunochemistry and bioconjugation techniques, our team has successfully developed specific antibodies for a wide range of **low-molecular-weight** (low MW) targets, including hormones, toxins, and pharmaceuticals. Strategic **hapten design and synthesis** plays a critical role in optimizing antibody binding and specificity, enabling the detection of analytes that are otherwise challenging to identify. Building upon these concepts, our group employs this rational hapten design to produce tailored antibodies,

ensuring the production of high-affinity antibodies tailored to the unique characteristics of each small molecule[1].

2.2.1 ANTIBODY PRODUCTION AGAINST LOW MW MOLECULES

The production of antibodies against small molecules is fundamental in several areas of biotechnology, such as environmental analysis, therapeutic drug monitoring, and diagnostics. Small molecules, in contrast to larger macromolecules, may be unable to trigger a strong immune response on their own because of their size and lack of structural complexity. The **design and synthesis of haptens** is a crucial strategy for addressing this obstacle.

Haptens are chemically related compounds to the target analyte that mimics its physico-chemical properties. Basically, the hapten is the target analyte that has a spacer arm ended with a chemical moiety to couple to a **carrier protein**. The introduction of the spacer arm is critical not to affect the inherent properties of the target analyte. The hapten-carrier complex is referred to as the **immunogen**. By conjugating the haptens to a high molecular weight carrier protein, the immune system is further stimulated and antibodies that specifically attach to the molecules of interest can be produced. A schematic representation of the antibody production strategy against small molecules can be seen in Figure 2.1.

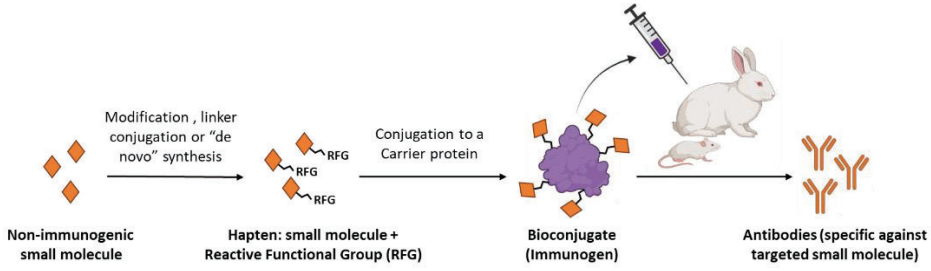

Figure 2.1. *Strategy for antibody production against small molecules. Small molecules cannot elicit an immune response on their own due to their low molecular weight. To enable this, they are modified, linked to spacers, or synthesized "de novo" to incorporate reactive functional groups (RFGs). These RFGs allow for covalent bonding with a high-molecular-weight carrier protein, resulting in an immunogen. When this immunogen is injected into animals, it elicits an immune response, leading to the production of specific antibodies against the target molecule.*

The **design** of the hapten and its **chemical structure** are crucial in the successful production of antibodies. The hapten needs to be properly designed to preserve the fundamental structural elements of the target molecule while adding

functional groups that facilitate successful conjugation to the carrier protein. This precise design ensures recognition by the immune system and promotes the production of highly specific antibodies.

Moreover, the immunogenicity and magnitude of the antibody response are highly dependent on the chemical structure of the hapten. The capacity of the immune system to identify the target molecule can be strengthened by **structural alterations**, such as the insertion of linkers or spacer arms, which improve the hapten's exposure to the carrier protein. These modifications must be meticulously designed to achieve an enhanced immunological response while preserving the hapten's structural integrity and similarity to the molecule of interest.

Synthesizing effective haptens poses significant challenges, including the selection of appropriate **reactive functional groups** (RFGs) for conjugation, the preservation of molecular epitopes, and the stability of the conjugate. One major challenge lies in ensuring that the conjugation of the hapten to the carrier protein does not alter its **immunogenic epitopes**, which are essential for antibody recognition. Furthermore, the RFGs must be carefully chosen to allow stable and efficient binding to the carrier without disrupting the structure of the target molecule.

To achieve an optimal immune response, various methods of synthesizing haptens have been developed, each tailored to address the specific challenges posed by the structure and reactivity of the target molecule:

- **Direct modification of the target molecule**: This approach involves adding RFGs, such as carboxyl groups (-COOH) or amino groups ($-NH_2$), directly to the small molecule for conjugation. This method is effective for structurally stable molecules, like certain drugs or environmental contaminants, where small modifications do not affect the immunogenicity or structure of the molecule.
- **“De novo” synthesis**: When direct modification is impractical, haptens can be synthesized from scratch to mimic essential structural features of the target molecule. This method is particularly useful for unstable or highly reactive molecules, where a structurally similar analog can serve as an immunogenic substitute.

- **Use of spacer arms and linkers**: Introducing spacer arms or linkers between the hapten and carrier protein improves the epitope's exposure to the immune system. Linkers such as polyethylene glycol (PEG) chains or aliphatic spacers provide flexibility, enhancing antibody accessibility and specificity by allowing the hapten to extend away from the carrier surface.

Hapten synthesis requires a careful balance between maintaining **structural similarity** to the target molecule, ensuring **stable conjugation** to the carrier, and maximizing the **immune response**. The development of haptens with high specificity and stability is essential for generating reliable antibodies, which are indispensable for applications in diagnostics, environmental monitoring, and therapeutic monitoring.

Through meticulous screening and optimization processes, the **Nb4D** has yield several antibodies applied for a variety of different purposes, contributing significantly to advancements in food safety, environmeltal monitoring, diagnosis and therapeutic applications.

To date, our team has effectively used its expertise of rational hapten design and **antibody production** to identify a variety of low-molecular-weight analytes, including **hormones**[2], **pesticides**[3], and **antibiotics**[4]. This expertise supports our ongoing efforts to innovate and refine immunoassay platforms for small molecule detection, contributing to advancements in diagnostic and monitoring technologies. More recently, our research has expanded to include the detection of **QSms**, compounds crucial for bacterial communication and biofilm formation. Specific strategies were developed to produce antibodies that target these signaling molecules with high sensitivity and specificity[5]. This advancement supports applications in bacterial infection **diagnostics** and **monitoring**, providing new tools to study and potentially disrupt pathogenic bacterial behaviors associated with QS.

Overall, the precedent work in our group demonstrates the versatility and impact of immunochemical approaches for monitoring a wide array of small compounds, contributing to both environmental and public health applications.

2.2.2 HAPTEN DESIGN FOR THE PRODUCTION OF ANTIBODIES AGAINST AIPS

For the purpose of identifying *S. aureus* AIPs, hapten design is very crucial. Acting as molecular signals, AIPs play a key role in the regulation of virulence factors in *S. aureus*. Due to their small size and the fact that certain AIPs are quite similar one to another (see Figure 1.33), antibody production against them is quite challenging. It is essential to identify each AIP individually to precisely track and gain insight into the QS processes of *S. aureus*, which may guide treatment approaches and infection control measures.

Accurate detection of individual AIPs requires the synthesis haptens that may produce antibodies against each particular AIP. **Specificity** is crucial in order to prevent cross-reactivity, which could lead to false positive results and compromise the reliability of the technique. By designing haptens that closely resemble the native structure of each AIP and coupling them to carrier proteins, it is feasible to produce antibodies capable of distinguishing between closely related AIPs.

AIPs present a significant challenge for recognition due to their **thiolactone ring**, which imparts a labile nature. Thiolactones are cyclic esters derived from mercapto acids and are typically unstable intermediates [6]. Hence, the thiolactone ring is prone to **hydrolysis** and other chemical transformations, which complicates the synthesis and preservation of haptens, as their low stability makes it difficult to maintain their structural integrity throughout these processes.

Park et al. (2007) addressed the labile stability of thiolactones in AIPs during the development of mAbs for AIP4 by implementing a chemical switch from the native thiolactone to a lactone-containing hapten. Their reasoning was based on the greater aminolytic **stability of lactones**, which ensured that the hapten conjugates remained structurally intact during the immunization process and subsequent immune response. This strategy was crucial in avoiding the generation of degradation products with unknown chemical and biological properties, an issue previously encountered with other QS molecules in their laboratory [7].

In our group, **two different approaches** were initially attempted to raise antibodies agains AIP4 and overcome the undersired unstability of the thiolactone ring, one conserving the original thiolactone structure and the other employing a more stable lactam.

. Two distinct immunizing haptens were produced, one with a heterologous structure (AIP4NH, including a lactam ring) and one with a homologous structure (AIP4S, containing the thiolactone ring) to AIP4. The aim was to evaluate the avidity of antibodies against AIP4 generated with a more stable but structurally distinct hapten against those produced with a hapten that mimics the same chemical structure of AIP4, although less stable due to hydrolysis.

The research conducted made it possible to directly compare the **avidity and specificity** of the antibodies produced against the two haptens. The study revealed a better detectability for the antibodies which was raised using as the immunizing hapten the thiolactone hapten despite the lactam hapten. Meaning, that, despite the better stability that offered the lactam ring, affect significantly the physico chemical properties of the native AIP4.

2.2.3 POLYCLONAL ANTIBODY PRODUCTION AGAINST AIP4

Antisera against AIP4NH-HCH (As376, As377, and As378) and AIP4S-HCH (As379, As380, and As381) were produced in female New Zealand white rabbits. This work was carried out by Dr. Enrique José Montagut.

The As380/AIP4S-BSA ELISA provided detectability values in the **high pM range**, being substantially higher compared with other antisera, with a limit of detection (LOD) of 0.22 ± 0.06 nM and a IC_{50} value of 2.90 ± 0.19 nM (Table 2.1). Therefore, in order to produce mAbs against the remaining *S. aureus* AIPs, the thiolactone hapten approach was selected.

It is important to note that lactone-type haptens are not exempt from the risk of hydrolysis. This susceptibility to degradation has been observed not only in the context of *S. aureus* AIPs but also in QSMs from other species, such as *P. aeruginosa*. Ones of the key signaling molecules in *P. aeruginosa* are the homoserine lactones (**HSLs**), which also contain a lactone ring, making them vulnerable to hydrolysis. As Debler et al. pointed out, lactone-based haptens are

at risk of degradation, which is an important consideration when designing stable and effective immunogens for antibody production [8] .

Although the thiolactone hapten strategy (AIP4S-HCH) enabled the production of antibodies with the highest avidity, concerns about its stability persisted. This led to the hypothesis that during the course of an infection, AIPs are initially released in their mature form, characterized by 7 to 9 amino acid residues and a thiolactone ring. However, once secreted, their structure is susceptible to modifications due to environmental changes within the host. Therefore, two different forms could be identified:

1) The native thiolactone form (**closed form**).

2) The linearized form (**open form**).

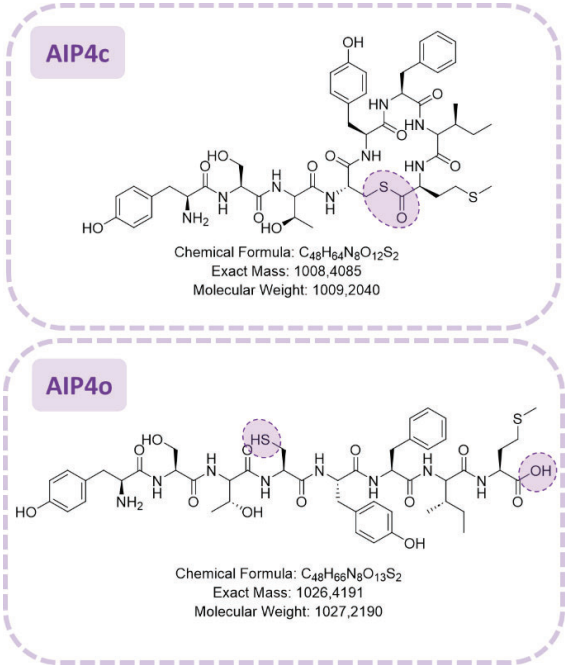

Figure 2.2. *Chemical structures of AIP4 cyclic (AIP4c) and linear (AIP4o) forms. The chemical formula, exact mass and molecular weight are specified for each molecule.*

To test this hypothesis, rabbit antisera produced with the AIP4S-HCH immunogen were tested against both the native form of AIP4 (AIP4 closed form: **AIP4c**) and the linear form of this peptide (AIP4 open form: **AIP4o**).

This screening method confirmed the previous hypothesis. Some of the antisera recognized AIP4o, and, surprisingly, the antiserum As381, which had not shown reactivity against AIP4c, was highly specific for detecting AIP4o. In light of these results, it was decided to re-optimize the assay As381/AIP4S-BSA for AIP4o.

Finally, **two competitive indirect ELISAs** were developed, each specific for one of the AIP4 forms: using **As380/AIP4S-BSA** for the detection of **AIP4c** and **As381/AIP4S-BSA** for **AIP4o**. The analytical parameters and calibration curves of both assays are shown in Figure 2.3. and Table 2.1.

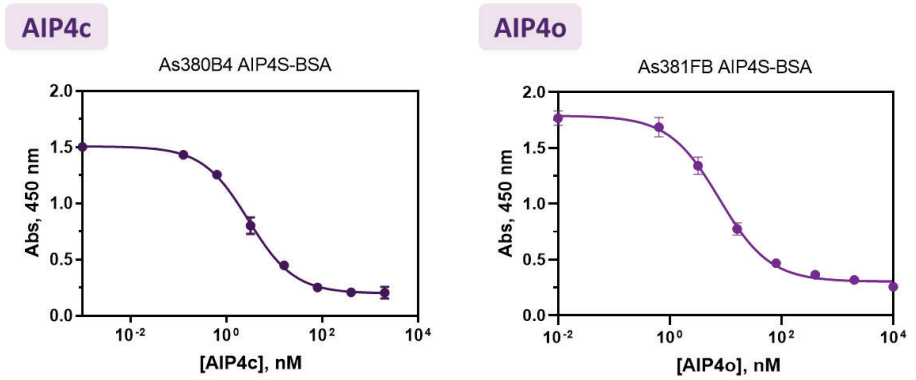

Figure 2.3. *Calibration curves of the ELISAs As380FB/AIP4S-BSA for the detection of AIP4c and As381FB/AIP4S-BSA for AIP4o in PBST. Absorbance was measured at 450 nm.*

Table 2.1. *Analytical parameters of As380B4/AIP4S-BSA and As381FB/AIP4S-BSA ELISAs.*

	As380B4/AIP4S-BSA	**As381FB/AIP4S-BSA**
A_{min}	0.15 ± 0.04	0.30 ± 0.03
A_{max}	1.46 ± 0.01	1.79 ± 0.06
Slope	-0.91 ± 0.03	- 0.96 ± 0.06
IC_{50} (nM)	2.89 ± 0.19	7.56 ± 0.68
Dynamic Range (nM)	0.68 ± 0.14 to 14.26 ± 0.93	1.96 ± 0.39 to 38.95 ± 3.14
LOD (nM)	0.22 ± 0.06	0.89 ± 0.25
R^2	0.996 ± 0.003	0.997 ± 0.001

For the As380B4/AIP4S-BSA ELISA, a concentration of 0.63 µg mL^{-1} of CA and As dilution 1/2000 were used. In the case of As381FB/AIP4S-BSA ELISA, the concentration of CA and As dilution were 0.078 µg mL^{-1} and 1/4000, respectively. The concentrations are expressed in nM. The results represent the average data values obtained from three separate assays conducted on three different days, with each assay performed at least in duplicate wells.

Utilizing the aforementioned immunoassays, Dr. Enrique José Montagut successfully detected AIP4 in **bacterial isolates** of *S. aureus* strains from the agr-IV group[9]. This achievement underscores the potential of AIPs as biomarkers for diagnosing infections caused by this pathogen. Additionally, several studies highlight the promising role of AIPs as markers with prognostic value[10, 11] or even for differentiating between colonization and infection[12-14], which is one of the greatest challenges in diagnosing infections caused by bacteria that are part of the natural microbiota in healthy individuals[15].

2.3 OBJECTIVES AND SCIENTIFIC STRATEGY

General Objective

Within this context, the main goal of this thesis was to improve the diagnostic efficacy of *S. aureus* infections by gaining a deeper understanding about the function the bacterial communication process known as QS and its role in *S. aureus* pathogenesis. Specifically, we aimed to investigate the correlation between the presence and concentration of *S. aureus* AIPs, both in culture media where clinical isolates are cultivated and in clinical respiratory samples, with the progression of the disease. This strategy attempted to assess the potential of these molecules as bimarkers for infection.

Specific Objectives

In order to accomplish this objective, we suggested creating immunochemical techniques to profile the expression of the four different signalling molecules of *S. aureus* QS (AIPs 1-4). The goal of this approach was to provide further knowledge on how these molecules function in the pathophysiology of *S. aureus*. The following specific objectives were accomplished in order to achieve this aim:

1. Design of haptens for the non-immunogenic QS molecules produced by *S. aureus* (AIPs 1-4).

2. Preparation of bioconjugates for the generation of specific monoclonal and polyclonal antibodies against *S. aureus* AIPs.

3. Development of single-analyte immunochemical analysis tools to build up fast and accurate diagnostic methods to:
    - Diagnose *S. aureus* infections discerning from colonizations.
    - Predict and manage infection progression throungh the quantification of AIPs.

4. Evaluation of the capacity to engange the immunochemical tools developed for phenotyping studies.

5. Assessment of the potential value of AIPs as biomarkers of infection by analyzing their profile in bacterial isolates and clinical samples obtained from patients suffering respiratory diseases.

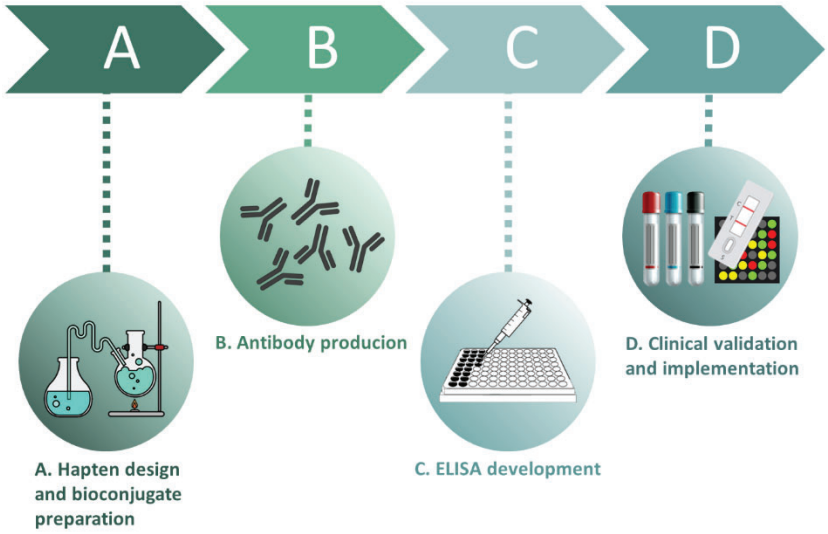

Figure 2.4. *Diagram on the methodology steps to be followed in order to yield the objectives of the present thesis research work.*

2.4 THESIS STRUCTURE

The structure of this thesis follows the scheme detailed below:

- **Immunoreagent production**:
  Chapter 3 describes the production of monoclonal and polyclonal antibodies against *S. aureus* AIPs.
- **ELISA development:**

Chapter 4 focuses on the development of indirect competitive ELISAs for the detection of AIP2, AIP2 and AIP3.

- **Bacterial isolates:**
  Chapter 5 details the optimization of the ELISAs for AIP detection in TSB culture medium and their potential application for both diagnostic and phenotyping purposes.
- **Respiratory samples:**
  Chapter 6 describes different treatment strategies to deal with low tract respiratory samples such as bronchial aspirate samples (BAS) or blonchoalveolar lavage (BAL) for direct AIP detection and quantification in such complex smaples.

2.5 BIBLIOGRAPHY

1. Marco, M.-P.; Gee, S.; Hammock, B. D., Immunochemical techniques for environmental analysis II. Antibody production and immunoassay development. *TrAC Trends in Analytical Chemistry* **1995,** *14* (8), 415-425.
2. Salvador, J. P.; Vila-Roca, E.; Monfort, N.; Ventura, R.; Marco, M. P., New approach based on immunochemical techniques for monitoring of selective estrogen receptor modulators (SERMs) in human urine. *J Pharm Biomed Anal* **2018,** *156*, 147-152.
3. Zacco, E.; Pividori, M. I.; Alegret, S.; Galve, R.; Marco, M. P., Electrochemical Magnetoimmunosensing Strategy for the Detection of Pesticides Residues. *Analytical Chemistry* **2006,** *78* (6), 1780-1788.
4. Pinacho, D. G.; Sánchez-Baeza, F.; Marco, M. P., Molecular Modeling Assisted Hapten Design To Produce Broad Selectivity Antibodies for Fluoroquinolone Antibiotics. *Analytical Chemistry* **2012,** *84* (10), 4527-4534.
5. Montagut, E. J.; Raya, J.; Martin-Gomez, M. T.; Vilaplana, L.; Rodriguez-Urretavizcaya, B.; Marco, M. P., An Immunochemical Approach to Detect the Quorum Sensing-Regulated Virulence Factor 2-Heptyl-4-Quinoline N-Oxide (HQNO) Produced by Pseudomonas aeruginosa Clinical Isolates. *Microbiol Spectr* **2022,** *10* (4), e0107321.
6. Finkelstein, M. B.; Dekant, W.; Kende, A. S.; Anders, M. W., .alpha.-Thiolactones as Novel Intermediates in the Cysteine Conjugate .beta.-Lyase-Catalyzed Bioactivation of Bromine-Containing Cysteine S-Conjugates. *Journal of the American Chemical Society* **1995,** *117* (37), 9590-9591.
7. Park, J.; Jagasia, R.; Kaufmann, G. F.; Mathison, J. C.; Ruiz, D. I.; Moss, J. A.; Meijler, M. M.; Ulevitch, R. J.; Janda, K. D., Infection Control by Antibody Disruption of Bacterial Quorum Sensing Signaling. *Chemistry & Biology* **2007,** *14* (10), 1119-1127.
8. Debler, E. W.; Kaufmann, G. F.; Kirchdoerfer, R. N.; Mee, J. M.; Janda, K. D.; Wilson, I. A., Crystal Structures of a Quorum-quenching Antibody. *Journal of Molecular Biology* **2007,** *368* (5), 1392-1402.
9. Montagut, E. J.; Acosta, G.; Albericio, F.; Royo, M.; Godoy-Tena, G.; Lacoma, A.; Prat, C.; Salvador, J. P.; Marco, M. P., Direct Quantitative Immunochemical Analysis of Autoinducer Peptide IV for Diagnosing and Stratifying Staphylococcus aureus Infections. *ACS Infect Dis* **2022,** *8* (3), 645-656.

10. Lee, S. O.; Lee, S.; Lee, J. E.; Song, K. H.; Kang, C. K.; Wi, Y. M.; San-Juan, R.; López-Cortés, L. E.; Lacoma, A.; Prat, C.; Jang, H. C.; Kim, E. S.; Kim, H. B.; Lee, S. H., Dysfunctional accessory gene regulator (agr) as a prognostic factor in invasive Staphylococcus aureus infection: a systematic review and meta-analysis. *Sci Rep* **2020,** *10* (1), 20697.
11. Schweizer, M. L.; Furuno, J. P.; Sakoulas, G.; Johnson, J. K.; Harris, A. D.; Shardell, M. D.; McGregor, J. C.; Thom, K. A.; Perencevich, E. N., Increased mortality with accessory gene regulator (agr) dysfunction in Staphylococcus aureus among bacteremic patients. *Antimicrob Agents Chemother* **2011,** *55* (3), 1082-7.
12. Gomes-Fernandes, M.; Laabei, M.; Pagan, N.; Hidalgo, J.; Molinos, S.; Villar Hernandez, R.; Domínguez-Villanueva, D.; Jenkins, A. T. A.; Lacoma, A.; Prat, C., Accessory gene regulator (Agr) functionality in Staphylococcus aureus derived from lower respiratory tract infections. *PLoS One* **2017,** *12* (4), e0175552.
13. Shopsin, B.; Drlica-Wagner, A.; Mathema, B.; Adhikari, R. P.; Kreiswirth, B. N.; Novick, R. P., Prevalence of agr dysfunction among colonizing Staphylococcus aureus strains. *J Infect Dis* **2008,** *198* (8), 1171-4.
14. Stulik, L.; Malafa, S.; Hudcova, J.; Rouha, H.; Henics, B. Z.; Craven, D. E.; Sonnevend, A. M.; Nagy, E., α-Hemolysin activity of methicillin-susceptible Staphylococcus aureus predicts ventilator-associated pneumonia. *Am J Respir Crit Care Med* **2014,** *190* (10), 1139-48.
15. Sakr, A.; Brégeon, F.; Mège, J. L.; Rolain, J. M.; Blin, O., Staphylococcus aureus Nasal Colonization: An Update on Mechanisms, Epidemiology, Risk Factors, and Subsequent Infections. *Front Microbiol* **2018,** *9*, 2419.

3 IMMUNOREAGENT PRODUCTION

3.1 CHAPTER PRESENTATION

This chapter discusses various strategies for producing antibodies against *S. aureus* AIPs and the preparation of the corresponding bioconjugates for both immunization and immunoassay development. Initially, based on the group's previous experience, the production of monoclonal antibodies (mAbs) was pursued using haptens that preserve the native thiolactone structure of the AIPs. Through a comprehensive screening process, the aim was to identify clones capable of producing antibodies specific to both the closed (thiolactone) and linear forms of the AIPs.

Given the challenges encountered, the production of polyclonal antibodies (pAbs) was explored as an alternative, given the prior success in the group in generating pAbs for AIP4. Lastly, recognizing that linear forms of AIPs are present in bacterial culture medium, a novel strategy was undertaken using immunogens presenting AIPs in their linear form. This innovative approach ultimately led to the production of a complete repertoire of antibodies capable of detecting all four AIPs of *S. aureus* (AIPs 1–4). These antibodies will later be implemented for the development of ELISAs. Chapter structure is depicted in Figure 3.1.

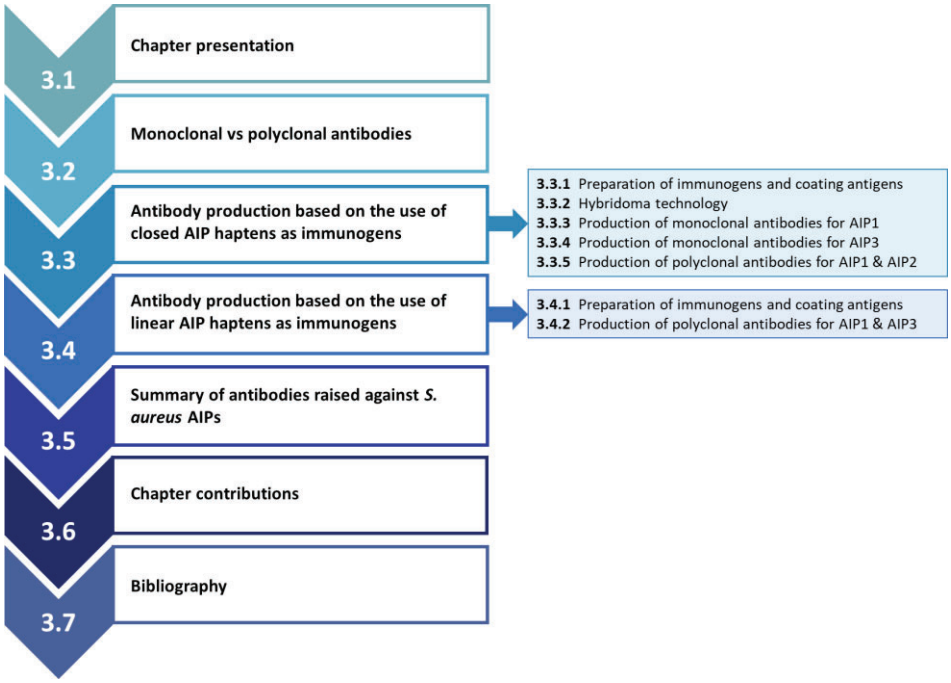

Figure 3.1. *Structure of Chapter 3.*

3.2 MONOCLONAL VS POLYCLONAL ANTIBODIES

The main difference between mAbs and pAbs lies in their production. MAbs are typically generated using hybridoma technology, where B-cells from an immunized animal are fused with myeloma cells to create hybrid cells that can be cloned and cultured indefinitely. This method ensures a consistent supply of identical antibodies. They are produced by identical immune cells derived from a single parent cell, resulting in a homogeneous population that binds to a single, specific epitope on an antigen. In contrast, pAbs are obtained by immunizing an animal and then collecting the serum, which contains a mix of antibodies produced by different B-cells. As their production is driven by multiple immune cells, hey constitute a heterogeneous mixture that recognizes multiple epitopes on the same antigen[1]. The main differences between mAbs and pAbs are illustrated in Figure 3.2 .

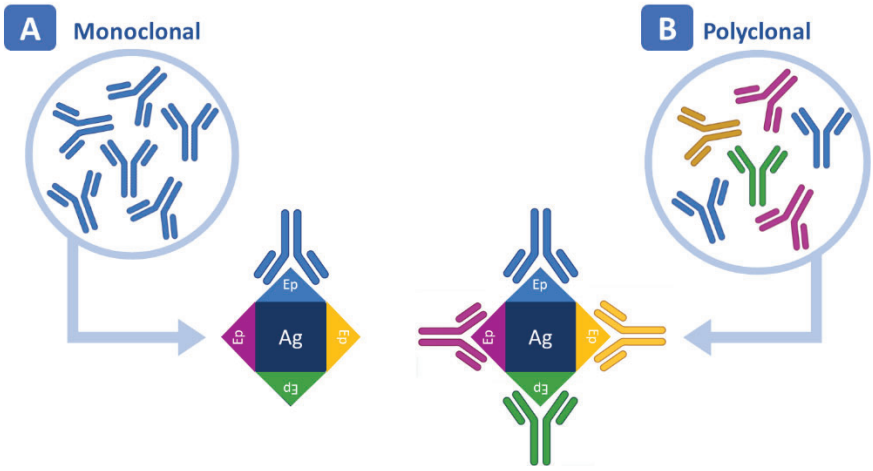

***Figure 3.2**. Schematic representation of A) Monoclonal and B) Polyclonal antibodies. Monoclonal antibodies are specific to a single epitope on an antigen, representing a uniform population of identical antibodies. In contrast, polyclonal antibodies are a mixture of different antibodies, recognizing multiple epitopes on the same antigen, resulting in broader heterogenicity and binding diversity. Ag.: antigen. Ep.: epitope.*

MAbs are characterized by unlimited source of antibodies by culturing the final hybridoma cell line. Their uniformity ensures consistent results across experiments and manufacturing batches. Additionally, mAbs can be engineered for specific applications, such as humanized versions for therapeutic use or labeled forms for imaging[2]. However, their production is tedious and expensive,

involving hybridoma technology or recombinant methods. Their high specificity can be also a limitation in cases of antigen variability, as mutations or conformational changes may prevent binding[3]. Despite these challenges, mAbs are widely applied in diagnostic tools like ELISAs and lateral flow assays[4], therapeutics for conditions such as cancer[5] and autoimmune diseases[6], and research techniques like flow cytometry[7] and imaging[8].

In contrast, pAbs are produced by multiple B-cell clones in response to an antigen, resulting in a heterogeneous mixture of antibodies that recognize and bind to multiple epitopes of the same antigen[9]. Their diversity can enhance the overall strength of the immune response, providing robust antigen detection in assays where recognizing multiple epitopes is beneficial. Additionally, having multiple epitopes leads to signal amplification, which is particularly useful in assays targeting low-abundance molecules[10].

pAbs are also easier and less expensive to produce, as they are generated by immunizing animals such as rabbits or goats, without the need for cell culture or extensive screening processes. They are also more stable than mAbs over a broad pH and salt concentration, reducing variability in long-term studies[1]. However, their heterogeneity can lead to batch-to-batch variability, impacting reproducibility, and their broader binding spectrum may result in higher background noise, reducing assay specificity. Despite these limitations, pAbs are commonly used in applications like Western blotting[11], immunohistochemistry[12], and immunoprecipitation[13], where their ability to detect multiple epitopes is advantageous. They are also frequently employed as secondary antibodies in immunoassays.

To date, reports on the production of antibodies targeting AIPs of *S. aureus* are extremely limited, and those available primarily focus on therapeutic applications rather than diagnostic purposes. Already published mAbs were designed to disrupt the *agr* QS system, a key mechanism regulating virulence factor expression in the bacteria. By inhibiting this system, the antibodies reduce the ability of this pathogen to cause infection, making them a promising tool in combating and mitigating the severity of *S. aureus* infections[14].

To our knowledge, the unique therapeutic application of antibodies against AIPs from *S. aureus* was developed by Park and colleagues. Their work involved the generation of a hydrolytically stable AIP4 hapten that led to the production of

the mAb AP4-24H11. This antibody specifically inhibits the *agr* QS system in *S. aureus*, significantly reducing the expression of virulence factors like α-hemolysin in vitro. In vivo studies demonstrated that AP4-24H11 effectively mitigates *S. aureus*-induced skin injury and enhances survival in a lethal mouse infection model, supporting its potential for prophylactic and therapeutic use against *S. aureus* infections [15].

The antibody previously mentioned is already patented and, while initially developed for therapeutic purposes, the authors recognize their potential for diagnostic and phrophylactic applications, highlighting the importance of further investigation into its utility for other clinical approaches[16].

3.3 ANTIBODY PRODUCTION BASED ON THE USE OF CLOSED AIP HAPTENS AS IMMUNOGENS

The production of the remaining AIPs (1 to3) was performed following the same strategy by Dr. E. Montagut. The same linker was used for the corresponding AIP for the preparation of the immunogens (see Figure 3.3). However, we decided to produce mAbs instead of producing pAbs.

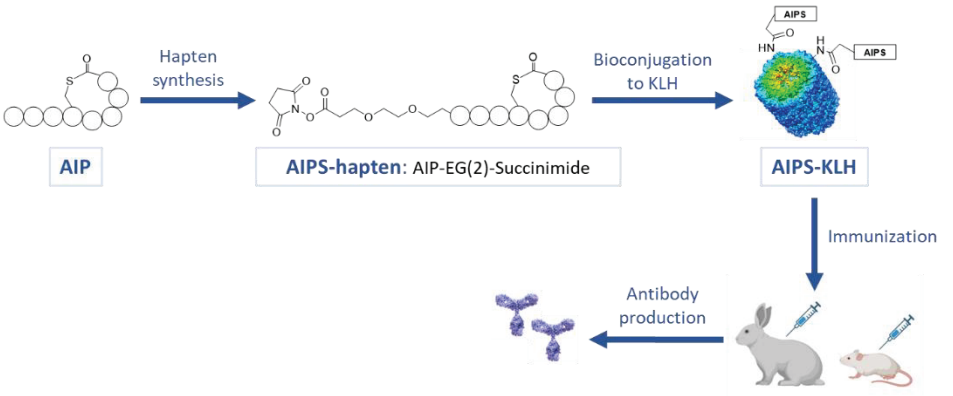

Figure 3.3. *Schematic representation of the process for antibody production against S. aureus AIPs using closed AIP haptens (AIPS-haptens) as immunogens.*

The previous studies performed by Dr. Montagut showed an unexpected result during the AIP4s-KLH immunization process. After the immunization, we obtained a pAb that recognized mainly the open form of the AIP, meaning that

the AIP4S was hydrolized and then, exposing to the immune system the open form of the AIP4. However, a partial bleeding obtained after the fourth immunization (As380 B4) showed an unexpected recognition profile: it recognized specifically the closed form. We have not any rational explanation to this behaviour just that during this immunization the majority of the pAbs produced were against a non-hydrolized KLH form. Thus, we consider to look for both open and close form during the cloning of the mAbs aiming to capture the antibodies that recognize the open and close form. This approach aimed to identify rigourously the clones producing the antibodies of our interest, each one of them specific for one of the six remaining targets: AIP1c, AIP1o, AIP2c, AIP2o, AIP3c and AIP3o. The chemical structures of the targeted molecules showing the differences between the linear and cyclic forms are shown in Figure 3.6.

3.3.1 PREPARATION OF IMMUNOGENS AND COATING ANTIGENS

In order to produce antibodies against all the AIPs of *S. aureus* (AIPs 1–4), the corresponding haptens were synthesized. Considering the previous work producing pAbs against AIP4 conducted by Dr. Enrique José Montagut, the synthetic strategy preserving their native thiolactone ring was selected. The haptens were then linked to a spacer arm at the N-terminal residue, consisting of two ethylene glycol units and ending N-hydrosuccinimide ester.

In addition to improving hydrophilicity and lowering antigenicity, this spacer arm ensures the majority of the peptide structure and distinctive AIP epitopes are efficiently exposed to the immune system. The chemical structures of the haptens, synthesized by MS4N group of Dra. Miriam Royo, are shown in Figure 3.4.

As described in Figure 3.5, haptens were linked to 2 different carrier proteins: Bovine serum albumin (BSA), to be used as the competitor, and keyhole limpet hemocyanin (KLH) conforming the immunogen. The conjugation process of the AIPS-haptens involved the direct nucleophilic attachment of amino groups of the lysine residue in the portein to the succinimide-activated carboxylic acid group of the hapten, forming a covalent linkage through amide bond formation.

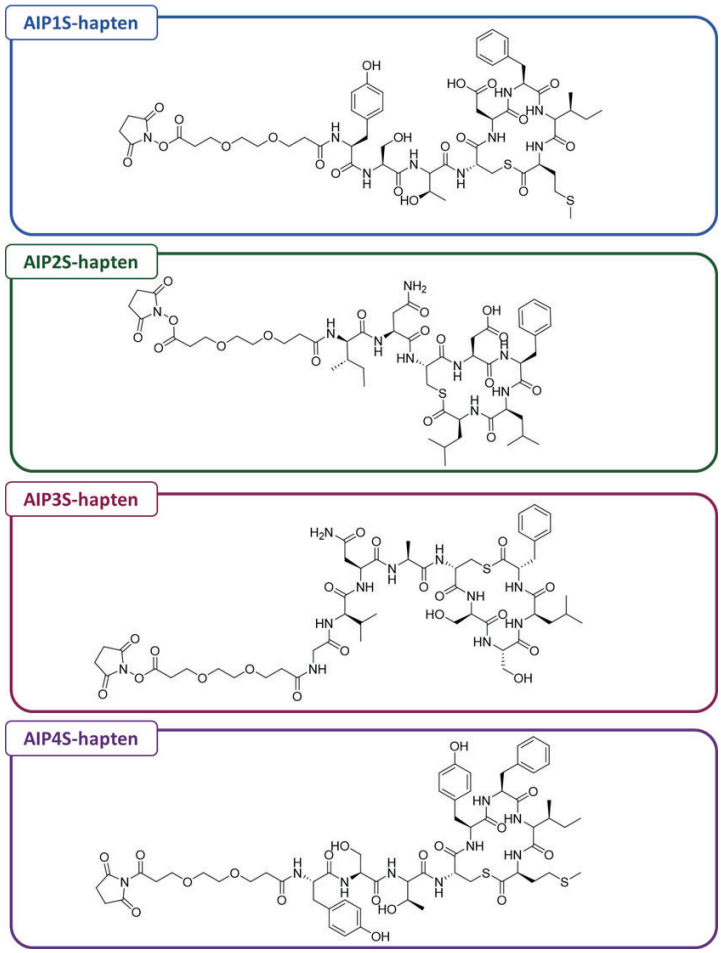

Figure 3.4. *Chemical structures of AIPS-haptens. Haptens following the synthetic strategy conserving the native thiolactone structure were sintetized for AIPs 1–4: AIP1S-hapten, AIP2S-hapten, AIP3S-hapten and AIP4S-hapten.*

This conjugation approach is widely used because it results in a stable amide linkage, effectively coupling the hapten to the protein, which is essential for producing immunogens[17]. KLH and HCH bioconjugates serve as strong antigens, promoting an immune response and facilitating the generation of antibodies specifically against the AIPs.

Since our group was producing antibodies with higher avidity using Keyhole limpet hemocyanin (KLH), this protein was selected for the synthesis of the remaining immunogens (AIP1S-KLH, AIP2S-KLH, AIP3S-KLH, AIP4S-HCH). In the case of the competitors, BSA was employed.

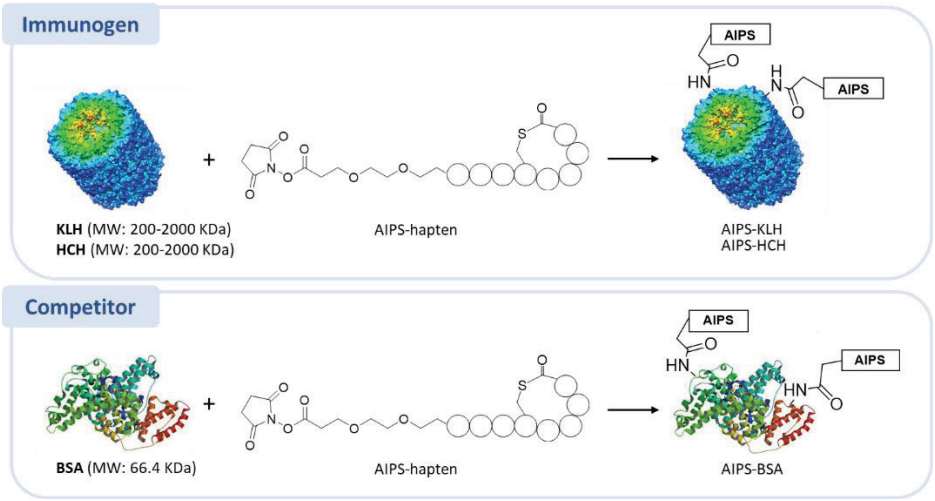

***Figure 3.5**. Bioconjugation of AIPS-haptens to carrier proteins. Haptens synthetized for each AIP following the thiolactone strategy were conjugated to either Keyhole limpet hemocyanin (KLH) (AIPS-haptens 1 to 3) or Horseshoe Crab Hemocyanin (HCH) (AIP4S-hapten) to give rise to the immunogens and to Bovine Serum Albumin (BSA) to constitute the competitor antigens.*

KLH/HCH conjugates could not be analyzed by MALDI-TOF MS due to their large molecular weight. To address this, BSA and KLH/HCH bioconjugates were prepared simultaneously under identical conditions, with the data from the BSA conjugates serving as a control for the bioconjugation process. Hapten densities for BSA bioconjugates are displayed in Table 3.1.

***Table 3.1.** Data on the hapten densities of all AIPS bioconjugates (1 to 4).*

Bioconjugate	HD
AIP1S-BSA	13
AIP2S-BSA	9
AIP3S-BSA	9
AIP4S-BSA	5

Hapten densities (HDs) of BSA conjugates were determined using MALDI-TOF-MS analysis.

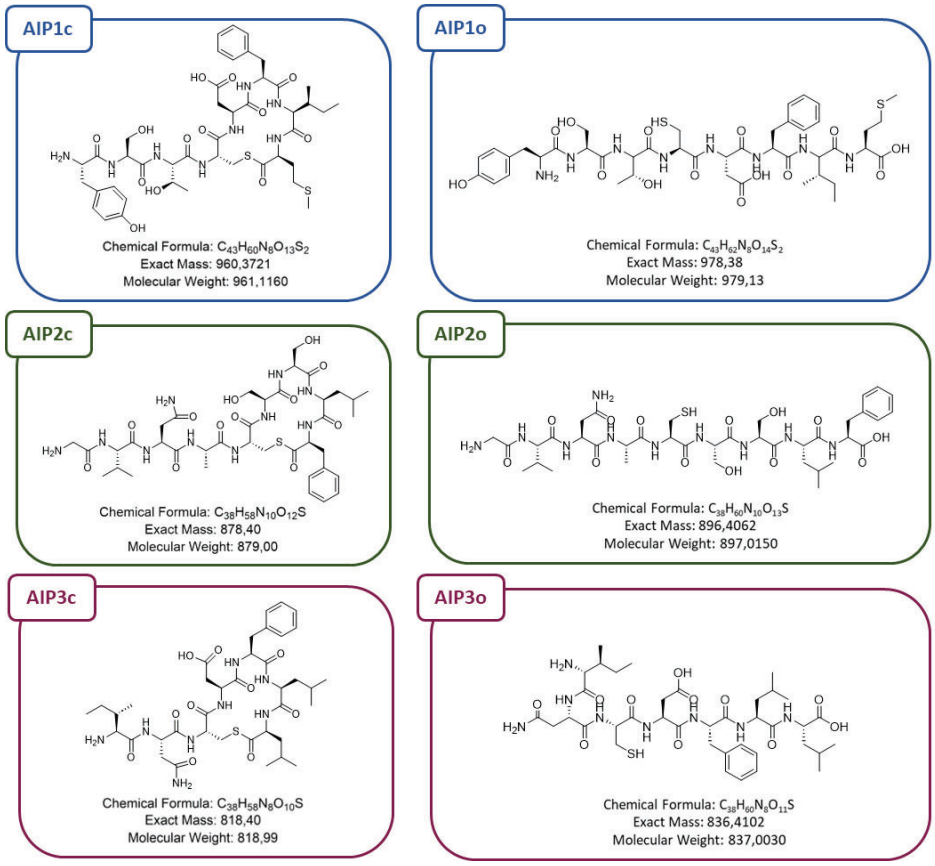

Figure 3.6. *Chemical structures of the closed and open forms of S. aureus AIP1, AIP2 and AIP3.*

3.3.2 HYBRIDOMA TECHNOLOGY

Hybridoma technology is a widely used method for producing mAbs, leading to highly specific antibodies derived from a single clone of B cells. This method combines the antibody-producing capability of B lymphocytes with the immortality of myeloma cells, resulting in hybrid cells known as hybridomas that can produce large quantities of specific antibodies indefinitely.

As described in Figure 3.7, the process begins with the immunization of animals, typically mice or rats, with the target antigen to elicit an immune response. The antigen may be presented in its native form (high MW molecules) or conjugated to a carrier protein (low MW molecules), and can be emulsified with an adjuvant to enhance the immune response. After repeated immunizations, the spleen is

extracted from the animal showing the strongest and most specific immune response to the antigen.

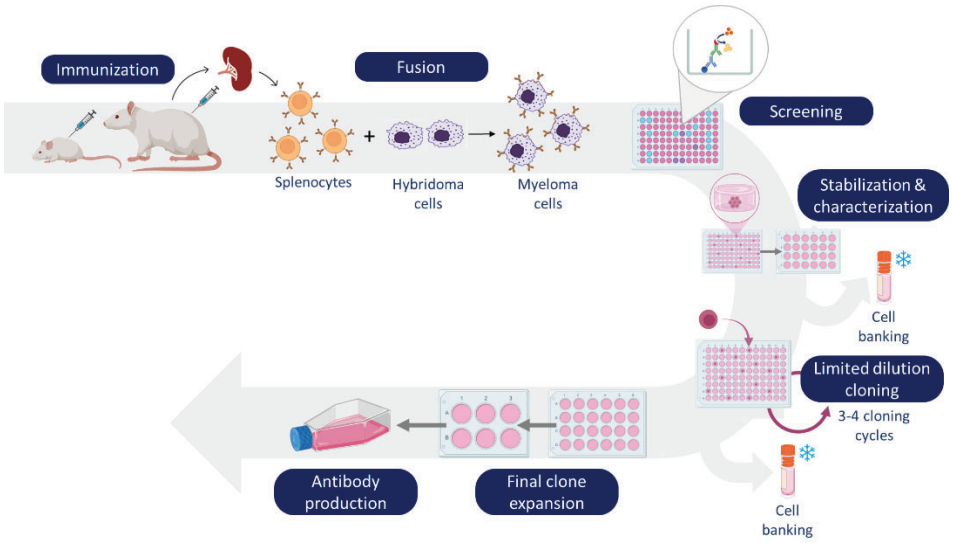

Figure 3.7. *Schematic representation of the hybridoma technology workflow for mAb production. The process involves several key steps: 1) Immunization of rats and mice to stimulate the production of antigen-specific B lymphocytes; 2) Fusion of B lymphocytes extracted from the spleen with myeloma cells to create hybridomas; 3) Screening of hybridoma supernatants via competitive ELISA to identify candidates with the desired recognition profile; 4) Stabilization and characterization of selected hybridomas, freezing both cells and supernatants of interest; 5) Cloning of hybridomas by isolating single cells to create identical clones, requiring 3–4 rounds of cloning, freezing clones and supernatants at each step; 6) Selection and expansion of final clones; and 7) Large-scale production of hybridoma cultures to obtain high quantities of the antibody of interest, followed by its purification.*

B lymphocytes from the spleen are then fused with myeloma cells (a type of immortal cancer cell line) using a fusion agent such as polyethylene glycol (PEG). Myeloma cells are immortal but lack the ability to produce antibodies, while B lymphocytes are short-lived but capable of producing specific antibodies. The resulting hybrid cells, known as hybridomas, combine these traits, producing antibodies indefinitely.

The fused cells are cultured in a selective medium known as HAT (hypoxanthine-aminopterin-thymidine) medium, which ensures that only hybridomas survive. Myeloma cells are unable to synthesize nucleotides in the presence of aminopterin, and unfused B cells die naturally after a short period.

The supernatants of the hybridoma cultures are then screened, typically using ELISA, to identify clones producing antibodies that specifically recognize the

target antigen. The initial hybridoma culture consists of a diverse population of antibody-producing cells, originating from various primary B-lymphocyte clones. Each clone secretes its own unique antibody into the culture medium, meaning that the antibodies at this stage are still polyclonal. This step ensures that only hybridomas producing antibodies with the desired specificity are selected for further development.

Once positive hybridomas are identified, they are cloned to ensure monoclonality. This is achieved isolating single cells by dilution into different culture wells and allowing them to grow into colonies. Several rounds of cloning are often necessary to confirm that the hybridomas produce identical antibodies. After cloning, the selected hybridoma clones are characterized to evaluate the specificity, affinity, and isotype of the antibodies they produce. For that purpose, the culture medium screened to select those hybridoma cells producing the desired antibodies. The positive wells are subjected to various cloning cycles and retested for activity until single-cell clones producing the desired antibody with optimal sensitivity and specificity for the target analyte are obtained. These hybridomas are then cryopreserved for long-term storage, along with their supernatants, to ensure the availability of both the cells and the antibodies.

Finally, the selected hybridomas are expanded in large-scale cultures to produce significant quantities of the desired antibody. The antibodies are secreted into the culture medium, from which they are collected and purified. Methods such as protein G affinity chromatography are commonly used to isolate the antibodies in a highly pure form.

3.3.3 PRODUCTION OF MONOCLONAL ANTIBODIES FOR AIP1

3.3.3.1 Immunization and antibody titer

4 BALB/c female mice and 4 Winstar female rats (6–8 weeks old) were immunized with 100 µg of AIP1S-KLH bioconjugate. After the initial dose, three additional immunizations were required in each case. Once completed the immunization period, the best candidates, both from rats and mice, were selected for spleen extraction and the subsequent production of mAbs, using

hybridoma technology. A scheme illustrating the different steps followed for mAb production is detailed in Figure 3.7.

Initially, it was necessary to select the best animal candidates (mice or rats) for spleen cell collection to proceed with the fusion with myeloma cells. As a starting point for animal selection, the focus was on individuals exhibiting the highest recognition of AIP1c. For this purpose, blood samples collected from all mice and rats after 10 days after the third immunization (Bleeding 3: B3) were compared. The selection of the animals that showed the best immune response was based on evaluating the avidity of the antisera from the final blood sample of each animal against the AIP1S-BSA bioconjugate using an indirect competitive ELISA.

The assay involved adding serial dilutions of the antisera to microplates coated with AIP1S-BSA and assessing their binding both in the absence the analyteand in the presence of 1 µM AIP1c or AIP1o. Figure 3.8 presents the absorbance values obtained under non-competitive and competitive conditions, along with the percentage of inhibition caused by the binding of antibodies to the target analyte. The spleens of the remaining animals were extracted and preserved in liquid nitrogen for potential future use. More detailed information about the immunization and production process can be found in Section 8.7.1

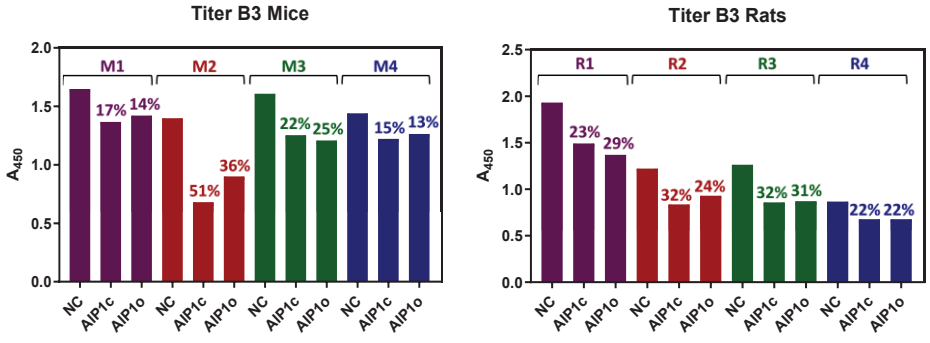

Figure 3.8. *Antibody titers corresponding to Bleeding 3 (B3) for mAb production against AIP1. The figure presents the antibody titers in B3 samples from the four immunized mice (M1-M4) on the left and the four immunized rats (R1-R4) on the right. The plates were coated with 1 µg mL^{-1} AIP1S-BSA. Blood samples were diluted 1:64,000 and analyzed under three conditions: B3 without competition (NC), B3 with competition using AIP1c, and B3 with competition using AIP1o. The competitors (AIP1c and AIP1o) were added at 1 µM. For each competitor, the percentage of inhibition is shown relative to the absorbance obtained under non-competitive conditions. This comparison highlights the differential recognition profiles of the antibodies in response to the closed (AIP1c) and open (AIP1o) forms of the antigen as well as the different stregths of the immune response.*

The antibody concentration shown in the Figure 3.8 corresponds to the dilution at which the absorbance under non-competitive conditions was closest to one. For both rats and mice, a dilution of 1:64,000 was selected, indicating very high antibody titers and reflecting a strong immune response. Notably, while R1 exhibited the highest absorbance, mice generally displayed higher titers overall, as their absorbance values exceeded one even at this dilution, suggesting the potential for further dilution.

Among the eight immunized animals, mouse 2 (M2) demonstrated the most selective recognition of AIP1c (Inhibition 51 %). On contrast, mouse 1 (M1) exhibited the strongest immune response overall, reflected by higher absorbance values (Abs: 1.64), with similar recognition profile comparing to mouse 4 (M4). Based on these results, it was decided to proceed with spleen fusions from both M1 and M2 in parallel to maximize the chances of generating hybridomas with optimal antibody production against AIP1c.

3.3.3.2 Screening for mAb selection

Our first goal was to specifically detect the closed forms of AIPs, as these represent their functional conformations. However, while detection of the linear forms of AIPs has not been previously reported, our group had prior experience successfully generating antibodies against open forms of AIPs. Based on this precedent and the hypothesis that a fraction of the AIPs released into the extracellular environment might adopt a linear form due to the physiological conditions of the medium, it was decided to include open forms of AIPs in the screening process.

Thus, the close form of AIP1 (AIP1c) and the open form (AIP1o) were used in the screening phase to identify clones specific for AIP1c or AIP1o. Hence, after performing the fusion, various rounds of screening and cloning were conducted, evaluating the avidity of antibodies for the AIP1S-BSA bioconjugate and the AIP1c and AIP1o analytes. The aim was to isolate a cell clone producing specific antibodies for AIP1c with minimum CR for AIP1o and viceversa.

The supernatants extracted from the production of the selected hybridoma clones were tested. This process involved analyzing the antibodies secreted by these clones into the culture medium to evaluate their binding affinity,

specificity, and suitability for further assay development. Testing these supernatants allows for efficient screening of antibody-producing clones and helps identify those with the desired characteristics for subsequent applications

Table 3.2. *Recognition percentages of AIP1c and AIP1o and absorbance values in the absence of competitors for the selected clones.*

Clone	Abs. (NC)	Competiton rate against AIP1c (%)	Competiton rate against AIP1o (%)
13.11.1.2.1	0.72	12.7	82.1
13.11.1.2.2	0.81	16.2	82.9
13.11.1.2.3	0.98	14.9	86.4
13.11.1.4.1	1.38	12.9	81.8
13.11.1.4.2	1.37	19.2	85.1
13.11.1.4.3	1.06	11.1	82.3
20.3.1.1.1	0.75	51.3	84.7
20.3.1.1.2	2.18	33.8	90.3
20.3.5.7.1	2.29	38.4	90.5
20.3.5.7.2	1.86	37.8	89.4
20.3.5.7.3	2.38	42.1	90.6
23.1.3.1.1	1.52	36.7	89.4
23.1.3.1.2	2.62	23.7	91.3
23.1.3.1.3	2.68	4.3	89.4
23.1.3.7.1	2.35	42	91.9
23.1.3.7.2	0.53	39.1	77.6
23.1.3.7.3	0.58	49.7	72.9

The table presents the data for 17 hybridomas selected in the fourth cloning round. Plates were coated with AIP1S-BSA at a concentration of 1 µg mL^{-1}, and competitors (AIP1c and AIP1o) were added at a concentration of 1 µM. The color scale represents the recognition of the analyte, with dark green indicating higher recognition and white indicating no recognition. The competition rate was calculated as the percentage reduction in absorbance due to competition, defined as the difference between the absorbance with competition and without competition, divided by the absorbance without competition, multiplied by 100. The final clones selected for mAb production are highlighted in blue.

Table 3.2 shows the competition rate of AIP1c and AIP1o on the ELISA carried out with the antibodies produced by the selected hybridomas in the fourth cloning cycle. As it can be observed, the hybridomas selected showed different recognition profiles for both analytes. For this reason, it was decided to select clones representing the three different recognition profiles observed.

Initially, the first clone selected was 23.1.3.7.1 according its highest recognition of AIP1c, with a competition rate of 42 % and a very high absorbance under non-

competitive conditions (Abs: 2.35). Similarly, 20.3.1.1.1 clone showed a slightly higher recognition of AIP1c (competition rate of 51.3 %) but its absorbance in the absence of competitors was much lower (Abs: 0.75). For this reason, this clone was excluded as a final candidate.

Another interesting clone was 23.1.3.1.3 which showed the highest selectivity between AIPo and AIP1c, with a competition rate of 89.4 % for AIP1o and 4.3 % for AIP1c. Lastly, the clone 13.11.1.4.1 showing partial recognition of AIP1c was included, reflecting another observed recognition profile.

3.3.3.3 Evaluation of recognition profiles

After selecting the three final clones mentioned above, their recognition profiles were evaluated against all four AIPs (1–4) of the agr QS system of *S. aureus*, in both their closed and linear forms. The objective of this experiment was to assess the selectivity of the mAbs for detecting AIP1 specifically, despite the structural similarities among the four molecules.

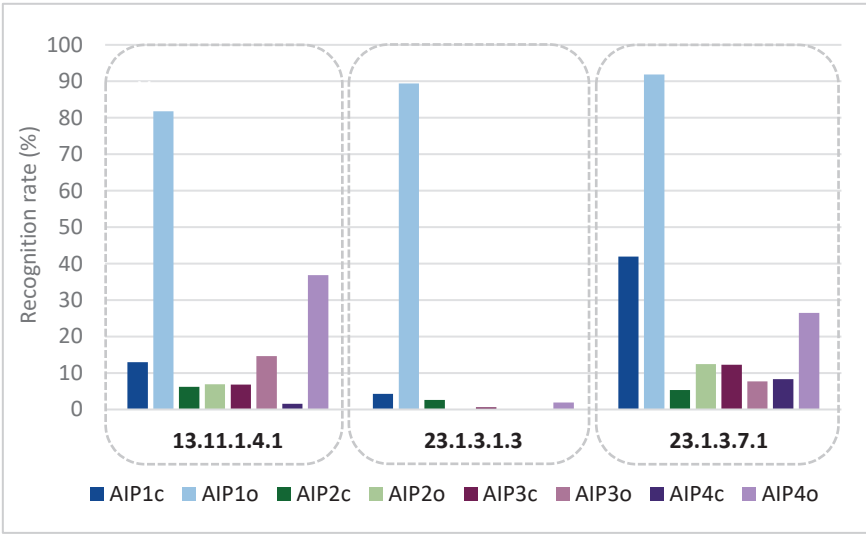

Figure 3.9. *Recognition profiles of the three final clones selected for AIP1 detection. For the indirect competitive ELISA, microplates were coated with 0.5 µg mL^{-1} of AIP1S-BSA bioconjugate, and the supernatants from the production of the selected clones were diluted 1/100 for the assay. The figure highlights the differential recognition capacities of the clones, focusing on their specificity for AIP1o.*

Figure 3.9 illustrates the recognition rates of the three selected clones against all AIPs. Clone 23.1.3.1.3 exhibited the highest specificity for detecting AIP1o. In

contrast, the other two clones (13.11.1.4.1 and 23.1.3.7.1) displayed some recognition of the other AIPs, particularly AIP4, with a stronger response to its linear form (AIP4o). This cross-recognition can be explained by the fact that AIP1 and AIP4 differ by only a single amino acid residue, making it more likely for the mAbs to recognize AIP4 more than the other two AIPs. Given that the mAbs primarily recognize AIP1o, it is reasonable to expect that their cross-recogniton with AIP4 would also be higher for its linear form (AIP4o). Despite their similarities, the two clones mentioned before differ in their recognition profiles for AIP1c and AIP1o, as previously discussed. These differences highlight their distinct binding properties and potential applications.

3.3.3.4 Search for AIP1c-recognizing clones

Although immunization was carried out with the AIP1 thiolactone bioconjugate (AIP1S-BSA), the screening process revealed a stronger recognition of the linear form, AIP1o. These results support our initial hypothesis, suggesting that under physiological conditions, AIPs are susceptible to hydrolysis and are predominantly found in their linear form.

However, since the functional form of AIPs is the closed form, a more exhaustive screening of previous cloning rounds was conducted to identify clones specifically recognizing AIP1c or, at least, displaying a stronger preference for the closed form over the linear form. To achieve this, a fusion was performed using mouse 3 (M3), as titration experiments indicated that this animal exhibited a higher recognition of the closed form in relation to the remaining mouse (M4). Additionally, four fusions were also performed using spleens extracted from rats.

Unfortunately, neither the mouse fusion (M3) nor the rat fusions (R1-R4) resulted successful. In a final attempt to produce mAbs capable of detecting AIP1c, the recognition profiles from previous cloning rounds were re-evaluated to identify and rescue promising hybridomas. These hybridomas were then subjected to additional rounds of cloning with the goal of isolating clones recognizing AIP1c.

Finally, despite all efforts, subsequent rounds of cloning resulted in AIP1c recognition rates of 30-40 %, while AIP1o was recognized to a greater extent (60-70 %). Based on these results, and considering that the previously selected clone

23.3.7.1 already exhibited an AIP1c recognition rate of 42 %, it was decided to proceed with the three previously selected final clones. The newly obtained clones were cryopreserved for potential use in future studies. Figure 3.10 shows a summary of the whole cloning and screening process to produce mAbs against AIP1 using the the hapten preserving the thiolactone (AIP1S-BSA) as immunogen.

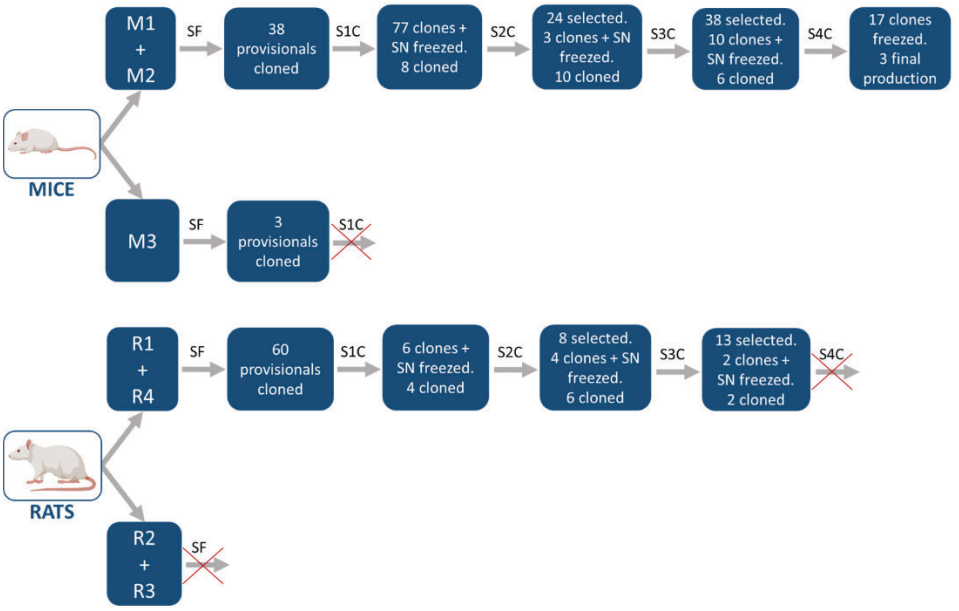

Figure 3.10. *Summary of the screening process for producing mAbs against AIP1 using the thiolactone hapten (AIP1S-BSA) strategy. The figure provides an overview of the screening strategy employed to develop mAbs targeting AIP1, guiding the selection and characterization of hybridomas with the desired recognition profiles. Abbreviations: SF: Screening after fusion; S1C, S2C, and S3C: Screening after the first, second, and third cloning rounds; SN: Supernatant.*

3.3.3.5 Final clones selected for AIP1 detection

In summary, after an exhaustive screening process, three final clones were selected for the production of mAbs against AIP1:

- 3 clones selected for AIP1 detection: 13.11.1.4.1 / 23.1.3.1.3 / 23.1.3.7.1

The selected clones were expanded and subsequently cultured for production in 10 Petri dishes, each containing 12 mL of medium. Following the cultivation, the yields obtained were 0.34 mg/mL for clone 13.11.1.4.1, 0.96 mg/mL for clone 23.1.3.1.3, and 0.85 mg/mL for clone 23.1.3.7.1. Then, they were purified using

Protein G affinity chromatography, a method that selectively binds to the Fc region of antibodies, ensuring a high level of purity. After purification, the antibodies were subjected to an indirect competitive ELISA to assess their binding affinity and specificity, ultimately determining the most promising candidate for further development (results discussed in Chapter 4).

3.3.4 PRODUCTION OF MONOCLONAL ANTIBODIES FOR AIP3

3.3.4.1 Immunization and antisera evaluation

In the same way as AIP1, 4 BALB/c female mice and 4 Winstar female rats (6-8 weeks old) were immunized, this time with 100 µg of AIP3S-KLH bioconjugate. Once completed the immunization period, the best candidates, both from rats and mice, were selected for spleen extraction and the subsequent production of mAbs, using hybridoma technology.

For the selection of animals from which spleens would be extracted for fusion, recognition of both AIP3c (closed form) and AIP3o (open form) was sought. The objective was to produce mAbs specific to each form of AIP3. To this end, blood samples collected from all mice and rats after 10 days after the third immunization (B3) were compared.

The selection of the animals that showed the best immune response was based on evaluating the avidity of the antisera from the final blood sample of each animal against the AIP3S-BSA bioconjugate using an indirect competitive ELISA.

As shown in Figure 3.11, the antibody titers in mice were significantly higher than those in rats, indicating a stronger immune response to the immunogen. For this reason, two mice were initially selected to begin the hybridoma production process. Mice 1 and 2 (M1 & M2) were chosen, with M1 exhibiting the highest overall signal and M2 showing the greatest recognition of AIP3c, the native and functional form.

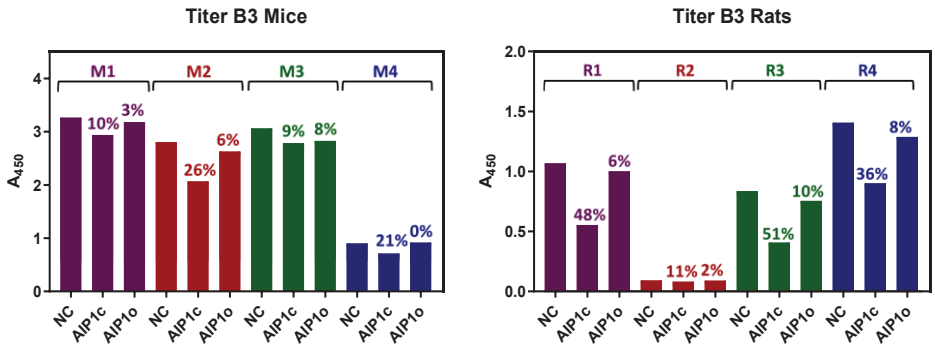

Figure 3.11. *Antibody titers in Blood 3 (B3) for mAb production against AIP3. The figure presents the antibody titers in B3 samples from the four immunized mice (M1–M4) on the left and the four immunized rats (R1–R4) on the right. The plates were coated with 1 µg mL^{-1} AIP3S-BSA. Blood samples were diluted 1:64,000 and analyzed under three conditions: B3 without competition (NC), B3 with competition using AIP1c, and B3 with competition using AIP1o. The competitors (AIP3c and AIP3o) were added at 1 µM. For each competitor, the percentage of inhibition is shown relative to the absorbance obtained under non-competitive conditions. This comparison highlights the differential recognition profiles of the antibodies in response to the closed (AIP3c) and open (AIP3o) forms of the antigen as well as the different stregths of the immune response.*

3.3.4.2 Screening for mAb selection

Table 3.3 shows the competition rate of AIP3c and AIP3o on the ELISA carried out with the antibodies produced by the hybridomas in the fourth cloning cycle.

Unlike the screening process for AIP1, all the hybridomas obtained for AIP3 exhibited a very similar recognition profile, with the exception of three of them. Notably, the majority of the clones were highly specific for AIP3c. Recognition of AIP3o was observed in only three clones, which predominantly showed higher recognition of AIP3c.These results were quite unexpected, as in the case of AIP1, the clones predominantly recognized the open form (AIP1o) and, despite extensive efforts, it was not possible to produce clones specifically capable of detecting the closed form (AIP1c).

43 clones were advanced to the fourth round of cloning and the three final clones were selected for the detection of AIP3 (highlighted in blue in Table 3.3). The three clones ultimately chosen for the production of mAbs against AIP3 were 2.5.2.2.3, 13.9.1.1.3 and 14.5.1.1.2.

Table 3.3. *Recognition percentages of AIP3c and AIP3o and absorbance values in the absence of competitors for the selected clones.*

Clone	Abs. (NC)	Competiton rate against AIP3c (%)	Competiton rate against AIP3o (%)
2.1.3.1.1	1.29	92.9	0
2.1.3.1.2	1.23	92.6	0
2.1.3.1.3	1.39	93.1	0
2.1.3.1.4	1.60	90.0	2.3
2.1.3.1.5	1.38	91.8	0
2.5.2.2.1	1.53	93.4	56.5
2.5.2.2.2	1.86	92.3	51.9
2.5.2.2.3	1.54	91.9	0
2.5.2.2.4	1.92	92.2	1.5
2.5.2.2.5	1.36	93.5	8.0
13.4.1.2.1	2.02	88.3	2.1
13.4.1.2.2	1.76	93.8	7.9
13.4.1.2.3	1.60	93.8	6.0
13.4 .1.2.4	1.70	92.8	0
13.4.1.2.5	1.79	92.7	0
13.4.1.2.6	1.66	94.1	4.3
13.4.1.2.7	1.44	94.1	12.8
13.4.1.2.8	1.39	85.4	5.9
13.4.1.2.9	1.71	92.9	2.4
13.4.2.2.1	1.91	91.8	0
13.4.2.2.2	1.81	93.3	0.9
13.4.2.2.3	1.81	94.0	5.3
13.4.2.2.4	1.47	93.8	0
13.4.2.2.5	1.73	92.9	0
13.4.2.2.6	1.68	94.7	74.5
13.9.1.1.1	1.76	94.4	11.1
13.9.1.1.2	1.74	93.8	2.2
13.9.1.1.3	1.70	93.9	1.8
13.9.1.1.4	1.07	94.1	5.9
13.9.1.1.5	1.27	93.7	0
14.5.1.1.1	1.09	92.7	0
14.5.1.1.2	1.82	89.3	0
14.5.1.1.3	1.90	91.1	6.5
14.5.1.1.4	1.56	92.9	9.8
14.5.1.1.5	1.32	90.5	0
14.5.1.1.6	1.29	88.8	0
14.5.3.1.1	1.91	59.6	0
14.5.3.1.2	1.89	86.4	0
14.5.3.1.3	1.78	70.8	0
14.5.3.1.4	2.05	70.8	0
14.5.3.1.5	1.88	79.8	8.4
14.5.3.1.6	2.04	81.4	6.0
14.5.3.1.7	1.89	81.4	6.0

The table presents data for 43 hybridomas from the fourth cloning round. Plates were coated with AIP3S-BSA (1 µg mL^{-1}), and competitors (AIP3c and AIP3o) were added at 1 µM. A color scale indicates analyte recognition, ranging from dark green (high recognition) to white (no recognition). The competition rate, expressed as a percentage, was calculated based on absorbance reduction due to competition. Final selected clones are marked in blue.

Following the final selection, the recognition profiles of the three selected clones were evaluated against all four AIPs of *S. aureus* in both their closed and open forms. As presented in Figure 3.12, this study revealed a completely unexpected recognition profile. While the three selected clones were highly specific for AIP3c and did not recognize AIP3o, it was surprising to find that they exhibited significant recognition of other AIPs, specifically AIP1 and AIP4. Since all three clones displayed the same recognition pattern, it was decided to proceed with their purification and subsequent characterization. The aim was to further enhance their specificity for AIP3 through additional optimization and analysis.

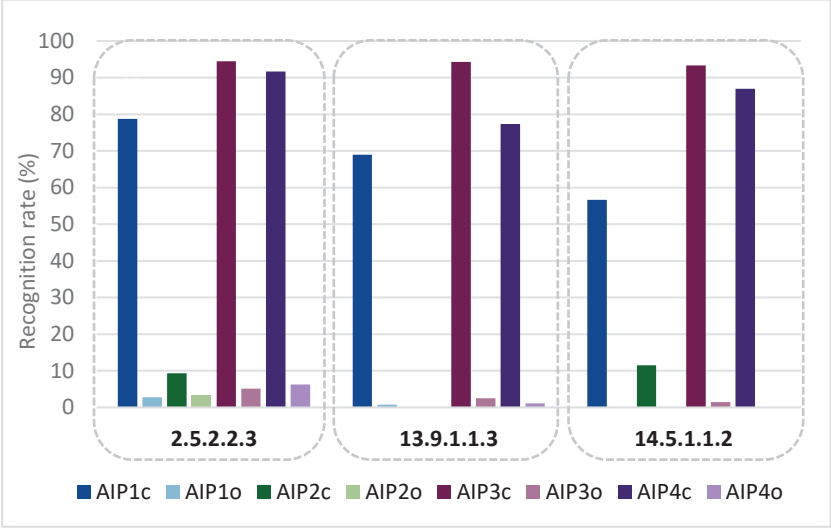

Figure 3.12. *Recognition profiles of the three final clones selected for AIP3 detection. For the indirect competitive ELISA, microplates were coated with 0.5 µg mL^{-1} of AIP3S-BSA bioconjugate, and the supernatants from the production of the selected clones were diluted 1/100 for the assay. The figure shows better recognition of AIP3c rather than AIP3o and an unexpected recognition profile of AIP1c ad AIP4c.*

Later, upon observing that the selected animals predominantly recognized AIP3c, it was decided to perform two additional fusions to identify clones capable of detecting AIP3o. Since attempts with mice had been unsuccessful in finding clones that recognized AIP3o, it was decided to try using rats instead. In this instance, rats 1 and 4 (R1 & R4) were selected for spleen extraction to proceed with the fusion process.

Despite extensive efforts, no clones specific to AIP3o could be isolated. Based on these results, the decision was made to continue with the three previously selected clones. Figure 3.13 presents a simplified diagram of the meticulous

screening process conducted for the selection of clones producing antibodies against AIP3c and AIP3o.

As a result, the thorough screening process carried out led to the selection of the following three final clones for the production of mAbs against AIP3:

- 3 clones selected for AIP3 detection: 2.5.2.2.3 / 13.9.1.1.3 / 14.5.1.1.2

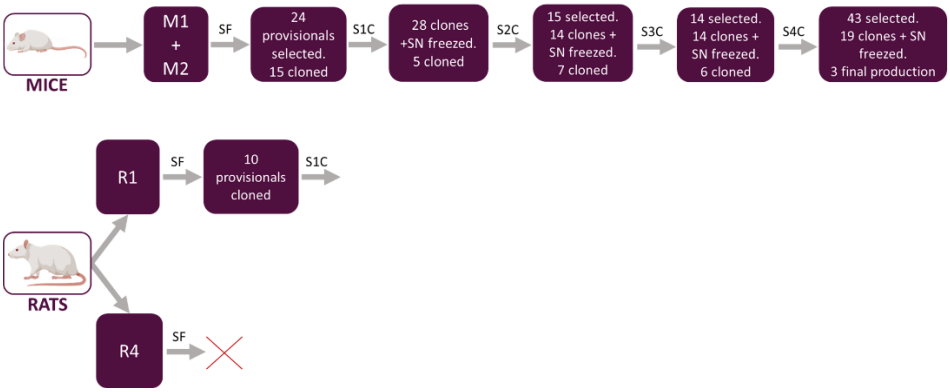

Figure 3.13. *Summary of the screening process for producing mAbs against AIP3 using the thiolactone hapten (AIP3S-KLH) strategy. The figure provides an overview of the screening strategy employed to develop mAbs targeting AIP3, guiding the selection and characterization of hybridomas with the desired recognition profiles. Abbreviations: SF: Screening after fusion; S1C, S2C, and S3C: Screening after the first, second, and third cloning rounds; SN: Supernatant.*

3.3.5 PRODUCTION OF POLYCLONAL ANTIBODIES FOR AIP1 & AIP2

The results obtained from the production of mAbs against AIP1 and AIP3 highlighted the inherent challenges in selecting antibodies with high specificity for each of the two structural forms (open and closed) of the AIPs. This difficulty in achieving form-specific recognition underscored the limitations of the monoclonal approach for this application.

Given these challenges, and considering the previous successful outcomes in our group with the production of pAbs targeting both structural forms, we decided to revise our strategy and shift towards the production of pAbs. This approach was expected to provide a broader epitope coverage and improve the likelihood of effective detection across the different structural forms of AIPs.

Since no clones specifically recognizing AIP1 in its thiolactone form nor AIP3 in its open forms could be isolated during the mAb production process, rabbits were immunized this time with the aim of producing pAbs. Likewise, in view of the laborious work involved in the production of mAbs and the difficulty in finding the desired recognition profiles, it was decided to produce pAbs as well for the detection of AIP2.

In his doctoral thesis, Dr. Montagut successfully produced pAbs against AIP4 and implemented them to 2 different ELISA assays, one specific for AIP4c and the other AIP4o. Based on these precedents, this approach aimed to determine whether similar results could be reproduced, with the goal of obtaining pAbs capable of specifically recognizing AIP1c, AIP3o, AIP2c and AIP2o.

With that purpose, firstly pAbs were produced for AIP1 and AIP2 to evaluate the effectiveness of the pAb production strategy in raising antibodies that recognise their linear and cyclic forms. To achieve this, New Zealand White rabbits were immunized using the same immunogens previously employed in the production of mAbs (AIP1S-KLH and AIP2S-KLH). Two rabbits were immunized with each immunogen (AIP1: 415-416; AIP2: 417-418), and antibodies were produced following a meticulously designed protocol that is routinely implemented within our research group (see Section 8.7.2).

The titers of the antisera from all four rabbits exhibited a very strong signal. The final blood samples (FBs) were tested against their corresponding AIP, both in the open and closed forms, to evaluate their recognition capabilities and assess competition. All the pAbs produced showed a predominant recognition of the open form. In the case of AIP1, the final antiserum from rabbit 415 (As415FB) demonstrated low competition, while As416 exhibited higher competition. The pAbs produced against AIP2 showed greater recognition overall, displaying high sensitivity to AIP2o (see Figure 3.14).

Surprisingly, all pAbs generated against AIP1 and AIP2 showed a stronger recognition of the open form of their corresponding AIP compared to the closed form. Based on these results, the production of mAbs for AIP3 was considered an exception, as it specifically detected the closed form without cross-reactivity with the open form. Aside from this particular case, both the mAbs and pAbs produced generally recognized the open form of the AIPs more effectively.

Moreover, the specific ELISAs for AIP4c and AIP4o that were successfully developed previously in our group by producing pAbs against AIP4S-KLH revealed an interesting observation: out of the four rabbits immunized, only one showed competition with AIP4c in the fourth partial blood sample (As380B4). This led to the hypothesis that, under physiological conditions, the majority of AIPs exist in their linear form. Additionally, due to the cyclic form being highly labile, given its lactone structure, these molecules can easily linearize.

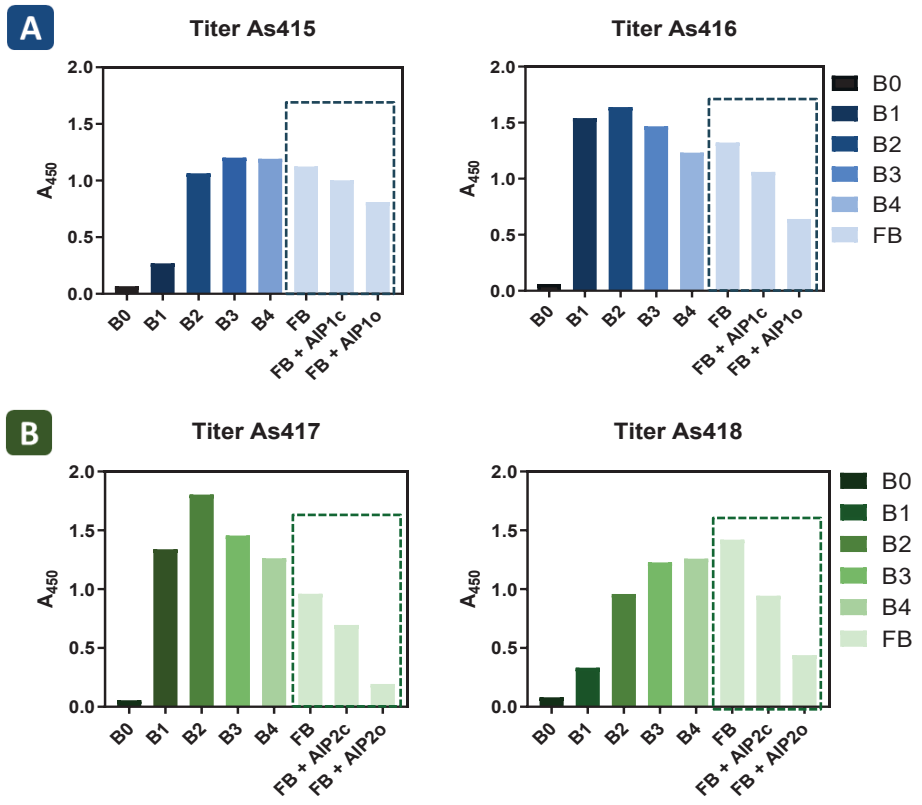

***Figure 3.14**. Titer analysis of antisera produced against A) AIP1S-KLH and B) AIP2S-KLH in four rabbits: As415 & As416 for AIP1, and As417 & As418 for AIP2. The figure displays the absorbance measured at 450 nm for the antisera obtained after each of the four immunizations (B1-B4) and the final blood sample (FB) collected at the end of the immunization period, compared to the preimmune blood sample (B0). Additionally, the figure shows the competition assays of the FBs of each rabbit against their corresponding AIP, in both linear and cyclic forms. The bioconjugates were coated at 1 µg mL^{-1}: A) AIP1S-BSA; B) AIP2S-BSA. The competitors were added at 1 µM. All samples were diluted 1/32,000.*

3.4 ANTIBODY PRODUCTION BASED ON THE USE OF LINEAR AIP HAPTENS AS IMMUNOGENS

Subsequent studies analyzing AIPs in culture medium revealed that a portion of the AIPs exists in their linear form. For this reason, the decision was made to directly focus on producing antibodies targeting the open form of AIPs. As will be discussed in later chapters, the detection of linear forms appears to be the most effective strategy. This approach is supported by the observation that linear forms are present in culture samples, and with a simple hydrolysis treatment, all AIP content can be converted into the linear form. This ensures that no AIPs are left unquantified.

The production of antibodies against the linear forms of AIPs has never been addressed before. Therefore, if antibodies generated through this strategy exhibit high avidity and specificity toward the linear form, they could be considered for patenting.

To address this, a strategic shift was made to produce pAbs by immunizing with haptens derived from the linear forms of AIPs (AIPL-haptens). This approach was chosen to enhance the likelihood of generating antibodies that specifically recognize the more stable and probably predominant linear forms of the AIPs, rather than the cyclic ones. By focusing on the linear structures, the aim was to develop antibodies with greater specificity and sensitivity, optimizing the overall effectiveness of antibody production for the detection of open forms.

3.4.1 PREPARATION OF IMMUNOGENS AND COATING ANTIGENS

The production of antibodies for the linear forms required the synthesis of the corresponding haptens and bioconjugated. The strategy followed is summarized in the Figure 3.15.

The haptens were designed introducing the spacer arm in the N-terminal side from the peptidic chain maintaining the hydrophilic nature of the spacer arm with a chemical entity of the peptidic chain. We decided to use the amine functional group as a chemical coupling entity to couple to a carrier protein. No

primary amines are in any AIP1–4, so it will allow the selective coupling by the N-terminal group.

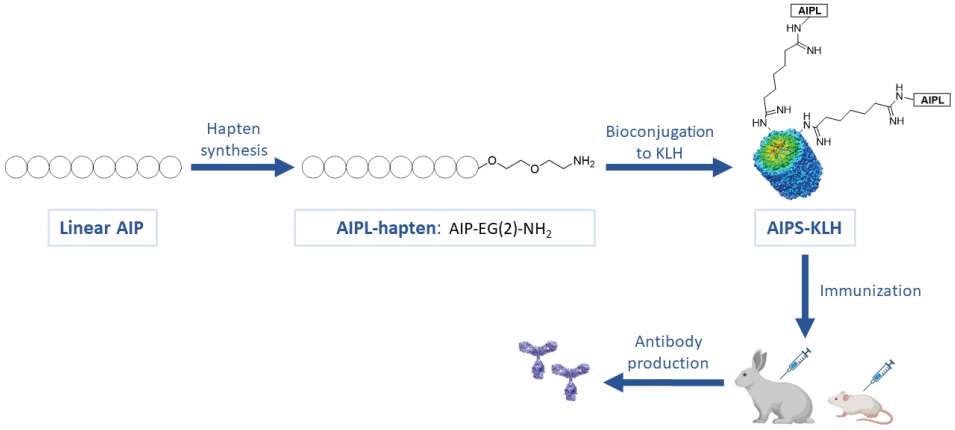

Figure 3.15. *Schematic representation of the process for antibody production against S. aureus AIPs using linear AIP haptens (AIPL-haptens) as immunogens.*

The synthesis of the linear AIPs (see Figure 3.6) and their respective haptens (AIPL-haptens) was carried out by the MS4N group. The chemical structures of AIPL-haptens are shown in Figure 3.16.

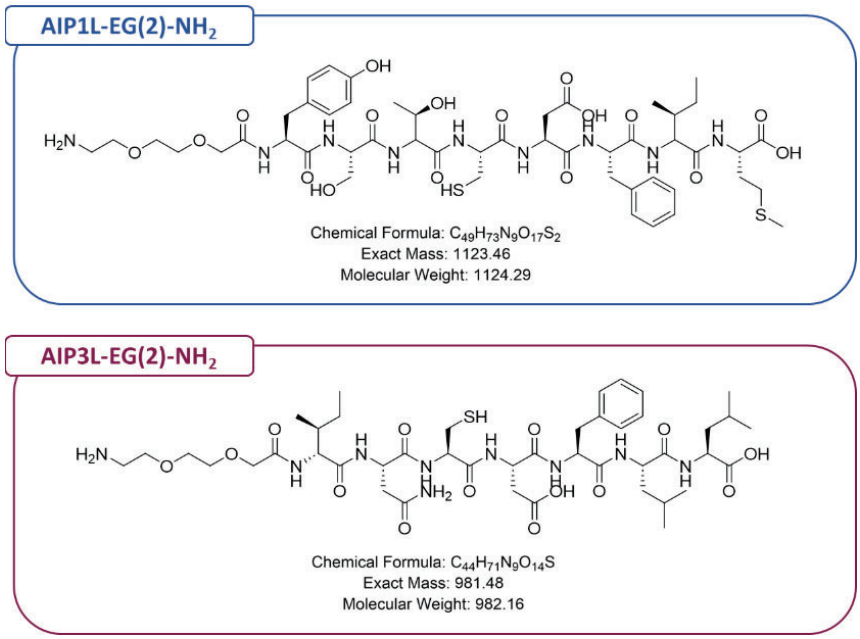

Figure 3.16. *Chemical structures of the linear haptens (AIPL-haptens) for AIP1 and AIP3.*

One of the potential drawbacks that can occur working with the linear forms of AIPs is the sulfur atom from cysteine residues tends to oxidize, leading to the formation of disulfide bonds. This oxidation process causes the molecules to form dimers, which can complicate the production, stability, and specificity of antibodies targeting these linear forms. Such structural changes may alter the epitope presentation, potentially affecting the immune response and antibody recognition. To get around this problem, we ensured that the monomer was form during the synthetic process, and also, preserve the hapten in dry and inert condition to avoid the oxidation.

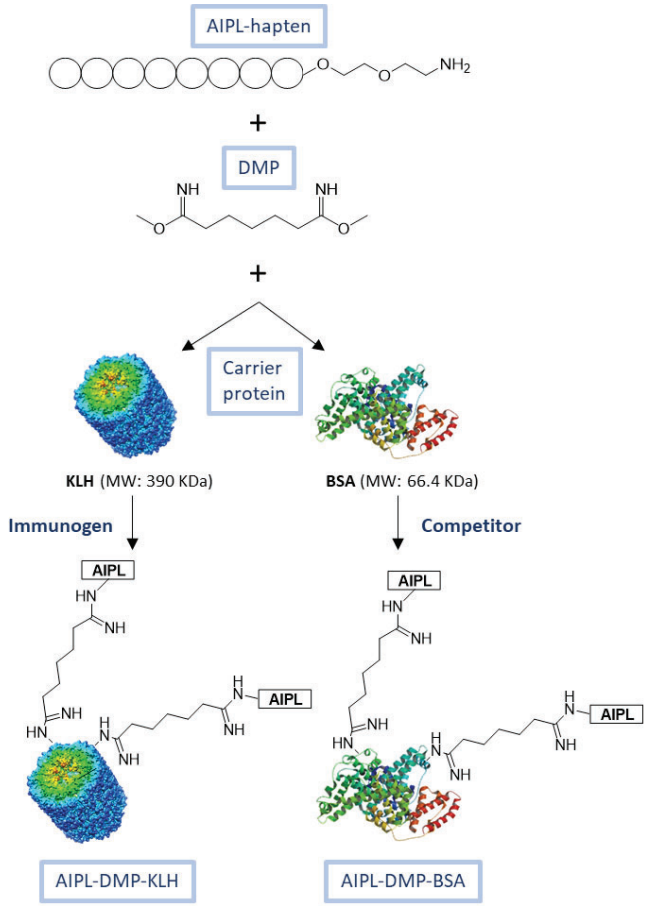

Figure 3.17. *Bioconjugation of AIPL-haptens to carrier proteins. AIPL-haptens were synthetized for each linear AIP (1–4) by the addition of a spacer arm constituted by two ethylene glycol units with a terminal active amino group (EG(2)-NH_2). Then, the haptens were conjugated to two different carrier proteins using DMP as a crosslinker: Keyhole limpet hemocyanin (KLH) to give rise to the immunogens and to Bovine Serum Albumin (BSA) to constitute the competitor antigens.*

The initial strategy used to couple the AIPL to the carrier proteins were using an homobifunctional crossliners like dimethyl pimelimidate (DMP), which specifically reacts with amino groups forming stable amide bonds. The reaction conditions were carefully optimized, regulating the molar ratios of reactants, adjusting the pH, and optimizing the reaction time to ensure the specific formation of the AIPL-DMP-protein conjugate. As in previous approaches, haptens were bioconjugated to two different carrier proteins: KLH and BSA (see Figure 3.17). The HDs of the AIP1L-DMP-BSA and AIP3L-DMP-BSA are shown in One of the potential drawbacks that can occur working with the linear forms of AIPs is the sulfur atom from cysteine residues tends to oxidize, leading to the formation of disulfide bonds. This oxidation process causes the molecules to form dimers, which can complicate the production, stability, and specificity of antibodies targeting these linear forms. Such structural changes may alter the epitope presentation, potentially affecting the immune response and antibody recognition. To get around this problem, we ensured that the monomer was form during the synthetic process, and also, preserve the hapten in dry and inert condition to avoid the oxidation. .

Table 3.4. *Data on the hapten densities AIPL bioconjugates.*

Bioconjugate	HD
AIP1L-DMP-BSA	8
AIP3L-DMP-BSA	4

Hapten densities (HDs) of BSA conjugates were determined using MALDI-TOF MS analysis.

3.4.2 PRODUCTION OF POLYCLONAL ANTIBODIES FOR AIP1 & AIP3

The goal of producing antibodies by immunizing with the linear forms of AIPs was, firstly, to obtain antibodies specific for AIP3o. As previously discussed, no clones with this recognition profile were identified during the screening process for mAbs. Additionally, the production of pAbs for AIP1o was also conducted because, at this stage, the characterization of mAbs for AIP1 was already in process, and it was observed that the IC_{50} in the ELISA was not as low as expected. For this reason, this strategy was adopted to achieve greater sensitivity.

Once the bioconjugates of the linear forms were synthesized, four New Zealand White rabbits were immunized to generate the corresponding pAbs. For that purpose, two of the rabbits (427, 428) were immunized with AIP1, and the other two (429, 430) with AIP3.

All the rabbits responded well to the new immunogen, producing high-titer pAbs and demonstrating a robust immune response. Unfortunately, one of the rabbits (427) had to be euthanised due to paralysis.

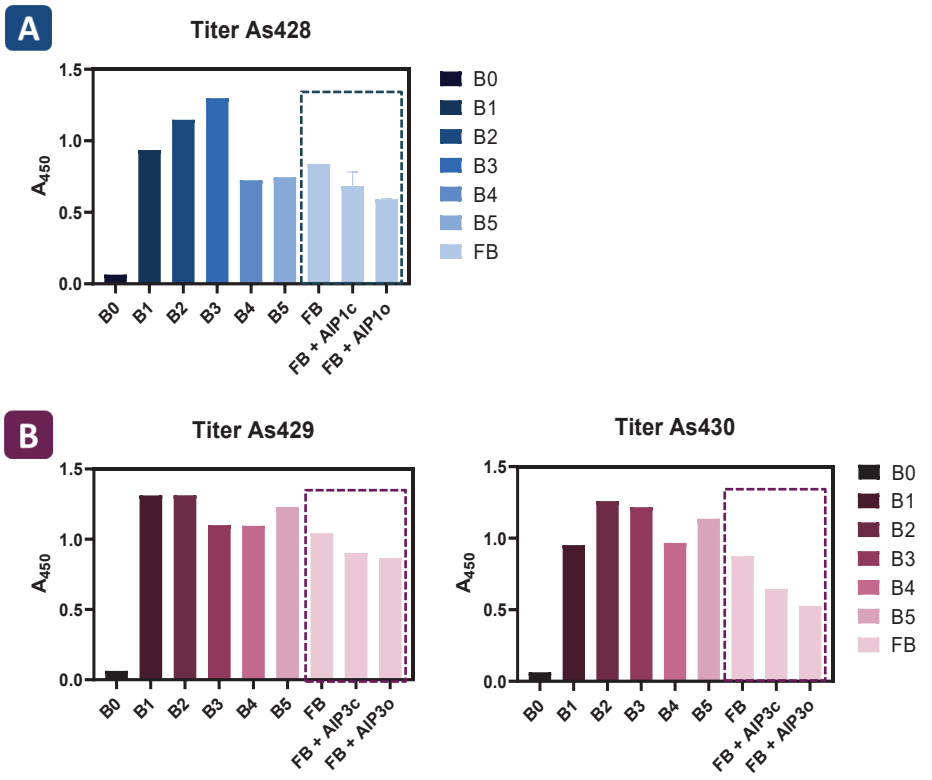

Figure 3.18. *Titer analysis of antisera produced against A) AIP1L-DMP-KLH and B) AIP3L-DMP-KLH in three rabbits: As428 for AIP1, and As429 & As430 for AIP3. The figure displays the absorbance measured at 450 nm for the antisera obtained after each of the four immunizations (B1-B4) and the final blood sample (FB) collected at the end of the immunization period, compared to the preimmune blood sample (B0). Additionally, the figure shows the competition assays of the FBs of each rabbit against their corresponding AIP, in both linear and cyclic forms. The bioconjugates were coated at 1 µg mL^{-1}: A) AIP1L-DMP-BSA; B) AIP2L-DMP-BSA. The competitors were added at 1 µM. All samples were diluted 1/32,000.*

Figure 3.18 displays the titers of the antisera collected and the competition assays of the final blood samples with both the cyclic and linear forms of the corresponding AIP in each case. Although the titers were high, there was minimal competition observed, with almost no recognition of the closed forms and slightly higher recognition of the open forms.

Given the lack of competition observed, our hypothesis was that antibodies had been produced against DMP, rather than specifically against the target AIPs. Since these are pAbs, it is possible that a fraction of the antibodies was, indeed, recognizing the linear form of the AIP, while another fraction was binding to the DMP spacer. This heterogeneity in the antibody population could explain the limited competition observed in the assays, as the presence of antibodies against the spacer could mask the detection of the target analytes.

To address this issue and enhance the competition results, different competitors were tested in the assays. The intention was to introduce heterology in the synthesis method by using competitors that were not synthesized with DMP strategy. By doing so, we aimed to increase the sensitivity of the immunochemical assays, ensuring that the recognition of our target analytes was not masked by CR with the DMP spacer. This strategy was designed to refine the specificity of the antibodies for the AIPs in their linear forms, improving the overall performance of the assays.

In the case of AIP1, we tested two different bioconjugates as competitor antigens to introduce heterology both in the conjugation method and in the analyte structure. The first bioconjugate, AIP1S-BSA, was designed to introduce heterology in the conjugation method, while the second, AIP4S-BSA, introduced heterology both in the conjugation method and in the analyte itself, different from AIP1 in just one amino-acid residue. However, despite these efforts, we were unable to achieve increased competition with either of these bioconjugates, indicating that the antibodies produced were not effectively recognizing the linear form of AIP1 in the presence of these competitors.

Since we already produced a mAb with increased sensitivity for identifying AIP1o, we decided to move forward with the immunoassay development employing the mAb 23. Consequently, the pAb428 was discarded from further analysis. This decision was made to ensure the highest possible sensitivity and specificity for AIP1o detection.

In contrast, for AIP3, we used the conjugate AIP3S-BSA, which was synthesized without DMP. This trial resulted encouraging, as it enabled competition with AIP3o (see Figure 3.19).

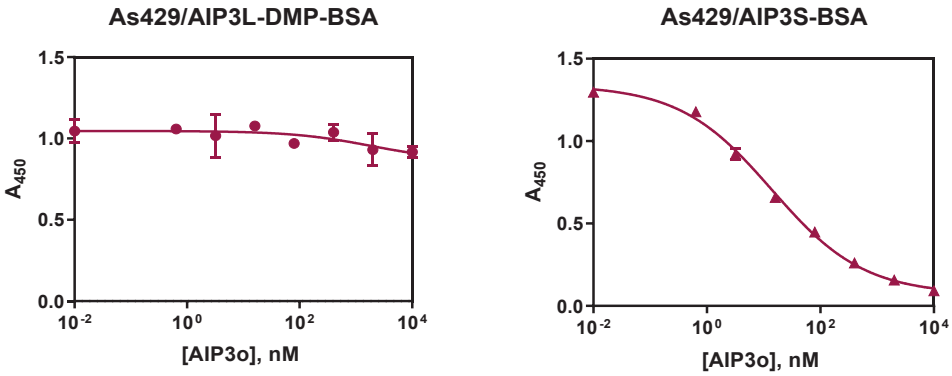

Figure 3.19. *Comparison of calibration curves for the ELISA developed with pAb As429 for the detection of AIP3o. Under homologous conditions (AIP3L-DMP-BSA), no competition is observed. In contrast, under heterologous conditions (AIP3S-BSA), AIP3c competes, resulting in a highly sensitive ELISA for its detection (IC_{50} 13.96 nM).*

Therefore, we successfully generated antibodies specifically targeting AIP3o, thereby completing the detection of all analytes in our target set. Given this achievement, we completed the entire set of antibodies required to recognize each of the four AIP variants produced by *S. aureus*.

Once the the antibody production process was accomplished, the next step was antibody implementation in the development of specific ELISAs. This phase involved optimizing the assay conditions to ensure reliable and sensitive detection of each AIP variant, thereby enabling the efficient detection of these bacterial signaling molecules.

3.5 SUMMARY OF ANTIBODIES RAISED AGAINST *S. AUREUS* AIPS

Figure 3.20 summarizes the antibodies that were ultimately produced and selected for subsequent implementation in the development of ELISAs. As a result of the extensive work discussed in this chapter, antibodies were successfully produced against the remaining target analytes. However, generating antibodies against both the open and closed forms of the AIPs proved challenging. The strategy of producing antibodies targeting the open forms of

the AIPs was determined to be the most optimal. This approach allows for the detection of both forms when the sample is subjected to hydrolysis, ensuring that all AIP content is converted into the linear form.

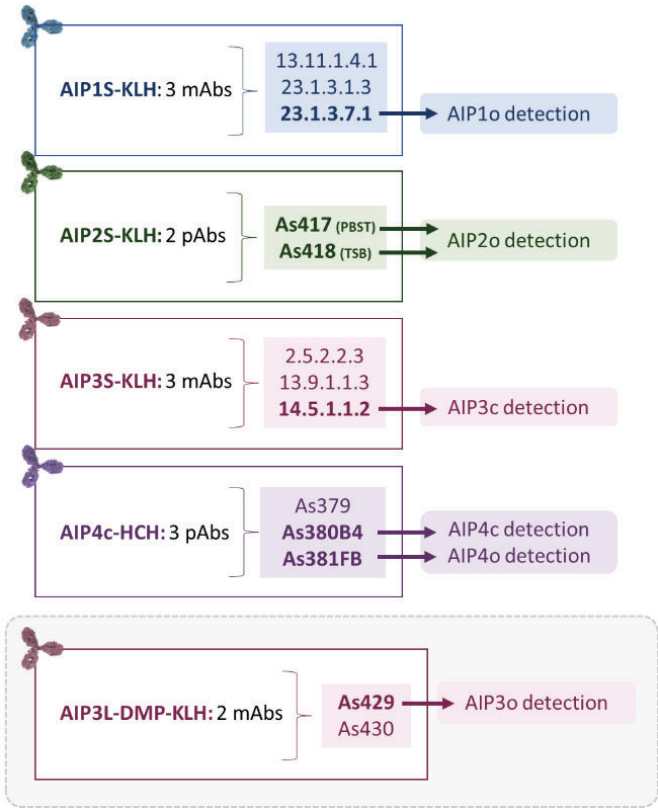

Figure 3.20. *Antibodies produced against S. aureus AIPs and the final clones selected for each target molecule. The upper section of the figure illustrates the antibodies produced for AIPs 1–4 of S. aureus using the strategy with thiolactone-structure haptens (AIPS-haptens). The antibodies against AIP4 were produced by Dr. Enrique José Montagut. The lower section highlights in gray the antibodies produced against AIP3 using the strategy with linear-structure haptens (AIPL-haptens). For each case, it is indicated whether mAbs or pAbs were produced. The final clone selected for ELISA implementation for each target molecule is shown in bold.*

3.6 CHAPTER CONTRIBUTIONS

Antibodies were successfully produced for the detection of the remaining three AIPs in *S. aureus* (antibodies for AIP4 were previously produce in our research group), significantly expanding the tools available for both diagnostic and therapeutic applications. The ability to detect all four types of AIPs opens numerous possibilities. As a diagnostic approach, these antibodies can be

employed in highly sensitive assays to monitor bacterial communication and virulence factor production in clinical samples, aiding in the early detection and management of infections. Therapeutically, these antibodies can be used to inhibit QS systems through QQ strategies, potentially reducing bacterial virulence and preventing the progression of infections. The development of these antibodies thus represents a major advancement in the field, providing a comprehensive set of tools for both the study and control of *S. aureus* and its associated infections.

3.7 BIBLIOGRAPHY

1. Lipman, N. S.; Jackson, L. R.; Trudel, L. J.; Weis-Garcia, F., Monoclonal Versus Polyclonal Antibodies: Distinguishing Characteristics, Applications, and Information Resources. *ILAR Journal* **2005,** *46* (3), 258-268.
2. Posner, J.; Barrington, P.; Brier, T.; Datta-Mannan, A., Monoclonal Antibodies: Past, Present and Future. In *Concepts and Principles of Pharmacology: 100 Years of the Handbook of Experimental Pharmacology*, Barrett, J. E.; Page, C. P.; Michel, M. C., Eds. Springer International Publishing: Cham, 2019; pp 81-141.
3. Aboul-Ella, H.; Gohar, A.; Ali, A. A.; Ismail, L. M.; Mahmoud, A. E. E.-R.; Elkhatib, W. F.; Aboul-Ella, H., Monoclonal antibodies: From magic bullet to precision weapon. *Molecular Biomedicine* **2024,** *5* (1), 47.
4. Ang, G. Y.; Chan, K. G.; Yean, C. Y.; Yu, C. Y., Lateral Flow Immunoassays for SARS-CoV-2. *Diagnostics (Basel)* **2022,** *12* (11).
5. Zahavi, D.; Weiner, L., Monoclonal Antibodies in Cancer Therapy. *Antibodies* **2020,** *9* (3), 34.
6. Hafeez, U.; Gan, H. K.; Scott, A. M., Monoclonal antibodies as immunomodulatory therapy against cancer and autoimmune diseases. *Current Opinion in Pharmacology* **2018,** *41*, 114-121.
7. Adan, A.; Alizada, G.; Kiraz, Y.; Baran, Y.; Nalbant, A., Flow cytometry: basic principles and applications. *Critical Reviews in Biotechnology* **2017,** *37* (2), 163-176.
8. Sehlin, D.; Fang, X. T.; Cato, L.; Antoni, G.; Lannfelt, L.; Syvänen, S., Antibody-based PET imaging of amyloid beta in mouse models of Alzheimer's disease. *Nature Communications* **2016,** *7* (1), 10759.
9. Ascoli, C. A.; Aggeler, B., Overlooked Benefits of using Polyclonal Antibodies. *BioTechniques* **2018,** *65* (3), 127-136.
10. Schwickart, M.; Vainshtein, I., Immunoassays. In *Nijkamp and Parnham's Principles of Immunopharmacology*, Parnham, M. J.; Nijkamp, F. P.; Rossi, A. G., Eds. Springer International Publishing: Cham, 2019; pp 243-253.
11. Pillai-Kastoori, L.; Schutz-Geschwender, A. R.; Harford, J. A., A systematic approach to quantitative Western blot analysis. *Analytical Biochemistry* **2020,** *593*, 113608.
12. Oumarou Hama, H.; Aboudharam, G.; Barbieri, R.; Lepidi, H.; Drancourt, M., Immunohistochemical diagnosis of human infectious diseases: a review. *Diagnostic Pathology* **2022,** *17* (1), 17.

13. Liu, L.; Qing, Y.; Shoaib, N.; Di, R.; Liu, H.; Li, Y.; Hu, Y.; Huang, Y.; Yu, G., Preparation of Polyclonal Antibody against ZmBT1 Protein and Its Application in Hormone-Regulated Starch Synthesis. *Agronomy* **2023,** *13* (7), 1805.
14. Otto, M., Critical Assessment of the Prospects of Quorum-Quenching Therapy for Staphylococcus aureus Infection. *International Journal of Molecular Sciences* **2023,** *24* (4), 4025.
15. Park, J.; Jagasia, R.; Kaufmann, G. F.; Mathison, J. C.; Ruiz, D. I.; Moss, J. A.; Meijler, M. M.; Ulevitch, R. J.; Janda, K. D., Infection Control by Antibody Disruption of Bacterial Quorum Sensing Signaling. *Chemistry & Biology* **2007,** *14* (10), 1119-1127.
16. Kim D. Janda (La Jolla, C., Gunnar F. Kaufmann (San Diego, CA), Junguk Park (San Diego, CA) US Patent ANTIBODY-MEDIATED DISRUPTION OF QUORUM SENSING IN BACTERIA. Feb 16, 2017.
17. Koniev, O.; Wagner, A., Developments and recent advancements in the field of endogenous amino acid selective bond forming reactions for bioconjugation. *Chem Soc Rev* **2015,** *44* (15), 5495-551.

4 ELISA DEVELOPMENT

4.1 CHAPTER PRESENTATION

Chapter 4 focuses on the development of immunochemical diagnostic techniques in an ELISA format from the previously described immunoreagents. The chapter begins by comparing the most commonly used ELISA formats and identifies the indirect competitive format as the optimal choice for the detection of AIPs. The goal is to develop and optimize these ELISAs to elucidate the role of these signaling molecules in the pathogenesis of *S. aureus*, as well as to evaluate their potential as biomarkers for diagnostic purposes.

Then, the chapter will provide a detailed characterization of the immunoreagents used in each assay, selecting the best combinations and optimal concentrations to achieve the highest sensitivity and specificity.

The chapter then will evaluate the performance of each developed ELISA against various physicochemical parameters to assess their robustness and establish the optimal procedural conditions. Finally, the accuracy and specificity of the assays will be studied, and the analytical characteristics that define each assay are presented. The steps and structure of the chapter are illustrated in Figure 4.1.

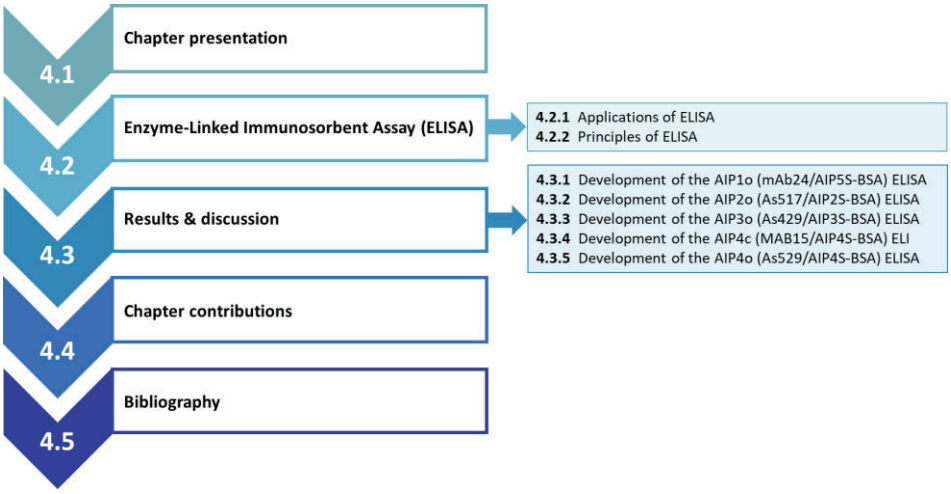

Figure 4.1. *Structure of Chapter 4.*

4.2 ENZYME-LINKED IMMUNOSORBENT ASSAY (ELISA)

Modern biomedical research and diagnostic procedures rely significantly on immunochemical techniques, which use the specificity of **antigen-antibody interactions** to identify and measure a wide range of biological molecules. They can be applied in an assort of tests and applications, such as flow cytometry, immunohistochemistry, Western blotting, and immunofluorescence, each with specific benefits for particular types of analysis. Among them, **ELISA** stands out for its versatility, sensitivity, and ease use. This technique has emerged as a gold standard for the accurate quantification multiple analytes. Because of its capacity to provide accurate and reproducible data, ELISA is an essential tool both in research and clinical settings[1].

ELISA is a widely used analytical technique for detecting and quatifying a broad range of antigens, including proteins (such as antibodies, membrane proteins, or glycoproteins), peptides, small molecules, and even complex organisms like viruses and bacteria. It is based on the precise interaction between antibodies and their specific antigens, allowing for targeted detection. In this technique, an enzyme is conjugated to an antibody or antigen, which, upon binding to its target, produces a measurable signal, often through a color change, fluorescence, or chemiluminescence. This signal indicates the presence and amount of the target molecule, making ELISA both specific and quantifiable[2].

4.2.1 APPLICATIONS OF ELISA

Its high sensitivity allows the detection of even trace amounts of analytes, together with its specificity, which ensures accurate identification of target molecules, ELISA has become an indispensable tool in various fields. Its versatility and relatively simple procedure make it highly suitable for applications in biotechnology, research, and clinical diagnostics. Furthermore, the high adaptability of this technique to different assay formats further expands its potential applications, solidifying its role as a powerful technique in both laboratory research and medical testing.

ELISA is extensively utilized in **food safety and environmental monitoring**to detect contaminants such as pesticides, mycotoxins, and other pollutants in

water, soil, and food products. Its high sensitivity and specificity make it an invaluable tool for monitoring and ensuring safety standards. It has been effectively applied to monitor pesticide residues in various matrices. For instance, ELISA has been applied to detect organophosphate **pesticides** in agricultural products, offering a rapid alternative to chromatographic methods[3, 4]. The effectiveness of ELISA in identifying carbamate residues in water and soil samples has also been demostrated, demostrating its versatility across different matrices[5]. These applications highlight the value of ELISA technique in monitoring pesticide contamination.

Mycotoxins, toxic secondary metabolites produced by fungi, pose significant health risks. ELISA is widely employed for their detection due to its rapidity and ease of use. Multiple studies highlight the application of ELISA in detecting mycotoxins like aflatoxins and ochratoxin A in food products, emphasizing its role in food safety[6, 7]. Beyond pesticides and mycotoxins, ELISA is used to detect various environmental **pollutants**. For example, the technique has been applied to monitor antibiotic residues in food[8, 9], water[10, 11] and soil[12, 13], ensuring compliance with environmental regulations.

In the **food industry**, ELISA is commonly employed to identify food **allergens** such as gluten, peanuts and soy[14-16]. It is also used to detect **foodborne pathogens** like *Salmonella*[17] and *Listeria monocytogenes*[18], in order to guarantee their safety. Moreover, ELISA can be applied to identify **adulterants**, such as undeclared meat species in processed foods, to ensure they meet quality standards[19].

Additionally, ELISA is widely used in **crop science** and **agricultural research**, contributing to disease management and ensuring the quality and safety of agricultural products. It is a valuable tool for identifying **plant pathogens**, enabling early detection and management of diseases. For instance, the European and Mediterranean Plant Protection Organization (EPPO) has established ELISA protocols for detecting bacterial pathogens in plants, such as *Xanthomonas campestris* and *Ralstonia solanacearum*, highlighting its effectiveness in plant disease diagnostics[20]. Another extended application is the detection **genetically modified organisms** (GMOs) in crops by identifying specific proteins expressed due to genetic modifications[21], facilitating compliance with regulatory requirements.

ELISA is also a pivotal analytical technique in **biotechnology** and **pharmaceutical research**, offering precise quantification and detection of various biomolecules. Its applications span several areas, such as the screening potential **drug candidates** by quantifying target proteins, enzymes, or receptors[22]. For instance, it has been employed to measure the binding affinity of monoclonal antibodies to specific antigens, facilitating the selection of therapeutic candidates[23].

In **pharmacokinetic studies**, ELISA quantifies drug concentrations in biological matrices, aiding in understanding absorption, distribution, metabolism, and excretion profiles. This is crucial for determining appropriate dosing regimens and ensuring therapeutic efficacy[24], as well as to evaluate immune responses in vaccine development[25]. This technique is also employed in the **quality control** of **biopharmaceuticals** to assess product consistency and potency. It quantifies specific proteins or contaminants, ensuring that products meet strict regulatory standards before market release[26].

ELISA constitutes a crucial tool for detecting disease-related biomarkers in **clinical diagnosis**[27]. It is suitable for measuring **hormone levels** associated with various conditions. For example, it is employed to detect and measure levels of thyroid hormones, specifically T4, T3 and TSH, which are critical for diagnosing and managing thyroid disorders[28]. It also serves to control Anti-Müllerian Hormone (AMH) levels to assess ovarian reserve in women, providing insights into fertility potential[29] and Luteinizing Hormone (LH), to assess ovulation timing, diagnose fertility issues, and evaluate reproductive health, particularly in conditions like polycystic ovary syndrome and menopause[30].

Additionally, ELISA is used to measure other markers such as the ones related with **tumors**, enabling early intervention. Some examples are carcinoembryonic antigen (CEA) highly associated with colorectal cancer[31], prostate-specific antigen (PSA) for prostate cancer screening[32] and cancer Antigen 125 (CA-125) for the diagnosis and monitoring of ovarian cancer[33].

ELISA is extensively used to diagnose and monitor viral, bacterial and parasitic infections by detecting **specific antigens or antibodies**. For instance, **HIV** detection often relies on ELISA to identify HIV-specific antibodies or antigens in blood samples, facilitating early diagnosis and monitoring of infection[34]. Similarly, ELISA helps diagnose illnesses like **hepatitis**[35] by detecting antibodies or viral antigens, allowing for effective treatment planning and reducing

transmission risks. Similarly, ELISA has proven its ability to adapt for detecting **emerging pathogens** such as the **SARS-CoV-2** virus responsible for COVID-19. ELISA tests were rapidly developed to detect both viral antigens and antibodies, playing a critical role in understanding the spread of the virus, identifying immune responses, and assessing vaccine efficacy[36].

ELISA is commonly applied to detect **bacterial pathogens**. For example, it is used to identify infections like **tuberculosis** (TB) by detecting *Mycobacterium tuberculosis*, especially useful in areas with high TB prevalence or limited diagnostic resources[37]. Finally, it is also a valuable tool in detecting **parasitic infections**, such as malaria and toxoplasmosis. In **malaria** diagnosis, ELISA can identify antigens specific to *Plasmodium* species, assisting in rapid diagnosis, epidemiological surveillance and blood donor screening[38]. For **toxoplasmosis**, ELISA detects antibodies against *Toxoplasma gondii*, allowing for timely treatment in immunocompromised patients or pregnant women where the parasite poses severe risks[39].

All things considered, the extensive applications of ELISA in multiple flields highlight its fundamental role in modern science and industry. Its continuing advancement and integration with new technologies hold up the possibility of increasing its usefulness and efficacy for addressing a variety of scientific and medical problems.

4.2.2 PRINCIPLES OF ELISA

ELISA uses the specificity of antibodies to bind to target antigens. Based on the principle of antigen-antibody interactions, antigens present in a sample can be detected and measured by and an enzyme-mediated colorimetric reaction. Briefly, the fundamental steps of this procedure may include covering a microplate with an antigen or antibody, blocking non-specific binding sites, adding the target analyte sample, and utilizing an antibody or antigen tagged with enzymes to detect the molecules of interest. The enzyme converts a substrate into a detectable signal, typically involving a color change, which is measured spectrophotometrically.

ELISAs are highly versatile, offering various assay types that can be tailored to detect specific molecules of interest. Each format is designed to suit different

types of targets, whether they are proteins, hormones, pathogens, or small molecules, allowing for precise and effective detection across a wide range of applications. According to the labelling method used, ELISAs can be classified as direct or indirect:

- **Direct ELISA:** the detection antibody is directly labeled with a signal-generating molecule, such as an enzyme, which binds specifically to the target antigen, allowing for a simpler and quicker assay with fewer steps. However, it lacks the signal amplification provided by a secondary antibody, making it less sensitive compared to other types.

- **Indirect ELISA:** the primary antibody that binds to the antigen is unlabeled, and a secondary antibody, labeled with the signal-generating molecule, binds to the primary antibody. This additional step increases assay sensitivity by amplifying the signal, as multiple secondary antibodies can bind to each primary antibody, enhancing the overall signal strength. The indirect format, therefore, is commonly used when greater sensitivity is required, despite involving more steps than the direct format.

In addition, ELISAs can be conducted in various formats, each offering unique advantages and applications. An illustration detailing the main ELISA configurations is shown in Figure 4.2.

- **Sandwich ELISA:** In sandwich ELISA, a capture antibody is immobilized and, subsequently the sample containing the target antigen is added to the plate. Then, another antibody, known as the detection antibody, is added. The detection antibody binds to an alternative epitope on the antigen, not interfering to the primary one. An additional enzyme-labelled antibody can be used to bind the detection antibody, or it can be directly enzyme-labelled. The epitopes required for the recognition must be far enought allowing simultaneous detection by two different antibodies. High molecular weight analytes are usually detected using a sandwich-type ELISA.

- **Competitive ELISA:** Competitive ELISA is based on the competition between the analyte and a third specie (competitor) for the binding to the antibody that has been immobilized in the wells. The more antigen is present in the sample, the less labelled molecule will attach to the antibody, providing a

lower signal. This method is particularly useful for measuring small molecules. The competitive ELISAs can be direct, when the competitor antigen is labelled with an enzyme that will catalyse the colorimetric reaction, or indirect, when the use of a secondary antibody labelled with this enzyme is required.

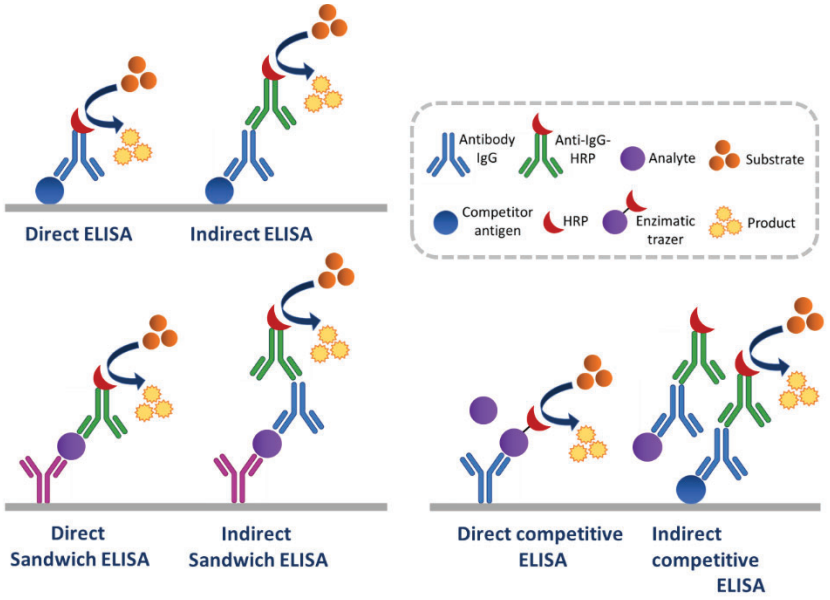

Figure 4.2. *Schematic representation of the main ELISA formats. Direct ELISA: The antigen is directly immobilized on the plate and detected by an enzyme-linked antibody. Indirect ELISA: The antigen is immobilized in the plate and detected by a primary antibody followed by an enzyme-linked secondary antibody. Sandwich ELISA: A capture antibody immobilized in the plate binds the antigen, which is then detected by a second antibody and an enzyme-linked secondary antibody. Indirect Competitive ELISA: The antigen in the sample competes with a known amount of antigen for binding to a primary antibody, which is then detected by an enzyme-linked secondary antibody. Direct Competitive ELISA: The antigen in the sample competes with an enzyme-linked antigen for binding to a capture antibody immobilized in the plate.*

All ELISA types rely on the chemical adsorption of a specific molecule, either an antibody or a competitor antigen, onto a solid surface. Typically, these assays are carried out on 96-well microtiter plates made of polystyrene, which have been specially treated to enhance the attachment of proteins. The process involves the step-by-step addition of necessary reagents, followed by washing steps to eliminate any unbound molecules. The final step in an ELISA assay generally involves an enzymatic reaction that generates a detectable signal. In most cases, this signal is colorimetric, where the enzyme catalyzes the conversion of a substrate into a chromophore, resulting in a color change that is directly proportional to the presence of the target molecule. This color change is typically

measured using a spectrophotometer, providing a quantitative or semi-quantitative readout of the analyte concentration[40].

In addition to the widely used colorimetric detection, other signal generation methods can also be employed in similar ELISA formats. These include fluorescent labeling, where the enzyme or secondary antibody is conjugated to a fluorophore that emits light upon excitation, and chemiluminescent labeling, where the enzyme catalyzes a reaction that emits light, which is then detected with a luminometer. Other advanced detection systems can also be adapted for specialized applications.

In **competitive ELISAs**, the higher concentrations of the analyte in the sample result in lower absorbance values because the sample analyte competes with a labelled analyte for binding sites. This inverse relationship is reflected in the calibration curve, where increased analyte concentrations lead to decreased absorbance. The same principle of comparing sample absorbance to a standard curve is used to determine analyte concentration.

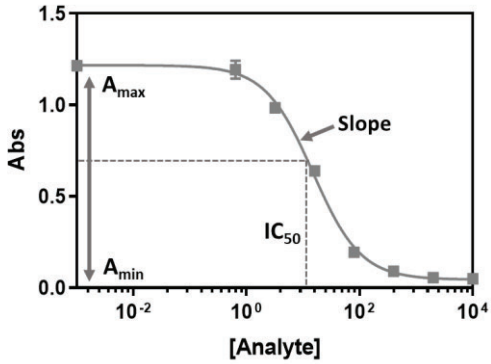

$$Y = A_{min} + \frac{A_{max} - A_{min}}{1 + \left(\frac{C}{IC_{50}}\right)^{hill\ slope}}$$

Figure 4.3. *Calibration curve of a competitive ELISA and its fitted equation. The curve is typically modeled using a four-parameter logistic (4PL) equation, which relates the absorbance to the concentration of the analyte. The equation is used to determine the concentration of unknown samples by comparing their absorbance to the standard curve generated by known concentrations, where: Y is the observed absorbance; A_{min} is the minimum absorbance value; A_{max} is the maximum absorbance value; C is the concentration of the analyte; IC_{50} is the concentration at which the response is halfway between the minimum and maximum absorbance and Hill Slope determines the steepness of the curve.*

As illustrated in Figure 4.3, the relationship between absorbance and concentration follows a **sigmoidal curve**, that be described using a four-parameter logistic model, which includes the following parameters: Maximum Absorbance (**A_{max}**), Minimum Absorbance (**A_{min}**), **IC_{50}** and **Hill Slope**. These four parameters collectively describe the sigmoidal relationship between absorbance

and analyte concentration in an ELISA, allowing for accurate quantification of the analyte based on the observed absorbance values.

4.3 RESULTS & DISCUSSION

4.3.1 DEVELOPMENT OF THE AIP1O (MAB23/AIP4S-BSA) ELISA

4.3.1.1 Selection of the best mAb candidate

As previously stated in Chapter 3, mAbs with high specificity for AIP1o were successfully obtained, demonstrated by their selective binding when tested against the four distinct AIP variants of *S. aureus* (see Table 4.1). The mAb 13.11.1.4.1 demonstrated the lowest percentage of inhibition against AIP1o (81.82 %) when its binding competition was assessed using indirect competitive ELISAs. Additionally, this antibody showed minor recognition of both AIP1 and AIP4 in their thiolactone forms (AIP1c and AIP4c).

The antibody 23.1.3.1.3 was found to be the most specific, with an inhibition percentage of 89.42 % for AIP1o and only 4.29 % for AIP1c. The recognition of other analytes by this antibody was less than 3 %. Finally, the mAb 23.1.3.7.1 showed the highest recognition of AIP1o, with an inhibition percentage of 91.91 %. However, this antibody also exhibited some cross-reactivity (CR) with the cyclic form of AIP1 (AIP1c), with an inhibition of 41.95 %, and a slight recognition of AIP4o at 26.52 %.

Table 4.1. *Competition rates of the three selected mAbs against the four S. aureus AIP variants in both their thiolactone (closed) and linearized (open) conformations.*

mAb	% AIP1c	% AIP1o	% AIP2c	% AIP2o	% AIP3c	% AIP3o	% AIP4c	% AIP4o
13.11.1.4.1	12.95	81.82	6.20	6.93	6.85	14.68	1.60	36.81
23.1.3.1.3	4.29	89.42	2.62	0.00	0.60	0.00	0.00	1.90
23.1.3.7.1	41.95	91.91	5.32	12.43	12.25	7.73	8.33	26.52

The results exhibit the inhibitory performance of the supernatants (diluted 1/100) extracted from the production of the selected hybridoma clones for the detection of AIP1 tested by indirect competitive ELISAs. A color scale indicates analyte recognition, ranging from dark green (high recognition) to white (no recognition). The mAbs produced against AIP1 exhibit high specificity for detecting the linear form of AIP1 (AIP1o).

Upon purification, each antibody was tested under both homologous and heterologous conditions, taking advantatge of other AIP haptens that were prepared using the same bioconjugation strategy. The introduction of heterology aimed to assess potential improvements in assay performance, in terms of specificity and sensibility, compared to the results observed under homologous conditions.

To explore the possibility of developing an ELISA under heterologous conditions, monodimensional titration experiments were conducted. In these experiments, the four CAs (AIP1S-BSA, AIP2S-BSA, AIP3S-BSA, and AIP4S-BSA) were tested with the three final mAbs.

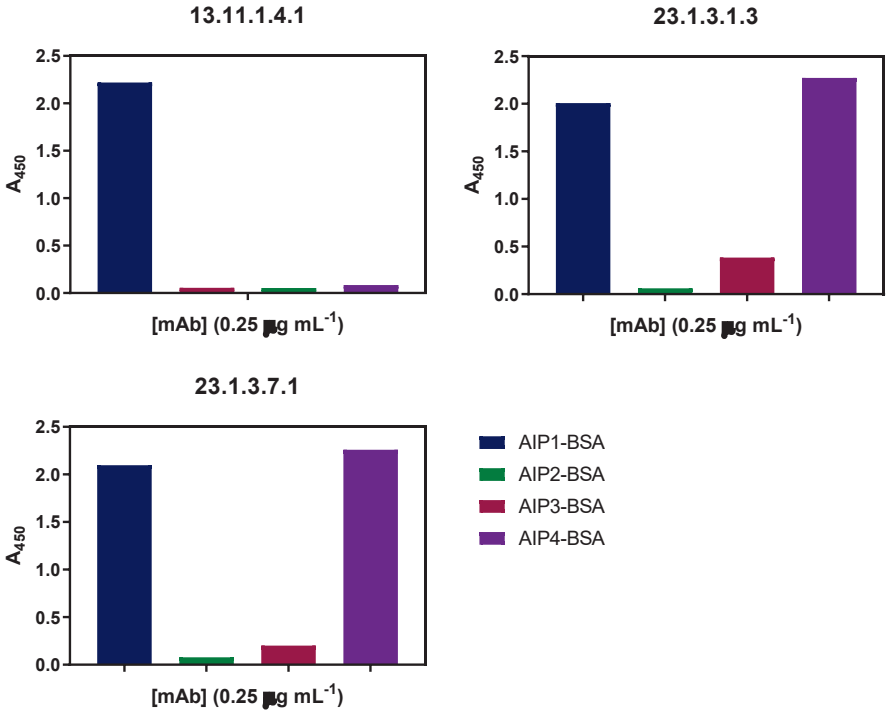

Figure 4.4. *Monodimensional titration experiments of the three selected mAbs for the detection of AIP1o. Each mAb was tested against conjugated antigens (CAs) for the four AIPs (AIP1S-BSA, AIP2S-BSA, AIP3S-BSA, and AIP4S-BSA). The mAb concentration was set at 2 µg mL^{-1} with 1/2 serial dilutions, while the CA concentration remained constant at 1 µg mL^{-1}. A mAb concentration of 0.25 µg mL^{-1} was selected to compare the absorbance achieved with different CAs.*

As shown in Figure 4.4, for the mAbs targeting AIP1o, the mAb 13.11.1.4.1 only recognized its homologous competitor (AIP1S-BSA), despite their high homology (see Figure 3.4 for reference to the chemical structures of CAs). In contrast, the

other two mAbs (23.1.3.1.3 and 23.1.3.7.1) exhibited strong recognition of both their homologous competitor (AIP1S-BSA) and the heterologous competitor for AIP4 (AIP4S-BSA).

According to this experiment, bi-dimensional titration experiments were conducted for each mAb using the CAs they were capable of recognizing. The purpose of these experiments was to determine the optimal concentrations of immunoreactants for the indirect competitive ELISAs (see Table 4.2). The aforementioned concentrations of immunoreagents were used to perform the competitive ELISAs.

The detailed data on the analytical parameters of the tested assays can be found in Table 4.2. In general, the best detectability was obtained when it was used clons 23.1.3.1.3 and 23.1.3.7.1 under heterologous conditions. This behaviour can be explained by the high affinity of these mAbs, which confers a high binding strength. This strong affinity allows the antibody to exhibit significant recognition of the competitor, thereby reducing its competition with the target analyte. Finally, **mAb23.1.3.7.1** (from now on referred to as **mAb23**) was chosen as the final candidate for further characterization, optimization, and development of the immunochemical assays. For ELISA development, heterologous conditions were selected (**mAb23/AIP4S-BSA**).

Table 4.2. *Analytical parameters of competitive indirect ELISAs for the detection of AIP1o using the three selected mAbs.*

[mAb] µg mL $^{-1}$	**13.11.1.4.1; 0.125**	**23.1.3.1.3; 0.03**	**23.1.3.1.3; 0.06**	**23.1.3.7.1; 0.015**	**23.1.3.7.1; 0.03**
[CA] µg mL $^{-1}$	**AIP1S-BSA; 0.5**	**AIP1S-BSA; 0.1**	**AIP4S-BSA; 0.6**	**AIP1S-BSA; 0.03**	**AIP4S-BSA; 0.4**
A_{min}	0.06	0.10	0.06	0.05	0.06
A_{max}	1.66	1.36	1.29	1.28	1.48
Hill Slope	-1.33	-1.11	-1.25	-1.05	-1.36
IC_{50} (nM)	655.80	89.45	42.18	54.64	34.97
R^2	0.998	0.996	0.998	0.998	0.998

The assays were optimized based on bi-dimensional titration results.

4.3.1.2 Physicochemical parameters optimization

Tehe optimization was carried outh testing various physicochemical parameters to enhance assay performance and reliability. The parameters examined included pH, ionic strength, pre-incubation time, competition time, and the percentage of Tween 20 in the buffer. Results are recorded in Figure 4.5.

pH: The pH of the buffer is critical for maintaining the stability and activity of both the antibody and the antigen. Different pH levels were tested to determine the optimal conditions that maximize the binding interaction between the mAb and its target AIP while minimizing non-specific binding. The assesment of tolerance to pH variations in mAb23/AIP4S-BSA ELISA revealed that the assay is robust within a pH range of 6.5–9.5, as the IC_{50} remains relatively stable throughout this interval. When pH levels were adjusted outside this range, specifically below 6.5 and above 9.5, significant changes in assay performance were observed. With pH levels above 9.5, there was an absence of signal. At pH levels below 6.5, the IC_{50} value increased significantly, indicating a substantial drop in sensitivity. This emphasizes the importance of conducting the assay within the optimal pH range to ensure robustness and reliability. Based on these results, a pH of 7.5 was selected for subsequent experiments.

Conductivity: Conductivity is a measure of a solution's ability to conduct electric current, which is directly related to the ionic strength of the solution. Ionic strength refers to the concentration of ions in the solution, which affects the overall charge environment. The ionic strength of the buffer can influence the electrostatic interactions between molecules. High ionic strength can shield electrostatic interactions, potentially reducing binding efficiency and sensitivity, while low ionic strength may enhance binding but increase non-specific interactions. By adjusting the conductivity, the assay conditions were fine-tuned to reduce non-specific interactions and improve the specificity of the antibody-antigen binding. At medium and high conductivity levels, the detectability of the assay remained consistent. However, it showed variability at low conductivities. In terms of sensitivity, the assay was robust across a conductivity range of 8.8 to 53.2 mS cm^{-1}. This consistency does not extend to A_{max}, which varies depending on conductivity. However, since the assay is routinely calibrated daily, fluctuations in A_{max} do not pose a significant problem. It was decided to continue using the standard conductivity of 15.8 mS cm^{-1}, as changes in conductivity did

not lead to any improvement, and it was determined to be optimal value in terms of both sensitivity and signal intensity.

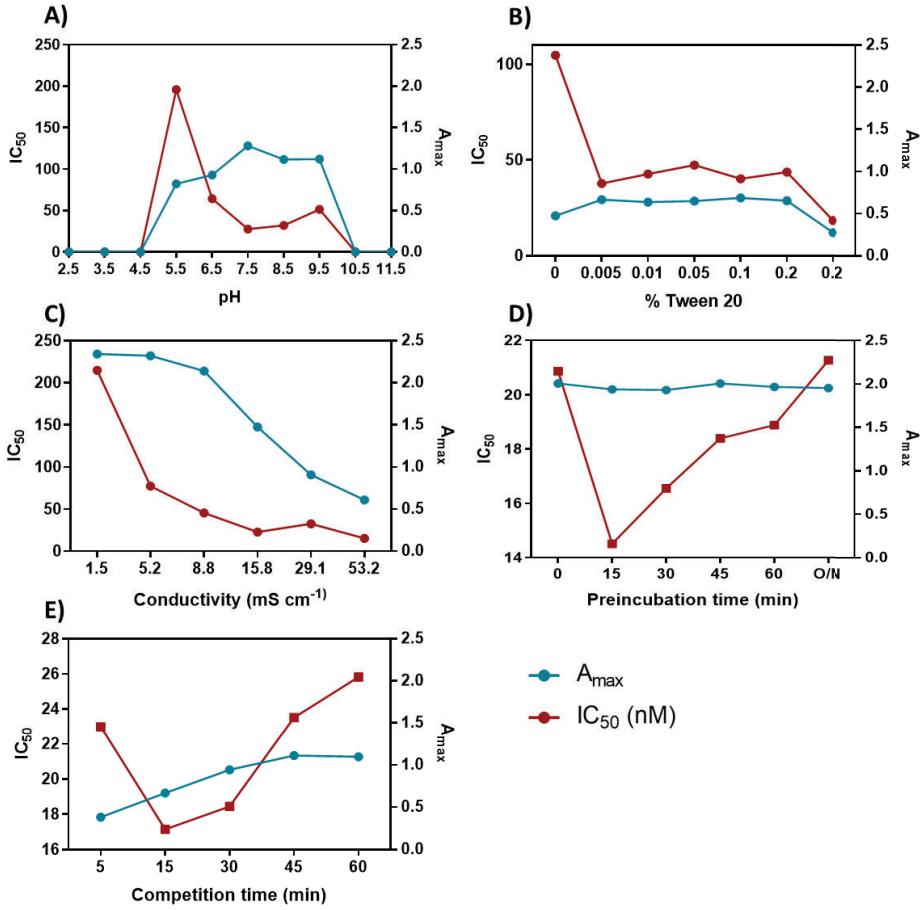

Figure 4.5. *Performance of the mAb23/AIP4S-BSA ELISA across various physicochemical parameters. Each graph corresponds to a specific parameter tested: A) pH; B) % Tween 20; C) Conductivity; D) Preincubation Time; and E) Competition Time. Optimal conditions for each parameter were selected by performing indirect competitive ELISAs and comparing the calibration curves obtained under the different conditions. These analyses helped determine the most favorable settings to ensure accurate and sensitive detection of AIP1o.*

Pre-incubation Time: Pre-incubation time refers to the duration during which the antibody and antigen are allowed to interact before the addition of any competitors or detection reagents. This parameter was varied to determine the optimal time needed for effective binding, ensuring the assay is both sensitive and reproducible. The pre-incubation time was also evaluated, with slight

modifications showing that a 15-minute pre-incubation of the analyte and antibody resulted in a marginal improvement in sensitivity. This adjustment will be considered in the context of optimizing other immunoassays, as it may provide additional benefits.

Competition Time: The competition time is the period during which the sample analyte competes with the labeled antigen for binding to the antibody. By varying this time, the goal was to identify the duration that provides the best balance between sensitivity and assay completion time, allowing for accurate detection of the analyte. The optimization of the competition time demonstrated that the best balance between A_{max} and sensitivity is achieved with a 30-minute competition period. It is important to note that this ELISA requires at least 15 minutes of competition time, since shorter times, such as 5 minutes, resulted in a significant loss of signal. While reducing the competition time could be considered for implementation in other devices, it would need a pre-incubation step to maintain assay performance (see Figure 4.5) to consult the performance of this ELISA when assessing the different parameters.

Percentage of Tween 20: Tween 20 is a surfactant commonly used in ELISA buffers to reduce non-specific binding by blocking non-target sites on the plate. Different concentrations of Tween 20 were tested to find the optimal percentaje that minimizes background noise while maintaining strong specific signals. Regarding Tween 20 concentration, the assay showed considerable robustness. The sensitivity remained consistent, with IC_{50} values ranging from 18.65 to 19.72 nM across Tween 20 concentrations from 0.005 % to 0.25 %. However, in the absence of Tween 20, the IC50 value increased to 34.59 nM, indicating a decrease in sensitivity. This suggests that while the assay can tolerate varying levels of Tween 20, its inclusion is necessary to maintain optimal performance by reducing non-specific binding. he results obtained align with the hypothesis that the detergent Tween 20 aids in solubilizing the peptide in aqueous conditions, as indicated by improved assay sensitivity when Tween 20 is present. Tween 20, a non-ionic surfactant, likely enhances peptide solubility by reducing hydrophobic interactions that can cause aggregation or precipitation in water-based solutions[41]. This solubilizing effect promotes better peptide dispersion, ensuring that more peptide molecules are freely available to interact with antibodies in the assay. These findings underscore the role of Tween 20 in improving peptide solubility and stabilizing assay conditions for more reliable measurements

By systematically evaluating these parameters, the ELISA protocols were fine-tuned to ensure optimal conditions for the detection of each AIP. This optimization process is crucial for developing robust, reliable, and sensitive assays suitable for various applications, including clinical diagnostics and research.

The final conditions of the assay, established after completing the optimization of physicochemical parameters, are summarized in Table 4.3.

Table 4.3. *Conditions selected for mAb23/AIP4S-BSA ELISA.*

	mAb23/AIP4S-BSA
[mAb] µg mL^{-1}	0.015
[CA] µg mL^{-1}	0.4
pH	7.5
Conductivity (mS cm^{-1})	15.8
Tween 20 (%)	0.05
Preincubation time (min)	0
Competition time (min)	30

4.3.1.3 Optimized calibration curve for mAb23/AIP4s-BSA ELISA

The reproducibility of the developed ELISA was performed by evaluating its parameters and performance across different days. This assessment involved conducting the ELISA assay on three separate days, with each assay performed, at least, in duplicate wells to ensure reproducibility and reliability of the results.

Table 4.4. *Analytical parameters of mAb23/AIP4S-BSA ELISA for AIP1o detection.*

	mAb23/AIP4s-BSA
A_{min}	0.06 ± 0.004
A_{max}	0.98 ± 0.10
Slope	-1.16 ± 0.07
IC_{50} (nM)	20.41 ± 2.47
Dynamic Range (nM)	5.74 ± 1.21 to 68.72 ± 2.91
LOD (nM)	2.49 ± 0.78
R^2	0.996 ± 0.001

The ELISAs were carried out in PBST. For the AIP1o ELISA, a concentration of 0.4 µg mL^{-1} of competitor antigen (AIP4S-BSA) and 0.015 µg mL^{-1} of antibody (mAb23) were used. For the AIP3c ELISA, 0.1 µg mL^{-1} of competitor antigen (AIP3S-BSA) and 0.063 µg mL^{-1} of antibody (mAb14) were employed. The results represent the average values of data obtained from three separate assays conducted on three different days, with each assay performed at least in duplicate wells.

For the ELISA targeting AIP1o, the combination of mAb23 and AIP4S-BSA at the optimized concentrations demonstrated the ability to detect AIP1o in PBST buffer with a LOD of 2.49 ± 0.78 nM, an IC_{50} value of 20.41 ± 2.47 nM and a dynamic range between 5.74 ± 1.21 to 68.72 ± 2.91 nM (see the analytical parameters of the assay on Table 4.4 and the corresponding calibration curve in Figure 4.6).

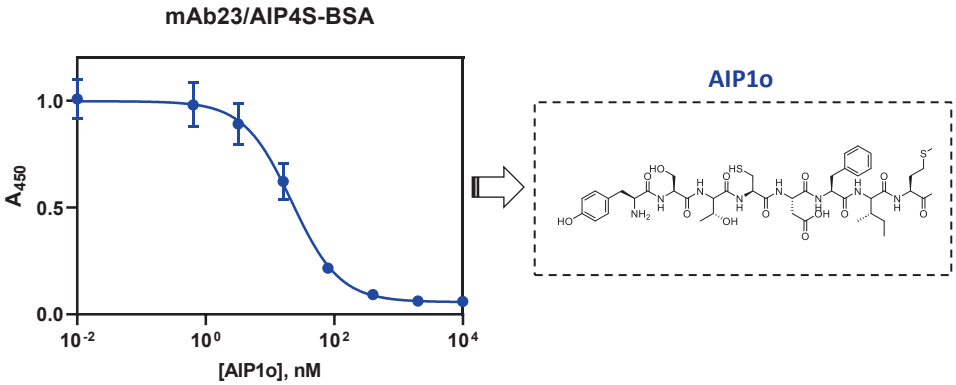

Figure 4.6. *Calibration curve of the mAb23/AIP4S-BSA ELISA for AIP1o detection. The assay was performed in PBST, under the conditions established (see Table 4.3). Each calibration point was measured in triplicates on the same ELISA plate and the results show the average and standard deviation of analysis made on three different days.*

4.3.1.4 Specificity evaluation

The analytes tested included all the AIPs of *S. aureus* in their open and closed forms. Additionally, six analytes corresponding to QS signaling molecules or virulence factors from *P. aeruginosa* were included.

These two pathogens commonly cause respiratory infections and, in patients with conditions such as cystic fibrosis, they are among the most aggravating pathogens, posing a significant threat to pleople suffering these diseases [42, 43]. Furthermore, it has been reported that QSMs of *P. aeruginosa* and *S. aureus* can interact with each other, influencing the behavior and virulence of both pathogens during co-infections. The QS systems of these two bacteria are not isolated but can interfere with one another. Specifically, *P. aeruginosa* can produce molecules that inhibit the QS systems of *S. aureus*, thereby reducing its virulence and altering the dynamics of infection. Conversely, *S. aureus* may also affect the QS signaling in *P. aeruginosa*, potentially leading to complex

interactions that can enhance or suppress the overall pathogenicity of the infection. These interactions highlight the importance of considering polymicrobial environments in understanding bacterial infections and developing effective treatment strategies [44]. Due to the frequent occurrence of co-infections by these pathogens, it is relevant to check whether the developed ELISAs exhibit CR with these analytes.

Table 4.5. *IC_{50} values and specificity results of mAb23/AIP4S-BSA ELISA using S. aureus AIPs and other QSMs from P. aeruginosa as analytes.*

	mAb23/AIP4S-BSA	
Analyte	IC_{50} (nM)	CR (%)
AIP1c	1251	1.4
AIP1o	16.98	100
AIP2c	>10,000	<0.2
AIP2o	>10,000	<0.2
AIP3c	>10,000	<0.2
AIP3o	>10,000	<0.2
AIP4c	>10,000	<0.2
AIP4o	618.90	2.7
Pyo	>10,000	<0.2
OH-phz	>10,000	<0.2
IQS	>10,000	<0.2
PQS	>10,000	<0.2
HHQ	>10,000	<0.2
HQNO	>10,000	<0.2

The table presents the IC_{50} values of the ELISAs when using molecules from the QS systems of S. aureus and P. aeruginosa as analytes and the corresponding cross-reactivity (CR) percentages with each analyte. The CR percentages were calculated following the equation: CR (%) = IC_{50}(Cross reactant)/IC_{50}(Analyte) x 100. Pyo: Pyocyanin; OH-pnz: Hydroxyphenazine; IQS: Integrated Quorum Sensing Signal, PQS: Pseudomonas Quinolone Signal; HHQ: 4-Hydroxy-2-Heptylquinoline (HHQ); HQNO: 4-Hydroxy-2-Heptylquinoline N-oxide.

As shown in Table 4.5, the mAb23/AIP4S-BSA ELISA was found to be highly specific for the detection of AIP1o, with a CR of only 1.4 % with AIP1c (IC_{50}=1251 nM), despite the identical amino acid composition of the two forms. This specificity highlights that the presence of the thiolactone ring in AIP1c significantly influences the immune response. When AIPs are in cyclic form, they adopt a three-dimensional conformation. The particular shape and rigidity provided by the thiolactone ring may expose certain amino acid residues more prominently, presenting distinct epitopes or binding sites, which are recognized by immune cells. As a result, a highly specific ELISA for AIP1o detection was

obtained, able to recognize unique epitopes present in AIP1o but not in AIP1c, thereby preventing CR with the linear peptide.

Additionally, this assay exhibited only 2.7 % CR with AIP4o (IC_{50}=618.90 nM), showing the ability to discriminate between AIP1 and AIP4 (refer to Table 4.5). These results are noteworthy, given that the two oligopeptides mentioned differ only at position 5 with an aspartic acid (D) residue in AIP1 and a tyrosine moiety (Y) in AIP4 (see Figure 4.7).

To identify the epitope of mAb23, the influence of the amino acid composition of AIP1 and AIP4 on recognition was studied, focusing on the physicochemical properties of the residues that make up these molecules. Figure 4.7 categorizes each amino acid by a specific color based on its properties: hydrophobic (nonpolar) amino acids include those with aliphatic chains or aromatic groups, while hydrophilic (polar) amino acids are further divided into neutral, positively charged (basic), or negatively charged (acidic).

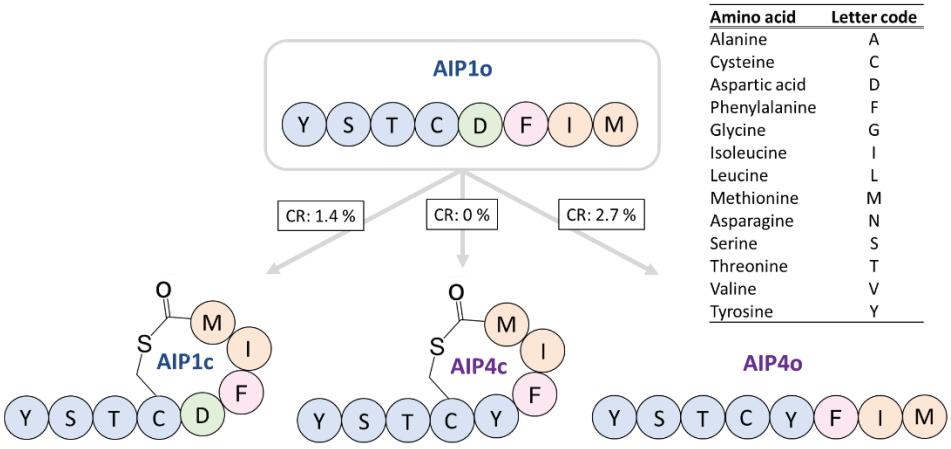

Amino acid	Letter code
Alanine	A
Cysteine	C
Aspartic acid	D
Phenylalanine	F
Glycine	G
Isoleucine	I
Leucine	L
Methionine	M
Asparagine	N
Serine	S
Threonine	T
Valine	V
Tyrosine	Y

Figure 4.7. *Simplified structures of S. aureus AIP1 and AIP4 in both their thiolactone and linear forms. The amino acid sequences of AIPs are illustrated, grouped in base of the physicochemical properties of their residues: nonpolar residues with aliphatic side chains are shown in orange, those with aromatic groups in pink, and polar residues are categorized into neutral (blue), acidic (green), and basic (purple). This classification emphasizes the compositional differences between AIP1 and AIP4 and provides insight into their potential impact on mAb23 recognition.*

As previously discussed, the presence of the thiolactone ring affects recognition. However, the recognition epitope of this antibody must include a distinguishing feature between AIP1c and AIP4c, as AIP4c is not recognized, while AIP1c exhibits a CR of 1.4 %. The only structural difference between these two molecules is the

substitution of aspartic acid (D) in AIP1c with tyrosine (Y) in AIP4c. This strongly suggests that this residue is part of the recognition epitope. Furthermore, mAb23 shows a CR of 2.7 % with AIP4o. AIP1o and AIP4o are structurally identical except for the D/Y residue substitution. While both residues are polar, aspartic acid (D) is acidic, whereas tyrosine (Y) is neutral. This difference supports the hypothesis that the recognition epitope of mAb23 includes this position, as the antibody displays high specificity for AIP1o with minimal recognition of AIP4o.

Although the exact number of residues comprising the mAb23 epitope cannot be determined with the current information, it is evident that this specific position is critical for recognition. These findings highlight the importance of residue D/Y in differentiating between AIP1 and AIP4 in both their closed and open forms.

4.3.1.5 Accuracy studies

The accuracy of the ELISA developed for detecting AIP1o using specific mAbs was thoroughly evaluated by preparing blind samples. These samples were spiked with varying concentrations of their targeting analyte, including concentrations both within and beyond the established dynamic range of the assays. The blind samples were then measured in triplicate on the same ELISA 96 well microplate to ensure consistency. To further validate the reliability of the results, the entire experiment was repeated over three different days, allowing for the assessment of reproducibility and accuracy under varying conditions. This approach ensured that the ELISAs were rigorously tested for their ability to accurately quantify AIP concentrations across a wide range of values.

As shown in Figure 4.8, the mAb23/AIP4S-BSA ELISA demonstrated high accuracy across all tested concentrations of AIP1o in PBST. Slight variations were observed at concentrations of 80 nM or higher, which is expected as these values approach the upper limit of quantification (ULOQ) of the dynamic range. The assay's performance is reflected by a slope of 0.96 and a regression coefficient (R^2) of 0.98, indicating a strong linear correlation and accurate quantification within the tested range.

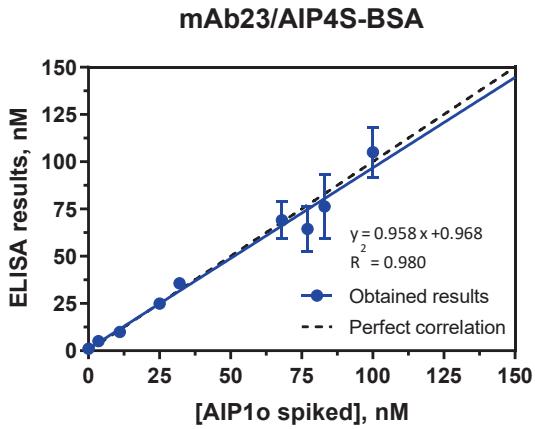

Figure 4.8. *Results of the accuracy studies for mAb13/AIP4S-BSA ELISA. The graph shows the linear regression analysis of the concentrations of AIP1o spiked and the concentrations measured by the ELISA. The samples were blind-spiked. Triplicates were performed for each concentration, and the mean and Standard deviation (SD) of the results from three different days are shown. The study was performed in PBST buffer.*

4.3.2 DEVELOPMENT OF THE AIP2O (AS417/AIP2S-BSA) ELISA

4.3.2.1 Antisera selection

To identify the best combination of the immunoreactants produced, monodimensional titration experiments were conducted. In these experiments, the performance of each pAb produced for the detection of AIP2o (As417 and As418) was tested.

The results shown in Figure 4.9 indicated that both pAbs only functioned effectively with their homologous bioconjugate (AIP2S-BSA), showing no significant recognition with other potential conjugates.

Following this, the avidity of the obtained antisera for the BSA conjugates was asessed by bidimensional titration experiments, allowing for the determination of the optimal immunoreagent concentrations for the indirect competitive ELISAs.

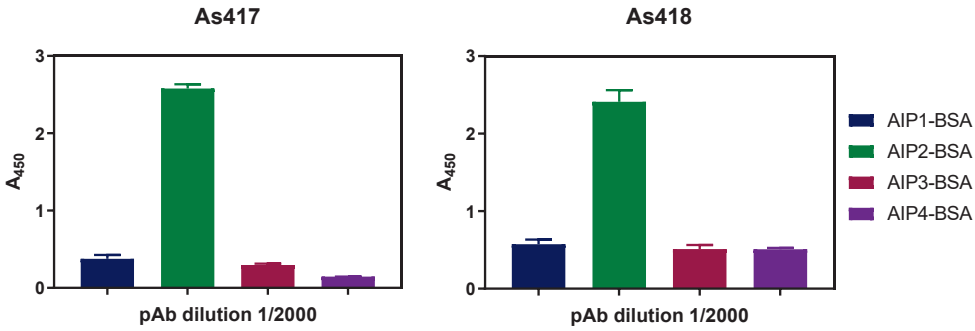

Figure 4.9. *Monodimensional titration experiments of the two selected pAbs for the detection of AIP2o. Each pAb was tested against conjugated antigens (CAs) for the four AIPs (AIP1S-BSA, AIP2S-BSA, AIP3S-BSA, and AIP4S-BSA). [CA] 1 µg mL^{-1}. The initial pAb dilution was set at 1/500, with 1/2 serial dilutions, while the CA concentration remained constant at 1 µg mL^{-1}. PAb dilution 1/2,000 was selected to compare the absorbance achieved with different CAs.*

By testing different combinations and concentrations of the pAbs and their corresponding bioconjugates, calibration curves for both AIP2o and AIP2c were generated to evaluate the sensitivity and performance of each assay. It was decided to test both in this early stage according the previous experience showed with AIP1 and AIP4 which the main recognition made was for the open form of the AIP.

Table 4.6. *Analytical parameters of the competitive indirect ELISAs for the detection of AIP2o using the two selected pAbs.*

pAB dilution	As417; 1/8000		As418; 1/16000	
Analyte	AIP2c	AIP2o	AIP2c	AIP2o
A_{min}	0.22	0.10	-0.17	0.17
A_{max}	0.96	0.92	1.35	1.31
Slope	-1.00	-0.74	-0.42	-0.74
IC_{50} (nM)	1,640.00	46.66	15,066.00	152.40
R^2	0.98	0.98	0.97	0.99

In all combinations the selected CA was AIP2S-BSA, at a concentration of 0.125 µg mL^{-1}.

The results obtained revealed that the ELISA using As417 was significantly more sensitive for AIP2o detection compared to the the one with As418, with an IC_{50} of 46.67 nM versus 152.4 nM, respectively. The analytical parameters of the different combinations tested are displayed in Table 4.6.

Based on these findings, the immunoreagent combination **As417FB/AIP2S-BSA** was selected for further characterization and optimization, as it demonstrated superior sensitivity and potential for accurate detection of AIP2o was.

4.3.2.2 Physicochemical parameters optimization

pH: The optimization was performed accordingly to section 4.3.1.2. As417/AIP2S-BSA ELISA demonstrated robust performance across a pH range of 5.5 to 8.5. At pH 4.5 and 9.5, the sensitivity of the assay is still maintained; however, there is a noticeable trend of increasing maximum signal. Although the assay is highly robust across a wide pH range, pH variations within this range did not offer any significant improvement and, outside it, the assay failed to function properly. Therefore, the standard pH of 7.5 was selected for the assay.

Percentage of Tween 20: Regarding the concentration of Tween 20, the ELISA showed considerable robustness, with A_{max} remaining constant regardless of Tween 20 levels. However, a slight improvement in IC_{50} was observed when the Tween 20 concentration was reduced to 0.01 % (33.36 nM) or 0.005% (34.12 nM), compared to the standard condition of 0.05 % Tween (39.85 nM). Despite this, the sensitivity gained was not significant enough to modify the standard conditions. It is important to note that the assay's performance significantly worsened when conducted in PBS, as IC_{50} values increased markedly. This finding confirmed the necessity of including Tween 20 in the buffer to maintain optimal assay conditions.

Conductivity: For ionic strength, no significant improvements were observed when testing different conductivities. Thus, the standard conditions were retained.

Preincubation time: The assay showed a marked improvement when a preincubation step was included. Although A_{max} remained constant, the IC_{50} was significantly reduced, resulting in enhanced sensitivity. Notably, a substantial improvement was observed with an overnight (O/N) preincubation at 4°C (from 32.93 to 11.79 nM), which provided the best results without adding time to the assay procedure. Based on this significant enhancement, the decision was made to incorporate this preincubation step into the standard protocol (see Figure 4.10 to compare the behaviour of this ELISA under the different parameters evaluated. The final conditios optimized for As417/AIP2S-BSA ELISA are shown in Table 4.7.

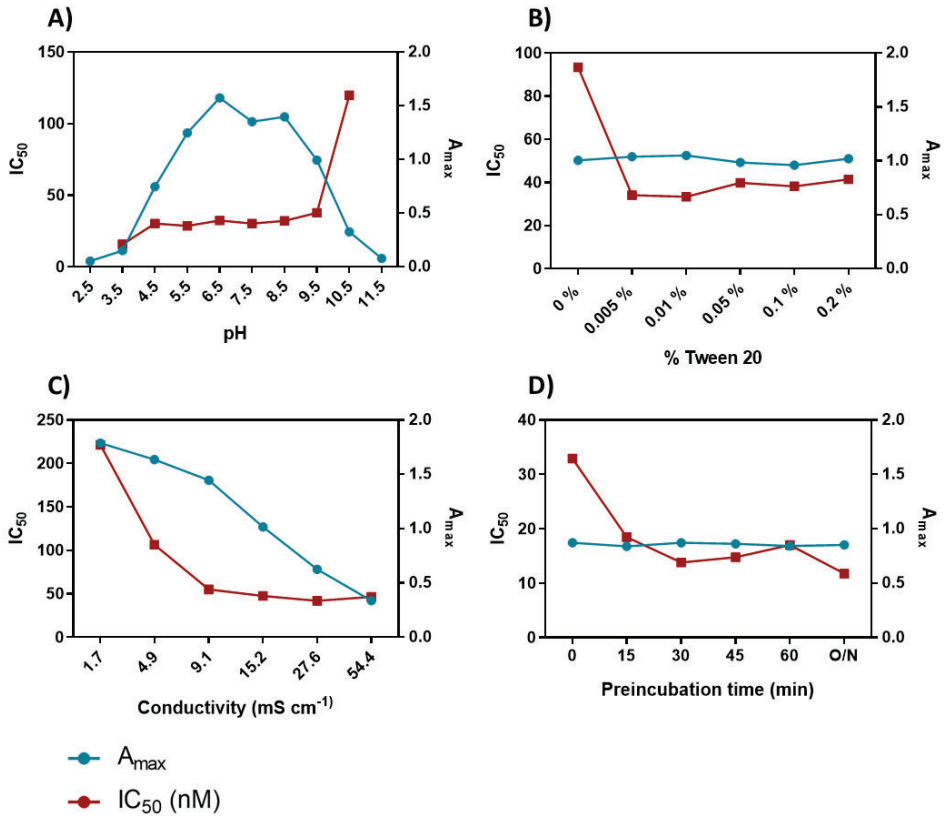

Figure 4.10. *Performance of the As417/AIP2S-BSA ELISA across various physicochemical parameters. Each graph corresponds to a specific parameter tested: A) pH; B) % Tween 20; C) Conductivity and D) Preincubation Time. Optimal conditions for each parameter were selected by performing indirect competitive ELISAs and comparing the calibration curves obtained under the different conditions. The study was conducted by testing each parameter individually, and if any modifications showed improvements, those parameters were then combined and tested together to assess their collective impact on the assay. These combinations were then compared against the standard conditions to determine if they provided any overall enhancement to the assay's performance.*

Table 4.7. *Conditions selected for As417/AIP2S-BSA ELISA.*

	As417/AIP2s-BSA
As dilution	1/8000
[CA] µg mL^{-1}	0.125
pH	7.5
Conductivity (mS cm^{-1})	15.2
Tween 20 (%)	0.05
Preincubation time (min)	O/N (4 °C)
Competition time (min)	30

4.3.2.3 Optimized calibration curve for As417/AIP2S-BSA ELISA

The As417/AIP2S-BSA ELISA assay showed a high sensitivity for AIP2o detection, with an IC_{50} value of 2.78 ± 0.16 nM and an LOD of 0.15 ± 0.02 nM. The dynamic range extends from 0.43 ± 0.03 to 23.67 ± 4.85 nM, offering a broad range for accurate quantification. Additionally, the R^2 value of 0.993 ± 0.004 reflects the high reliability and accuracy of the assay, with minimal variability across measurements. Overall, these values suggest that the assay is both sensitive and reliable, capable of detecting low concentrations of AIP2o with high precision (see calibration curve in Figure 4.11 and the analytical parameters of the assay in Table 4.8).

Table 4.8. *Analytical parameters of As417/AIP2S-BSA ELISA for AIP2o detection in PBST.*

	As417/AIP2S-BSA
A_{min}	0.11 ± 0.008
A_{max}	1.12 ± 0.07
Slope	-0.67 ± 0.06
IC_{50} (nM)	2.78 ± 0.16
Dynamic Range (nM)	0.43 ± 0.03 to 23.67 ± 4.85
LOD (nM)	0.15 ± 0.02
R^2	0.993 ± 0.004

The results represent the average data values obtained from three separate assays conducted on three different days, with each assay performed at least in duplicate wells.

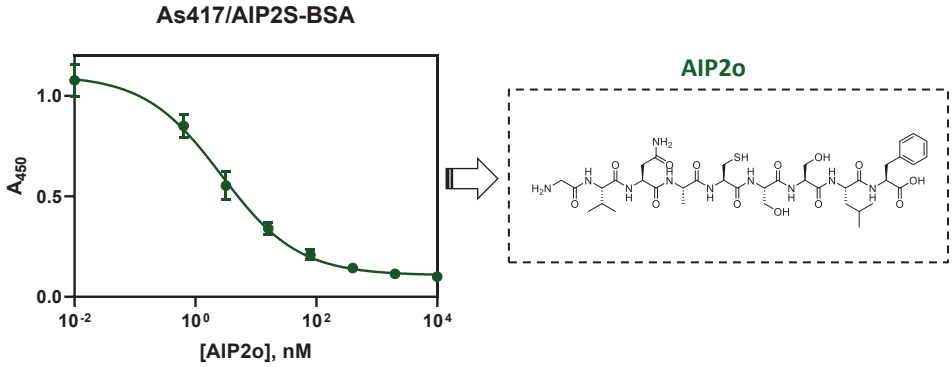

Figure 4.11. *Calibration curve of the As417/AIP2S-BSA ELISA for AIP2o detection. The assay was performed in PBST, under the conditions established (see Table 4.7). Each calibration point was measured in triplicates on the same ELISA plate and the results show the average and standard deviation of analysis made on three different days.*

4.3.2.4 Specificity evaluation

Similar to the approach outlined in section 4.3.1.4, the specificity of this assay was evaluated using a wide range of analytes as potential cross-reactants. In this instance, in addition to the analytes previously tested, two additional QSMs from *P. aeruginosa* were included in the evaluation.

As shown in Table 4.9, results for the As417/AIP2S-BSA ELISA were remarkable, demonstrating exceptional specificity for detecting AIP2o. These results were obtained before the O/N preincubation optimization. Because of that, the sensitivity of the assay at this point was worse, as reflected in a higher IC_{50}.

Table 4.9. *IC_{50} values and specificity results of As417/AIP2S-BSA ELISA using S. aureus AIPs and other QSMs from P. aeruginosa as analytes.*

	As417/AIP2S-BSA	
Analyte	IC_{50} (nM)	CR (%)
AIP1c	>10,000	<0.4
AIP1o	>10,000	<0.4
AIP2c	2.63	100
AIP2o	>10,000	<0.4
AIP3c	>10,000	<0.4
AIP3o	>10,000	<0.4
AIP4c	>10,000	<0.4
AIP4o	>10,000	<0.4
Pyo	>10,000	<0.4
OH-phz	>10,000	<0.4
IQS	>10,000	<0.4
PQS	>10,000	<0.4
HHQ	>10,000	<0.4
HQNO	>10,000	<0.4
C4-HSL	>10,000	<0.4
3-oxo-C12-HSL	>10,000	<0.4

The tested analytes included all the AIPs from S. aureus in both their closed and open forms, as well as the following Quorum-sensing molecules (QSMs) from P. aeruginosa: Pyocyanin (Pyo), Hydroxyphenazine (OH-pnz), Integrated Quorum Sensing Signal (IQS), Pseudomonas Quinolone Signal (PQS), 4-Hydroxy-2-Heptylquinoline (HHQ), 4-Hydroxy-2-Heptylquinoline N-oxide (HQNO), C4-HSL (N-butanoyl-L-homoserine lactone) and 3-oxo-C12-HSL (N-(3-oxododecanoyl)-L-homoserine lactone). The table presents the IC_{50} values of the ELISAs when using these molecules as analytes and the corresponding cross-reactivity (CR) percentages with each analyte. The CR percentages were calculated following the equation: CR (%) = IC_{50}(Cross reactant)/IC_{50}(Analyte) x 100.

Out of the 15 molecules tested, the assay showed no CR with any of them, which underscores its precision. Furthermore, it exhibited only a 1 % CR with AIP2c (IC_{50}=2629 nM), despite the fact that it was used during the immunization process (see). This low level of CR with AIP2c is particularly impressive, given the close structural similarity between AIP2o and AIP2c. This level of specificity is highly desirable in diagnostic applications, as it ensures that the assay can accurately detect the target analyte without interference from other substances, even in complex biological samples. The outstanding performance of this ELISA makes it a powerful tool for the specific detection of AIP2o.

4.3.2.5 Accuracy studies

The accuracy studies were conducted as described in section 4.3.1.5. The ELISA developed for detecting AIP2o demonstrated particularly high accuracy at lower analyte concentrations and, notably, around its IC_{50} value, where it quantifies the analyte most effectively. As the concentration of AIP2o increases, there is a slight reduction in accuracy, which is a common occurrence as assays approach its ULPQ. Despite this, the assay remains highly precise.

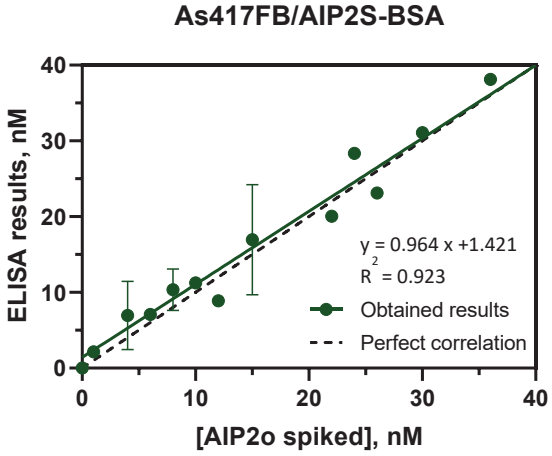

Figure 4.12. *Results of the accuracy studies for As417/AIP2S-BSA. The graph shows the linear regression analysis of the concentrations of AIP2o spiked and the concentrations measured by the ELISAs. The samples were blind-spiked. Triplicates were performed for each concentration, and the mean and Standard deviation (SD) of the results from three different days are shown. The study was performed in PBST buffer.*

Out of the 13 spiked concentrations of AIP2o tested, variability was observed in only 3 of them, indicating consistent performance across a broad range of concentrations (accuracy results are displayed in Figure 4.12). This level of precision underscores the robustness of the assay. It suggests that the ELISA can reliably quantify AIP2o even in challenging conditions, making it an excellent tool for sensitive and precise measurements. The low variability and high consistency across different concentrations highlight the assay's reliability, making it well-suited for both research and clinical applications where accurate quantification is critical.

4.3.3 DEVELOPMENT OF THE AIP3C (MAB14/AIP3S-BSA) ELISA

4.3.3.1 Selection of the best mAb candidate

In the case of AIP3, the supernatants extracted from the production of the selected hybridoma clones displayed greater sensitivity in recognizing AIP3c, with inhibitory percentajes over 93 %. However, it is noteworthy that these antibodies also exhibited CR with other AIPs, specifically AIP1 and AIP4, thereby diminishing their specificity for AIP3c.

Table 4.10. *Competition rates of the three selected mAbs for AIP3 detection against the four S. aureus AIP variants in both their thiolactone (closed) and linearized (open) conformations.*

mAbs	% AIP1c	% AIP1o	% AIP2c	% AIP2o	% AIP3c	% AIP3o	% AIP4c	% AIP4o
2.5.2.2.3	78.70	2.75	9.28	3.42	94.43	5.17	91.66	6.25
13.9.1.1.3	69.00	0.79	0.00	0.00	94.27	2.47	77.35	1.12
14.5.1.1.2	56.64	0.00	11.54	0.00	93.32	1.42	86.98	0.00

The results exhibit the inhibitory performance of the supernatants (diluted 1/100) extracted from the production of the selected hybridoma clones for the detection of AIP1 tested by indirect competitive ELISAs. A color scale indicates analyte recognition, ranging from dark green (high recognition) to white (no recognition). The mAbs produced for AIP3 detection are highly sensitive to the thiolactone form of AIP3 (AIP3c), although they show reduced specificity as they also recognize AIP1c and AIP4c to a lesser extent.

Surprisingly, unlike AIP1, the antibodies generated for AIP3 recognized the native thiolactone form of this peptide (AIP3c) while showing very little recognition of the linear form of AIP3 (1.4–5.2 %). The mAb 2.5.2.2.3 exhibited the highest CR towards both AIP1c (78.60 %) and AIP4c (91.66 %). The mAb 13.9.1.1.3

demonstrated slightly lower competition with AIP4c (77.35 %) compared to the other two antibodies, although it remained elevated. Finally, the mAb 14.5.1.1.2, while significantly recognizing AIP4c (86.98 %), showed the lowest percentage of inhibition towards AIP1c at 56.6 %. In light of these results, it was decided to proceed with the characterization of monoclonal antibodies 13.9.1.1.3 and 14.5.1.1.2. The competition rates of the clones selected for mAb production against AIP3 are illustrated in Table 4.10.

As previously described, the assays were rigorously tested under heterologous conditions to assess potential improvements in specificity and sensibility, compared to the results observed under homologous conditions.

For that purpose, monodimensional titration experiments were conducted and the CAs for AIPs 1-4 (AIP1S-BSA, AIP2S-BSA, AIP3S-BSA, and AIP4S-BSA) were tested with the two final mAbs selected for AIP3c detection (refer to Figure 4.13). The mAb 13.9.1.1.3 recognized all the competitor antigens except for AIP2S-BSA. Meanwhile, the mAb 14.5.1.1.2 showed a strong preference for its homologous competitor (AIP3S-BSA) and, to a lesser extent, recognized the competitors for AIP1 and AIP4 (AIP1S-BSA and AIP4S-BSA).

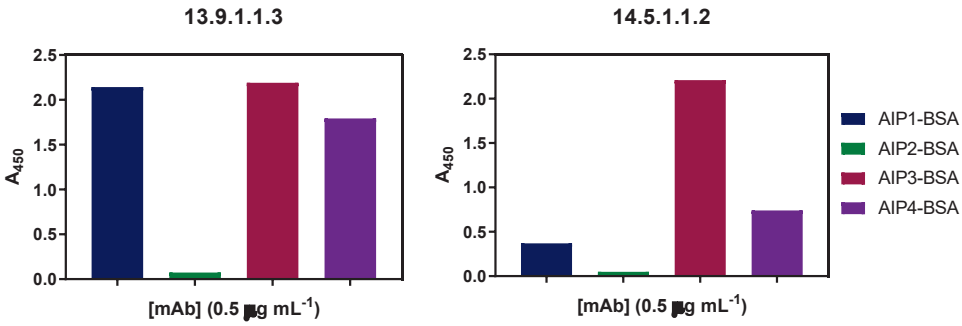

Figure 4.13. *Monodimensional titration experiments of the three selected mAbs for the detection of AIP3c. Each mAb was tested against conjugated antigens (CAs) for the four AIPs (AIP1S-BSA, AIP2S-BSA, AIP3S-BSA, and AIP4S-BSA). The mAb concentration was set at 2 µg mL^{-1} with 1/2 serial dilutions, while the CA concentration remained constant at 1 µg mL^{-1}.*

These results provided valuable insights into the CR and potential application of these mAbs under heterologous assay conditions, guiding further development and optimization of the ELISA protocols. Based on them, bi-dimensional titration experiments were conducted for each mAb using the CAs they were capable of

recognizing. The purpose of these experiments was to determine the optimal concentrations of immunoreactants for the indirect competitive ELISAs.

The two selected mAbs demonstrated similar IC_{50} values for AIP3c detection, indicating comparable binding affinities (see Table 4.11). Ultimately, **mAb 14.5.1.1.2** (**mAb 14**) was chosen as the final candidate due to its slightly higher specificity compared to the others.

***Table 4.11**. Analytical parameters of the competitive indirect ELISAs for the detection of AIP3c using the two selected mAbs.*

[mAb]; µg mL^{-1}	**13.9.1.1.3; 0.125**	**13.9.1.1.3; 0.125**	**14.5.1.1.2; 0.06**
[CA]; µg mL^{-1}	**AIP1S-BSA; 1.25**	**AIP3S-BSA; 0.125**	**AIP3S-BSA; 0.1**
A_{min}	0.07	0.07	0.04
A_{max}	1.41	1.12	1.22
Slope	-1.27	-1.17	-1.03
IC_{50} (nM)	21.61	19.76	14.94
R^2	0.998	0.990	0.997

The assays were optimized based on bi-dimensional titration results.

In relation to the above, the best combination of immunoreagents was selected for further development and optimization was **mAb14/AIP3S-BSA.**

4.3.3.2 Physicochemical parameters optimization

pH: For the ELISA targeting AIP3c, the optimization of pH revealed improvements in the assay, in terms of both sensitivity and signal intensity, at more acidic pH levels (ranging from 6.5 to 3.5). Since the assay was initially performed in PBST, which does not buffer effectively in this acidic range, an alternative buffer, composed of citrate and Na_2HPO_4, was used to provide better buffering capacity at lower pH levels (pH 2 to 8). When comparing the ELISA parameters under standard conditions (PBST, pH 7.5) with those obtained using the alternative buffer across the acidic pH range to be studied (3.5–7.5), no significant differences were observed (see Figure 4.14 B). Consequently, it was decided to continue using the standard conditions, as this would allow for greater consistency across ELISAs for different AIPs and facilitate potential multiplexed assays or in-parallel single-analyte ELISAs on the same sample. The results

obtained from evaluating the physicochemical characteristics of the ELISA for AIP3c can be found in Figure 4.14 and the final conditions selected for mAb14/AIP3S-BSA ELISA are stated in Table 4.12.

Percentage of Tween 20: Variations regarding Tween 20 did not significantly influence the assay, indicating that this ELISA is robust against variations in Tween 20 concentration. However, it was necessary to include Tween 20. The assay performed slightly better at 0.01 % Tween compared to the standard concentration of 0.05 % (IC_{50}: 4.86 nM vs 7.49 nM). Although this slight increase in sensitivity was noted, the assay was already very sensitive under standard conditions, with greater signal intensity as well.

Competition time: The optimal competition time was determined to be 30 minutes, ensuring the best balance between signal strength and assay sensitivity. Notably, the assay also performed well with a competition time of 15 minutes, which is of interest as it could shorten processing times in future applications.

Preincubation time: No significant differences were observed, as the assay performed equally well without preincubation across all tested preincubation times. Thus, including a preincubation step did not enhance the assay's performance.

Conductivity: The ELISA showed considerable robustness across different conductivities. Susprisingly, the standard conductivity (15.8 mS cm^{-1}) yielded the worst performance of the assay, showing higher IC_{50} values. The best conductivity was identified as 8.8 mS cm^{-1}, and it was combined with 0.01 % Tween 20 to evaluate whether these modifications and their various combinations would offer improvements over the standard conditions. This study revealed that the best combinations were I) 0.05 % Tween 20 with 15.8 mS cm^{-1} and II) 0.01 % Tween 20 with 15.8 mS cm^{-1} (see Figure 4.14 E). However, the assay's performance in both combinations was nearly identical in terms of signal and specificity, leading to the decision to continue using the standard conditions.

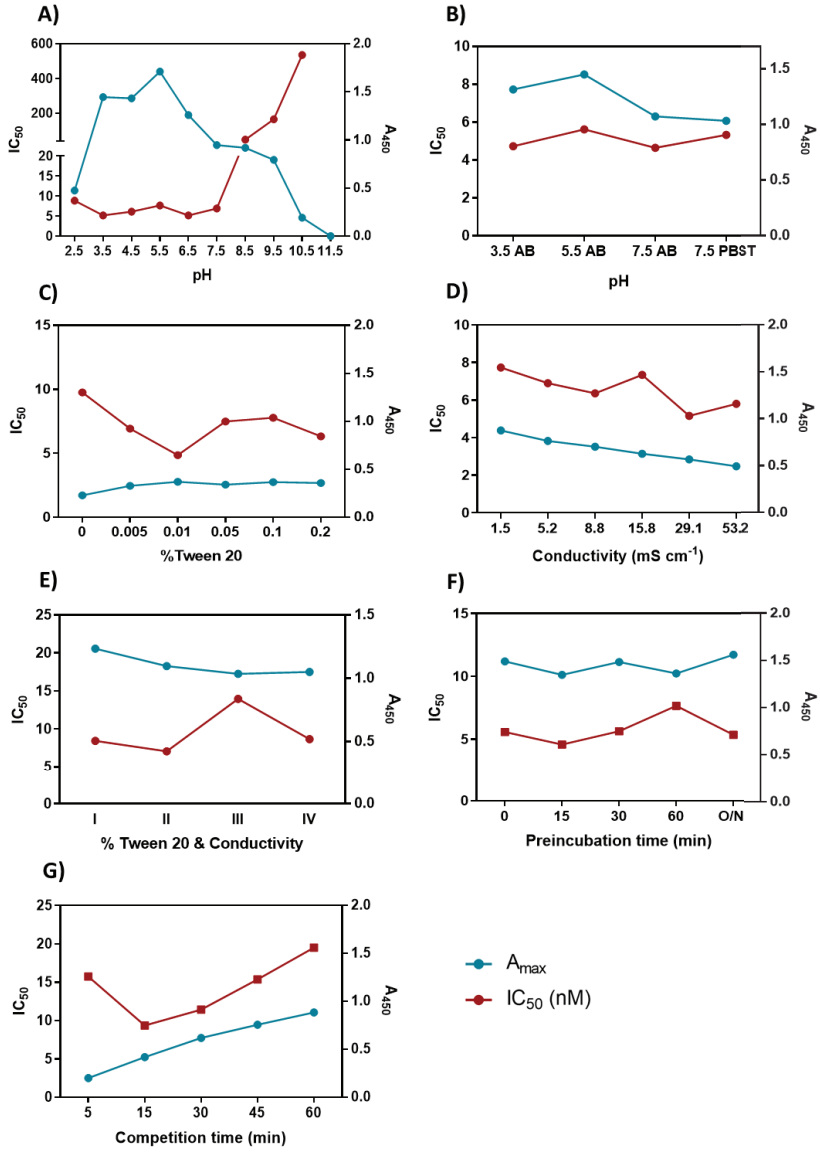

Figure 4.14. *Performance of the mAb14/AIP3S-BSA ELISA across various physicochemical parameters. Each graph corresponds to a specific parameter tested: A) pH in PBST; B) pH in the alternative buffer (AB) tested for low pH values vs PBST; C) % Tween 20; D) Conductivity; E) Different combinations of % Tween 20 and Conductivity (I: 0.05 % T and 16 mS cm^{-1}; II: : 0.01 % T and 16 mS cm^{-1}; III: : 0.05 % T and 8 mS cm^{-1}; IV: : 0.15 % T and 8 mS cm^{-1}); F) Preincubation Time; and G) Competition Time. Optimal conditions for each parameter were selected by performing indirect competitive ELISAs and comparing the calibration curves obtained under the different conditions. The study was conducted by testing each parameter individually, and if any modifications showed improvements, those parameters were then combined and tested together to assess their collective impact on the assay. These combinations were then compared against the standard conditions to determine if they provided any overall enhancement to the assay's performance.*

Table 4.12. *Conditions selected for mAb14/AIP3S-BSA ELISA.*

	mAb14/AIP3S-BSA
[mAb] µg mL^{-1}	0.06
[CA] µg mL^{-1}	0.1
pH	7.5
Conductivity (mS cm^{-1})	15.8
Tween 20 (%)	0.05
Preincubation time (min)	0
Competition time (min)	30

4.3.3.3 Optimized calibration curve for mAb14/AIP3S-BSA ELISA

The ELISA developed for the detection of AIP3c, mAb14/AIP3S-BSA, demonstrated a LOD of 0.67 ± 0.07 nM in PBST buffer, indicating a higher sensitivity compared to the AIP1o assay. The IC_{50} for this assay was 6.54 ± 0.67 nM and the dynamic range determined to be between 1.67 ± 0.53 nM and 27.66 ± 6.38 nM (see the analytical parameters of the assays on Table 4.13 and the corresponding calibration curve in Figure 4.15).

Table 4.13. *Analytical parameters of mAb14/AIP3S-BSA ELISA for AIP3c detection.*

	mAb14/AIP3S-BSA
A_{min}	0.06 ± 0.004
A_{max}	0.98 ± 0.10
Slope	-1.16 ± 0.07
IC_{50} (nM)	20.41 ± 2.47
Dynamic Range (nM)	5.74 ± 1.21 to 68.72 ± 2.91
LOD (nM)	2.49 ± 0.78
R^2	0.996 ± 0.001

The ELISAs were carried out in PBST. For the AIP3c ELISA, 0.1 µg mL^{-1} of competitor antigen (AIP3S-BSA) and 0.06 µg mL^{-1} of antibody (mAb14) were employed. Concentrations are expressed in nM. The results represent the average values of data obtained from three separate assays conducted on three different days, with each assay performed at least in duplicate wells.

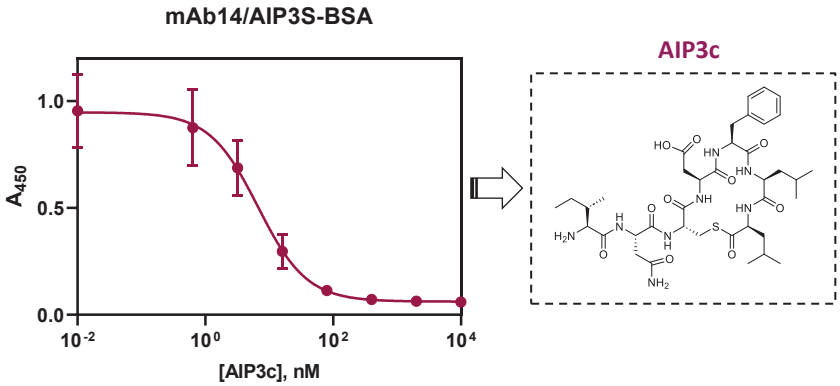

Figure 4.15. *Calibration curves of mAb14/AIP3S-BSA ELISA for AIP3c detection. The assays were performed in PBST, under the conditions established (see Table 4.12). Each calibration point was measured in triplicates on the same ELISA plate and the results show the average and standard deviation of analysis made on three different days.*

4.3.3.4 Specificity studies

The specificity study results for the mAb14/AIP3S-BSA ELISA were unexpected. Unlike previous assays, this assay showed CR with other non-related AIPs (AIP1 and AIP4). Although highly sensitive for the detection of AIP3c, this ELISA showed some recognition of AIP4c, with a CR of 15.9 % (IC_{50}=38.97 nM). Regarding the detection of AIP3o, there is minimal recognition, with a CR of 4 % (IC_{50}=153.70 nM). The IC_{50} values and CR percentajes of all the analytes tested are displayed in Table 4.14.

The recognition of AIP4c by the antibody is quite unexpected, as AIP3c and AIP4c are structurally quite different. However, through optimization and characterization of the assay, by adjusting the concentrations of immunoreactants, the specificity was significantly improved compared to the preliminary results, where this antibody recognized AIP3c and AIP4c almost equally (competiton rates: 93.32 % for AIP1c and 86.98 % for AIP4c). These findings underscore the importance of optimizing ELISA conditions to achieve high specificity and minimize CR, particularly when working with closely related analytes. In any case, mAb14 also recognized AIP1c to a significant extent, while the current results indicate a CR of only 2 % with AIP1c (IC_{50}=297.80 nM).

Table 4.14. *IC_{50} values and specificity results of mAb14/AIP3S-BSA ELISA using S. aureus AIPs and other QSMs from P. aeruginosa as analytes.*

mAb14/AIP3S-BSA		
Analyte	IC_{50} (nM)	CR (%)
AIP1c	297.80	2.0
AIP1o	>10,000	<0.06
AIP2c	>10,000	<0.06
AIP2o	>10,000	<0.06
AIP3c	6.07	100
AIP3o	153.70	4.0
AIP4c	38.27	15.9
AIP4o	>10,000	<0.06
Pyo	>10,000	<0.06
OH-phz	>10,000	<0.06
IQS	>10,000	<0.06
PQS	>10,000	<0.06
HHQ	>10,000	<0.06
HQNO	>10,000	<0.06

A concentration of 10 µM was used for each analyte. The tested analytes included all the AIPs from S. aureus in both their closed and open forms, as well as the following Quorum-sensing molecules (QSMs) from P. aeruginosa: Pyocyanin (Pyo), Hydroxyphenazine (OH-pnz), Integrated Quorum Sensing Signal (IQS), Pseudomonas Quinolone Signal (PQS), 4-Hydroxy-2-Heptylquinoline (HHQ), and 4-Hydroxy-2-Heptylquinoline N-oxide (HQNO). The table presents the IC_{50} values of the ELISAs when using these molecules as analytes and the corresponding cross-reactivity (CR) percentages with each analyte. The CR percentages were calculated following the equation: CR (%) = IC_{50}(Cross reactant)/IC_{50}(Analyte) x 100.

With the aim to understand the observed CR, the chemical structures of the AIPs were compared to identify any shared epitopes. By analyzing structural similarities, attempts were made to identify specific epitopes that might explain why mAb14 recognizes both AIP1 and AIP4, despite their structural differences from AIP3.

By a detailed examination of conserved amino acid motifs that could be responsible for cross-recognition, initially it was proposed that the shared epitope might be the aspartic acid (D) residue, which could explain the recognition of AIP1. However, the hypothesis that the epitope of mAb14 is located on the aspartic acid residue does not explain the CR results obtained. Specifically, AIP4, which lacks this residue (shared between AIP1 and AIP3), shows greater recognition by mAb14 (see Figure 4.16). This observation led us to consider whether the physicochemical properties of the amino acids composing

each AIP might also play a role in determining recognition, potentially due to differences in their isoelectric points.

Amino acid	Letter code
Alanine	A
Cysteine	C
Aspartic acid	D
Phenylalanine	F
Glycine	G
Isoleucine	I
Leucine	L
Methionine	M
Asparagine	N
Serine	S
Threonine	T
Valine	V
Tyrosine	Y

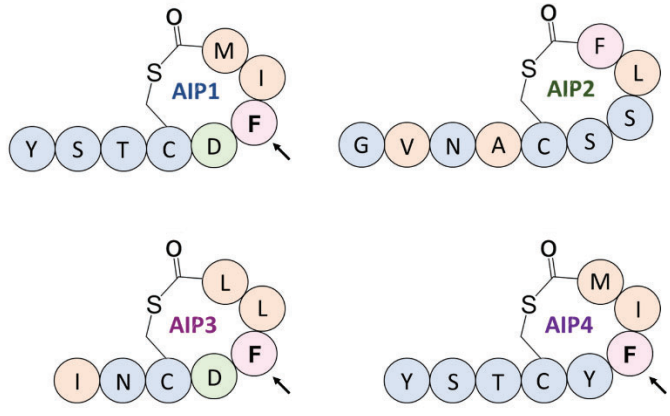

Figure 4.16. *Simplified structures of AIPs from S. aureus (1 to 4). The amino acid sequences of AIPs are illustrated, grouped in base of the physicochemical properties of their residues: nonpolar residues with aliphatic side chains are shown in orange, those with aromatic groups in pink, and polar residues are categorized into neutral (blue), acidic (green), and basic (purple). This classification emphasizes the compositional differences between AIPs and provides insight into their potential impact on mAb14 recognition.*

To explore this possibility, Figure 4.16 illustrates each amino acid categorized by a different color according to its properties. Hydrophobic (apolar) amino acids include those with aliphatic chains or aromatic groups, while hydrophilic (polar) amino acids are subdivided into neutral, positively charged (basic), or negatively charged (acidic). The figure clearly shows that AIP2 differs significantly from AIP3 based on its composition and properties, evidencing why there is no CR of mAb14 with AIP2.

A closer examination of the chemical structures of the four AIPs reveals that the phenylalanine (F) shared by AIP1, AIP3, and AIP4 is directly adjacent (as illustrated in Figure 4.17) to the residue differing between AIP1 (aspartic acid, D) and AIP4 (tyrosine, T). This observation suggests that the epitope recognized by mAb14 likely encompasses, at least, the phenylalanine residue common to the three molecules and the variable residue between AIP1 and AIP4.

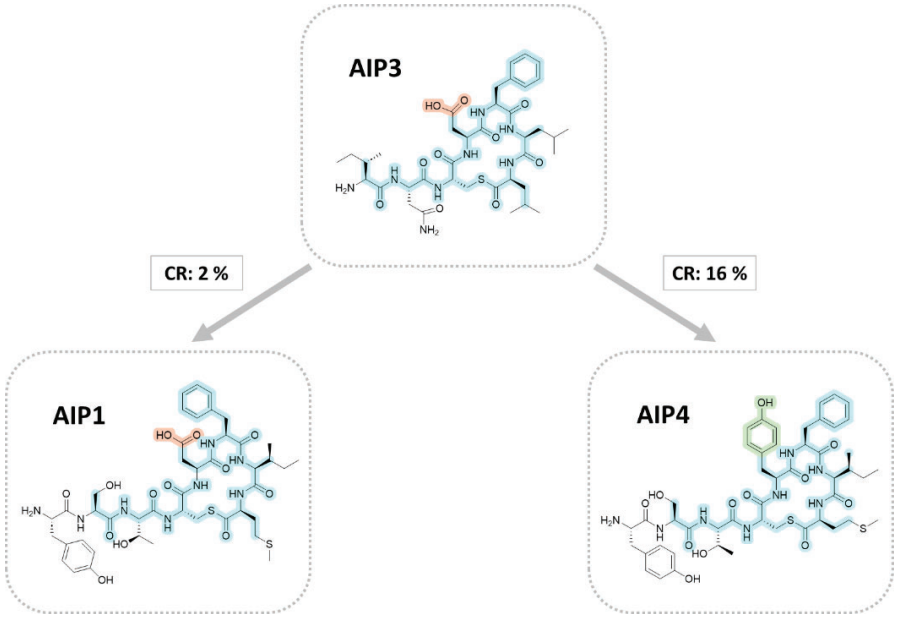

Figure 4.17. *Chemical structures of AIP1, AIP3, and AIP4 highlighting shared and variable residues. Specific regions are highlighted: common residues are shown in blue, the aspartic acid residue shared by AIP1 and AIP3 is highlighted in orange, and the tyrosine residue unique to AIP4 (compared with AIP1) is marked in green. The cross-reactivity (CR) of mAb14 is 2 % for AIP1 and 16 % for AIP4, illustrating the unexpected differential recognition by the antibody.*

Moreover, considering again the physicochemical properties of the residues, AIP1 and AIP4 both contain a methionine (M) and an isoleucine (I) adjacent to phenylalanine (F). AIP3, on the other hand, has two leucines (L) in these positions. Despite these differences, all these residues share similar properties as they are nonpolar residues with aliphatic side chains. It is possible that the epitope encompasses these positions, and although AIP1 and AIP4 share two of these residues, the critical difference between AIP1 and AIP3 lies in the substitution of aspartic acid (D) with tyrosine (Y), as previously mentioned. These two amino acids have completely different properties: D is polar and acidic, while Y is polar and neutral. The epitope might also involve two additional residues: the cysteine (C) common to all AIPs and the adjacent residue, which is a threonine (T) in AIP1 and AIP4, and an asparagine (N) in AIP3. All these residues share similar characteristics, as they are polar and neutral (see Figure 4.16).

Based on this reasoning, the homologies between the three molecules are illustrated in blue in Figure 4.17, while the residue shared by AIP1 and AIP3 is highlighted in orange, and the distinctive residue of AIP4 is shown in green. This

could explain why, although the recognition profile of mAb14 was initially unexpected, it shows a slight recognition of AIP4 and a higher CR with AIP3.

4.3.3.5 Accuracy studies

The mAb14/AIP3S-BSA ELISA resulted quite accurate at detecting low concentrations of AIP3c, with only minor variations. However, at higher concentrations (above 20 nM), the assay tended to underestimate the concentration, particularly near its limit of quantification. This is evident from the slope of 0.89 and an R^2 value of 0.90, suggesting a slight deviation from linearity at higher analyte concentrations but still maintaining reasonable accuracy at lower concentrations (see Figure 4.18).

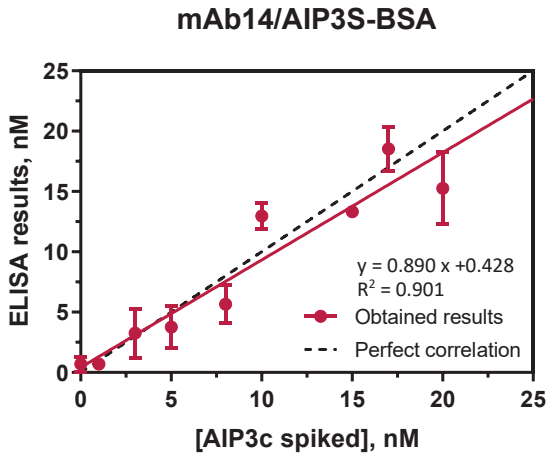

Figure 4.18. *Results of the accuracy studies for mAb14/AIP3S-BSA ELISA. The graphs show the linear regression analysis of the concentrations of analyte spiked (AIP1 or AIP3) and the concentrations measured by the ELISAs. The samples were blind-spiked. Triplicates were performed for each concentration, and the mean and Standard deviation (SD) of the results from three different days are shown. The study was performed in PBST buffer.*

4.3.4 DEVELOPMENT OF THE AIP3O (AS429/AIP3S-BSA) ELISA

4.3.4.1 Antisera selection

After discovering that both pAbs, As429 and As430, competed for the recognition of AIP3o under heterologous conditions, bi-dimensional titration

experiments were conducted with the AIP3 homologous (AIP3L-DMP-BSA) and heterologous (AIP3S-BSA) bioconjugates. As displayed in Table 4.15, the indirect competitive ELISAs performed with the selected concentrations of immunoreactants revealed that, while both pAbs were capable of recognizing AIP3o, As429 demonstrated higher sensitivity.

These results shown in Table 4.15 suggest that the pAbs produced for detecting AIP3o recognize the crosslinker (DMP), as evidenced by the high values obtained in the A_{min} for As429. A similar behavior was expected for As430; however, in this case, no calibration curve was obtained. The issue of nonspecific recognition was resolved by introducing heterology through the use of a CA prepared via a different conjugation method (active ester). This bioconjugate (AIP3S-BSA) does not contain DMP, eliminating the interference caused by the spacer arm.

Table 4.15. *Analytical parameters of the competitive indirect ELISAs for the detection of AIP3o using the two selected mAbs in homologous and heterologous conditions.*

pAB dilution	**As429; 1/8000**	**As429; 1/32000**	**As430; 1/16000**	**As430; 1/32000**
[CA]; µg mL^{-1}	**AIP3S-BSA; 0.25**	**AIP3L-DMP-BSA; 0.12**	**AIP3S-BSA; 0.25**	**AIP3L-DMP-BSA; 0.06**
A_{min}	0.07	0.81	0.03	~ -41.43
A_{max}	1.34	1.03	1.24	1.85
Slope	-0.53	-1.35	-0.50	~ -0.08
IC_{50} (nM)	13.96	819.30	36.24	~ 3.72e+025
R^2	1.00	0.72	0.99	0.70

Furthermore, in this case, the heterology introduced is double: while the immunogen used was the linear form of AIP3 (AIP3L-DMP-KLH), the CA is based on the thiolactone structure. In some cases, pAbs can exhibit very high avidity. In competitive assays, such high avidity can result in exceptionally strong binding to the homologous CA, making it difficult for the analyte to effectively compete. By introducing heterology, the binding affinity is slightly reduced, allowing the analyte to displace the CA more efficiently and thus improving assay performance.

This strategy significantly enhanced the competitive response and underscored the importance of introducing heterology to achieve optimal assay sensitivity. As a result of this approach, two ELISAs were developed (one with As429 and another with As430) for the detection of AIP3o. However, the assay with As429

demonstrated superior sensitivity. Based on these results, As429 was chosen for further characterization and optimization due to its superior sensitivity. This work was performed in collaboration with Nerea Castro Agirre (PhD candidate).

4.3.4.2 Physicochemical parameters optimization

The optimization was performed as detailed in section 4.3.1.2.

pH: The results of the As429/AIP3S-BSA ELISA indicate a high level of robustness across a pH range of 2.5 to 7.5, with the assay performing better at more acidic pH levels. However, at pH 4.5, an increase in the IC_{50} is observed, which does not align with the expected trend and might be attributed to a pipetting error. Above pH 7.5, the IC_{50} increases significantly as the environment becomes more basic. While there is a slight gain in sensitivity at pH levels below 7.5, it was decided to maintain a more neutral pH of 7.5, as the assay is already highly sensitive, and the difference in performance is minimal. Additionally, maintaining standard buffer conditions allows for greater consistency when conducting multiple assays in parallel, especially when modifications do not result in substantial improvements.

Percentaje of Tween 20: The assay is very robust and performs well even in the absence of this surfactant, which is unlike the previously optimized ELISAs. This suggests that the assay could be conducted in PBS. However, the standard condition of 0.05 % Tween was selected to ensure consistency with other assays.

Conductivity: The A_{max} increases as the salt concentration decreases, leading to lower conductivity. Conversely, the IC_{50} shows a slight increase as conductivity increases. Therefore, the standard conductivity of 15.2 mS cm^{-1} was chosen, as it provided the best ratio between these two parameters, ensuring both strong signal and sensitivity.

Preincubation time: When evaluating this parameter, it was found that preincubating the analyte and primary antibody resulted in a higher signal (A_{max}), with this effect becoming more pronounced with (O/N) preincubation at 4°C. While there were slight fluctuations in IC_{50}, the sensitivity of the ELISA was not compromised. However, to prioritize one of our main goals, which is reducing diagnostic time, it was decided to proceed with the assay without preincubation. Nonetheless, it is noted that the ELISA for detecting AIP4o (As381FB/AIP4S-BSA)

requires overnight (O/N) preincubation, and this ELISA also performs well under those conditions. This preincubation step may then be added to the protocol for both tests, making it possible to perform both simultaneously and simplifying the workflow.

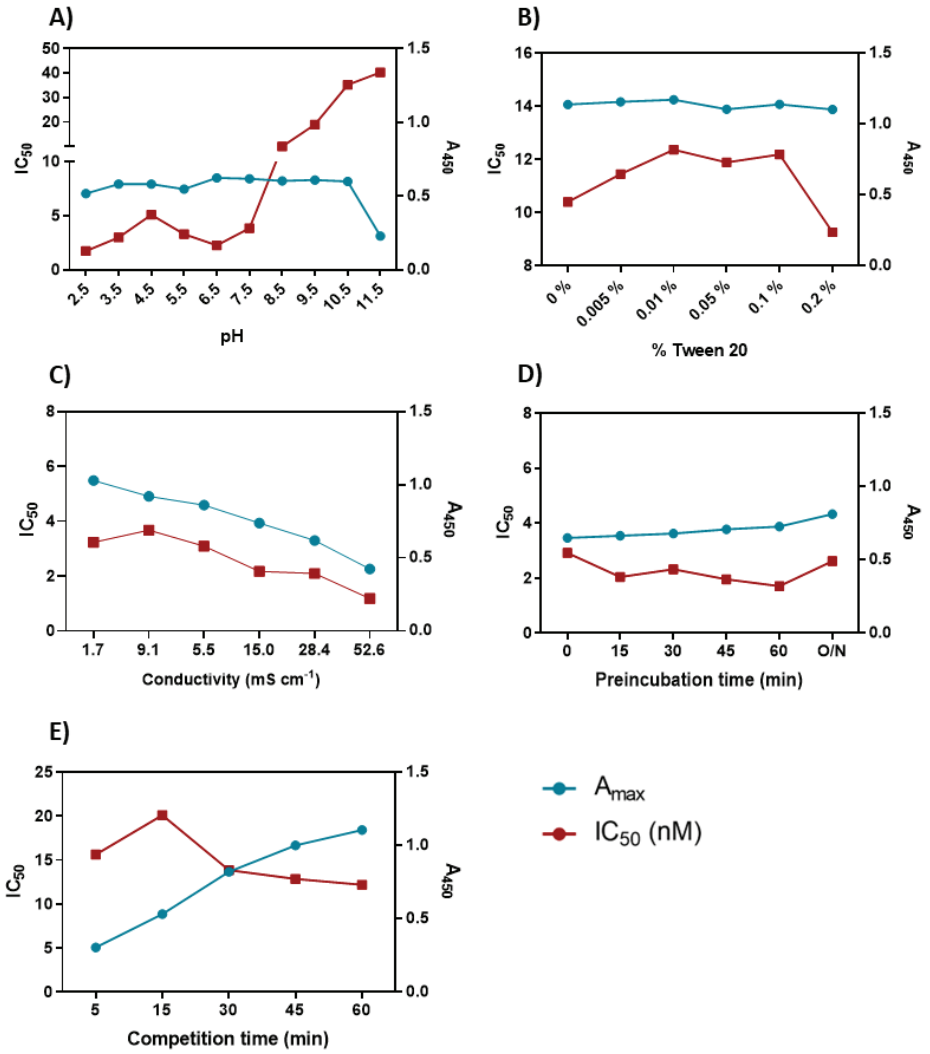

Figure 4.19. *Performance of the As429/AIP3S-BSA ELISA across various physicochemical parameters. Each graph corresponds to a specific parameter tested: A) pH; B) % Tween 20; C) Conductivity and D) Preincubation Time. Optimal conditions for each parameter were selected by performing indirect competitive ELISAs and comparing the calibration curves obtained under the different conditions. The study was conducted by testing each parameter individually, and if any modifications showed improvements, those parameters were then combined and tested together to assess their collective impact on the assay. These combinations were then compared against the standard conditions to determine if they provided any overall enhancement to the assay's performance.*

Competition time: Both A_{max} and IC_{50} improved with longer competition times. Although increasing the competition time to 45-60 minutes enhanced A_{max}, the gain in sensitivity was not substantial. Extending the competition time would compromise our goal of minimizing assay duration for future diagnostic applications. Therefore, a standard competition time of 30 minutes was determined to be optimal, balancing assay performance with the need for a rapid diagnostic process. The behaviour of the assay under the different paratemers evaluated is showed in Figure 4.19 and the final conditions selected for the assay are specified in Table 4.16.

Table 4.16. *Conditions selected for As429/AIP3S-BSA ELISA.*

	As429/AIP3S-BSA
As dilution	1/16000
[CA] µg mL^{-1}	0.06
pH	7.5
Conductivity (mS cm^{-1})	15.0
Tween 20 (%)	0.05
Preincubation time (min)	0
Competition time (min)	30

4.3.4.3 Optimized calibration curve for As429/AIP3S-BSA ELISA

Table 4.17 presents the analytical parameters for the As429/AIP3S-BSA ELISA, indicating its overall sensitivity and reliability. The IC_{50} value of 2.19 ± 0.02 nM reflects the concentration at which the assay signal is reduced by half, demonstrating that the assay is highly sensitive and capable of detecting low analyte concentrations effectively. The dynamic range, which spans from 0.36 ± 0.04 to 15.87 ± 3.65 nM, indicates that the assay can accurately quantify the analyte across a broad concentration range, making it versatile for various sample types. The LOD is very low at 0.13 ± 0.02 nM, further emphasizing the assay's high sensitivity. The R^2 value of 0.994 ± 0.004 indicates excellent linearity and consistency in the assay's performance, with minimal variability between replicates. These results suggest that the As429/AIP3S-BSA ELISA is a robust and reliable method for detecting and quantifying AIP3o in samples with high precision and accuracy (see calibration graph in Figure 4.20).

Table 4.17. *Analytical parameters of As429/AIP3S-BSA ELISA for AIP3o detection in PBST.*

	As429/AIP3S-BSA
A_{min}	0.07 ± 0.01
A_{max}	0.80 ± 0.17
Slope	-0.71 ± 0.08
IC_{50} (nM)	2.19 ± 0.02
Dynamic Range (nM)	0.36 ± 0.04 to 15.87 ± 3.65
LOD (nM)	0.13 ± 0.02
R^2	0.994 ± 0.004

For this ELISA, a concentration of 0.063 µg mL^{-1} of competitor antigen (AIP2S-BSA) was used. The As417 was diluted 1/16000. Concentrations are expressed in nM. The results represent the average data values obtained from three separate assays conducted on three different days, with each assay performed at least in duplicate wells.

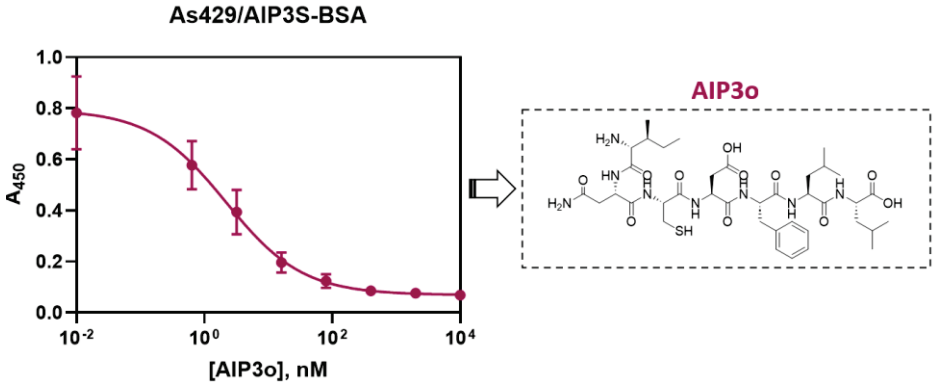

Figure 4.20. *Calibration curve of the As429/AIP3S-BSA ELISA for AIP3o detection. The assay was performed in PBST, under the conditions established (see Table 4.16). Each calibration point was measured in triplicates on the same ELISA plate and the results show the average and standard deviation of analysis made on three different days.*

4.3.4.4 Specificity evaluation

The specificity results were obtained using the same methodology described in section 4.3.2.4. It should be noted that on the day the specificity study was conducted, the ELISAs targeting AIP3 showed a signal that was higher than expected for both the closed (AIP3c) and open (AIP3o) forms. This unexpected increase in signal likely contributed to a higher IC_{50} value for the assay, indicating reduced sensitivity under these conditions. Even so, the As429/AIP3S-BSA ELISA

demonstrated high specificity, showing CR with none of the 15 potential cross-reactants tested (refer to Table 4.18).

Table 4.18. *IC_{50} values and specificity results of As429/AIP3S-BSA ELISA using S. aureus AIPs and other QSMs from P. aeruginosa as analytes.*

	As429/AIP3S-BSA	
Analyte	IC_{50} (nM)	CR (%)
AIP1c	>10,000	<0.05
AIP1o	>10,000	<0.05
AIP2c	>10,000	<0.05
AIP2o	>10,000	<0.05
AIP3c	1878	<0.05
AIP3o	4.71	100
AIP4c	>10,000	<0.05
AIP4o	>10,000	<0.05
Pyo	>10,000	<0.05
OH-phz	>10,000	<0.05
IQS	>10,000	<0.05
PQS	>10,000	<0.05
HHQ	>10,000	<0.05
HQNO	>10,000	<0.05
C4-HSL	>10,000	<0.05
3-oxo-C12-HSL	>10,000	<0.05

A concentration of 10 µM was used for each analyte. The tested analytes included all the AIPs from S. aureus in both their closed and open forms, as well as the following Quorum-sensing molecules (QSMs) from P. aeruginosa: Pyocyanin (Pyo), Hydroxyphenazine (OH-pnz), Integrated Quorum Sensing Signal (IQS), Pseudomonas Quinolone Signal (PQS), 4-Hydroxy-2-Heptylquinoline (HHQ), 4-Hydroxy-2-Heptylquinoline N-oxide (HQNO), C4-HSL (N-butanoyl-L-homoserine lactone) and 3-oxo-C12-HSL (N-(3-oxododecanoyl)-L-homoserine lactone). The table presents the IC_{50} values of the ELISAs when using these molecules as analytes and the corresponding cross-reactivity (CR) percentages with each analyte. The CR percentages were calculated following the equation: CR (%) = IC_{50}(Cross reactant)/IC_{50}(Analyte) x 100.

The high specificity of this assay is particularly notable given that AIP3c is structurally very similar to AIP3o, except that it forms a thiolactone ring in its cyclic form. This finding highlights the ELISA's ability to distinguish between the open and closed forms of the same molecule, which is a significant achievement. This level of specificity is crucial in applications where accurate identification of the exact molecular form is essential, such as in studies of bacterial communication or in clinical diagnostics where CR with similar molecules could lead to false positives or misleading results. The results affirm that the ELISA is a

reliable tool for the selective detection of AIP3o, ensuring that the assay's outputs are very selective to the target analyte.

4.3.4.5 Accuracy studies

The studies were conducted as described in section 4.3.1.5. The accuracy of the As429/AIP3S-BSA ELISA was assessed by quantifying the same spiked blind samples across three different days. The ELISA demonstrated high precision based on the results from two of the days. However, on the third day, slight differences in quantification were observed. This variation is reflected in Figure 4.21, where the standard deviation for some points on the linear regression line is evident.

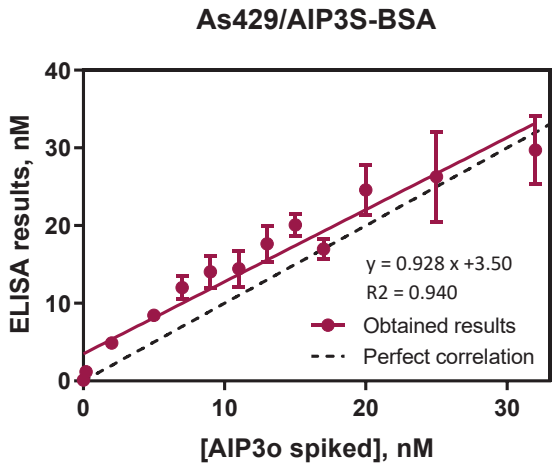

Figure 4.21. *Results of the accuracy studies for As429/AIP3S-BSA. The graph shows the linear regression analysis of the concentrations of AIP3o spiked and the concentrations measured by the ELISAs. The samples were blind-spiked. Triplicates were performed for each concentration, and the mean and Standard deviation (SD) of the results from three different days are shown. The study was performed in PBST buffer.*

The results suggest that the assay exhibits minimal inter-day variations, indicating that the ELISA generally performs consistently across multiple days. However, slight fluctuations in accuracy can occur, which is expected, especially when measurements exceed the linear dynamic range of the assay. Within this optimal range, the ELISA quantifies AIP3o reliably, but outside of it, even small differences in experimental conditions can lead to remarkable disparities in quantification. This emphasizes the importance of maintaining conditions within

the linear range to ensure precise and accurate results and highlights the need for careful interpretation of data when working near or beyond this range.

In terms of accuracy, the ELISA tends to slightly overestimate the concentrations, which impacts its overall accuracy to a small extent. This is evident in the graph, where the regression line sits above the line representing perfect correlation between the spiked and measured concentrations. Although this ELISA may not seem as accurate as others, the measured concentrations do not deviate significantly from the original values.

It is important to note that, given the high sensitivity of this assay, it operates within very low analyte concentration ranges. As a result, even a small quantification error can appear magnified. Despite these minor discrepancies, the ELISA still provides reasonably accurate measurements, making it a useful tool for detecting low concentrations of AIP3o.

4.4 CHAPTER CONTRIBUTIONS

- Highly sensitive ELISAs capable of specifically detecting three of the AIPs from *S. aureus*, accounting for both the open (linear) and closed (cyclic) forms of these peptides have been developed.

- The full set of immunochemical assays necessary for detecting all four types of AIPs present in *S. aureus* has been completed, representing a significant step forward in the ability to monitor QS activity and bacterial communication with high specificity and sensitivity.

- This research has provided a new tool that could offer crucial clinical information for the more effective and rapid diagnosis of *S. aureus* infections. By enabling the detection of AIPs with high sensitivity, this advancement enhances the diagnostic process, allowing for the identification of infections at earlier stages.

- When implemented in other formats, such as PoC devices, this technology could become a key instrument in reliably diagnosing these infections, significantly reducing diagnostic timeframes. The ability to quickly and

accurately diagnose *S. aureus* infections can lead to more timely and targeted treatments, potentially improving patient outcomes and curbing the spread of resistant strains.

4.5 BIBLIOGRAPHY

1. Drijvers, J. M.; Awan, I. M.; Perugino, C. A.; Rosenberg, I. M.; Pillai, S., Chapter 7 - The Enzyme-Linked Immunosorbent Assay: The Application of ELISA in Clinical Research. In *Basic Science Methods for Clinical Researchers*, Jalali, M.; Saldanha, F. Y. L.; Jalali, M., Eds. Academic Press: Boston, 2017; pp 119-133.
2. Crowther, J., *The ELISA Guidebook*. 2009; Vol. 516.
3. Khan, N. S.; Pradhan, D.; Choudhary, S.; Saxena, P.; Poddar, N. K.; Jain, A. K., Immunoassay-based approaches for development of screening of chlorpyrifos. *Journal of Analytical Science and Technology* **2021,** *12* (1), 32.
4. Xu, L.; Zhang, X.; Abd El-Aty, A. M.; Wang, Y.; Cao, Z.; Jia, H.; Salvador, J. P.; Hacimuftuoglu, A.; Cui, X.; Zhang, Y.; Wang, K.; She, Y.; Jin, F.; Zheng, L.; Pujia, B.; Wang, J.; Jin, M.; Hammock, B. D., A highly sensitive bio-barcode immunoassay for multi-residue detection of organophosphate pesticides based on fluorescence anti-quenching. *Journal of Pharmaceutical Analysis* **2022,** *12* (4), 637-644.
5. Xu, L.; Abd El-Aty, A. M.; Eun, J. B.; Shim, J. H.; Zhao, J.; Lei, X.; Gao, S.; She, Y.; Jin, F.; Wang, J.; Jin, M.; Hammock, B. D., Recent Advances in Rapid Detection Techniques for Pesticide Residue: A Review. *J Agric Food Chem* **2022,** *70* (41), 13093-13117.
6. Jafari, S.; Burr, L.; Migliorelli, D.; Galve, R.; Marco, M. P.; Campbell, K.; Elliott, C.; Suman, M.; Sturla, S. J.; Generelli, S., Smartphone-based magneto-immunosensor on carbon black modified screen-printed electrodes for point-of-need detection of aflatoxin B1 in cereals. *Analytica Chimica Acta* **2022,** *1221*, 340118.
7. Agriopoulou, S.; Stamatelopoulou, E.; Varzakas, T., Advances in Analysis and Detection of Major Mycotoxins in Foods. *Foods* **2020,** *9* (4), 518.
8. Guercetti, J.; Pascual, N.; Aviñó, A.; Eritja, R.; Salvador, J. P.; Marco, M. P., DNA-directed immobilization fluorescent immunoarray for multiplexed antibiotic residue determination in milk. *Analytical and Bioanalytical Chemistry* **2024**.
9. Liu, M.; Sang, Y.; Zhang, J.; Li, J.; Yu, W.; Zhang, F.; Wang, X., Development of a Broad-Specific Competitive ELISA for First-Generation Cephalosporin Antibiotics in Animal-Derived Foods Samples. *Bulletin of Environmental Contamination and Toxicology* **2021,** *107* (2), 215-220.
10. Shelver, W. L.; Shappell, N. W.; Franek, M.; Rubio, F. R., ELISA for Sulfonamides and Its Application for Screening in Water Contamination. *Journal of Agricultural and Food Chemistry* **2008,** *56* (15), 6609-6615.
11. Kim, S. C.; Carlson, K., Quantification of human and veterinary antibiotics in water and sediment using SPE/LC/MS/MS. *Anal Bioanal Chem* **2007,** *387* (4), 1301-15.
12. Aga, D. S.; O'Connor, S.; Ensley, S.; Payero, J. O.; Snow, D.; Tarkalson, D., Determination of the Persistence of Tetracycline Antibiotics and Their Degradates in Manure-Amended Soil Using Enzyme-Linked Immunosorbent Assay and Liquid Chromatography−Mass Spectrometry. *Journal of Agricultural and Food Chemistry* **2005,** *53* (18), 7165-7171.
13. Shi, X.; Zhang, S.; Zhang, Y.; Geng, Y.; Wang, L.; Peng, Y.; He, Z., Novel and simple analytical method for simultaneous determination of sulfonamide, quinolone,

tetracycline, macrolide, and chloramphenicol antibiotics in soil. *Analytical and Bioanalytical Chemistry* **2022,** *414* (22), 6497-6506.

14. Poms, R. E.; Klein, C. L.; Anklam, E., Methods for allergen analysis in food: a review. *Food Addit Contam* **2004,** *21* (1), 1-31.
15. Scharf, A.; Kasel, U.; Wichmann, G.; Besler, M., Performance of ELISA and PCR Methods for the Determination of Allergens in Food: An Evaluation of Six Years of Proficiency Testing for Soy (Glycine max L.) and Wheat Gluten (Triticum aestivum L.). *Journal of Agricultural and Food Chemistry* **2013,** *61* (43), 10261-10272.
16. Jayasena, S.; Smits, M.; Fiechter, D.; de Jong, A.; Nordlee, J.; Baumert, J.; Taylor, S. L.; Pieters, R. H.; Koppelman, S. J., Comparison of Six Commercial ELISA Kits for Their Specificity and Sensitivity in Detecting Different Major Peanut Allergens. *Journal of Agricultural and Food Chemistry* **2015,** *63* (6), 1849-1855.
17. Di Febo, T.; Schirone, M.; Visciano, P.; Portanti, O.; Armillotta, G.; Persiani, T.; Di Giannatale, E.; Tittarelli, M.; Luciani, M., Development of a Capture ELISA for Rapid Detection of Salmonella enterica in Food Samples. *Food Analytical Methods* **2019,** *12* (2), 322-330.
18. Cavaiuolo, M.; Paramithiotis, S.; Drosinos, E.; Ferrante, A., Development and optimization of an ELISA based method to detect Listeria monocytogenes and Escherichia coli O157 in fresh vegetables. *Analytical methods* **2013,** *5*, 4622–4627.
19. Mandli, J.; El Fatimi, I.; Seddaoui, N.; Amine, A., Enzyme immunoassay (ELISA/immunosensor) for a sensitive detection of pork adulteration in meat. *Food Chemistry* **2018,** *255*, 380-389.
20. Venbrux, M.; Crauwels, S.; Rediers, H., Current and emerging trends in techniques for plant pathogen detection. *Front Plant Sci* **2023,** *14*, 1120968.
21. Liu, W.; Meng, L.; Liu, X.; Liu, C.; Jin, W., Establishment of an ELISA Method for Quantitative Detection of PAT/pat in GM Crops. *Agriculture* **2022,** *12* (9), 1400.
22. Fu, W.; Chen, Y.; Wang, K.; Hettinghouse, A.; Hu, W.; Wang, J.-Q.; Lei, Z.-N.; Chen, Z.-S.; Stapleford, K. A.; Liu, C.-j., Repurposing FDA-approved drugs for SARS-CoV-2 through an ELISA-based screening for the inhibition of RBD/ACE2 interaction. *Protein & Cell* **2021,** *12* (7), 586-591.
23. Strohner, P.; Staatz, A.; Sarrach, D.; Steiss, J.-O.; Becher, G., The recoveryELISA – a newly developed immunoassay for measurement of therapeutic antibodies and the target antigen during antibody therapy. *Clinical Chemistry and Laboratory Medicine (CCLM)* **2012,** *50* (7), 1263-1269.
24. Garzon, V.; Salvador, J.-P.; Marco, M.-P.; G.-Pinacho, D.; Bustos, R.-H., Development and ELISA Characterization of Antibodies against the Colistin, Vancomycin, Daptomycin, and Meropenem: A Therapeutic Drug Monitoring Approach. *Antibiotics* **2024,** *13* (7), 600.
25. Han, L.; An, C.; Liu, D.; Wang, Z.; Bian, L.; He, Q.; Liu, J.; Wang, Q.; Liu, M.; Mao, Q.; Hang, T.; Wang, A.; Gao, F.; Tan, D.; Liang, Z., Development of an ELISA Assay for the Determination of SARS-CoV-2 Protein Subunit Vaccine Antigen Content. *Viruses* **2023,** *15* (1), 62.
26. Rey, G.; Schuetz, F.; Schroeder, D.; Kaluschke, C.; Wendeler, M. W.; Hofmann, I.; Dumbliauskas, E.; Obrdlik, P., Automated ELISA for potency measurements of therapeutic antibodies and antibody fragments. *Journal of Pharmaceutical and Biomedical Analysis* **2024,** *245*, 116141.
27. Tsurusawa, N.; Chang, J.; Namba, M.; Makioka, D.; Yamura, S.; Iha, K.; Kyosei, Y.; Watabe, S.; Yoshimura, T.; Ito, E., Modified ELISA for Ultrasensitive Diagnosis. *Journal of Clinical Medicine* **2021,** *10* (21), 5197.
28. Islam, K. N.; Ihara, M.; Dong, J.; Kasagi, N.; Mori, T.; Ueda, H., Micro Open-Sandwich ELISA to Rapidly Evaluate Thyroid Hormone Concentration from Serum Samples. *Bioanalysis* **2010,** *2* (10), 1683-1687.

29. Kumar, A.; Kalra, B.; Patel, A.; McDavid, L.; Roudebush, W. E., Development of a second generation anti-Müllerian hormone (AMH) ELISA. *Journal of Immunological Methods* **2010,** *362* (1), 51-59.
30. Bernard, D. J.; Ongaro, L., The Ultrasensitive Luteinizing Hormone (LH) ELISA Gets a New Lease on Life. *Endocrinology* **2022,** *163* (10), bqac123.
31. Yokoyama, S.; Takeuchi, A.; Yamaguchi, S.; Mitani, Y.; Watanabe, T.; Matsuda, K.; Hotta, T.; Shively, J. E.; Yamaue, H., Clinical implications of carcinoembryonic antigen distribution in serum exosomal fraction-Measurement by ELISA. *PLoS One* **2017,** *12* (8), e0183337.
32. Łupicka-Słowik, A.; Grzywa, R.; Leporowska, E.; Procyk, D.; Oleksyszyn, J.; Sieńczyk, M., Development and evaluation of an immunoglobulin Y-based ELISA for measuring prostate specific antigen in human serum. *Annals of Laboratory Medicine* **2019,** *39* (4), 373-380.
33. Wang, Y. S.; Ren, S. F.; Jiang, W.; Lu, J. Q.; Zhang, X. Y.; Li, X. P.; Cao, R.; Xu, C. J., CA125-Tn ELISA assay improves specificity of pre-operative diagnosis of ovarian cancer among patients with elevated serum CA125 levels. *Ann Transl Med* **2021,** *9* (9), 788.
34. de la Rica, R.; Stevens, M. M., Plasmonic ELISA for the ultrasensitive detection of disease biomarkers with the naked eye. *Nature Nanotechnology* **2012,** *7* (12), 821-824.
35. Kim, S.-H., ELISA for Quantitative Determination of Hepatitis B Virus Surface Antigen. *in* **2017,** *17* (6), 451-459.
36. Amanat, F.; Stadlbauer, D.; Strohmeier, S.; Nguyen, T. H. O.; Chromikova, V.; McMahon, M.; Jiang, K.; Arunkumar, G. A.; Jurczyszak, D.; Polanco, J.; Bermudez-Gonzalez, M.; Kleiner, G.; Aydillo, T.; Miorin, L.; Fierer, D. S.; Lugo, L. A.; Kojic, E. M.; Stoever, J.; Liu, S. T. H.; Cunningham-Rundles, C.; Felgner, P. L.; Moran, T.; García-Sastre, A.; Caplivski, D.; Cheng, A. C.; Kedzierska, K.; Vapalahti, O.; Hepojoki, J. M.; Simon, V.; Krammer, F., A serological assay to detect SARS-CoV-2 seroconversion in humans. *Nature Medicine* **2020,** *26* (7), 1033-1036.
37. Kim, J.; Tran, V. T.; Oh, S.; Jang, M.; Lee, D. K.; Hong, J. C.; Park, T. J.; Kim, H.-J.; Lee, J., Clinical Trial: Magnetoplasmonic ELISA for Urine-based Active Tuberculosis Detection and Anti-Tuberculosis Therapy Monitoring. *ACS Central Science* **2021,** *7* (11), 1898-1907.
38. Mangano, V. D.; Perandin, F.; Tiberti, N.; Guerriero, M.; Migliaccio, F.; Prato, M.; Bargagna, L.; Tais, S.; Degani, M.; Verra, F.; Bisoffi, Z.; Bruschi, F., Risk of transfusion-transmitted malaria: evaluation of commercial ELISA kits for the detection of anti-Plasmodium antibodies in candidate blood donors. *Malaria Journal* **2019,** *18* (1), 17.
39. Robert-Gangneux, F.; Dardé, M. L., Epidemiology of and diagnostic strategies for toxoplasmosis. *Clin Microbiol Rev* **2012,** *25* (2), 264-96.
40. Hayrapetyan, H.; Tran, T.; Tellez-Corrales, E.; Madiraju, C., Enzyme-Linked Immunosorbent Assay: Types and Applications. In *ELISA: Methods and Protocols*, Matson, R. S., Ed. Springer US: New York, NY, 2023; pp 1-17.
41. Liu, Y.; Liu, M.; Yan, H.; Liu, H.; Liu, J.; Zhao, Y.; Wu, Y.; Zhang, Y.; Han, J., Enhanced solubility of bisdemethoxycurcumin by interaction with Tween surfactants: Spectroscopic and coarse-grained molecular dynamics simulation studies. *Journal of Molecular Liquids* **2021,** *323*, 115073.
42. Shoaib, A.; Lone, N. A.; Yi, X., Co-infection with Pseudomonas aeruginosa impacts virulence of Staphylococcus aureus and intensifies the severity of infection. *Pak J Pharm Sci* **2020,** *33* (5), 1933-1937.
43. Nguyen, A. T.; Oglesby-Sherrouse, A. G., Interactions between Pseudomonas aeruginosa and Staphylococcus aureus during co-cultivations and polymicrobial infections. *Appl Microbiol Biotechnol* **2016,** *100* (14), 6141-6148.
44. Magalhães, A. P.; Jorge, P.; Pereira, M. O., Pseudomonas aeruginosa and Staphylococcus aureus communication in biofilm infections: insights through network and database construction. *Crit Rev Microbiol* **2019,** *45* (5-6), 712-728.

45. Park, J.; Jagasia, R.; Kaufmann, G. F.; Mathison, J. C.; Ruiz, D. I.; Moss, J. A.; Meijler, M. M.; Ulevitch, R. J.; Janda, K. D., Infection Control by Antibody Disruption of Bacterial Quorum Sensing Signaling. *Chemistry & Biology* **2007,** *14* (10), 1119-1127.
46. Junio, H. A.; Todd, D. A.; Ettefagh, K. A.; Ehrmann, B. M.; Kavanaugh, J. S.; Horswill, A. R.; Cech, N. B., Quantitative analysis of autoinducing peptide I (AIP-I) from Staphylococcus aureus cultures using ultrahigh performance liquid chromatography-high resolving power mass spectrometry. *J Chromatogr B Analyt Technol Biomed Life Sci* **2013,** *930*, 7-12.

5 BACTERIAL ISOLATES

5.1 CHAPTER PRESENTATION

In this chapter, the results obtained from the implementation of ELISAs for the measurement of AIPs in culture broth derived from S. aureus clinical and reference isolates will be discussed. After the optimization of ELISAs for AIPs, Tryptic Soy Broth (TSB) was selected as the culture medium for growing the different S. aureus clinical isolates. The primary objective of this chapter is the implementation of the developed ELISAs for the detection and quantification of AIPs in the culture supernatant of *S. aureus* isolates. These ELISAs were optimized to ensure sensitive and specific detection of AIPs in a matrix as complex as TSB.

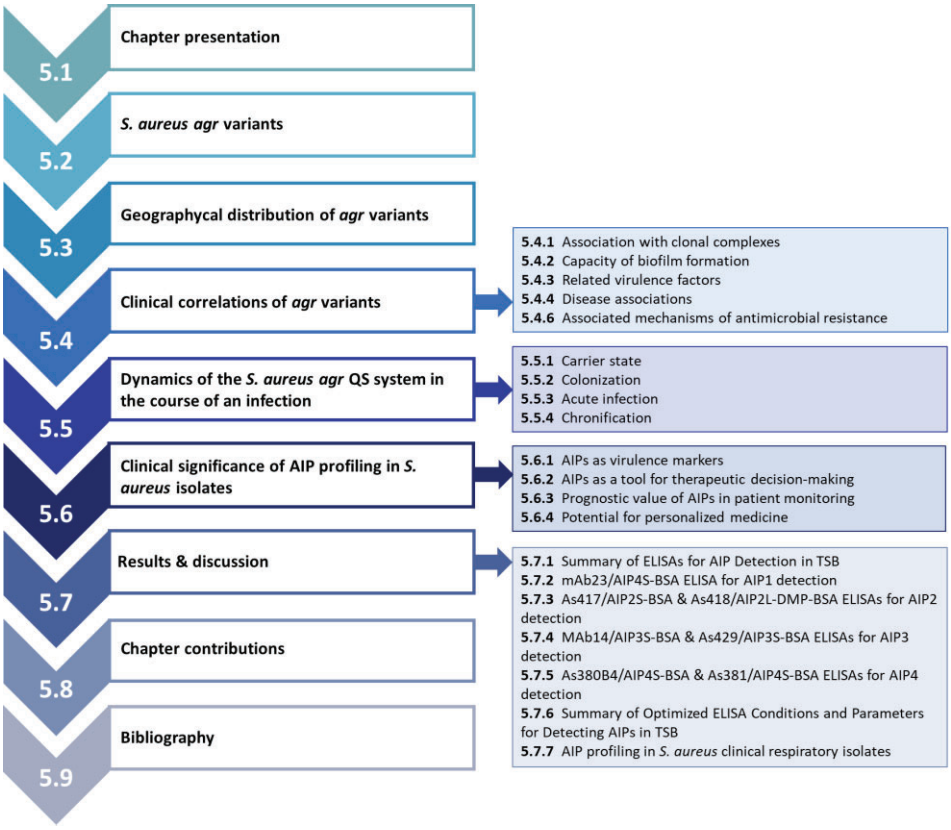

Figure 5.1. *Structure of Capter 5.*

The successful implementation and optimization of these ELISAs culminated in a highly sensitive and specific assay capable of profiling *S. aureus* strains representing the four agr groups. This chapter highlights how the developed technology enables the reliable detection and quantification of AIPs directly from the culture supernatants, providing insights into the QS dynamics of S. aureus.

Furthermore, the results obtained introduce this technology as a diagnostic and phenotyping tool, offering significant potential for various clinical applications. Its utility for identifying agr group-specific AIPs and phenotyping *S. aureus* strains makes it a valuable tool for infection monitoring, therapeutic guidance, and further understanding the virulence mechanisms of this bacterium. This work underscores the clinical relevance of AIP profiling as a step forward in improving the management of *S. aureus* infections. Figure 5.1 provides an overview on the structure of this chapter.

5.2 *S. AUREUS AGR* VARIANTS

Based on the structure and sequence of AIPs and their corresponding receptors, *S. aureus* strains are classified into four *agr* groups: *agr*-I, *agr*-II, *agr*-III, and *agr*-IV. Each *agr* group produces a unique AIP[1], which can activate its own receptor (intra-group activation) while inhibiting the receptors of other groups (inter-group inhibition)[2].

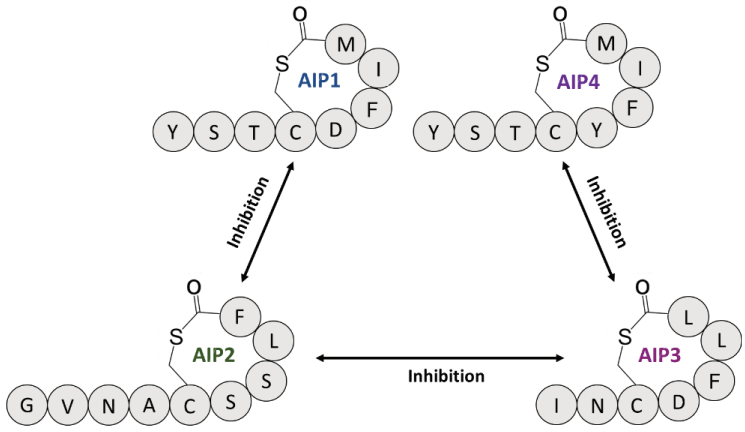

Figure 5.2. *Inhibitory interactions between the AIPs produced by the four agr groups of Staphylococcus aureus. Each AIP activates its corresponding agr group while inhibiting others.*

The inhibitory interactions between de different AIPs are shown in Figure 5.2. This specificity plays a critical role in bacterial communication and competition during colonization and infection. Understanding the *agr* groups is essential for studying S. aureus pathogenicity, strain phenotyping, and developing targeted therapeutic and diagnostic approaches.

5.3 GEOGRAPHICAL DISTRIBUTION OF *AGR* VARIANTS

The distribution of *S. aureus agr* variants shows a significant correlation with specific geographic regions, reflecting the dominance of particular clonal types across different parts of the world. This regional distribution is directly related to the way the *agr* system influences the production of virulence factors and bacterial interference, which in turn affects the success and prevalence of particular clones in different areas.

***Agr*-I** is predominantly found in Europe and parts of South America, including major clones such as the Iberian, Brazilian, Portuguese, Hungarian, Berlin, and EMRSA-15 clones (epidemic MRSA). These clones have consistently dominated in Europe, with significant dissemination of the Brazilian clone in South America, except in regions like Colombia where *agr* group II predominates. In German hospitals during the 1990s and early 2000s, *agr*-I clones, such as the Northern German (ST247), Hannover (ST254), Berlin (ST45), and Barnim (ST22) clones, were particularly widespread[3-5].

Clones from ***agr*-II** group, including the Pediatric and NY/Japan clones, are significantly widespread in Japan and North America. Though they are more frequently isolated in Japan and the US, these clones are also present in several European countries. In some regions, such as Portugal, *agr*-II clones such as the Pediatric clone have coexisted with *agr*-I clones in healthcare settings. This has highlighted the complex dynamics of agr group distribution within the same geographic area[5, 6].

***Agr*-III**, though less common than groups I and II, is mostly prevalent in Europe and is represented by the EMRSA-16 clone. Given their geographic distribution, *agr*-III strains may be more confined in European hospitals, which could explain their unique epidemiological patterns[3, 4].

***Agr*-IV** strains, though less frequently studied, have been associated with specific geographic regions, particularly in Europe. Despite being less widespread, *agr*-IV strains are noticeably more prevalent in several European regions, which may indicate that they have adapted to the local environment or are under selective pressure in areas where this kind of infections are more prevalent[7-9].

5.4 CLINICAL CORRELATIONS OF *AGR* VARIANTS

The pathogenic potential of a *S. aureus* strain is significantly influenced by its *agr* group, which is determined by the type of AIP it produces. The interaction between different AIP types is crucial, as cross-inhibition among them can influence bacterial competition and the dynamics of co-infections[10]. This means that the quantification of AIPs not only reveals the activity level of the *agr* system but also offers insights into the strain's virulence profile and its potential behavior in polymicrobial environments[11, 12].

This section will discuss the correlations described so far between the agr group of *S. aureus* strains with several of these clinical characteristics, which may actually influence the course of infection and the type of infection caused.

Some studies have attempted to associate *agr* variants with the distribution of clonal lineages, antibiotic resistance profile, biofilm formation capacity and the expression of virulence factors. However, despite some correlations were reported, the available literature on the relationship between specific agr groups of *S. aureus* and certain clinical conditions is quite limited. Establishing precise associations is challenging due to the complex interplay of various factors such as geographic distribution and environmental conditions. These variables underscore the need for more comprehensive, region-specific studies to better understand the clinical relevance of agr group variations.

Understanding the distribution and implications of each *agr* variant can be extremely helpful for effective diagnosis, treatment, and infection control in clinical settings. By identifying the specific *agr* group, clinicians could better predict the strain's virulence, anticipate potential co-infection scenarios, and adjust treatment strategies accordingly. This knowledge is also valuable for designing targeted interventions and improving infection control measures,

ultimately enhancing patient outcomes and reducing the spread of highly virulent or resistant strains.

5.4.1 ASSOCIATION WITH CLONAL COMPLEXES

A **clonal complex (CC)** refres to a group of genetically related strains that share a common ancestor, identified through genetic analysis like multilocus sequence typing (MLST). Within each CC, there are **lineages**, which are subgroups of strains that have diverged from the common ancestor but still retain significant genetic similarity. Essentially, a CC groups together closely related strains, while lineages within these complexes represent more specific evolutionary branche. Lineages often correlate with specific *agr* groups, influencing their virulence, biofilm formation, and the types of infections they cause. This association reflects the evolutionary history and adaptation of the lineages to various ecological niches and infection types[4, 13].

***Agr*-I** is predominantly found in **CC8, CC25, CC22, CC45** and **CC395**[6, 14]. This is the most common *agr* variant found in clinical isolates, particularly in strains causing invasive infections. These lineages are frequently implicated in HAIs, including MRSA strains. These strains are particularly associated with severe, invasive diseases, highlighting the significant role of *agr*-I group in the pathogenicity of *S. aureus* in healthcare settings[4].

Clonal lineages **CC5, CC12**, and **CC15** are typically associated with ***agr*-II**[6, 14]. This group is often involved in HA-MRSA infections, especially in clinical scenarios where biofilm formation is crucial, such as chronic wound infections or infections involving implanted medical devices. The ability of *agr*-II strains to form biofilms makes them particularly resilient in these contexts, contributing to their persistence and difficulty in treatment[14].

***Agr*-III** is most frequently linked to the **CC30**[6, 14]. This group is notable for leading to toxin-mediated diseases, including those driven by TSST-1. The strong association between agr-III and these toxin-driven conditions highlights the severity of infections caused by *S. aureus* strains belonging to this group[9].

Lastly, ***agr*-IV** is predominantly associated with **CC121**[6, 14]. Although less common than the other agr groups, it plays a significant role in specific clinical conditions,

particularly in generalized exfoliative syndromes such as bullous impetigo. The link between *agr*-IV and these syndromes draws attention to how serious infections carried on by this particular group can be[4].

5.4.2 CAPACITY OF BIOFILM FORMATION

Biofilm formation, a critical factor in chronic and device-related infections, varies significantly among the different *agr* groups in *S. aureus*. *Agr*-II and *agr*-III are the primary biofilm producers, with ***agr*-II** strains, especially MRSA, demonstrating a particularly **high capacity** for **biofilm formation**. This characteristic makes *agr*-II strains especially problematic in chronic infections (e.g., osteomyelitis and endocarditis) and those involving medical devices[15]. However, for ***agr*-III** strains the degree of biofilm formation is **variable**. While some studies suggest that *agr*-III strains are less likely to form biofilms, other research indicates that, under certain conditions, these strains can indeed produce substantial biofilms that contribute to their persistence in chronic infections and resistance to treatment[16, 17]. The virulence factors involved include extracellular matrix-binding proteins, which aid in bacterial adhesion and initial colony formation[17].

In contrast, ***agr*-I** strains, although primarily associated with virulent toxin production, generally have a **lower capacity** for biofilm formation compared to the previously mentioned groups. This lower biofilm-forming ability might explain why *agr*-I strains are more frequently linked to acute infections rather than chronic ones[16].

***Agr*-IV** strains, though less common, are equipped with SpA, MSCRAMM proteins and collagen-degrading enzymes. These factors enable to form biofilms that are not only large and resistant to antibiotics but also particularly **challenging to treat**, highlighting their potential role in difficult-to-manage infections[16].

5.4.3 RELATED VIRULENCE FACTORS

The distribution of virulence factors, including toxin genes, adhesins, and enzymes, is strongly associated with *agr* phylogeny, influencing the clinical manifestations and severity of infections caused by different *agr* variants[4].

***Agr*-I** strains are frequently linked to severe invasive infections due to their ability to produce potent **toxins** such as **hla** and **PVL**. These toxins are instrumental in the pathogenesis of serious conditions like necrotizing pneumonia and sepsis, making *agr*-I a significant marker of virulence in clinical settings[4]. Furthermore, *agr*-I strains also express **surface proteins** like **SpA**, which contribute to immune evasion by binding the Fc region of antibodies[6, 18].

***Agr*-II** strains are associated with the production of **biofilm-associated factors** like polysaccharide intercellular adhesin (**PIA**) and **FnBPs** facilitates robust biofilm formation, contributing to the persistence and antibiotic resistance observed in these infections[16].

***Agr*-III** is strongly associated with **toxin-mediated diseases**, notably toxic shock syndrome (TSS), due to the production of **TSST-1**. This toxin acts as a superantigen, triggering an overwhelming immune response that can lead to severe and rapid disease progression[4].

***Agr*-IV** strains, while less common, are closely linked with **exfoliative toxins** (ETs) which are responsible for conditions like staphylococcal scalded skin syndrome (SSSS) and bullous impetigo. ETs disrupt the epidermal layer, leading to widespread skin damage and detachment. Additionally, *agr*-IV strains can produce **enterotoxins**, which are implicated in staphylococcal food poisoning, underscoring their broad virulence potential[4, 9, 19].

5.4.4 DISEASE ASSOCIATIONS

Reflecting their distinct virulence profiles and mechanisms of pathogenesis, each *agr* variant in *S. aureus* can be more closely related with some particular diseases. These associations are critical for understanding the clinical impact of different *agr* groups and for selecting appropriate therapeutic strategies.

Agr groups **I and II** are predominantly linked to **suppurative infections**, which involve the formation of pus and include severe conditions. ***Agr*-I** is particularly associated with **HAIs**, where the environment favors the spread and persistence of highly virulent strains. These strains are frequently isolated from patients with endocarditis and bacteremia, where their virulence factors, such as hla and SpA, play a significant role in tissue destruction and immune evasion. The strong

association of *agr*-I with HAIs underscores the need for more strict infection control measures in healthcare settings to prevent the spread of these highly pathogenic strains[4].

On the other hand, ***agr*-II** strains are more commonly associated with **chronic wound infections**, which are characterized by prolonged inflammation and delayed healing, often due to the biofilm-forming capacity of these strains. The ability to form robust biofilms allows *agr*-II strains to persist in wounds, resist antibiotic treatment, and evade the host immune response, leading to chronicity and increased morbidity in affected patients. This association highlights the role of *agr*-II in difficult-to-treat conditions that require comprehensive management strategies, including advanced wound care and prolonged antibiotic therapy[4].

In contrast, ***agr*-III** and ***agr*-IV** are primarily associated with **toxin-mediated diseases**, which are characterized by the production of specific toxins that lead to severe clinical syndromes. ***Agr*-III** strains are frequently involved in cases of **TSS**, a life-threatening condition caused by the overproduction of TSST-1[13]. This toxin induces a massive immune response, leading to symptoms such as high fever, rash, and hypotension, which can rapidly progress to multi-organ failure if not promptly treated. The strong link between *agr*-III and TSS makes this *agr* group particularly concerning in in infections associated with tampon use and in clinical settings, especially after surgical interventions[20].

***Agr*-IV** strains are associated with generalized exfoliative syndromes such as **bullous impetigo** and **SSSS**[21]. These conditions are caused by exfoliative toxins (eta and etb), which cleave the desmosomes in the epidermis, leading to blistering and widespread skin detachment[4]. The implication of *agr*-IV in these diseases highlights its role in dermatological conditions where skin integrity is severely compromised, often affecting neonates and young children who are particularly vulnerable to these toxins[22]. These syndromes necessitate rapid diagnosis and treatment to prevent complications and ensure effective management.

5.4.5 ASSOCIATED MECHANISMS OF ANTIMICROBIAL RESISTANCE

Research on the association between *agr* variants and antibiotic resistance in *S. aureus* has revealed significant insights crucial for managing and treating

infections, especially MRSA. The established link between specific *agr* groups and resistance mechanisms underscores the value of *agr* typing in clinical microbiology. Understanding these correlations can help clinicians to anticipate resistance patterns more accurately and guide therapeutic strategies effectively, making agr typing a promising tool for personalizing targeted treatments.

***Agr*-I** is strongly linked to high levels of resistance to **beta-lactam** antibiotics, especially **methicillin**, and is commonly associated with HA-MRSA strains[23]. These strains frequently carry mutations in the *mecA* gene, which PBP2a, leading to their resistance to beta-lactams[24]. Moreover, *agr*-I strains have been observed to exhibit MDR, particularly to aminoglycosides and fluoroquinolones, making them particularly challenging to treat in healthcare settings[13, 15, 25]. The high incidence of these strains in hospital environments underlines the necessity of understanding its resistance mechanisms to develop effective treatment strategies.

S. aureus strains grouped as ***agr*-II** are notably associated with resistance to **glycopeptides**, such as **vancomycin**, and with a strong ability to form biofilms. Biofilm formation significantly enhances resistance to various antibiotics by providing a protective barrier that limits drug penetration. These strains often carry the *vanA* gene cluster, directly contributing to vancomycin resistance, a trend frequently observed in CA-MRSA[6, 23]. The capacity of biofilm formation in *agr*-II strains also correlates with resistance to **macrolides** and **lincosamides**, further complicating treatment approaches in infections where these strains are involved.

***Agr*-III** is primarily associated with toxin-mediated virulence and display resistance to protein synthesis inhibitors like **tetracyclines** and **aminoglycosides**[4]. Although *agr*-III strains are less frequently linked to widespread antibiotic resistance compared to *agr*-I and *agr*-II, their emergence in community settings, particularly in the context of PVL-positive MRSA, poses a growing concern. Moreover, there is an increasing relevance of *agr*-III strains in non-hospital environments, where their resistance profiles are becoming more prominent.

Interestingly, ***agr*-IV** strains are the only ones that have **not acquired** the ***mecA*** gene which encodes PBP2a and confers resistance to beta-lactam antibiotics [9]. *Agr* group IV, while less commonly studied, was linked to resistance against

against **rifampin** and **trimethoprim**[23]. The limited incidence of this group emphasizes the need for continued research to fully understand its impact on treatment outcomes, especially in regions where the diseases associated to this group are prevalent.

5.4.6 SUMMARY ON REPORTED CORRELATIONS

Table 5.1 summarizes all the reported correlations discussed in Section 5.4:

Table 5.1. *Summary on the correlations between each agr variant and different bacterial or clinical features.*

Attribute	*agr*-I	*agr*-II	*agr*-III	*agr*-IV
Clonal Complexes	CC8, CC25, CC22, CC45, and CC395	CC5, CC12, and CC15	CC30	CC121
Biofilm Formation	Lower capacity.	High capacity, especially MRSA.	Variable biofilm formation	Large, antibiotic-resistant biofilms.
Virulence Factors	Toxins: hla and PVL. Surface proteins: SpA	Biofilm-associated factors: PIA and FnBPs	TSST-1	Exfoliative toxins and enterotoxins
Diseases	Healthcare-associated infections like endocarditis and bacteremia	Chronic wound infections and device-related infections	Toxin-mediated diseases: e.g. toxic shock syndrome	Exfoliative syndromes: bullous impetigo, SSSS
Antimicrobial Resistance	Methicillin (HA-MRSA); MDR to aminoglycosides and fluoroquinolones	Glycopeptides (e.g. vancomycin)	Tetracyclines and aminoglycosides	Rifampin and trimethoprim. Not beta-lactam resistant

5.5 DYNAMICS OF THE *S. AUREUS AGR* QS SYSTEM IN THE COURSE OF AN INFECTION

As detailed in Section 1.7 (Chapter 1), the *agr* system is crucial for the dynamic control of *S. aureus* virulence factor expression. By responding to changes in bacterial population density, this system allows *S. aureus* to strategically modulate its behavior during different stages of infection, optimizing its ability to colonize, evade the immune response, and cause disease.

The activation of the *agr* system varies significantly depending on the stage of the infection and the surrounding environment. When the system is activated by high concentrations of AIPs, RNAIII is produced, which is a key regulatory

molecule that controls the expression of numerous genes involved in virulence. In the meantime, RNAIII downregulates the expression of surface adhesins, which are more important during the initial stages of infection for colonization. This regulatory switch from adhesin production to toxin production reflects a strategic shift from stable colonization to active infection, allowing *S. aureus* to effectively invade and damage host tissues during the acute phase of infection [26-28].

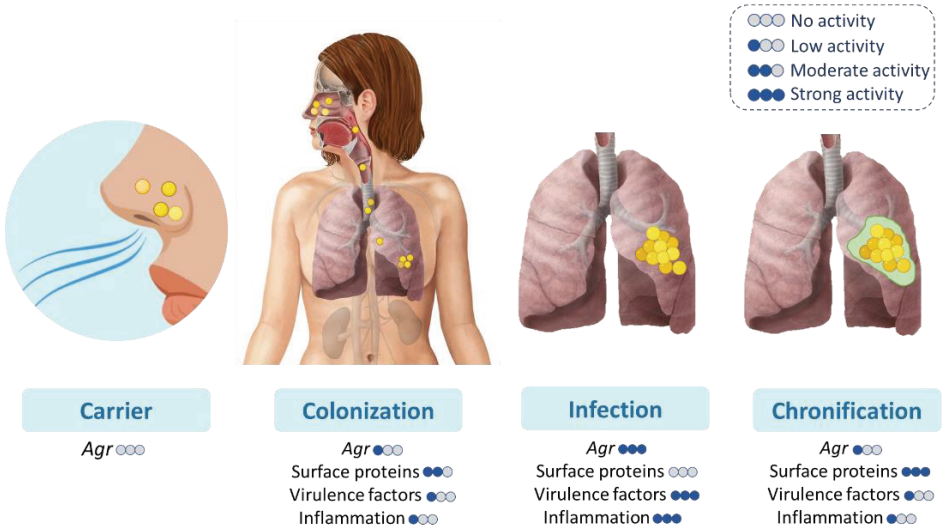

Figure 5.3. *Schematic representation of the regulation (activation/inactivation) of the agr QS system during the course of a low tract respiratory infection. The figure illustrates the four stages of an infection: carrier state, colonization, acute infection, and chronification. For each stage, the activity of the agr system is indicated along with its modulation of virulence factor expression and adhesion mechanisms. Additionally, the inflammatory response triggered at each stage is detailed, showing how the agr system dynamically influences the progression and outcome of the infection. This illustration provides a clear overview of the role of the agr system in transitioning from colonization to active infection and its impact on the host's immune response.*

A thorough examination of the variations in the *agr* system activation/deactivation and the expected AIP profile at the several stages of infection is provided below (see Figure 5.3 for a graphical representation summarizing all the content).

5.5.1 CARRIER STATE

The carrier state, or being a carrier, refers to an asymptomatic individual who harbors a pathogen without showing any signs or symptoms of an infection. Carriers can harbor the bacteria intermittently or persistently, serving as reservoirs and potentially transmitting the pathogen to others, especially in healthcare settings[29]. Clinically, carriers do not require treatment unless they are at high risk of developing an infection or are in situations where transmission to vulnerable individuals could occur, such as in surgical settings or in individuals with compromised immune systems[30].

In the context of *S. aureus*, it resides asymptomatically in the nostrils, skin, or other mucosal surfaces, where it constitutes part of the normal flora in healthy individuals[29]. During this phase, the *agr* system remains in a low activity state due to the typically low bacterial density. AIP levels are minimal, which likely serves as an adaptive strategy to avoid triggering the host's immune response. By keeping virulence factor production low, *S. aureus* can maintain a commensal relationship with the host, persisting without causing harm[1, 27].

5.5.2 COLONIZATION

Colonization refers to the process by which *S. aureus* establishes itself on a host surface, such as the skin or mucous membranes, without causing an active infection or disease. During colonization, the bacteria adhere to epithelial cells and begin to multiply, forming a stable microbial community. Even while colonization is usually asymptomatic and can last for an extended period of time, it is an antecedent to infection, particularly in immunocompromised people or in situations where the skin or mucosal barrier has been weakened. Clinically speaking, colonization possesses significance since it raises the possibility of infection and transmission, especially in hospitals, where colonized people may infect other patients or medical personnel[31].

During colonization, *S. aureus* begins to establish itself in new niches within the host. The bacterial density increases slightly to avoid provoking a strong immune response[32]. In this state, the agr system is either inactivated or showing low activity[33, 34]. The bacterium focuses on adhesion and immune evasion rather than virulence, minimizing the production of aggressive virulence factors and leading

to the expression of surface proteins that facilitate attachment to host tissues[32]. Thus, low AIP levels during colonization enable the bacteria to establish themselves in host tissues without triggering a strong inflammatory response.

5.5.3 ACUTE INFECTION

An acute infection is characterized by the rapid onset of symptoms resulting from the active multiplication of the pathogenic microorganisms, leading to inflammation and tissue damage. Acute *S. aureus* infections can manifest in various forms, including skin and soft tissue infections (such as abscesses, cellulitis, and impetigo), bacteremia, endocarditis, and pneumonia. These infections are typically marked by local signs of inflammation (redness, warmth, swelling, and pain) and systemic symptoms such as fever[35]. Acute infections often require prompt medical intervention, including antibiotics, to prevent complications and limit the spread of the infection. The severity of the infection is influenced by both the virulence of the *S. aureus* strain and the host's immune response[36].

Regarding the activity of the *agr* QS system, it reaches its peak activity during acute infections, where the bacterial population density increases rapidly. The high density triggers a substantial rise in AIP levels, leading to full activation of the system. This results in the upregulation of a wide array of virulence factors, including hemolysins, proteases, and other toxins that facilitate tissue invasion and immune evasion[10]. The acute phase is characterized by rapid bacterial proliferation, significant tissue damage, and a strong inflammatory response from the host. This phase is often associated with severe clinical symptoms due to the aggressive nature of the infection[36].

5.5.4 CHRONIFICATION:

Chronic infections can be defined as those that persist over an extended period, often due to inadequate initial treatment or the presence of underlying health conditions that compromise the immune system and limit the host's ability to clear the infection. From a clinical perspective, an infection is considered chronic when it lasts for more than three months despite appropriate treatment, or

when it recurs after apparently successful therapy. These infections are typically associated with ongoing symptoms, such as low-grade inflammation, pain, or dysfunction of the affected area, and may show intermittent exacerbations.

When an infection caused by *S. aureus* chronifies, it can be long-lasting and persistent. Clinically, these infections are challenging to treat and often require prolonged antibiotic therapy, sometimes in combination with surgical removal of infected devices or tissue. Chronic *S. aureus* infections are particularly problematic in patients with CF, osteomyelitis, or endocarditis, where they can lead to ongoing inflammation, tissue damage, and serious complications[37].

In chronic infections, the dynamics of the *agr* system changes significantly. The activation of this system may be low or intermittent, which is often associated with a reduced bacterial density or the presence of mutations in the *agr* operon that impede its function (*agr*-). These mutations or downregulations lead to decreased production of virulence factors, allowing *S. aureus* to evade immune detection and persist within the host over extended periods[38]. This adaptive strategy helps them survive long-term within the host is crucial for *S. aureus* to establish a persistent infection, often leading to prolonged and difficult-to-treat infections[39].

Biofilm formation is a critical aspect of chronic *S. aureus* infections, as they can be adhered to surfaces such as medical devices (e.g., catheters, implants, prosthetic joints, etc.) or damaged tissues[25]. They provide a protective environment that defends *S. aureus* from antibiotics and immune cells, making the infection difficult to eradicate. The structural complexity and regulation of biofilms allow *S. aureus* strains to survive in hostile environment and persist in chronic infections, becoming a significant concern in clinical settings, particularly in infections that are difficult to manage with conventional therapies[40].

Within a biofilm, *agr* activity is typically reduced, leading to lower AIP levels. This reduction in *agr* activity is beneficial for biofilm stability, as it decreases the production of dispersal factors and toxins that could disrupt the biofilm structure. At the initial stage of biofilm formation, the concentration of AIPs is low, which prevents the *agr* system from being activated. This decreased activity makes it easier for bacteria to initially adhere to surfaces and form microcolonies.

As the biofilm evolves, AIP concentration rises because the growing bacterial population produces more of them. The *agr* system, which controls the expression of virulence factors and genes linked to biofilms, can be partially activated by this elevated AIP level. This will help the bacteria remain within the biofilm and survive. In a mature biofilm, AIP levels are typically high, potentially triggering *agr* activation and promoting biofilm dispersal. This activation of dispersal mechanisms, induced by high AIP concentrations, allows bacteria to leave the biofilm and spread to new sites within the host, potentially leading to new foci of infection[41, 42].

5.6 CLINICAL SIGNIFICANCE OF AIP PROFILING IN *S. AUREUS* ISOLATES

The detection and quantification of AIPs in clinical isolates of *S. aureus* are highly valuable for the better understanding of its pathogenic potential. As previously explained in Section 1.7, AIPs initiate the activation of the *agr* system once their concentration reaches a threshold level, triggering the expression of virulence genes in a coordinated manner. Therefore, measuring AIP levels provides insights into the activation state of the *agr* system, which is directly linked to to the ability of this pathogen to cause an infection.

Furthermore, the *agr* system is not uniform across all *S. aureus* strains. It is divided into four major groups (*agr* I-IV) based on the sequence variation in the AIPs and their corresponding receptors. Each *agr* group is associated with different patterns of virulence, biofilm formation, and clinical outcomes, making the identification of the specific *agr* type in clinical isolates highly valuable for tailoring appropriate therapeutic and infection control strategies. Thus, identifying the specific AIP variants produced by a certain bacterial strain and measuring their concentrations within a clinical sample can be really helpful for assessing virulence, informing therapeutic strategies, and guiding infection control measures.

5.6.1 AIPS AS VIRULENCE MARKERS

As mentioned beforehand, the *agr* system controls the expression of numerous virulence factors, such as toxins, proteases, and surface proteins that facilitate tissue invasion and immune evasion. When the concentration of AIPs reaches a certain threshold, the system is activated, leading to a coordinated expression of these virulence genes.

High levels of AIPs in a clinical isolate suggest an upregulated *agr* system, indicating that the bacteria are in a virulent state, actively expressing factors that enhance their pathogenicity. Therefore, quantifying AIP levels in clinical isolates can provide a direct indication of the degree of *agr* activation, and consequently, the virulence potential of a *S. aureus* strain. This information is highly valuable for clinicians, as it can influence the aggressiveness of the treatment approach.

5.6.2 AIPS AS A TOOL FOR THERAPEUTIC DECISION-MAKING

In addition to serving as a marker of virulence, AIP quantification can guide therapeutic decisions, particularly in the context of developing or applying quorum sensing inhibitors (QSIs) as complementary treatments. The key role of the *agr* system in regulating virulence mechanisms makes it an attractive target for novel therapeutic strategies. By disrupting AIP signaling, QSIs can potentially attenuate the expression of virulence factors, reducing the severity of infection without exerting selective pressure for antibiotic resistance[43].

Understanding the specific AIP profile of a *S. aureus* clinical isolate allows for more personalized therapeutic approaches. For instance, the identification of high AIP levels might prompt the use of QSIs combined with conventional antibiotics to diminish the virulence of the bacteria and improve patient outcomes. This approach could be particularly valuable in treating infections caused by MDR *S. aureus* strains, where traditional antibiotics alone may be insufficient[44].

5.6.3 PROGNOSTIC VALUE OF AIPS IN PATIENT MONITORING

AIP profiling in *S. aureus* clinical isolates can provide significant prognostic value, particularly in the context of patient monitoring and the management of ongoing or recurrent infections. AIPs serve as biomarkers for the activation of the *agr* system, which regulates the pathogenic potential of the bacterium. Monitoring AIP levels in patients, especially those at high risk for severe or recurrent infections, will offer to clinicians a powerful tool for predicting disease progression, anticipating exacerbations, and adapting treatment strategies providing a personalized approach.

5.6.3.1 Infection onset and severity prediction

As AIPs are directly involved in the regulation of virulence in *S. aureus*, their increased levels can provide early indications of infection onset or the likelihood of an upcoming exacerbation. In patients who are colonized with *S. aureus* or who have suffered recurrent infections, periodic monitoring of AIP levels can reveal the activation of the *agr* system before clinical symptoms become apparent. Elevated AIP levels may signal that the bacterium is transitioning from a quiescent state to an active virulent phase, enabling clinicians to intervene early, potentially preventing the full development of an infection.

In high-risk patient populations, such as those with chronic conditions, immunosuppression, or implanted medical devices, the ability to detect and respond to rising AIP levels could be of particular interest. For example, in patients with CF or chronic wounds, monitoring AIP levels could help predict the likelihood of infection outbreaks, allowing for preventive measures in treatment plans, such as the initiation of targeted antibiotics or the use of QSIs.

5.6.3.2 Treatment guidance during chronic infections

In the context of chronic infections, such as those associated with biofilm formation on medical devices or in tissues, AIP monitoring offers a method for assessing the effectiveness of ongoing treatment. A reduction in AIP levels could indicate successful suppression of the *agr* system and a corresponding decrease in virulence factor expression, suggesting that the infection is under control.

Conversely, persistently high or rising AIP levels might indicate treatment failure, the presence of resistant bacterial populations, or the potential for relapse, prompting a re-evaluation of the therapeutic approach.

For patients undergoing long-term antibiotic therapy, AIP levels can serve as an important marker of treatment efficacy, helping to avoid unnecessary prolongation of therapy or, conversely, to signal the need for more aggressive intervention if standard treatments are not achieving the desired effect.

5.6.3.3 Anticipation of relapses and management of exacerbations

In patients with a history of recurrent *S. aureus* infections, monitoring AIP levels could help predict the likelihood of recurrence, providing valuable prognostic information. This information could be used to implement preventive measures, such as prophylactic antibiotic use, decolonization strategies, or even the use of experimental therapies aimed at disrupting QS and preventing the reactivation of virulent *S. aureus* populations.

Furthermore, in patients with chronic conditions where *S. aureus* plays a role in disease exacerbations, such as in chronic obstructive pulmonary disease (COPD)[45], CF[46] or atopic dermatitis[47], monitoring AIP levels may aid in anticipating future episodes and adjusting treatment plans. Early intervention in response to rising AIP levels could mitigate the severity of exacerbations and improve patient outcomes.

5.6.4 POTENTIAL FOR PERSONALIZED MEDICINE

The integration of AIP monitoring into routine clinical practice may represent a step towards personalized medicine in the management of *S. aureus* infections. By customizing treatment programs based on the unique *agr* profile and AIP activity of the infecting strain, clinicians could adapt therapeutic strategies to meet the specific needs of individual patients.

Inhibiting the *agr* system can effectively reduce the virulence of *S. aureus*, making infections easier to treat and less likely to result in severe outcomes. By targeting the *agr* system, therapies can disrupt QS mechanisms, thereby

downregulating the expression of virulence factors[48]. This approach is particularly useful in treating infections caused by antibiotic-resistant strains, such as MRSA, where traditional antibiotic therapies may be less effective. Ongoing research is focused on developing small molecules and peptides that can interfere with AIP signaling, offering an alternative to combact *S. aureus* infections without relying excusively on antibiotics[48, 49].

As the understanding of AIP dynamics in infection progresses, their relevance in individualized patient care is likely to grow, making AIP monitoring a valuable component to guide treatment decisions in *S. aureus* infections. This approach could reduce the risk of overtreatment, minimize the development of resistance, and enhance overall patient outcomes.

5.7 RESULTS & DISCUSSION

5.7.1 SUMMARY OF ELISAS FOR AIP DETECTION IN TSB

As a reminder, *Table 5.2* provides an overview of the ELISAs developed for each AIP, which will be implemented for their detection in TSB.

Table 5.2. *Overview of Developed ELISAs to be implemented for AIP detection in TSB.*

ELISA	AIP detected
mAb23/AIP4S-BSA	AIP1o
As417/AIP2S-BSA	AIP2o
As418/AIP2L-DMP-BSA	AIP2o
mAb14/AIP3S-BSA	AIP3c
As429/AIP3S-BSA	AIP3o
As380/AIP4S-BSA	AIP4c
As381/AIP4S-BSA	AIP4o

5.7.2 MAB23/AIP4S-BSA ELISA FOR AIP1 DETECTION

5.7.2.1 Matrix effect evaluation

The implementation of the developed ELISAs for the detection of *S. aureus* AIPs in culture media is a critical approach for understanding the role of QS in *S. aureus* pathogenicity. *S. aureus* is commonly cultured in TSB, a medium widely used due to its suitability for supporting the growth and proliferation of this bacterium. TSB is a rich, non-selective, complex medium composed of enzymatic digests of casein and soybean meal, which provide an abundant source of amino acids, peptides, and other nitrogenous compounds necessary for bacterial metabolism. Additionally, TSB contains glucose as a readily metabolizable carbohydrate source, sodium chloride to maintain osmotic balance, and dipotassium phosphate as a buffering agent to stabilize the pH during bacterial growth. TSB is commonly used for the preparation of bacterial inocula, maintaining bacterial cultures, and in experiments requiring large volumes of bacterial cells. The use of TSB is particularly advantageous when growing *S. aureus* in large quantities for further testing, such as antibiotic susceptibility or biochemical assays[50].

Despite its benefits for bacterial culture, TSB poses certain challenges when it comes to detecting AIPs using ELISA. The complexity of this medium, with its high protein content and various other components, can interfere with the ELISA by causing non-specific binding to the antibodies, thereby increasing background noise and potentially leading to false-positive results. Furthermore, the presence of glucose and buffer components like dipotassium phosphate can influence the pH of the medium, altering antigen-antibody interactions and affecting the activity of HRP. Sodium chloride, another component of TSB, may also impact protein-protein interactions, which could lead to altered assay performance[51].

To address the potential matrix effect of the medium, ELISA performance must be carefully evaluated when applied to samples derived from TSB. The evaluation is carried out by comparing the calibration curve generated in PBST with calibration curves prepared in TSB and in TSB diluted at different ratios. All curves are generated on the same ELISA plate to eliminate inter-plate variability and ensure a direct comparison of the effects of TSB on the assay's performance.

This approach allows for a clear assessment of how the presence of TSB and its dilution levels influence the analytical parameters of the ELISA. The final aim is to determine any possible effect caused by TSB components and to identify the optimal dilution factor that minimizes them to achieve the best possible balance between sensitivity, specificity, and robustness. The matrix effect evaluation is crucial for optimizing the ELISA, ensuring that it provides accurate and reliable measurements of AIPs even in the presence of complex media like TSB.

In this point, it is important to highlight the novel hypothesis that emerged during this research, which led to a pivotal shift in our approach. The thiolactone ring in AIPs is known for its labile nature which suggests that, when a *S. aureus* strain grows in culture media or under physiological conditions, this bond may break, resulting in the peptides adopting a linear form.

Given this possibility, we revised our strategy to focus on detecting the linear forms of AIPs. This approach is optimal because, if the AIPs remain in their thiolactone form, they can be easily converted to their linear forms by a simple treatment. Specifically, for the detection of AIP1 and AIP2, it became necessary to implement a sample treatment step to break any existing thiolactone bonds, as the antibodies we produced are specific for the linear forms (AIP1o and AIP2o).

The selected treatment involves treating the samples with a basic solution, by adding sodium hydroxide (NaOH). This alkaline environment facilitates the cleavage of the thiolactone ring in AIPs, converting them to their linear form. This treatment proved to be effective in linearizing the AIPs with a treatment time of 15 minutes established to ensure complete conversion to the linear form. After this period, the samples are neutralized to a pH of 7.5 to stop the reaction (see detailed procedure in materials & methods Section 8.6.3).

Consequently, the matrix effect of mAb23/AIP4S-BSA ELISA (AIP1o detection) was evaluated using TSB that had undergone this treatment, referred to as hydrolyzed TSB (TSB-h). The NaOH treatment ensures that the total AIP amount in the samples is fully linearized, enabling reliable detection with the ELISAs that specifically detect the linear AIPs. For the ELISAs designed to detect AIP3 and AIP4, hydrolysis treatment is unnecessary, as specific assays have been developed to target both the open (linear) and closed (thiolactone) forms of

these AIPs. This allows for accurate detection without the need to convert the peptides to their linear form.

The matrix effect study revealed that the ELISA for detecting **AIP1o** experienced significant interference caused by the TSB medium. As shown in Figure 5.4, the presence of undiluted TSB had a considerable impact on the assay's performance, drastically reducing the signal (0.50 in TSB compared to 0.92 in PBST). However, when the TSB was diluted 1/2 in PBST, the signal was substantially recovered (0.80), while the sensitivity of the ELISA remained nearly unaffected (24.39 nM in TSB 1/2 versus 20.57 nM in PBST) (see Table 5.3).

Further dilution of the TSB resulted in a slight increase in absorbance, though without any meaningful gains in signal strength, and it led to a noticeable decrease in assay sensitivity. Based on these findings, 1/2 dilution of TSB was selected as the optimal condition for mitigating the matrix effect in this assay. This dilution effectively balances the recovery of signal strength with minimal loss of sensitivity, ensuring more reliable detection of AIP1o in TSB.

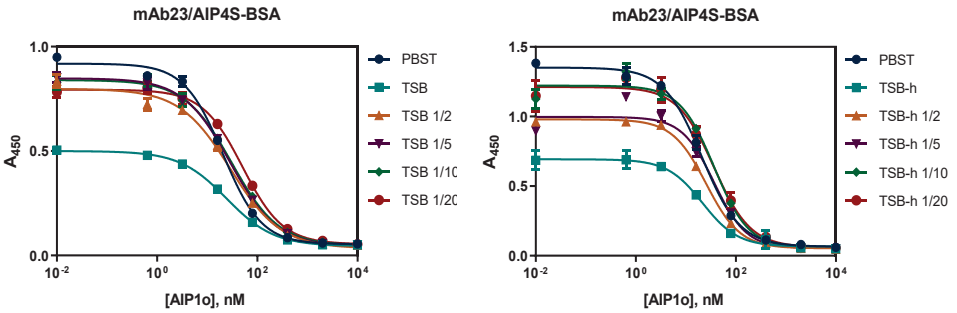

Figure 5.4. *Calibration curves for the competitive indirect ELISA mAb23/AIP4S-BSA conducted in PBST, TSB, TSB-h and various dilutions in PBST. The results are presented as the mean values with standard deviations from duplicate measurements. The conditions of the indirect competitive ELISAs used are specified in Table 5.17.*

As for TSB-h, although it has a notable effect on the assay's signal, it affects its sensitivity to a lesser extent. Overall, the interferences caused by TSB-h do not significantly compromise the performance of the assay. According to the data presented in Figure 5.4, when comparing the calibration curve obtained in PBST with that in undiluted TSB-h, the A_{max} notably decreased from 1.35 to 0.69. Despite this reduction in signal intensity, the IC_{50} value remained consistent at

21 nM in both cases (refer to Table 5.4). This suggests that while the signal in undiluted TSB is lower, it is still within a workable range for the assay

However, it is important to consider that if the concentrations of immunoreactants were adjusted to achieve an A_{max} of 1 in TSB-h, the IC_{50} would likely increase, indicating a potential decrease in assay sensitivity. The matrix effect of TSB-h on the assay's sensitivity becomes more evident as TSB-h is progressively diluted in PBST. As the dilution factor increases, the A_{max} gradually recovers, yet the sensitivity, as indicated by the IC_{50}, does not fully return to the levels observed in PBST (refer to Table 5.4).

The optimal dilution appears to be TSB-h 1/2, where the A_{max} approaches 1 (0.97), and the IC_{50} remains close to that observed in PBST (25.57 nM compared to 21.05 nM in PBST). This finding suggests that the assay can be performed directly in TSB-h, though with some compromise on signal intensity (see Table 5.4). The 1/2 dilution achieves a balance, providing a near-optimal signal while maintaining similar sensitivity to that achieved in PBST, making it a practical choice for detecting AIPs in *S. aureus* culture broths.

Table 5.3. *Analytical parameters of the competitive indirect ELISA mAb23/AIP4S-BSA conducted in PBST, TSB and various dilutions in PBST.*

Parameters	PBST	TSB	TSB 1/2	TSB 1/5	TSB 1/10	TSB 1/20
A_{min}	0.05	0.04	0.03	0.04	0.05	0.05
A_{max}	0.92	0.50	0.80	0.85	0.84	0.79
Slope	-1.13	-0.92	-0.86	-0.93	-0.92	-1.08
IC_{50} (nM)	20.57	24.39	28.74	28.70	30.94	50.79
R^2	0.996	0.999	0.993	0.999	0.997	0.998

Table 5.4. *Analytical parameters of the competitive indirect ELISA mAb23/AIP4S-BSA conducted in PBST, TSB-h and various dilutions in PBST.*

Parameters	PBST	TSB-h	TSB-h 1/2	TSB-h 1/5	TSB-h 1/10	TSB-h 1/20
A_{min}	0.07	0.07	0.05	0.05	0.06	0.06
A_{max}	1.35	0.69	0.98	1.00	1.22	1.21
Slope	-1.14	-1.23	-1.28	-1.35	-1.26	-1.18
IC_{50} (nM)	21.05	21.52	25.57	36.78	36.70	36.52
R^2	0.997	0.985	0.999	0.981	0.988	0.987

5.7.2.2 Sample treatment for the quantification of the total amount of AIP1 in bacterial culture

Despite having a complete set of assays for detecting the four AIPs of *S. aureus*, specific ELISAs for both the open and closed forms of each AIP have not been developed. For AIP3 and AIP4, two separate ELISAs are available, each specific to the closed or open form. However, for AIP1 and AIP2, a single ELISA has been developed for each, specifically recognizing the open form.

Because bacterial culture samples may contain both cyclic (closed) and linear (open) forms of AIPs, for AIP1 and AIP2 it is necessary to treat the sample to ensure that the total AIP content is converted to the linear form, allowing for accurate quantification. To address this, a simple treatment protocol was established, involving the addition of 0.1 M NaOH for 15 minutes (see Section 8.6.3).

5.7.2.3 UPLC-MS analysis of AIP1c hydrolysis kinetics subjected to NaOH treatment

To determine the optimal hydrolysis treatment time required to fully hydrolyze the total AIP content in a sample, the kinetics of the hydrolysis process were studied using UPLC-MS taking AIP1 as a model. A solution of ACN:H_2O (10:90) was spiked with 10 µM AIP1c, and hydrolysis was initiated by adding 20 µL of 5 N NaOH to 980 µL of the spiked sample. To stop the hydrolysis reaction, pH was neutralized to 7.5.

The hydrolyzed samples were analyzed by UPLC-ToF MS under positive ionization. The results provide information on the progression of the hydrolysis reaction by monitoring the mass-to-charge ratios (m/z). As positive ionization MS was employed to analyze the samples, both the exact mass of the neutral molecule (M) and the m/z ratio corresponding to the singly protonated ion ($[M+H]^+$) were considered during spectral analysis, reflecting the addition of a proton: AIP1c ($[M]^+$= 960 m/z; $[M+1]^+$= 961 m/z) and AIP1o ($[M]^+$= 978 m/z; $[M+1]^+$= 979 m/z). The objective was to select the minimum time required to confirm the full conversion of AIP1c to AIP1o. The predominant forms detected in the MS analysis were the protonated exact masses ($[M+1]^+$). Refer to Figure 5.5 for the structures of AIP1 and their corresponding exact masses.

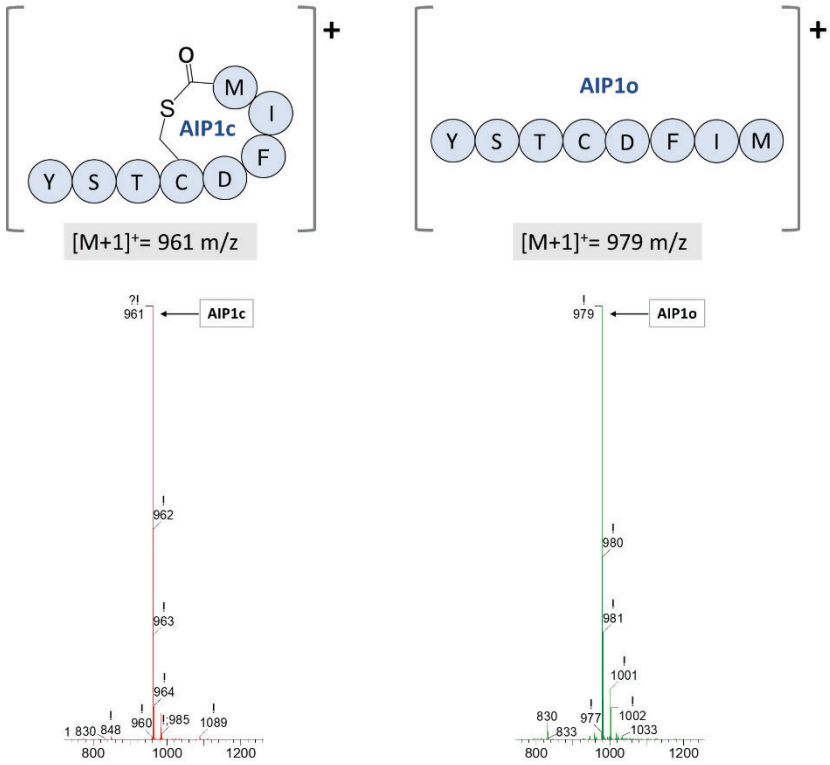

Figure 5.5. *Simplified structures, mass spectra and exact protonated masses ([M+1]+) of AIP1 in its thiolactone (AIP1c) and linear (AIP1o) forms.*

In this study, The Total Ion Chromatogram (TIC) and the extracted ion chromatograms (EICs) corresponding to the exact masses of both the closed (AIP1c) and open (AIP1o) forms of AIP1 were compared. This comparison aimed to determine the relative abundances of these forms under different conditions: untreated, 5 minutes post-treatment with NaOH, and 15 minutes post-treatment. Additionally, mass spectra were analyzed at each time point to identify the predominant ion species.

The TIC provides an overview of all ionized species detected over time, while EICs focus on specific m/z values corresponding to the target analytes. By overlaying the EICs for AIP1c and AIP1o onto the TIC, we assessed changes in their relative intensities across the different treatment conditions. This approach allowed for the monitoring of the interconversion between the closed and open forms of AIP1 induced by NaOH treatment.

Mass spectral analysis at each time point further elucidated the structural dynamics of AIP1. By calculating the area under the curve (AUC) of the peaks corresponding to AIP1c and AIP1o, the predominant form under each condition was determined. The retention times for the predominant forms detected in the mass spectrometry analysis were determined to be 3.00 minutes for AIP1c and 2.65 minutes for AIP1o. This comprehensive analysis provided insights into the stability and transformation of AIP1 in response to alkaline treatment.

The results of the chromatograms and mass spectra at different treatment times are discussed bellow (see Table 5.5).

- **Initial time point (0 min):** the chromatogram exhibits a dominant peak corresponding to the intact thiolactone form of AIP1 (AIP1c), indicating that the peptide predominantly exists in its cyclic structure. The linear form (AIP1o) is present in negligible amounts, as the relative abundance of the closed form constitutes nearly the entirety of the sample. This observation is corroborated by the mass spectrum, which displays a clear peak corresponding to AIP1c, while no peaks corresponding to AIP1o are detected. These findings suggest that, under the conditions studied, AIP1 maintains its thiolactone configuration, with minimal conversion to the open form.

- **Second time point (5 min):** the chromatogram reveals a significant decrease in the relative abundance of AIP1c, indicating substantial hydrolysis of the thiolactone ring. Concurrently, the mass spectrum displays a new peak with an m/z value corresponding to the linear form, AIP1o, confirming the conversion of AIP1c to AIP1o. A minor peak corresponding to AIP1c is also present, suggesting that the hydrolysis is nearly complete but not absolute.

- **Final time point (15 min):** chromatographic analysis indicates that the peak corresponding to AIP1c remains significantly diminished compared to AIP1o, suggesting a near-complete conversion to the linear structure. MS analysis corroborates this finding, displaying a prominent peak at the m/z value corresponding to AIP1o, while the previously observed residual peak for AIP1c is no longer detectable. These results suggest that the hydrolysis of AIP1c to AIP1o was fully completed.

Table 5.5. *Kinetic analysis of AIP1 hydrolysis using UPLC-ToF MS.*

Time (min)	AUC AIP1c	AUC AIP1o
0	1180	19
5	58	5138
15	17	1307

The table presents the area under the curve (AUC) for AIP1c and AIP1o at three time points. Pre-treatment data indicate that AIP1 predominantly exists in its cyclic form (AIP1c). At 5 minutes post-treatment, a drastical decrease in AIP1c is observed, with a concurrent emergence of AIP1o, suggesting near-complete hydrolysis. By 15 minutes, AIP1c is practically undetectable, confirming full conversion to the linear form (AIP1o).

The mass spectra confirmed the efficiency and kinetics of the hydrolysis process. The disappearance of the AIP1c peak and the corresponding increase in the AIP1o peak provide direct evidence of the reaction. Monitoring the intensity of these peaks over time allowed to determine the optimal hydrolysis duration to achieve complete conversion, which in this case likely occurs between 5 and 15 minutes based on the described time points. Based on these results, a 15-minute treatment was established.

5.7.2.4 Accuracy studies in TSB 1/2 and TSB-h 1/2

As discussed earlier in this chapter, the ELISAs mAb23/AIP4S-BSA (for AIP1o) and As418/AIP2L-DMP-BSA showed no matrix effect from the hydrolysis treatment in TSB. Based on these findings, accuracy and recovery studies were conducted to validate the reliability of the quantification of these assays in TSB.

Accuracy studies involved comparing the AIP concentrations measured by ELISA to the real spiked concentrations in both hydrolyzed and non-hydrolyzed TSB. A linear regression analysis was performed to evaluate the relationship between the measured and spiked concentrations, providing insight into the assay's accuracy and reliability. This approach allowed to determine how well the ELISA quantifications aligned with the known values.

In recovery studies, samples were spiked with known AIP concentrations, subjected to hydrolysis treatment, and quantified using the corresponding indirect competitive ELISAs to determine if the total spiked AIP content could be accurately measured. As illustrated in Figure 5.6, four parallel sample conditions were analyzed:

A. **AIPc spiked in TSB**: in this condition, all the AIP is in its closed thiolactone form (AIPc). Since the ELISAs for detecting AIP1 and AIP2 are specific to the open form (AIPo), it sould not be quantificable, serving as a negative control.
B. **AIPc spiked in TSB and hydrolyzed:** here, the sample containing AIPc undergoes hydrolysis treatment. If the hydrolysis is complete, converting all AIPc into AIPo, the recovery should be 100 %. This condition tests the efficiency of the hydrolysis process.
C. **AIPo spiked in TSB:** this is a positive control in which the sample contains AIPo without undergoing hydrolysis. It demonstrates that the ELISA accurately quantifies the open form and serves as a reference for comparison.
D. **AIPo spiked in TSB and hydrolyzed**: this condition is a control to check whether the hydrolysis treatment induces any interferences in the ELISA. If there are no interferences, the quantification should be identical to the previous condition, where AIPo is analyzed without hydrolysis.

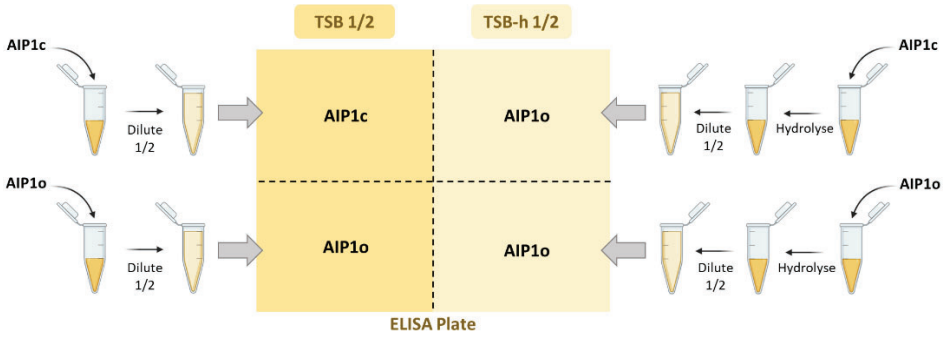

Figure 5.6. *Simplified design of the recovery study. The figure illustrates the four parallel sample conditions tested: A) spiked with AIPc without hydrolysis, B) spiked with AIPc and hydrolyzed, C) spiked with AIPo without hydrolysis, and D) spiked with AIPo and hydrolyzed. This design was used to evaluate whether hydrolysis treatment effectively converted 100 % of AIPc to AIPo, whether the treatment caused any interferences in the ELISAs, and to test the accuracy of quantification after sample treatment.*

To perform de an accuracy study, various concentrations of AIP1o were blind spiked. The results, shown in Figure 5.7, revealed that the mAb23-ELISA quantified AIP1o fairly well in TSB 1/2, with a slight overestimation. In contrast, in hydrolyzed TSB (TSB-h 1/2), the assay showed an underestimation of the

concentrations, which became more pronounced as the concentration of AIP1o increased.

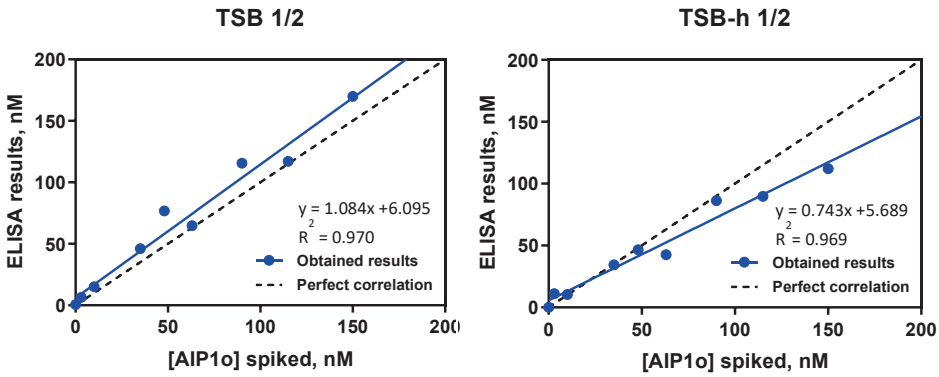

Figure 5.7. *Results of the accuracy studies of mAb/AIP4S-BSA in TSB ½ and TSB-h ½. The graphs show the linear regression analysis of the concentrations of AIP1o spiked and the concentrations measured by ELISA. The samples were blind-spiked. Triplicates were performed for each concentration.*

5.7.2.5 Recovery studies on TSB 1/2

Given these findings, recovery studies were planned to determine whether the assay could successfully convert and quantify the total AIP1c content in bacterial culture samples, ensuring accurate measurements after sample treatment.

Table 5.6. *Recovery results of AIP1o spiked in TSB ½.*

AIP1o Spiked (nM)	AIP1o Quantifyed (nM)	Recovery (%)	N
20	18.39 ± 0.13	92 ± 0.9	2
40	35.36 ± 4.80	88.4 ± 13.8	4
80	68.26 ± 8.29	85.32 ± 12.0	4
160	128.25 ± 15.27	80.16 ± 13.5	2

The table presents the concentration of AIP1o quantified in TSB ½ and the corresponding recovery percentages. Samples were analyzed using the As417/AIP2S-BSA ELISA, and the recovery was calculated based on the quantified AIP1o relative to the spiked concentration.

Surprisingly, despite confirming that the hydrolysis treatment effectively converts the total AIP content of the sample into its linear form, the quantification results did not show a 100 % recovery. In the case of the sample spiked with AIP1c without treatment (containing only AIP1c), no signal was detected, which is expected since the mAb23-ELISA specifically detects the open

form. When TSB was spiked with the open form (AIP1o), the quantification was fairly accurate near the IC_{50} value of the assay (28.16 nM), with a slight underestimation that increased gradually as the values deviated further from the IC_{50} (refer to Table 5.6).

However, when TSB samples were spiked with both AIP1c and AIP1o and then subjected to hydrolysis treatment (containing only AIP1o), a consistent recovery of approximately 50 % was observed across multiple experiments (refer to Table 5.7). For the samples spiked with AIP1c, initially it was suspected that hydrolysis was incomplete, explaining the lower recovery. However, since samples spiked with AIP1o (already spiked in the linear form) and subjected to the same treatment also showed a 50 % recovery, this hypothesis was ruled out.

Table 5.7. *Recovery results of AIP1c spiked in TSB and quantified after hydrolysis treatment.*

AIP1c Spiked (nM)	Mean AIP1o Quantifyed (nM)	N	Recovery (%)	
40	22.75 ± 8.83	5	56.9	
80	40.06 ± 3.49	5	50.1	
160	86.07 ± 11.59	3	53.8	
			53.5 ± 2.8	**Mean**

The table shows consistent recovery percentages over time for AIP1c after hydrolysis treatment. A final recovery rate of 53.5 % was assumed for subsequent analyses.

These results, consistent over time, led to the hypothesis that potential interferences from the hydrolysis treatment could be affecting the recovery. However, revisiting the matrix effect evaluation in TSB treated with hydrolysis demonstrated no such interferences. As shown in Figure 5.4, despite the treatment affecting the assay signal (A_{max}: 1.35 vs 0.98) the sensitivity remains uncompromised when the hydrolyzed TSB (TSB-h) is diluted 1/2. (IC_{50}: 21.05 nM vs 25.57 nM), further complicating the explanation for this unexpected outcome.

As previously discussed in Chapter 3, one of the main challenges with linear forms of AIPs is their potential to form disulfide bonds due to the free thiols generated after thiolactone hydrolysis. Given the quantification issues observed during sample hydrolysis, the hypothesis that the linear forms might be forming disulfide bonds, leading to the formation of dimers, was proposed. This could explain the recovery yields around 50 % after hydrolysing the samples.

To address this, it was hypothesized that adding a reducing agent to the samples could break any disulfide bonds that had formed, preventing AIP dimerization. This would ensure that the AIPs remain fully accessible, allowing for accurate quantification.

Based on this new hypothesis, it was decided to test whether the addition of reducing agents could improve quantification. Reducing agents are chemical compounds capable of donating electrons to break disulfide bonds between cysteine residues in proteins or other thiol-containing molecules. By disrupting these bonds, they prevent the formation of dimers and ensure that molecules remain in their monomeric state, making them fully accessible for detection and quantification.

Initially, DTT (dithiothreitol) was tested at a concentration of 0.1 %. While the quantification improved slightly, the enhancement was not significant enough to resolve the recovery issue. Subsequently, TCEP (tris(2-carboxyethyl)phosphine) was tested at a concentration of 10 µM. The addition of TCEP successfully addressed the quantification problem, with only a slight underestimation observed.

Table 5.8. *Recovery results of AIP1c spiked in TSB and quantified after hydrolysis treatment followed by TCEP addition.*

AIP1c Spiked (nM)	Mean AIP1o Quantifyed (nM)	N	Recovery (%)	
35	16.36 ± 3.93	4	46.7	
40	38.30 ± 2.04	2	95.8	
48	23.31 ± 5.89	4	48.6	
63	33.46 ± 6.10	4	53.1	
80	60.40 ± 20.35	6	75.5	
90	44.09 ± 11.67	4	49	
150	79.47 ± 19.73	4	53	
160	144.14 ± 19.27	2	90.1	
220	130.97 ± 38.65	4	59.5	
	+TCEP		**61.2 ± 17.8**	**Mean**

The table highlights significant variability in quantification across six different days, despite some measurements being relatively accurate. Considering the results obtained over six days, an average recovery rate of 55.39 % was calculated, indicating that the quantification issues were not resolved with the addition of TCEP.

However, as shown in Table 5.8 , the results with TCEP were not reproducible. In several experiments, despite adding TCEP, the recovery remained around 55 %. This inconsistency raised further questions about whether the formation of dimers was indeed the underlying issue. To evaluate this hypothesis before testing other reducing agen ts, a study was conducted using MALDI-TOF MS.

To investigate the potential dimerization of AIP1 during hydrolysis and the effectiveness of reducing agents in preventing it, three experimental conditions were analyzed using MALDI-TOF MS: 1) untreated AIP1c, representing the native cyclic form of the molecule; 2) AIP1c treated with NaOH for 15 minutes, to evaluate the complete hydrolysis of AIP1c into its linear form (AIP1o) and the potential formation of dimers; and 3) AIP1c treated with NaOH for 15 minutes followed by TCEP addition, to assess whether the reducing agent prevents dimerization by breaking disulfide bonds and ensuring the molecule remains in its monomeric state. These conditions were chosen to better understand the impact of hydrolysis and reduction on AIP1 stability and quantification.

As illustrated in Figure 5.8, the mass spectrum of untreated AIP1c revealed a major peak at 962 m/z, corresponding to the closed thiolactone form of AIP1 (AIP1c) with an additional hydrogen. This confirms the presence of AIP1 in its native cyclic form prior to hydrolysis.

After treating AIP1c with NaOH, no peak corresponding to the closed form (AIP1c) was detected, indicating complete conversion of the cyclic form to its linear form (AIP1o). The spectrum displayed two major peaks: one at 1002 m/z, corresponding to AIP1o with a sodium ion, and another at 980 m/z, corresponding to AIP1o with an additional hydrogen. These peaks confirm the successful hydrolysis of AIP1c into AIP1o. However, minor peaks were observed at 1957 and 1979 m/z, which are consistent with the mass of AIP1 dimers. This suggests that disulfide bond formation occurred between AIP1 molecules, leading to dimerization during hydrolysis.

When TCEP was added after hydrolysis, the same two peaks corresponding to AIP1o (980 and 1002 m/z) were detected as in the previous condition. However, the dimer peaks observed earlier at 1957 and 1979 m/z were no longer present. This indicates that the addition of TCEP successfully broke the disulfide bonds, preventing dimer formation and maintaining AIP1 in its monomeric linear form.

AIP1c (0 min)

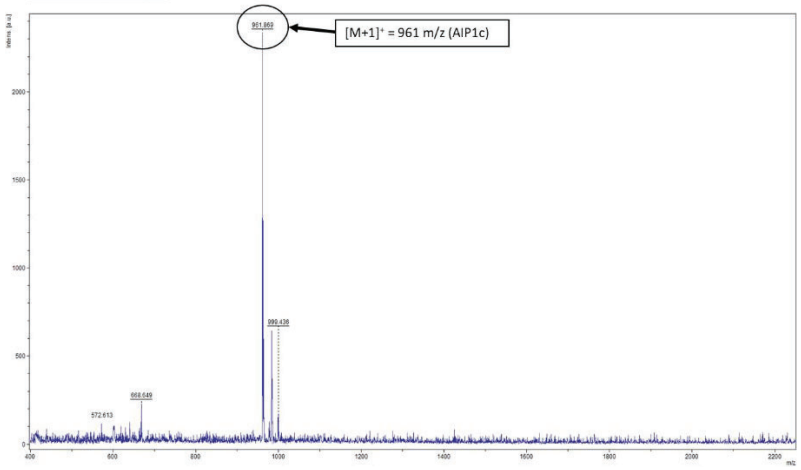

AIP1c (15 min)

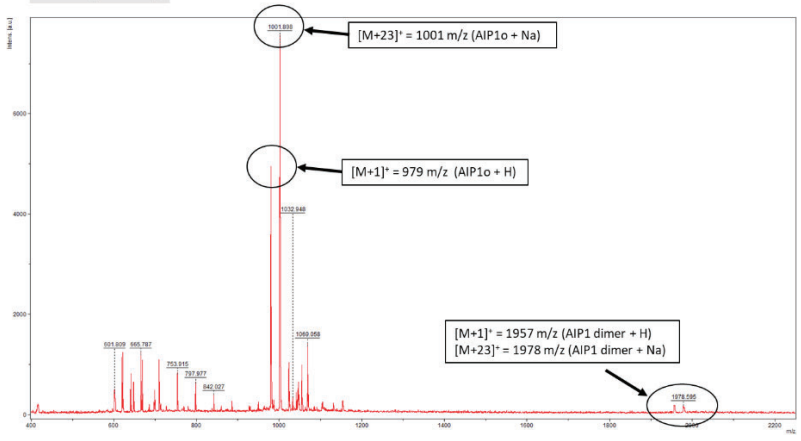

AIP1c (15 min + TCEP)

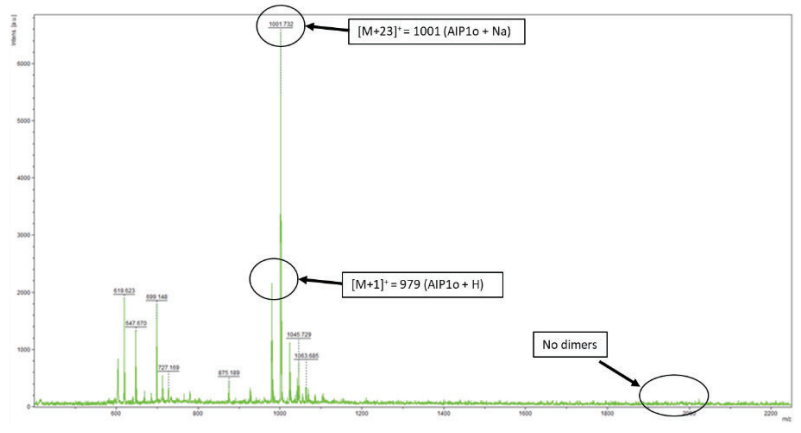

Figure 5.8. *Dimerization study of AIP1o analyzed by MALDI-TOF. The mass spectra show the following conditions: 1) AIP1c untreated: the detected mass corresponds to the closed AIP1 form + 1 hydrogen (962 m/z). 2) AIP1c treated with NaOH for 15 minutes: No AIP1c is detected, indicating complete conversion. A major peak at 1002 m/z (AIP1o + 1 sodium) and another peak at 980 m/z (AIP1o + 1 hydrogen) are observed. Minor peaks at 1957 and 1979 m/z suggest the presence of dimers. 3) AIP1c treated with NaOH for 15 minutes followed by TCEP addition: The same two peaks corresponding to AIP1o (980 and 1002 m/z) are observed as in spectrum B. The peaks corresponding to dimers (1957 and 1979 m/z) are no longer detected.*

However, although these results suggest that dimers can form during hydrolysis and that TCEP is effective in ensuring that AIPs remain in their monomeric state, they do not fully explain the recovery percentage observed when quantifying hydrolyzed samples. While dimers are present, they are in quantities that are practically negligible compared to the monomeric AIP. Therefore, dimer formation is discarded as the primary factor affecting quantification.

Given these findings and the consistency of the results, it was decided to assume a recovery of approximately 50 %. To proceed with the quantification of AIPs in bacterial cultures, four different controls of a known concentration of AIP1c and AIP1o were included in each experiment.

In the plate of non-hydrolysed TSB, the AIP1c control serves as a negative control, as it should not be detected, while the AIP1o control serves as a positive control, indicating the assay's functionality. In the hydrolyzed TSB plate (TSB-h), both controls are expected to be quantifiable. The AIP1c control will confirm whether the conversion to the linear form (AIP1o) is complete, while the AIP1o control will assess the accuracy of the assay and determine if any interferences are present. This approach ensures the reliability of the quantification process under both conditions. The results obtained were then normalized based on these controls to ensure accurate and consistent quantification.

5.7.3 AS417/AIP2S-BSA & AS418/AIP2L-DMP-BSA ELISAS FOR AIP2 DETECTION

5.7.3.1 Matrix effect evaluation

As417/AIP2S-BSA: In contrast to the previous results, the ELISA for detecting AIP2o showed a pronounced matrix effect of both TSB and TSB-h. As stated in Figure 5.9, when the assay is performed directly in undiluted media, the A_{max}

barely reaches 0.1, indicating that the assay is essentially non-functional under these conditions. Despite the ELISA having a very low IC_{50} in PBST, the sensitivity is completely lost in TSB, with the IC_{50} increasing dramatically (see Table 5.9 and Table 5.10). This ELISA performs almost identically in both media, regardless of the hydrolysis treatment, highlighting the substantial impact that TSB has on the assay, severely compromising its performance.

Even after diluting either the TSB or the TSB-h 20 times in PBST, the assay parameters do not recover sufficiently. The A_{max} states in both cases under 0.5, which is still too low to provide reliable results, and the IC_{50} remains high, far from the sensitivity levels achieved in PBST (refer to Table 5.9 and Table 5.10). This poses a significant problem, as the assay is unable to detect low levels of AIP2 in culture media where *S. aureus* strains from the agr-II group have been grown.

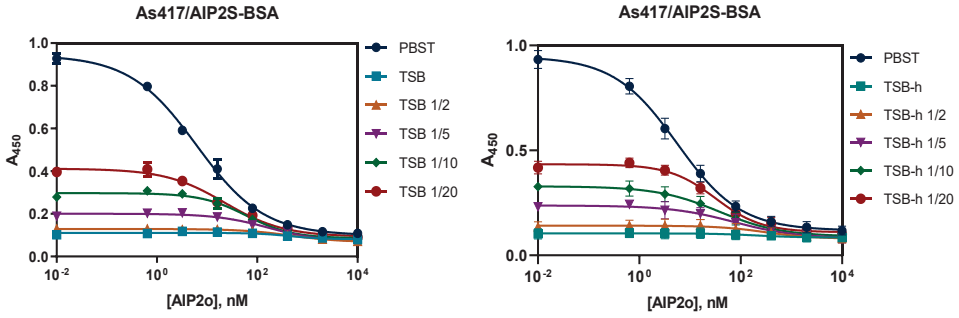

Figure 5.9. *Calibration curves for the competitive indirect ELISA As417/AIP2S-BSA conducted in PBST, TSB, TSB-h and various dilutions in PBST. The results are presented as the mean values with standard deviations of analysis measured by duplicates. In the case of TSB-h, the analysis was repeated on three different days. The conditions of the indirect competitive ELISAs used are specified in Table 5.17.*

Table 5.9. *Analytical parameters of the competitive indirect ELISA As417/AIP2S-BSA conducted in PBST, TSB and various dilutions in PBST.*

Parameters	PBST	TSB	TSB 1/2	TSB 1/5	TSB 1/10	TSB 1/20
A_{min}	0.10	0.08	0.07	0.07	0.09	0.09
A_{max}	0.94	0.11	0.13	0.20	0.30	0.41
Slope	-0.65	-1.29	-0.86	-0.83	-0.95	-0.73
IC_{50} (nM)	6.16	444.50	473.00	167.00	61.06	22.47
R^2	0.997	0.820	0.991	0.983	0.978	0.986

Table 5.10. *Analytical parameters of the competitive indirect ELISA As417/AIP2S-BSA conducted in PBST, TSB-h and various dilutions in PBST.*

Parameters	PBST	TSB-h	TSB-h 1/2	TSB-h 1/5	TSB-h 1/10	TSB-h 1/20
A_{min}	0.12	0.08	0.08	0.08	0.09	0.11
A_{max}	0.95	0.10	0.14	0.24	0.33	0.43
Slope	-0.69	-1.01	-0.92	-0.69	-0.71	-0.96
IC_{50} (nM)	5.59	205.90	309.90	73.30	37.08	31.71
R^2	0.988	0.122	0.483	0.812	0.917	0.967

Despite these efforts, immunoreactant concentrations were adjusted based on bidimensional titration experiments to develop an assay for AIP2 detection in TSB 1/2. Figure 5.10 presents the optimized calibration curves for the As417/AIP2S-BSA ELISA in TSB 1/2 and TSB-h 1/2.

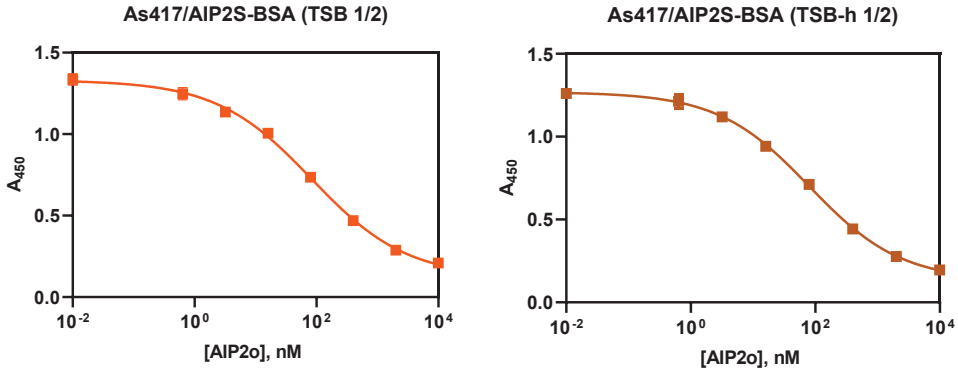

Figure 5.10. *Optimized calibration curves for the ELISA As417/AIP2S-BSA in TSB 1/2 and TSB-h 1/2. Due to the significant matrix effect observed in TSB, the concentrations of immunoreactants were adjusted to work under these conditions: CA at 1.2 µg/mL and As at a 1/4000 dilution.*

As shown in Table 5.11, the analytical parameters were improved in both matrices. However, the sensitivity of this ELISA in culture medium remains significantly lower compared to the other ELISAs, with IC_{50} values around 80 nM in both cases. Nevertheless, it was decided to proceed with this assay to evaluate whether this level of sensitivity would be sufficient for detecting AIP2 in bacterial isolates until a more sensitive assay could be developed.

Given these results, it was decided to explore the use of another previously discarded pAb for the detection of AIP2, to assess whether this alternative ELISA is less affected by TSB. The purpose was to develop a more sensitive ELISA that can accurately detect AIP2 in TSB, allowing for the effective monitoring of AIP2

levels in *S. aureus* culture broths, even in the presence of the complex medium components

Table 5.11. *Analytical parameters of the As417/AIP2S-BSA ELISA optimized in TSB 1/2 and TSB-h 1/2.*

Parameters	TSB 1/2	TSB-h 1/2
A_{min}	0.12	0.13
A_{max}	1.33	1.27
Slope	-0.55	-0.59
IC_{50} (nM)	82.73	80.12
R^2	0.997	0.998

- **As418/AIP2L-DMP-BSA:** As an alternative, the pAb As418 was selected. This Ab was initially discarded due to its lower sensitivity for the detection of AIP2 compared to As417. However, it was reconsidered and tested in a heterologous combination using newly synthesized competitor antigens based on the linear forms of AIPs.

The matrix effect of the As418/AIP2L-DMP-BSA ELISA was evaluated in TSB to determine its performance in the presence of this complex medium. This evaluation was crucial to assess whether the As418 pAb could offer a viable solution for detecting AIP2 in TSB, given the previous challenges encountered with the As417/AIP2S-BSA ELISA.

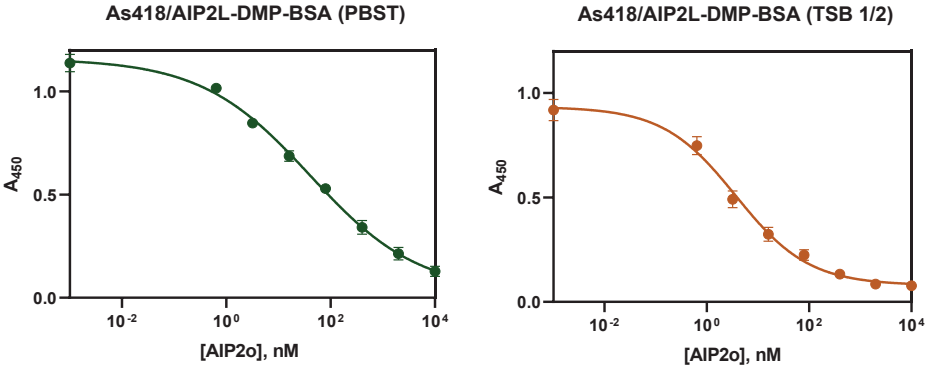

Figure 5.11. *Calibration curve for the competitive indirect ELISA As418/AIP2L-DMP-BSA optimized in TSB 1/2. The results are presented as the mean values with standard deviations from duplicate measurements in three different days. The conditions of the indirect competitive ELISAs in TSB 1/2 are specified in Table 5.17. The same conditions were used for PBST.*

Since all other assays were successfully optimized to function effectively with TSB diluted 1/2 with PBST, efforts were made to optimize this ELISA to operate under the same dilution conditions. The goal was to achieve consistent assay performance across different ELISAs while minimizing the matrix effects of TSB, allowing for reliable detection of AIP2 even at this specific dilution.

Finally, by employing the CA AIP2L-DMP-BSA, an ELISA with high sensitivity for the detection of AIP2o was successfully developed, achieving an IC_{50} of 3.71 nM (mean value obtained with N=3) in TSB 1/2 (refer to Figure 5.11 and Table 5.12). However, even though the ELISA developed with As418 demonstrates higher sensitivity in TSB 1/2, its performance in PBST was inferior to the developed ELISA As417/AIP2S-BSA ELISA previously developed (see Table 5.12). Therefore, from then on, As418-ELISA was chosen exclusively for assays conducted in culture media.

Table 5.12. *Comparison of the analytical parameters obtained for the As418/AIP2L-DMP-BSA ELISA in PBST and TSB 1/2. The plates were coated with a concentration of 0.125 µg mL^{-1} of CA, and the As dilution was 1/8000. This ELISA demonstrates higher sensitivity in TSB 1/2.*

Parameters	PBST	TSB 1/2
A_{min}	0.03	0.08
A_{max}	1.16	0.93
Slope	-0.42	-0.61
IC_{50} (nM)	40.37	3.71
R^2	0.99	0.98

5.7.3.2 Sample treatment for the quantification of the total amount of AIP2 in bacterial culture

Given that the ELISA developed for the detection of AIP2 is specific to the linear form, similar to the one targeting AIP1, it is necessary to hydrolyze the sample to ensure that the entire AIP content is converted into its linear form for accurate quantification. To achieve this, the culture sample in TSB is subjected to the hydrolysis treatment described in Section 8.6.3. This step guarantees te total conversion of AIP2 from its thiolactone form to its linear form, enabling precise and reliable measurement of the total AIP concentration.

5.7.3.3 Accuracy studies in TSB 1/2 and TSB-h 1/2

As discussed in section 5.7.3, although the As417-ELISA was initially implemented for the detection of AIP2 in TSB, a second assay (As418-ELISA) was later developed, offering reduced matrix effects and greater sensitivity in culture medium. However, some of the initial studies were performed using the As417-ELISA, as it was the assay optimized at that time.

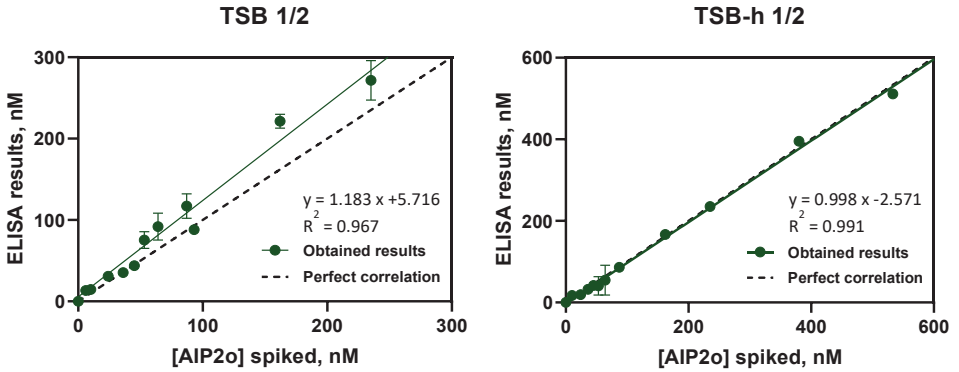

***Figure 5.12**. Results of the accuracy studies of As417/AIP2S-BSA in TSB ½ and TSB-h ½. The graphs show the linear regression analysis of the concentrations of AIP2o spiked and the concentrations measured by ELISA. The samples were blind-spiked. Triplicates were performed for each concentration, and the mean and Standard deviation (SD) of the results of two different days for TSB ½ and three different days for TSB-h ½ are shown.*

According to the accuracy studies performed, the As417/AIP2S-BSA ELISA, despite exhibiting matrix effects, proved to be fairly accurate for quantifying AIP2. Figure 5.12 illustrates the accuracy results, comparing how the ELISA measurements align with the actual concentrations in blind spiked samples.

As shown, in TSB diluted 1/2, the assay overestimates the concentrations, likely due to matrix effects, and becomes less accurate at higher concentrations. However, in hydrolyzed TSB (TSB-h 1/2), the quantification is highly accurate, even across a broader range of concentrations.

Based on these findings, four positive controls were included as a reference to determine the accuracy of the assay and to normalize the data based on it, following the same approach used for AIP1.

After implementing the As418-AIP2S-BSA ELISA in TSB, which offered improved sensitivity compared to the previous assay, its accuracy was evaluated. The

results of this study, illustrated in Figure 5.13, demonstrated that the As418-ELISA was quite accurate, with only slight deviations observed.

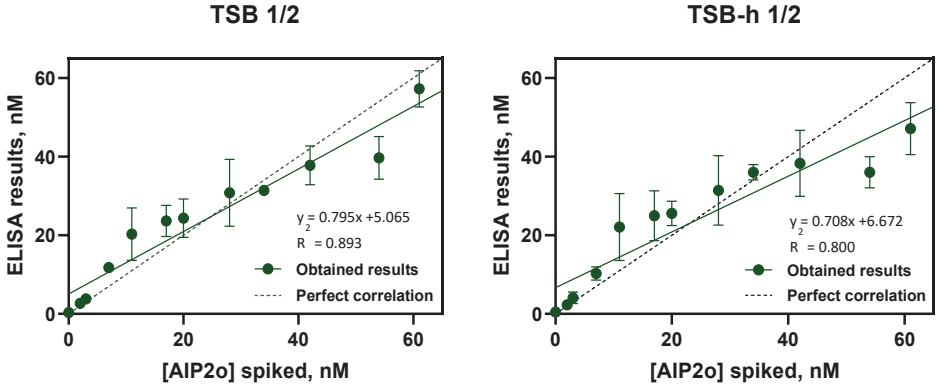

***Figure 5.13**. Results of the accuracy studies As418/AIP2L-DMP-BSA in TSB ½ and TSB-h ½. The graphs show the linear regression analysis of the concentrations of AIP2o spiked and the concentrations measured by ELISA. A detailed view of the spiked concentration range is show in each case. The samples were blind-spiked. Triplicates were performed for each concentration, and the mean and Standard deviation (SD) of the results of three different days are shown.*

In Figure 5.13, an expanded view of the region corresponding to the spiked concentration range is provided for each medium analyzed (TSB 1/2 and TSB-h 1/2), allowing for a more detailed examination of the data within this range. It is important to note that the concentration range used in this study was very narrow, as the IC_{50} of the As418-ELISA is significantly lower than that of the previous assay (TSB ½: 3.70 nM vs 87.43 nM and TSB-h ½: 4.81 nM vs 67.83 nM). Consequently, minor variations in quantification are magnified, potentially appearing as larger errors.

As in the previous assays, given the preliminary stage of the study, the same controls were included to ensure that the quantification of AIP production in bacterial isolates was reliable.

5.7.4 MAB14/AIP3S-BSA & AS429/AIP3S-BSA ELISAS FOR AIP3 DETECTION

5.7.4.1 Matrix effect evaluation

- **mAb14/AIP3S-BSA:** In the case of the ELISA for **AIP3c** detection, TSB slightly affected the signal. In undiluted TSB, the IC_{50} was lower, but this was due to a worsening of the hill slope (-0.56). When the TSB was diluted 1/2, the A_{max} increased slightly, and the slope recovered to -0.86 (see Table 5.13).

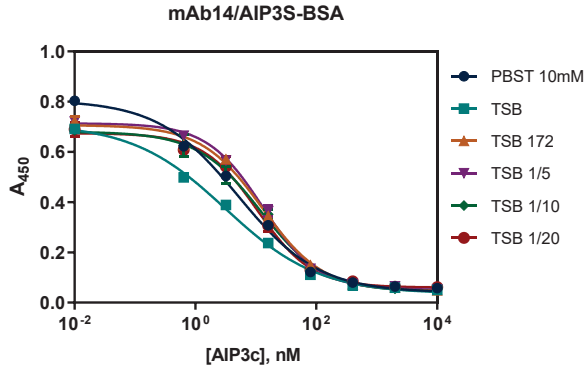

Figure 5.14. *Calibration curves for the competitive indirect mAb14/AIP3S-BSA conducted in PBST, TSB, and various dilutions of TSB. The results are presented as the mean values with standard deviations from duplicate measurements. The conditions of the indirect competitive ELISAs used are specified in Table 5.17.*

Table 5.13. *Analytical parameters of the competitive indirect ELISA mAb14/AIP3S-BSA conducted in PBST, TSB and various dilutions in PBST.*

Parameters	PBST	TSB	TSB 1/2	TSB 1/5	TSB 1/10	TSB 1/20
A_{min}	0.04	0.04	0.05	0.05	0.04	0.06
A_{max}	0.81	0.71	0.71	0.71	0.68	0.67
Slope	-0.65	-0.56	-0.86	-0.95	-0.83	-0.96
IC_{50} (nM)	5.15	3.15	12.81	12.88	12.23	10.62
R^2	0.995	0.996	0.996	0.997	0.994	0.993

Similar to the ELISAs for detecting AIP4o and AIP1o, the assay could be performed directly in undiluted TSB (refer to Figure 5.14). However, the 1/2 dilution was chosen to standardize all assays. This standardization ensures

consistency across different ELISAs, allowing for more reliable comparisons and easier implementation in various experimental conditions.

- **As429/AIP3S-BSA:** As for **AIP3o** assay, the effect of TSB was most noticeable in the A_{max}. Sensitivity remained good across all TSB dilutions, comparable to that obtained in PBST. However, both the A_{max} and the hill slope were affected. In undiluted TSB, the slope was too low to produce a reliable curve. When the TSB was diluted 1/2, a well-defined calibration curve was obtained. As TSB was further diluted, the A_{max} gradually improved, but the differences were not very significant (see Figure 5.15). As showed in Table 5.14, with a 1/2 dilution, the signal was already quite strong (two-day average A_{max}: 0.74). Based on these findings, 1/2 dilution was selected, consistent with the conditions selected for the previous ELISAs.

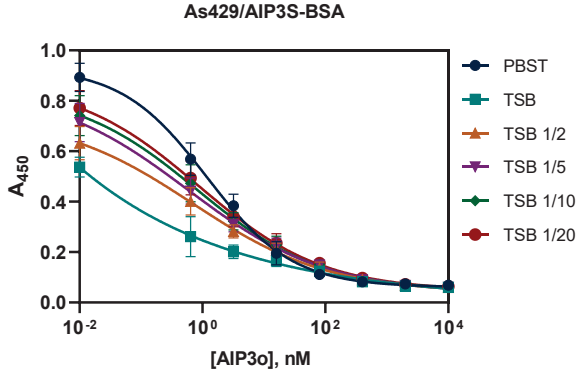

Figure 5.15. *Calibration curves for the competitive indirect As429/AIP3S-BSA conducted in PBST, TSB, and various dilutions of TSB. The results are presented as the mean values with standard deviations of analysis made on two different days measured by duplicates each day. The conditions of the indirect competitive ELISAs used are specified in Table 5.17.*

Table 5.14. *Analytical parameters of the competitive indirect ELISA As429/AIP3S-BSA conducted in PBST, TSB and various dilutions in PBST*

Parameters	PBST	TSB	TSB 1/2	TSB 1/5	TSB 1/10	TSB 1/20
A_{min}	0.06	0.01	0.04	0.04	0.05	0.05
A_{max}	0.93	~ 50,43	0.74	0.86	0.85	0.88
Slope	-0.62	~ -0,1727	-0.39	-0.38	-0.43	-0.43
IC_{50} (nM)	1.18	~ $3{,}770e^{-14}$	0.70	0.59	0.84	0.87
R^2	0.99	0.96	0.97	0.98	0.97	0.98

5.7.4.2 Accuracy studies in TSB ½

- **mAb14/AIP3S-BSA:** This ELISA demonstrates high accuracy for the detection of **AIP3c** in TSB 1/2. Given the low IC_{50} value (6.68 nM, see Table 5.17), the working range is narrow, and small variations can become magnified. Despite this issue, the assay is very accurate, particularly at lower concentrations, ensuring reliable detection within the concentration range studied. These results are illustrated in Figure 5.16.

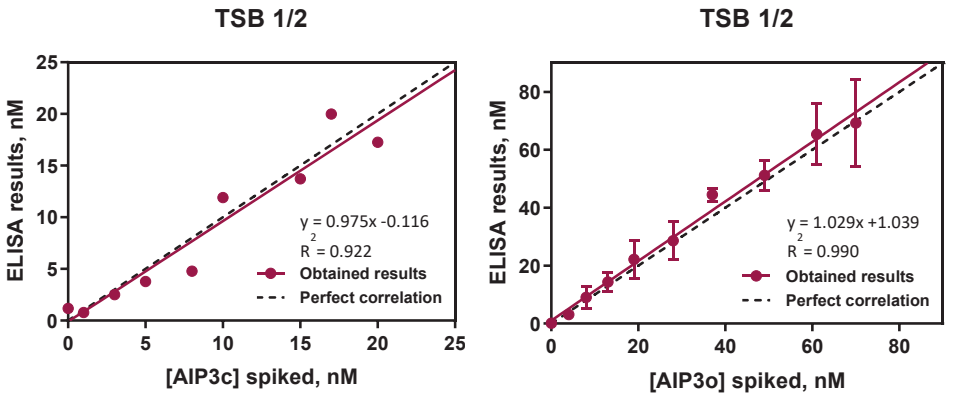

***Figure 5.16**. Results of the accuracy studies for mAb14/AIP3S-BSA and As429/AIP3S-BSA in TSB ½. The graph shows the linear regression analysis of the concentrations of AIP3 spiked (AIP3c for mAb14-ELISA and AIP3o for As429-ELISA) and the concentrations measured by ELISAThe samples were blind-spiked. For As429-ELISA, Triplicates were performed for each concentration, and the mean and Standard deviation (SD) of the results of three different days are shown.*

- **As429/AIP3S-BSA:** In the case of the ELISA for **AIP3o** detection, it also proved to be highly accurate across the entire concentration range studied. Inter-day variations were observed at higher concentrations, but these are justified as they are closer to the upper limit of quantification (see Figure 5.16).

5.7.5 AS380B4/AIP4S-BSA & AS381/AIP4S-BSA ELISAS FOR AIP4 DETECTION

For the ELISAs targeting AIP4, the results previously obtained by Dr. Enrique José Montagut were replicated to ensure their reproducibility before proceeding with the measurement of bacterial isolates.

5.7.5.1 Matrix effect evaluation

- **As380B4/AIP4S-BSA:** The ELISA designed for the detection of **AIP4c** exhibited a significant matrix effect when conducted in undiluted TSB. In this condition, the assay resulted non-functional, as it failed to produce a clear calibration curve. While the signal was slightly impacted, the most pronounced effect was on the IC_{50}, which made this ELISA ineffective in undiluted TSB (refer to Figure 5.17 and Table 5.15.

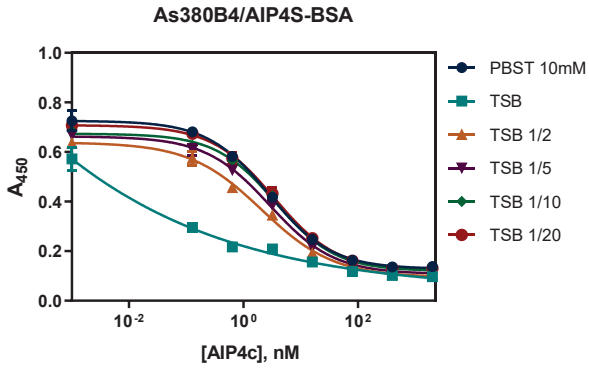

Figure 5.17. *Calibration curves for the competitive indirect as380B4/AIP4S-BSA conducted in PBST, TSB, and various dilutions of TSB. The results are presented as the mean values with standard deviations from duplicate measurements. The conditions of the indirect competitive ELISAs used are specified in Table 5.17.*

Table 5.15. *Analytical parameters of the competitive indirect ELISA As380/AIP4S-BSA conducted in PBST, TSB and various dilutions in PBST.*

Parameters	PBST	TSB	TSB 1/2	TSB 1/5	TSB 1/10	TSB 1/20
A_{min}	0.13	0.04	0.09	0.11	0.12	0.12
A_{max}	0.73	~ 4,086	0.64	0.66	0.67	0.71
Slope	-0.80	-0.17	-0.69	-0.77	-0.83	-0.79
IC_{50} (nM)	2.84	~ $1{,}552e^{-8}$	2.09	2.87	3.64	3.44
R^2	1.00	0.99	1.00	1.00	1.00	1.00

However, upon diluting the TSB 1/2 with PBST, the assay's sensitivity was effectively restored. At this dilution, the assay performed well, with the A_{max} nearly identical to that observed in PBST, indicating that the maximum signal was not compromised. Moreover, the low IC_{50} of this ELISA was maintained (1.93 nM) demonstrating that there was no significant loss in sensitivity at this dilution (see Table 5.15). These results indicate that the ELISA for AIP4c can be reliably

conducted in TSB diluted 1/2 without sacrificing assay performance. This dilution effectively mitigates the matrix effects of TSB, allowing for accurate detection of AIP4c while maintaining both the signal intensity and sensitivity of the assay.

- **As381/AIP4S-BSA:** In the case of the ELISA targeting **AIP4o**, the matrix effect of TSB presented a completely different profile. Unlike previous assay, this ELISA could be conducted in undiluted TSB with only a slight compromise in signal and sensitivity (see Figure 5.18). As evidenced by Table 5.16, while the A_{max} in TSB did decrease, it remained relatively high at 0.87, and the IC_{50} stayed very close to the value observed in PBST. It's important to note that this study was conducted without O/N pre-incubation, as the primary objective was to determine whether TSB interferes with the assay. This lack of pre-incubation accounts for lower sensitivity compared to previous results.

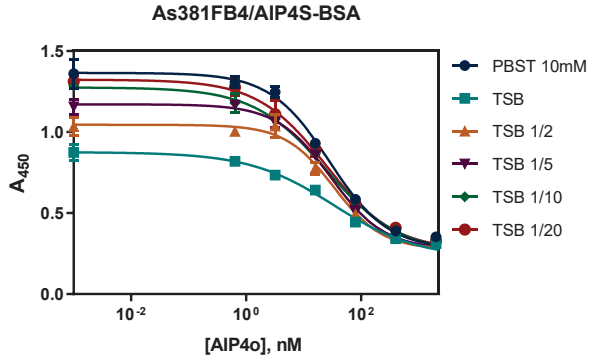

Figure 5.18. *Calibration curves for the competitive indirect As381FB/AIP4S-BSA conducted in PBST, TSB, and various dilutions of TSB. The results are presented as the mean values with standard deviations from duplicate measurements. The conditions of the indirect competitive ELISAs used are specified in Table 5.17.*

Table 5.16. *Analytical parameters of the competitive indirect ELISA As381/AIP4S-BSA conducted in PBST, TSB and various dilutions in PBST.*

Parameters	PBST	TSB	TSB 1/2	TSB 1/5	TSB 1/10	TSB 1/20
A_{min}	0.28	0.22	0.28	0.28	0.26	0.27
A_{max}	1.37	0.88	1.05	1.17	1.28	1.32
Slope	-0.85	-0.59	-1.03	-0.93	-0.69	-0.73
IC_{50} (nM)	27.84	33.25	33.39	29.29	24.99	24.33
R^2	0.992	0.989	0.984	0.993	0.995	0.992

Although the ELISA can function in undiluted TSB, the performance improves with a 1/2 dilution, where the IC_{50} remains stable, and the A_{max} increases to 1.05 (see Table 5.16). Both dilution conditions are considered viable, with the choice depending on the specific requirements of the rest of the assays.

5.7.6 SUMMARY OF OPTIMIZED ELISA CONDITIONS AND PARAMETERS FOR DETECTING AIPS IN TSB

The final conditions and parameters of the calibration curves after implementing and optimizing all the ELISAs developed for the detection of AIPs in TSB are presented in Table 5.17.

Table 5.17. *Analytical Conditions and Parameters of the ELISAs for detecting AIPs in TSB 1/2 and TSB-h 1/2.*

ELISA	Matrix	AIP detected	[Ab] µg/ml; Dil.	[CA] µg/ml	IC_{50} (nM)	Optimized cond.
mAb23/AIP4S-BSA	TSB 1/2	AIP1o	0.03	0.40	28.16 ± 8.10	Standard
	TSB-h 1/2	AIP1c + AIP1o	0.03	0.40	18.79 ± 1.77	Standard
As417/AIP2S-BSA	TSB 1/2	AIP2o	1/4,000	1.20	87.49 ± 3.3	O/N preincubation
	TSB-h 1/2	AIP2c + AIP2o	1/4,000	1.20	68.32 ± 6.84	O/N preincubation
As418/AIP2L-DMP-BSA	TSB 1/2	AIP2o	1/16,000	0.13	3.70 ± 0.72	O/N preincubation
	TSB-h 1/2	AIP2c + AIP2o	1/16,000	0.13	4.81 ± 1.33	O/N preincubation
mAb14/AIP3S-BSA	TSB 1/2	AIP3c	0.06	0.10	6.68 ± 3.38	Standard
As429/AIP3S-BSA	TSB 1/2	AIP3o	1/16,000	0.08	3.76 ± 1.00	O/N preincubation
As380/AIP4S-BSA	TSB 1/2	AIP4c	1/3,000	0.75	3.18 ± 0.95	Standard
As381/AIP4S-BSA	TSB 1/2	AIP4o	1/8,000	0.25	4.94 ± 0.86	O/N preincubation

For each ELISA, the selected concentrations of immunoreactants (antibody and coating antigen) are presented. The concentration of the competitor for the calibration curves is set at 10 µM, except for the As380-ELISA, where the curve starts at 2 µM, followed by serial 1/8 dilutions. The IC_{50} value of each assay is indicated (N=3), along with the optimized conditions, if applicable.

5.7.7 AIP PROFILING IN *S. AUREUS* CLINICAL RESPIRATORY ISOLATES

In this chapter, the clinical significance of *agr* typing and AIP profiling in *S. aureus* has been underscored. These techniques are essential for gaining insights into the nature of infections, including their severity, progression, and potential outcomes. Traditionally, *agr* typing has been carried out using techniques like genome-sequencing[52, 53], PCR[16, 54], and microarrays[55]. Although these methods

are highly effective, they are also associated with several limitations. They often involve extensive labor and are time-consuming, requiring the extraction and preparation of high-quality DNA. Additionally, these approaches generally require specialized skills and trained personnel.

Similarly, AIP profiling has been recognized for its potential in understanding QS mechanisms and their impact on virulence. MS has been the gold standard for detecting and quantifying AIPs directly from culture media. However, this method also has significant limitations. It is highly labor-intensive, requiring extensive sample preparation, and the equipment involved is both expensive and technically demanding. Furthermore, the availability of MS equipment in clinical settings is limited, and few studies have utilized this approach due to the complexity and resource requirements.

The technology developed in this work presents a significant advancement by allowing both *agr* typing and AIP profiling to be conducted simultaneously using ELISA. This approach offers several advantages over traditional methods. ELISA is faster, cost-effective, and accessible, making it feasible for use in virtually any clinical laboratory. The simplicity and speed of ELISA reduce the time to obtain results, which is critical in clinical settings where timely decision-making is essential. Moreover, the ability to perform both *agr* typing and AIP profiling in a single assay streamlines the diagnostic process, providing comprehensive data in a more efficient manner.

With the aim of validating the immunochemical tools developed, the production profiles of AIPs in various *S. aureus* strains representative of different *agr* groups were analysed. Specifically, eight strains were selected: four from *agr* group I (two of them being reference strains), one from *agr* group II, one from *agr* group III, and two from *agr* group IV. These strains, provided by the Hospital Universitari Germans Trias i Pujol, were intended to provide a comprehensive overview of AIP production across different *agr* groups.

The classification of the strains according to their *agr* allele was initially performed using the Clondiag Staphylococcus aureus Genotyping Kit 2.0 (Alere Technologies GmbH, Jena, Germany). This initial classification was subsequently validated through WGS to confirm the *agr* group assignment for each strain. The characteristics of the strains used in this study are summarized in Table 5.18.

Table 5.18. *Features of the eight Staphylococcus aureus strains selected for this study, including their reference, agr system classification (determined by WGS), and the study group to which they belong based on their origin.*

Strain reference	*Agr* system	Study group
6	I	Pneumonia
197	I	Pneumonia
Newman	I	Reference
USA300	I	Reference
3	II	Tracheobronchitis
32	III	Carrier
48	IV	Colonization
165	IV	Tracheobronchitis

The selected strains were grown in TSB and AIP levels were quantified at 13 different time points, ranging from 0 to 48 hours. Growth curves were generated by measuring the OD600 at each of these time points. Interestingly, as shown in Figure 5.19, all strains exhibited similar growth profiles, with no significant differences in growth patterns despite their belonging to different *agr* groups or their clinical origins. This consistent growth behavior across strains ensured that any differences observed in AIP production could be attributed to the *agr* group differences rather than variations in growth rates.

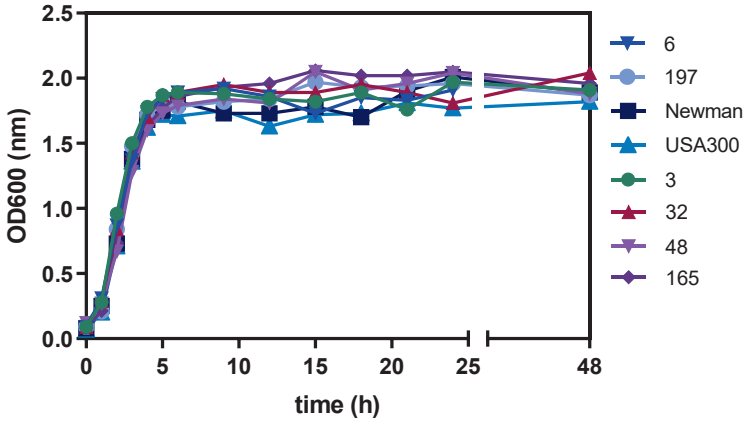

Figure 5.19. *Representation of the growth curves showing OD600 as a function of time (h) for the eight S. aureus strains, including both clinical isolates and reference strains, used in the AIP profiling study.*

A critical component of this study involved AIP profiling to verify the reliability and specificity of the ELISAs. The primary objective was to determine whether the technology here developed could accurately detect the AIP corresponding to the *agr* group of each strain without CR with AIPs from other groups. Since each strain produces a unique AIP determined by its *agr* group, the accuracy of our detection method was essential. The ELISAs developed for this purpose were designed to be highly specific to each AIP, ensuring no or very little CR and reliable results.

5.7.7.1 *Agr*-I strains

In the four *S. aureus* strains belonging to *agr*-I (6, 197, Newman and USA300), AIP1 was successfully detected throughout the growth experiments. The AIP1 levels exhibited an increasing trend, which was consistent with the exponential phase of bacterial growth. As the bacteria entered the exponential growth phase, the production of AIP1 increased steadily, reflecting the activation of the agr quorum-sensing system.

Interestingly, a decline in AIP1 levels was observed after reaching the peak, which may be attributed to cell death. This decline suggests that the accumulation of AIP1 is closely tied to the viability of the bacterial population, further underscoring the dynamic nature of AIP production in response to bacterial growth phases.

AIP1 was detected as early as 2 hours of bacterial growth (see Figure 5.20), which is particularly significant given that the *agr*-I strains, often associated with HAIs, are known for their enhanced pathogenicity. The ability to identify and quantify AIP1 so quickly can facilitate more rapid diagnostic and therapeutic decisions, potentially improving patient outcomes by enabling timely interventions based on the *agr* type of the *S. aureus* strain involved.

The concentration of AIP1 in the strains typed as *agr*-I reached up to 345 nM, which represents a substantial production level, reflecting robust QS activity. This concentration indicates that the QS system is fully activated during the exponential phase, driving the expression of virulence factors regulated by the agr system. The precise measurement and detection of AIP1 at these levels

further affirm the reliability and accuracy of the ELISA used in this study, demonstrating its capability to quantify AIP1 production across different stages of bacterial growth.

For the first time, AIPs have been detected in their linear form, validating our initial hypothesis regarding the lability of the thiolactone ring. Additionally, the contribution of the linear forms to the total amount of AIP1 in the samples was analyzed. The bar graphs in Figure 5.20 show that AIP1o (open AIP1) was detected in all four isolates. Notably, AIP1o accounted for approximately 40% of the total AIP1 quantified in the samples, highlighting the importance of a tool capable of detecting both forms to determine the true concentration of AIPs in a sample.

This is particularly valuable as AIPs have not yet been detected in clinical samples. The high sensitivity of the developed ELISAs and their ability to detect the total AIP content could overcome these limitations, potentially enabling the detection of AIPs in clinical samples for the first time.

Figure 5.20 clearly illustrates that only AIP1 was detected in the strains classidied as agr-I, with no CR observed with AIPs from other *agr* groups. This specificity strongly corroborates the correct classification of these strains. The absence of detection of any other AIPs further confirms the high specificity of the ELISA developed for AIP1, validating that these strains indeed belong to *agr* group I.

Surprisingly, one of the *S. aureus* strains, previously characterized as *agr*-IV by Clondiag, exhibited an *agr*-I phenotype based on our ELISA results. Clondiag is a diagnostic platform known for its molecular testing capabilities, which employs a microarray-based system that uses specific probes to detect different *agr* groups. It utilizes four probes targeting the *agr* operon: a general *agr* probe (detecting all *agr* groups), and specific probes for *agr*B, *agr*C, and *agr*D genes. According to Clondiag's analysis, the strain 197 tested positive for *agr*-IV across all four probes. However, it also tested positive for *agr*-I in two of these probes: the general *agr* probe and the *agr*D probe, leading to an ambiguous result.

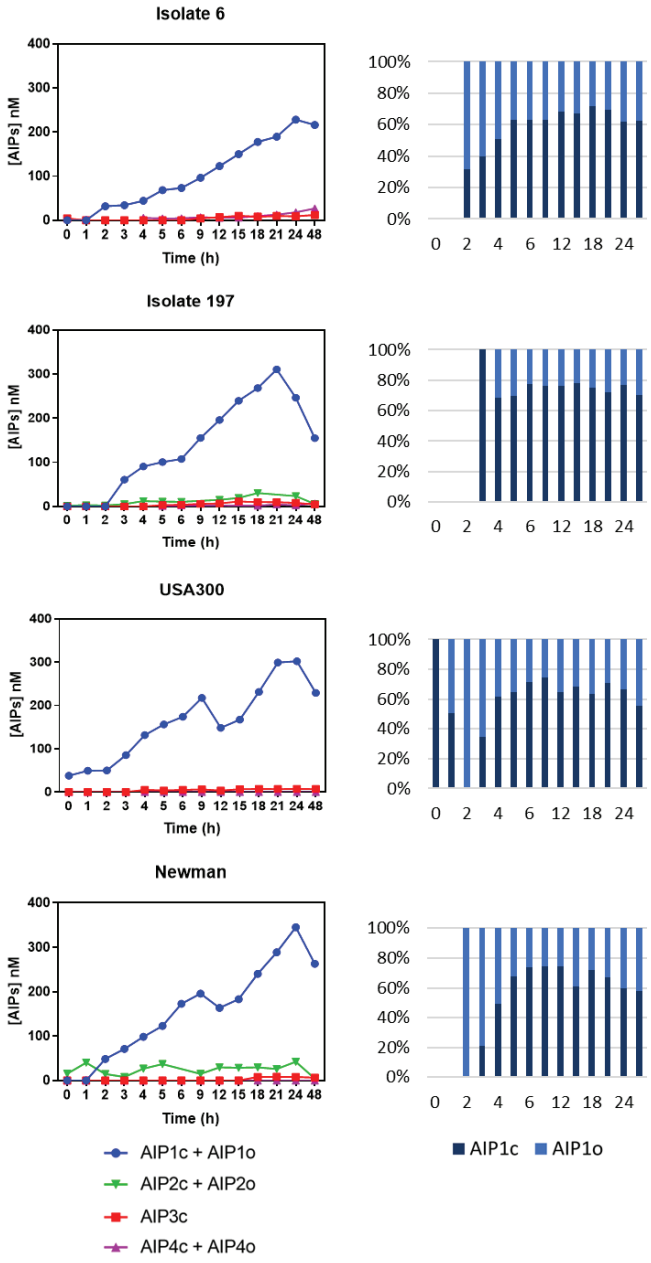

Figure 5.20. *AIP production profiles of four S. aureus agr-I isolates and contribution of AIP1c/AIP1o to total AIP1 amount. The isolates belong to two clinical respiratory strains (6 and 197) and two reference strains (Newman and USA300). AIP3o was not quantified because no sample remained by the time this ELISA was developed. For isolates 6 and USA300, AIP2 was not quantified due to a failed assay and insufficient sample for repetition. The profiles clearly classify all four isolates as agr-I type. The bar graphs on the right indicate that approximately 40 % of the quantified AIP1 is in its linear form, emphasizing the importance of detecting this fraction to determine the total AIP1 levels. The conditions of the indirect competitive ELISAs used are specified in Table 5.17.*

In contrast, our ELISA clearly detected AIP1, the signal molecule specific to *agr*-I, with no evidence of AIP4, which is indicative of *agr*-IV. This discrepancy indicated that the Clondiag result was likely incorrect. WGS later confirmed that the strain was indeed *agr*-I, not *agr*-IV as Clondiag had initially suggested, thereby validating the accuracy of our ELISA.

The *agr* operon, which includes the *agrBDCA* genes, contains regions that are highly variable between different *agr* groups, especially within *agr*B and *agr*C, as well as the entirety of *agr*D (see Figure 5.21). This hypervariable region is critical for distinguishing between *agr* types. The Clondiag platform, however, relies on conserved sequences within these genes to differentiate between *agr* groups. In this case, it appears that the probe targeting *agr*D may have cross-reacted or misidentified the strain due to insufficient specificity in detecting the variant unique to *agr*-IV, resulting in an erroneous classification.

A)

Strain reference	*Agr* typing (Clondiag)	*agr*-I				*agr*-II				*agr*-III				*agr*-IV			
		Total	*agr*B-I	*agr*C-I	*agr*D-I	Total	*agr*B-II	*agr*C-II	*agr*D-II	Total	*agr*B-III	*agr*C-III	*agr*D-III	Total	*agr*B-IV	*agr*C-IV	*agr*D-IV
6	I	POS	POS	POS	POS	NEG	NEG	NEG	NEG	NEG	NEG	NEG	NEG	NEG	NEG	NEG	NEG
197	IV	NEG	POS	POS	NEG	NEG	NEG	NEG	NEG	NEG	NEG	NEG	NEG	POS	POS	POS	POS
3	II	NEG	NEG	NEG	NEG	POS	POS	POS	POS	NEG	NEG	NEG	NEG	NEG	NEG	NEG	NEG
32	III	NEG	NEG	NEG	NEG	NEG	NEG	NEG	NEG	POS	POS	POS	POS	NEG	NEG	NEG	NEG
48	IV	NEG	AMB	POS	NEG	NEG	NEG	NEG	NEG	NEG	NEG	NEG	NEG	POS	POS	POS	POS
165	IV	NEG	AMB	POS	NEG	NEG	NEG	NEG	NEG	NEG	NEG	NEG	NEG	POS	POS	POS	POS

B)

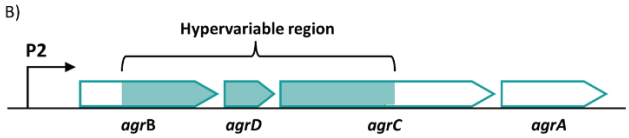

Figure 5.21. *Classification of the agr groups for the six clinical S. aureus isolates selected for AIP-profiling study. A) Results of the probes used for agr allele determination obtained through the Clondiag microarray. "POS" indicates a positive probe, "NEG" indicates a negative probe, and "AMB" denotes an ambiguous result. The results are shown for each of the four agr types, including the total agr classification and the specific alleles for agrB, agrC, and agrD. B) Schematic representation of the hypervariable region (highlighted in blue) within the agrBDCA locus, which gives rise to the different agr groups.*

Our ELISA, however, showed no such CR and was able to unambiguously identify the strain as *agr*-I. This ability to accurately distinguish between *agr* groups, even those as closely related as *agr*-I and *agr*-IV, underscores the reliability and specificity of our method. The ELISA's capacity to discern between these two *agr* groups, which share significant homology in certain regions of the *agr* operon, highlights its potential as a robust diagnostic tool.

This finding not only demonstrates the specificity of our ELISA in detecting AIP1 without CR with AIP4 but also emphasizes the limitations of traditional molecular

typing methods, which can occasionally produce ambiguous results. The ability of the immunochemical tools developed to reliably differentiate between *agr* groups with closely related sequences offers a powerful advantage in clinical diagnostics, where accurate identification of *agr* types can significantly impact the understanding and treatment of *S. aureus* infections.

5.7.7.2 *Agr*-II strain

In the case of *agr*-II, we had access to only a single clinical isolate genotyped within this group. Regarding the AIP profile obtained for isolate 3, the study was conducted exclusively using the ELISA As417/AIP2S-BSA. Initially, the bacterial isolate studies were performed using this immunoassay. However, after resolving matrix effect issues and achieving improved sensitivity with the implementation of the ELISA As418/AIP2L-DMP-BSA, this newer assay was subsequently used for the rest of the analyses. We intended to repeat all measurements across the eight isolates included in this study with the improved ELISA. Unfortunately, in some cases, the sample volume was insufficient to do so.

Despite the fact that the ELISA developed with As418 is the most optimal for quantifying AIPs in TSB, the earlier assay developed with As417, while less sensitive, still proved to be quite accurate. Therefore, as there was not enough sample to conduct this experiment again with As418-ELISA, for isolate 3, the results obtained with the assay developed with As417 are presented.

As shown in Figure 5.22, isolate 3 is clearly categorized within the *agr*-II group, as high levels of AIP2 were detected, significantly exceeding those of other AIPs. Nevertheless, there is clearly a matrix effect of TSB in this ELISA as AIP2 can be quantified even at time 0. This highlights the need to measure more samples classified within the *agr*-II group by As418-ELISA.

Isolate 3 did not show any CR with AIP3 or AIP4. However, quantifiable levels of AIP1 reaching up to 66.36 nM were detected. Although AIP1 was also detected, the levels of AIP2 were clearly superior, making it straightforward to classify this strain within the correct *agr* variant. These results indicate that, even though an assay showing some matrix effect (As417/AIP2S-BSA) was used this time, the

identification and categorization of the isolate as *agr*-II was correct, reinforcing the reliability of this technique as a phenotyping tool.

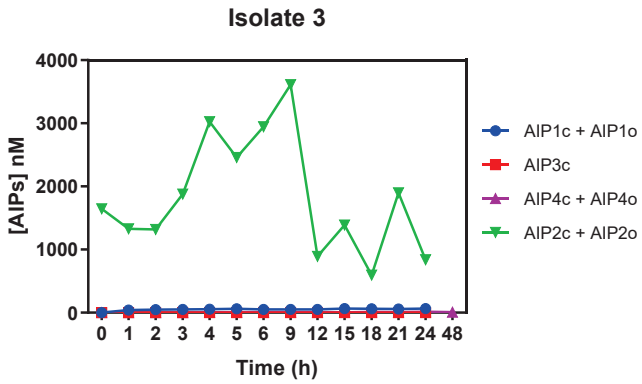

Figure 5.22. *AIP production profiles of a S. aureus agr-II isolate. Isolate 3 belongs to a clinical respiratory strain. AIP3o was not quantified because no sample remained by the time this ELISA was developed. The profiles clearly classify the isolate as agr-II type, although the As417/AIP2S-BSA ELISA shows some matrix effect of the TSB medium. The conditions of the indirect competitive ELISAs used are specified in Table 5.17.*

Since each *S. aureus* strain is expected to produce only the AIP corresponding to its *agr* group, these results suggest that the AIP1 assay might be experiencing some interferences. Initially, it was hypothesized that the interferences observed could be related to the hydrolysis process required for quantifying the totality of AIP1 in the sample (AIP1o + AIP1c). However, this hypothesis was discarded because the sample corresponding to 0 h of growth, which underwent the same hydrolysis treatment, showed no detectable AIP1 levels (remaining below the LLOQ). Moreover, when we separately analyzed AIP1o levels (by diluting the TSB 1/2 without hydrolysis) versus total AIP1 levels (subjecting the TSB to hydrolysis and then diluting 1/2 to quantify both AIP1c and AIP1o), AIP1 was still detected in isolate 3 in both cases. This confirms that the ELISA for detecting AIP1 is not influenced by the hydrolysis treatment.

After ruling out the hydrolysis treatment as the cause, it was considered the possibility that the growth of bacteria in TSB could alter the sample's physicochemical parameters, such as pH, leading to interferences in the ELISA. However, this hypothesis was also dismissed, as previous results demonstrated no detection of AIP1 in *agr*-IV isolates. If there were matrix effect due to changes in the TSB over time, it would have been reflected in those results as well.

5.7.7.3 *Agr*-III strain

As for *agr*-III, we initially had only one genotyped sample belonging to this group, similar to the situation with *agr*-II. This limitation poses a challenge, as it only allows us to obtain preliminary results, which must be validated by increasing the sample size in future studies. Despite this limitation, we proceeded to analyze this isolate using ELISAs for AIP1, AIP3, and AIP4. Unfortunately, due to insufficient sample volume, we were unable to analyze AIP2.

Recognizing that limited sample volume was a recurring issue, we explored the possibility of obtaining frozen stocks of these strains to generate new growth curves using the same isolates, thereby completing our study. While we were able to retrieve some of the strains, we were unable to obtain strain 32, which restricted our ability to conduct further analyses. Nevertheless, Figure 5.23 presents the results obtained with the ELISAs that were possible to run on this isolate.

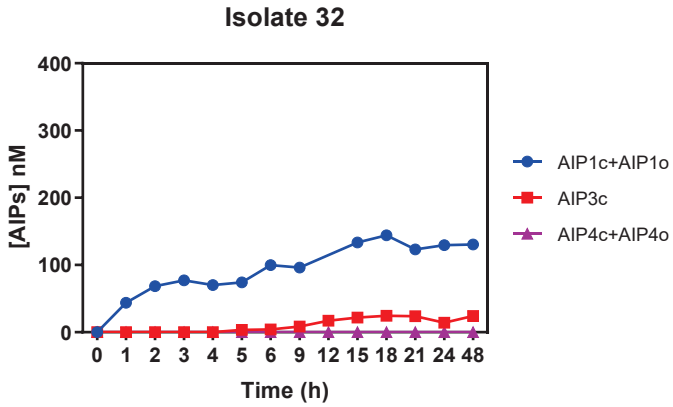

Figure 5.23. *AIP production profiles of a S. aureus agr-III isolate. Isolate 32 belongs to a clinical respiratory strain. AIP3o was not quantified because no sample remained by the time this ELISA was developed. The figure shows an unexpected profile where AIP1 is quantified in an isolate classified as agr-III, suggesting a possible interference. The results do not allow for accurate phenotyping of isolate 32, as the quantification of AIP3o is missing. AIP2 was not quantified doe to insufficient sample volume. The conditions of the indirect competitive ELISAs used are specified in Table 5.17.*

Strain 32, although genotyped as *agr*-III, showed very low levels of AIP3c. Unfortunately, we could not analyze this strain with the ELISA for AIP3o (AS429/AIP3o-DMP-BSA), so we were only able to quantify the linear fraction of AIP3, not the total amount. Given our initial hypothesis that a significant portion of the total AIP3 might be in the linear form, it is possible that this strain

expresses much higher levels of AIP3 than what we were able to measure using the AIP3c ELISA (mAb14/AIP3S-BSA).

Regarding the other AIPs, there was no CF detected with AIP4. However, similar to what was observed with the *agr*-II strain, AIP1 was detected (up to 144.19 nM) in a strain that theoretically should not produce this signaling peptide. As with the strain 3, no AIP1 was detected at time 0, ruling out interference caused by the hydrolysis treatment.

To definitively discard potential interference due to changes in the culture medium caused by bacterial growth, two negative control strains were analyzed (refer to Figure 5.24). One of these was from another species, specifically *Staphylococcus epidermidis*. Although this species also produces AIPs, they are different from those produced by *S. aureus*, so they should not interfere with our assays. The other control was *S. aureus* RN6911, an *agr*-negative strain where the *agr* locus has been replaced with the tetracycline resistance gene (tetM), rendering it incapable of producing any AIP.

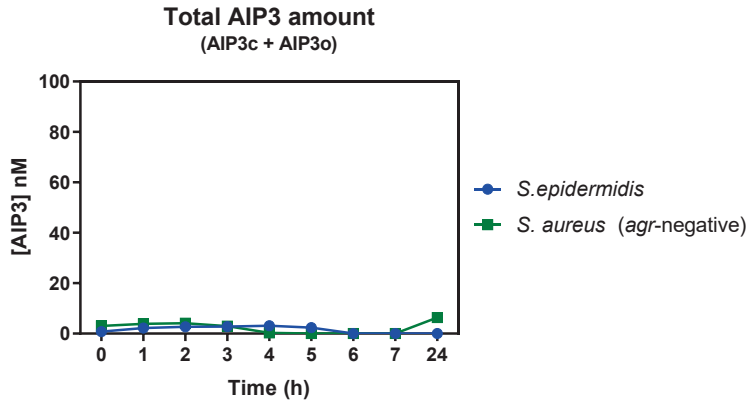

Figure 5.24. *AIP3 production profile in two negative controls. The figure shows the AIP3 production profile in two negative strains: A) S. epidermidis strain and B) S. aureus strain with a mutated agr locus, incapable of producing AIPs. AIP3c was quantified by mAb14/AIP3-BSA ELISA and for AIP3o the As429/AIP3S-BSA ELISA was used. No AIP3 was detected in either isolate, indicating that the assay is not affected by potential interferences caused by changes in TSB due to bacterial growth. The conditions of the indirect competitive ELISAs used are specified in Table 5.17.*

The results, matching those shown in Figure 5.23, indicated that there was no matrix effect from the growth of these two strains. However, these analyses were conducted by a PhD student, Nerea Castro, as part of a different study that employed ELISAs for detecting AIP3c and AIP3o. The results on that investigaton

confirmed that these strains could be used as negative controls and that they do not cause interference in the assays for detecting AIP3. Nevertheless, it remains possible that the AIP1 ELISA could experience interference due to bacterial growth, as demonstrated in Chapter 4, where each assay was shown to respond differently to variations in physicochemical parameters. Therefore, it would be highly helpful to conduct the same study using the ELISA for AIP1 to further investigate this possibility.

For now, while the detection of AIP1 in an *agr*-II and *agr*-III isolates is unexpected and suggests a potential matrix effect, the exact cause of this phenomenon remains unclear. It is evident that more isolates need to be analyzed, particularly from these two *agr* variants, as conclusions cannot be reliably drawn from the examination of a single strain. Although we currently have access to a much larger collection of isolates, their analysis was beyond the scope of this thesis. The study of these additional isolates will be crucial for gaining a better understanding of the results obtained and clarifying the underlying factors responsible for the inconclusive findings.

5.7.7.4 *Agr*-IV strains

In the case of *agr*-IV, two bacterial isolates, 48 and 165, were analyzed. Despite AIP1 and AIP4 being the most structurally similar molecules, differing only by a single amino acid substitution (D/Y), AIP1 was surprisingly not detected in the *agr*-IV group isolates. This result was unexpected, as the ELISAs designed to detect AIP2 and AIP3, which have no CR with AIP1, were still able to detect AIP1 in *agr*-II and *agr*-III isolates. This initially suggested that the AIP1 assay might have some interferences, potentially due to the hydrolysis treatment of the sample. However, such an effect was not observed in the *agr*-IV isolates.

Given these results, the hypothesis that hydrolysis treatment generates interferences was discarded, as such effect should have been observed in the *agr*-IV isolates as well. Since only one isolate was analyzed for the *agr*-II and *agr*-III groups, additional isolates from these groups should be measured to confirm if these results are reproducible and draw conclusions.

Regarding AIP4 production in the *agr*-IV isolates, both isolates demonstrated very similar profiles, with detectable levels of AIP4 increasing over time. These

findings reinforce the reliability of ELISA-based detection method here developed, which accurately quantified AIP4 in both *agr*-IV isolates. However, the concentrations of AIP4 were lower than those observed for AIP1 in the *agr*-I strains. Notably, AIP4 production began later, around 4-5 hours into the growth phase, compared to the earlier onset of AIP1 detection (see Figure 5.25).

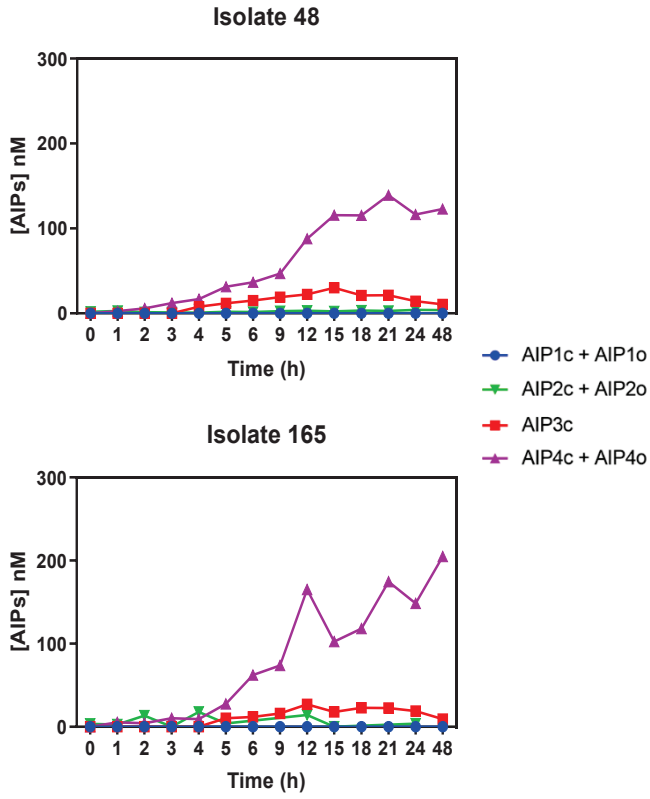

Figure 5.25. *AIP production profiles of two S. aureus agr-IV isolates. Isolates 48 and 165 belong to clinical respiratory strains. AIP3o was not quantified because no sample remained by the time this ELISA was developed. The results allow for accurate phenotyping of both isolates within agr-IV group. The conditions of the indirect competitive ELISAs used are specified in Table 5.17.*

Low levels of AIP3 were detected in both isolates, and a small amount of AIP2 was observed in isolate 165. However, these concentrations were negligible compared to the levels of AIP4 detected. When examining the individual strains, strain 48 exhibited a production profile more consistent with its growth curve, showing a steady increase in AIP4 levels. In contrast, strain 165 displayed more fluctuating AIP4 levels, with higher peak concentrations (204.87 nM) compared

to strain 48 (139.19 nM). As shown in the AIP production profiles in Figure 5.25, it is evident that both isolates exhibit the agr-IV phenotype.

5.8 CHAPTER CONTRIBUTIONS

- Highly sensitive ELISAs have been implemented for the detection of all AIPs produced by *S. aureus* in bacterial culture medium (TSB), previously unreported.

- For the first time, the detection of linear forms of AIPs in *S. aureus* bacterial culture medium has been reported. This highlights the importance of quantifying both the closed and linear fractions of AIPs to accurately measure the total AIP levels produced by a bacterial isolate.

- A novel ELISA-based technique has been developed for phenotyping *S. aureus* strains based on their *agr* group, achieving a clinical sensitivity of 75% in the preliminary study performed. This demonstrates the potential of the technology as a phenotyping tool, which requires further validation to establish its clinical utility.

5.9 BIBLIOGRAPHY

1. Novick, R. P., Autoinduction and signal transduction in the regulation of staphylococcal virulence. *Mol Microbiol* **2003,** *48* (6), 1429-49.
2. Malone, C.; Boles, B.; Horswill, A., Biosynthesis of Staphylococcus aureus Autoinducing Peptides by Using the Synechocystis DnaB Mini-Intein. *Applied and environmental microbiology* **2007,** *73*, 6036-44.
3. Traber, K. E.; Lee, E.; Benson, S.; Corrigan, R.; Cantera, M.; Shopsin, B.; Novick, R. P., agr function in clinical Staphylococcus aureus isolates. *Microbiology (Reading)* **2008,** *154* (Pt 8), 2265-2274.
4. Jarraud, S.; Mougel, C.; Thioulouse, J.; Lina, G.; Meugnier, H.; Forey, F.; Nesme, X.; Etienne, J.; Vandenesch, F., Relationships between Staphylococcus aureus genetic background, virulence factors, agr groups (alleles), and human disease. *Infect Immun* **2002,** *70* (2), 631-41.
5. Oliveira, D. C.; Tomasz, A.; de Lencastre, H., Secrets of success of a human pathogen: molecular evolution of pandemic clones of meticillin-resistant Staphylococcus aureus. *Lancet Infect Dis* **2002,** *2* (3), 180-9.

6. Peacock, S. J.; Moore, C. E.; Justice, A.; Kantzanou, M.; Story, L.; Mackie, K.; O'Neill, G.; Day, N. P., Virulent combinations of adhesin and toxin genes in natural populations of Staphylococcus aureus. *Infect Immun* **2002,** *70* (9), 4987-96.
7. Grundmann, H.; Aanensen, D. M.; van den Wijngaard, C. C.; Spratt, B. G.; Harmsen, D.; Friedrich, A. W., Geographic distribution of Staphylococcus aureus causing invasive infections in Europe: a molecular-epidemiological analysis. *PLoS Med* **2010,** *7* (1), e1000215.
8. Monk, A. B.; Curtis, S.; Paul, J.; Enright, M. C., Genetic analysis of Staphylococcus aureus from intravenous drug user lesions. *J Med Microbiol* **2004,** *53* (Pt 3), 223-227.
9. Wright, J. S., 3rd; Traber, K. E.; Corrigan, R.; Benson, S. A.; Musser, J. M.; Novick, R. P., The agr radiation: an early event in the evolution of staphylococci. *J Bacteriol* **2005,** *187* (16), 5585-94.
10. Thoendel, M.; Kavanaugh, J. S.; Flack, C. E.; Horswill, A. R., Peptide Signaling in the Staphylococci. *Chemical Reviews* **2011,** *111* (1), 117-151.
11. Geisinger, E.; Isberg, R. R., Interplay Between Antibiotic Resistance and Virulence During Disease Promoted by Multidrug-Resistant Bacteria. *J Infect Dis* **2017,** *215* (suppl_1), S9-s17.
12. Canovas, J.; Baldry, M.; Bojer, M. S.; Andersen, P. S.; Grzeskowiak, P. K.; Stegger, M.; Damborg, P.; Olsen, C. A.; Ingmer, H., Cross-Talk between Staphylococcus aureus and Other Staphylococcal Species via the agr Quorum Sensing System. *Front Microbiol* **2016,** *7*, 1733.
13. Gomes, A. R.; Vinga, S.; Zavolan, M.; de Lencastre, H., Analysis of the Genetic Variability of Virulence-Related Loci in Epidemic Clones of Methicillin-Resistant Staphylococcus aureus. *Antimicrobial Agents and Chemotherapy* **2005,** *49* (1), 366-379.
14. Holtfreter, S.; Grumann, D.; Schmudde, M.; Nguyen, H. T. T.; Eichler, P.; Strommenger, B.; Kopron, K.; Kolata, J.; Giedrys-Kalemba, S.; Steinmetz, I.; Witte, W.; Bröker, B. M., Clonal Distribution of Superantigen Genes in Clinical Staphylococcus aureus Isolates. *Journal of Clinical Microbiology* **2007,** *45* (8), 2669-2680.
15. Ikonomidis, A.; Vasdeki, A.; Kristo, I.; Maniatis, A. N.; Tsakris, A.; Malizos, K. N.; Pournaras, S., Association of biofilm formation and methicillin-resistance with accessory gene regulator (agr) loci in Greek Staphylococcus aureus clones. *Microbial Pathogenesis* **2009,** *47* (6), 341-344.
16. Cafiso, V.; Bertuccio, T.; Santagati, M.; Demelio, V.; Spina, D.; Nicoletti, G.; Stefani, S., agr-Genotyping and transcriptional analysis of biofilm-producing Staphylococcus aureus. *FEMS Immunology & Medical Microbiology* **2007,** *51* (1), 220-227.
17. Khoramrooz, S. S.; Mansouri, F.; Marashifard, M.; Malek Hosseini, S. A. A.; Akbarian Chenarestane-Olia, F.; Ganavehei, B.; Gharibpour, F.; Shahbazi, A.; Mirzaii, M.; Darban-Sarokhalil, D., Detection of biofilm related genes, classical enterotoxin genes and agr typing among Staphylococcus aureus isolated from bovine with subclinical mastitis in southwest of Iran. *Microbial Pathogenesis* **2016,** *97*, 45-51.
18. Foster, T. J., The Staphylococcus aureus "superbug". *J Clin Invest* **2004,** *114* (12), 1693-6.
19. Bukowski, M.; Wladyka, B.; Dubin, G., Exfoliative Toxins of Staphylococcus aureus. *Toxins* **2010,** *2* (5), 1148-1165.
20. Atchade, E.; De Tymowski, C.; Grall, N.; Tanaka, S.; Montravers, P., Toxic Shock Syndrome: A Literature Review. *Antibiotics* **2024,** *13* (1), 96.
21. Ladhani, S.; Garbash, M., Staphylococcal Skin Infections in Children. *Pediatric Drugs* **2005,** *7* (2), 77-102.
22. Brazel, M.; Desai, A.; Are, A.; Motaparthi, K., Staphylococcal Scalded Skin Syndrome and Bullous Impetigo. *Medicina* **2021,** *57* (11), 1157.
23. Javdan, S.; Narimani, T.; Shahini Shams Abadi, M.; Gholipour, A., Agr typing of Staphylococcus aureus species isolated from clinical samples in training hospitals of Isfahan and Shahrekord. *BMC Res Notes* **2019,** *12* (1), 363.

24. Turner, N. A.; Sharma-Kuinkel, B. K.; Maskarinec, S. A.; Eichenberger, E. M.; Shah, P. P.; Carugati, M.; Holland, T. L.; Fowler, V. G., Methicillin-resistant Staphylococcus aureus: an overview of basic and clinical research. *Nature Reviews Microbiology* **2019,** *17* (4), 203-218.
25. Rimi, S. S.; Ashraf, M. N.; Sigma, S. H.; Ahammed, M. T.; Siddique, M. P.; Zinnah, M. A.; Rahman, M. T.; Islam, M. S., Biofilm formation, agr typing and antibiotic resistance pattern in methicillin-resistant Staphylococcus aureus isolated from hospital environments. *PLoS One* **2024,** *19* (8), e0308282.
26. Tan, L.; Huang, Y.; Shang, W.; Yang, Y.; Peng, H.; Hu, Z.; Wang, Y.; Rao, Y.; Hu, Q.; Rao, X.; Hu, X.; Li, M.; Chen, K.; Li, S., Accessory Gene Regulator (agr) Allelic Variants in Cognate Staphylococcus aureus Strain Display Similar Phenotypes. *Front Microbiol* **2022,** *13*, 700894.
27. Cheung, G. Y.; Wang, R.; Khan, B. A.; Sturdevant, D. E.; Otto, M., Role of the accessory gene regulator agr in community-associated methicillin-resistant Staphylococcus aureus pathogenesis. *Infect Immun* **2011,** *79* (5), 1927-35.
28. Queck, S. Y.; Jameson-Lee, M.; Villaruz, A. E.; Bach, T. H.; Khan, B. A.; Sturdevant, D. E.; Ricklefs, S. M.; Li, M.; Otto, M., RNAIII-independent target gene control by the agr quorum-sensing system: insight into the evolution of virulence regulation in Staphylococcus aureus. *Mol Cell* **2008,** *32* (1), 150-8.
29. Aryee, A.; Edgeworth, J. D., Carriage, Clinical Microbiology and Transmission of Staphylococcus aureus. In *Staphylococcus aureus: Microbiology, Pathology, Immunology, Therapy and Prophylaxis*, Bagnoli, F.; Rappuoli, R.; Grandi, G., Eds. Springer International Publishing: Cham, 2017; pp 1-19.
30. Wertheim, H. F.; Melles, D. C.; Vos, M. C.; van Leeuwen, W.; van Belkum, A.; Verbrugh, H. A.; Nouwen, J. L., The role of nasal carriage in Staphylococcus aureus infections. *Lancet Infect Dis* **2005,** *5* (12), 751-62.
31. Becker, K., Colonization and Persistence Strategies of Staphylococcus aureus. In *Staphylococcus aureus: Interplay between Bacteria and Hosts*, Nakane, A.; Asano, K., Eds. Springer Nature Singapore: Singapore, 2024; pp 1-40.
32. Weidenmaier, C.; Goerke, C.; Wolz, C., Staphylococcus aureus determinants for nasal colonization. *Trends in Microbiology* **2012,** *20* (5), 243-250.
33. Li, P.; Schulte, J.; Wurpts, G.; Hornef, M. W.; Wolz, C.; Yazdi, A. S.; Burian, M., Transcriptional Profiling of Staphylococcus aureus during the Transition from Asymptomatic Nasal Colonization to Skin Colonization/Infection in Patients with Atopic Dermatitis. *International Journal of Molecular Sciences* **2024,** *25* (17), 9165.
34. Burian, M.; Wolz, C.; Goerke, C., Regulatory Adaptation of Staphylococcus aureus during Nasal Colonization of Humans. *PLOS ONE* **2010,** *5* (4), e10040.
35. Tong, S. Y.; Davis, J. S.; Eichenberger, E.; Holland, T. L.; Fowler, V. G., Jr., Staphylococcus aureus infections: epidemiology, pathophysiology, clinical manifestations, and management. *Clin Microbiol Rev* **2015,** *28* (3), 603-61.
36. Tong Steven, Y. C.; Davis Joshua, S.; Eichenberger, E.; Holland Thomas, L.; Fowler Vance, G., Staphylococcus aureus Infections: Epidemiology, Pathophysiology, Clinical Manifestations, and Management. *Clinical Microbiology Reviews* **2015,** *28* (3), 603-661.
37. David, M. Z.; Daum, R. S., Treatment of Staphylococcus aureus Infections. In *Staphylococcus aureus: Microbiology, Pathology, Immunology, Therapy and Prophylaxis*, Bagnoli, F.; Rappuoli, R.; Grandi, G., Eds. Springer International Publishing: Cham, 2017; pp 325-383.
38. Suligoy, C. M.; Lattar, S. M.; Noto Llana, M.; González, C. D.; Alvarez, L. P.; Robinson, D. A.; Gómez, M. I.; Buzzola, F. R.; Sordelli, D. O., Mutation of Agr Is Associated with the Adaptation of Staphylococcus aureus to the Host during Chronic Osteomyelitis. *Front Cell Infect Microbiol* **2018,** *8*, 18.

39. Kong, K.-F.; Vuong, C.; Otto, M., Staphylococcus quorum sensing in biofilm formation and infection. *International Journal of Medical Microbiology* **2006,** *296* (2), 133-139.
40. Idrees, M.; Sawant, S.; Karodia, N.; Rahman, A., Staphylococcus aureus Biofilm: Morphology, Genetics, Pathogenesis and Treatment Strategies. *International Journal of Environmental Research and Public Health* **2021,** *18* (14), 7602.
41. Boles, B. R.; Horswill, A. R., agr-Mediated Dispersal of Staphylococcus aureus Biofilms. *PLOS Pathogens* **2008,** *4* (4), e1000052.
42. Beenken Karen, E.; Blevins Jon, S.; Smeltzer Mark, S., Mutation of sarA in Staphylococcus aureus Limits Biofilm Formation. *Infection and Immunity* **2003,** *71* (7), 4206-4211.
43. Naga, N. G.; El-Badan, D. E.; Ghanem, K. M.; Shaaban, M. I., It is the time for quorum sensing inhibition as alternative strategy of antimicrobial therapy. *Cell Communication and Signaling* **2023,** *21* (1), 133.
44. Kalia, V. C., Quorum sensing inhibitors: An overview. *Biotechnology Advances* **2013,** *31* (2), 224-245.
45. Flora, M.; Perrotta, F.; Nicolai, A.; Maffucci, R.; Pratillo, A.; Mollica, M.; Bianco, A.; Calabrese, C., Staphylococcus Aureus in chronic airway diseases: An overview. *Respiratory Medicine* **2019,** *155*, 66-71.
46. Goss, C. H.; Muhlebach, M. S., Review: Staphylococcus aureus and MRSA in cystic fibrosis. *Journal of Cystic Fibrosis* **2011,** *10* (5), 298-306.
47. Geoghegan, J. A.; Irvine, A. D.; Foster, T. J., Staphylococcus aureus and Atopic Dermatitis: A Complex and Evolving Relationship. *Trends in Microbiology* **2018,** *26* (6), 484-497.
48. Tan, L.; Li, S. R.; Jiang, B.; Hu, X. M.; Li, S., Therapeutic Targeting of the Staphylococcus aureus Accessory Gene Regulator (agr) System. *Front Microbiol* **2018,** *9*, 55.
49. Vasquez, J. K.; Tal-Gan, Y.; Cornilescu, G.; Tyler, K. A.; Blackwell, H. E., Simplified AIP-II Peptidomimetics Are Potent Inhibitors of Staphylococcus aureus AgrC Quorum Sensing Receptors. *Chembiochem* **2017,** *18* (4), 413-423.
50. Chen, X.; Thomsen, T. R.; Winkler, H.; Xu, Y., Influence of biofilm growth age, media, antibiotic concentration and exposure time on Staphylococcus aureus and Pseudomonas aeruginosa biofilm removal in vitro. *BMC Microbiology* **2020,** *20* (1), 264.
51. Terato, K.; Do, C. T.; Cutler, D.; Waritani, T.; Shionoya, H., Preventing intense false positive and negative reactions attributed to the principle of ELISA to re-investigate antibody studies in autoimmune diseases. *Journal of Immunological Methods* **2014,** *407*, 15-25.
52. Monecke, S.; Coombs, G.; Shore, A. C.; Coleman, D. C.; Akpaka, P.; Borg, M.; Chow, H.; Ip, M.; Jatzwauk, L.; Jonas, D.; Kadlec, K.; Kearns, A.; Laurent, F.; O'Brien, F. G.; Pearson, J.; Ruppelt, A.; Schwarz, S.; Scicluna, E.; Slickers, P.; Tan, H. L.; Weber, S.; Ehricht, R., A field guide to pandemic, epidemic and sporadic clones of methicillin-resistant Staphylococcus aureus. *PLoS One* **2011,** *6* (4), e17936.
53. Lacoma, A.; Laabei, M.; Sánchez-Herrero, J. F.; Young, B.; Godoy-Tena, G.; Gomes-Fernandes, M.; Sumoy, L.; Plans, O.; Arméstar, F.; Prat, C., Genotypic and Phenotypic Characterization of Staphylococcus aureus Isolates from the Respiratory Tract in Mechanically-Ventilated Patients. *Toxins (Basel)* **2021,** *13* (2).
54. COTAR, A.-I.; DINU, S.; CHIFIRIUC, C.; BANU, O.; IORDACHE, C.; LIXANDRU, M.; DRACEA, O.; BUCUR, M.; LAZAR, V., Molecular markers of quorum-sensing and virulence gene regulators in Staphylococcus aureus strains isolated from biofilm associated infections. **2008**.
55. Monecke, S.; Slickers, P.; Ehricht, R., Assignment of Staphylococcus aureus isolates to clonal complexes based on microarray analysis and pattern recognition. *FEMS Immunology & Medical Microbiology* **2008,** *53* (2), 237-251.

6 RESPIRATORY SAMPLES

6.1 CHAPTER PRESENTATION

This chapter focuses on the development and optimization of immunochemical techniques for the detection of *S. aureus* AIPs in complex biological samples, specifically bronchoalveolar samples (BAS). The primary objective is to identify a sample treatment method that facilitates better handling of BAS samples by reducing their viscosity and liquefying them. Additionally, the treatment aims to homogenize the samples, ensuring consistency and enabling reliable comparison during AIP quantification.

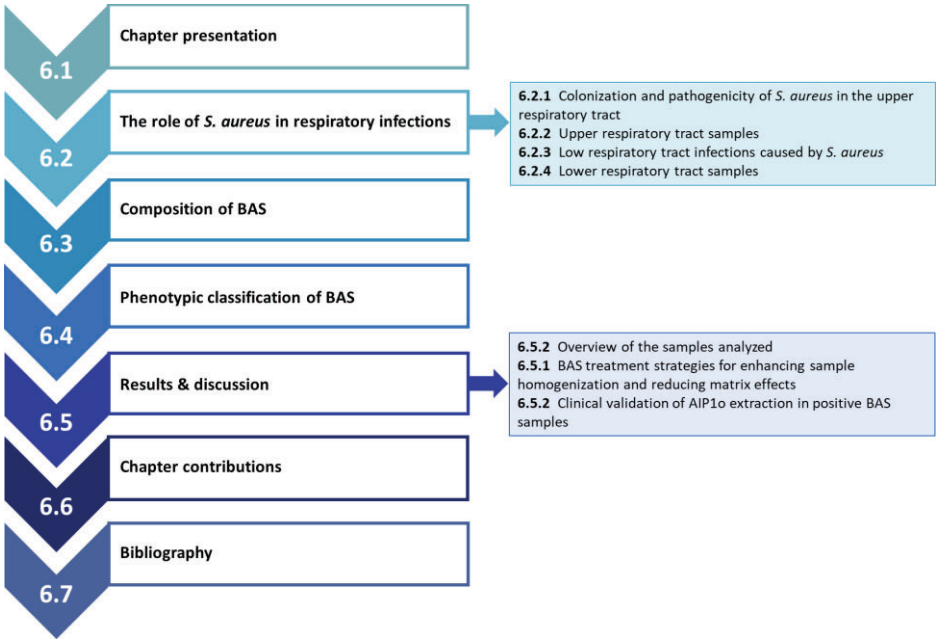

Figure 6.1. *Structure of Capter 6.*

The chapter begins introducing concepts concerning sample treatment and explains strategies used to overcome the matrix interferenes and avoid sample heterogeneity. After testing multiple treatment strategies, immunoaffinity-based approaches are introduced as a solution.

The use of immunoaffinity columns (IACs) is explored, detailing their advantatges and preparation. Promising results in detecting AIP1o in spiked PBS samples by IACs are discussed. The chapter also examines the application of these techniques in clinical settings, presenting results from a pilot study with BAS and

BAL samples from ICU patients suffering *S. aureus* respiratory infections. The potential to quantify AIPs reliably by ISCs in challenging clinical samples is highlighted and real AIP levels in direct clinical samples are reported for thr first time. The different sections of this chapter are outlined in Figure 6.2.

6.2 THE ROLE OF *S. AUREUS* IN RESPIRATORY INFECTIONS

As detailed before in Chapter 1*, S. aureus* is a versatile and opportunistic pathogen that plays a significant role in a wide array of human infections, ranging from mild skin infections to fatal systemic diseases[1]. Regarding respiratory infections, *S. aureus* poses a major threat, particularly in vulnerable populations such as hospitalized patients, individuals with compromised immune systems, and those with pre-existing respiratory conditions. While *S. aureus* is frequently associated with upper respiratory tract (URT) colonization, its involvement in LRTIs poses more severe clinical challenges, often leading to conditions such as pneumonia, bronchiectasis, lung abscesses, and in some cases, life-threatening complications like sepsis or acute respiratory distress syndrome[2].

6.2.1 COLONIZATION AND PATHOGENICITY OF *S. AUREUS* IN THE UPPER RESPIRATORY TRACT

S. aureus commonly colonizes the URT, particularly the nasal cavity, where it can persist asymptomatically in a significant portion of the population. However, under certain conditions, such as immune suppression or epithelial damage, it can transition from a commensal organism to a pathogen[3]. Using surface adhesins, it adheres to epithelial surfaces and can cause localized infections like sinusitis or pharyngitis. Of greater concern, *S. aureus* can invade deeper tissues or disseminate to the lower respiratory tract (LRT). Its multiple virulence factors and its capacity for immune evasion contribute to severe tissue damage and inflammation in the lungs[4, 5], leading to potentially life-threatening outcomes in individuals with pre-existing lung conditions or those who are immunocompromised[6].

6.2.2 UPPER RESPIRATORY TRACT SAMPLES

Samples from the URT are easier and less invasive to collect, making them essential for clinical diagnostics. They provide valuable information for detecting localized infections[7], monitoring asymptomatic carriers[3], and assessing the respiratory microbiome[8]. URT samples are particularly important during respiratory outbreaks or pandemics, as they enable rapid, non-invasive diagnostics to control disease spread[9].

URT samples can be collected through various methods, each with specific advantages and limitations. **Nasal swabs** are one of the most common non-invasive techniques, involving the collection of epithelial cells and mucus from the anterior nares. They are widely used for detecting viral pathogens like influenza and bacterial carriers such as *S. aureus*[3], particularly in large-scale screenings during outbreaks. **Throat swabs** are another widely used method, particularly for diagnosing bacterial infections like *S. pyogenes* in cases of pharyngitis[10]. Both nasal and throat swabs are easy to perform but are limited in their ability to detect pathogens in the lower respiratory tract. **Nasopharyngeal aspirates**, a more invasive approach, involve suctioning mucus from the nasopharynx, providing more concentrated samples ideal for detecting pathogens like respiratory syncytial virus (RSV) and influenza[11], especially in clinical and pediatric settings. Each method serves as a critical tool for diagnosing and monitoring respiratory infections, although their utility may vary depending on the specific respiratory region or pathogen of interest.

6.2.3 LOW RESPIRATORY TRACT INFECTIONS CAUSED BY *S. AUREUS*

S. aureus is a major concern in lower respiratory tract infections (LRTIs) due to its ability to cause severe and rapidly progressing diseases like pneumonia. While the lower respiratory tract is protected by immune defenses such as mucociliary clearance and alveolar macrophages, *S. aureus* can evade or disrupt these mechanisms[12, 13]. Pneumonia caused by S. aureus can be classified as community-acquired (CAP) or hospital-acquired (HAP), with MRSA being a significant cause of severe HAP and VAP, particularly in hospital settings[14, 15]. In community settings, pneumonia often follows viral infections like influenza, which weaken the respiratory epithelium and allow bacterial invasion[13, 14]. Once established, *S.*

aureus causes tissue damage through toxins like PVL and forms biofilms that protect it from immune responses and antibiotics, complicating treatment and recovery while contributing to chronic inflammation[14].

6.2.4 LOWER RESPIRATORY TRACT SAMPLES

LRT samples are essential for diagnosing infections in the deeper parts of the respiratory system. Common types include **sputum**, which is collected through coughing and is useful but prone to contamination by upper respiratory flora; **bronchoalveolar lavage (BAL)**, an invasive procedure providing samples from the alveoli and bronchioles, ideal for diagnosing severe infections like pneumonia and opportunistic diseases; **tracheal aspirates**, obtained via suction in mechanically ventilated patients to diagnose nosocomial infections such as VAP; and **bronchial aspirate samples (BAS),** collected directly from the bronchi using a bronchoscope, valuable for diagnosing lung infections in intubated patients or those unable to produce sputum naturally. Each sample type offers distinct advantages and diagnostic applications, depending on the clinical context.

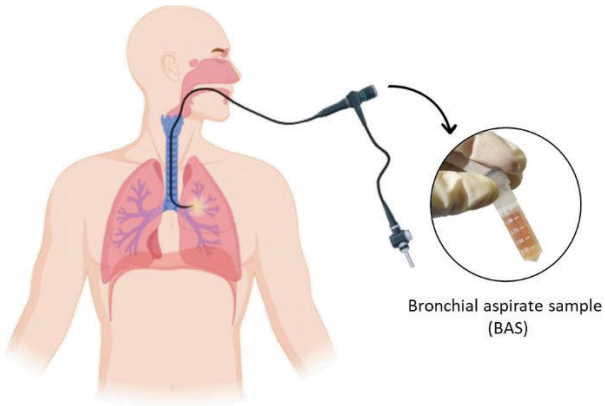

Figure 6.2. *Schematic representation of the procedure for obtaining a bronchial aspirate sample (BAS). The process involves collecting respiratory secretions from the lower airway using a bronchoscope.*

6.3 COMPOSITION OF BAS

In contrast to sputum, BAS are collected using controlled techniques like bronchoscopy or a suction catheter (see Figure 6.2), which minimizes the likelihood of contamination from saliva or flora present in the URT. This sample-collection methodologies ensure a more accurate representation of the conditions and pathogens present in the lower airways, especially in clinical settings where precision is essential for diagnosis and treatment.

The composition of BAS closely resembles that of sputum, as both are primarily composed of pulmonary mucus originating from the LRT. This mucus contains a variety of immune cells, such as neutrophils and macrophages, as well as cellular debris shed from the respiratory epithelium. Additionally, both BAS and sputum harbor pathogens like bacteria, viruses, and fungi that can cause infections in the lungs (see Figure 6.3). The presence of these immune cells and pathogens reflects the body's response to inflammation or infection within the bronchi and bronchioles, making both sample types valuable for diagnosing respiratory diseases.

Pulmonary mucus is typically produced as a response to inflammation or infection in the respiratory system, such as bronchitis, pneumonia, or chronic conditions like CF[16]. It is primarily composed of a network of mucins (MUC5AC and MUC5B). These glycoproteins create a gel-like matrix that traps inhaled particles, pathogens, and cellular debris, providing an essential protective function. However, in diseases like CF, this mucus becomes abnormally thick and difficult to clear, leading to chronic infections and airway obstruction[17].

Another key component of pulmonary mucus are immune cells, predominantly neutrophils, which release DNA and actin as they respond to infections. This extracellular DNA-actin complex forms a secondary network, further increasing the viscosity. In CF and chronic bronchitis, this DNA-actin network contributes to the thick, sticky nature of the mucus, exacerbating respiratory difficulties[16]. This rigid structure, along with the dense mucin network, makes it harder for the body to clear the mucus, leading to recurrent infections and inflammation.

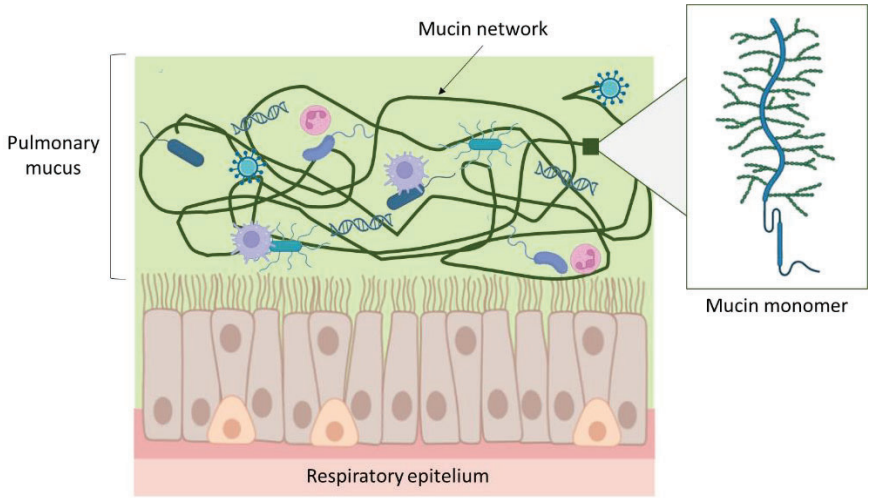

Figure 6.3. *Composition of pulmonary mucus. Pulmonary mucus is a highly complex matrix composed primarily of interconnected mucins, which are large glycoproteins with extensive carbohydrate side chains. These mucins form a dense network through disulfide bonds and other interactions, creating the structural backbone of the mucus. Embedded within this network are bacteria, viruses, immune cells, extracellular DNA, and various other components.*

One of the significant challenges in managing respiratory conditions like CF is breaking down these networks to improve mucus clearance. Treatments often include mucolytics[18] to disrupt the mucin gel and DNase enzymes[19] to degrade the extracellular DNA, thereby reducing the viscosity and facilitating better airway clearance.

6.4 PHENOTYPIC CLASSIFICATION OF BAS

BAS samples can be classified into different phenotypes based on observable factors such as color, consistency, and density of the samples[20]. Through this methodology, BAS samples analyzed in this work were categorized into three primary groups: mucoid, purulent, and bloody. Mucoid samples were generally less viscous and either clear or slightly opaque, indicating a lower level of infection or inflammation. In contrast, purulent samples were thicker and more viscous, often exhibiting a yellow or green coloration, which is indicative of pus and a higher degree of infection. Bloody samples contained visible blood (redish colour), which could signal more severe tissue damage or an advanced infection within the respiratory tract.

This phenotypic classification provided a reference for understanding the physical properties of the BAS samples, which was essential for evaluating the success of treatments aimed at reducing sample viscosity and achieving homogenization for diagnostic analyses. The phenotypic characteristics and classification criteria used to characterize the BAS samples in this research are outlined in Figure 6.4.

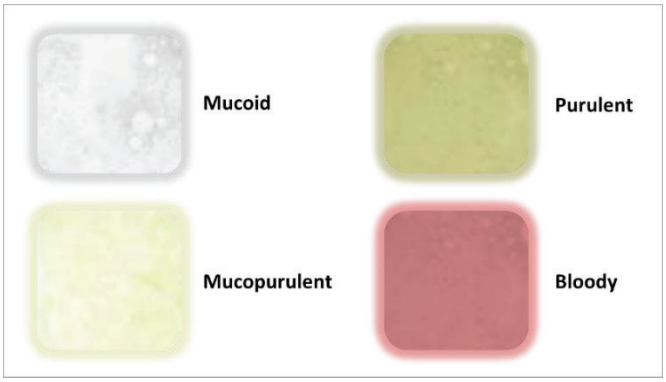

Figure 6.4. *Color chart for the phenotypic classification of BAS. The classification is based on color and consistency. Transparent and liquid samples are classified as saliva or mucoid. Slightly thicker and yellowish samples are mucopurulent. Green, highly viscous samples are purulent, and red samples, due to the presence of blood, are classified as bloody.*

6.5 RESULTS & DISCUSSION

6.5.1 OVERVIEW OF THE SAMPLES ANALYZED

The lower respiratory tract samples used in the following studies correspond to BAS (except one BAL sample), selected due to the availability of stock. As stated before, BAS samples are more challenging to obtain as they require invasive methods, such as bronchoscopy, compared to sputum. However, they offer a significant advantage for detecting *S. aureus* because this pathogen is part of the nasopharyngeal flora of healthy individuals, leading to a high risk of contamination and false positives when using sputum samples[21].

The samples were provided by the Microbiology Department at Hospital Universitari Germans Trias i Pujol and were obtained from intubated patients in

the ICU, where bronchoscopy is feasible. Sample volume was quite limited, ranging approximately between 0.5 and 1.8 mL, depending on the specific sample.

Table 6.1. *Classification of blank BAS samples (negative for S. aureus) used in the studies described in Chapter 6. The colors correspond to the phenotypic classification color chart presented in Section 6.4.*

Negative samples (BAS)	
Sample Ref.	Phenotype
R46	Purulent
R47	Bloody
R59	Purulent
R76	Purulent
R92	Mucoid
R93	Purulent
R94	Mucopurulent
R95	Mucoid
R108	Mucoid
R140	Bloody
R450	Mucoid
BAS2	Purulent
BAS5	Purulent-bloody

Table 6.2. *Classification of S. aureus-positive BAS/BAL samples used in the studies described in Chapter 6. The colors correspond to the phenotypic classification color chart presented in Section 6.4.*

Positive samples (BAS/BAL)			
Type	Sample Ref.	Phenotype	*agr* group
BAS	218	Mucopurulent	I
BAS	221	Purulent-bloody	I
BAL	221	Mucoid	I

A total of 13 blank samples and 3 positive samples were analyzed. Blank samples were defined as those with a negative culture for *S. aureus*. Positive samples showed a positive culture for *S. aureus* and were further genotyped by whole-genome sequencing. The phenotypic characteristics of the BAS/BAL samples included in this chapter are summarized in Table 6.1 (for negative samples) and Table 6.2 (for positive samples).

6.5.2 BAS TREATMENT STRATEGIES FOR ENHANCING SAMPLE HOMOGENEIZATION AND REDUCING MATRIX EFFECTS

While profiling AIPs in bacterial isolates has significant clinical value, the primary aim of this research is to enable the direct detection of *S. aureus* infections directly from clinical samples, without the need for prior culturing. Given the high incidence of *S. aureus* as one of the main pathogens causing LTR infections, this study seeks to detect AIPs in BAS, which could offer crucial insights into *S. aureus* infections and potentially lead to improved diagnostic tools and therapeutic strategies.

However, this goal presents a considerable challenge, as the detection of AIPs directly from clinical samples has not yet been documented. Consequently, there is no established reference data or baseline information regarding the concentration of these signaling molecules in LRT samples. This lack of prior research complicates the development of detection methods, as it is unknown what range of concentrations or conditions might be encountered in such clinical samples. Thus, this study attempts, to quantify AIPs in BAS for the first time, adding complexity to the experimental design and assay validation.

BAS are inherently difficult to handle due to their complexity, heterogeneity, and high viscosity. These factors not only impede sample manipulation but also complicate the extraction of AIPs, as they become trapped within the complex mucin-DNA-actin network.

The primary objective of this research was to develop a methodology to reduce the viscosity of BAS, thereby facilitating easier processing and analysis. To address this purpose, Figure 6.5 illustrates the four main strategies addessed: 1) the addition of reducing agents, which break disulfide bonds between proteins, thereby disrupting structural protein networks; 2) treatment with DNase I, which degrades the DNA network that significantly contributes to the viscosity of mucus; 3) treatment with proteinase K, which specifically cleaves proteins at serine residues, breaking down protein structures; and 4) the addition of H_2O_2, which, through the catalytic activity of catalase, generates bubbles that indiscriminately disrupt the network structure. These approaches target different components of the matrix, aiming to reduce viscosity and improve sample handling.

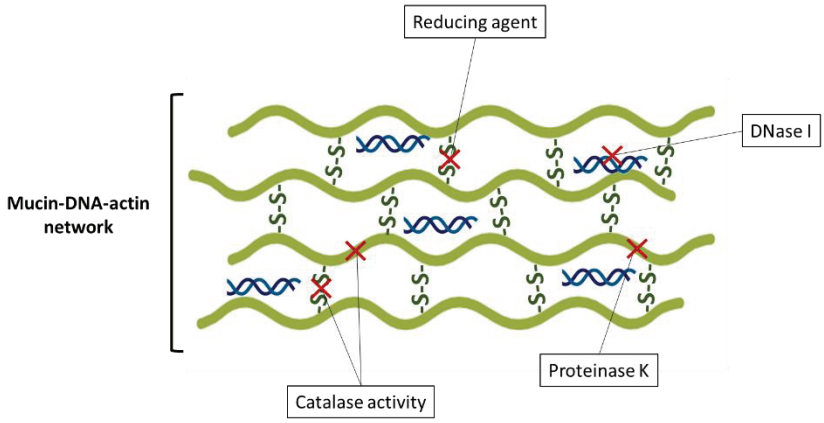

Figure 6.5. *Overview of the four main strategies evaluated for reducing mucus viscosity: 1) reducing agents to disrupt disulfide bonds, 2) DNase I to degrade DNA networks, 3) proteinase K to cleave proteins, and 4) H_2O_2 to generate bubbles via catalase activity, breaking the structural network.*

6.5.2.1 Proteinase K

To address the challenge of breaking down the complex mucus network that constitutes BAS, we initially focused on targeting the mucins, which are the primary glycoprotein components of pulmonary mucus. Mucins form a dense and viscous gel that traps particles and pathogens, making it difficult to extract or detect AIPs. To disrupt this mucin network, it was decided to use Proteinase K (PK), a serine protease known for its ability to degrade proteins efficiently.

The decision to use PK was based on prior successful experiments conducted by Dr. Juan Raya, a member of our research group, who had previously used this enzyme to treat sputum samples. Given the positive results from those studies, it was decided to adopt the same strategy as a starting point.

However, a potential complication arose concerning the detection of AIPs. Since AIPs are signaling molecules composed of short peptide chains, the use of PK could theoretically degrade these peptides, making them undetectable in the subsequent ELISAs. This concern was particularly relevant because most AIPs, with the exception of AIP3, contain serine residues in their structure (see Figure 6.6). As PK targets serines, there was a risk that the enzyme would not only digest the mucins but also degrade the AIPs, rendering them undetectable.

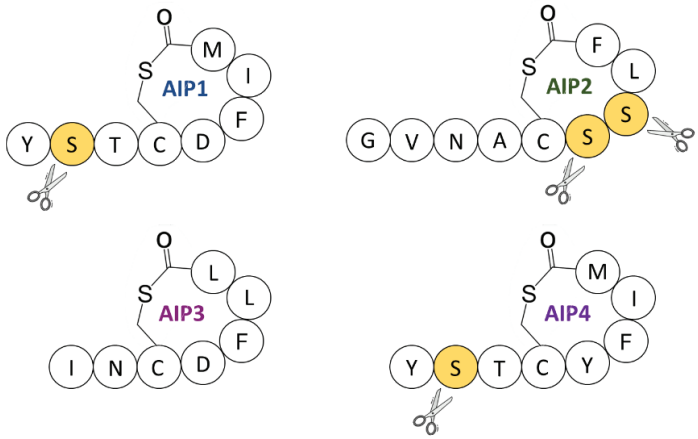

Figure 6.6. *Structures of AIPs I–IV from S. aureus, highlighting the serine residues targeted by Proteinase K. The serine residues, marked in yellow, serve as critical restriction sites for Proteinase K, an enzyme with serine-protease activity.*

Despite these concerns, it was decided to proceed with the experiment, as the exact epitope recognized by the antibodies impemented in the ELISAs was not fully known. In particular, some of the assays employed pAbs, which recognize multiple epitopes on the target molecule. This raised the possibility that the AIPs could still be detected even after partial degradation by PK, depending on where the digestion occurred relative to the antibody recognition site. As a result, this methodology was tested, hoping that the enzyme might degrade the mucins while leaving the critical regions of the AIPs intact, allowing their successful detection in the ELISA.

PK requires calcium chloride ($CaCl_2$) as a cofactor to maintain its stability and catalytic activity. The presence of calcium ions helps to stabilize the structure of the enzyme, especially around the active site, enabling it to efficiently cleave peptide bonds. The enzyme works optimally at elevated temperatures. These conditions enhance the activity of PK, allowing it to break down the mucin networks in BAS. Taking this into consideration, a procedure to treat BAS specimens for 4 hours at 55°C was stabished following various examples where proteinase K was used for sputum treatment[22-24].

To stop the action of PK after the digestion phase, a serine protease inhibitor known as phenylmethylsulfonyl fluoride (PMSF) is used. PMSF acts by irreversibly binding to the serine residue in the active site of serine proteases like PK This covalent modification of the serine residue prevents further enzymatic activity,

effectively halting the digestion process. PMSF is widely used in protease inhibition to preserve the integrity of other proteins or peptides in a sample after proteolytic treatment.

Given the specific conditions required for PK activity, it was crucial to evaluate whether these factors would interfere with the ELISA assays developed for detecting AIPs. Each of these components, when used together and separately, could potentially influence the sensitivity or accuracy of the ELISA. Therefore, before applying the enzymatic treatment, it was determined wether the presence of calcium chloride, the elevated temperature, or the addition of PMSF affected the assay performance. These tests were essential to ensure that the ELISA could still reliably detect AIPs under the conditions used for PK digestion, without introducing false positives or negatives due to interference from the treatment process.

It was determined wether $CaCl_2$, required for PK activity, interfered with the ELISAs. Using the mAb23/AIP4S-BSA ELISA as a model, the results indicated that the presence of $CaCl_2$ slightly reduced the signal in the assay but did not affect the IC_{50} (refer to Table 6.3). This suggests that $CaCl_2$ does not drastically compromise the assay's performance, allowing for the detection of AIPs with minimal loss of sensitivity under these conditions.

The effects of other treatment conditions (incubation at 55°C, the addition of PMSF, and PK treatment) were also evaluated by comparing four calibration curves on the same ELISA plate. As displayed in Figure 6.7, neither the elevated temperature nor PMSF caused any interference with the assay, meaning that both conditions are compatible with AIP1 detection via ELISA. However, when PK was introduced, the parameters of the calibration curve were significantly altered (seeTable 6.3), resulting in a poorly defined curve. This indicated that PK digestion severely affected the ability of the assay to detect AIP1, likely due to the degradation of this peptidic signaling molecules.

These findings confirmed the initial hypothesis: the use of PK to treat BAS samples is not effective for detecting AIPs, as the enzyme's proteolytic activity degrades the AIPs, making them undetectable by ELISA. However, previous antecedents demonstrated that PK treatment was successful for the detection of non-peptidic molecules, suggesting that this method may still be useful for analyzing other biomarkers in LTR samples.

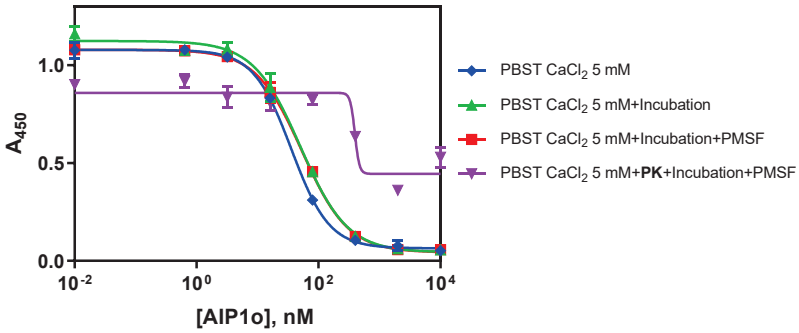

Figure 6.7. *Evaluation of the potential interferences of Proteinase K (PK) treatment conditions and its effect on AIP1 detection. The curves were obtained using the ELISA mAb23/AIP4S-BSA. The antibody concentration was set to 0.015 µg mL^{-1} and CA concentration to 0.4 µg mL^{-1}. Neither the incubation at 55°C nor the presence of PMSF interfered with the assay performance. However, the treatment with PK is not suitable for AIP1 detection, as it led to the degradation of the peptide.*

Table 6.3. *Analytical parameters of the calibration curves obtained under different conditions for Proteinase K treatment: A) PBST with 5 mM $CaCl_2$, B) PBST with 5 mM $CaCl_2$ + Incubation, C) PBST with 5 mM $CaCl_2$ + Incubation + PMSF, and D) PBST with 5 mM $CaCl_2$ + PK + Incubation + PMSF.*

Parameters	A	B	C	D
A_{min}	0.06	0.04	0.04	0.44
A_{max}	1.08	1.12	1.08	0.86
Slope	-1.39	-1.12	-1.14	~ -11,72
IC_{50} (nM)	35.86	50.44	53.62	~ 394,5
R^2	0.998	0.995	0.998	0.892

Based on these results, the study concluded that alternative treatment methods should be explored to preserve the integrity of AIPs in BAS samples. These methods need to effectively break down the mucus and other components that complicate sample handling and analysis, without compromising the molecular targets.

6.5.2.2 DNase I

As previously discussed in Section 6.3, DNA, together with actin, forms a critical network that significantly contributes to the structural integrity of BAS. This network is particularly prominent in patients with cystic fibrosis, where the extracellular DNA content is higher. Given the key role of this DNA/actin network

in the viscosity of BAS, the effectiveness of DNase I treatment was evaluated as a strategy to disrupt this network.

As illustrated in Figure 6.8, DNase I specifically targets DNA molecules, catalyzing the hydrolysis of phosphodiester bonds within the DNA, and breaking it into smaller oligonucleotide fragments.

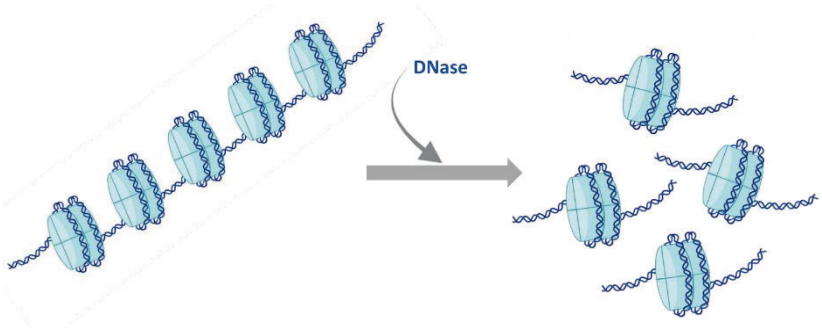

Figure 6.8. *Mechanism of action of DNase I. This en hydrolyzes phosphodiester bonds in DNA, breaking it down into smaller fragments.*

DNase I treatment was tested in clinical BAS. Initially, BAS R46, which was classified as purulent, highly viscous, and difficult to manipulate, was treated with DNase I (8 U mL^{-1}) according to the specifications outlined in Section 8.11.1.2. After treatment, three different dilutions (1/2, 1/5, and 1/10) were prepared, and each dilution was used as the matrix for a competitive indirect ELISA calibration curve, using the mAb23/AIP4S-BSA system with AIP1o as the analyte. These calibration curves were compared with a standard curve (PBST) and a PBST curve subjected to the same DNase I treatment. The goal was to assess whether the DNase I treatment (2 U mL^{-1} after treatmemt) caused interference in the ELISA and whether it could resolve the matrix effect issues commonly associated with BAS.

DNase I requires $CaCl_2$ and magnesium chloride ($MgCl_2$) as cofactors to function effectively[25]. Before testing this combined treatment on BAS samples, it was evaluated whether these cofactors would interfere with the ELISA used to detect AIPs. According to Figure 6.9, the calibration curves were nearly identical when $CaCl_2$ and $MgCl_2$ were added, indicating that the addition of these cofactors does not interfere with the assay.

No significant interference from the DNase I treatment was observed in the ELISA. However, the matrix effect problem in the BAS was not fully resolved. According to Table 6.4, aclear reduction in A_{max} was noted in the calibration curves corresponding to treated BAS, and signal recovery improved with increased dilution in PBST. Despite diluting the sample up to 10 times, the matrix effect was still not completely eliminated (refer to Figure 6.9). BAS R46 was particularly thick, and after treatment, the solution remained heterogeneous.

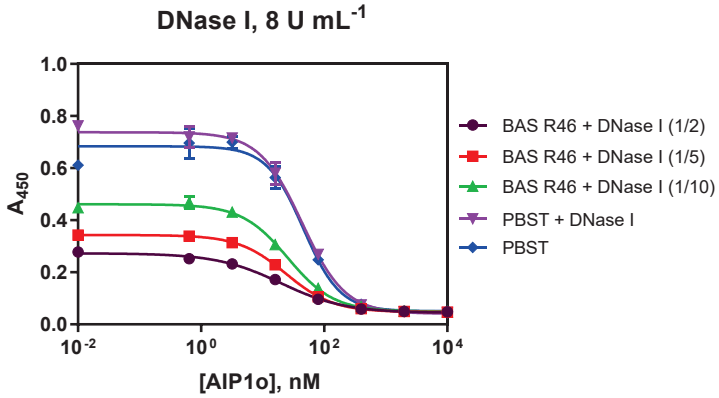

Figure 6.9. *Evaluation of BAS treatment with DNase I (8 U/ mL^{-1}). The calibration curve under normal conditions (PBST) is compared to the curve in PBST with DNase I and three curves corresponding to a mucoid BAS sample (R46) treated with DNase I and diluted 1/1, 1/5, or 1/10. DNase I treatment did not interfere with the assay performance. However, the matrix effect of the BAS sample persisted, even after diluting the sample 10 times after treatment. The curves were obtained using the ELISA mAb23/AIP4S-BSA. The antibody concentration was set to 0.015 µg mL^{-1} and CA concentration to 0.4 µg mL^{-1}.*

Table 6.4. *Analytical parameters of BAS R46 (negative for S. aureus) treated with DNase I at different dilutions, compared to calibration curves in PBST with DNase I and PBST alone.*

Parameters	R46 + DNase (1/2)	R46 + DNase (1/5)	R46 + DNase (1/10)	PBST + DNase	PBST
A_{min}	0.04	0.05	0.05	0.04	0.05
A_{max}	0.27	0.34	0.46	0.74	0.68
Slope	-0.83	-1.13	-1.16	-1.24	-1.46
IC_{50} (nM)	19.77	23.78	25.65	43.92	45.93
R^2	0.997	0.997	0.996	0.996	0.989

For the following experiment, a 1/5 dilution was chosen as a reference to dilute the samples as little as possible so as not to compromise sensitivity. Using this dilution as a reference, three BAS samples of different phenotypes were treated with DNase I: R46 (mucoid), R47 (bloody and purulent), and R92 (mucoid). The

aim of this experiment was to study how the treatment affected BAS samples with different BAS phenotypes and to evaluate whether the calibration curves generated from these matrices were homogeneous and exhibited similar behaviors.

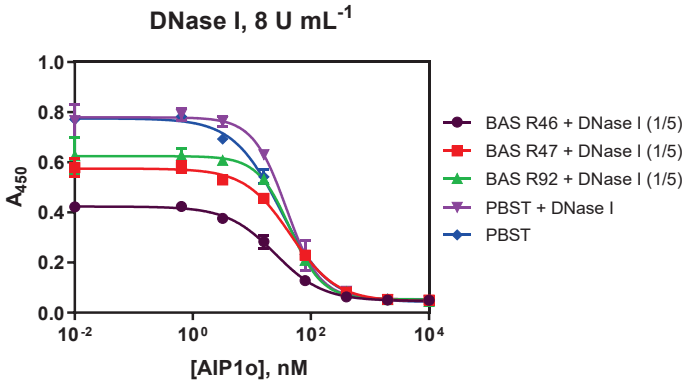

Figure 6.10. *Evaluation of BAS treatment with DNase I (8 U/ mL^{-1}). The calibration curve under normal conditions (PBST) is compared to the curve in PBST with DNase I and three curves corresponding to different BAS treated with DNase I and diluted 1/5 (R46: mucoid; R47: sanguinolent and purulent and R92: mucoid). BAS R47 and R92 exhibited similar behavior despite their completely different phenotypes. The curves were obtained using the ELISA mAb23/AIP4S-BSA. The antibody concentration was set to 0.015 µg mL^{-1} and CA concentration to 0.4 µg mL^{-1}.*

Table 6.5. *Analytical parameters of BAS R46, R47 and R92 (negative for S. aureus) treated with DNase I and diluted 1/5, compared to calibration curves in PBST with DNase I and PBST alone.*

Parameters	R46 + DNase (1/5)	R47 + DNase (1/5)	R92 + DNase (1/5)	PBST + DNase	PBST
A_{min}	0.05	0.05	0.05	0.05	0.04
A_{max}	0.42	0.58	0.62	0.78	0.78
Slope	1.40	1.66	1.64	1.59	1.49
IC_{50} (nM)	24.84	45.56	43.94	38.42	30.68
R^2	0.996	0.996	0.993	0.994	0.998

As shown in Figure 6.10, BAS R46 exhibited the same behavior as in the previous experiment. However, BAS samples R47 and R92 showed very similar behaviors, despite having different phenotypes. Both of these samples were visually homogeneous, unlike BAS R46, which remained heterogeneous with suspended particles after treatment, despite being R46 and R92 being the same BAS phenotype. As shown in Table 6.5, the analytical parameters for BAS R47 and R92 are nearly identical, whereas BAS R46 exhibits lower A_{max}, IC_{50}, and slope values.

To further confirm these results, an additional study was conducted comparing five BAS were tested in parallel. The A_{max} was compared under various conditions: a) the reference buffer (PBST, since its behavior was identical to that of DNase I-treated PBST); b) each BAS sample treated and diluted 1/5 without spiking (zero); c) each BAS treated, diluted 1/5, and then spiked with 30 nM of AIP1o and d) each BAS treated and spiked with 30 nM of AIP1o before diluting it 1/5. The phenotypic classification of the five BAS tested in this study is detailed in Figure 6.11.

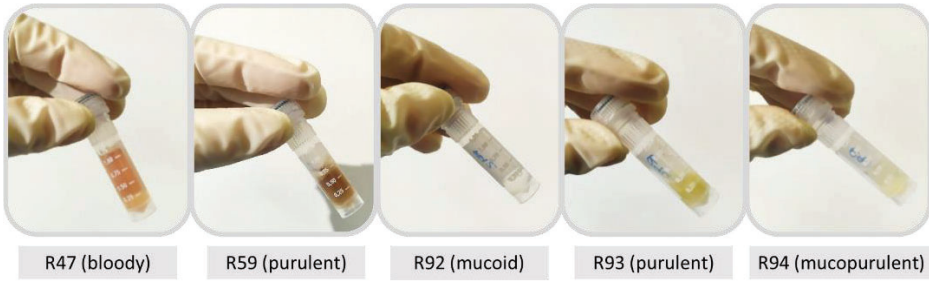

Figure 6.11. *Phenotypic classification of the 5 fresh BAS samples treated in parallel with DNase I.*

As shown in Figure 6.12, the DNase I treatment was ineffective in eliminating the matrix effect issues in BAS, as the A_{max} values for the treated samples (zeros) were consistently lower compared to the standard conditions. Additionally, the DNase I treatment required a centrifugation step.

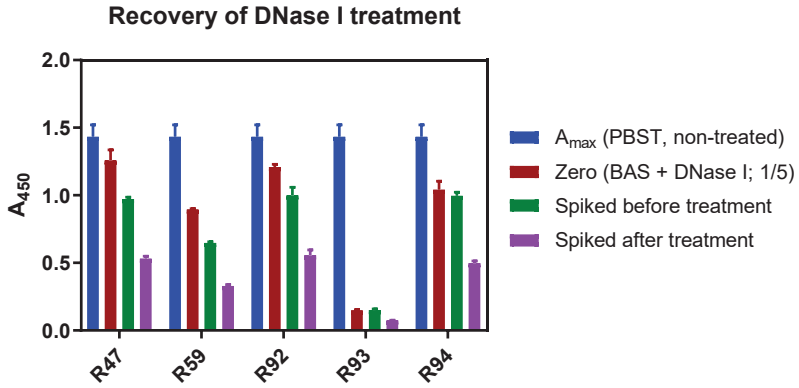

Figure 6.12. *Recovery study of freeze-dried BAS samples treated with DNase I (8 U mL^{-1}). Five clinical BAS samples were analyzed, comparing absorbance in PBST, the zero control (BAS treated with DNase I), DNase I-treated BAS spiked post-treatment, and BAS spiked prior to DNase I treatment. Samples were spiked with 30 nM of AIP1o. DNase I treatment interferes with the signal and matrix effect persists in the treated BAS. Additionally, analyte loss occurs during the treatment process, compromising the recovery. The antibody concentration was set to 0.015 µg mL^{-1} (mAb23) and CA concentration to 0.4 µg mL^{-1} (AIP4S-BSA).*

When comparing the A_{max} values for BAS samples spiked before and after treatment, a clear increase in inhibition was observed when the samples were spiked after treatment. This suggests that analyte loss occurred during some stage of the treatment process, most likely during the phase separation in the centrifugation step, given that the DNase I itself does not interfere with the ELISA. Besides that, the variability in the behavior of the treated BAS samples was evident.

Due to the difficulty in manipulating BAS and the significant phenotypic differences between them, the next step was to standardize the samples to enable meaningful comparisons and evaluate whether DNase I treatment acted uniformly across all samples. While the phenotypic variations were evident, the most notable difference was in the consistency of the samples. Some were much more viscous, and it was hypothesized that this variability was due to differences in water content, making certain samples more diluted than others. This discrepancy made it challenging to compare the samples directly.

Table 6.6. *Relationship between fresh weight and dry weight of clinical BAS.*

BAS	Phenotype	Wet weight (mg)	Dry weight (mg)	Dry/wet %
R47	Bloody	479.5	6.60	1.4
R59	Purulent	550.3	44.30	8.1
R76	Purulent	768.0	67.6	8.8
R92	Mucoid	124.0	1.30	1.1
R95	Mucoid	119.8	1.40	1.2
R108	Mucoid	91.9	3.20	3.5
R140	Bloody	667.7	76.0	11.4

The samples were weighed fresh and after water removal by freeze-drying. The results show highly variable percentages, indicating that the water content in BAS differs significantly among clinical samples.

To address this, the decision was made to standardize the samples based on their dry weight. The water content was removed from the samples by freeze-drying. As shown in Table 6.6, the correlation between dry weight and wet weight varied significantly. Purulent samples had a much higher dry residue content, while the mucoid samples were composed mostly of water, with very little solid residue. The sanguineous samples showed more variability in their composition.

Once the samples were lyophilized, they were treated with 8 U mL^{-1} of DNase I, using a concentration of 10 mg mL^{-1} of dry BAS as a reference (see procedure in Section 8.11.1.2). The calibration curves of 3 freeze-dried BAS treated with

DNase I in two different days were compared. From this experiment it was concluded that DNase I treatment alone did not homogenize the samples effectively, as some parts of the residue remained suspended even after sonication. This variability is evident in graph A) of Figure 6.13 and Table 6.7 A), where significant differences are seen between the three treated BAS (R59, R76, and R140).

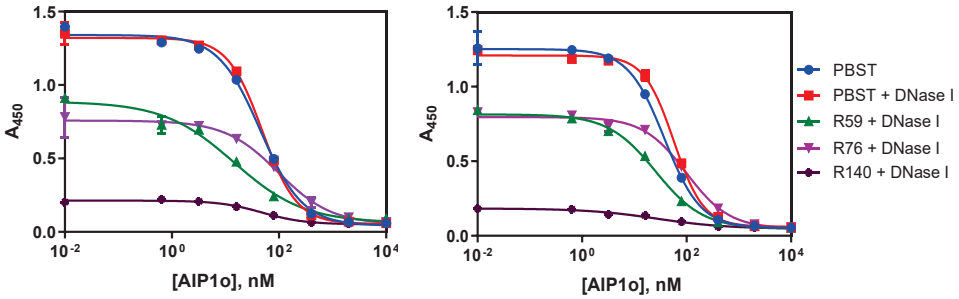

Figure 6.13. *Evaluation of DNase I treatment in freeze-dried BAS samples. A) Calibration curves in PBST, PBST + DNase I, and three freeze-dried BAS samples (10 mg mL^{-1}) treated with DNase I are compared. B) The same experiment was performed with an additional centrifugation step. The antibody concentration was set to 0.015 µg mL^{-1} (mAb23) and CA concentration to 0.4 µg mL^{-1} (AIP4S-BSA). Samples were treated with 8 U mL^{-1} of DNase I. No significant differences were observed between the two approaches, indicating that centrifugation does not improve sample homogenization. DNase I treatment alone does not resolve the matrix effect issues in the ELISA.*

To address this issue, an additional centrifugation step was introduced after DNase I treatment. Despite this, as shown in graph B) of Figure 6.13, the behavior of the supernatants remained almost identical to the previous assay. According to Table 6.7 B), there are significant differences in the analytical parameters corresponding to the three ssamples treated, especially evidenced by the lower Amax and slopes in BAS R140 and a higher IC_{50} value in BAS R76. The results obtained indicate that the DNase I treatment, even with centrifugation, was not sufficient to fully homogenize the samples.

These findings confirm that DNase I treatment alone is insufficient to homogenize BAS samples or resolve matrix effect issues, prompting the need for alternative sample processing methods to improve consistency and detection accuracy.

Table 6.7. *Analytical parameters of three BAS samples negative for S. aureus (R59, R76, and R140), freeze-dried and treated with DNase I, compared to calibration curves in PBST with DNase I and PBST alone.*

A)

Parameters	PBST	PBST + DNase	R59 + DNase	R76 + DNase	R140 + DNase
A_{min}	0.04	0.05	0.06	0.05	0.05
A_{max}	1.34	1.32	0.89	0.76	0.21
Slope	-1.10	-1.35	-0.66	-0.87	-1.08
IC_{50} (nM)	44.77	48.74	14.27	97.10	47.84
R^2	0.997	0.998	0.988	0.981	0.990

B)

Parameters	PBST	PBST + DNase	R59 + DNase	R76 + DNase	R140 + DNase
A_{min}	0.05	0.06	0.05	0.05	0.05
A_{max}	1.25	1.21	0.81	0.80	0.18
Slope	-1.25	-1.52	-0.96	-1.05	-0.65
IC_{50} (nM)	37.70	57.07	25.68	99.08	27.15
R^2	0.997	0.998	0.997	0.995	0.973

In Table A, the samples were not centrifuged, while in Table B, a centrifugation step was included

6.5.2.3 Combined treatment: DNAse I + Reducing agent (DTT)

Based on a study conducted by R. Ghanem and colleagues on the rheology of sputum samples, a new sample processing method was explored, combining DNase I with a reducing agent. Rheology, which refers to the measurement of viscosity and flow properties of a substance, was key in understanding how to reduce the viscosity of sputum in patients with CF. The study compared how sputum rheology changed after treatment with NAC or DNase I, with DNase I being administered as Pulmozyme® (dornase alfa)[16]. Pulmozyme® is a therapeutic enzyme commonly used in CF patients, which breaks down the extracellular DNA that contributes to the thick, sticky consistency of pulmonary mucus[26].

Reducing agents and DNases operate through distinct mechanisms. As previously discussed, DNase I specifically targets DNA molecules, catalyzing the hydrolysis of phosphodiester bonds within the DNA, and breaking it into smaller oligonucleotide fragments (refer to Figure 6.8).

On the other hand, reducing agents, such as DTT, disrupt the structural integrity of proteins by cleaving disulfide bonds, which are crucial for maintaining the

stability of the tertiary and quaternary structures. This reduction leads to protein denaturation, resulting in the loss of functional conformation (see Figure 6.14).

In the context of mucus, reducing agents specifically target the disulfide bonds between cysteine residues in mucin proteins, which are responsible for the thick, gel-like structure of mucus. By breaking these bonds, the mucus becomes less viscous and easier to handle, which is crucial for both clinical treatment and laboratory analysis.

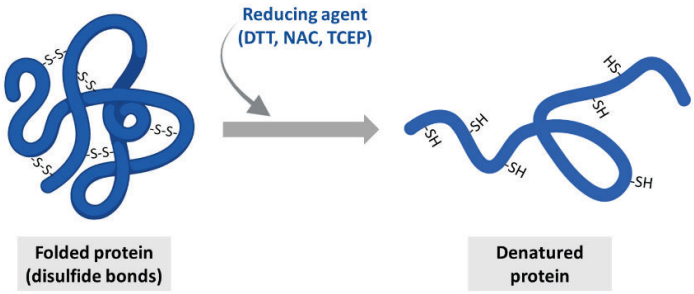

Figure 6.14. *Mechanism of action of reducing agents. These agents cleave disulfide bonds, leading to protein denaturation and loss of tertiary structure.*

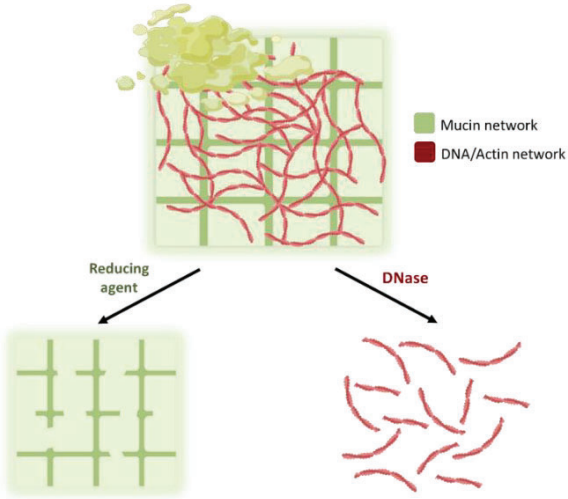

Figure 6.15. *Schematic representation of BAS structure and the effects of two treatment strategies. BAS is composed of two interconnected networks: the mucin network and the DNA/actin network. DNase specifically disrupts the DNA/actin network by hydrolyzing DNA, while reducing agents break the mucin network by cleaving disulfide bonds within mucin molecules. Adapted from Ghanem, R., et al. (2021)[16].*

This combined approach aimed to reduce the viscosity and heterogeneity of the mucus by targeting the two main structural components of pulmonary mucus:

the DNA-actin network and the mucin network. As illustrated in Figure 6.15, in this processing method, DNase is responsible for disrupting the DNA-actin network, while the reducing agent breaks the mucin network[16].

An interference study was conducted that included both agents, DNase I, and DTT, either individually or in combination. The results revealed that DNase I did not interfere with the ELISA for detecting AIP1. However, in all calibration curves where DTT was added, there was a significant increase in the IC_{50}, as shown in Figure 6.16 and Table 6.8. This increase in IC_{50} indicated interference caused by DTT, which affected the sensitivity of the ELISA.

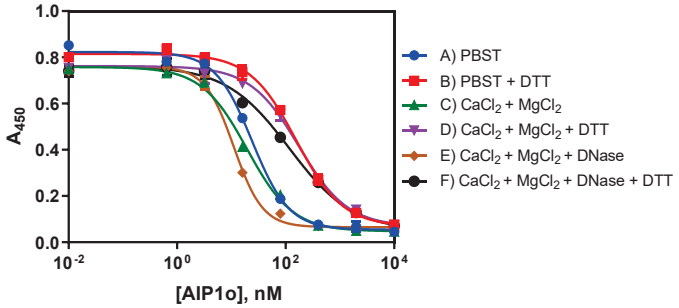

Figure 6.16. *Assessment of potential interferences caused by DNase I and DTT treatments. The antibody concentration was set to 0.015 µg mL^{-1} (mAb23) and CA concentration to 0.4 µg mL^{-1} (AIP4S-BSA). DNase I treatment did not interfere with the assay performance, neither its cofactors. In contrast, DTT treatment affected the assay sensitivity.*

Table 6.8. *Analytical parameters for the calibration curves in the interference study of DNase I and DTT treatments.*

	A	B	C	D	E	F
A_{min}	0.05	0.07	0.05	0.07	0.07	0.05
A_{max}	0.82	0.81	0.76	0.76	0.76	0.76
Hill Slope	-1.27	-1.01	-1.03	-0.96	-1.63	-0.75
IC_{50} (nM)	23.95	**156.70**	19.50	**175.70**	11.08	**117.20**
R^2	0.997	0.997	0.997	0.994	0.996	0.995

The tested conditions (A–F) correspond to the calibration curves illustrated in Figure 6.16. Conditions B, D, and F are highlighted, as the addition of DTT under these scenarios caused interferences that compromised the sensitivity of the ELISA.

Given these results, it was decided to first evaluate the effects of various reducing agents on the ELISA individually before testing them in combination with DNase I. This step was necessary to identify the most suitable reducing

agent that would minimize interference while still providing the desired reduction in sample viscosity for easier manipulation and analysis.

6.5.2.4 Reducing agents

As outlined above, reducing agents are chemical compounds that donate electrons to other molecules, facilitating the breaking of disulfide bonds. Given the well-documented effectiveness of both NAC and DTT in minimizing mucus viscosity in clinical and laboratory settings, the use of these reducing agents was considered an optimal approach for processing BAS samples. Since these methods are well-established in routine hospital laboratory practice, applying them to treat BAS samples for the detection of AIPs was a logical and widely accepted choice.

One commonly-used reducing agent for this purpose is N-acetylcysteine (NAC). NAC acts by disrupting the disulfide bonds in mucins, leading to a significant reduction in mucus viscosity. This mechanism has made NAC a popular choice for respiratory treatments, particularly for patients with COPD[27] and CF[28], as it helps clear thick mucus from the lungs. NAC is frequently used in hospital laboratories as well, where it is employed to treat LTR samples, reducing their viscosity to facilitate diagnostic procedures such as the detection of pathogens or biomarkers[29].

Dithiothreitol (DTT) was also considered in this study due to its stronger reducing power compared to NAC. DTT contains two thiol (–SH) groups, whereas NAC has only one, which allows DTT to reduce disulfide bonds more efficiently (their chemical structures are displayed in Figure 6.17). This makes DTT particularly effective in breaking down mucus in thicker or more viscous samples, where greater reduction power is needed.

DTT is widely used in clinical laboratories to reduce mucus viscosity for easier sample manipulation, especially in diagnostic contexts involving sputum or bronchial aspirates[29]. However, contrary to NAC, DTT is not typically used for direct clinical treatment of patients. While NAC is frequently administered to patients to reduce mucus viscosity and improve lung function, DTT is primarily a laboratory reagent. For example, DTT is found in commercial products such as

Sputasol and Sputolysin, which are used in clinical laboratories rather than directly in patient care, to liquefy mucus samples for analysis[17].

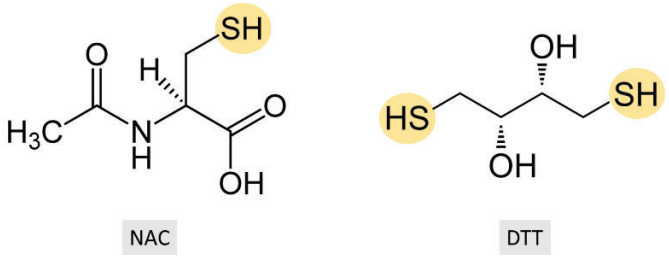

Figure 6.17. *Chemical structures of N-acetylcysteine (NAC) and dithiothreitol (DTT). Thiol groups are highlighted in yellow. DTT contains two thiol groups, resulting in a higher reducing power compared to NAC, which has only one thiol group.*

Before applying the reducing agents directly to BAS, and considering the previous results with DNase Iand DTT treatment, it was studied if these agents would interfere with the immunochemical assays developed to detect AIPs, specifically the ELISA for AIP1 detection. Separate experiments were performed for DTT and NAC by comparing a standard calibration curve (using PBST) against five calibration curves containing increasing concentrations of each reducing agent.

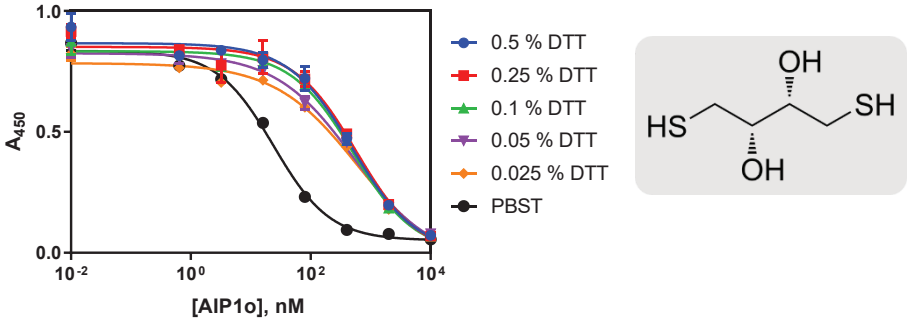

Figure 6.18*. Evaluation of potential interferences caused by DTT treatment. The calibration curve in PBST without DTT is compared to curves obtained with varying percentages of DTT. The results demonstrate that DTT interferes with the ELISA assay, even at very low concentrations, compromising its sensitivity. The antibody concentration was set to 0.015 µg mL^{-1} (mAb23) and CA concentration to 0.4 µg mL^{-1} (AIP4S-BSA).*

The results for DTT confirmed the prior concerns based on experiments combining DNase I and DTT treatments. The data revealed significant interference in the ELISA assay when DTT was present, particularly affecting the sensitivity of the assay (see Figure 6.18). As shown in Table 6.9, while the A_{max}

remained largely unchanged, there was a considerable increase in the IC_{50} value, even at the lowest concentration of DTT (0.025 %). This shift in IC_{50} indicates a loss of sensitivity, meaning the assay could no longer reliably detect low levels of AIP1.

Table 6.9. *Analytical parameters from the interference study comparing different percentages of DTT diluted in PBST with PBST alone.*

Parameters	0.5 % DTT	0.25 % DTT	0.1 % DTT	0.05 % DTT	0.025 % DTT	PBST
A_{min}	-0.004	-0.01	-0.004	-0.04	-0.06	0.05
A_{max}	0.87	0.85	0.83	0.83	0.78	0.83
Slope	-0.81	-0.83	-0.83	-0.67	-0.63	-0.92
IC_{50} (nM)	496.60	573.20	507.40	514.50	606.80	23.90
R^2	0.985	0.980	0.990	0.994	0.988	0.995

Since there are no established reference concentrations for AIPs in BAS samples, this loss of sensitivity posed a major limitation, potentially leading to false negatives and making these treatments unreliable for detecting AIPs in clinical samples. As a result, it was concluded that DTT was unsuitable for treating BAS samples intended for AIP detection, as the assay would not reach the necessary sensitivity threshold.

After observing the strong interference caused by DTT, it was hypothesized that NAC, having a weaker reducing power, might cause less interferences to the ELISA. To test this, lower concentrations of NAC were used. However, the results in Figure 6.19 revealed that NAC also caused interference in the assay, primarily affecting its sensitivity (see IC_{50} values in Table 6.10).

At the highest NAC concentration tested (0.01 %, equivalent to 0.1 mg mL^{-1}), the IC_{50} was ten times higher than under standard conditions. Even at a very low concentration of NAC (0.005 mg mL^{-1}), which is far below concentrations commonly reported in the literature[27], the sensitivity of the assay could not be restored (refer to Figure 6.19). These findings indicate that neither DTT nor NAC are suitable treatments for BAS samples with te aim to detect AIPs.

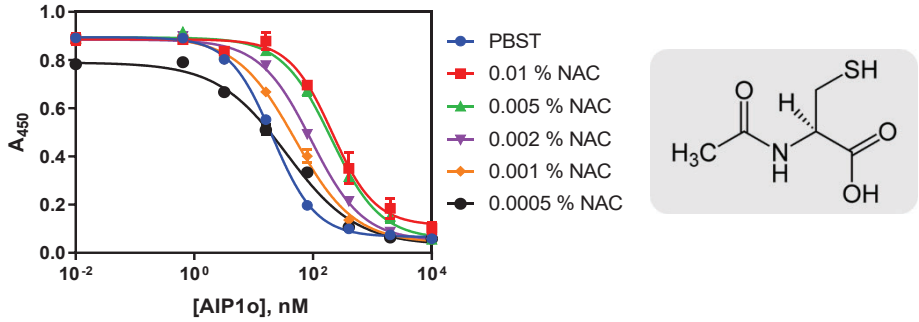

Figure 6.19. *Evaluation of potential interferences caused by NAC treatment. The calibration curve in PBST without NAC is compared to curves obtained with varying percentages of NAC. The results demonstrate that NAC interferes with the ELISA assay, even at very low concentrations, compromising its sensitivity. The antibody concentration was set to 0.015 µg mL^{-1} (mAb23) and CA concentration to 0.4 µg mL^{-1} (AIP4S-BSA).*

Table 6.10. *Analytical parameters from the interference study comparing different percentages of NAC diluted in PBST with PBST alone.*

Parameters	PBST	10 % NAC	5 % NAC	2 % NAC	1 % NAC	0.05 % NAC
A_{min}	0.07	0.11	0.06	0.05	0.04	0.03
A_{max}	0.89	0.89	0.89	0.88	0.90	0.79
Slope	-1.19	-1.20	-1.04	-1.00	-0.88	-0.74
IC_{50} (nM)	20.89	209.20	201.80	93.16	50.07	35.95
R^2	0.999	0.991	0.995	0.998	0.996	0.994

Given the limitations observed with DTT and NAC, an alternative reducing agent, TCEP (tris(2-carboxyethyl) phosphine), was selected for evaluation. TCEP acts as a potent reducing agent through its central phosphorus atom, which exists in a trivalent state. The phosphorus atom donates electrons to cleave disulfide bonds, converting them into free thiol groups (the chemical structure of TCEP can be found in Figure 6.20).

The results shown in Figure 6.20 demonstrated that, at a concentration of 0.01 mM, TCEP also caused interference in the ELISA for detecting AIPs. However, in comparison to DTT and NAC, the interference was significantly lower. The IC_{50} increased to 73.92 nM with the addition of TCEP, compared to 27.78 nM in PBST alone (refer to Table 6.11). Despite this, it was decided to test TCEP in real BAS samples to assess whether this concentration could adequately liquefy and homogenize the samples.

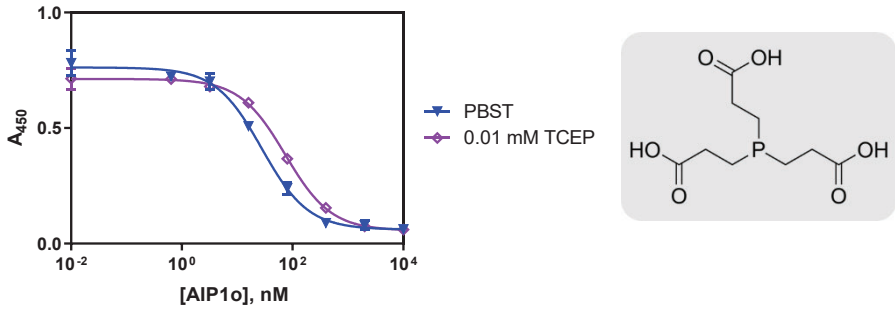

Figure 6.20. *Evaluation of potential interferences caused by TCEP treatment. The calibration curve in PBST without NAC is compared to a curve containing 0.01 mM of TCEP. The results demonstrate that the selected TCEP concentration interferes slightly the ELISA assay. The antibody concentration was set to 0.015 µg mL^{-1} (mAb23) and CA concentration to 0.4 µg mL^{-1} (AIP4S-BSA).*

Table 6.11. *Analytical parameters from the interference study comparing PBST containing 0.01 mM TCEP with PBST alone.*

Parameters	PBST	PBST + TCEP
A_{min}	0.06	0.06
A_{max}	0.76	0.71
Slope	-1.04	-1.05
IC_{50} (nM)	27.78	73.92
R^2	0.994	0.998

To assess its effectiveness, three BAS samples (R59, R76 and R140) of different phenotypes (see Table 6.6) were treated with 0.04 mM TCEP (for details of the treatment, refer to Section 8.11.1.3). After treatment, calibration curves were generated for each of the BAS samples, and the results were compared (TCEP concentration after treatment is 0.01 mM). During treatment, it became evident that TCEP at this concentration was not fully effective in liquefying the samples. The samples remained heterogeneous, with particles in suspension that blocked pipette tips, making handling difficult.

Furthermore, as shown in Figure 6.21, the calibration curves for the three BAS samples, despite undergoing the same treatment, were markedly different one form another. As evidenced in Table 6.12, the addition of TCEP drastically increases the IC_{50}. Furthermore, the matrix effect issues in BAS samples are not resolved, as absorbance values are significantly lower in the presence of the different samples. This suggests that the TCEP treatment was insufficient in eliminating the matrix effect and failed to homogenize the behavior of the BAS

samples in the ELISA. Consequently, this treatment did not meet the objective of standardizing the samples for reliable detection of AIPs.

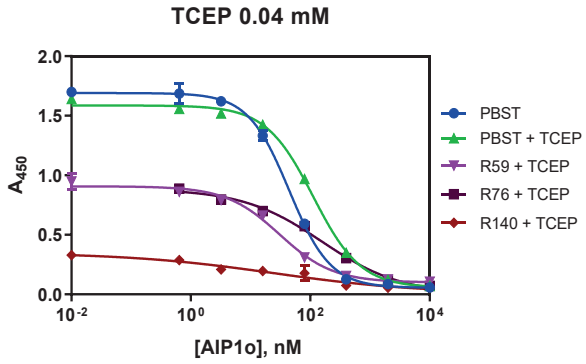

Figure 6.21. *Evaluation of TCEP treatment in freeze-dried BAS samples. Calibration curves in PBST, PBST + TCEP, and three BAS samples (10 mg mL^{-1}) treated with 0.04 mM of TCEP are compared. TCEP treatment alone does not resolve the matrix effect issues in the ELISA as samples show very heterogeneous behaviour. The antibody concentration was set to 0.015 µg mL-1 (mAb23) and CA concentration to 0.4 µg mL-1 (AIP4S-BSA).*

Table 6.12. *Analytical parameters of three BAS samples negative for S. aureus (R59, R76, and R140), freeze-dried and treated with TCEP, compared to calibration curves in PBST with TCEP and PBST alone.*

Parameters	PBST	PBST + TCEP	R59 + TCEP	R76 + TCEP	R140 + TCEP
A_{min}	0.05	0.06	0.10	0.00	0.01
A_{max}	1.69	1.59	0.91	0.89	0.35
Slope	-1.26	-1.09	-0.97	-0.65	-0.35
IC_{50} (nM)	44.36	111.90	30.53	157.40	24.36
R^2	0.998	0.998	0.989	0.992	0.928

6.5.2.5 Enzimatic liquefaction

In a recent study published by Clemente and colleagues[30], a new technique for the rapid liquefaction of respiratory samples in just one minute was presented. This method relies on the generation of oxygen bubbles through the activity of bacterial catalase upon the addition of hydrogen peroxide (H_2O_2) to liquify the sputum. The catalase enzyme, which is naturally produced by many bacterial species found in respiratory samples, breaks down hydrogen peroxide into water and oxygen. The rapid release of oxygen in the form of bubbles helps to

mechanically disrupt and liquefy the mucus, making the sample easier to handle for further analysis (see Figure 6.22).

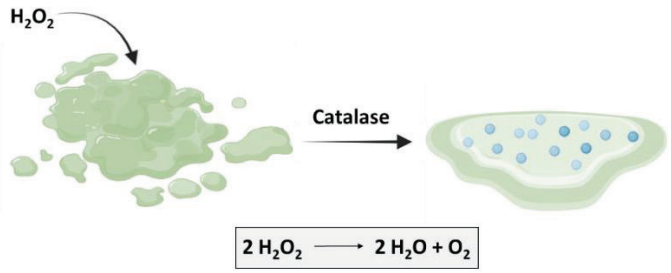

Figure 6.22. *Mechanism of action of catalase. Catalase catalyzes the decomposition of hydrogen peroxide (H_2O_2) into water (H_2O) and oxygen (O_2). The release of oxygen bubbles disrupts the structure of the BAS, causing it to disaggregate and reducing its viscosity.*

Given the simplicity and speed of this sample processing technique, it was tested in this study to determine its effectiveness for BAS samples.

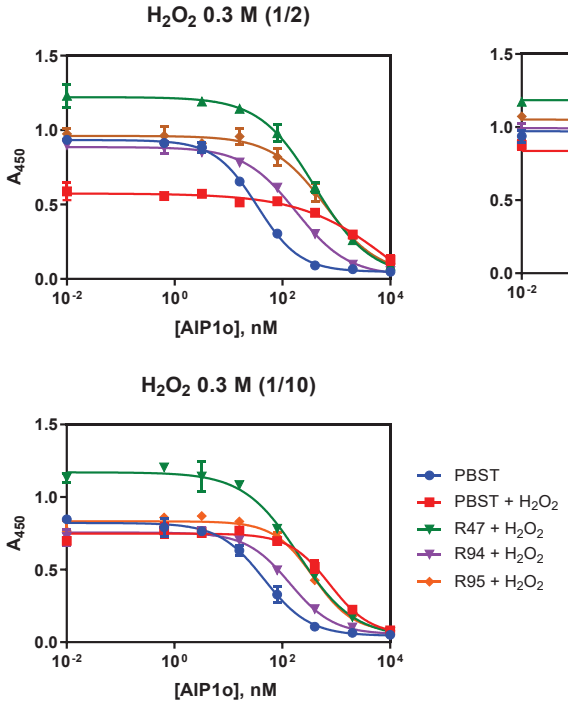

Figure 6.23. *Evaluation of H_2O_2 treatment in BAS samples. Calibration curves in PBST, PBST + H_2O_2, and three BAS treated with 0.3 M of H_2O_2 in a ratio 20:1 (v/w) are compared. H_2O_2 treatment does not resolve the matrix effect issues in the ELISA as samples show very heterogeneous behaviour. The antibody concentration was set to 0.015 µg mL^{-1} (mAb23) and CA concentration to 0.4 µg mL^{-1} (AIP4S-BSA).*

Three BAS samples with different phenotypes were selected for treatment following the protocol described by A. Clemente and colleagues, based the addition of 0.3 M of H_2O_2 in a ratio 20:1 (v/w)[30] (see Section 8.11.1.5 for further details). The selected samples were: R47 (bloody), R94 (mucopurulent), and R95 (mucoid). After treatment, each sample was diluted 1/2, 1/5, and 1/10 with PBST. Calibration curves were then carried out using these dilutions as matrix, and the results were compared to a curve generated from PBST treated with hydrogen peroxide and diluted under the same conditions.

Table 6.13. *Analytical parameters of H_2O_2 treatment for three BAS samples negative for S. aureus (R47, R93, and R94) tested at three different dilutions: 1/2, 1/5, and 1/10.*

1/2

Parameters	PBST	PBST + H_2O_2 (1/2)	R47 + H_2O_2 (1/2)	R93 + H_2O_2 (1/2)	R94 + H_2O_2 (1/2)
A_{min}	0.05	-0.35	0.01	0.02	0.03
A_{max}	0.93	0.57	1.22	0.89	0.96
Slope	-1.10	-0.52	-0.84	-0.90	-0.88
IC_{50} (nM)	33.88	11117.00	400.90	177.80	620.20
R^2	0.999	0.975	0.996	0.997	0.988

1/5

Parameters	PBST	PBST + H_2O_2 (1/5)	R47 + H_2O_2 (1/5)	R93 + H_2O_2 (1/5)	R94 + H_2O_2 (1/5)
A_{min}	0.06	-0.03	0.05	0.04	0.06
A_{max}	0.97	0.84	1.19	0.99	1.05
Slope	-1.23	-0.77	-0.88	-1.02	-0.94
IC_{50} (nM)	26.16	1334.00	312.70	118.20	380.10
R^2	0.996	0.984	0.997	0.993	0.985

1/10

Parameters	PBST	PBST + H_2O_2 (1/10)	R47 + H_2O_2 (1/10)	R93 + H_2O_2 (1/10)	R94 + H_2O_2 (1/10)
A_{min}	0.04	0.05	0.03	0.05	0.07
A_{max}	0.82	0.75	1.17	0.76	0.83
Slope	-1.03	-1.16	-0.85	-1.08	-1.18
IC_{50} (nM)	46.20	756.00	200.90	138.50	374.00
R^2	0.993	0.987	0.992	0.993	0.984

The results in Figure 6.23 revealed that, at a 1/2 dilution, hydrogen peroxide caused significant interference in the ELISA, affecting the accuracy of the assay. However, as the samples were diluted further, there was greater homogeneity in their behavior. Despite this improvement, even at a 1/10 dilution, significant heterogeneity remained, and the presence of hydrogen peroxide still interfered with the ELISA, compromising its sensitivity. Although the calibration curve in

PBST treated with hydrogen peroxide recovered much of the signal after a 1/10 dilution, the interference issues were still apparent, severely affecting the assay's overall sensitivity (see Table 6.13).

To effectively evaluate the potential interferences of H_2O_2 on the ELISA, calibration curves were generated under standard conditions (PBST) and compared with those created in the presence of H_2O_2 at various dilutions. The results demonstrated significant interference caused by H_2O_2, even when the samples were diluted up to 20 times (see Figure 6.24). This level of dilution is not a feasible option, as diluting the samples beyond 1/20 would likely compromise the sensitivity of the ELISA, as indicated in Table 6.13, especially given that the concentrations of AIPs in BAS remain unknown. Such extensive dilution would ultimately limit the assay's effectiveness in detecting low levels of AIPs.

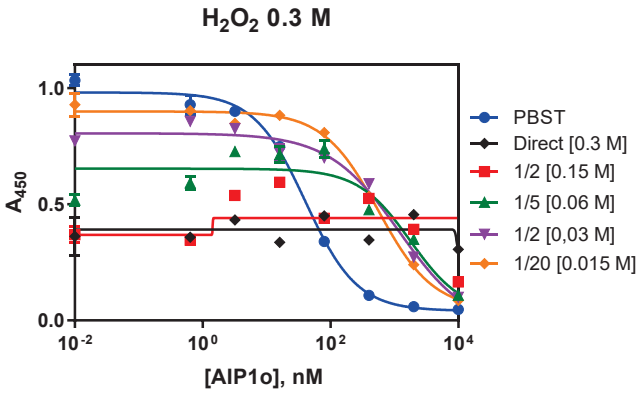

Figure 6.24. *Assessment of potential interferences caused by H_2O_2 treatment. The antibody concentration was set to 0.015 µg mL^{-1} (mAb23) and CA concentration to 0.4 µg mL^{-1} (AIP4S-BSA). H_2O_2 interferes with the assay performance even diluting the sample 20 times.*

An additional challenge encountered during the treatment process was the formation of excessive oxygen bubbles due to the catalase activity of the microbial flora present in the BAS samples. Bubbles made pipetting and sample manipulation difficult after the treatment.

To address this, an incubation step with Sodium azide (NaN_3) for 1 hour was introduced to inhibit catalase activity after treating the samples. NaN_3 is known to irreversibly bind to the heme group of the catalase, effectively inhibiting its activity and preventing further oxygen production[31]. The inhibition of catalase by NaN_3 occurs due to the specific interaction between the azide ion (N_3^-) and the

iron (Fe^{3+}) in the heme group of the enzyme. The azide ion binds to the Fe^{3+}, forming an inactive complex (Fe^{3+}-N_3) that blocks the active site and prevents the enzyme from interacting with hydrogen peroxide (H_2O_2). As visualized in Figure 6.25, this inhibition avoids the catalytic breakdown of H_2O_2 into water and oxygen, making the enzyme inactive. This approach allowed for easier handling of the samples post-treatment and reduced challenges caused by the bubbles.

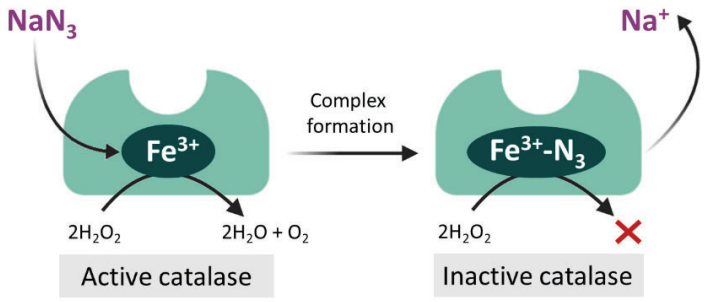

Figure 6.25. *Mechanism of catalase inhibition by sodium azide (NaN_3). The azide ion (N_3^-) binds to the Fe^{3+} in the heme group of the enzyme, forming an inactive Fe^{3+}-N_3 complex that blocks the active site and prevents hydrogen peroxide (H_2O_2) breakdown.*

To determine whether the addition of NaN_3 that inhibits catalase activity and stops bubble formation would improve the sample handling process, BAS samples treated with H_2O_2 alone and with H_2O_2 combined with NaN_3 were compared on the same day. Additionally, a sonication step was removed from the initial protocol, as it contributed to the excessive bubble formation. The same three BAS samples (R47, R94, and R95) were treated, and the effect of adding NaN_3 was evaluated.

As shown in Figure 6.26, the same interferences caused by H_2O_2 were still evident in two of the BAS samples (R47 and R95), even after adding NaN_3. In the case of R94, the loss of signal due to interference was partially resolved, but the IC_{50} remained high (refer to Table 6.14). These results suggest that, while inhibiting catalase with NaN_3 helped reduce bubbling and improve sample handling, it did not fully address the interference from H_2O_2 in the ELISA.

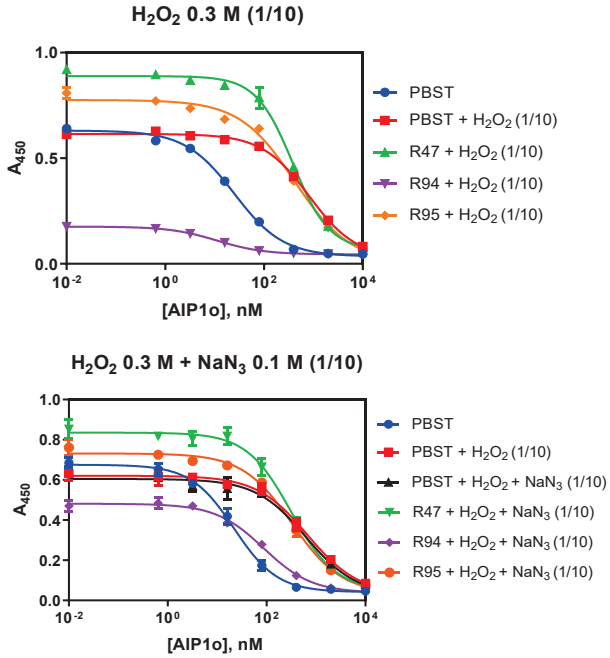

Figure 6.26. *Evaluation of NaN_3 addition for catalase inactivation after H_2O_2 treatment of BAS. On the top, calibration curves in PBST, PBST + H_2O_2 diluted 1/10, and three BAS treated with 0.3 M of H_2O_2 in a ratio 20:1 (v/w) are compared. On the bottom, te same calibration curves are performed after 1h incubation with NaN3 (0.1 M). NaN_3 does not solve the interference problems of H_2O_2 treatment. The antibody concentration was set to 0.015 µg mL^{-1} (mAb23) and CA concentration to 0.4 µg mL^{-1} (AIP4S-BSA).*

Table 6.14. *Analytical parameters of H_2O_2 treatment for three BAS samples negative for S. aureus (R47, R94, and R95).*

A) Parameters	PBST	PBST + H_2O_2 (1/10)	R47 + H_2O_2 (1/10)	R94 + H_2O_2 (1/10)	R95 + H_2O_2 (1/10)
A_{min}	0.03	0.03	0.07	0.04	0.01
A_{max}	0.63	0.61	0.89	0.18	0.78
Slope	-0.87	-0.91	-1.17	-0.91	-0.78
IC_{50} (nM)	24.90	820.20	382.80	11.08	416.30
R^2	0.997	0.998	0.996	0.997	0.992

B) Parameters	PBST	PBST + H_2O_2 (1/10)	PBST + H_2O_2 + NaN_3 (1/10)	R47 + H_2O_2 + NaN_3 (1/10)	R94+ H_2O_2 + NaN3 (1/10)	R95 + H_2O_2 + NaN_3 (1/10)
A_{min}	0.03	0.03	0.07	0.04	0.01	0.01
A_{max}	0.63	0.61	0.89	0.18	0.78	0.78
Slope	-0.87	-0.91	-1.17	-0.91	-0.78	-0.78
IC_{50} (nM)	24.90	820.20	382.80	11.08	416.30	416.30
R^2	0.997	0.998	0.996	0.997	0.992	0.992

Table A) shows the results for treatment with H_2O_2 alone, while Table B) presents the results for H_2O_2 combined with sodium azide (NaN_3). All samples were diluted 1/10 after the treatment.

In an attempt to remove the remaining H_2O_2 after sample processing, the first strategy tested was to neutralize it by adding sodium nitrite ($NaNO_2$). The ability of $NaNO_2$ to neutralize H_2O_2 was evaluated, and calibration curves were generated at various dilutions after the neutralization process (for 15 minutes). However, the results in Figure 6.27 revealed that $NaNO_2$ was ineffective in eliminating the H_2O_2 interference. A significant increase in IC_{50} values was observed at all dilutions tested, as shown in Table 6.15. This finding highlighted the need for alternative methods to eliminate H_2O_2 from the samples to avoid compromising the assay sensitivity.

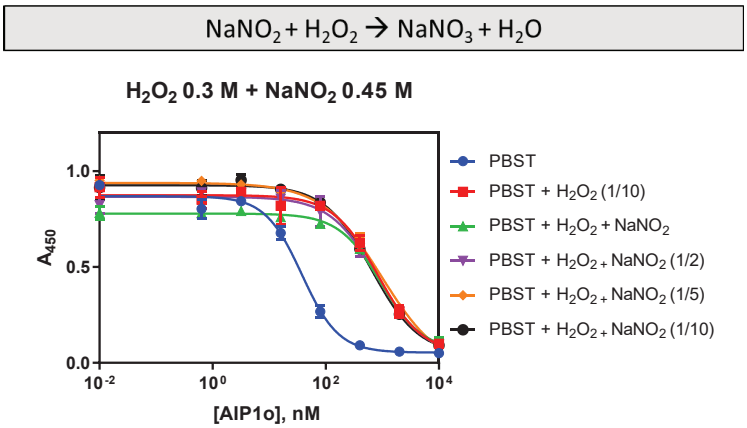

Figure 6.27. *Evaluation of $NaNO_2$ addition for H_2O_2 neutralization. Calibration curves in PBST, PBST + H_2O_2 diluted 1/10 and PBST + H_2O_2 + $NaNO_2$ at three different dilutions are compared. $NaNO_2$ does not solve the interference problems of H_2O_2 treatment as the sensibility of the ELISA is not recovered. The antibody concentration was set to 0.015 µg mL^{-1} (mAb23) and CA concentration to 0.4 µg mL^{-1} (AIP4S-BSA).*

Table 6.15. *Analytical parameters from the study evaluating the addition of $NaNO_2$ for H_2O_2 neutralization.*

Parameters	PBST	PBST + H_2O_2 (1/10)	PBT + H_2O_2 + $NaNO_2$	PBST + H_2O_2 + $NaNO_2$ (1/2)	PBST + H_2O_2 + $NaNO_2$ (1/5)	PBST + H_2O_2 + $NaNO_2$ (1/10)
A_{min}	0.05	0.05	0.06	0.04	-0.04	0.04
A_{max}	0.87	0.87	0.78	0.87	0.94	0.93
Slope	-1.58	-2.92	-2.97	-2.90	-2.99	-2.81
IC_{50} (nM)	37.77	824.00	931.10	801.40	982.30	649.40
R^2	0.990	0.981	0.996	0.987	0.996	0.993

In a last attempt before discarding this methodology, sodium dithionite ($Na_2S_2O_4$) was tested for its ability to neutralize the remaining H_2O_2 and eliminate the matrix effect in BAS samples. Unlike the previous attempts, 1h incubation with 0.1 M $Na_2S_2O_4$ appeared to be effective in homogenizing the treated BAS

samples. Although it did not completely resolve the interference issues compared to the standard PBST curve, the two BAS samples tested (R47 and R95) showed homogeneity both between each other and also in comparison to the treated PBST curve (see Figure 6.28).

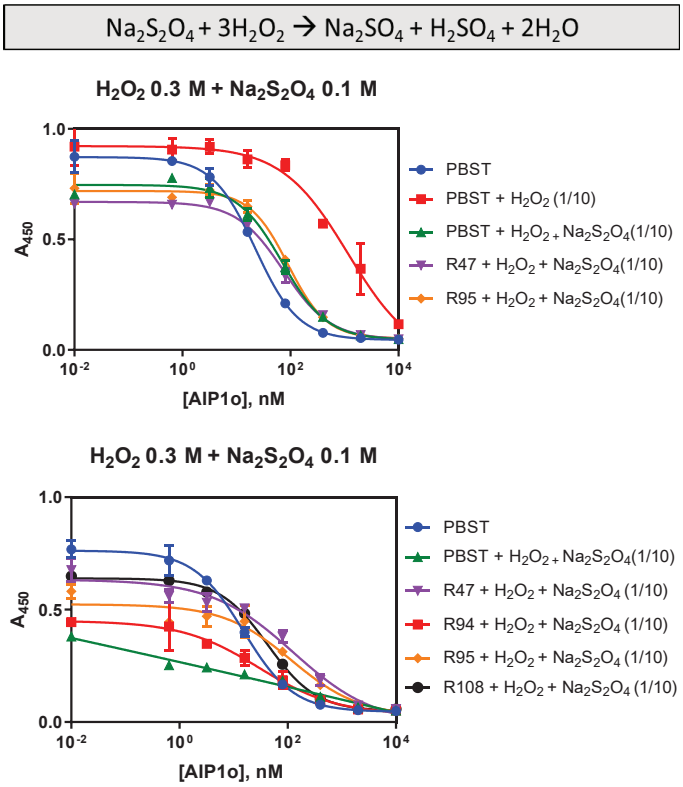

***Figure 6.28**. Evaluation of $Na_2S_2O_4$ addition for H_2O_2 neutralization after BAS treatment. Calibration curves in PBST, PBST + H_2O_2 + $Na_2S_2O_4$ dilutes 1/10 and four BAS treated following the same procedure are compared. $Na_2S_2O_4$ does not solve the interference problems of H_2O_2 treatment as no reproducible results were obtained to homogenize the bahaviour of the samples. The antibody concentration was set to 0.015 µg mL^{-1} (mAb23) and CA concentration to 0.4 µg mL^{-1} (AIP4S-BSA).*

Encouraged by these results, the methodology was expanded to test additional BAS samples to assess consistency. However, upon treating four different BAS samples, the initial results could not be reproduced. As showed in Figure 6.28, the behavior of the two previously treated BAS samples did not align with their earlier results, and there was significant variability among the newly tested samples in terms of A_{max} and IC_{50} (see Table 6.16 B). This lack of reproducibility, combined with persistent heterogeneity, led to the decision to discard this

treatment approach due to its unreliability for consistent BAS processing and ELISA assay performance.

Table 6.16. *Analytical parameters from the study evaluating the addition of $Na_2S_2O_4$ for H_2O_2 neutralization.*

A)

Parameters	PBST	PBST + H_2O_2 (1/10)	PBST + H_2O_2 + $Na_2S_2O_4$ (1/10)	R47 + H_2O_2 + $Na_2S_2O_4$ (1/10)	R95 + H_2O_2 + $Na_2S_2O_4$ (1/10)
A_{min}	0.05	-0.05	0.05	0.05	0.05
A_{max}	0.87	0.92	0.75	0.67	0.72
Slope	-1.35	-3.07	-1.85	-1.87	-1.96
IC_{50} (nM)	22.34	1162.00	70.32	74.31	90.42
R^2	0.997	0.974	0.992	0.997	0.994

B)

Parameters	PBST	PBST + H_2O_2 + $Na_2S_2O_4$ (1/10)	R47 + H_2O_2 + $Na_2S_2O_4$ (1/10)	R94 + H_2O_2 + $Na_2S_2O_4$ (1/10)	R95 + H_2O_2 + $Na_2S_2O_4$ (1/10)	R108 + H_2O_2 + $Na_2S_2O_4$ (1/10)
A_{min}	0.05	~ -5,560	-0.01	0.03	0.02	0.05
A_{max}	0.76	~ 2,487	0.63	0.45	0.52	0.64
Slope	-0.94	~ -0,01470	-0.57	-0.61	-0.69	-0.97
IC_{50} (nM)	15.26	~ $3{,}180e^{28}$	126.30	29.67	118.10	42.75
R^2	0.995	0.974	0.972	0.958	0.953	0.998

6.5.2.6 AIP extraction by organic solvents

The matrix effect of BAS persisted despite all the treatments tested, posing significant challenges to the efficient detection of *S. aureus* AIPs. Given the difficulties encountered in directly detecting AIPs within the BAS matrix, a new strategy was adopted: instead of attempting to modify the matrix, AIPs were extracted from it to enable their detection and quantification.

This approach involved the use of organic solvents, starting with methanol, to selectively isolate the AIPs. This strategy aimed to skip the complications of matrix effects, by working with a purified product.

The choice of methanol was based on the polar nature of AIPs. It effectively solubilizes AIPs due to their similar polarity, which favors their extraction. To evaluate whether methanol could efficiently extract AIPs, the BAS sample R450

(mucoid phenotype) was spiked with AIP4o at three concentrations: A) 4 µM, B) 400 nM and C) 40 nM. An unspiked portion of the sample was also treated, serving as a blank to determine if this extraction method introduced interferences in the ELISA. For this study, the selected ELISA system was As381/AIP4S-BSA.

The spiking was performed one day prior to the treatment, and the samples were mixed using a vortex to ensure uniform penetration of AIP4o into the matrix. The following day, the samples were treated with methanol, sonicated for 15 minutes to disrupt the mucus and enhance AIP accessibility, and centrifuged at 10,000 rpm for 10 minutes. After centrifugation, the phases were separated (see Figure 6.29), and the organic phase was collected for quantification via ELISA.

To ensure the samples fell within the working range of the ELISA, different dilutions were prepared, resulting in varying residual methanol concentrations: Sample A) 0.5 % methanol and Samples B) and C) 5 % methanol. Each sample was interpolated into a calibration curve prepared under the same conditions.

Table 6.17. *Results of AIP4o extraction from BAS R450 (negative for S. aureus) using methanol.*

	Sample	AIP4o quantified (nM)	Recovery (%)
A)	**BAS R450: 4000 nM AIP4o**	2352.90	58.82
	Blank	405.50	
	+ Control: 5 nM AIP4o	7.63	
	+ Control: 10 nM AIP4o	11.24	
	- Control	<LLOQ	
B)	**BAS R450: 400 nM AIP4o**	613.02	153.25
	Blank	3.59	
	+ Control: 5 nM AIP4o	6.82	
	+ Control: 10 nM AIP4o	14.36	
	- Control	<LLOQ	
C)	**BAS R450: 40 nM AIP4o**	95.32	238.29
	Blank	3.59	
	+ Control: 5 nM AIP4o	6.82	
	+ Control: 10 nM AIP4o	14.36	
	- Control	<LLOQ	

Methanol extraction introduces interferences in the ELISA, as evidenced by the quantification of blank (non-spiked) samples and significant overestimation in the ELISA for two of the spiked samples. Blank stands for non-spiked BAS, subjected to the same treatment. The antibody dilution was set to 1/4000 (As381) and CA concentration to 0.078 µg mL^{-1} (AIP4S-BSA).

The results displayed in Table 6.17 revealed that the methanol treatment introduced interferences in the ELISA, as the blanks were quantifiable, indicating non-specific signals. Additionally, at lower spiked concentrations of AIP4o, the ELISA exhibited poor quantification and significant overestimation, suggesting that the extraction method was not sufficiently robust at the tested concentration range. However, the positive and negative controls performed correctly, confirming that the issue was not with the ELISA itself but rather due to interferences introduced during the treatment process.

Based on these findings, an additional step was implemented to remove the organic solvent from the sample to minimize interferences and improve the accuracy of AIP quantification. After extraction, the organic solvent was removed using a vacuum concentrator (SpeedVac), which evaporates it under reduced pressure. This step is critical, as it eliminates any residual solvent that could interfere with the ELISA. Once the organic solvent was evaporated, the extracted AIPs were reconstituted in the optimal assay buffer (PBST) to proceed with their detection and quantification.

To evaluate this new procedure, five organic solvents were selected: ethyl acetate (AcOEt), chloroform ($CHCl_3$), dichloromethane (CH_2Cl_2), diethyl ether (Et_2O), and n-butanol (n-BuOH). Water-immiscible solvents were selected this time to ensure a phase separation during the extraction process. This approach allows the AIPs to be efficiently extracted into the pure solvent phase, isolating them from the aqueous matrix. Using an immiscible solvent offers the added advantage of simplifying subsequent steps, as the AIPs are concentrated in a solvent that is easier to evaporate, reducing sample processing time.

In this study, a 10 mM PBS solution was spiked with 1 nmol of AIP4o, and 500 µL of this spiked solution were extracted with 500 µL of each solvent. Then, 200 µL of the organic phase were collected, evaporated in a SpeedVac, and reconstituted in 500 µL of 10 mM PBST. Several dilutions were prepared to ensure the samples fell within the ELISA working range.

As shown in Table 6.18, the most promising solvents for AIP4o extraction were ethyl acetate (ρ= 0.90 g cm^{-3}) and n-butanol (ρ= 0.81 g cm^{-3}), both of which have densities lower than water. This is advantageous as it allows for easier recovery of the organic phase, which remains on top of the aqueous phase, avoiding matrix effects from the BAS. Despite this, both solvents introduced interferences

in the ELISA. AcOEt showed an initially low recovery (31 %) when quantified directly, but recovery improved with increasing dilutions, reaching 89 % when diluting 50 times. On the other hand, the n-BuOH extract consistently overestimated the results at all dilution levels. Both the positive and negative controls performed as expected, confirming that the ELISA quantified correctly.

Table 6.18. *Recovery results after AIP4o extraction from spiked PBS using five organic solvents.*

Sample	AIP4o quantified (nM)
AcOEt direct	248.08
AcOEt 1/10	275.33
AcOEt 1/25	508.55
AcOEt 1/50	715.04
$CHCl_3$ direct	<LLOQ
$CHCl_3$ 1/10	<LLOQ
$CHCl_3$ 1/25	<LLOQ
$CHCl_3$ 1/50	<LLOQ
CH_2Cl_2 Direct	7.91
CH_2Cl_2 1/10	<LLOQ
CH_2Cl_2 1/25	<LLOQ
CH_2Cl_2 1/50	<LLOQ
Et_2O Direct	6.46
Et_2O 1/10	<LLOQ
Et_2O 1/25	<LLOQ
Et_2O 1/50	<LLOQ
n-BuOH Direct	>HLOQ
n-BuOH 1/10	1091.21
n-BuOH 1/25	1115.59
n-BuOH 1/50	1254.67
AIP4o [10 nM]	10.99
AIP4o [20 nM]	17.37
AIP4o [40 nM]	40.17
Zero	<LLOQ

***LLOQ: 9.04nM**

The table shows the percentage of recovery in the sample reconstituted in PBST and at different dilutions. The most promising solvents are ethyl acetate (AcOEt) and n-butanol (n-BuOH), although the quantification is not entirely accurate due to potential interferences from solvent residues. The antibody dilution was set to 1/4000 (As381) and CA concentration to 0.078 µg mL-1 (AIP4S-BSA).

Based on these results, it was decided to perform extractions with AcOEt and n-BuOH from blank BAS samples (negative for *S. aureus*) spiked with AIP4o,

ensuring that the total solvent content was completely evaporated before reconstituting the pellet to minimize interferences.

After testing both solvents, n-BuOH was determined to be the most suitable for AIP extraction from BAS, despite the promising performance of AcOEt in PBS. As visualized in Figure 6.29, n-BuOH treatment efficiently separated the aqueous phase from the organic phase, extracting AIPs into the organic phase, which remained on the top layer. The detailed procedure is outlined in Figure 8.2**,** from Section 8.11.1.6.

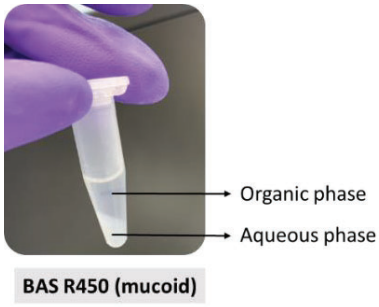

Figure 6.29. *Phase separation after n-BuOH treatment. BAS R450 (mucoid) after treatment is shown. The organic phase (containing the extracted AIPs) is visible at the top, while the aqueous phase remains at the bottom.*

Table 6.19. *Recovery of AIP4o from spiked BAS R450 (negative for S. aureus) using n-BuOH extraction.*

	[AIP4o] spiked (nM)	[AIP4o] detected (nM)
BAS	2000	1336.48
	200	111.31
	20	12.41
	Blank	1.09
Controls	10	13.25
	20	21.40
	Zero	<LLOQ

Recovery (%): 55.7 - 66.8

***LLOQ: 1.28 nM**

The table shows recovery percentages ranging from 55.7 % to 66.8 % across the spiked concentration range. The antibody dilution was set to 1/4000 (As381) and CA concentration to 0.078 µg mL^{-1} (AIP4S-BSA).

The recovery percentages of AIP4o from spiked BAS samples ranged between 55.7 % and 66.8 % (see Table 6.19). The recovery rates were relatively low, and, in addition, the quantification of the blank sample (negative BAS without spiking, subjected to the same treatment) revealed detectable levels, suggesting the presence of some matrix effect. Given the unknown concentration of AIPs in BAS,

it was unclear whether this methodology could achieve the required sensitivity. Thus, alternative approaches AIP detection in BAS were were investigated.

6.5.2.7 Affinity purification: funcionalized magnetic particles (mAb23-MPs)

Due to the interferences caused by organic solvents in the ELISA and the relatively low recovery rates, an alternative strategy was tested: the extraction of AIPs using immunoaffinity techniques. Initially, the purification strategy was approached using Invitrogen™ Dynabeads™ MyOne™ Tosylactivated magnetic beads. These beads are pre-activated with tosyl groups (-$CH_3C_6H_4SO_2$) on their surface, which are highly reactive for the amine groups present in proteins. When an antibody is added to the activated beads, the tosyl groups react with the antibody's amine groups, forming stable amide bonds. This covalent bond securely attaches the antibody to the surface of the beads. Once functionalized, the beads are coated with the antibody, enabling specific binding of the target analyte when introduced into a sample. Then, as illustrated in Figure 6.30, the target analyte can be easily isolated using a magnet.

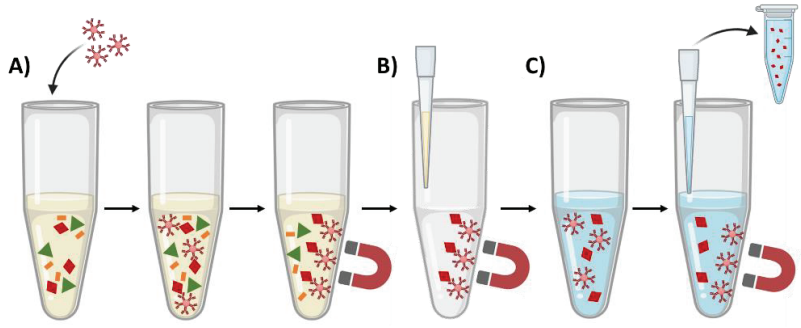

Figure 6.30. *Steps of affinity purification using antibody-functionalized magnetic particles. The figure illustrates the main steps involved in the process: A) Sample loading, where the target analyte binds specifically to the antibody immobilized on the magnetic particles; B) Washing, to remove unbound and non-specifically bound components; and C) Elution, where the analyte is released from the antibody using a dissociation buffer, while the magnetic particles are retained using a magnet. This process enables selective purification of the analyte from the sample.*

In this case, due to the higher prevalence of *S. aureus* strains from the *agr*-I group, the mAb23 (specific for AIP1o) was selected to functionalize the magnetic microparticles. The functionalization process achieved a coupling efficiency of 84.3 % (see Section 8.11.1.8, and the resulting functionalized particles were

named mAb23-MPs (refer to Figure 6.31 to see a simplified representation of the resulting particles).

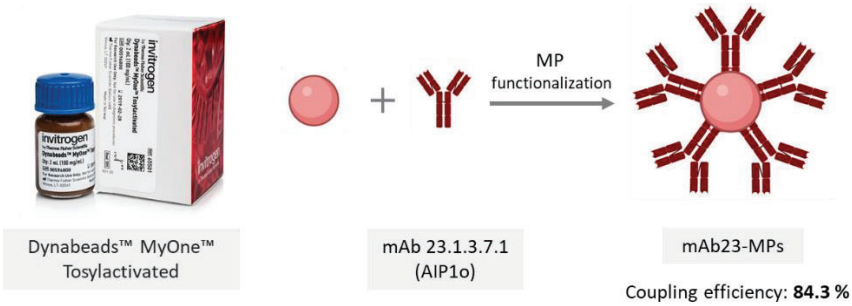

Figure 6.31. *Schematic representation of the functionalization process for mAb23-MPs. Magnetic microparticles were functionalized with the mAb23 antibody (specific for AIP1o) with a coupling efficiency of 84.3%.*

As in the case of the IAC, once the analyte is captured and the washes are completed, a dissociation buffer must be used to disrupt the antibody-antigen interaction and release the analyte from the magnetic particles (MPs), which remain bound to the magnet. This process allows the purified AIP to be recovered in the dissociation buffer.

To achieve this, an acidic dissociation buffer strategy was initially tested. A 0.1 M glycine buffer at pH 2.7 (Gly-HCl) was used. PBS samples spiked with 20, 100, and 200 nM of AIP1o were prepared, along with a blank sample (PBS without AIP1o). All samples were submitted to the extraction procedure with mAb23-MPs detailed in Section 8.11.1.8.

The results revealed that while quantification was not perfect, the recovery was reasonably good for a first attempt. However, despite optimizing the salt concentration and Tween levels in the extract and adjusting the pH to 7.5, interferences were observed in the ELISA. These interferences were evident since AIP1o was quantified in the blank sample, indicating the presence of non-specific signals, likely caused by residual glycine buffer or incomplete separation of MPs during the extraction process. Additionally, for the same spiked concentration of AIP1o, higher dilutions of the sample in PBST resulted in better recovery percentages, suggesting that dilution minimized the interferences affecting the ELISA (see Table 6.20). These results highlight the need for further optimization of the extraction process to eliminate interferences and improve quantification accuracy.

Table 6.20. *Results of AIP1o extraction from PBS spiked with mAb23-MPs using Gly-HCl as the dissociation buffer.*

Dissociation buffer	AIP1o spiked (nM)	AIP1o quantified (nM)	Dilution
Gly-HCl	Blank	12.65	No
		31.90	1/2
	20	15.52	No
		29.26	1/2
	100	78.49	1/2
		108.70	1/5
		144.24	1/10
	200	82.81	1/2
		136.09	1/5
		232.60	1/10
	+ Control 20	20.15	
	+ Control 10	15.81	
	Zero	13.62	

The buffer was used at a concentration of 0.1 M and pH 2.7. Interferences from the buffer were observed. The antibody concentration was set to 0.03 µg mL^{-1} (mAb23) and CA concentration to 0.6 µg mL^{-1} (AIP4S-BSA).

To address the interferences observed in the ELISA, a basic dissociation buffer was tested this time to evaluate whether it did not cause interferences. A 0.1 M citric acid buffer adjusted to pH 3 with NaOH (CA-NaOH) was selected. The extraction procedure was repeated with PBS spiked with 25 nM of AIP1o, using the two dissociation buffers in parallel: Gly-HCl and CA-NaOH. Additionally, a PBST blank was included, referring to a PBST sample without AIP1o that was submitted the entire extraction procedure with the MPs.

In this experiment, a significant underestimation was observed in the Gly-HCl extract, which was inconsistent with previous results. The PBST blank was not quantified, indicating that the MPs did not interfere with the ELISA. For the CA-NaOH extract, the recovery was 64.3 %. Moreover, in addition to low recovery rates, in both cases interferences persisted, as evidenced by the quantification of the zero control. This suggests that the dissociation buffers themselves interfered with the ELISA. Additionally, blank samples were also quantified, further confirming the presence of non-specific signals (see Table 6.21).

Table 6.21. *Results of AIP1o extraction from PBS spiked with mAb23-MPs using Gly-HCl or CA-NaOH as dissociation buffers.*

Buffer	Sample	[AIP1o] nM
PBST	Blank (MPs)	<LLOQ
	+ Control 25 nM	29.50
	Zero	1.36
Gly-HCl	25 nM (MPs)	<LLOQ
	Blank (MPs)	<LLOQ
	+ Control 25 nM	40.70
	Zero	20.74
CA-NaOH	25 nM (MPs)	16.09
	Blank (MPs)	5.36
	+ Control 25 nM	17.12
	Zero	5.86

Gly-HCl buffer was used at a concentration of 0.1 M and pH 2.7. CA-NaOH buffer was used at a concentration of 0.1 M and pH 3. Interferences from the buffers were observed. The antibody concentration was set to 0.03 µg mL^{-1} (mAb23) and CA concentration to 0.3 µg mL^{-1} (AIP4S-BSA).

The manipulation of the magnetic particles was an additional challenge. The separation of magnetic particles was performed using a magnetic rack in a 96-well plate format, which was designed by the Instituto de Microelectrónica de Barcelona (IMB-CNM, CSIC).

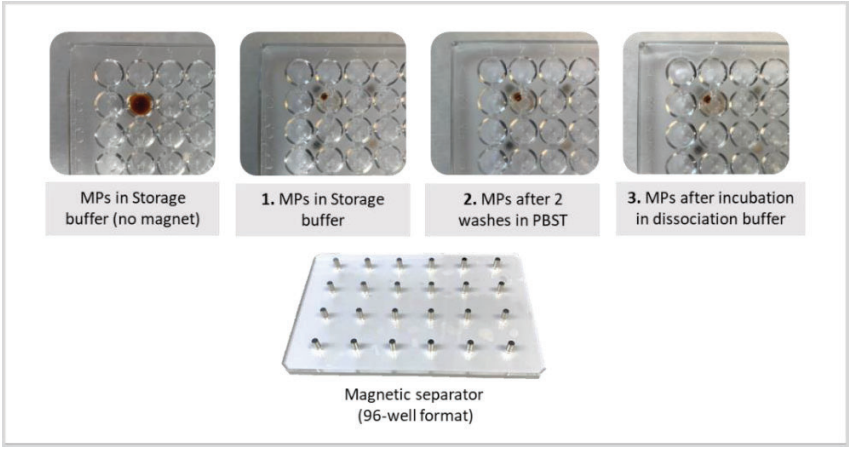

Figure 6.32. *Separation of magnetic particles (MPs) using a magnet. The figure illustrates the separation of MPs with the use of a 96-well plate format magnetic rack. The separation of MPs in steps 2 and 3 was not complete, potentially leading to interferences in the ELISA.*

However, ensuring their complete separation from the sample resulted quite difficult (see Figure 6.32). Given these difficulties and the lack of satisfactory results, another affinity-based purification approach was considered.

6.5.2.8 Affinity purification: immunoaffinity column (As381-IAC)

Since the purification strategy using mAb23-MPs did not yield satisfactory results, an alternative immunoaffinity approach was explored. This time, a HiTrap NHS-Activated HP 1 mL immunoaffinity column was functionalized with the As381 antibody, specific for AIP4o. The goal remained the same: to extract AIP4o from BAS samples to enable accurate quantification using ELISA.

The HiTrap NHS-Activated HP column is designed for covalently coupling ligands, such as antibodies, to the column matrix through their primary amines. The functionalization process involves the reaction between the N-hydroxysuccinimide (NHS) ester groups on the column and the primary amine groups present on the antibody (As381 in this case and previously purified). This reaction forms a stable amide bond, immobilizing the antibody on the column. The coupling efficiency of the antibody in the IAC was 80%, and the theoretical retention capacity was calculated to be 5.83 µg of AIP4o (see Section 8.11.1.7).

Once functionalized, the column is prepared for for immunoaffinity purification, which involves the following steps (see Figure 6.33):

1. **Loading the sample**: The sample containing the target analyte (AIP4o in this case) is loaded onto the column. As the sample passes through, the AIP4o binds to the immobilized antibodies due to their high specificity for the analyte.
2. **Washing steps**: Once the sample has passed through, washing steps are performed to remove non-specifically bound components. These washes ensure that only the target analyte remains bound to the column, improving the purity of the final elution.
3. **Elution of the analyte**: Finally, the analyte (AIP4o) is eluted from the column using an elution buffer that disrupts the antibody-antigen interaction. The eluted fraction contains the purified AIP4o, ready to be quantified using ELISA.

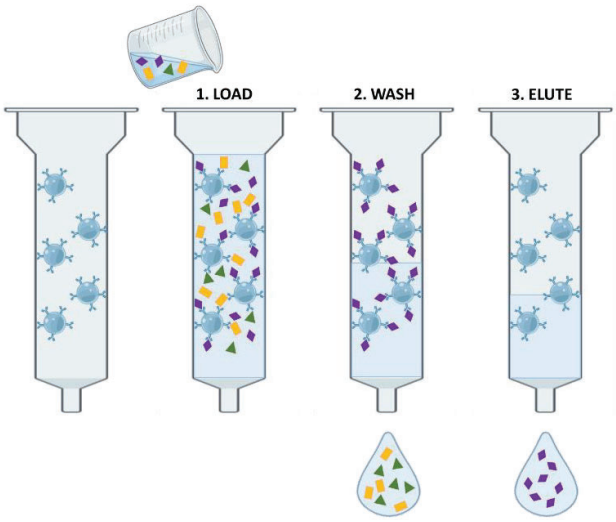

Figure 6.33. *Schematic representation of the steps involved in purification using an immunoaffinity column. The column contains immobilized antibodies on the stationary phase. 1) Load: The sample, containing the target analyte along with other components, is loaded onto the column. 2) Wash: The column is washed to remove undesired components and non-specific interactions. 3) Elute: The specifically bound analyte is eluted using a buffer that disrupts the antibody-antigen interaction, obtaining the purified analyte.*

A HiTrap 1 mL column was prepared by immobilizing the As381 antibody specific for AIP4o detection (see procedure in Section 8.11.1.7). Once the column was functionalized, the next step was to determine the most optimal elution buffer. Elution buffers are used in immunoaffinity purification to disrupt the specific interaction between the immobilized antibody and the target analyte, allowing the analyte to be released and collected. For AIP4o extraction, identifying the buffer that ensures efficient elution without degrading the analyte or antibody was critical to optimizing the purification process.

An interference study of the As381/AIP4S-BSA ELISA to various organic solvents was conducted to assess its tolerance. The solvents tested included methanol, ethanol, and acetonitrile. The results, shown in Figure 6.34, revealed that ethanol and methanol were the best tolerated solvents, with methanol performing slightly bette since, for similar IC_{50} values, a smaller decrease in A_{max} is observed (see Table 6.22). In both cases, while there was some loss in assay sensitivity, the ELISA was able to tolerate up to 5 % solvent in assay conditions, equivalent to 10 % in the sample as it is diluted 1/2 with antibody addition (in PBST).

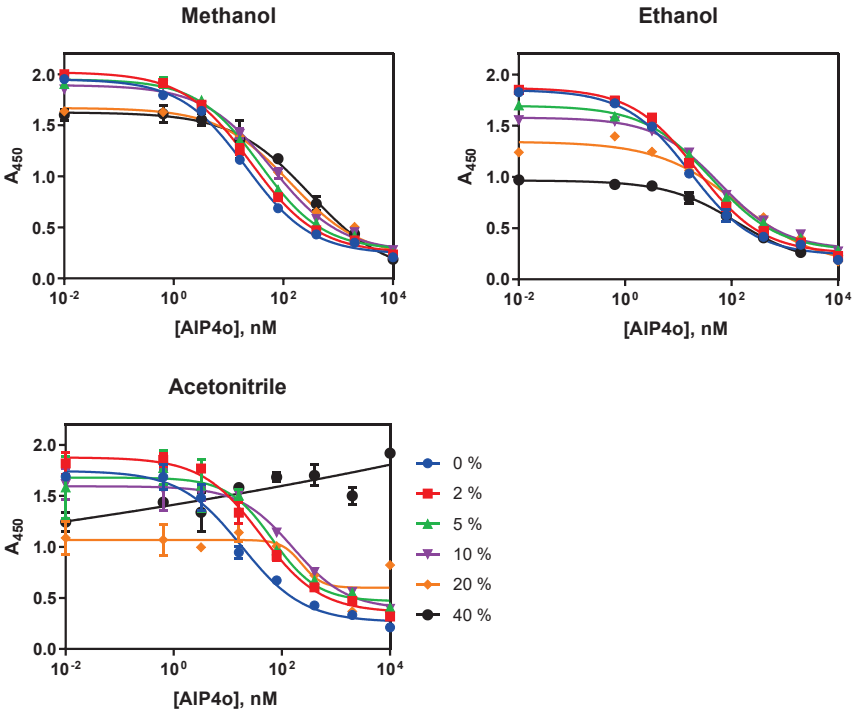

Figure 6.34. *Assessment of potential interferences caused by organic solvents in As381/AIP4S ELISA. Calibration curves were performed in PBST with increasing concentrations (0 %–40 %) of different organic solvents. Methanol is the most optimal eluent as the assay tolerales 5 % of this solvent, corresponding to 10 % in the sample, with slight loss of sensititity. The antibody dilution was set to 1/4000 (As381) and CA concentration to 0.078 µg mL^{-1} (AIP4S-BSA).*

Based on these findings, methanol was selected as the eluent in this procedure. The next step was to determine the optimal methanol concentration for eluting the analyte, ensuring that the analyte could be recovered in the smallest possible volume to maximize its concentration in the final purified sample.

To address this, 500 nM of AIP4o was loaded onto the IAC, and elution was performed using PBS with increasing percentages of MeOH: first 5 mL of PBS containing 20 % MeOH, followed by 5 mL of PBS containing 40 % MeOH. The elution profile results, shown in Figure 6.35, indicate that very little analyte was recovered at both 20 % and 40 % MeOH concentrations. Based on these findings, a higher concentration of MeOH, specifically 60 %, was tested.

Table 6.22. *Analytical parameters from the solvent tolerance study using the As381/AIP4S ELISA: A) Methanol, B) Ethanol, and C) Ethyl acetate.*

A) Methanol

Parameters	PBST	2 % MeOH	5 % MeOH	10 % MeOH	20 % MeOH	40 % MeOH
A_{min}	0.24	0.25	0.28	0.26	0.20	0.03
A_{max}	1.95	2.02	1.95	1.89	1.67	1.63
Slope	-0.73	-0.71	-0.75	-0.69	-0.66	-0.61
IC_{50} (nM)	20.70	25.49	37.67	62.69	134.40	302.80
R^2	0.997	0.998	0.996	0.995	0.991	0.985

B) Ethanol

Parameters	PBST	2 % EtOH	5 % EtOH	10 % EtOH	20 % EtOH	40 % EtOH
A_{min}	0.23	0.25	0.28	0.29	0.13	0.15
A_{max}	1.85	1.87	1.70	1.58	1.34	0.97
Slope	-0.71	-0.71	-0.68	-0.72	-0.57	-0.66
IC_{50} (nM)	16.80	22.85	41.77	60.43	137.80	127.30
R^2	0.996	0.997	0.997	0.994	0.970	0.992

C) Acetonitrile

Parameters	PBST	2 % ACN	5 % ACN	10 % ACN	20 % ACN	40 % ACN
A_{min}	0.26	0.36	0.47	0.39	0.60	~ 0,02655
A_{max}	1.75	1.88	1.68	1.59	1.07	~ 30,33
Slope	-0.76	-0.79	-1.04	-0.87	-2.31	~ 0,02852
IC_{50} (nM)	18.11	41.08	66.95	160.00	233.20	~ $1{,}829e^{46}$
R^2	0.984	0.988	0.941	0.973	0.702	0.643

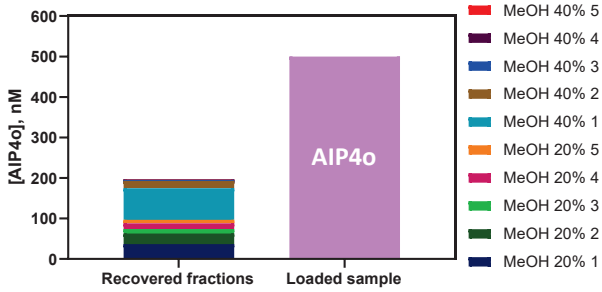

Figure 6.35. *Elution profile of AIP4o from the IAC using PBS with increasing percentages of MeOH: 20% and 40%. The results indicate low analyte recovery at both concentrations.*

As illustrated in Figure 6.36, using 60 % MeOH resulted in 100 % analyte recovery, with a slight overestimation. In view of these results, PBS containing 60 % MeOH

was identified as the optimal elution buffer, effectively eluting all the analyte retained in the column.

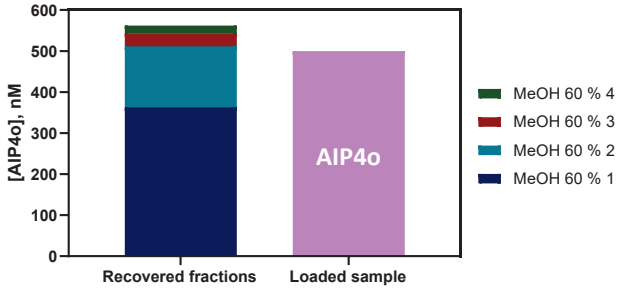

Figure 6.36. *Elution profile of AIP4o from the IAC using PBS with 60% MeOH. The results demonstrate 100 % analyte recovery with a slight overestimation.*

After extensive testing, a purification protocol was successfully established using the immunoaffinity column functionalized with immobilized As381 (As381-IAC) for the effective purification of AIP4. The elution profile of the column was characterized using PBS spiked with AIP4c and AIP4o.

First, the column was conditioned with PBS containing 60 % methanol (PBS 60 % MeOH) to remove any residual AIP4 or impurities that may have been retained. The column was then rinsed with PBS to eliminate methanol residues. Subsequently, 1 mL of PBS spiked with 500 nM AIP4c was loaded onto the column, which corresponds to 10 % of its theoretical binding capacity (see Section 8.11.1.7 for details on how it as calculated). The column was washed with PBS to remove non-specifically bound components, followed by elution with 4 mL of the eluent (PBS 60 % MeOH). The target analyte, AIP4o, is expected to be recovered in these four fractions. Afterwards, PBS with 90 % MeOH was applied to completely clean the column, followed by reconditioning with PBS to prepare it for a second round of purification.

In the second round, 1 mL of PBS spiked with 500 nM AIP4o was loaded onto the column and the same procedure was repited. All eluted fractions (1 mL each) were collected throughout the process and diluted to a final concentration of 10 % MeOH, the maximum solvent concentration tolerated by the ELISA.

Finally, all fractions were analyzed using two ELISAs to detect AIP4: As380/AIP4S-BSA (for AIP4c) and As381/AIP4S-BSA (for AIP4o). Quantification was performed

using calibration curves prepared with 10 % MeOH to mimic the same conditions as the eluted fractions.

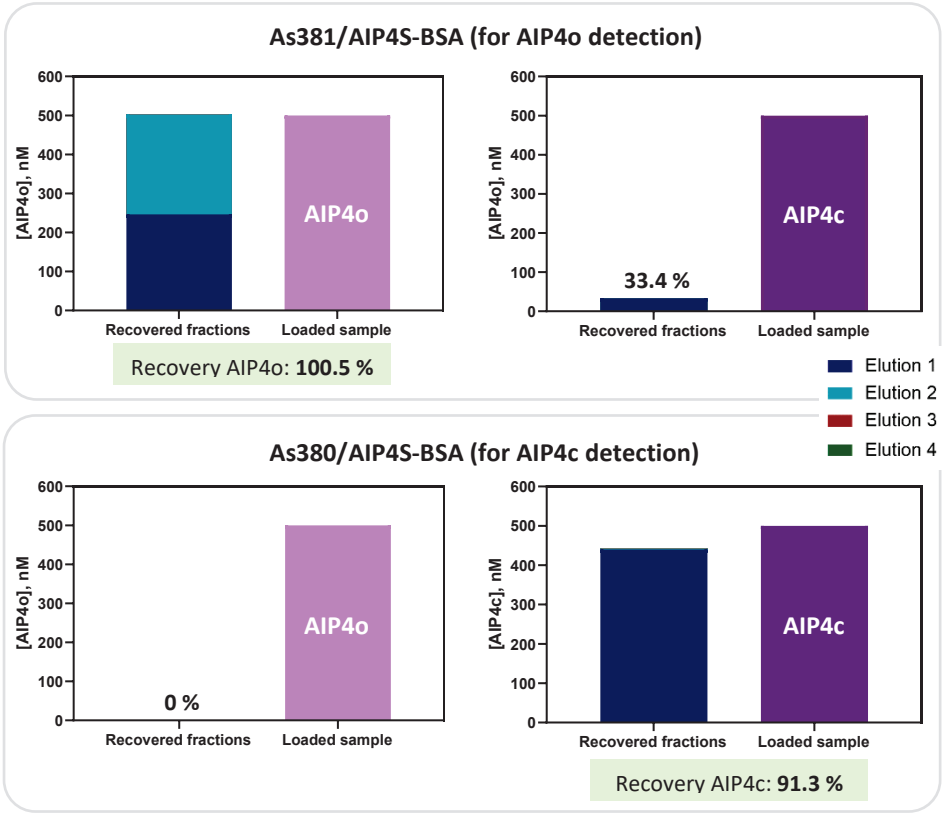

Figure 6.37. *Purification performance of As381-IAC for AIP4. The As381-IAC column achieved a 100.5 % recovery of spiked AIP4o in just two fractions (1 mL each), minimizing sample dilution. For AIP4c, a recovery of 91.28 % was observed, indicating that the column retains both closed and linear forms of AIP4. For As380/AIP4S-BSA ELISA, the antibody dilution was set to 1/4000 and CA concentration to 0.625 µg mL^{-1}. For As381/AIP4S-BSA ELISA, the antibody dilution was set to 1/24000 and CA concentration to 0.25 µg mL^{-1}.*

As shown in Figure 6.37, the As381-IAC successfully purified the entire AIP4o content spiked in the sample, achieving a recovery of 100.5 %. Furthermore, all the analyte was recovered in just two fractions, minimizing sample dilution. This is particularly important for AIPs, as their concentration in clinical respiratory samples is unknown. The ability to purify AIPs at the highest possible concentration is a key advantage for detecting even small amounts of these analytes. When the eluates were quantified for AIP4c using the As381/AIP4S-BSA ELISA, only 33.40 nM of AIP4c was detected. This can be explained by the 2 % CR of this ELISA with AIP4c.

However, results from the sample spiked with AIP4c were unexpected. While the As380/AIP4S-BSA ELISA in an indirect competitive format was highly specific for detecting AIP4c with no CR with AIP4o, quantification of the eluates suggested the opposite. When measuring AIP4c eluates, the recovery was 91.28 %, indicating that in this format, the column is not specific for AIP4o but instead retains both AIP4 in its closed and linear forms. Importantly, the specificity of the ELISA was confirmed, as the eluted AIP4o was not detected with this assay, demonstrating that the quantified AIP4c was indeed the analyte retained. One explanation for this behaviour remains on the fact that the AIP4c is recognized in a non-competitive format, being able that the antibody specific AIP4o also recognize the AIP4o. Working in a competitive format is more restric and enhance the biorecognition for the AIP4o. The fact that the antibody increases the cross-reactivity profile in a non-competitive format is well-known within the scientific community and proven in our research group[32].

Given these highly promising results, the next step was to purify spiked BAS samples containing AIP4, which was the ultimate goal of this technique. Due to the high viscosity of BAS, which makes it difficult to handle, the samples needed to be pretreated before loading onto IAC to prevent obstruction. To achieve this, the samples were treated with DTBA (dithiobutylamine) 5 mM, a reducing agent similar to DTT but with enhanced performance. Its chemical structure is shown in Figure 6.38. DTBA acts more rapidly than DTT, homogenizing and liquefying the sample within just 5 minutes, making it easier to manipulate.

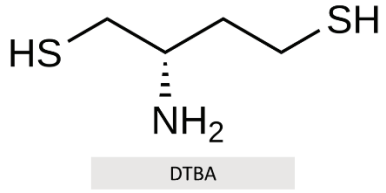

Figure 6.38. *Chemical structure of DTBA. DTBA (dithiobutylamine) is the selected reducing agent for the pretreatment of respiratory samples. It contains two thiol groups and acts more rapidly than DTT, making it highly effective for reducing sample viscosity.*

After treatment, the samples were spiked with 500 nM AIP4o, and the same purification protocol described previously was performed. With this methodology, there is no concern regarding potential interferences caused by the reducing agent (in this case, DTBA) in the ELISA, as a thorough clean-up of the treated sample is performed. Through successive washes, it is ensured that

only the AIP remains retained in the IAC, effectively removing any potential matrix effects from the sample or interferences from the treatment.

Unfortunately, unlike in PBS, purification in BAS was not successful, with only 13 % of the analyte being recovered. Given this result, it was hypothesized that larger molecules in the BAS might obstruct the retention of AIP4o on the column. To address this, the sample was filtered using 0.22 µm and 0.45 µm filters before loading onto the IAC. However, filtration did not solve the problem. Recovery was even lower, with only 3.6 % recovery for the 0.22 µm filter and 7.2 % recovery for the 0.45 µm filter. These results led to the exploration of an alternative affinity-based purification method that did not involve the use of columns.

6.5.2.9 Affinity purification: immunoaffinity spin columns (mAb23-ISCs)

Due to the promising results and consistency of the IAC purification strategy, it was decided to test a similar approach to address the challenges encountered. As previously discussed, the primary issue with the IAC was the inability to recover AIPs when processing BAS samples. Additionally, IACs are labor-intensive and time-consuming, requiring elution at a flow rate of 1 mL/min.

To overcome these limitations, a new strategy was adopted using smaller-volume immunoaffinity columns designed for purification through centrifugation. Specifically, Pierce™ NHS-Activated Agarose Spin Columns were employed. Similar to the IACs, these spin columns have an NHS-activated agarose resin, allowing the covalent coupling of the antibody, in this case, mAb23.

As represented in Figure 6.39, the functionalization occurs by a reaction between the NHS groups on the resin and the primary amines present on the antibody, forming stable amide bonds that immobilize the antibody onto the resin. As outlined in Section 8.11.1.9, the conjugation yield of the antibody in the ISCs was 100 %, and the theoretical binding capacity of the column was estimated to be 20 nmol of AIP1o.

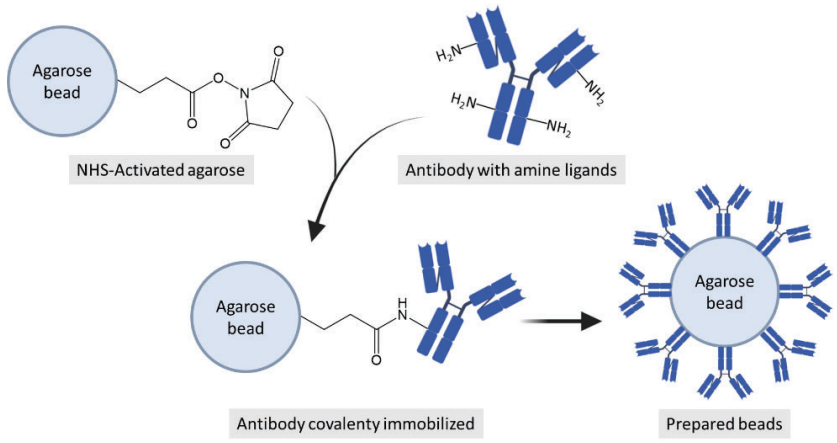

Figure 6.39. *Antibody coupling to NHS-Activated Agarose Spin Columns. The agarose beads in the column are functionalized with NHS-activated groups. Upon adding the antibody, these groups react with the primary amines on the antibody, forming a covalent bond that immobilizes the antibody onto the beads. This results in antibody-coupled beads, ready to be used in affinity purification.*

By reducing the column volume and utilizing centrifugal force instead of pressure from a syringe, this approach is expected to prevent obstruction when processing BAS samples. Centrifugation may help the entire sample to pass through the column, allowing the AIPs to bind to the immobilized antibody.

From a practical point of view, this method offers significant advantages for potential implementation in clinical laboratories. It is user-friendly, greatly reduces processing time, and requires a smaller sample volume, which is particularly important given that the volume of BAS is often quite limited.

Two columns were prepared, referred to as mAb23 immunoaffinity spin columns (mAb23-ISCs) 1 and 2, to evaluate the effectiveness of this new approach. Once the columns were prepared and characterized, AIP1o extraction with PBS containing 60 % of methanol was tested. This eluent was selected as it yielded the best results in the case of the As381-IAC. However, in the case of the mAb23-ISCs, it proved ineffective, as no analyte was recovered.

Before considering a new eluent, it was decided to test whether a higher percentage of methanol could achieve a satisfactory recovery rate for AIP1o. PBS containing 90 % methanol (PBS 90 % MeOH) was tested. As shown in *Table 6.23*, this methanol concentration proved effective, achieving 100 % recovery of the analyte loaded onto the ISC, with a slight overestimation.

Table 6.23. *Quantification results of AIP1o recovered by mAb23-ISC#1 from a spiked PBS sample using PBS 90 % MeOH as eluent.*

Elution fraction	AIP1o recovered (nM)	AIP1o recovered (nmol)
1	224.81	0.09
2	336.96	0.13

Recovery: **112.5 %**

The sample was spiked with 500 nM of AIP1o, equivalent to 0.1 nmol. The table shows the amount of AIP1o quantified in the first two elution factions, with a total recovery of 112.5 %. In the rest on the fractions, no analyte was detected.

Ultimately, PBS 90 % MeOH was chosen as the elution buffer. Since the ELISA tolerates up to 10 % methanol in the sample, all eluted fractions were diluted 1/9 after elution to remain at the same percentage and avoid interferences in the ELISA.

Table 6.24. *Quantification results of AIP1o recovered by mAb23-ISC#1 from a spiked PBS sample.*

Sample	AIP1o (nM)	
Load	<LLOQ	
Wash 1	<LLOQ	
Wash 2	<LLOQ	
Elution 1	202.84	→ 0.04 nmol
Elution 2	126.01	→ 0.03 nmol
Elution 3	114.38	→ 0.02 nmol
Elution 4	<LLOQ	
Elution 5	<LLOQ	
Conditioning 1	<LLOQ	
Conditioning 2	<LLOQ	
Conditioning 3	<LLOQ	
+Control 30 nM	33.69	
Zero PBST	<LLOQ	

Recovery: **88.6 %**

The sample was spiked with 500 nM of AIP1o, equivalent to 0.1 nmol. The table shows the amount of AIP1o quantified in all collected fractions, with a total recovery of 88.6 %.

In a first trial, 200 µL of PBS spiked with 0.1 nmol of AIP1o (corresponding to the retention volume of the column) were used. The protocol began with a conditioning step using PBS 90 % MeOH, followed by PBS. The spiked sample (PBS, 0.1 nmol AIP1o) was then loaded onto the column and incubated for 30 minutes in end-to-end rotation to promote binding. After binding, the column was washed with PBS and then eluted with PBS 90 % MeOH, incubating the sample with the eluent in the same manner as during the binding step. A more

detailed description of the procedure can be found in Figure 8.4 from Section 8.11.1.9.

Finally, the collected fractions were analyzed using the mAb23/AIP4S-BSA ELISA. A total of three fractions were required to elute AIP1o, achieving a recovery of 88.6 % (refer to Table 6.24).

In a second experiment, both columns (mAb23-ISC #1 and #2) were tested in parallel to evaluate their respective performance. For each column, two samples spiked with different amounts of AIP1o (0.1 nmol and 0.2 nmol) were processed.

Table 6.25. *AIP1o quantification and recovery by mAb23-ISCs #1 and #2 from PBS spiked at two concentrations.*

mAb23-ISC	AIP1o spiked	AIP1o recovered (nM)	AIP1o recovered (nmol)	Recovery %
1	1000 nM (0.2 nmol)	848.39	0.17	84.8
2	1000 nM (0.2 nmol)	826.53	0.17	82.7

For each ISC, the table presents the quantified AIP1o in elution fractions at spiked concentration of 1 µM. The results are expressed in both concentration and absolute amounts, along with the recovery percentages. The antibody concentration was set to 0.016 µg mL^{-1} (mAb23) and CA concentration to 0.7 µg mL^{-1} (AIP4S-BSA; HD=4).

Figure 6.40. *Appearance of BAS2 before and after DTBA treatment. Classified as a purulent phenotype sample, the BAS2 showed high viscosity. After treatment, a homogeneous non-sticky sample was obtained.*

Table 6.25 shows that both mAb23-ISC#1 and mAb23-ISC#1 performed well for the spiked concentration, with recovery rates of 114.3 % for ISC#1 and 82.7 % for ISC #2. Given the ability of the columns to efficiently purify AIP1o with high recovery percentages, the next step was to test the extraction from BAS samples

spiked with AIP1o. Blank BAS samples (negative for *S. aureus*) were processed using the same protocol as for the IAC (see Section 8.11.1.3), with treatment using DTBA. The first sample tested was BAS2, a purulent-type BAS (see Figure 6.40), spiked with 0.1 nmol of AIP1o. As visualized in Table 6.26, the recovery was successful, with 82.7 % of the analyte recovered in the eluted fractions, reporting for the first time AIP detection in respiratory clinical samples.

Table 6.26. *Quantification results of AIP1o in fractions collected during the purification process by mAb23-ISCs of spiked BAS2.*

Sample	AIP1o (nM)	AIP1o (nmol)	
Load	16.31	0.003	
Wash 1	26.09	0.01	
Wash 2	22.26	0.004	
Elution 1	189.00	0.04	Recovery: **88.6 %**
Elution 2	224.48	0.04	
Elution 3	<LLOQ	<LLOQ	
Conditioning 1	19.00	0.004	
Conditioning 2	<LLOQ	<LLOQ	
Conditioning 3	<LLOQ	<LLOQ	

The BAS2 sample was spiked with 500 nM of AIP1o (equivalent to 0.1 nmol). The recovery from the elution fractions was 82.7 %. The antibody concentration was set to 0.016 µg mL-1 (mAb23) and CA concentration to 0.7 µg mL-1 (AIP4S-BSA; HD=4).

To further validate these findings, a second BAS sample, BAS5 (purulent-bloody phenotype, negative for *S. aureus*), was processed (see Figure 6.41). BAS5 was splitten into two fractions, one spiked with 0.1 nmol and the other with 0.05 nmol of AIP1o. The aim was to verify consistency with the BAS2 recovery for the same spiked concentration and to evaluate the ability of this methodology to efficiently purify smaller amounts of AIP1o, refining the sensitivity of the technique given the unknown AIP concentration in patient BAS samples with *S. aureus* respiratory infections.

This time, the results were again successful, with 79.3 % recovery for the 0.1 nmol spiked sample, consistent with previous results in PBS and BAS2. Additionally, for the 0.05 nmol sample, the recovery was even higher at 91 %. The results are presented in Table 6.27.

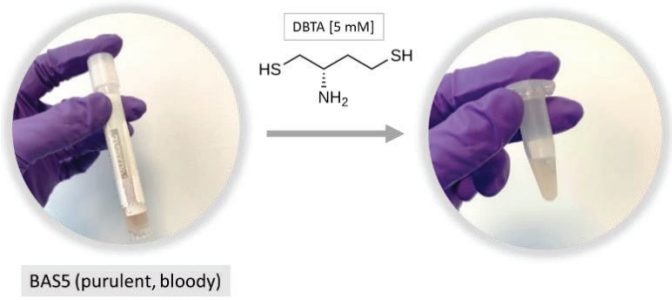

Figure 6.41. *Appearance of BAS5 (purulent-bloody type) before and after treatment with DTBA [5 mM]. The treatment reduces viscosity in 5 minutes, making the sample homogeneous and easy to handle.*

Table 6.27. *AIP1o quantification and recovery by mAb23-ISCs from BAS5 spiked at two concentrations.*

AIP1o spiked	AIP1o recovered (nM)	AIP1o recovered (nmol)	Recovery %
500 nM (0.1 nmol)	396.39	0.08	79.28
250 nM (0.05 nmol)	227.57	0.05	91.03

The table presents the quantified AIP1o in elution fractions at spiked concentrations of 500 nM and 250 nM. The results are expressed in both concentration and absolute amounts, along with the recovery percentages. The antibody concentration was set to 0.016 µg mL^{-1} (mAb23) and CA concentration to 0.7 µg mL^{-1} (AIP4S-BSA; HD=4).

BAS5 was processed again, this time spiked with 0.025 nmol of AIP1o. For mAb23-ISC#2 the results were successful once more, with 80.5 % recovery of the analyte. However, mAb23-ISC#1 showed high overestimation, possibly due to uneluted AIP1o or remaining BAS from previous experiments (refer to Table 6.28). This indicated that the columns must be properly conditioned before use, employing a high percentage of organic solvent to wash away any residual analyte or sample that may remain bound. Finally, to confirm that the recovered analyte was indeed AIP1o and not due to matrix effects or interferences from the BAS sample or treatment, BAS5 without spiking was processed in both columns in parallel.

Table 6.28. *AIP1o quantification and recovery by mAb23-ISCs #1 and #2 from BAS5 spiked.*

mAb23-ISC	AIP1o spiked	AIP1o recovered (nM)	AIP1o recovered (nmol)	Recovery %
1	150 nM (0.025 nmol)	363.87	0.07	242.58
2	150 nM (0.025 nmol)	120.81	0.02	80.54

For each ISC, the table presents the quantified AIP1o in elution fractions at spiked concentration of 150 nM. The results are expressed in both concentration and absolute amounts, along with the recovery percentages. The antibody concentration was set to 0.008 µg mL-1 (mAb23) and CA concentration to 0.7 µg mL-1 (AIP4S-BSA; HD=4).

Table 6.29. *Evaluation of the clinical specificity of mAb23-ISCs #1 and #2 in negative BAS (BAS5).*

mAb23-ISC	Sample	AIP1o recovered (nM)	AIP1o recovered (nmol)
1	Conditioning 1	697.89	0.14
	Conditioning 2	531.50	0.11
	Conditioning 3	<LLOQ	<LLOQ
	Conditioning 4	<LLOQ	<LLOQ
	Conditioning 5	<LLOQ	<LLOQ
	Elution 1	<LLOQ	<LLOQ
	Elution 2	<LLOQ	<LLOQ
	Elution 3	<LLOQ	<LLOQ
2	Conditioning 1	563.84	0.11
	Conditioning 2	553.80	0.11
	Conditioning 3	<LLOQ	<LLOQ
	Conditioning 4	<LLOQ	<LLOQ
	Conditioning 5	<LLOQ	<LLOQ
	Elution 1	530.40	0.11
	Elution 2	<LLOQ	<LLOQ
	Elution 3	<LLOQ	<LLOQ

The figure shows the performance of the spin columns in identifying negative samples, ensuring no cross-reactivity or non-specific binding when processing BAS. The samples tested was BAS5, non-spiked with AIP1o. The antibody concentration was set to 0.008 µg mL^{-1} (mAb23) and CA concentration to 0.7 µg mL^{-1} (AIP4S-BSA; HD=4).

As shown in Table 6.29, mAb23-ISC#1 did not quantify any AIP1o in the eluted fractions, confirming the absence of interferences or matrix effects and that the recoveries in previous assays corresponded to the spiked AIP1o. In contrast, mAb23-ISC#2 detected 0.11 nmol of AIP1o in one of the eluted fractions. This column was subjected to several washes with PBS 90 % MeOH to ensure that any

remaining AIP1o was completely eluted, guaranteering reliable quantification of the following BAS to be processed.

Based on the results obtained, we can conclude that this approach is highly effective, significantly minimizing matrix interferences and enhancing the reliability of AIP1o detection in complex BAS samples. Therefore, a pilot clinical validation study was conducted, measuring BAS samples from patients with lower respiratory tract infections caused by *S. aureus*.

6.5.3 CLINICAL VALIDATION OF AIP1O EXTRACTION IN POSITIVE BAS SAMPLES

To conduct this study, three samples provided by the IGTP were analyzed. These samples were obtained from intubated patients in the ICU, two of which were BAS samples (BAS218 and BAS221), and one was a bronchoalveolar lavage (BAL221). All samples tested positive for *S. aureus* in bacterial culture. Additionally, the *S. aureus* strains were isolated and characterized through genome sequencing, confirming their classification as *agr-I* group, which ensures the production of AIP1. The purification of positive samples was carried out using the latest technique developed, based on the extraction of AIPs with immunoaffinity spin columns.

First, a bronchoalveolar lavage (BAL) sample was analyzed. BAL is a fluid sample collected from the lower respiratory tract by washing the bronchi and alveoli with saline solution, typically via bronchoscopy. BAL samples are more liquid and homogeneous compared to BAS, making them easier to manipulate. As a result, this sample was not treated with DTBA, as such pretreatment was unnecessary.

The extraction results revealed that the AIP1o content in BAL221 was relatively low (0.02 nmol). Since no reference values exist for comparison, it is unclear whether this concentration is within the expected range. However, as BAL is a diluted sample, it was hypothesized that AIP concentrations would be lower compared to BAS samples. To verify this result, the same BAL sample was processed again, quantifying slightly higher but still low AIP1o concentrations this time (0.04 nmol, equivalent to 210.79 nM). The quantification results in BAL sample are displayed in Figure 6.42.

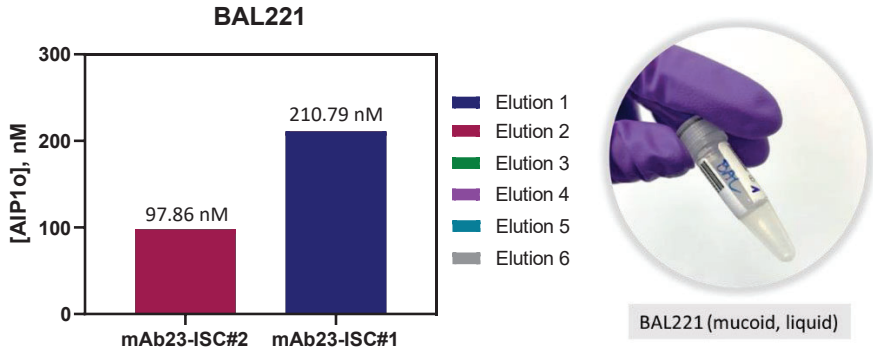

Figure 6.42. *Quantification results of AIP1o in BAL221. The figure shows the AIP1o levels extracted fromvBAL221 on two different days, using a different column each day (mAb23-ISC #1 or #2). The sample, being homogeneous and liquid, was not treated with DTBA. Low levels of AIP1o were quantified, eluted the first two fractions. The antibody concentration was set to 0.008 µg mL^{-1} (mAb23) and CA concentration to 0.7 µg mL^{-1} (AIP4S-BSA; HD=4).*

To test this hypothesis, BAS221 sample (bloody phenotype, highly viscous and difficult to handle) was analyzed next (see Figure 6.43). This sample was pretreated with DTBA before extraction with the mAb23-ISC. The extracted AIP1o content was much higher, at 0.42 nmol (equivalent to 2.1 µM), supporting the hypothesis that AIP concentrations in BAS are higher than in BAL. Furthermore, all collected fractions were analyzed and no analyte was detected in the pre-elution fractions. This confirmed that the column was properly washed, with no residual sample or non-specifically bound material, ensuring that the eluted fractions contained only the specific target, AIP1o.

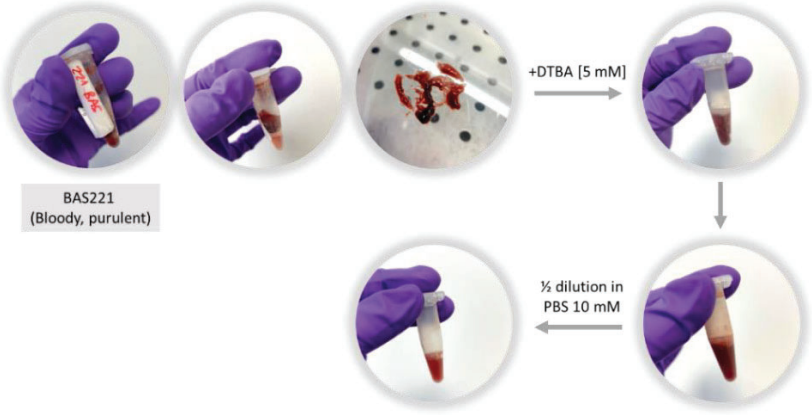

Figure 6.43. *Pretreatment of BAS221 with DTBA. BAS221 was classified as bloody and purulent, being highly viscous and difficult to handle. It was treated with DTBA (5 mM) for 5 minutes with vortexing and then diluted 1/2 in 10 mM PBS. This process successfully disaggregated the mucus, resulting in a homogeneous solution.*

To confirm the reproducibility of the technique, a second extraction of BAS221 was performed. The results (see Figure 6.44) were consistent with the first extraction, recovering 0.42 nmol of AIP1o form the sample (equivalent to 2.42 µM). While the results appear reliable, validating the technique with the reference technique for AIP detection, mass spectrometry, would be of great interest to fully validate the developed method.

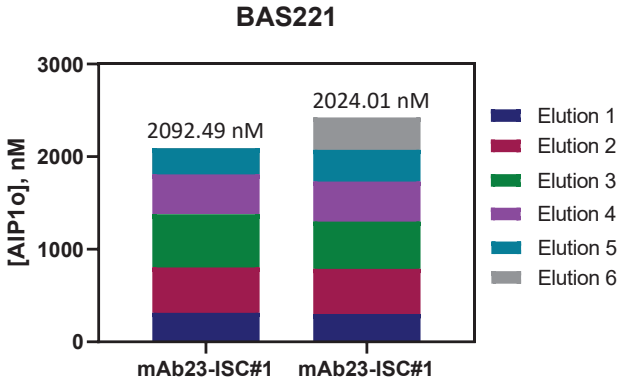

Figure 6.44. *Quantification results of AIP1o in BAS221. The figure shows the AIP1o levels extracted from BAS221 on two different days, using the same column both days to check reproducibility (mAb23-ISC#1). The sample, being highly viscous and containing blood, was pre-treated with DTBA. Comparing to BAL, high levels of AIP1o were quantified in all or almost all eluted fractions. The antibody concentration was set to 0.008 µg mL^{-1} (mAb23) and CA concentration to 0.7 µg mL^{-1} (AIP4S-BSA; HD=4).*

Next, the BAS218, classified as mucopurulent (a completely different phenotype), was analyzed (see its appearance in Figure 6.45). The extracted AIP1o amount was very similar to BAS SA221, with 0.40 nmol (equivalent to 1.99 µM) being recovered (refer to Figure 6.46).

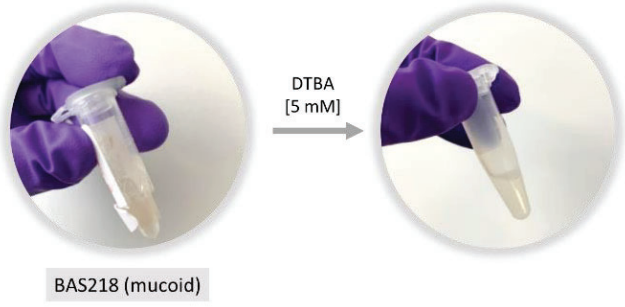

Figure 6.45. *Appearance of BAS218 before and after treatment with DTBA. BAS218, classified as a mucoid phenotype and less viscous, becomes completely liquid and homogeneous after treatment with DTBA.*

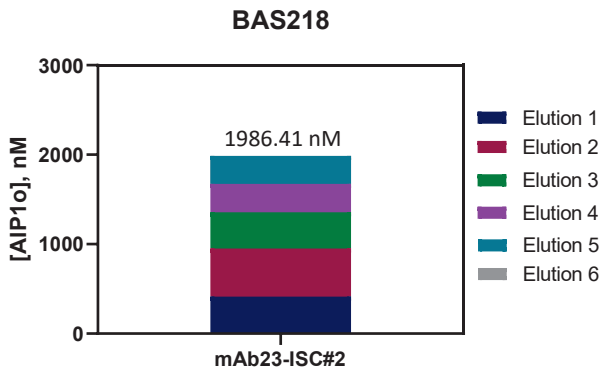

***Figure 6.46**. Quantification results of AIP1o in BAS218. The figure shows the AIP1o levels extracted form BAS218 using the mAb23-ISC#2. The sample, being classified as mucoid, was pre-treated with DTBA. High levels of AIP1o were quantified, very similar to those detected in BAS221. The antibody concentration was set to 0.008 µg mL^{-1} (mAb23) and CA concentration to 0.7 µg mL^{-1} (AIP4S-BSA; HD=4).*

In short, the pilot clinical validation study yielded promising results, despite the limited number of samples analyzed. The results of the AIP1 quantification in clinical samples are summarized in Table 6.30. Future steps will focus on conducting a more comprehensive clinical validation study, incorporating a larger set of clinical samples to further confirm the robustness and reliability of the developed technique.

***Table 6.30.** Summary of AIP1o quantification results in clinical lower respiratory tract samples (BAS/BAL).*

Sample	mAb23-ISC	AIP1o recovered (nM)	AIP1o recovered (nmol)
BAL221	2	97.86	0.02
	1	210.79	0.04
BAS221	1	2092.49	0.42
	1	2424.01	0.42
BAS218	2	1986.41	0.4

The table presents the results obtained using the extraction method based on mAb23-ISCs.

6.6 CHAPTER CONTRIBUTIONS

- Immunoaffinity-based approaches (IACs, MPs and ISCs) are introduced as innovative techniques for the detection of *S. aureus* AIPs in complex biological samples, such as BAS.

- Different protocols for processing of challenging matrices like BAS are described.

- Spin columns (ISCs) are proposed as a practical and efficient alternative to traditional immunoaffinity columns to be implemented in clinical settings; offering reduced time, smaller sample volumes, and simplified operation.

- The effectiveness of the developed methods in extracting and quantifying AIPs, both in spiked PBS samples and in complex clinical respiratory matrices, is provided.

- The capacity for AIP detection of the developed methodology in clinical samples is demonstrated through a pilot study involving BAS and BAL from patients with *S. aureus* respiratory infections, and AIP levels in these samples are reported for the first time.

6.7 BIBLIOGRAPHY

1. Tong, S. Y.; Davis, J. S.; Eichenberger, E.; Holland, T. L.; Fowler, V. G., Jr., Staphylococcus aureus infections: epidemiology, pathophysiology, clinical manifestations, and management. *Clin Microbiol Rev* **2015,** *28* (3), 603-61.
2. Liu, G. Y., Molecular Pathogenesis of Staphylococcus aureus Infection. *Pediatric Research* **2009,** *65* (7), 71-77.
3. Wertheim, H. F. L.; Melles, D. C.; Vos, M. C.; van Leeuwen, W.; van Belkum, A.; Verbrugh, H. A.; Nouwen, J. L., The role of nasal carriage in Staphylococcus aureus infections. *The Lancet Infectious Diseases* **2005,** *5* (12), 751-762.
4. Duhaniuc, A.; Păduraru, D.; Nastase, E. V.; Trofin, F.; Iancu, L. S.; Sima, C. M.; Dorneanu, O. S., Multidrug-Resistant Bacteria in Immunocompromised Patients. *Pharmaceuticals (Basel)* **2024,** *17* (9).
5. Verkaik, N. J.; de Vogel, C. P.; Boelens, H. A.; Grumann, D.; Hoogenboezem, T.; Vink, C.; Hooijkaas, H.; Foster, T. J.; Verbrugh, H. A.; van Belkum, A.; van Wamel, W. J., Anti-staphylococcal humoral immune response in persistent nasal carriers and noncarriers of Staphylococcus aureus. *J Infect Dis* **2009,** *199* (5), 625-32.

6. Sakr, A.; Brégeon, F.; Mège, J. L.; Rolain, J. M.; Blin, O., Staphylococcus aureus Nasal Colonization: An Update on Mechanisms, Epidemiology, Risk Factors, and Subsequent Infections. *Front Microbiol* **2018,** *9*, 2419.
7. Kumpitsch, C.; Koskinen, K.; Schöpf, V.; Moissl-Eichinger, C., The microbiome of the upper respiratory tract in health and disease. *BMC Biology* **2019,** *17* (1), 87.
8. Li, J.; Jing, Q.; Li, J.; Hua, M.; Di, L.; Song, C.; Huang, Y.; Wang, J.; Chen, C.; Wu, A. R., Assessment of microbiota in the gut and upper respiratory tract associated with SARS-CoV-2 infection. *Microbiome* **2023,** *11* (1), 38.
9. Péré, H.; Podglajen, I.; Wack, M.; Flamarion, E.; Mirault, T.; Goudot, G.; Hauw-Berlemont, C.; Le, L.; Caudron, E.; Carrabin, S.; Rodary, J.; Ribeyre, T.; Bélec, L.; Veyer, D., Nasal Swab Sampling for SARS-CoV-2: a Convenient Alternative in Times of Nasopharyngeal Swab Shortage. *J Clin Microbiol* **2020,** *58* (6).
10. Worrall, G.; Hutchinson, J.; Sherman, G.; Griffiths, J., Diagnosing streptococcal sore throat in adults: randomized controlled trial of in-office aids. *Can Fam Physician* **2007,** *53* (4), 666-71.
11. Frayha, H.; Castriciano, S.; Mahony, J.; Chernesky, M., Nasopharyngeal swabs and nasopharyngeal aspirates equally effective for the diagnosis of viral respiratory disease in hospitalized children. *J Clin Microbiol* **1989,** *27* (6), 1387-9.
12. Wang, R.; Braughton, K. R.; Kretschmer, D.; Bach, T. H.; Queck, S. Y.; Li, M.; Kennedy, A. D.; Dorward, D. W.; Klebanoff, S. J.; Peschel, A.; DeLeo, F. R.; Otto, M., Identification of novel cytolytic peptides as key virulence determinants for community-associated MRSA. *Nat Med* **2007,** *13* (12), 1510-4.
13. Gillet, Y.; Issartel, B.; Vanhems, P.; Fournet, J. C.; Lina, G.; Bes, M.; Vandenesch, F.; Piémont, Y.; Brousse, N.; Floret, D.; Etienne, J., Association between Staphylococcus aureus strains carrying gene for Panton-Valentine leukocidin and highly lethal necrotising pneumonia in young immunocompetent patients. *Lancet* **2002,** *359* (9308), 753-9.
14. Labandeira-Rey, M.; Couzon, F.; Boisset, S.; Brown, E. L.; Bes, M.; Benito, Y.; Barbu, E. M.; Vazquez, V.; Höök, M.; Etienne, J.; Vandenesch, F.; Bowden, M. G., Staphylococcus aureus Panton-Valentine leukocidin causes necrotizing pneumonia. *Science* **2007,** *315* (5815), 1130-3.
15. Vardakas, K. Z.; Matthaiou, D. K.; Falagas, M. E., Incidence, characteristics and outcomes of patients with severe community acquired-MRSA pneumonia. *Eur Respir J* **2009,** *34* (5), 1148-58.
16. Ghanem, R.; Roquefort, P.; Ramel, S.; Laurent, V.; Haute, T.; Le Gall, T.; Aubry, T.; Montier, T., Apparent Yield Stress of Sputum as a Relevant Biomarker in Cystic Fibrosis. *Cells* **2021,** *10* (11).
17. Meldrum, O. W.; Chotirmall, S. H., Mucus, Microbiomes and Pulmonary Disease. *Biomedicines* **2021,** *9* (6), 675.
18. Henke, M. O.; Ratjen, F., Mucolytics in cystic fibrosis. *Paediatric Respiratory Reviews* **2007,** *8* (1), 24-29.
19. Storey, S.; Wald, G., Novel agents in cystic fibrosis. *Nature Reviews Drug Discovery* **2008,** *7* (7), 555-556.
20. Murray, M. P.; Pentland, J. L.; Turnbull, K.; MacQuarrie, S.; Hill, A. T., Sputum colour: a useful clinical tool in non-cystic fibrosis bronchiectasis. *European Respiratory Journal 34* (2), 361-364.
21. Popova, G.; Boskovska, K.; Arnaudova-Danevska, I.; Smilevska-Spasova, O.; Jakovska, T., Sputum Quality Assessment Regarding Sputum Culture for Diagnosing Lower Respiratory Tract Infections in Children. *Open Access Maced J Med Sci* **2019,** *7* (12), 1926-1930.
22. Yuan Liang, L. X., Clinical sputum specimen liquefaction treatment method. **2020**.
23. Yu, F.; Qiu, T.; Zeng, Y.; Wang, Y.; Zheng, S.; Chen, X.; Chen, Y., Comparative Evaluation of Three Preprocessing Methods for Extraction and Detection of Influenza A Virus Nucleic Acids from Sputum. *Front Med (Lausanne)* **2018,** *5*, 56.

24. Peng, J.; Lu, Y.; Song, J.; Vallance, B. A.; Jacobson, K.; Yu, H. B.; Sun, Z., Direct Clinical Evidence Recommending the Use of Proteinase K or Dithiothreitol to Pretreat Sputum for Detection of SARS-CoV-2. *Front Med (Lausanne)* **2020,** *7*, 549860.
25. Guéroult, M.; Picot, D.; Abi-Ghanem, J.; Hartmann, B.; Baaden, M., How Cations Can Assist DNase I in DNA Binding and Hydrolysis. *PLOS Computational Biology* **2010,** *6* (11), e1001000.
26. Zitter, J. N.; Maldjian, P.; Brimacombe, M.; Fennelly, K. P., Inhaled Dornase alfa (Pulmozyme) as a noninvasive treatment of atelectasis in mechanically ventilated patients. *Journal of Critical Care* **2013,** *28* (2), 218.e1-218.e7.
27. Sadowska, A. M.; Manuel-y-Keenoy, B.; De Backer, W. A., Antioxidant and anti-inflammatory efficacy of NAC in the treatment of COPD: Discordant in vitro and in vivo dose-effects: A review. *Pulmonary Pharmacology & Therapeutics* **2007,** *20* (1), 9-22.
28. Guerini, M.; Condrò, G.; Friuli, V.; Maggi, L.; Perugini, P., N-acetylcysteine (NAC) and Its Role in Clinical Practice Management of Cystic Fibrosis (CF): A Review. *Pharmaceuticals* **2022,** *15* (2), 217.
29. Saraswathy Veena, V.; Sara George, P.; Jayasree, K.; Sujathan, K., Comparative analysis of cell morphology in sputum samples homogenized with dithiothreitol, N-acetyl-L cysteine, Cytorich(®) red preservative and in cellblock preparations to enhance the sensitivity of sputum cytology for the diagnosis of lung cancer. *Diagn Cytopathol* **2015,** *43* (7), 551-8.
30. Clemente, A.; Alba-Patiño, A.; Rojo-Molinero, E.; Russell, S. M.; Borges, M.; Oliver, A.; de la Rica, R., Rapid Detection of Pseudomonas aeruginosa Biofilms via Enzymatic Liquefaction of Respiratory Samples. *ACS Sensors* **2020,** *5* (12), 3956-3963.
31. Ma, X.; Deng, D.; Chen, W., Inhibitors and Activators of SOD, GSH-Px, and CAT. *Enzyme inhibitors and activators* **2017,** *29*, 207-224.
32. Salvador, J. P.; Sánchez-Baeza, F.; Marco, M. P., A high-throughput screening (HTS) immunochemical method for the analysis of stanozolol metabolites in cattle urine samples. *J Chromatogr B Analyt Technol Biomed Life Sci* **2010,** *878* (2), 243-52.

7 CONCLUSIONS

1. The present PhD thesis represents a significant advance in the study of *Staphylococcus aureus* QS molecules. It reports for the first time an innovative diagnostic strategy capable of accurate, reproducible and robust detection and quantification of four existing AIP variants, corresponding to the different *agr S. aureus* genotypes. The methodologies developed herein are much faster and more straightforward than any of the techniques available for this purpose.

- *Antibodies and microplate-based ELISAs have been developed that can detect S. aureus AIPs in the low nM range (IC_{50} values in buffer: 20.41 nM for AIP1o; 2.70 nM for AIP2o; 6.54 nM for AIP3c; and 2.19 nM for AIP3o) in just 1.30h.*

2. To our knowledge, this study reports for the first time the detection of the linear forms of the AIPs from *S. aureus* in biological samples. Hence, the analytical techniques developed in this work allow identification and quantification of these linear AIPs in culture media where clinical isolates had been grown. The presence of such hydrolysed forms has never been reported before, but their detection could open new avenues on the investigation of the *S. aureus* QS and have significant impact for developing new diagnostic and/or therapeutic strategies targeting *S. aureus* communication pathways.

3. Despite the stability studies performed previously by other members of the research team indicated that thiolactones exhibit a certain degree of stability in neutral or slightly basic media over time, our studies have demonstrated that the thiolactone ring is probably hydrolized under physiological conditions. Hence immunization of mice and rabbits with bioconjugates prepared with the cyclic AIPs predominantly generate antibodies against their linear form. Efforts invested addressed to isolate hybridoma cell clones producing monoclonal antibodies recognizing the AIP cyclic forms were unsuccessful.

4. Studies conducted in *S. aureus* clinical and reference isolates have further demonstrated that measuring the linear forms of AIPs is a most effective strategy to detect this pathogen. Despite the cyclic peptides have been identified as the active autoinducers, our studies have shown, that under the bacterial culture conditions employed, a significant proportion of AIPs are in their linear form. Since, conversion of the cyclic peptides into the linear forms can be accomplished introducing a short hydrolysis step, the quantification of these linear peptides confers enhanced sensitivity to the technologies here reported

allowing for more accurate and timely detection of QS signalling molecules in *S. aureus.*

5. Although the number of clinical isolates that have been measured in this research work is limited, preliminary results indicate that the immunochemical methodologies here developed can accurately classify *S. aureus agr* strains with a specificity exceeding 75 %.

6. With the immunochemical technologies here reported it has been possible to quantify for the first time AIPs in complex low tract respiratory samples without prior culture. Notably, AIP concentrations of approximately 2 µM have been detected in bronchial aspirate samples (BAS). This represents the first time that quantitative data on AIP concentrations in such clinical specimens is reported.

To conclude, this work demostrates significant progress in the detection, quantification, and understanding of *S. aureus* AIPs. The technologies developed represent a step forward in sensitivity, speed, and scalability compared to traditional techniques, such as mass spectrometry. These findings suggest that implementing these methodologies in clinical settings could revolutionize the diagnosis and management of *S. aureus* infections, providing valuable tools for studying QS dynamics, phenotyping strains, and informing clinical decisions. Future research should focus on expanding the clinical validation, particularly to correlate AIP levels with patient outcomes and validating the results obtained with a reference technique such as mass spectrometry, which would provide definitive confirmation of accuracy.

8 MATERIALS & METHODS

8.1 CHEMICALS AND BIOCHEMICALS

All chemical substances and proteins used were purchased from Sigma-Aldrich except **Goat Anti-Mouse-IgG-HRP** (Ref. P0447; from Agilent Dako in Glostrup, Denmark and Carpinteria, California, USA).

AIP haptens and analytes were synthesized by the "Multivalent Systems for Nanomedicine" group at IQAC-CSIC. The stock solutions of AIPs 1-4 used as standards were prepared in DMSO at 10 mM and stored at -20°C. TSB broth (Sigma Aldrich) was prepared by dissolving 30 g of MH powder in 1 L of deionized water, following the manufacturer's instructions. The resulting liquid medium was then autoclaved at 121°C for 15 minutes.

8.2 EQUIPMENT

The pH and conductivity of all buffers and solutions were measured using a pH-meter pH 540 GLP and a conductimeter LF 340 (WTW, Weilheim, Germany) respectively. Polystyrene microtiter plates (Maxisorp, Roskilde, Denmark) were employed for the ELISAs, while dilution plates were procured from Nirco (Barberà del Vallés, Spain). Washing steps were conducted using a Biotek ELx465 (Biotek Inc.). Absorbances were recorded at 450 nm using a Thermo Scientific MultiSkan GO (Thermo Fisher Scientific, Waltham, MA, USA) in single wavelength mode. Competitive curves were analyzed using a four-parameter logistic equation in GraphPad Prism 7.0 software (GraphPad Software Inc., San Diego, CA, USA) according to the formula: $y = B(A-B)/[1 - (x/C)D]$, where A represents the maximum absorbance, B the minimum absorbance, C the concentration producing 50% of the maximal absorbance, and D the slope at the inflection point of the sigmoid curve. Unless stated otherwise, presented data represent the average of at least two well replicates. The matrix-assisted laser desorption ionization time-of-flight mass spectrometer (MALDI-TOF-MS) utilized for hapten density (HD) calculation of bioconjugates was a Bruker autoflex III Smartbeam spectrometer (Billerica, Massachusetts). The autoclave is the Presoclave II 75 from Selecta and the centrifuge is the 5810 R from Eppendorf.

8.3 BUFFERS

Phosphate buffer saline (PBS): 10 mM phosphate buffer and 0.8 % saline solution (pH 7.5). **Coating buffer:** 50 mM bicarbonate-carbonate buffer (pH 9.6). **PBST:** PBS with 0.05 % Tween 20 (pH 7.5). **Citrate buffer:** 40 mM sodium citrate solution (pH 5.5). **TMB solution:** 0.01 % of 3,3',5,5'- tetramethylbenzidine (TMB) and 0.004 % H_2O_2 prepared in citrate buffer. **Borate buffer:** 0.2 M sodium borate/boric acid (pH 9.7).

8.4 PREPARATION OF OF BIOCONJUGATES

8.4.1 AIPS-HAPTEN BIOCONJUGATION

Thiolactone hapten bioconjugates (AIP4S-BSA and AIP4S-HCH). A solution of each AIPS-hapten (2.82 mg AIP1S, 2.63 mg AIP2S, 2.47 mg AIP3S and 1.56 mg AIP4S) in anhydrous DMF (0.1 mL) was added dropwise over the protein solutions (BSA or KLH, 2.5 mg mL-1, 2 mL in PBS 10mM buffer). The mixtures were left stirring 4h at RT and the bioconjugates were subsequently purified by dialysis against 0.5 mM PBS (5 x 5 L) and Milli-Q water (1 x 5L), and stored freeze dried at -80 ºC. A small fraction (20 µL) of each AIPS-BSA conjugates was kept for MALDI-TOF analysis, resulting in HDs of 13 (AIP1S), 9 (AIP2S), 9 (AIP3S) and 5 (AIP4S) per molecule of BSA.

8.4.2 AIPL-HAPTEN BIOCONJUGATION

The haptens used in this study were AIPL-PEG(2)-NH_2, which consist of the AIPL moiety linked to a spacer arm composed of two polyethylene glycol (PEG) units and terminated with an amino group (NH_2). The conjugation was carried out using dimethyl pimelimidate dihydrochloride (DMP·2HCl) as a crosslinker. A solution of DMP·2HCl was prepared by dissolving 3.92 mg of the reagent in 1.5 mL of borate buffer (pH 9.7). Separately, a solution of each hapten was prepared: 3.4 mg of hapten AIP1o and 2.97 mg of hapten AIP3o were dissolved in 600 µL of a 1:1 mixture of acetonitrile (ACN) and water (H_2O). The DMP solution was added

to the hapten solutions on an ice bath with gentle stirring to initiate the activation reaction.

In parallel, carrier protein solutions were prepared. For each hapten, a solution of 2 mg of keyhole limpet hemocyanin (KLH) was prepared by mixing 1515 µL of concentrated KLH stock with 1485 µL of borate buffer. Similarly, two solutions of 17.25 mg of bovine serum albumin (BSA) were prepared by dissolving the protein in 4.5 mL of borate buffer. The activated hapten-DMP mixture was then added dropwise to the BSA and KLH solutions, which were stirred during the addition. The reaction mixtures were gently stirred (280 rpm) for 4 hours, followed by overnight incubation at 4°C to complete the conjugation.

The resulting hapten-protein conjugates were stored at 4°C for further use in downstream applications. A small fraction (20 µL) of each AIPL-BSA conjugates was kept for MALDI-TOF analysis, resulting in HDs of 8 (AIP1L) and 4 (AIP3L) per molecule of BSA.

8.5 MALDI-TOF MS ANALYSIS AND HD CALCULATION

Hapten densities of the conjugates were calculated by MALDI-TOF-MS by comparing the molecular weight recorded on the MALDI spectra of the native proteins to that of the BSA-AIP bioconjugates. For this purpose, the bioconjugates were combined with a freshly prepared matrix (trans-3,5-dimethoxy-4-hydroxycinnamic acid, 10 mg mL^{-1} in 70:30 ACN/H_2O with 0.1 % HCOOH) following the 'sandwich' sample preparation method. The bioconjugate aliquot was diluted by half using ACN with 0.2 % HCOOH. Subsequently, 2 µL of the matrix was applied to the MALDI plate and dried, followed by the addition of the bioconjugate solution (2 µL, 2 to 5 mg mL^{-1} in 1:1 ACN/H_2O, 0.1 % HCOOH), allowed to dry again, and finally, 2 µL of the matrix solution was added over again. The resulting dried spot underwent analysis by MALDI-TOF-MS. Hapten densities were calculated through the equation: [MW(conjugate)-MW(native protein)]/[MW(hapten)-MW(lost atoms)].

8.6 AIP HYDROLISIS

8.6.1 STUDY OF AIP1 HYDROLYSIS KINETICS BY UPLC-TOF MS

A solution of ACN:H_2O (10:90) was spiked with 10 µM AIP1c, and hydrolysis was initiated by adding 20 µL of 5 N NaOH to 980 µL of the spiked sample. To stop the hydrolysis reaction, pH was neutralized to 7.5 by the addition of 5 N HCl. Samples were analyzed using Ultra-Performance Liquid Chromatography coupled with Time-of-Flight Mass Spectrometry (UPLC-ToF MS). A spiked sample containing AIP1o was used as a positive control to determine the retention time, while additional samples spiked with AIP1c were hydrolyzed for 5 and 15 minutes to assess hydrolysis kinetics. The mass range was set to detect ions with an m/z of 100-1500, enabling the identification of both AIP1o and its hydrolyzed product. The instrument was operated in both positive and negative ionization modes. Sample Injection: a fixed ratio of 70 % acetonitrile and 30 % water was used for 2 minutes to condition the system. Chromatographic Gradient: the elution gradient progressed from 10 % ACN to 100 % ACN in water over a span of 5 minutes, providing separation of AIP1 compounds based on their polarity. Samples were injected into the UPLC system and separated on a reverse-phase column optimized for small molecules. The retention times were recorded and compared with the positive control (AIP1o) to identify AIP1c and its hydrolyzed products. The data were processed to determine the peak intensities and retention times of each analyte, facilitating the evaluation of hydrolysis after 5 and 15 minutes.

8.6.2 HYDROLYSIS PROCEDURE TO TRANSFORM AIPS INTO LINEAR ANALYTES

For the hydrolysis of the AIPs, 2 µL of a 1 mM stock in DMSO was added to 48 µL of a 0.1 M NaOH solution. The solution was vortexed several times over 15 minutes, followed by 1/40 dilution in the corresponding buffer or solution. The concentration of the hydrolyzed stock is 10 mM.

8.6.3 CULTURE SAMPLE HYDROLYSIS FOR THE LINEARIZATION OF TOTAL AIP CONTENT

For the hydrolysis procedure, 980 µL of the supernatant form bacterial culture was mixed with 20 µL of 5 N NaOH and incubated for 15 minutes with vortexing. After hydrolysis, 110 µL of 100 mM PBST was added to the sample, and the pH was adjusted to 7.5 by adding 76 µL of 1 N HCl. Finally, the hydrolyzed sample was diluted 1/2 in 10 mM PBST.

8.7 ANTIBODY PRODUCTION

8.7.1 MONOCLONAL ANTIBODY PRODUCTION

BALB/c female mice (6-8 weeks old) and Winstar female rats (6 weeks old) were immunized with AIP1S-KLH and AIP3S-KLH, 4 rats and 4 mice in each case. The first dose consisted of 100 µg of conjugate injected intraperitoneally as an emulsion of PBS and complete Freund's adjuvant. In addition, 3 booster injections were given at 3-week intervals using the same dose of immunogen emulsified in incomplete Freund's adjuvant. Mice and rats selected as spleen donors for hybridoma production received a final injection of 100 µg of antigen in PBS 4 days prior to fusion.

P3-X63/Ag 8.653 murine myeloma cells (ATCC, Rockville, MD) were cultured in supplemented Dulbecco's Modified Eagle Medium (high-glucose DMEM with 2 mM alanylglutamine, 1 mM minimum nonessential amino acids, and 25 µg mL-1 gentamicin supplemented with 10% (v/v) fetal bovine serum (FBS)). Mouse spleen lymphocytes were fused with myeloma cells at a 4:1 ratio using PEG 1500 (Roche Applied Science, Mannheim, Germany) as a fusing agent. The fused cells were cultured in 96-well culture plates at a density of 2 x 105 cells/100 µl of 15 % FBS supplemented DMEM per well. After 24h, hypoxanthine-aminopterin-thymidine (HAT) selection medium (10% FBS supplemented DMEM with 100 µM hypoxathine, 0.4 µM aminopterine, 16 µM thymidine, 2% Hybridoma Fusion and Cloning Supplement (HFCS, Roche)) was added (100 µl well-1). Subsequently, 10 days after cell fusion, culture supernatants were screened by performing indirect ELISA assays, coating the corresponding plates with 1.0 µg mL-1 PC1-BSA

conjugate, in order to select the hybridomas that were able to recognize AIP1 and AIP3 with high affinity. The chosen hybridomas were then cloned four times by the limiting dilution method using HAT medium without aminopterine (HT) medium, supplemented with 15% FBS and 1% HFCS. Finally, stable antibody-producing clones were expanded and cryopreserved in liquid nitrogen and the resulting supernatants containing mAbs were purified by protein G affinity chromatography (HiTrap Protein G HP antibody purification columns, Cytiva). Hybridoma technology procedure for mAb production is detailed in Figure 8.1.

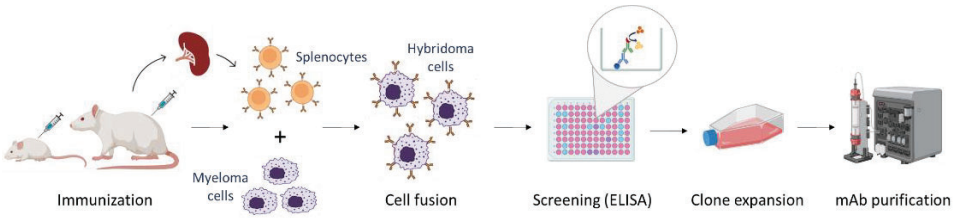

Figure 8.1. *Hybridoma technology for mAb production. Mice and rats were immunized using the correspondieng AIP-bioconjugates. Spleen lymphocytes (splenocytes) were fused with murine mieloma cells to obtain the corresponding hybridoma cells. Hybridomas were then cloned and a selection was made by ELISA screening. The selected clones were expanded and the productions were purified to obtain the produced mAbs.*

8.7.2 POLYCLONAL ANTIBODY PRODUCTION

Antibody production has been performed with the support of the Custom Antibody Service (CAbS, CIBER-BBN, IQAC-CSIC). Eight female New Zealand white rabbits weighing 1-2 kg were immunized with AIP1S-KLH (x2), AIP2S-KLH (x2), AIP1L-DMP-KLH (x2) and AIP3L-DMP-KLH (x2) following the established protocols in our research group. Immunizations were carried out in the animal facility of the Research and Development Center (CID) of the Spanish Research Council (CSIC) Registration Number: B9900083, employing approved procedures that avoid unnecessary treatments and minimize suffering of the animals. The protocol used in accordance with the institutional guidelines under a license from the local government (DAAM 7463) and approved by the Institutional Animal Care and Use Committee at the CID-CSIC. The antisera (As) obtained by immunization with the different haptens were named as follows: As415, As416 (AIP1S-KLH); As417, As418 (AIP2S-KLH); As428 (AIP1L-DMP-KLH) and As429, As430 (AIP3L-DMP-KLH). The animals were exsanguinated after 5-6 immunizations, and the final blood was collected in vacutainer tubes provided

with a serum separation gel. Antisera were obtained by centrifugation at 4°C for 10 min at 10 000 rpm, then stored at -80°C in the presence of preservative 0,02 % sodium azide. The antibody titer was assessed during the immunization process through non-competitive indirect ELISA. Microtiter plates were coated with a fixed concentration of the corresponding BSA conjugates (1 mg mL^{-1}) and the avidity of the produced antibodies was measured by preparing serial dilutions of the corresponding As.

8.8 PURIFICATION PROCEDURES

8.8.1 PURIFICATION OF CONJUGATES

The purification of conjugates was carried out through dialysis using Spectra/Por membranes sourced from Spectrumlabs (Piraeus, Greece, EU) with a molecular weight cut-off of 12-14 kDa. Alternatively, purification was conducted using ÄKTA Prime Plus equipment with two HiTrap desalting columns from GE Healthcare (Chicago, IL, USA).

8.8.2 PURIFICATION OF MONOCLONAL ANTIBODIES

Monoclonal antibodies (mAbs) were purified using HiTrap Protein G columns (Cytiva, Uppsala, Sweden). The purification procedure was carried out according to the manufacturer's instructions with minor modifications. The columns were equilibrated with binding buffer (10 mM PBS, pH 7.4), and the antibody-containing sample was loaded onto the column at a flow rate of 1 mL/min. After washing with binding buffer to remove unbound proteins, the antibodies were eluted with elution buffer (0.1 M glycine-HCl, pH 2.7) at a flow rate of 5 mL/min. Elution fractions of 1.8 mL were collected in tubes containing 200 µL of neutralization buffer (100 mM PBS, pH 7.5, with 5 % [v/v] NaOH 5N). The fractions corresponding to the elution peak, as determined by UV absorbance at 280 nm, were grouped. The pH of the resulting sample was adjusted to 7.4 using 1 N NaOH. The sample was then filtered through a 0.2 µm syringe filter with low protein binding (Millipore, Burlington, MA, USA) to ensure sterility and remove

particulates. The antibody concentration was determined by measuring the absorbance at 280 nm using a spectrophotometer. Finally, the purified antibodies were aliquoted and stored at -20°C until use.

8.9 ELISAS

8.9.1 SCREENING FOR BEST MAB CANDIDATE SELECTION

The ELISA was performed using 96-well microplates, which were coated with 0.5 µg mL^{-1} of the corresponding BSA bioconjugates. For monoclonal antibodies (mAbs) against AIP1, the wells were coated with AIP1S-BSA, while for mAbs against AIP3, AIP3S-BSA was used. Plates were incubated overnight at 4°C to allow efficient binding of the bioconjugates to the wells. After incubation, the plates were washed with 10 mM PBST using an automated plate washer to remove unbound material. For the assay, 50 µL of PBST was added to the wells in non-competitive assays, or 50 µL of competitor solution (AIPc or AIPo) at a concentration of 1 µM was added for competitive assays. Subsequently, 50 µL of the supernatants from the production of the selected monoclonal clones, previously diluted 1/100 in PBST, were added to the wells. The plates were incubated for 30 minutes at room temperature. Following incubation, the plates were washed. Then, 100 µL per well of goat anti-mouse IgG-HRP diluted 1/12,000 in PBST was added. The plates were incubated for another 30 minutes at room temperature. After washing the plates again to remove unbound secondary antibody, 100 µL per well of OPD substrate solution was added to initiate the colorimetric reaction. The reaction was allowed to develop for approximately 30 minutes at room temperature in the dark, monitoring visually for sufficient colour development. If the colour developed quickly, the reaction was stopped earlier. To stop the reaction, 50 µL per well of 4 N sulfuric acid (H_2SO_4) was added. The absorbance of each well was measured at 490 nm using a spectrophotometer.

8.9.2 NON-COMPETITIVE INDIRECT MONODIMENSIONAL TITRATION (1D ELISAS).

The ELISA plates with 96 wells each were coated with the different antigen combinations tested at a concentration of 1 $mg \cdot mL^{-1}$ in coating buffer. They were left overnight at 4°C. Subsequently, the plates were washed four times with 300 µL of PBST each. Then, 100 µL of anti-serum dilutions were added per well (seven 1/2 dilutions starting from 1/500 dilution for pABs or 2 $\mu g\ mL^{-1}$ concentration for mAbs, with the final dilution being PBST). After washing the plates, a solution of secondary antibody (goat anti-rabbit IgG-HRP 1/6000 in PBST for polyclonal antibodies and goat anti-mouse IgG-HRP 1/12,000 in PBST for monoclonal antibodies) was added (100 µL per well) and incubated for an additional 30 minutes at room temperature. The plates were washed again, and then 100 µL of substrate solution (TMB) was added to each well and left for 30 minutes at room temperature in the dark. The enzymatic reaction was stopped by adding 50 µL of 4 N H_2SO_4 solution to each well, and the absorbance was read at 450 nm.

8.9.3 NON-COMPETITIVE INDIRECT BIDIMENSIONAL TITRATION (2D ELISAS).

A microtiter plate was coated with varying concentrations of the corresponding coating antigen, ensuring that each row contained a different concentration (ranging from 10 $\mu g \cdot mL^{-1}$ to 10 $ng \cdot mL^{-1}$, and zero in coating buffer, 100 $\mu L \cdot well^{-1}$). The plate was left overnight at 4ºC. Subsequently, the plate was washed (4 x 300 µL, PBST), and different concentrations of antiserum were added (ranging from 1/100 to 1/6400, and zero in the assay buffer, 100 $\mu L \cdot well^{-1}$). The plate was incubated for 30 minutes at room temperature, followed by a washing step (4 x 300 µL, PBST). Next, 100 µL/well of goat anti-rabbit IgG-HRP (1/6000 in PBST) was added, and the plate was incubated for an additional 30 minutes at RT. Subsequently, the plate was washed (4 x 300 µL, PBST), and the substrate solution (100 µL/well) was added, incubating another 30 minutes at room temperature, shielded from light. The enzymatic reaction was stopped by adding 4M H_2SO_4 (50 µL·well-1), and the absorbance was finally read at 450 nm.

8.9.4 COMPETITIVE INDIRECT ELISAS

ELISA mAb23/AIP4S-BSA for the detection of AIP1o in buffer. Microtiter plates were coated with 0.4 µg mL^{-1} of AIP4S-BSA in coating buffer and left overnight at 4°C. The following day, the microtiter plate was washed four times with 300 µL of PBST. Then, 50 µL of a solution of AIP1o (AIP1 hydrolyzed) ranging from 10 µM to 0.64 nM in PBST were added to a 96-well plate. Subsequently, 50 µL of mAb23 at a concentration of 0.015 µg mL^{-1} in PBST were added over the analyte. The mixture was left for 30 minutes at room temperature. After another round of washing (4 x 300 µL, PBST), a solution of goat anti-mouse IgG-HRP (1/12,000 in PBST) was added and incubated for an additional 30 minutes at room temperature. Following this, another wash step (4 x 300 µL, PBST) was performed, and then 100 µL of substrate solution was added to each well and left for 30 minutes at room temperature in the dark. The enzymatic reaction was stopped by the addition of 50 µL of 4 N H_2SO_4 solution to each well, and the absorbance was measured at 450 nm.

ELISA As417/AIP2S-BSA for the detection of AIP2o in buffer. Microtiter plates were coated with 0.125 µg mL^{-1} of AIP2S-BSA in coating buffer and left overnight at 4°C. The same day, 75 µL of solutions of AIP2o (AIP2 hydrolyzed) ranging from 10 µM to 0.64 nM in PBST were added to a non-treated 96-well plate. Then, 75 µL of a 1/1500 dilution of As417 in PBST As420 were added over the analyte. The mixture was left overnight at 4°C. The following day, the microtiter plate was washed four times with 300 µL of PBST. Afterwards, 100 µL per well of the analyte/As mixture were added and left for 30 minutes at room temperature. After another round of washing (4 x 300 µL, PBST), a solution of goat anti-rabbit IgG-HRP (1/6,000 in PBST) was added and incubated for an additional 30 minutes at room temperature. Following this, another wash step (4 x 300 µL, PBST) was performed, and then 100 µL of substrate solution was added to each well and left for 30 minutes at room temperature in the dark. The enzymatic reaction was stopped by the addition of 50 µL of 4 N H_2SO_4 solution to each well, and the absorbance was measured at 450 nm.

ELISA mAb14/AIP3S-BSA for the detection of AIP3c in buffer. Microtiter plates were coated with 0.1 µg mL^{-1} of AIP4S-BSA in coating buffer and left overnight at 4°C. The following day, the microtiter plate was washed four times with 300 µL of PBST. Then, 50 µL of a solution of AIP3o (AIP3 hydrolyzed) ranging from 10 µM to 0.64 nM in PBST were added to a 96-well plate. Subsequently, 50 µL of

mAb14 at a concentration of 0.06 µg mL^{-1} in PBST were added over the analyte. The mixture was left for 30 minutes at room temperature. After another round of washing (4 x 300 µL, PBST), a solution of goat anti-mouse IgG-HRP (1/12,000 in PBST) was added and incubated for an additional 30 minutes at room temperature. Following this, another wash step (4 x 300 µL, PBST) was performed, and then 100 µL of substrate solution was added to each well and left for 30 minutes at room temperature in the dark. The enzymatic reaction was stopped by the addition of 50 µL of 4 N H_2SO_4 solution to each well, and the absorbance was measured at 450 nm.

ELISA As429/AIP3S-BSA for the detection of AIP3o in buffer. Microtiter plates were coated with 0.062 µg mL^{-1} of AIP2S-BSA in coating buffer and left overnight at 4°C. The following day, the microtiter plate was washed four times with 300 µL of PBST. Then, 50 µL of AIP3o (AIP3 hydrolyzed) ranging from 10 µM to 0.64 nM in PBST were added to a microtiter 96-well plate. Subsequently, 50 µL of a 1/16,000 dilution of As429 in PBST were added over the analyte. After another round of washing (4 x 300 µL, PBST), a solution of goat anti-rabbit IgG-HRP (1/6,000 in PBST) was added and incubated for an additional 30 minutes at room temperature. Following this, another wash step (4 x 300 µL, PBST) was performed, and then 100 µL of substrate solution was added to each well and left for 30 minutes at room temperature in the dark. The enzymatic reaction was stopped by the addition of 50 µL of 4 N H_2SO_4 solution to each well, and the absorbance was measured at 450 nm.

8.9.5 CROSS-REACTIVITY STUDIES

They were conducted for each of the optimized assays. Both the non-hydrolyzed and hydrolyzed forms of the AIPs were used as cross-reactants. A non-competitive indirect ELISA, as previously described, was performed by adding these molecules as analytes at concentrations ranging from 10 µM to 0.64 nM. The cross-reactivity (CR) was calculated using the formula: CR (%) = IC_{50}(Cross reactant)/IC_{50}(Analyte) x 100.

8.9.6 ACCURACY STUDIES

Calibration curves were generated following the procedure described for each indirect competitive ELISA. Blindly spiked samples with known concentrations of the analyte were quantified by interpolation on the calibration curve and the absorbance values were recorded for each concentration. These values were used to interpolate the concentrations of unknown samples based on the calibration curve, which was typically fitted using a four-parameter logistic regression model. A regression line was constructed to assess how closely the quantified values matched the known concentrations. The linearity of the regression was used to validate the assay's accuracy.

8.9.7 MATRIX EFFECT ASSAY*:*

The same procedure described in Section 8.9.4 for the indirect competitive ELISAs for AIP 1-4 detection in buffer was followed, but the analyte dilutions were prepared in PBST, sterile TSB and TSB diluted 1/2, 1/5, 1/10 and 1/20.

8.9.8 ACCURACY STUDIES IN TSB ½ AND TSB-H ½

The procedure described in Section 8.9.6 was followed, replacing PBST with TSB medium. For the accuracy study in TSB diluted 1/2, samples were blindly spiked with AIP1o or AIP2o in TSB and diluted 1/2. The calibration curve was prepared by serially diluting the analyte in TSB 1/2 and subsequently adding the corresponding primary antibody in PBST. For hydrolyzed TSB (TSB-h), samples were spiked in TSB, hydrolyzed as outlined in Section 8.6.2, and then diluted 1/2 in PBST. The calibration curve for hydrolyzed samples was prepared using TSB subjected to the same hydrolysis treatment. This was done by mixing 9.8 mL of TSB with 200 µL of 5 N NaOH, vortexing for 15 minutes, and then adding 1.1 mL of 100 mM PBST. The pH was adjusted to 7.5 by adding 153 µL of HCl 5N, and the mixture was diluted 1/2 in PBST 10mM.

8.9.9 AIP1 RECOVERY STUDIES FROM SPIKED TSB SAMPLES

Sterile TSB medium was spiked with AIP1c and AIP1o at three different concentrations (typically 40, 80, and 160 nM, although other concentrations were tested). For each spiked sample, one fraction was diluted 1/2 in PBST, while another fraction underwent the hydrolysis procedure as follows: 5 uL of 5N NaOH were added to 245 µL of the supernatant extracted from culture samples, vortexing for 15 minutes, and 27.8 µL of 100 mM PBST were added. Then, pH was adjusted to 7.5 by adding 22 µL of 1N HCl and the sample was diluted 1/2 in 10 mM PBST. In total, 12 spiked samples were analyzed in each assay: 3 samples spiked with AIP1c; 3 samples spiked with AIP1c and hydrolyzed; 3 samples spiked with AIP1o and 3 samples spiked with AIP1o and hydrolyzed. For analysis, two different calibration curves were used: one prepared in TSB diluted 1/2 and the other in hydrolyzed TSB diluted 1/2 (TSB-h 1/2). Non-hydrolyzed samples were quantified using the calibration curve in TSB 1/2, while hydrolyzed samples were quantified using the calibration curve in TSB-h 1/2.

8.9.10 INDIRECT COMPETITIVE ELISAS FOR AIP DETECTION IN CULTURE MEDIA

ELISA mAb23/AIP4S-BSA for the detection of AIP1o in TSB 1/2. Microtiter plates were coated with 0.4 µg mL^{-1} of AIP4S-BSA in coating buffer and left overnight at 4°C. The following day, the microtiter plate was washed four times with 300 µL of PBST. Then, 50 µL of a solution of AIP1o (AIP1 hydrolyzed) ranging from 10 µM to 0.64 nM in TSB 1/2 were added to a 96-well plate. Subsequently, 50 µL of mAb23 at a concentration of 0.03 µg mL^{-1} in PBST were added over the analyte. The mixture was left for 30 minutes at room temperature. After another round of washing (4 x 300 µL, PBST), a solution of goat anti-mouse IgG-HRP (1/12,000 in PBST) was added and incubated for an additional 30 minutes at room temperature. Following this, another wash step (4 x 300 µL, PBST) was performed, and then 100 µL of substrate solution was added to each well and left for 30 minutes at room temperature in the dark. The enzymatic reaction was stopped by the addition of 50 µL of 4 N H_2SO_4 solution to each well, and the absorbance was measured at 450 nm.

ELISA As418/AIP2L-DMP-BSA for the detection of AIP2o in TSB 1/2. Microtiter plates were coated with 0.125 µg mL^{-1} of AIP2S-BSA in coating buffer and left overnight at 4°C. The same day, 75 µL of solutions of AIP2o (AIP2 hydrolyzed) ranging from 10 µM to 0.64 nM in TSB 1/2 were added to a non-treated 96-well plate. Then, 75 µL of a 1/16,000 dilution of As418 in PBST As420 were added over the analyte. The mixture was left overnight at 4°C. The following day, the microtiter plate was washed four times with 300 µL of PBST. Afterwards, 100 µL per well of the analyte/As mixture were added and left for 30 minutes at room temperature. After another round of washing (4 x 300 µL, PBST), a solution of goat anti-rabbit IgG-HRP (1/6,000 in PBST) was added and incubated for an additional 30 minutes at room temperature. Following this, another wash step (4 x 300 µL, PBST) was performed, and then 100 µL of substrate solution was added to each well and left for 30 minutes at room temperature in the dark. The enzymatic reaction was stopped by the addition of 50 µL of 4 N H_2SO_4 solution to each well, and the absorbance was measured at 450 nm.

ELISA mAb14/AIP3S-BSA for the detection of AIP3c in TSB 1/2. Microtiter plates were coated with 0.1 µg mL^{-1} of AIP4S-BSA in coating buffer and left overnight at 4°C. The following day, the microtiter plate was washed four times with 300 µL of PBST. Then, 50 µL of a solution of AIP3o (AIP3 hydrolyzed) ranging from 10 µM to 0.64 nM in TSB 1/2 were added to a 96-well plate. Subsequently, 50 µL of mAb14 at a concentration of 0.06 µg mL^{-1} in PBST were added over the analyte. The mixture was left for 30 minutes at room temperature. After another round of washing (4 x 300 µL, PBST), a solution of goat anti-mouse IgG-HRP (1/12,000 in PBST) was added and incubated for an additional 30 minutes at room temperature. Following this, another wash step (4 x 300 µL, PBST) was performed, and then 100 µL of substrate solution was added to each well and left for 30 minutes at room temperature in the dark. The enzymatic reaction was stopped by the addition of 50 µL of 4 N H_2SO_4 solution to each well, and the absorbance was measured at 450 nm.

ELISA As429/AIP3S-BSA for the detection of AIP3o in TSB 1/2. Microtiter plates were coated with 0.08 µg mL^{-1} of AIP2S-BSA in coating buffer and left overnight at 4°C. The following day, the microtiter plate was washed four times with 300 µL of PBST. Then, 50 µL of AIP3o (AIP3 hydrolyzed) ranging from 10 µM to 0.64 nM in TSB 1/2 were added to a microtiter 96-well plate. Subsequently, 50 µL of a 1/16,000 dilution of As429 in PBST were added over the analyte. After another round of washing (4 x 300 µL, PBST), a solution of goat anti-rabbit IgG-HRP

(1/6,000 in PBST) was added and incubated for an additional 30 minutes at room temperature. Following this, another wash step (4 x 300 µL, PBST) was performed, and then 100 µL of substrate solution was added to each well and left for 30 minutes at room temperature in the dark. The enzymatic reaction was stopped by the addition of 50 µL of 4 N H_2SO_4 solution to each well, and the absorbance was measured at 450 nm.

ELISA As380/AIP4S-BSA for the detection of AIP4c in TSB 1/2. Microtiter plates were coated with 0.75 µg mL^{-1} of AIP2S-BSA in coating buffer and left overnight at 4°C. The following day, the microtiter plate was washed four times with 300 µL of PBST. Then, 50 µL of AIP4c ranging from 2 µM to 0.13 nM in TSB 1/2 were added to a microtiter 96-well plate. Subsequently, 50 µL of a 1/3,000 dilution of As380 in PBST were added over the analyte. After another round of washing (4 x 300 µL, PBST), a solution of goat anti-rabbit IgG-HRP (1/6,000 in PBST) was added and incubated for an additional 30 minutes at room temperature. Following this, another wash step (4 x 300 µL, PBST) was performed, and then 100 µL of substrate solution was added to each well and left for 30 minutes at room temperature in the dark. The enzymatic reaction was stopped by the addition of 50 µL of 4 N H_2SO_4 solution to each well, and the absorbance was measured at 450 nm.

ELISA As381/AIP4S-BSA for the detection of AIP4o in TSB 1/2. Microtiter plates were coated with 0.25 µg mL^{-1} of AIP4S-BSA in coating buffer and left overnight at 4°C. The same day, 75 µL of solutions of AIP4o (AIP4 hydrolyzed) ranging from 10 µM to 0.64 nM in TSB 1/2 were added to a non-treated 96-well plate. Then, 75 µL of a 1/8,000 dilution of As418 in PBST As381 were added over the analyte. The mixture was left overnight at 4°C. The following day, the microtiter plate was washed four times with 300 µL of PBST. Afterwards, 100 µL per well of the analyte/As mixture were added and left for 30 minutes at room temperature. After another round of washing (4 x 300 µL, PBST), a solution of goat anti-rabbit IgG-HRP (1/6,000 in PBST) was added and incubated for an additional 30 minutes at room temperature. Following this, another wash step (4 x 300 µL, PBST) was performed, and then 100 µL of substrate solution was added to each well and left for 30 minutes at room temperature in the dark. The enzymatic reaction was stopped by the addition of 50 µL of 4 N H_2SO_4 solution to each well, and the absorbance was measured at 450 nm.

8.10 BACTERIAL ISOLATES

Samples. Six clinical *S. aureus* isolates were retrospectively selected from a collection of strains in the Hospital Universitari Germans Trias i Pujol. Strains were isolated from respiratory specimens obtained from patients under mechanical ventilation admitted at the intensive care unit. Isolates were stored at -80°C in a maintenance freezing medium (Oxoid TP, 15731). Strains were identified as *S. aureus* by conventional assays (Gram staining, selective culture media, coagulase test) and antibiotic susceptibility testing. Strains were initially genotypically characterized by means of a DNA microarray (Clondiag) and further confirmed by genome sequencing. According to sequencing results, they were classified as *agr*-I (strains 6 and 197); *agr*-II (strain 3); *agr*-III (strain 32) and *agr*-IV (strains 48 and 165). Two *S. aureus* reference strains were also included, USA300 and Newman, both *agr*-I.

Bacterial growth curves. The bacterial isolates and two *S. aureus* reference strains (USA300 and Newman, both *agr*-I) were cultured overnight at 37ºC in TSB (5mL). The day after, dilutions 1/50 in fresh TSB were prepared and the optical density at 600 nm (OD600) measured. Then the resulting solutions were shaken at 37°C until the selected time of growth was completed. When the time was finished, aliquots were extracted for Colony Forming Units (CFUs) and OD600 measurement.

Supernatants for ELISA analysis. the aliquots extracted from different growth times were centrifuged 10 min at 3000 g and stored at -20°C for AIP concentration measurement using the corresponding ELISAs developed in this work (for AIP1, AIP2 and AIP3 detection) or previously developed in our group (AIP4 detection).

8.11 LOW TRACT RESPIRATORY SAMPLES (BAS/BAL)

Samples. Blank and positive BAS/BAL samples for *S. aureus* were selected by Dr. Alicia Lacoma from the Microbiology Department at Hospital Universitari Germans Trias i Pujol. Samples were obtained from intubated patients in the ICU. Blank samples were those with a negative culture for *S. aureus*. Positive samples

showed a positive culture for *S. aureus* and were genotyped by whole-genome sequencing. All samples were stored in cryovials and kept at -40°C until use.

8.11.1 TREATMENT STRATEGIES

8.11.1.1 Proteinase K

Each calibration point was prepared separately, starting at a concentration of 10 µM. For each point, 800 µL of sample was prepared. Four calibration curves were generated under different conditions: A) Samples were prepared in 10 mM PBST (pH 7.5) containing 5 mM $CaCl_2$. B) Identical to condition A but with an additional incubation step at 55°C for 4 hours with agitation at 750 rpm. C) Samples were prepared by mixing 400 µL of 10 mM PBST (pH 7.5) containing 10 mM $CaCl_2$ with 400 µL of proteinase K solution (stock at 1 mg/mL, Tritirachium album, Sigma Aldrich). The mixture was incubated under the same conditions as in B. D) Similar to condition C, but 8 µL of 100 mM PMSF (Penylmethanesulfonyl fluoride, Thermo Fisher) in isopropanol was added to reach a final concentration of 1 mM in the sample. The resulting solutions were analyzed immediately using ELISA.

8.11.1.2 DNase I

10 mg of BAS was weighed on a precision balance and 1 mL of a solution with 2 U mL^{-1} of DNase I (ThermoFisher, 90083) in buffer (10 mM PBS pH 7.5, 0.1 mM $CaCl_2$, 2.5 mM $MgCl_2$) were added. The reaction was incubated at 37°C for 15 minutes and then at room temperature stirring at 1000 rpm for 30 minutes. The resulting solution was centrifuged at 10000 xg for 20 minutes and the resulting supernatants were analyzed by ELISA.

8.11.1.3 Reducing agents

TCEP treatment. 10 mg of BAS was weighed on a precision balance, and 250 µL of the solution with 0.04 mM TCEP in 10 mM pH 7.5 PBST were added. The mixture was incubated for 30 minutes stirring vigorously (1200 rpm). Then, 750 µL of 10 mM pH 7.5 PBST were added and the resulting solution was directly analyzed by ELISA.

DTBA treatment (prior to immunoaffinity extraction). In a 1.5 mL Eppendorf tube, 150 µL of BAS were mixed with 150 µL of 10 mM DTBA (Dithiobutylamine) solution. The mixture was vortexed for 5 minutes to ensure thorough mixing and proper treatment. The treated sample was then ready for subsequent purification steps.

8.11.1.4 Combined treatment: DNase I + DTT

300 mg of BAS (approximately 400 µL) was weighed and mixed with 500 µL of PBS, followed by the addition of 100 µL of 10 times concentrated DNase buffer (10 mM PBS pH 7.5, 1 mM $CaCl_2$, 25 mM $MgCl_2$) and 20.4 µL of 100 U mL^{-1} DNase. The mixture was incubated at 37°C for 15 minutes. Subsequently, 102 µL of 2 % DTT was added, and the mixture was incubated for 30 minutes at room temperature with agitation at 1000 rpm. After incubation, the sample was centrifuged at 100,000 ×g for 20 minutes, and the supernatant was collected. To the collected supernatant, 83 µL of 100 mM was added. The total volume added during the procedure was 722 µL, combined with the initial BAS volume (~400 µL), resulting in a final total volume of 1122 µL. The dilution factor for BAS was calculated to be 1.55, corresponding to a concentration of 41.55 mg/mL BAS in the final solution. Serial dilutions were subsequently prepared for ELISA measurement.

8.11.1.5 Enzymatic liquefaction

H_2O_2. 75 mg of BAS was weighed and mixed with 1.5 mL of 0.3 M H_2O_2. The mixture was allowed to react for 1 minute. Following this, the sample was diluted in proportions of 1:2, 1:5, or 1:10 by adding 10 times concentrated PBST to adjust the buffer conditions (final conditions: 10 mM PBST, pH 7.5, 0.05 % Tween 20). The final ratio of BAS to solution was calculated to be 20:1 (w/v).

H_2O_2 + NaN_3/$Na_2S_2O_4$. 75 mg of BAS was weighed and mixed with 750 µL of 0.3 M H_2O_2. The mixture was allowed to react for 1 minute. Subsequently, 0.1 M NaN_3 or 0.1 M $Na_2S_2O_4$ was added, and the sample was incubated for 1 hour at room temperature. After incubation, the sample was diluted 1:10 by adding 10 times concentrated PBST to adjust the buffer conditions (final conditions: 10 mM

PBST, pH 7.5, 0.05 % Tween 20). In this case, the final ratio of BAS to solution was 10:1 (w/v).

8.11.1.6 Organic solvents: n-ButOH

AIP4 was hydrolyzed following the procedure described in Section 8.6.2, resulting in a stock solution of AIP4o at 400 µM. Three aliquots of BAS (125 µL each) were spiked with AIP4o at different levels: A) 4000 nM by adding 1.25 µL of the 400 µM AIP4o stock: B) by adding 12.5 µL of a 4 µM AIP4o solution, and C) by adding 1.25 µL of the 4 µM AIP4o solution. A negative control sample was also prepared by subjecting a BAS aliquot to the same procedure without spiking with AIP4o.The samples were vortexed for 5 minutes to ensure proper mixing and incubated overnight at 4°C to allow integration of AIP4o into the BAS matrix. The next day, 250 µL of n-butanol (n-ButOH) was added to each sample, followed by vortexing for 5 minutes. The samples were then centrifuged at 10,000 ×g for 10 minutes, and 100 µL of the supernatant was carefully collected using a Hamilton syringe. The supernatants were evaporated in a SpeedVac, and the resulting pellets were reconstituted in 200 µL of PBST. Finally, serial dilutions of the reconstituted samples were prepared for analysis by ELISA. The steps involved in this procedure are detailed in Figure 8.2.

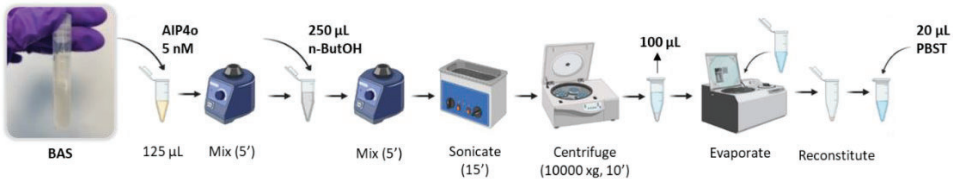

Figure 8.2. *Procedure for AIP4o extraction by n-ButOH.*

8.11.1.7 Immunoaffinity column (As381-IAC)

IgG purification by ammonium sulfate ($(NH_4)_2SO_4$ ***) precipitation.*** The antibody purification protocol follows the ammonium sulfate precipitation method described by Manson, M. M., *Immunochemical Protocols* (Humana Press, 1992). A saturated solution of ammonium sulfate was prepared 24 hours in advance. The antiserum (As381, 600 µL) was cooled in a 1.5 mL Eppendorf vial with a small stir bar in an ice/water bath. 400 µL of saturated ammonium sulfate solution was then added dropwise to achieve a final saturation of 50 %. The mixture was

stirred gently overnight at 4°C to allow antibody precipitation. The sample was centrifuged at 4,000 rpm for 20 minutes at 4°C, and the supernatant was carefully discarded. The resulting pellet was resuspended in 300 µL of 10 mM PBS. The resuspended antibody was further purified by dialysis against 0.5 mM PBS (four times with 5 L each) followed by Milli-Q water (once with 5 L). The purified antibody was lyophilized and stored at -40°C, while working aliquots (1 mg/mL in 10 mM PBS) were kept at 4°C for immediate use.

Antibody Coupling to HiTrap™ NHS-Activated HP Column. A HiTrap™ NHS-activated HP column (1 mL volume, Cytiva) was used for the antibody coupling process. The coupling buffer was prepared as 0.2 M $NaHCO_3$ with 0.5 M NaCl, pH 8. A total of 18 mg of the lyophilized antibody (As381) was dissolved in 1.8 mL of coupling buffer to prepare the ligand solution. The column was first washed to remove 100 % isopropanol by flushing with cold 1 mM HCl (kept on ice bath). Two washes with 3 mL of HCl were performed at a flow rate of 1 mL/min. Immediately afterward, the ligand solution was added to the column, and the top and bottom caps were securely placed. The column was incubated for 45 minutes at 25°C. Following incubation, 1 mL of coupling buffer was injected into the column, and 1 mL of the eluate (containing the ligand solution) was collected. This eluate was re-injected into the column and incubated again for 45 minutes at 25°C to enhance binding efficiency. After this step, 1 mL of coupling buffer was injected, and the eluate was collected. This eluate was lyophilized and weighed to calculate the binding efficiency. The next step was washing and deactivation. Two buffers were prepared for this process: Buffer A: 0.5 M ethanolamine, 0.5 M NaCl, pH 8.3 and Buffer B: 0.1 M sodium acetate, 0.5 M NaCl, pH 4. The column was washed sequentially with 6 mL of Buffer A, followed by 6 mL of Buffer B, and then another 6 mL of Buffer A. The column was then incubated for 45 minutes at room temperature. After incubation, another washing sequence was performed: 6 mL of Buffer B, 6 mL of Buffer A, and 6 mL of Buffer B. Finally, 6 mL of binding buffer (10 mM PBS, pH 7.5) was injected. At this point, the column was ready for use. For storage, a solution of 0.05 M Na_2HPO_4 and 0.1 M NaN_3, pH 7, was used.

Calculation of theoretical column capacity. The volume of As381 purified by ammonium sulfate precipitation was 1.8 mL. For coupling to the column, 10 mg of this antibody were loaded (1 mL of lyophilized As381 dissolved in coupling buffer at a concentration of 10 mg mL^{-1}). Out of the total As381 loaded, 2 mg were not retained, meaning that 8 mg were successfully bound to the column, equivalent to 5.33×10^5 nmol. The theoretical binding capacity of the column

was calculated based on the following assumptions: I) 10% of the polyclonal antibodies in the As381 pool specifically recognize AIP4o. II) 50% of the immobilized antibodies are correctly oriented on the column surface. III) Each antibody has two binding sites (valences). Based on these assumptions, the estimated retention capacity was calculated to be 5.83 µg of AIP4o.

AIP4o extraction procedure by As381-IAC. The column was conditioned by passing 2 mL of 60 % MeOH in 10 mM PBS buffer (pH 7.5), followed by 5 mL of PBS buffer, maintaining a flow rate of 1 mL/min throughout the process. To prepare the sample for loading, 1 mL of PBS, TSB, or BAS was doped with 0.5 µM AIP4o, corresponding to 10 % of the column's theoretical capacity. To spike the samples, AIP4 (10 mM stock in DMSO) was hydrolyzed according to the procedure described in Section 8.6.2 to obtain a 400 µM AIP4o stock solution. Next, 25 µL of the 400 µM stock was diluted into 975 µL of the sample (PBS, TSB, or BAS) to prepare a 10 µM working solution. A final 1:20 dilution was then performed by mixing 100 µL of the 10 µM solution with 1900 µL of the sample matrix to achieve a final concentration of 0.5 µM. 1 mL of the spiked sample was loaded onto the column and incubated at room temperature for 5 minutes to promote binding. The column was then washed by passing 6 mL of 20% MeOH in PBS at a flow rate of 1 mL/min to remove unbound material. Bound analytes were eluted by passing 4 mL of 60% MeOH in PBS through the column, and the eluate, containing the retained analyte, was collected in fractions. After elution, the column was reconditioned by injecting 4 mL of PBS. For storage, 2 mL of 0.1% NaN_3 in PBS were injected, and the column was stored at 4°C for future use. The eluted fractions were prepared for ELISA analysis by adjusting the solution to 10 % MeOH in 10 mM PBST (pH 7.5) containing 0.05 % Tween 20, with a conductivity of 15 mS cm^{-1}, ensuring consistent assay conditions between samples and the calibration curve.

8.11.1.8 Functionalized magnetic particles (mAb23-MPs)

Functionalization of the MPs with mAb23. The magnetic particles (MPs) used for this procedure were Dynabeads™ MyOne™ Tosylactivated (Thermo Fisher Scientific). Four buffers were prepared following the manufacturer's guidelines: Buffer A (0.1 M Borate Buffer, pH 9.5), Buffer C (3 M Ammonium Sulfate in Buffer A, pH 9.5), Blocking Buffer (10 mM PBST with 0.05% Tween and 0.5% BSA), and Storage Buffer (PBST with 0.1% BSA). To begin, 200 µL of MPs (100 mg mL^{-1}) were

transferred into a 1.5 mL Eppendorf tube and placed on a magnetic rack for 3 minutes to allow the separation of the particles. The supernatant was discarded, and the MPs were washed with 300 µL of Buffer A. This step was repeated two more times, each time placing the tube on the magnetic rack for 3 minutes and discarding the supernatant. Subsequently, 400 µL of mAb 23.1.3.7.1 at a concentration of 2 mg mL^{-1} in Buffer A were added to the MPs. The antibody had been purified and concentrated using Vivaspin® Turbo 4 concentrators (Sartorius, 50 kDa cutoff). Initially, the Vivaspin device was prewashed with 4 mL of Milli-Q water to remove glycerin and sodium azide, centrifuged at 4000 ×g for 5 minutes at 20°C. After prewashing, 2 mL of the antibody solution (measured at 0.958 mg mL^{-1} by NanoDrop) were loaded and centrifuged at 4000 ×g for 1 minute, repeating this process five times while ensuring the membrane did not dry out. After concentration, the waste was measured and confirmed to contain no antibody loss. Buffer A was added in 1 mL increments, followed by centrifugation at 4000 ×g for 3 minutes, until the final concentration of 2 mg mL^{-1} was achieved. To initiate coupling, 200 µL of Buffer C were added to the MPs and incubated overnight at 37°C with orbital shaking to prevent particle aggregation. The next day, the MPs were separated using a magnetic rack for 2 minutes, and the supernatant was discarded. The unbound antibody concentration was measured using NanoDrop at 0.221 mg mL^{-1}, indicating a coupling efficiency of 88.95 %. Blocking was performed by adding 600 µL of Blocking Buffer to the MPs and incubating overnight at 37°C without shaking. The following day, the MPs were separated using a magnetic rack, and the supernatant was discarded. The MPs were then washed twice with 1 mL of Storage Buffer, each time using the magnetic rack for 2 minutes and discarding the supernatant. Finally, the functionalized MPs were resuspended in 1 mL of Storage Buffer and stored at 4°C for future use.

AIP1o extraction procedure by mAb23-MPs. The magnetic rack in a 96-well plate format, provided by the Centro Nacional de Microelectrónica (CNM), was used for this procedure. First, 25 µL of magnetic particles (MPs) functionalized with mAb 23.1.3.7.1 were taken. The MPs, stored at a concentration of 20 mg mL^{-1} in storage buffer, were placed on the magnetic rack to allow separation. Once separated, the supernatant was discarded. The MPs were washed twice with 200 µL of 10 mM PBS, followed by resuspension in 200 µL of sample (PBS spiked with 50 nM AIP1o). The mixture was incubated for 30 minutes on an IKA MS 3 basic shaker in a 96-well plate format, allowing the analyte to bind to the MPs. After

incubation, the MPs were placed on the magnetic rack for separation, and the supernatant was collected for later quantification by ELISA to determine the unbound AIP1o. The MPs were then washed twice with 200 µL of 10 mM PBS, discarding the supernatant after each wash. Subsequently, the MPs were resuspended in 200 µL of either Gly-HCl (pH 2.7) or CA-NaOH (pH 3), followed by incubation for 30 minutes on the IKA MS 3 basic shaker in the same plate format. This step allowed the analyte to dissociate from the MPs. The MPs were again placed on the magnetic rack, and 100 µL of the supernatant containing the analyte was collected. For Gly-HCl, 12.5 µL of 10× PBS (100 mM, pH 7.5) containing 4.5 % 5N NaOH was added, while for CA-NaOH, 12.5 µL of 10 × PBS containing 36 % 5N NaOH was added. In both cases, 12.5 µL of 10× Tween (0.5 %) was also added. The samples were prepared for quantification by ELISA, including multiple dilutions as needed. The procedure is illustrated in Figure 8.3.

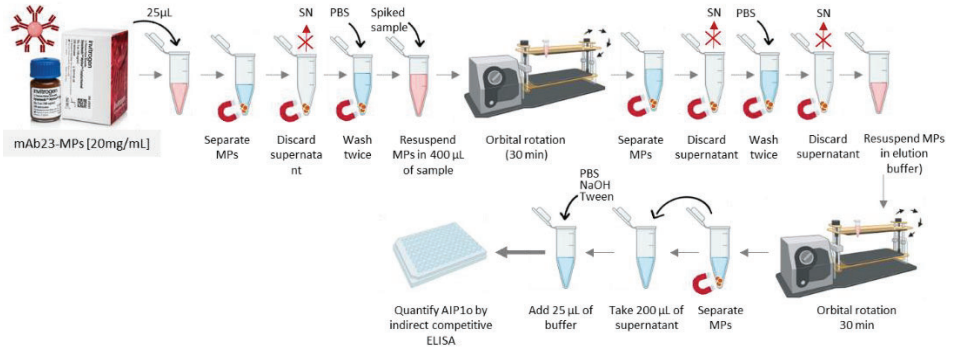

Figure 8.3. *Procedure for AIP1o extraction by mAb23-MPs.*

8.11.1.9 Immunoaffinity spin columns (mAb23-ISCs)

Functionalization of the ISCs with mAb23. Pierce NHS-Activated Agarose spin columns (0.2 mL) were used for antibody immobilization and subsequent column preparation. Antibody Immobilization: to begin, the antibody was concentrated, and the buffer was exchanged to 10 mM PBS. A total of 400 µL of the antibody solution (containing 3.02 mg of mAb) was added to the dry resin in the spin columns. The antibody was introduced into the resin either by applying pressure with a syringe or by centrifugation at low speed. Both caps were placed on the column, and it was incubated for 4 hours at room temperature to allow binding.

After incubation, the caps were removed, and the column was placed in a collection tube. The column was centrifuged at 1000 ×g for 1 minute, and the flow-through was collected. The column was then washed by adding 400 µL of Coupling/Wash buffer (10 mM PBS, pH 7.5) and centrifuging at 1000 ×g for 1 minute. This washing step was repeated. Blocking of Remaining Active Sites: to block the remaining active sites on the resin, 400 µL of Quenching buffer (1 M Tris, pH 7.4) was added to the column. The buffer was introduced into the resin either by applying pressure with a syringe or by centrifugation at low speed. The column was capped at both ends and incubated for 15 minutes at room temperature. After incubation, the caps were removed, and the column was placed in a collection tube. Washing: the column was centrifuged at 1000 ×g for 1 minute to remove the Quenching buffer, then washed with 400 µL of Coupling/Wash buffer. The washing step was followed by centrifugation at 1000 × g for 1 minute. Storage: for storage, 1.5 mL of Storage buffer (PBS with 0.05 % NaN_3) was added to the column. The column was centrifuged at 1000 ×g until only 0.5–1 mL of buffer remained above the resin bed. Finally, the column was capped at both ends and stored upright at 4°C for future use.

Calculation of the retention capacity of mAb23-ISCs. In the immunoaffinity spin columns (ISCs), 400 µL of mAb 23.1.3.7.1 at a concentration of 7.54 mg mL^{-1} were loaded. According to the coupling efficiency study conducted using the Bradford assay on the fractions collected during antibody immobilization, no antibody was detected in these fractions. This indicates that the antibody was completely retained on the column, suggesting that the entire quantity (3 mg of mAb23) was successfully immobilized. To calculate the theoretical binding capacity, the following parameters were considered: the antibody volume (0.4 mL), its concentration (7.54 mg mL^{-1}), the molecular weight of the antibody (150,000 Da), the fact that each antibody possesses two paratopes, and the assumption that 50 % of the antibodies are correctly oriented on the column. Based on these factors, the theoretical binding capacity of the column was estimated to be 20 nmol of AIP1o.

AIP1o extraction procedure by mAb23-ISCs. The conditioning step began with spinning the column at 1000 ×g for 2 minutes to remove the flowthrough. Subsequently, 200 µL of 10 mM PBS was added, followed by centrifugation at 1000 ×g for 1 minute, and the flowthrough was discarded. This process was repeated twice. For elution, 200 µL of PBS with 90 % methanol was added to the column, incubated for 3 minutes with end-to-end rotation, and then centrifuged

at 1000 ×g for 2 minutes. This step was repeated four times to ensure thorough elution. The column was reconditioned by adding 200 µL of 10 mM PBS, spinning at 1000 ×g for 1 minute, and discarding the flowthrough. This step was performed four times. For the load step, 200 µL of BAS treated with DTBA was added to the column. The column was incubated for 30 minutes with end-to-end rotation (Program 63, velocity 30), followed by centrifugation at 1000 ×g for 1 minute to remove unbound components. The wash step involved adding 200 µL of 10 mM PBS, spinning the column at 1000 ×g for 1 minute, and discarding the flowthrough. This process was repeated four times to thoroughly wash the column. For the second elution, 100 µL of PBS with 90 % methanol was added, incubated for 3 minutes with end-to-end rotation, and centrifuged at 1000 ×g for 2 minutes. This step was repeated three times. Following elution, the column was washed again by adding 200 µL of 10 mM PBS, spinning at 1000 ×g for 1 minute, and discarding the flowthrough. This step was repeated three times. Finally, for storage, 400 µL of storage buffer (PBS with 0.05 % NaN_3) was added, and the column was centrifuged at 1000 ×g for 1 minute to remove excess flowthrough. Another 400 µL of storage buffer was added, and the column was stored upright at 4°C for further use. Figure 8.4 illustrates the steps of the extraction procedure.

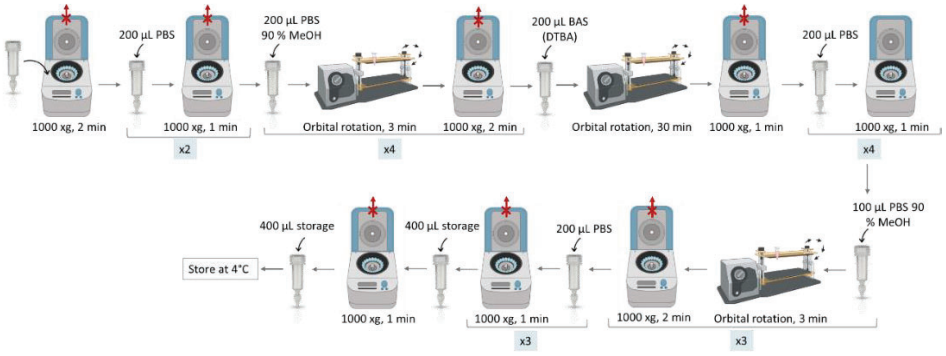

Figure 8.4. *Procedure for AIP1o extraction by mAb23-ISCs.*

9 ACRONYMS & ABBREVIATIONS

9.1 ACRONYMS AND ABBREVIATIONS

A. baumannii	*Acinetobacter baumannii*
Ab	Antibody
Abs.	Absorbance
AcOEt	Ethyl acetate
Ag	Antigen
Agr	Accessory gene regulator
AHLs	N-acyl homoserine lactones
AI	Autoinducer
AIDS	Acquired immunodeficiency syndrome
AIP	Autoinducing Peptide
AIP4NH-hapten	Lactam AIP hapten
AIPc	AIP closed
AIPc	AIP closed form
AIPL-hapten	Linear AIP hapten
AIPo	AIP open
AIPo	AIP open form
AIPS-hapten	Thiolactone AIP hapten
A_{max}	Maximum Absorbance
AMH	Anti-Müllerian Hormone
A_{min}	Minimum Absorbance
AMR	Antimicrobial resistance
ARDS	Acute respiratory distress syndrome
As	Antiserum
AST	Antimicrobial susceptibility testing
AUC	Area under the curve
B0	Preimmune blood
BAL	Bronchoalveolar lavage
BAS	Bronchial aspirate samples
BHI	Brain Heart Infusion
BSA	Bovine serum albumin
CA	Competitor Antigen
CA 125	Cancer Antigen 125
$CaCl_2$	Calcium chloride
CA-MRSA	Community-Associated MRSA
CAP	Community-acquired pneumonia
CC	Clonal complex

CEA	Carcinoembryonic antigen
CF	Cystic fibrosis
ClfB	Clumping factor B
cm	Centimeter
COPD	Chronic obstructive pulmonary disease
CR	Cross Reactivity
CRP	C-reactive protein
DMP	Dimethyl pimelimidate
DTT	Dithiothreitol
E. coli	*Escherichia coli*
E. faecium	*Enterococcus faecium*
EG	Ethylene glycol
ELISA	Enzyme-linked immunosorbent assay
EMRSA	Epidemic MRSA
Ep	Epitope
EPL	Extracellular polysaccharide
ETs	Exfoliative toxins
EU	European Union
FB	Final blood
FISH	Fluorescence in situ hybridization
FnBP	Fibrinogen-binding protein
GMO	Genetically modified organism
HAIs	Hospital-acquired infections
HA-MRSA	Healthcare-Acquired MRSA
HAP	Hospital-acquired pneumonia
HCH	Horseshoe crab hemocyanin
HHQ	4-Hydroxy-2-Heptylquinoline
HIV	Human immunodeficiency virus
Hla	Alpha-hemolysin
Hlg	Gamma-hemolysin
HQNO	4-Hydroxy-2-Heptylquinoline N-oxide
HRP	Horseradish peroxidase
HSL	Homoserine lactone
HSV	Herpes simplex virus
IAC	Immunoaffinity column
IC_{50}	Half-maximal inhibitory concentration
IE	Infective endocarditis
IFAs	Immunofluorescence Assays
IL-6	Interleukin-6

IQS	Integrated Quorum Sensing Signal
ISC	Immunoaffinity spin column
K. pneumoniae	*Klebsiella pneumoniae*
KLH	Keyhole limpet hemocyanin
L	Liter
LAMP	Loop-mediated isothermal amplification
LC	Liquid chromatography
LC-MS	Liquid chromatography-mass spectrometry
LFAs	Lateral Flow Assays
LFIA	Lateral Flow Immunoassay
LH	Luteinizing Hormone
LLOQ	Lower Limit of Quantification
LLOQ	Lower limit of quantification
LOD	Limit of Detection
Log	Logarithm
LOQ	Limit of Quantification
LPS	Lipopolysaccharide
LRTIs	Lower respiratory tract infections
LTA	Lipoteichoic acid
m/z	mass-to-charge ratio
mAb	Monoclonal Antibody
mAb	Monoclonal antibody
mAb 14	mAb 14.5.1.1.2
mAb23	mAb 23.1.3.7.1
MALDI-TOF	Matrix-Assisted Laser Desorption/Ionization Time-of-Flight
mAb14	mAb 14.5.1.1.2
MDR	Multidrug-resistant
MeOH	Methanol
MH	Mueller-Hinton
Min	Minute
MLS	Macrolides, Lincosamides, and Streptogramins
MLST	Multilocus sequence typing
MP	Magnetic particle
MRSA	Methicillin-resistant *S. aureus*
MS	Mass spectrometry
mS	Millisiemens
MS4N	Multivalent Systems for Nanomedicine
MSA	Mannitol salt agar

MSCRAMMs	Microbial surface components recognizing adhesive matrix molecules
MW	Molecular weight
NAC	N-acetylcysteine
Nb4D	Nanobiotechnology for Diagnostics
n-BuOH	Butanol
NGS	Next Generation Sequencing
NHS	N-hydroxysuccinimide
nM	Nanomolar
nm	Nanometer
O/N	Overnight
OD600	Optical density at 600 nm
OH-pnz	Hydroxyphenazine
OPD	o-phenylenediamine dihydrochloride
P. aeruginosa	*Pseudomonas aeruginosa*
pAb	Polyclonal Antibody
PBP	Penicillin-binding protein
PBS	Phosphate-buffered saline
PBST	Phosphate-buffered saline supplemented with Tween 20
PCR	Polymerase Chain Reaction
PCT	Procalcitonin
PEG	Polyethylene glycol
PIA	Polysaccharide intercellular adhesin
PK	Proteinase K
PMSF	Phenylmethylsulfonyl fluoride
PoC	Point-of-Care
PQS	*Pseudomonas* Quinolone Signal
PSA	Prostate-Specific Antigen
PSMs	Phenol-soluble modulins
PVDF	Polyvinylidene fluoride
PVL	Panton-Valentine leukocidin
Pyo	Pyocyanin
q-PCR	Real-Time PCR
QQ	Quorum Quenching
QS	Quorum Sensing
QSI	Quorum sensing inhibitor
QSM	Quorum Sensing Molecule
R^2	Regression coefficient
RFG	Reactive functional group

RSV	Respiratory syncytial virus
S. aureus	*Staphylococcus aureus*
S. pneumoniae	*Streptococcus pneumoniae*
S. pyogenes	*Streptococcus pyogenes*
SAB	*S. aureus* bacteremia
SCCmec	Staphylococcal chromosomal cassette mec
SD	Standard deviation
SIA	Succinimidil iodoacetate
SpA	*S. aureus* protein A
SSSS	Staphylococcal scalded skin syndrome
SSTIs	Skin and soft tissue infections
TB	Tuberculosis
TCEP	Tris(2-carboxyethyl)cphosphine
tetM	Tetracycline resistance ribosomal protection gene
TMB	3,3',5,5'-tetramethylbenzidine
TSB	Tryptic Soy Broth
TSS	Toxic shock syndrome
TSST-1	Toxic shock syndrome toxin-1
ULOQ	Upper limit of quantification
UPLC	Ultrahigh-Performance Liquid Chromatograph
URTIs	Upper respiratory tract infections
US	United States
UTIs	Urinary tract infections
VISA	Vancomycin-intermediate *S. aureus*
VRSA	Vancomycin-resistant *S. aureus*
WGS	Whole Genome Sequencing
WHO	World Health Organization